Publishing House ASV

begell house, inc. publishers

Scientific coordination is carried out by the Russian Academy of Architecture and Construction Sciences (RAACS)

Volume 20 • Issue 4 • 2024

ISSN 2588-0195 (Online)
ISSN 2587-9618 (Print) Continues ISSN 1524-5845

International Journal for

Computational Civil and Structural Engineering

Международный журнал по расчету гражданских и строительных конструкций

https://ijccse.iasv.ru/

DOI: 10.22337/2587-9618
GICID: 71.0000.1500.2830

Scientific coordination is carried out by the Russian Academy of Architecture and Construction Sciences (RAACS)

PUBLISHER

ASV Publishing House
(ООО «Издательство АСВ»)
19/1,12, Yaroslavskoe Shosse, 120338, Moscow, Russia
Tel. +7(925)084-74-24; E-mail: iasv@iasv.ru; Интернет-сайт: http://iasv.ru/

ADVISORY EDITORIAL BOARD

EDITORIAL TEAM

INVITED REVIEWERS

AIMS AND SCOPE

The aim of the Journal is to advance the research and practice in structural engineering through the application of computational methods. The Journal will publish original papers and educational articles of general value to the field that will bridge the gap between high-performance construction materials, large-scale engineering systems and advanced methods of analysis.

The scope of the Journal includes papers on computer methods in the areas of structural engineering, civil engineering materials and problems concerned with multiple physical processes interacting at multiple spatial and temporal scales. The Journal is intended to be of interest and use to researches and practitioners in academic, governmental and industrial communities.

ОБЩАЯ ИНФОРМАЦИЯ О ЖУРНАЛЕ

International Journal for Computational Civil and Structural Engineering

(Международный журнал по расчету гражданских и строительных конструкций)

Международный научный журнал "International Journal for Computational Civil and Structural Engineering (Международный журнал по расчету гражданских и строительных конструкций)" (IJCCSE) является ведущим научным периодическим изданием по направлению «Инженерные и технические науки», издаваемым, начиная с 1999 года (ISSN 2588-0195 (Online); ISSN 2587-9618 (Print) Continues ISSN 1524-5845). В журнале на высоком научно-техническом уровне рассматриваются проблемы численного и компьютерного моделирования в строительстве, актуальные вопросы разработки, исследования, развития, верификации, апробации и приложений численных, численно-аналитических методов, программно-алгоритмического обеспечения и выполнения автоматизированного проектирования, мониторинга и комплексного наукоемкого расчетно-теоретического и экспериментального обоснования напряженно-деформированного (и иного) состояния, прочности, устойчивости, надежности и безопасности ответственных объектов гражданского и промышленного строительства, энергетики, машиностроения, транспорта, биотехнологий и других высокотехнологичных отраслей.

В редакционный совет журнала входят известные российские и зарубежные деятели науки и техники (в том числе академики, члены-корреспонденты, иностранные члены, почетные члены и советники Российской академии архитектуры и строительных наук). Основной критерий отбора статей для публикации в журнале − их высокий научный уровень, соответствие которому определяется в ходе высококвалифицированного рецензирования и объективной экспертизы, поступающих в редакцию материалов.

Журнал входит в Перечень ВАК РФ ведущих рецензируемых научных изданий, в которых должны быть опубликованы основные научные результаты диссертаций на соискание ученой степени кандидата наук, на соискание ученой степени доктора наук по научным специальностям и соответствующим им отраслям науки:

- 1.1.8 – Механика деформируемого твердого тела (технические науки),
- 1.2.2 – Математическое моделирование численные методы и комплексы программ (технические науки),
- 2.1.1 – Строительные конструкции, здания и сооружения (технические науки),
- 2.1.2 – Основания и фундаменты, подземные сооружения (технические науки),
- 2.1.5 – Строительные материалы и изделия (технические науки),
- 05.23.07 – Гидротехническое строительство (технические науки),
- 2.1.9 – Строительная механика (технические науки)

В Российской Федерации журнал индексируется Российским индексом научного цитирования (РИНЦ).

Журнал входит в базу данных Russian Science Citation Index (RSCI), полностью интегрированную с платформой Web of Science. Журнал имеет международный статус и высылается в ведущие библиотеки и научные организации мира.

Издатели журнала – *Издательство Ассоциации строительных высших учебных заведений /АСВ/* (Россия, г. Москва) и до 2017 года *Издательский дом Begell House Inc*. (США, г. Нью-Йорк). Официальными партнерами издания является *Российская академия архитектуры и строительных наук* (РААСН), осуществляющая научное курирование издания, и *Научно-исследовательский центр СтаДиО* (ЗАО НИЦ СтаДиО).

Цели журнала – демонстрировать в публикациях российскому и международному профессиональному сообществу новейшие достижения науки в области вычислительных методов решения фундаментальных и прикладных технических задач, прежде всего в области строительства.

Задачи журнала:

• предоставление российским и зарубежным ученым и специалистам возможности публиковать результаты своих исследований;

• привлечение внимания к наиболее актуальным, перспективным, прорывным и интересным направлениям развития и приложений численных и численно-аналитических методов решения фундаментальных и прикладных технических задач, совершенствования технологий математического, компьютерного моделирования, разработки и верификации реализующего программно-алгоритмического обеспечения;

• обеспечение обмена мнениями между исследователями из разных регионов и государств.

Тематика журнала. К рассмотрению и публикации в журнале принимаются аналитические материалы, научные статьи, обзоры, рецензии и отзывы на научные публикации по фундаментальным и прикладным вопросам технических наук, прежде всего в области строительства. В журнале также публикуются информационные материалы, освещающие научные мероприятия и передовые достижения Российской академии архитектуры и строительных наук, научно-образовательных и проектно-конструкторских организаций.

Тематика статей, принимаемых к публикации в журнале, соответствует его названию и охватывает направления научных исследований в области разработки, исследования и приложений численных и численно-аналитических методов, программного обеспечения, технологий компьютерного моделирования в решении прикладных задач в области строительства, а также соответствующие профильные специальности, представленные в диссертационных советах профильных образовательных организациях высшего образования.

Редакционная политика. Политика редакционной коллегии журнала базируется на современных юридических требованиях в отношении авторского права, законности, плагиата и клеветы, изложенных в законодательстве Российской Федерации, и этических принципах, поддерживаемых сообществом ведущих издателей научной периодики.

За публикацию статей плата с авторов не взымается. Публикация статей в журнале бесплатная. На платной основе в журнале могут быть опубликованы материалы рекламного характера, имеющие прямое отношение к тематике журнала.

Журнал предоставляет непосредственный открытый доступ к своему контенту, исходя из следующего принципа: свободный открытый доступ к результатам исследований способствует увеличению глобального обмена знаниями.

Индексирование. Публикации в журнале входят в системы расчетов индексов цитирования авторов и журналов. «Индекс цитирования» – числовой показатель, характеризующий значимость данной статьи и вычисляющийся на основе последующих публикаций, ссылающихся на данную работу.

Авторам. Прежде чем направить статью в редакцию журнала, авторам следует ознакомиться со всеми материалами, размещенными в разделах сайта журнала (интернет-сайт Российской академии архитектуры и строительных наук (http://raasn.ru); подраздел «Издания РААСН» или интернет-сайт Издательства АСВ (http://iasv.ru); подраздел «Журнал IJCCSE»): с основной информацией о журнале, его целями и задачами, составом редакционной коллегии и редакционного совета, редакционной политикой, порядком рецензирования направляемых в журнал статей, сведениями о соблюдении редакционной этики, о политике авторского права и лицензирования, о представлении журнала в информационных системах (индексировании), информацией о подписке на журнал, контактными данными и пр. Журнал работает по лицензии Creative Commons типа cc by-nc-sa (Attribution Non-Commercial Share Alike) – Лицензия «С указанием авторства – Некоммерческая – Копилефт».

Рецензирование. Все научные статьи, поступившие в редакцию журнала, проходят обязательное двойное слепое рецензирование (рецензент не знает авторов рукописи, авторы рукописи не знают рецензентов).

Заимствования и плагиат. Редакционная коллегия журнала при рассмотрении статьи проводит проверку материала с помощью системы «Антиплагиат». В случае обнаружения многочисленных заимствований редакция действует в соответствии с правилами COPE.

Подписка. Журнал зарегистрирован в Федеральном агентстве по средствам массовой информации и охраны культурного наследия Российской Федерации. Индекс в общероссийском каталоге РОСПЕЧАТЬ − 18076.

По вопросам подписки на международный научный журнал “International Journal for Computational Civil and Structural Engineering (Международный журнал по расчету гражданских и строительных конструкций)” обращайтесь в Агентство «Роспечать» (Официальный сайт в сети Интернет: http://www.rosp.ru/) или в издательство Ассоциации строительных вузов (АСВ) в соответствии со следующими контактными данными:

ООО «Издательство АСВ»

Юридический адрес: 129337, Россия, г. Москва, Ярославское ш., д. 26, офис 705;

Фактический адрес: 129337, Россия, г. Москва, Ярославское ш., д. 19, корп. 1, 5 этаж, офис 12 (ТЦ Соле Молл);

Телефоны: +7 (925) 084-74-24;

Интернет-сайт: www.iasv.ru. Адрес электронной почты: iasv@iasv.ru.

Контактная информация. По всем вопросам работы редакции, рецензирования, согласования правки текстов и публикации статей следует обращаться к главному редактору журнала академику РААСН *Сидорову Владимиру Николаевичу* (адреса электронной почты: sidorov.vladimir@gmail.com, sidorov@iasv.ru, iasv@iasv.ru, sidorov@raasn.ru) или к техническому редактору журнала советнику РААСН *Кайтукову Таймуразу Батразовичу* (адреса электронной почты: tkaytukov@gmail.com; kaytukov@raasn.ru). Кроме того, по указанным вопросам, а также по вопросам размещения в журнале рекламных материалов можно обращаться к генеральному директору ООО «Издательство АСВ» *Никитиной Надежде Сергеевне* (адреса электронной почты: iasv@iasv.ru, nsnikitina@mail.ru, ijccse@iasv.ru).

Журнал становится технологичнее. Издательство АСВ с сентября 2016 года является членом Международной ассоциации издателей научной литературы (Publishers International Linking Association (PILA)), осуществляющей свою деятельность на платформе CrossRef. Оригинальным статьям, публикуемым в журнале, будут присваиваться уникальные номера (индексы DOI – Digital Object Identifier), что значительно облегчит поиск метаданных и местонахождение полнотекстового произведения. DOI – это система определения научного контента в сети Интернет.

С октября 2016 года стал возможен прием статей на рассмотрение и рецензирование через онлайн систему приема статей Open Journal Systems на сайте журнала (электронная редакция): https://ijccse.iasv.ru.

Автор имеет возможность следить за продвижением статьи в редакции журнала в личном кабинете Open Journal Systems и получать соответствующие уведомления по электронной почте.

В феврале 2018 года журнал был зарегистрирован в Directory of open access journals (DOAJ) (это один из самых известных поисковых сервисов в мире, который предоставляет открытый доступ к материалам и индексирует не только заголовки журналов, но и научные статьи), в сентябре 2018 года включен в продукты EBSCO Publishing.

В ноябре 2020 года журнал начал индексироваться в международной базе Scopus.

International Journal for
Computational Civil and Structural Engineering
(Международный журнал по расчету гражданских и строительных конструкций)
Volume 20, Issue 4 ***2024***

Scientific coordination is carried out by the Russian Academy of Architecture and Construction Sciences (RAACS)

CONTENTS

International Journal for
Computational Civil and Structural Engineering
(Международный журнал по расчету гражданских и строительных конструкций)
Volume 20, Issue 4 ***2024***

Scientific coordination is carried out by the Russian Academy of Architecture and Construction Sciences (RAACS)

СОДЕРЖАНИЕ

DOI:10.22337/2587-9618-2024-20-4-14-22

DETERMINATION OF PARAMETERS OF AN EXPERIMENTAL MODEL OF A MULTI-STOREY STEEL FRAME

Youssef H. Hamaty, Alexander T. Tusnin
Moscow State University of Civil Engineering (National Research University), Moscow, RUSSIA

Abstract: The load-bearing capacity of the structure can be accurately determined on large models made from the same material (or a material with similar elastic properties) as the actual structure. The scale of the model can be 1/5-1/6. This depends not only on the actual dimensions of the structure but also on the material of the model. Experience shows that for metal and concrete models, it is reasonable to adopt a scale of 1/5-1/15. Previous studies show that analysis based on the calculation of an idealized multi-story steel frame structure without considering imperfections does not fully reflect the actual performance of the steel frame and may not always ensure the load-bearing capacity of the building and the operational requirements for permissible frame displacements. It is interesting to compare some approximate data on the cost of testing in kind with the cost of testing the model. Thus, full-scale tests of large-panel buildings erected on subsidence soils ac-count for 10 to 30% of the cost of the buildings themselves. The cost of such tests on models would be 2-3%, that is, 5-10 times cheaper. The provided data indicates the feasibility of using modeling in the design of structures. The research results can be used to refine and develop building codes and standards, enabling the calculation and design of multi-story buildings that account for the actual performance of the steel frame-work.

Keywords: multi-storey buildings, installation and Fabrication errors, rigid frame, steel constructions, linear calculation, nonlinear calculation, geometric imperfections

ОПРЕДЕЛЕНИЕ ПАРАМЕТРОВ ЭКСПЕРИМЕНТАЛЬНОЙ МОДЕЛИ МНОГОЭТАЖНОГО СТАЛЬНОГО КАРКАСА

Ю. Хамати, А.Р. Туснин
Национальный исследовательский Московский государственный строительный университет
(НИУ МГСУ); г. Москва, РОССИЯ

Аннотация: Несущую способность конструкции можно достаточно точно определить на крупных моделях, изготовленных из того же материала (или близкого к нему по своим упругим свойствам), что и сама конструкция. Масштаб модели может быть 1/5-1/6. Это зависит не только от натурных размеров сооружения, но и от материала модели. Опыт показывает, что при металлических, бетонных и армоцементных моделях масштаба целесообразно принимать 1/5-1/15. Проведённые ранее исследования показывают, что анализ, основанный на расчете идеализированной многоэтажной стальной каркасной конструкции без учёта несовершенств, не полностью отражает действительную работу стального каркаса и не всегда может обеспечить несущую способность здания и эксплуатационные требования по допустимым перемещениям каркасов. Интересно сопоставить некоторые примерные данные стоимости испытаний в натуре со стоимостью испытания модели. Так, натурные испытания крупнопанельных зданий, возводимых на просадочных грунтах, составляют от 10 до 30% стоимости самих зданий. Стоимость подобных испытаний на моделях составила бы 2-3%, т.е. дешевле в 5-10 раз. Приведенные данные указывают на целесообразность использования моделирования при проектировании сооружений. Результаты исследований могут быть использованы для уточнения и разработки строительных норм и стандартов, что даст возможность расчёта и проектирования многоэтажных зданий с учётом действительной работы стального каркаса.

Ключевые слова: многоэтажные здания, погрешность монтажа и изготовления, рамный каркас, стальные конструкции, линейный расчет, нелинейный расчет, геометрические несовершенства

INTRODUCTION

A significant portion of urban development consists of multi-story buildings. These buildings can be categorized as public, industrial, or residential based on their purpose. Buildings over 75 meters in height are referred to as high-rise buildings, while those exceeding 100 meters are considered unique structures. [1-2]. Multi-storey buildings are characterized by the fact that a large building is being built on a relatively small area of development. The steel frame of a multi-storey building is a spatial system of load-bearing structural elements of the rod type, providing its necessary rigidity, stability and strength. In addition to columns, floor beams and vertical connections, hard disks of floors are formed, ensuring effective load transfer to vertical connections [3-6]. The choice of the structural frame scheme affects material consumption, building cost, operational expenses, and assembly labor intensity. In addition to ensuring the load-bearing capacity of the frame, it is essential to eliminate excessive horizontal and vertical displacements as well as unacceptable fluctuations [7-8]. The experience and practice of constructing multi-story steel frames in residential buildings in the Russian Federation are still limited. It is necessary to develop structural solutions that ensure fast and high-quality frame montage. The frame, mounted even from perfectly made structures, often has deviations of the columns from the vertical position, which leads to a decrease in the bearing capacity of the structure [9-10].

The load-bearing capacity of the structure can be accurately determined using large-scale models made from the same material (or a material with similar elastic properties) as the actual structure. The scale of the model can be 1/5-1/6. This depends not only on the actual dimensions of the structure but also on the material of the model. This depends not only on the actual dimensions of the structure but also on the material of the model. Experience shows that for metal and concrete models, it is reasonable to adopt a scale of 1/5-1/15.

The relevance of the work is to study the effect of the installation error on the operation of the steel frame of a multi-storey building. The research results can be used to refine and develop building codes and standards, enabling the calculation and design of multi-story buildings that account for the actual performance of the steel framework.

METHODS

The calculation of steel frames can be performed using several methods (Fig.1).

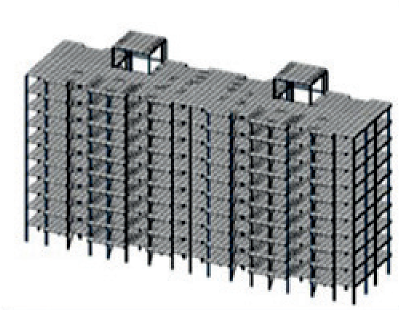

	Perfect shape	Initial imperfections	Linear material	Non-linear material
(1) Fist-order elastic analysis	x		x	
(2) Second-order elastic analysis		x	x	
(3) First-order plastic analysis	x			x
(4) Second-order plastic analysis		x		x

a) Different structural analysis methods

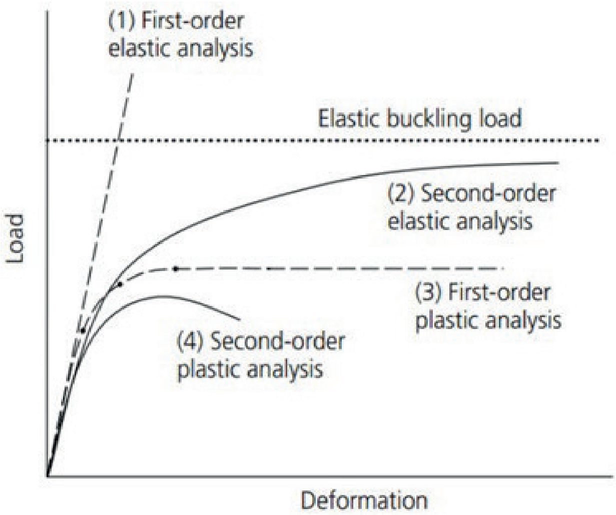

b) Load-deformation curve for different analysis types

Figure 1. General characteristics of steel frame calculation methods [11-14]

1. Calculation in an elastic formulation without taking into account the geometric nonlinearity of the structure – First-order elastic analysis.
2. Calculation in an elastic formulation taking into account the geometric nonlinearity of the structure – Second-order elastic analysis.
3. The calculation takes into account the physical nonlinearity of the material (the development of plastic deformations of steel is allowed), but without taking into account the geometric nonlinearity of the structure – First-order plastic analysis.
4. Calculation taking into account physical and geometric nonlinearity – Second-order plastic analysis.

Previous studies show that the analysis based on the calculation of an idealized multi-storey steel frame structure without taking into account imperfections does not fully reflect the actual operation of the steel frame and cannot always provide the bearing capacity of the building and the operational requirements for permissible movements of the frames [15-16].

The evaluation of the testing of the frame with rigid conjugations in reality was performed using the example of the frame of a 6-storey residential building. The height of the floor is 3.0 m. In the transverse direction, the frame consists of 3 spans, the step of the columns is 8.0 m. Steel columns and beams C345 (Fig.2). The columns of the frame are made of I-beams 20K2, crossbars of I-beams 40B1.

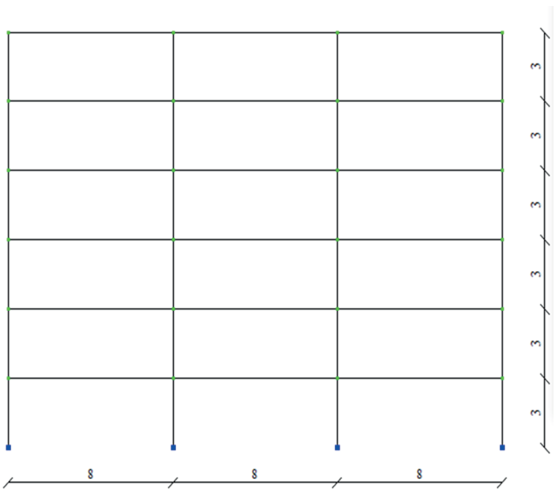

Figure 2. Geometry of the full-scale frame

A multi-storey frame structure was developed to test the multi-storey frame in the laboratory. The total number of floors in the model is 6, the frame with rigid conjugations , the floor height is 0.45 m. In the transverse direction, the frame consists of 3 spans, the step of the columns is 1.2 m. The steel of the columns and beams is C245 (Fig.3). The columns of the frame in the model are made of square pipes 45x5 mm, crossbars of rectangular pipes 70x50x5 mm.

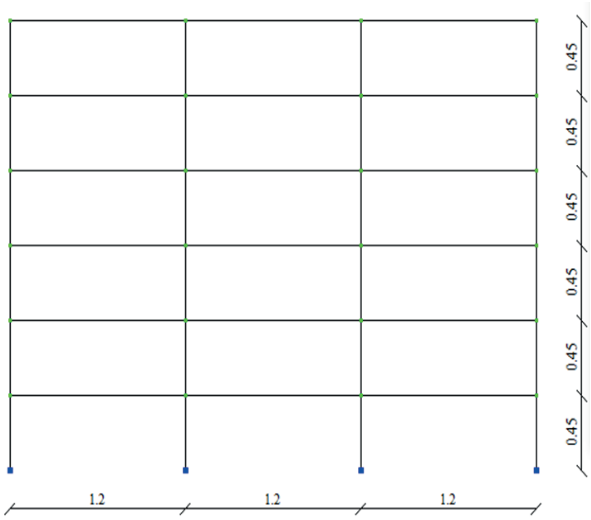

Figure 3. Geometry of the frame model

The frame is a load-bearing core system in which the columns and beams are rigidly connected to each other, and the columns are rigidly attached to the foundation. Due to the rigid attachment of the frame elements to each other, spatial stability and rigidity in the plane of the transverse frame are ensured.

The weight of the steel frame is taken into account by the cross sections of the elements when calculating by computing complexes. When determining the load from the own weight of the frame, the load reliability coefficient equal to 1.05 and the construction coefficient 1.2 are taken into account, taking into account the presence of ribs, linings, shapes and support plates. The load on the steel floor crossbars is determined taking into account the width of the loading area equal to the step of the transverse frames.

For the IV snow region, the normative snow load is 2.0 kPa, the calculated 2.8 kPa. For the IV wind region, the standard wind pressure is 0.48 kPa. The calculated wind load on the frame is determined taking into account the current norms and is 0.59 kPa for the top of the frame. In terms of bearing capacity, the distribution of wind load over the entire height of the building is assumed to be constant and equal to the value of the wind load at the top of the building.
To carry out the calculation, a finite element core model of the frame for a flat frame was formed. The calculation was performed using the LIRA-CAD 2021 computing complex. Table 1 shows the types of stiffness of the finite elements of a full-scale multi-storey frame.

Table 1. Types of stiffness of the frame elements

Type of stiffness	Name of the element	The cross section in reality
1	Columns	20K2[1]
2	Beams	40B1[2]

The load[3] was applied to the calculation scheme in the form of 5 loads:
1 loading: dead load – the weight of load-bearing structures;
2 loading: dead load – the weight of the enclosing structures;
3 Loading: live load;
4 loading: snow load;
5 Loading: wind load.
For the main load-bearing elements of the frame (columns and beams) the stress state is described by the formula
For the main load-bearing elements of the frame (columns and beams) the stress state is described by the formula

$$\sigma = \frac{N}{A} \pm \frac{M}{W} \quad (1)$$

where N – axial force, M – bending moment, A – cross-sectional area, W – the moment of resistance of the section.
The geometric dimensions of the model are taken from the condition of its placement in the laboratory. The scale of the model is 1.2/8=0.45/3=0.15. The section of the column was chosen taking into account the adopted design decision of the frame attachment points to the power floor. These parameters are used as the initial parameters for determining the remaining characteristics of the model.
Let's determine the remaining parameters of the laboratory model from the conditions of similarity of a full-scale multi -storey frame . since the effect of the column deviation from the vertical on the operation of the frame is being investigated, first of all, the stress-strain state of the column will determine the parameters of the laboratory structure.
Normal stresses in the column arise from the action of an axial force and a bending moment, which can be represented as the sum of two moments: from the eccentric action of the axial force and bending moment from the horizontal load.

$$\sigma = \frac{N}{A} \pm \frac{(Ne + kTH)}{W} \quad (2)$$

where e – the eccentricity of the axial force application, T – horizontal force equivalent to wind load, k – the fraction of the moment of the horizontal force in the column under study, H – building height.
Let's transform this expression to a dimensionless form. Let's introduce scale transformations for all values included in the specified expression,

$$\sigma = \sigma_0\bar{\sigma};\ N = n_0\overline{N};\ A = a_0\bar{A};\ T = n_0\bar{T};\ e = l_0\bar{e};\ H = l_0\overline{H};\ W = w_0\overline{W} \quad (3)$$

1 GOST R 57837-2017. Hot-rolled steel I-beams with parallel shelf faces. Technical conditions
2 GOST R 57837-2017. Hot-rolled steel I-beams with parallel shelf faces. Technical conditions
3 SP 20.13330.2016. Loads and impacts. (Updated version of SNiP 2.01.07—85*.)

Here, the "O" index marks the scales, and the letters with dashes at the top indicate the corresponding dimensional values.
Let the choice of scale be unlimited for now. Substituting these transformations into the initial expression, we get:

$$\sigma_0\bar{\sigma} = \frac{n_0\bar{N}}{a_0\bar{A}} \pm \frac{n_0 l_0(\bar{N}\bar{e} + k\bar{T}\bar{H})}{w_0\bar{W}} \quad (4)$$

In order for equation (4) to become dimensionless, the condition must be fulfilled:

$$\sigma_0 = \frac{n_0}{a_0} = \frac{n_0 l_0}{w_0} \quad (5)$$

This equality, which represents a restriction imposed on the freedom to choose scales, is called the coupling equation. The equation contains two coupling equations and five scales. Therefore, three scales can be chosen arbitrarily, and two are found from the coupling equations as functions of three arbitrary scales.
Values $\frac{n_0}{a_0\sigma_0} = 1$ and $\frac{n_0 l_0}{\sigma_0 w_0} = 1$, obtained from the coupling equations are called similarity criteria.
The initial equation (1), which determines the stress state of the frame, can be represented in a dimensionless form. A dimensionless equation called the law of similarity:

$$\bar{\sigma} = \frac{\bar{N}}{\bar{A}} \pm \frac{\bar{M}}{\bar{W}} \quad (6)$$

The number of independent coupling equations (*t*) is less than the number of scales (*n*). Therefore, some of the scales can be chosen arbitrarily, and the rest can be determined using coupling equations. At the same time, there should be no scales with interdependent dimensions among the arbitrarily selected scales. So, for example, if, among arbitrary scales, we choose the scale of force n_0, the scale of the cross sectional area a_0 и σ_0 — the stress scale, then an arbitrary choice of any two of them would already determine the choice of the third one due to the ratio

$$\sigma_0 = \frac{n_0}{a_0} \quad (7)$$

$$\sigma_0 = \frac{n_0 l_0}{w_0} \quad (8)$$

In the above scale restriction condition, we can choose three arbitrary non-interconnected scales, for example σ_0; a_0; m_0, and the remaining scales will be determined from the coupling equation.
Thus, arbitrarily selected scales should have independent dimensions.
From the example considered, it can be seen that with the help of scale transformations, at the same time, the choice of scales must be subordinated to the following restrictions:
From the total number of *n*-scales, you should choose arbitrarily *k*-scales with independent dimensions; as arbitrarily selected scales, the corresponding parameters should be taken from among the terms included in the considered physical equation; n — k-scales, having dependent dimensions, they must be determined by solving the coupling equations that are obtained by introducing scale transformations into the original physical equation [17-18].

RESULTS AND DISCUSSION

In the table 2 the characteristics of the cross sections of the columns of nature and model are presented.

Table 2. Characteristics of column cross sections

Type of columns	Profile	(A), cm^2	(W), cm^3
Nature	20K2	63,53	471,60
Model	45x5 mm	7,57	8,38

Taking into account the given dimensions at the beginning of the article (Fig. 2 and 3), we find l_0:

$$l_0 = \frac{\bar{e}}{e} = \frac{\overline{H}}{H}$$

$$l_0 = \frac{1{,}2}{8} = \frac{0{,}45}{3} = 0{,}150$$

Taking into account the geometric characteristics of the column of the full-scale structure and the model, we determine the scales for the cross-sectional area and the moment of resistance:

$$a_0 = A/\bar{A}$$
$$a_0 = \frac{7{,}57}{63{,}53} = 0.119$$
$$w_0 = W/\overline{W}$$
$$w_0 = \frac{8{,}38}{471{,}60} = 0.0178$$

From equation (7) and assuming $\sigma_0 = 1$, we get this

$$a_0 = n_0 \quad (9)$$
$$n_0 = 0.119$$

Let's check whether the selected column of the model satisfies the similarity criteria of equation (5, 7, 8).

Fulfilling the condition (7):

$$\sigma_{0column} = \frac{0{,}119}{0{,}119} = 1$$

Fulfilling the condition (8):

$\sigma_{0column} = \frac{0{,}119 \cdot 0{,}15}{0{,}0178} = 1{,}002 \approx 1$. The margin of error is less than 1%

Let's define the required beam parameters:

$$A_{beam} = 0.119 * 72.16 = 8.60 \text{ cm}^2$$
$$W_{beam} = 0.0178 * 1011.1 = 18.00 \text{ cm}^3$$

A rectangular tube with a cross section has the closest area and moment of resistance 70x50x5.

In the table 3 the characteristics of the cross sections of the beams of nature and model are presented.

Table 3. Characteristics of cross sections of beams

Type of beams	Profile	(A), см^2	(W), см^3
Nature	40B1	72,16	1011,10
Model	70x50x5	10,57	18,84

The error for the selected profile in terms of cross-sectional area is (10.-8.6)/8.6 = 22.91%, by the moment of resistance (18.84-18)/18 = 4.67%, Due to the fact that, first of all, the bending characteristics of the beam determine the moment transmitted to the column.

The selected profiles are accepted for further construction of the model structure.

In the table 4 shows the scale factors used in the development of the model.

Table 4. Scale factors for columns

The scale factor of the dimensions	l_0	0,150
Stress scale factor	σ_0	1,000
The scale factor of the force	n_0	0,119
Area scale factor	a_0	0,119
The scale factor of the moment of resistance	w_0	0,0178

CONCLUSION

It is interesting to compare some approximate data on the cost of testing in kind with the cost of testing the model. Thus, full-scale tests of large-panel buildings erected on subsidence soils account for 10 to 30% of the cost of the buildings themselves. The cost of such tests on models would be 2-3%, that is, 5-10 times cheaper.

These data indicate the expediency of using modeling in the design of structures.

In order to effectively use modeling methods in building design, it is necessary, in addition to developing research methodology issues, to improve existing ones, create special measuring equipment and devices, generalize experience and develop a number of new methods of model manufacturing technology, have specialized production groups for model manufacturing in laboratories.

It should be noted that in order to determine the parameters of the experimental model, it is important first of all to calculate the scale coefficients of the frame size (l_0), area (a_0) and moment of resistance (w_0) based on the available data. The geometric dimensions of the model are taken from the condition of its placement in the laboratory. The section of the column was chosen taking into account the adopted design decision of the frame attachment points to the power floor.

When checking whether the matched column meets the similarity criteria, the error turned out to be less than 1%. When checking the satisfaction of the selected beam with the similarity criteria based on the scale coefficients of the column, an error of 22.91% was found.

REFERENCES

1. **Kudishin Yu.I., Belenya E.I., Ignatyeva V.S.** (2008) Metallicheskie konstruktsii: uchebnik dlya stud. vyssh. ucheb. zavedenii [Metal Structures: Textbook for University Students]. Moscow: Publishing Center "Akademiya". 688 p. (in Russian)
2. **Turyeva A.V.** (2013) Steel Frame of a Multi-Storey Building: Advantages and Stiffness Assurance. Paper present-ed at the XIV International Youth Scientific Conference "Severgeoekotekh-2013," Part V, Ukhta, Russia, March 20–22, 2013, pp. 88–92.
3. **Tusnin A.R., Rybakov V.A., Nazmeeva T.V.** (2020) Proektirovanie metallicheskikh konstruktsiy. Chast' 2: «Me-tallicheskie konstruktsii. Spetsial'nyy kurs» [Design of Metal Structures. Part 2: "Metal Structures. Special Course"]. Moscow: Pero. (in Russian)
4. **Lebed E.V., Ibragimov A.M.** (2020) Proektirovanie metallicheskogo karkasa mnogoetazhnogo zdaniya [Design of the Steel Frame of a Multistory Building]. Moscow: MISI-MGSU. (in Russian).
5. **Lebedev E.V.** (2017) Kompyuternye tekhnologii v proektirovanii prostranstvennykh metallicheskikh karkasov zdaniy [Computer Technologies in the Design of Spatial Steel Frames for Buildings]. Moscow: MISI-MGSU. (in Russian)
6. **Hart F., Henn V., Sontag H.** (1977) Atlas of Steel Structures: Multi-Storey Buildings. London.
7. **Dhiman S., Nauman M., Islam N.** (2015) Behaviour of Multistory Steel Structure with Different Types of Bracing Systems. International Refereed Journal of Engineering and Science (IRJES), vol. 4, no. 1, pp. 70–82.
8. **Novoselov, A.A.** (2017). The influence of the type of connections on the deformability of the frame of a multi-storey building with a steel frame. Paper presented at the Issues of construction and engineering equipment of railway transport facilities: Materials of a scientific and practical conference, Novosibirsk, 22 March 2017. Siberian State Transport University, Novosibirsk, 27–34.
9. **Konin, D.V**. (2010) Statisticheskaya otsenka netochnostey montazha kolon metallicheskikh karkasov vysotnykh zdaniy [Statistical assessment of inaccuracies in the installation of columns of metal frames of high-rise build-ings], Stroitelnaya mekhanika i raschet sooruzheniy, 2010, no. 6(233), pp. 12-19.
10. **Fisher, J.W., Pense, A.W.** (1987) Experience with use of heavy W shapes in tension. Engineering Journal, vol. 2, no. 24, pp. 63–77.
11. **Nassr, A.A., Razaqpur, A.G., Tait, M.J., Campidelli, M., Foo, S.** (2013) Strength and stability of steel beam col-umns under blast load. International Journal of Impact Engineering, vol. 2, no. 55, pp. 34–48.
12. **Khamati, Yu.R., Tusnin, A.R.** (2023) Rabota svyazyevikh stal'nykh karkasov s uchetom pogreshnostey montazha i

izgotovleniya [Work of joint steel frames considering installation and manufacturing errors], Stroitel'stvo: nau-ka i obrazovanie, 2023, no. 13(1), pp. 22–40.

13. **Chladný, E., Stujberová, M.** (2013) Frames with unique global and local imperfection in the shape of the elastic buckling mode (Part 1). Stahlbau, vol. 82, no. 8, pp. 609–617.
14. **Baláz, I., Koleková, Y.** (2012) Structures with UGLI imperfections. Paper presented at the 18th International Con-ference Engineering Mechanics, Svratka, 2012, pp. 61–86.
15. **Vedyakov, I.I., Konin, D.V., Odessa, P.D.** (2014) Stal'nye konstruktsii vysotnykh zdaniy [Steel Structures of High-Rise Buildings], Moscow: ASV Publishing House, 272 p.
16. **Khamati, Yu.R., Tusnin, A.R.** (2023) Rabota ramnykh stal'nykh karkasov s uchetom pogreshnostey montazha i izgotovleniya [Work of frame steel structures considering installation and manufacturing errors], Stroitel'stvo: nauka i obrazovanie, 2023, no. 13(3), pp. 6–28.
17. **Smirnov, V.V., Svitsov, M.A., Shileeva, A.Yu., Shikhova, E.N., Ponikarova, Yu.E.** (2015) Analiz defektov i povrezhdeniy metallo-konstruktsiy zdaniy metallurgicheskikh proizvodstv [Analysis of defects and damages of metal structures in buildings of metallurgical productions], European science, 2015, no. 8(9), pp. 51–54.
18. **Pitlyuk, D.A.** (1965) Raschet stroitel'nykh konstruktsiy na osnove modelirovaniya [Calculation of Building Struc-tures Based on Modeling], Moscow: Leningrad Publishing House, 152 p.

СПИСОК ЛИТЕРАТУРЫ

1. **Кудишин Ю.И., Беленя Е.И., Игнатьева В.С.** Металлические конструкции: учебник для студ. высш. учеб. заведений // М.: Изд. центр «Академия», 2008. – 688 с.
2. **Турьева, А.В.** Стальной каркас многоэтажного здания: преимущества и обеспечение жесткости // Севергеоэкотех-2013: материалы XIV международной молодежной научной конференции: в 5-ти частях, Ухта, 20–22 марта 2013 года. Том Часть V. – Ухта: Ухтинский государственный технический университет, 2013. С. 88-92.
3. **Туснин А.Р., Рыбаков В.А., Назмеева Т.В.** Проектирование металлических конструкций. Часть 2: «Металлические конструкции. Специальный курс» // Учебник для ВУЗов – М.: Издательство «Перо», 2020 – 436 с.
4. **Лебедь Е.В., Ибрагимов А.М.** Проектирование металлического каркаса многоэтажного здания [Электронный ресурс]: учебно-методическое пособие – М.: Издательство МИСИ – МГСУ, 2020. – 84 с.
5. **Лебедев Е.В.** Компьютерные технологии в проектировании пространственных металлических каркасов зданий: учебное пособие. – М.: Издательство МИСИ – МГСУ, 2017. – 140 с.
6. **Hart F., Henn V., Sontag H.** Atlas of steel structures. Multi-storey buildings. London, 1977, 351 pages.
7. **Dhiman S., Nauman M., Islam N.** Behaviour of Multistory Steel Structure with Different Types of Bracing Systems // International Refereed Journal of Engineering and Science (IRJES), 2015, No. 1(4), pp. 70–82.
8. **Новоселов, А.А.** Влияние типа связей на деформативность каркаса многоэтажного здания со стальным каркасом // Вопросы строительства и инженерного оборудования объектов железнодорожного транспорта: Материалы научно-практической конференции, Новосибирск, 22 марта 2017 года / СГУПС. – Новосибирск: Сибирский государственный университет путей сообщения, 2017. – С. 27-34.

9. **Конин, Д.В.** Статистическая оценка неточностей монтажа колонн металлических каркасов высотных зданий // Строительная механика и расчет сооружений, 2010, № 6(233). – С. 12-19.
10. **Fisher J.W., Pense A.W.** Experience with Use of Heavy W Shapes in Tension // Engineering Journal, 1987, No. 2(24), pp. 63-77.
11. **Nassr A.A., Razaqpur A.G., Tait M.J., Campidelli M., Foo S.,** Strength and stability of steel beam columns under blast load // International Journal of Impact Engineering, 2013, No. 2(55), pp 34-48.
12. **Хамати Ю.Р., Туснин А.Р**. Работа связевых стальных каркасов с учетом погрешностей монтажа и изготовления // Строительство: наука и образование, 2023, № 13(1). С. 22-40.
13. **Chladný E., Stujberová M**. 2013. Frames with unique global and local imperfection in the shape of the elastic buckling mode (Part 1). // Stahlbau, 2013, No. 82(8), pp. 609-617.
14. **Baláz I., Koleková Y**. Structures with UGLI imperfections. // 18th International Conference Engineering Mechanics. Svratka, 2012, pp. 61-86.
15. **Ведяков И.И., Конин Д.В., Одесский П.Д.** Стальные конструкции высотных зданий. М.: Изд-во АСВ, 2014. – 272 с.
16. **Хамати Ю.Р., Туснин А.Р.** Работа рамных стальных каркасов с учетом погрешностей монтажа и изготовления. // Строительство: наука и образование, 2023, № 13(3). С. 6-28.
17. **Смирнов В.В., Свитцов М.А., Шилеева А.Ю., Шихова Е.Н., Поникарова Ю.Е**. Анализ дефектов и повреждений металлических конструкций зданий металлургических производств // European science, 2015, №8 (9). С. 51-54.
18. **Питлюк Д.А.** Расчет строительных конструкций на основе моделирования. М. : Изд-во Ленинград, 1965. –152 с.

Yusef Radwan Khamati — Candidate of Technical Sciences, Researcher of the Department of Metal and Wooden Structures, Engineer, National Research Moscow State University of Civil Engineering (NRU MGSU); 129337, Moscow, Yaroslavskoe Shosse, 26; YoussefHamaty@outlook.com

Alexander Romanovich Tusnin — Doctor of Technical Sciences, Associate Professor, Professor of the Department of Metal and Wooden Structures, Director of the Institute of Civil Engineering; National Research Moscow State University of Civil Engineering (NRU MGSU); 129337, Moscow, Yaroslavskoe Shosse, 26; TusninAR@mgsu.ru

Юсеф Радуан Хамати — кандидат технических наук, исследователь кафедры металлических и деревянных конструкций, инженер, Национальный исследовательский Московский государственный строительный университет (НИУ МГСУ); 129337, г. Москва, Ярославское шоссе, д. 26; YoussefHamaty@outlook.com

Александр Романович Туснин — доктор технических наук, доцент, профессор кафедры металлических и деревянных конструкций, Директор института ПГС; Национальный исследовательский Московский государственный строительный университет (НИУ МГСУ); 129337, г. Москва, Ярославское шоссе, д. 26; TusninAR@mgsu.ru

CONVERGENCE STUDY ON ASYMMETRICALLY FLEXURAL PROBLEM OF COLD-FORMED CHANNEL SECTIONS

***Huy Hoang Vu* [1], *Quoc Anh Vu* [1], *Cao Hung Pham* [2]**

[1] Faculty of Civil Engineering, Hanoi Architectural University, Hanoi, VIETNAM
[2] School of Civil Engineering, The University of Sydney, Sydney, AUSTRALIA

Abstract: Current Direct Strength Method equations computing flexural strength of cold-form members were reported to be over-conservative when applied to members bent about the asymmetrical axis. Finite Element Analysis was used to develop new equations. However, the convergence study, which ensures the accuracy of the Finite Element Analysis result, has not been presented clearly. Thus, this paper performed a convergence study on the strength problem of channel-section asymmetrically flexural members having the web in compression. 33 cold-form channel cross-sections utilized in Oey and Papagelis' study were modeled into ABAQUS to calculate the elastic buckling moment and the ultimate strength. Two factors affected the accuracy of the models, i.e., the mesh size, being 5 mm, *D*/20, *D*/40, and *D*/60, and the member length, ranging from 0.3*D* to 7*D*, where *D* is the cross-section height, were examined. The investigation shows that the seeding method considering the local buckling of the web is the most justifiable. Therefore, the seed size being 1/40 the cross-section height is suggested. This seed size is proven to produce results with reasonable accuracy. To avoid the end effect as well as the influence of incorrect half-wavelength, it is recommended that the member length should be chosen as greater than or equal to two times the cross-section height, and the lengthier the better.

Keywords: Convergence study, cold-formed, thin-walled, channel section, asymmetrical axis, Finite Element Analysis, Finite Element Method

ИССЛЕДОВАНИЕ СХОДИМОСТИ РЕШЕНИЯ ЗАДАЧИ НЕСИММЕТРИЧНОГО ИЗГИБА ХОЛОГНУТЫХ ШВЕЛЛЕРОВ

***Гуй Хоанг Ву* [1], *Куок Анх Ву* [1], *Као Хунг Фам* [2]**

[1] Факультет гражданского строительства, Ханойский архитектурный университет, Ханой, ВЬЕТНАМ
[2] Факультет гражданского строительства, Сиднейский университет, Сидней, АВСТРАЛИЯ

Аннотация: Используемые в настоящее время уравнения метода прямой оценки прочности для оценки несущей способности подверженных изгибу конструкций из холодногнутых профилей являются слишком консервативными применительно к конструкциям, изогнутым вокруг асимметричной оси. Для построения новых уравнений было использовано моделирование методом конечных элементов. Однако исследование сходимости решения, которое бы обеспечивало необходимую точность результатов расчета по методу конечных элементов, ранее не было представлено в явном виде. Таким образом, в данной работе было проведено исследование сходимости решения задачи о несущей способности при несимметричном изгибе швеллеров со сжатой стенкой. В ABAQUS были смоделированы 33 поперечных сечения холодно гнутых швеллеров, рассмотренные ранее в исследовании Оэя и Папагелиса. Вычислялись момент потери устойчивости в упругой постановке и прочность сечений. На точность моделей влияли два фактора: размер сетки разбиения (5 мм, D/20, D/40 и D/60) и длина конструктивного элемента (от 0,3D до 7D, где D - высота сечения). Исследование показало, что наиболее оправданным является шаг разбиения, позволяющей учесть местную потерю устойчивости стенки швеллера. Поэтому предлагается использовать размер сетки разбиения, равный 1/40 высоты стенки. Доказано, что такой размер ячейки сетки разбиения позволяет получить результаты с достаточной точностью. Чтобы избежать краевых эффектов, а также влияния неправильной длины полуволны, рекомендуется выбирать длину элемента больше или равной двукратной высоте поперечного сечения, при этом чем больше длина, тем лучше.

Ключевые слова: Исследование сходимости, холодно гнутые профили, тонкостенные профили, швеллер, ось симметрии, конечно-элементный анализ, метод конечных элементов

1 INTRODUCTION

The ultimate strength problem of cold-form members bent about the asymmetrical axis using the Direct Strength Method (DSM) is under investigation due to the finding that the current DSM analytical equations for the flexural member listed in relevant codes, i.e., AISI S100 [1] and AS/NZS 4600:2018 [2] are over-conservative for this type of member. Finite Element Analysis (FEA) is the primary tool for calibrating the newly efficient equations.

A convergence study is an important step in ensuring the accuracy of the Finite Element Analysis result. Some studies have been carried out on many types of problems. For example, a mesh convergence study was conducted by Hemesh Patil and P. V. Jeyakarthikeyan (2018) [3] using ANSYS on the hub of the automotive clutch disc assembly. Abdulsalam (2021) [4] has investigated the meshing sensitivity of Abaqus/CAE software to the problem of compact tension specimens. The resultant stresses and strains were discussed. Aron (2024) [5] analyzed displacement versus force, stress-strain relationship, maximum force, and stress for a series of mesh sizes of a rectangular hollow steel column using ABAQUS. On the problem of cold-formed steel channels bent about the asymmetrical axis, Oey and Papangelis (2021) [6] has utilized a mesh size comprising 97 nodes along the cross-section and extruding at 5 mm increments along the longitudinal length of the member. A finer element sizes were employed at the corners of the channel sections. The method produced the largest mesh size of 12 x 5 mm. To avoid the end effect on the instability of the web, the length of the member was chosen as 5 times the section height. However, no details about the convergence study were provided.

To more effectively deal with the mesh convergence problem in Abaqus/CAE, D. H. Vu (2022) [7] has introduced a method that uses the integrated Python script to refine automatically the mesh and update the system.

The literature review shows that the convergence problem of channel cross-section cold-formed members bent about the asymmetrical axis with the compressive web using Finite Element Analysis has not been discussed clearly. Therefore, it will be presented in this paper. Python scripts are a great help to solve a series of analogous problems with varying parameters.

2 MATERIALS AND METHODS

ABAQUS/CEA 2020 was selected to solve FEA problems in this study. Its reliability has been validated against the buckling problem of the cold-formed plain C-section member bending about its asymmetrical axis [8].

The full 3D shape of plain channel cross-section simply-supported beams subjected to bending about the asymmetrical axis having the web in compression was modeled into the software as a shell (see Fig. 1). The shell was then meshed into S4R elements [9, 10]. S4R is a 4-node, quadrilateral, stress/displacement shell element with reduced integration and a large-strain formulation. The mesh density is a factor causing the error of the FEA result and therefore was taken into account for the study.

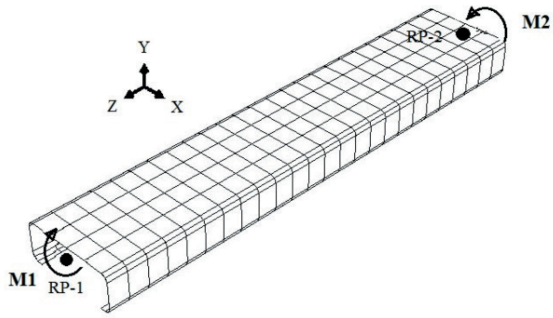

Figure 1. Model in ABAQUS

Member sections are 33 cross-sections utilized in Oey and Papangelis's study [6]. Thus, the modeling in this study can be verified in Section 3.1 by the results from that paper.

ABAQUS's "Rigid Body" constraint combined with "Reference Point" was used to facilitate the assignment of loads and support conditions at the member ends. Research shows that the function is useful but also results in some errors because it prevents the edges of plate elements from deforming freely [11]. "Rigid Body"'s end effect and the influence of member length is the second subject to be investigated.

To model a simple beam, one end reference point was assigned a boundary condition eliminating the transition in all three directions (Pinned type, $U_1 = U_2 = U_3 = 0$), the remaining point in x- and y- directions (ZASYMM type, $U_1 = U_2 = UR_3 = 0$). All three rotational restraints were free. The loads are a pair of opposite-sign concentrated moments applied on reference points in the cross-section's symmetrical plane ($y0z$ plane) which causes the web to be compressed. The magnitude of moments is 1 kN.m for the buckling problem. The value of the critical moment archived from the buckling problem was then assigned to reference points in the same process to simulate the load of the ultimate strength problem.

The Ramberg-Osgood material model was used which best describes the behavior of high-strength steel [6, 12]. The grades of steel are G450, G500, and G550 [13] associated with each cross-sectional as outlined in [6]. The elastic modulus E and the Poisson ratio v are 200000 MPa and 0.3, respectively.

Four seed sizes were investigated in this study. The first is a fixed size of 5 mm. This seed size was used by Oey and Papagelis [6] to mesh the longitudinal edge of the member. In their study, Oey and Papagelis recognized that the buckling of the web dominates the behavior of channel members bent about the asymmetrical axis when the web is in compression. This phenomenon can also be seen in Fig. 5. Thus, seed sizes related to the web width, represented by the cross-section height D, were considered. They are relative seed sizes of D/20, D/40, and D/60.

A "Buckle" step of the "Linear Perturbation" category was derived from the original one to solve the buckling problem in the elastic range of materials. As for the ultimate strength, the "Static, Risk" step dealing with non-linear analysis was added. Appropriate values of parameters of the above steps were carefully selected to ensure the convergence of problems.

Geometry imperfection [14] was also taken into account in the ultimate strength problem. The imperfection surface adopted the first local buckling mode [15] of the web with the largest magnitude of 0.66t [6, 16], where t is the thickness of the cross-section.

3 RESULTS

3.1 Model's input validation

First, the correctness of the modeling process was checked by comparison to the result obtained by Oey and Papangelis [6]. The member length is taken as five times the cross-section height according to [6].

The term "Similarity" is defined in this paper to describe how close one value is to another. It is designated as the ratio between two numbers. The similarity being equal to unity means that two values are equal and close to unity means that one value is in good accuracy compared to the other.

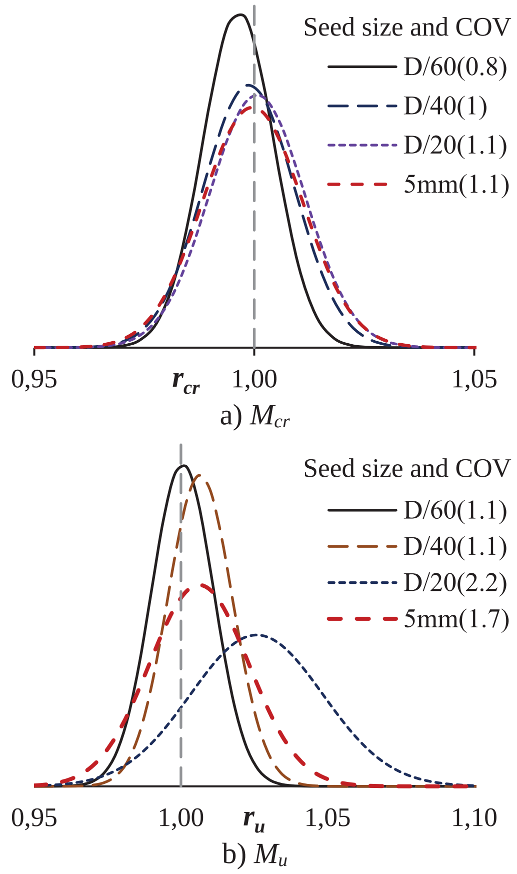

Figure 2. Normal distribution of similarities to Oey's research

The critical moments M_{cr} and ultimate strengths M_u of 33 cross-sections were determined using ABAQUS for four seeding methods. The similarities between these moments and the result of Oey and Papangelis were computed, where r_{cr} and r_u. represent the ratio between two buckling moments and that of two ultimate strengths, respectively. The probability density function (PDF) for each case of seeding was built in a process detailed in Section 3.2. Finally, these functions were summarized and plotted in Fig. 2.

The outcome shows that the buckling moments and the ultimate moments archived from models in this study are nearly identical to those calculated by Oey and Papangelis. The means of similarities are very close to 1. The biggest is 1.026 belonging to the $D/20$ seed size case in calculating M_u. The other means are within 1% of unity. The corresponding coefficient of variance COV is also small, about 1 to 2 percent. It means that the models are reliable. Then the next phase was carried out and presented in the next sections.

3.2 Mesh density assessment

The convergence study is to compare the results of one mesh density to those of the next finer density until the difference between the two adjacent densities is acceptable. Three seed sizes, $D/20$, $D/40$, and $D/60$, were based on the governing buckling mode of the cross-section. i.e., the local buckling of the web. They establish a series of similar seeding methods. The mesh size of 5 mm is of intermediate accuracy and does not have a solid base. Thus, it is not important and excluded from the study. The remaining three seed sizes form two pairs for comparison, $D/20$ to $D/40$, and $D40$ to $D/60$. Thus, the similarities between the coarser and the finer ($D/20$ over $D/40$, $D/40$ over $D/60$) in a pair will be calculated (it is different from Section 3.1 where all the values are compared to the Oey and Papangelis's). Intervals were determined and the number of similarities inside each interval was counted and shown as column diagrams in Fig. 3. The mean value μ, the standard deviation σ, and the coefficient of variation COV were computed and listed in Table 1. The associated probability density functions (PDF) are also shown in Fig. 3.

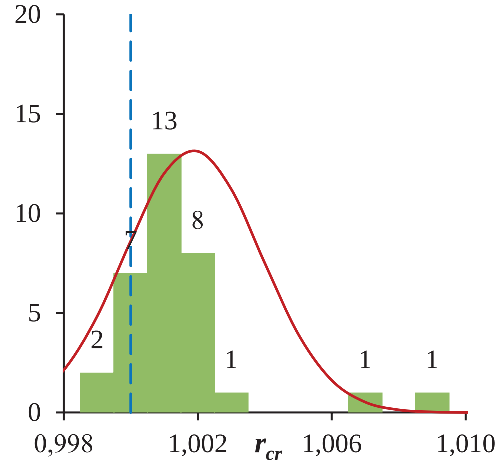

a) Similarities of M_{cr} ($D/20$ to $D/40$)

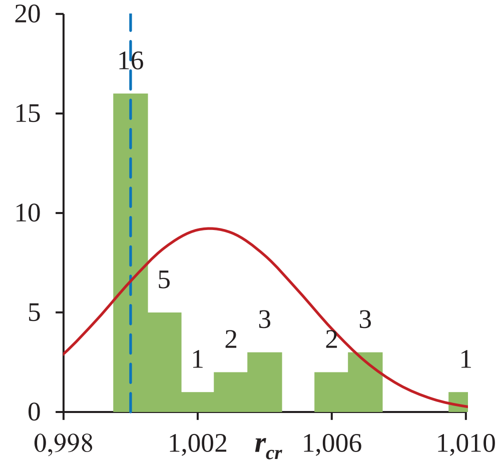

b) Similarities of M_{cr} ($D/40$ to $D/60$)

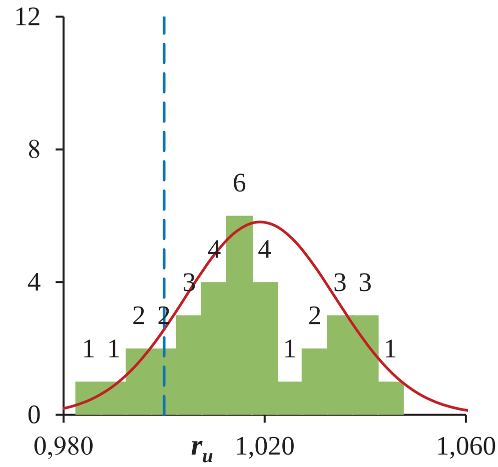

c) Similarities of M_u ($D/20$ to $D/40$)

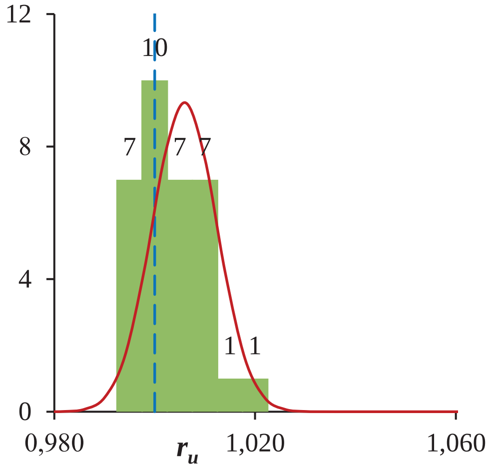

d) Similarities of M_u (D/40 to D/60)

Figure 3. Probability density of ratio between values in a pair of mesh sizes

Fig. 3a, Fig. 3b and Table 1 show that the effectiveness of meshing methods of D/20 and D/40 are analogous. The mean values are the same and very close to unity. The COVs are both small. The maximum error rate is only 1%. Thus, both mesh sizes, D/20 and D/40, are suitable for the buckling moment determination.

Table 1. Statistical values in Fig. 3

Item	M_{cr}		M_u	
Seedzise	D/20	D/40	D/20	D/40
μ	1.002	1.002	1.019	1.006
σ	0.00202	0.00288	0.01497	0.00641
COV (%)	0.20	0.29	1.47	0.64
ε_{max} (%)	1.0	1.0	4.7	2.3

For the ultimate moment, there is a big difference between Fig. 3c, and Fig. 3d. The values in Fig. 3d associated with the seed size of D/40 is more compact, which means that it is more reliable than seed size D/20 (Fig. 3c). The mean value of seed size D/40 is closer to unity than that of seed size D/20. The COV and the maximum error of seed size D/40 are a half smaller than those of seed size D/20. As for the seed size D/40, its mean value of 1.006, the COV of only 0.64%, and the maximum error of 2.3% are all within the expected range. Therefore, the seed size of D/40 is suitable for the current problem.

3.3 Member's end effect discussion

Three channel cross-sections of C152x64x19x2.4, C203x76x19x1.9, and C400x125x31x3.2 with a series of member length to cross-section height ratios (length/height ratio for short) including 0.3, 0.5, 0.7, 1, 2, 3, 4, 5, 6, and 7 were modeled in ABAQUS using the seed size of D/40. The elastic buckling moments and the ultimate strengths were determined and plotted against the L/D ratios in Fig. 4.

It can be observed that the trends of curves concerning three cross-sections are the same for both critical buckling moment and ultimate strength. In the small length/height ratio range, i.e., $L/D < 1$, the end constraint causes a large effect on the buckling moment while having little impact on the ultimate strength. The end effect fades after the member length exceeds two times the cross-section height for both critical buckling moment and ultimate strength with maximum differences to the values of $L/D = 7$ being 0.88% for the former and 1.1% for the latter.

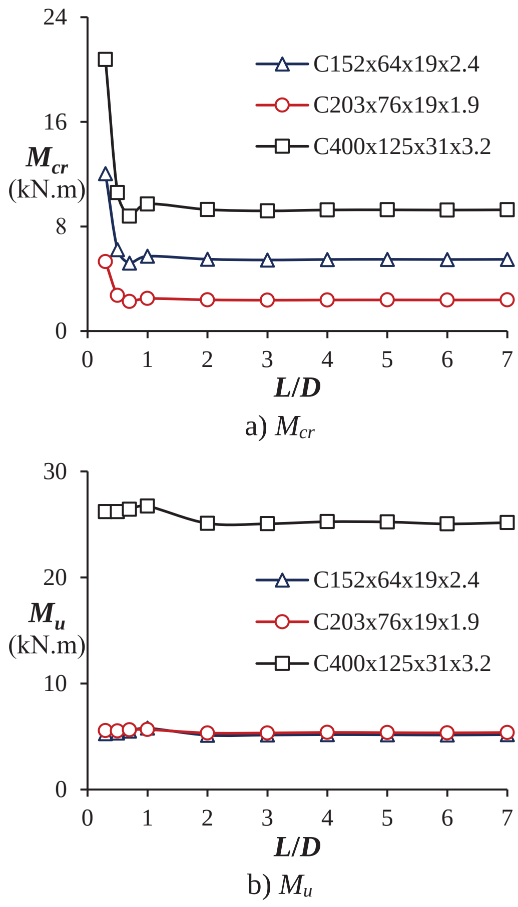

a) M_{cr}

b) M_u

Figure 4. The moments with respect to L/D ratio

Therefore, it can be concluded that the length/height ratio greater than or equal to 2 gives sufficient accuracy.

The effect of the member length on the buckling moment can be easily seen from the buckle shapes in Fig. 5. The number of half-waves is always a whole number. Thus, different member lengths result in different half-wavelengths, as seen in Fig. 5c and Fig. 5d. As the member length increases, this effect reduces. Especially, when the member length is less than and equal to *D*, only one half-wave is observed (see Fig. 5a and Fig. 5b). The half-wavelength is equal to the member length. It explains the large change in the early stage of the critical moment curve. Since the ultimate moment is related to the buckling moment through the imperfection, its value can be seen to have a certain variation over the short member length range.

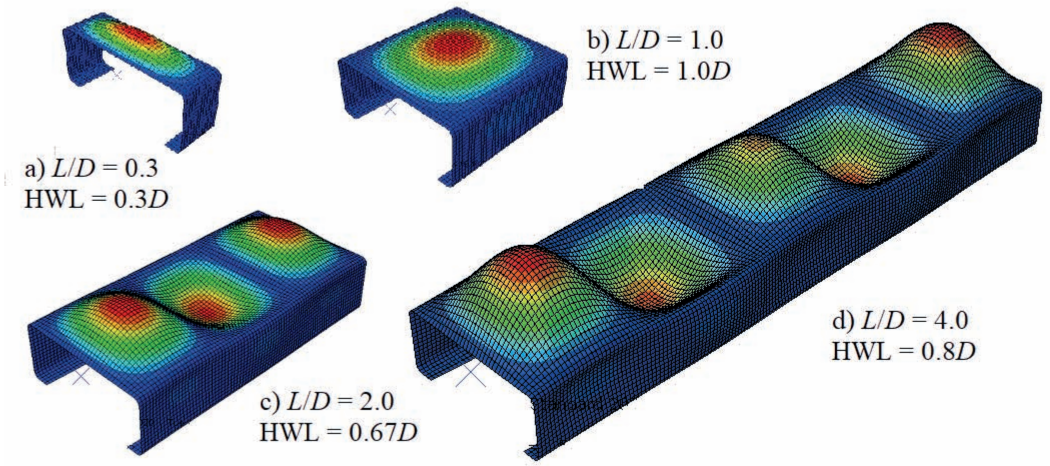

Figure 5. The half-wavelength with respect to L/D ratio

4 CONCLUSION

Convergence of the FEA elastic buckling and non-linear strength problems of cold-form channel cross-section members bent about the asymmetrical axis having the web in compression was investigated. The meshing method and reasonable member length were discussed.

The mesh size of *D*/40 is recommended for the current problem. Compared to Oey and Papagelis's meshing solution, the mesh size of 1/40 of the web depth is simpler. The method is more justifiable because it allows for the dominated buckling mode of the cross-section, i.e., the local buckling of the web. The method also gives a high accuracy with a mean similarity of 1.006 and COV of 0.64% compared to the next meshing step.

Another factor affecting the accuracy of the current problem is the member length. The lower bound of the member length to cross-section height ratio to eliminate the end effect is 2. It shows that the ratio of 5 utilized in Oey and Papagelis's study is conservative. Lower values may be considered to reduce the number of elements and thus the calculation time.

REFERENCES

1. AISI, AISI S100-16 North American Specification for the Design of Cold-Formed Steel Structural Members, 2016 Edition. 2016, American Iron and Steel Institute.
2. AS/NZS 4600:2018 Cold-formed steel structures. 2018, Australian/New Zealand Standard.
3. **Patil, H. and P.V. Jeyakarthikeyan,** Mesh Convergence Study and Estimation of Discretization Error of Hub in Clutch Disc with Integration of ANSYS, in 2nd International Conference on Advances in Mechanical Engineering (ICAME 2018).

2018, IOP Publishing Ltd: Kattankulathur, India.

4. **Abdulsalam, H.,** Mesh Sensitivity Assessment on 2D and 3D Elastic Finite Element Analysis on a Compact Tension Specimen Geometry Using Abaqus/CAE Software, in 4th International Conference/Training Workshop on Energy for Sustainable Development in Africa 11th - ICTWESDA 2020. 2021, IOP Publishing Ltd: University of Nigeria, Nsukka, Enugu State, Nigeria.
5. **Aron, M.A.H.,** The Mesh Convergence Analysis of a Rectangular Hollow Steel Column Using ABAQUS, in Department of Civil Engineering. 2024, Rajshahi University of Engineering & Technology: Bangladesh.
6. **Oey, O. and J. Papangelis**, Behavior of cold-formed steel channels bent about the minor axis. Thin-Walled Structures, 2021. Vol. 164.
7. **Vu, D.H.**, Developing Python scripting for mesh convergence in ABAQUS, in Journal of Science and Technique. A Section on Special Construction Engineering. 2022: Hanoi, Vietnam.
8. **Vu, H.H., Q.A. Vu, and C.H. Pham**. Evaluation of the software's reliability in solving the buckling problem of the cold-formed plain c-section member bending about its asymmetrical axis. in Structural Health Monitoring & Engineering Structures Conference, Da Nang, Vietnam. 2023. International Journal of Civil Engineering, Springer.
9. SIMULIA. http://130.149.89.49:2080/v2016 /index.html. 2016 [cited 2024 Aug, 9th].
10. SIMULIA, Abaqus/CAE User's Manual. 2011, Providence, RI, USA: Dassault Systèmes Simulia Corp.
11. **Vu, H.H.,** Accurate model for simply-supported plates, in XXVII International Scientific Conference on Advance in Civil Engineering "Construction the Formation of Living Environment" (FORM-2024). 2024, E3S Web of Conferences.
12. **Gardner, L. and X. Yun,** Description of stress-strain curves for cold-formed steels. Construction and Building Materials, 2018. Vol. 189: p. 527–538.
13. **Australia, S.,** AS 1397:2021 Continuous hot-dip metallic coated steel sheet and strip - Coatings of zinc and zinc alloyed with aluminum and magnesium. 2021, Standards Australia.
14. **Schafer, B.W., Z. Li, and C.D. Moen**, Computational modeling of cold-formed steel. Thin-Walled Structures, 2010. Vol. 48(Issues 10–11): p. 752-762.
15. **Yu, C. and B.W. Schafer**, Simulation of cold-formed steel beams in local and distortional buckling with applications to the direct strength method. Journal of Constructional Steel Research, 2007. Volume 63(Issue 5): p. 581-59.
16. **Schafer, B.W. and T. Pekoz**, Computational modeling of cold-formed steel: characterizing geometric imperfections and residual stresses. Journal of Constructional Steel Research, 1998. Vol. 47(3): p. 193–210.

СПИСОК ЛИТЕРАТУРЫ

1. AISI, AISI S100-16 North American Specification for the Design of Cold-Formed Steel Structural Members, 2016 Edition. 2016, American Iron and Steel Institute.
2. AS/NZS 4600:2018 Cold-formed steel structures. 2018, Australian/New Zealand Standard.
3. **Patil, H. and P.V. Jeyakarthikeyan,** Mesh Convergence Study and Estimation of Discretization Error of Hub in Clutch Disc with Integration of ANSYS, in 2nd International Conference on Advances in Mechanical Engineering (ICAME 2018). 2018, IOP Publishing Ltd: Kattankulathur, India.
4. **Abdulsalam, H.,** Mesh Sensitivity Assessment on 2D and 3D Elastic Finite Element Analysis on a Compact Tension Specimen Geometry Using Abaqus/CAE Software, in 4th

International Conference/Training Workshop on Energy for Sustainable Development in Africa 11th - ICTWESDA 2020. 2021, IOP Publishing Ltd: University of Nigeria, Nsukka, Enugu State, Nigeria.
5. **Aron, M.A.H.,** The Mesh Convergence Analysis of a Rectangular Hollow Steel Column Using ABAQUS, in Department of Civil Engineering. 2024, Rajshahi University of Engineering & Technology: Bangladesh.
6. **Oey, O. and J. Papangelis**, Behavior of cold-formed steel channels bent about the minor axis. Thin-Walled Structures, 2021. Vol. 164.
7. **Vu, D.H.**, Developing Python scripting for mesh convergence in ABAQUS, in Journal of Science and Technique. A Section on Special Construction Engineering. 2022: Hanoi, Vietnam.
8. **Vu, H.H., Q.A. Vu, and C.H. Pham**. Evaluation of the software's reliability in solving the buckling problem of the cold-formed plain c-section member bending about its asymmetrical axis. in Structural Health Monitoring & Engineering Structures Conference, Da Nang, Vietnam. 2023. International Journal of Civil Engineering, Springer.
9. SIMULIA. http://130.149.89.49:2080/v2016/index.html. 2016 [cited 2024 Aug, 9th].
10. SIMULIA, Abaqus/CAE User's Manual. 2011, Providence, RI, USA: Dassault Systèmes Simulia Corp.
11. **Vu, H.H.,** Accurate model for simply-supported plates, in XXVII International Scientific Conference on Advance in Civil Engineering "Construction the Formation of Living Environment" (FORM-2024). 2024, E3S Web of Conferences.
12. **Gardner, L. and X. Yun,** Description of stress-strain curves for cold-formed steels. Construction and Building Materials, 2018. Vol. 189: p. 527–538.
13. **Australia, S.,** AS 1397:2021 Continuous hot-dip metallic coated steel sheet and strip - Coatings of zinc and zinc alloyed with aluminum and magnesium. 2021, Standards Australia.
14. **Schafer, B.W., Z. Li, and C.D. Moen**, Computational modeling of cold-formed steel. Thin-Walled Structures, 2010. Vol. 48(Issues 10–11): p. 752-762.
15. **Yu, C. and B.W. Schafer**, Simulation of cold-formed steel beams in local and distortional buckling with applications to the direct strength method. Journal of Constructional Steel Research, 2007. Volume 63(Issue 5): p. 581-59.
16. **Schafer, B.W. and T. Pekoz**, Computational modeling of cold-formed steel: characterizing geometric imperfections and residual stresses. Journal of Constructional Steel Research, 1998. Vol. 47(3): p. 193–210.

Гуй Хоанг, Ву - магистр, преподаватель, факультет гражданского строительства, Ханойский архитектурный университет (HAU), Km 10, Nguyen Trai Street, Thanh Xuan District, Hanoi, 11400, Vietnam, hoangvh@hau.edu.vn

Куок Ань, Ву - кандидат технических наук, доцент, руководитель отдела стальных и деревянных конструкций, факультет гражданского строительства, Ханойский архитектурный университет (HAU), Km 10, Nguyen Trai Street, Thanh Xuan District, Hanoi, 11400, Vietnam, hoangvh@hau.edu.vn

Као Хунг, Фам - доктор философии, доцент, старший преподаватель, Школа гражданского строительства, Сиднейский университет, Сидней, NSW 2006, Австралия, caohung.pham@sydney.edu.au

Huy Hoang, Vu – Master, Lecturer, Faculty of Civil Engineering, Hanoi Architectural University (HAU), Km 10, Nguyen Trai Street, Thanh Xuan District, Hanoi, 11400, Vietnam, hoangvh@hau.edu.vn

Quoc Anh, Vu – Ph.D, Associate professor, Head of Division of Steel and Timber Structures, Faculty of Civil Engineering, Hanoi Architectural University (HAU), Km 10, Nguyen Trai Street, Thanh Xuan District, Hanoi, 11400, Vietnam, hoangvh@hau.edu.vn

Cao Hung, Pham – Ph.D., Associate professor, Senior Lecturer, School of Civil Engineering, The University of Sydney, Sydney NSW 2006, Australia, caohung.pham@sydney.edu.au

NUMERICAL MODELING OF WAVE-ICE INTERACTION WITH A SINGLE SUPPORT

Izmail G. Kantarzhi, Maksim S. Afonyushkin

National Research Moscow State University of Civil Engineering, Moscow, RUSSIA

Abstract: The change in the joint wave-ice load acting on a freestanding hydraulic structure under conditions of ice freezing to the support is considered. The existing scientific works on this problem were analyzed and the appropriate research method was chosen. The topic of the article is relevant in the light of active development of the Arctic part of Russia and construction of new hydraulic structures, which require more accurate methods of determining ice and wave loads. The novelty of the work lies in the analysis of the joint impact of the wave and ice floe on the structure. Numerical modeling in LS-DYNA program and analytical methods presented in normative documents were used for the study. Verification of the model by loads was performed by comparing numerical data with the results of analytical calculation. Changes in the horizontal forces of wave and ice floe pressure on the structure, as well as the wave impact on the ice floe were obtained. Dependences of changes in these forces and their ratios on the ice floe length were plotted. In the course of analyzing the results it was determined that the ice floe pressure force on the structure changes most significantly. The cyclic character of changes in the wave and ice forces was also revealed. Presumably, this is due to the dynamic nature of ice breakup and the effect of "ice floe surfacing-submergence". In further research, it is recommended to apply the developed model for different scenarios involving other types of ice and types of structures. The results of the paper can be used to develop more accurate methods for analytical calculation of the impact of waves and ice on structures.

Keywords: Mathematical models, ice, waves, numerical modeling, ice loads, wave loads, LS-DYNA

ЧИСЛЕННОЕ МОДЕЛИРОВАНИЕ ВЗАИМОДЕЙСТВИЯ ВОЛН И ЛЬДА С ОДИНОЧНОЙ ОПОРОЙ

И.Г. Кантаржи, М.С. Афонюшкин

Национальный исследовательский Московский государственный строительный университет, г. Москва, РОССИЯ

Аннотация: Рассмотрено изменение совместной волно-ледовой нагрузки, действующей на отдельно стоящее гидротехническое сооружение в условиях примерзания льда к опоре. Был проведен анализ существующих научных работ по данной проблеме и выбран соответствующий метод исследования. Тема статьи актуальна в свете активного освоения арктической части России и строительства новых гидротехнических сооружений, требующих более точные методы определения ледовых и волновых нагрузок для обеспечения безопасности строительства. Новизна работы заключается в анализе совместного воздействия волны и льдины на сооружение. Для проведения исследования использовались численное моделирование в программе LS-DYNA и аналитические методы, представленные в нормативных документах. Верификация модели по нагрузкам была выполнена путем сравнения численных данных с результатами аналитического расчета. Получены изменения горизонтальных сил давления волны и льдины на сооружение, а также воздействия волны на льдину. Построены графики зависимостей изменений этих сил и их соотношений от длины льдины. В ходе анализа результатов определено, что наиболее значительно изменяется сила давления льдины на сооружение. Также был выявлен циклический характер изменения волновой и ледовой сил. Предположительно, это связано с динамическим характером разрушения льда и эффектом "всплытие-погружение льдины". В дальнейших исследованиях рекомендуется применять разработанную модель для различных сценариев, включающих другие типы льда и виды конструкций. Результаты статьи могут быть использованы для разработки более точных методик аналитического расчета воздействия волн и льда на сооружения.

Ключевые слова: математические модели, лед, волны, численное моделирование, ледовые нагрузки, волновые нагрузки, совместные нагрузки, LS-DYNA

INTRODUCTION

To date, the joint impact of waves and ice on structures remains poorly studied. The approach adopted in the regulatory documents is to separately determine the wave and ice loads on a structure using a combination factor. This method does not take into account hydraulic effects arising from the impact of waves on the ice floe, such as ice floe surfacing and submergence, as well as redistribution of ice debris in the water. In addition, the nature of changes in ice and wave loads on the structure depending on the ice field length, wavelength and other characteristics is unknown.

The purpose of this paper is to investigate the wave-ice effect on a freestanding support and then analyze the dependencies of each of the loads on the wavelength of the wave and ice field. The objective of the paper is to study the changes in the load on the structure caused by the factors of ice freezing with the support and the impact of a single surface wave.

To solve this problem, a numerical model was developed in the LS-DYNA program. The structure in the model is designed as a vertical support of square cross-section, but any other shape of the cross-section of the structure can be used. The wave impacts the ice floe, causing it to collide with the structure, which leads to an increase in the kinetic energy of the ice floe motion and intense changes in the load on the ice floe and the support. The horizontal forces of wave and ice floe impact on the structure were measured in the model. The research methods include analysis of numerical simulation results and comparison with the results of calculations performed by analytical methods.

Numerical modeling studies of wave-ice interaction use models in which each ice floe is treated as a separate fundamental degree of freedom. According to the data from the paper Kantarzhi I. G., 2023 [1], this type of models allows to take into account many different physical and mechanical phenomena and provides high predictive accuracy of calculations.

Numerical calculations in this work are performed through the use of LS-DYNA program, which is actively used to analyze the impact of ice load on structures in other studies. The main purpose of such works is the correct selection of physical and mechanical properties of ice, as well as modeling of plausible processes of crack formation with subsequent failure. The Cohesive Element Method (CEM), which allows creating additional layers with unique properties between the volumetric finite elements of the ice floe, is particularly widespread.

In the study of Gurtner A., 2009 [2], the impact of an ice floe on a rigid lighthouse and its foundation was analyzed in order to determine the nature of stress redistribution in the structure. The model was built correctly, but with significant simplifications: ice thickness and velocity were not taken into account, and the hydraulic effects of water were completely ignored (the ice floe moved on a rigid smooth surface). These limitations were corrected in a subsequent study by Gurtner A., 2010 [3].

In a study by Daiyan H., 2011 [4], the variation of ice load on an inclined structure is considered as a function of the friction coefficient between the ice floe and the structure, as well as the inclination angle of the structure. The Arbitrary Lagrangian-Eulerian (ALE) method is used for modeling the aquatic environment, which is also used in this paper.

In the paper by Pang S. D., 2015 [5], the effect of mesh size and finite element shape on the magnitude of ice load applied to a cylindrical structure is studied. It is found that the use of CEM method gives ice load results that are directly proportional to the mesh size. The use of octahedral hexahedrons facilitates mesh construction but limits crack propagation along orthogonal trajectories, which makes the use of tetrahedral meshes preferable.

In Herrnring H., 2019 [6], the accuracy of a CEM model for simulating ice splitting under tension is analyzed. It is found that larger elements of the generated mesh due to their non-uniform distributed volume reduce the peak normal stresses, which may be the reason for requiring higher tensile forces when modeling coarse mesh ice.

In a study by Zhan K., 2020 [7], the dependence of ice loading on the inclination angle of the structure and ice thickness is studied. It is found that the CEM method reliably models the load changes due to the formation of ice debris. According to the calculation results, the increase in the inclination angle led to a decrease in the vertical load, which can be explained by a reduction in the formation of new debris. The results of the work were confirmed by comparison with experimental data.

Recommendations on the application of the CEM method are presented in Herrnring H., 2018 [8], where the advantages and disadvantages of this method for modeling the interaction of ice with structures are considered. Among the advantages, the preservation of the full volume of the ice floe in the defragmented state and the ability to model arbitrary crack propagation trajectories are noted. Major disadvantages include mass loss during ice breakup and high computational resource requirements.

For the latter two reasons, the CEM method was not applied to ice modeling in this work.

Among the studies dealing with numerical modeling of ice-structure interaction that do not use the coupling element method are the following works.

In the study by Mintu S., 2018 [9], an ice floe interaction model with a cone structure is developed using Smoothed Particle Hydrodynamics (SPH) and Computational Fluid Dynamics (CFD) technique. This has achieved high accuracy of results, but the SPH method, like the CEM method, requires significant computational resources.

In a study by Jeon S., 2020 [10], numerical modeling of the interaction of flat ice with structures was performed using the Drucker-Prager plasticity model and erosion model, which contributed to modeling the rapid loss of the ice floe's bearing capacity characteristic of brittle ice failure.

In the work of Jang H. S., 2024 [11], a collapsible foam model with damping and stretching constraints, as well as the already mentioned Drucker-Prager model that takes into account various yield criteria including dynamic strain rate, were used to model the impact of an ice floe on marine structures. The results showed that the yield criterion in the Drucker-Prager model within the elastic-plastic framework most adequately reflects the realism of ice impact loads.

There are very few studies devoted to direct numerical modeling of simultaneous wave and ice impact on structures.

One of them is the work of Behnen J., 2021 [12], which presents a model of wave, ice and structure interaction created in the LS-DYNA program. It compares different water modeling methods such as CFD, ALE and SPH in terms of computational time, but no analysis of the direct changes in the ice load acting on the structure.

Most of the works on the subject are devoted to experimental study of the problem.

The paper by D. J. McGovern (2014) investigates the impact of an ice floe on a structure under the influence of different waves. With irregular waves, impacts can occur at any time, whereas with regular waves, impacts can occur at crests. As the wavelength decreases, the probability of impact increases.

The work of S. Mintu (2021) studies the impact of waves on a hexagonal support at different ice concentrations and wavelengths. It is found that analytical methods accurately determine the average ice loads, but the prediction of impulsive loads remains unpredictable.

A study by A. Tsarau (2017) evaluates ice loads on a cylindrical structure when regular waves pass through an ice field. The aim is to determine the changes in the vertical displacement of the ice, the hydrodynamic force of the wave and the impact force of the ice floe. In all cases, an increase in ice load with increasing wave height was observed.

METHODS

The Mohr-Coulomb model is used to model the ice frozen to the structure. The physical-mechanical and geometric characteristics of the ice floe are taken as follows: density ρ_i = 900 kg/m^3, Young's modulus E = 5,2 GPa, shear modulus G = 2 GPa, Poisson's ratio ν = 0.3, angle of internal friction φ = 30°, cohesion c = 0.5 MPa, shear strength R_s = 0.85 MPa, compressive strength R_c = 1.82 MPa, tensile strength R_e = 0.57 MPa, thickness h_d = 0.4 m, width B = 5 m, length L varies from 1 to 10 m.

The CONSTRAINED_TIED_NODES_FAILURE keyword is used to model the breakage of ice into debris, which allows breaking the connection between nodes of a common solid element when a certain value of plastic volumetric strain is reached, which was assumed to be 0.35% according to [16].

The edge nodes of the ice floe are constrained to move towards the y-axis.

MAT_VACUUM, which is a virtual vacuum modeling material, is used to model air.

For water modeling, ALE method and MAT_NULL material are used, the characteristics of which are presented in Table 1.

Table 1. Properties of water. Source: [17].

Quantity	Unit of measurement	Value
Density ρ_w	kg/m^3	1000.00
Dynamic viscosity μ_d	Pa*s	0.001

The state of water is described by the Gruneisen equation [18] (1):

$$p = \frac{\rho_0 C^2 \mu\left[1+\left(1-\frac{\gamma_0}{2}\right)\mu-\frac{a}{2}\mu^2\right]}{\left[1-(S_1-1)\mu-S_2\frac{\mu^2}{\mu+1}-S_3\frac{\mu^3}{(\mu+1)^2}\right]^2}+(\gamma_0+a\mu)E, \quad (1)$$

where p – water pressure, ρ_0 – initial density of water, C = 1500 m/s – speed of sound in water. S_1 = 1.75, S_2 = 0, S_3 = 0 – shock adiabatic slope coefficients, γ_0 = 0.28 – Gruneisen coefficient characterizing the thermal pressure from the vibrating atoms, a = 0 – coefficient characterizing the slope of the graph of dependence of the Gruneisen coefficient on the volume, $\mu = \rho/\rho_0$ – 1, ρ – current water density, E – internal energy per unit volume of water. Values are taken according to [19].

To create a wave, the model uses a rigid body of triangular shape [20] (Fig. 1), where the short side a_b is taken to be equal to the wave height h ($a_b = h$) and the long side b_b is taken to be half the wavelength λ ($b_b = 0.5\lambda$). The body moves in a cycle, sinking into the water and then rising, thus creating waves, according to law (2):

$$f(t)=0.5h\sin(2\pi t/T), \quad (2)$$

where t is time, T is wave period.

The water depth d was modeled so that the ratio d/λ was kept constant. The calculations are performed at two wavelengths equal to 16 m and 32 m, so the depth was assumed to be 3 m and 6 m, respectively.

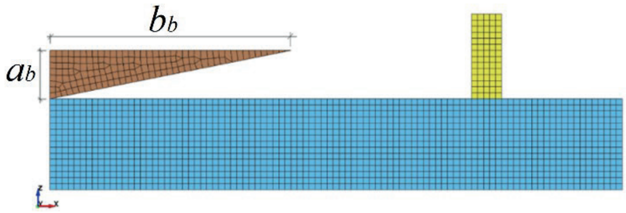

Figure 1. Wave modeling. Source: Compiled by the authors

The boundary conditions for the model are reproduced by the CONSTRAINED_GLOBAL keyword, which defines a global plane of boundary conditions-restrictions around the model.

The dimensions of the structure are a = 1; b = 1 m, and the height is 5.8 m. The base nodes are motion and rotation constrained.

The contact between the ice floe and the structure is reproduced by the CONTACT_AUTOMATIC_SURFACE_TO_SURFACE keyword. The coefficient of static friction is 0.2. The coefficient of dynamic friction is 0.1 [19].

The contact of ice floe debris with each other is reproduced by the CONTACT_AUTOMATIC_SINGLE_SURFACE keyword. The coefficient of static friction is 0.1. The coefficient of dynamic friction is 0.05 [19].

The gravitational force in the model is accounted for by the LOAD_BODY_Z keyword.

The model is shown in Fig. 2.

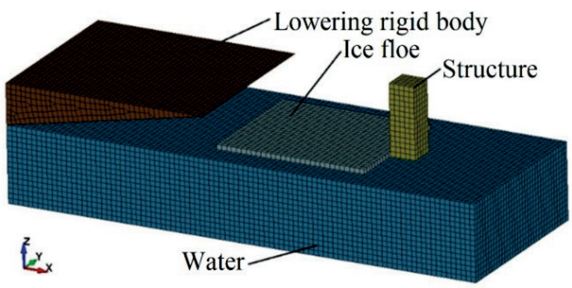

Figure 2. A model of wave, ice and structure interaction. Source: Compiled by the authors

Verification of the model by ice load.

The model described above is used, but without the rigid body – wave-producer (Fig. 3). The velocity vector $V = 1$ m/s is applied to the back side of the ice floe. The graph of the time dependence of the horizontal force on the ice floe is shown in Fig. 4.

The results obtained from the model are compared with the analytical calculation according to SP 38.13330.2018. The formula for determining the horizontal force of ice impact on a vertical structure $F_{c,w}$ is presented below (3):

$$F_{c,w} = 2.2*10^{-3}Vh_d\sqrt{Ak_V\rho_w R_c} = 2.2*10^{-3}*1*0.4*\sqrt{3*1*1000*1.82} = 0.065 \text{ MN} = 65.02 \text{ kN} \quad (3)$$

where $A = 3b^2 = 3*1^2 = 3$ m^2 – the maximum area of the ice field affecting the structure; k_V – ice deformation velocity coefficient – it is taken equal to 1.0, because not the first ice movement is taken into account, but the entire ice floe movement.

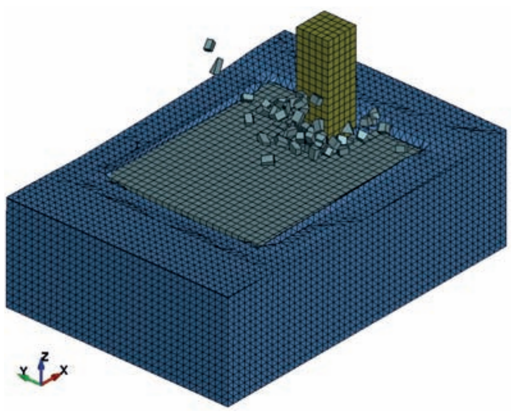

Figure 3. Model of ice floe-structure interaction. Source: Compiled by the authors

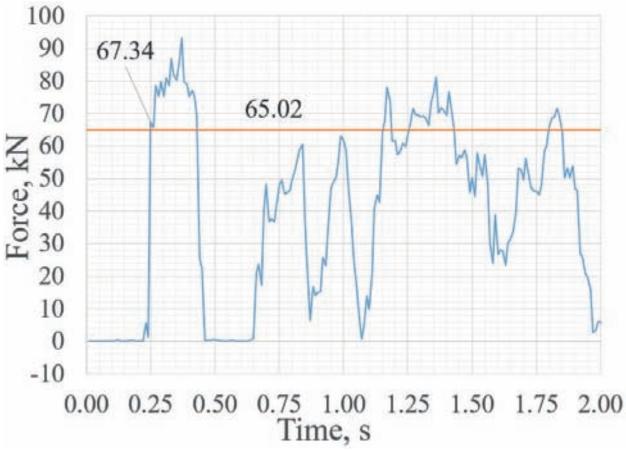

Figure 4. Graph of change in the horizontal component of the ice floe impact force on the structure. Blue line – results obtained from the model. Orange line – calculation according to SP 38.13330.2018. Source: Compiled by the authors

The first ice breaking against the structure occurred at a reaction force equal to 67.34 kN, which is approximately equal to the ice force obtained analytically – 65.02 kN. Subsequently, due to the formation of ice debris, the loads either increase (debris gets stuck between the ice floe and the structure) or decrease (debris goes to the bottom or piles up on the ice floe).

The nature of the loading is cyclic, which can lead to dynamic effects.

Verification of the model by wave loading.

The model described in the first section is used, but without the ice floe. Verification is performed for waves of height $h = 1.6$ m with lengths $\lambda = 16$ m (Fig. 5, *a*) and $\lambda = 32$ m (Fig. 5, *b*). The plots of the changes in the wave force on the structure are presented in Fig. 6. and Fig. 7.

The model results are compared with the analytical calculation according to SNiP 2.06.04-82. The maximum force of the wave impact on the structure Q_{max} is determined by formula (4):

$$Q_{max} = Q_{i,max}\delta_i + Q_{v,max}\delta_v, \quad (4)$$

where $Q_{i,max}$ is the inertial component of the wave force on the structure (5):

$$Q_{i,max} = 0.25\rho wg\pi b^2hk_v\alpha_i\beta_i, \quad (5)$$

where $Q_{v,max}$ is the velocity component of the wave force on the structure (6):

$$Q_{v,max} = 0.083\rho wgbh^2 k_v^2 \alpha_v \beta_v, \qquad (6)$$

δ_i and δ_v – coefficients of combination of inertial and velocity components of the wave impact force on the structure, depending on the distance between the top of the wave and the center of the structure x, m: for λ = 16 m x = 1.6 m, corresponding to the calculation time t = 1.5 s (Fig. 8, *a*); for λ = 32 m x = 4.1 m, corresponding to the calculation time t = 1.4 s (Fig. 8, *b*), is taken; k_v – coefficient depending on the relative size of the structure; α_i and α_v – inertial and velocity coefficients of depth; β_i and β_v – inertial and velocity coefficients of the obstacle shape.
The calculations are presented in Table 2.

Table 2. Calculation of the wave force on a freestanding structure according to SNiP 2.06.04-82. Source: Compiled by the authors

λ, m	16	32
d, m	3	6
k_v	1	1
α_i	0.9	0.875
α_v	2.1	1.5
β_i	1.6	1.6
β_v	1.6	1.6
$Q_{i,max}$, kN	17.74	17.25
$Q_{v,max}$, kN	7.03	5.02
δ_i	1	0.9
δ_v	0.6	0.4
Q_{max}, kN	21.96	17.53

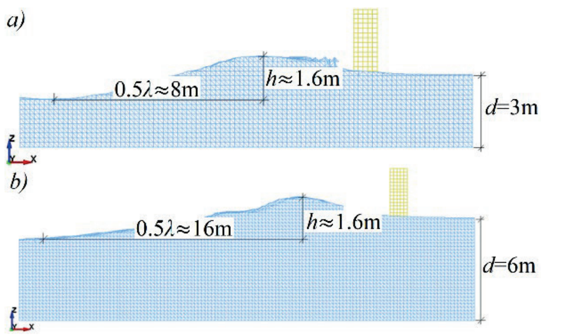

Figure 5. Wave-structure interaction model: a – at λ = 16 m, b – at λ = 32 m. Source: Compiled by the authors

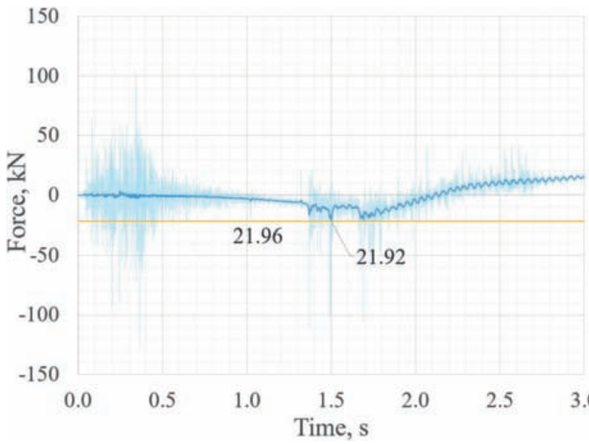

Figure 6. Graph of the change in horizontal wave force on the structure at λ = 16 m. Cyan line – results obtained from the model for the structure. Blue line – smoothed results from the model. Orange line – calculation according to SNiP 2.06.04-82. Source: Compiled by the authors

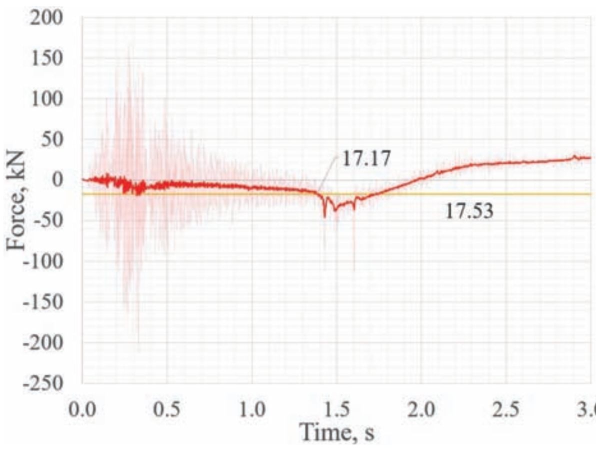

Figure 7. Graph of change of horizontal wave force on the structure at λ = 32 m. Pink line – results obtained from the model. Red line – smoothed results from the model. Orange line – calculation according to SNiP 2.06.04-82. Source: Compiled by the authors.

In both cases, the numerical (21.92 kN and 17.17 kN) and analytical (21.96 kN and 17.53 kN, respectively) methods give almost completely convergent results.

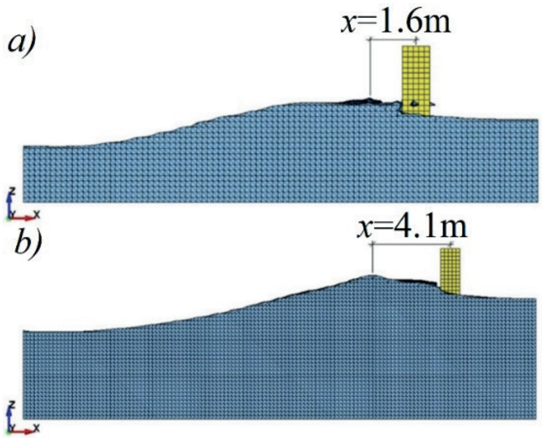

Figure 8. Coordinates of the wave top: a – at time t = 1.5 s for λ = 16 m, b – at time t = 1.4 s for λ = 32 m. Source: Compiled by the authors

RESULTS AND DISCUSSION

The model described at the beginning of the paper is used. Eleven calculations were performed for wavelengths $\lambda = 16$ m and $\lambda = 32$ m, respectively, with ice floe length L ranging from 0 to 10 m each. The wave pressure force per running meter of ice floe F_{wi}, the ice floe pressure force on the structure F_{is}, the wave pressure force on the structure F_{ws}, and the total horizontal force on the structure F_s were measured. For each load, the average values were taken at the moment of the most active interaction with the structure. The values of force ratios $F_{wi}^{\lambda=16m}/F_{wi}^{\lambda=32m}$ and $F_s^{\lambda=16m}/F_s^{\lambda=32m}$ are presented in Table 3.

Table 3. Dependence of the ratios $F_{wi}^{\lambda=16m}/F_{wi}^{\lambda=32m}$ and $F_s^{\lambda=16m}/F_s^{\lambda=32m}$ on the ice floe length. Source: Compiled by the authors

L, m	$F_{wi}^{\lambda=16m}/F_{wi}^{\lambda=32m}$	$F_s^{\lambda=16m}/F_s^{\lambda=32m}$
0	1	1
1	0.59	0.45
2	0.47	0.60
3	0.90	0.76
4	0.81	0.56
5	0.79	0.49
6	0.74	0.62
7	0.72	0.81
8	0.65	0.57
9	0.63	0.46
10	0.46	0.42

Graphs of changes in horizontal forces F_{wi}, F_{is} and F_{ws} are shown in Fig. 9.

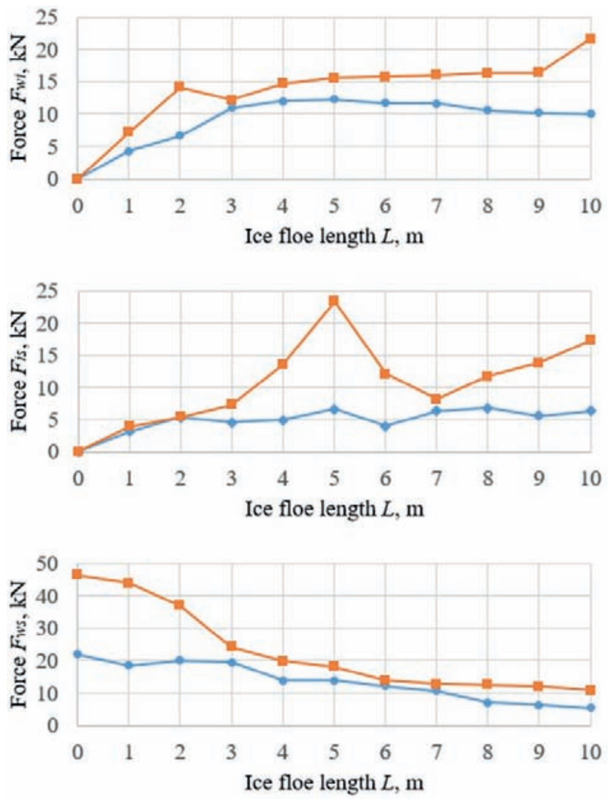

Figure 9. Dependence of forces F_{wi}, F_{is} and F_{ws} on L at λ = 16 m (blue line) and λ = 32 m (orange line). Source: Compiled by the authors

As Fig. 9 shows, the pattern of variation of the wave force on running meter of ice floe F_{wi} and structure F_{ws}, starting from $L = 3$ m becomes almost linear. While the force F_{is} exhibits cycles, and the peak values of the cycles are larger the longer the wavelength of the wave.

Graphs of changes in the F_{is}/F_{ws} and F_{wi}/F_{ws} ratios are shown in Fig. 10.

Figure 10 shows the cyclic dependence for the F_{wi}/F_{ws} and F_{is}/F_{ws} ratios on L. And, while the variation of F_{is}/F_{ws} remains linear enough to approximate this relationship by a linear function of the form $f(L) = aL + b$ (red dashed line in Fig. 10), F_{wi}/F_{ws} varies significantly, allowing the function to be averaged as follows (7):

$$f(L) = kL + g|\sin(aL+b)| + c, \quad (4)$$

where k, g, a, b and c are some values depending on the wavelength and height of the wave, ice thickness and strength, and other parameters. For the blue dashed line in Fig. 10, this function has the form: $f(L) = 0.117L - 0.2|\sin(L - 2)|$ when $L \geq 2$ m. And for orange – $f(L) = 0.1L - 0.79|\sin(0.6L)| + 0.79$ at $L \geq 3$ m. It should be noted that in order to use dependences of the type (7) for practical calculations, it is necessary to relate the cyclic nature of loads to the physics of the interaction process between the wave, ice floe and structure.

The plots of the change in F_s are shown in Fig. 11. Fig. 11 also shows the cyclic character of the decrease of the total horizontal force on the structure with the growth of the ice floe length.

The plots of changes in the ratios $F_{wi}^{\lambda=16m}/F_{wi}^{\lambda=32m}$ and $F_s^{\lambda=16m}/F_s^{\lambda=32m}$ are shown in Fig. 12.

Fig. 12 shows that the ratio of loads $F_{wi}^{\lambda=16m}/F_{wi}^{\lambda=32m}$ for $L \geq 3$m changes rather linearly – by 0.04 per 1 m of ice floe length.

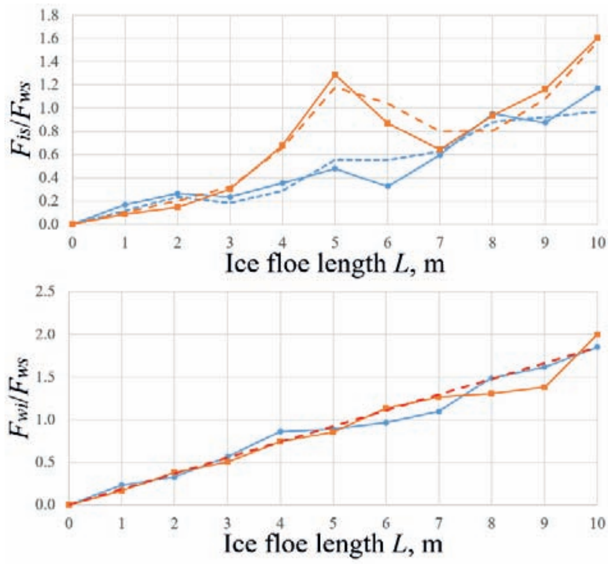

Figure 10. Dependence of F_{is}/F_{ws} and F_{wi}/F_{ws} ratios on L at λ = 16 m (blue line) and λ = 32 m (orange line). Blue dashed line – smoothed F_{is}/F_{ws} function at λ = 16 m; orange dashed line – smoothed F_{is}/F_{ws} function at λ = 32 m; red dashed line – linearization of F_{wi}/F_{ws} function. Source: Compiled by the authors

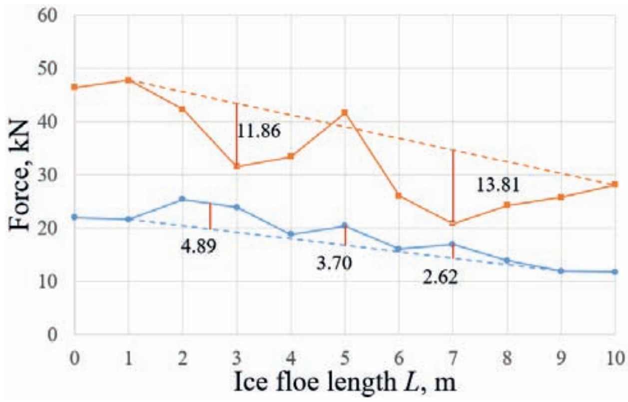

Figure 11. Dependence of force F_s on L at λ = 16 m (blue line) and λ = 32 m (orange line). Source: Compiled by the authors

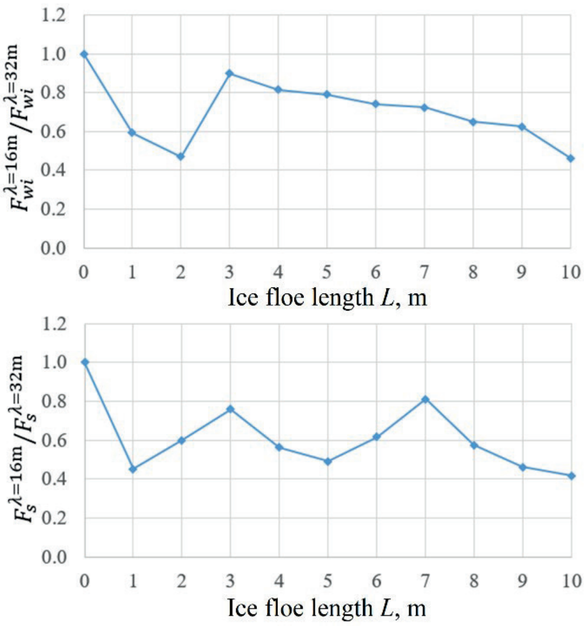

Figure 12. Dependence of $F_{wi}^{\lambda=16m}/F_{wi}^{\lambda=32m}$ and $F_s^{\lambda=16m}/F_s^{\lambda=32m}$ on L. Source: Compiled by the authors

The dependence of $F_s^{\lambda=16m}/F_s^{\lambda=32m}$ also changes cyclically, where the coefficient of the force ratio F_s changes from 0.4 to 0.8 with further decrease. It can also be noted that the ice force will change over time, and not only because of further wave action and ice breakup. During the interaction with the wave, the ice floe first rises (Fig. 13, *a*) and then falls (Fig. 13, *b*), causing a change in the horizontal component of the force. As the length of the ice floe increases, the load peaks decrease and almost reach zero, but as the wavelength increases, the forces continue to increase due to the stronger influences of the ice floe surfacing-submergence effect, decreasing to zero only when L reaches 10m.

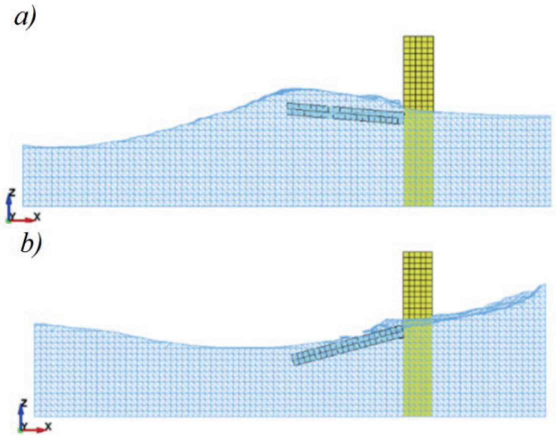

Figure 13. Changing the position of the ice floe: a – surfacing, b – sinking. Source: Compiled by the authors

CONCLUSION

A study analyzing the change in the total wave-ice load on a free-standing vertical support in the case of ice freezing with the structure has been carried out, with the development and verification of a numerical model in the LS-DYNA program. The following conclusions can be drawn from the results of the work:

1. The dependence between the forces of wave and ice impact on the structure at different wavelengths with keeping constant the ratio of water depth to wavelength d/λ has been established. It turned out that the pressure force from the ice floe changes most noticeably, and not only the peak values of the loads differ, but also the character of their distribution depending on the ice floe length.
2. The cyclic nature of the dependence of wave pressure forces on ice and ice pressure on the structure on the ice floe length was determined. When developing the normative method of calculation for wave loads acting on streamlined barriers, these dependencies can be used.
3. The character of the change of the wave pressure force on ice and the total force acting on the structure depending on the length of the wave and ice floe is revealed. The variation of the wave pressure force with a sufficiently long ice field was found to be linear, whereas the total force acting on the structure also varied cyclically. This information may be useful in determining the general law of variation of wave-ice load on structures.
4. In further research, it is advisable to continue using the developed numerical model to analyze the changes in loads depending on the thickness and physical and mechanical properties of ice. Similar calculations should also be carried out for structures of other shapes and designs. In the end, combining the methods of normative documents and the results of the numerical model, it is possible to develop more accurate methods for calculating the wave-ice impact on hydraulic structures.

ACKNOWLEDGEMENTS

The research was founded by the National Research Moscow State University of Civil Engineering (grant for fundamental and applied scientific research, project No. 38-234/130).

REFERENCES

1. **Kantarzhi I. G., Afonyushkin M. S.** (2023) *Development of models of ice interaction with waves and structures*. Paper presented at the International Scientific and Practical Symposium "The Future of the Construction Industry: Challenges and Development Prospects" (FCI-2023), Moscow, 18–22 September, 2023. doi:10.1051/e3sconf/202345702036
2. **Gurtner A., Bjerkas M., Kuehnlein W. L., Jochmann P., Konuk I.** (2009) Numerical Simulation of Ice Action to a Lighthouse. Proceedings of the *28th ASME International Conference on Ocean, Offshore and Arctic*

Engineering OMAE2009, Honolulu, 31 May–5 June, vol. 5, pp. 175–183. doi:10.1115/OMAE2009-80164
3. **Gurtner A., Bjerkas M., Forsberg J., Hilding D.** (2010) Numerical modelling of a full scale ice event. Proceedings of the *20th IAHR International Symposium on Ice, Lahti, 14–18 June*, pp. 1142–1157.
4. **Daiyan H., Sand B.** (2011) *Numerical Simulation of the Ice-Structure Interaction in LS-DYNA*. Paper presented at the 8th European LS-DYNA Conference, Strasbourg, 23–24 May, 2011.
5. **Pang S. D., Zhang J., Poh L. H., Law E., Yap K. T.** (2015) The modelling of ice-structure interaction with cohesive element method: Limitations and challenges. Proceedings of the *23rd International Conference on Port and Ocean Engineering under Arctic Conditions, Trondheim, 14–18 June*, pp. 476–489.
6. **Herrnring H., Kellner L., Kubiczek J. M., Ehlers S**. (2019) *A cohesive model for ice and its verification with tensile splitting tests*. Paper presented at the 12th European LS-DYNA Conference, Strasbourg, 14–16 May, 2019.
7. **Zhan K., Wan D., Yuan Z.** (2020) Cohesive Element Method for Ice Load on Conical Structures. Proceedings of the *30th International Ocean and Polar Engineering Conference, Shanghai, 11–16 October*, pp. 743–749.
8. **Herrnring H., Kellner L., J. Kubiczek M., Ehlers S.** (2018) *Simulation of Ice-Structure Interaction with CZM-Elements*. Paper presented at the 15th German LS-Dyna Forum 2018, Bamberg, 24th October, 2018.
9. **Mintu S., Molyneux D**. (2018) Simulation of Ice-Structure Interactions Using a Coupled SPH-DEM Method. Proceedings of the *OTC Arctic Technology Conference 2018, Houston, 5–7 November*, pp. 139–154. doi:10.4043/29139-MS
10. **Jeon S., Kim Y**. (2020) Numerical simulation of level ice-structure interaction using damage-based erosion model. *Ocean Engineering*, vol. 220, no 1, id. 108485. doi:10.1016/j.oceaneng.2020.108485
11. **Jang H. S., Hwang S., Yoon J., Lee J. H.** (2024) Numerical Analysis of Ice–Structure Impact: Validating Material Models and Yield Criteria for Prediction of Impact Pressure. *Journal of Marine Science and Engineering*, vol. 12, no 2, id. 229. doi:10.3390/jmse12020229
12. **Behnen J.** (2021) *Simulation of Wave-Ice-Structure Interaction* (Master Thesis), Hamburg: Hamburg University of Technology.
13. **McGovern D. J., Bai W.** (2014) Experimental study of wave-driven impact of sea ice floes on a circular cylinder. *Cold Regions Science and Technology*, vol. 108, pp. 36–48. doi:10.1016/j.coldregions.2014.08.008
14. **Mintu S., Molyneux D**. (2021) Experimental Study of Combined Wave and Ice Loads on a Fixed Offshore Structure. Proceedings of the *40th ASME International Conference on Ocean, Offshore and Arctic Engineering OMAE2021, Virtual Conference, 21–30 June*, vol. 7, id. V007T07A010. doi:10.1115/OMAE2021-66442
15. **Tsarau A., Sukhorukov S., Herman A., Evers K. U., Loset S.** (2017). Loads on Structure and Waves in Ice (LS-WICE) project, Part 3: Ice-structure interaction under wave conditions. Proceedings of the *24th International Conference on Port and Ocean Engineering under Arctic Conditions, Busan, 11–16 June*, pp. 560–567.
16. **Kim H., Kedward K. T.** (2000) Modeling Hail Ice Impacts and Predicting Impact Damage Initiation in Composite Structures, *AIAA Journal*, vol. 38, no 7, pp. 1278–1288. doi:10.2514/2.1099
17. **Tran K. Q., Hakansson L., Trinh T. T.** (2017) CFD pre-study of Nozzle reactor for fast hydrothermal liquefaction. Proceedings of the *9th International Conference on Applied Energy (ICAE2017), Cardiff, 21–24 August*, vol. 142, pp. 861–866. doi:10.1016/j.egypro.2017.12.138
18. **Hallquist J. O.** (2006) Equation of State Models. *LS-DYNA: Theoretical manual*,

Livermore: Livermore Software Technology Corporation, pp. 475–477.
19. **Salganik E. A., Shkhinek K. N.** (2014) Ice induced vibrations of offshore structures. *Magazine of Civil Engineering*, vol. 48, no 4, pp. 72–107. doi:10.5862/MCE.48.8
20. **Li X., Sui Y., Meng Y., Zhang X., Khayyer A., He M., Liang D.** (2024) Theory for plunger-type wavemakers to generate second-order Stokes waves and Smoothed Particle Hydrodynamics verification. *Applied Ocean Research*, vol. 153, id. 104244. doi:10.1016/j.apor.2024.104244

СПИСОК ЛИТЕРАТУРЫ

1. **Kantarzhi I. G., Afonyushkin M. S.** (2023) Development of models of ice inter-action with waves and structures. Paper presented at the International Scientific and Practical Symposium "The Future of the Construction Industry: Challenges and Development Prospects" (FCI-2023), Mos-cow, 18–22 September, 2023. doi:10.1051/e3sconf/202345702036
2. **Gurtner A., Bjerkas M., Kuehnlein W. L., Jochmann P., Konuk I.** (2009) Numer-ical Simulation of Ice Action to a Light-house. Proceedings of the 28th ASME In-ternational Conference on Ocean, Offshore and Arctic Engineering OMAE2009, Hono-lulu, 31 May–5 June, vol. 5, pp. 175–183. doi:10.1115/OMAE2009-80164
3. **Gurtner A., Bjerkas M., Forsberg J., Hilding D.** (2010) Numerical modelling of a full scale ice event. Proceedings of the 20th IAHR International Symposium on Ice, Lahti, 14–18 June, pp. 1142–1157.
4. **Daiyan H., Sand B.** (2011) Numerical Simulation of the Ice-Structure Interaction in LS-DYNA. Paper presented at the 8th European LS-DYNA Conference, Strasbourg, 23–24 May, 2011.
5. **Pang S. D., Zhang J., Poh L. H., Law E., Yap K. T.** (2015) The modelling of ice-structure interaction with cohesive element method: Limitations and challenges. Proceedings of the 23rd International Conference on Port and Ocean Engineering under Arctic Conditions, Trondheim, 14–18 June, pp. 476–489.
6. **Herrnring H., Kellner L., Kubiczek J. M., Ehlers S.** (2019) A cohesive model for ice and its verification with tensile split-ting tests. Paper presented at the 12th Eu-ropean LS-DYNA Conference, Strasbourg, 14–16 May, 2019.
7. **Zhan K., Wan D., Yuan Z.** (2020) Cohesive Element Method for Ice Load on Conical Structures. Proceedings of the 30th International Ocean and Polar Engineering Conference, Shanghai, 11–16 October, pp. 743–749.
8. **Herrnring H., Kellner L., J. Kubiczek M., Ehlers S**. (2018) Simulation of Ice-Structure Interaction with CZM-Elements. Paper presented at the 15th German LS-Dyna Forum 2018, Bamberg, 24th October, 2018.
9. **Mintu S., Molyneux D**. (2018) Simulation of Ice-Structure Interactions Using a Coupled SPH-DEM Method. Proceedings of the OTC Arctic Technology Conference 2018, Houston, 5–7 November, pp. 139–154. doi:10.4043/29139-MS
10. **Jeon S., Kim Y.** (2020) Numerical simulation of level ice-structure interaction using damage-based erosion model. Ocean Engineering, vol. 220, no 1, id. 108485. doi:10.1016/j.oceaneng.2020.108485
11. **Jang H. S., Hwang S., Yoon J., Lee J. H.** (2024) Numerical Analysis of Ice–Structure Impact: Validating Material Models and Yield Criteria for Prediction of Impact Pressure. Journal of Marine Sci-ence and Engineering, vol. 12, no 2, id. 229. doi:10.3390/jmse12020229
12. **Behnen J.** (2021) Simulation of Wave-Ice-Structure Interaction (Master Thesis), Hamburg: Hamburg University of Tech-nology.
13. **McGovern D. J., Bai W.** (2014) Experimental study of wave-driven impact of sea ice floes on a circular cylinder. Cold Regions Science and Technology, vol. 108, pp.

36–48. doi:10.1016/j.coldregions.2014.08.008

14. **Mintu S., Molyneux D**. (2021) Experi-mental Study of Combined Wave and Ice Loads on a Fixed Offshore Structure. Pro-ceedings of the 40th ASME International Conference on Ocean, Offshore and Arctic Engineering OMAE2021, Virtual Confer-ence, 21–30 June, vol. 7, id. V007T07A010. doi:10.1115/OMAE2021-66442
15. **Tsarau A., Sukhorukov S., Herman A., Evers K. U., Loset S.** (2017). Loads on Structure and Waves in Ice (LS-WICE) project, Part 3: Ice-structure interaction under wave conditions. Proceedings of the 24th International Conference on Port and Ocean Engineering under Arctic Condi-tions, Busan, 11–16 June, pp. 560–567.
16. **Kim H., Kedward K. T.** (2000) Modeling Hail Ice Impacts and Predicting Impact Damage Initiation in Composite Structures, AIAA Journal, vol. 38, no 7, pp. 1278–1288. doi:10.2514/2.1099
17. **Tran K. Q., Hakansson L., Trinh T. T**. (2017) CFD pre-study of Nozzle reactor for fast hydrothermal liquefaction. Proceed-ings of the 9th International Conference on Applied Energy (ICAE2017), Cardiff, 21–24 August, vol. 142, pp. 861–866. doi:10.1016/j.egypro.2017.12.138
18. **Hallquist J. O.** (2006) Equation of State Models. LS-DYNA: Theoretical manual, Livermore: Livermore Software Technology Corporation, pp. 475–477.
19. **Salganik E. A., Shkhinek K. N.** (2014) Ice induced vibrations of offshore structures. Magazine of Civil Engineering, vol. 48, no 4, pp. 72–107. doi:10.5862/MCE.48.8
20. **Li X., Sui Y., Meng Y., Zhang X., Khayyer A., He M., Liang D**. (2024) The-ory for plunger-type wavemakers to gener-ate second-order Stokes waves and Smoothed Particle Hydrodynamics verifi-cation. Applied Ocean Research, vol. 153, id. 104244. doi:10.1016/j.apor.2024.104244

Izmail G. Kantrazhi – Dr. Sc., Professor, Professor of the Department of Hydraulics and Hydraulic Engineering, Department of Hydraulics and Hydraulic Engineering, Moscow State University of Civil Engineering (National Research University) (MSUCE), 12933, 26, Yaroslavskoe Shosse, Moscow, Russian Federation, kantardgi@yandex.ru.

Maksim S. Afonyushkin — postgraduate, Department of "Hydraulics and Hydrotechnical Engineering", Federal State Budget Educational Institution of Higher Education "Moscow State University of Civil Engineering (National Research University)", MGSU, 26, Yaroslavskoye shosse, Moscow, 129337, Russia, kanz@mgsu

Кантаржи Измаил Григорьевич — доктор технических наук, профессор, профессор кафедры ГиГС, кафедра Гидравлики и гидротехнического строительства, Федеральное государственное бюджетное образовательное учреждение высшего образования «Национальный исследовательский Московский государственный строительный университет» (НИУ МГСУ), дом 26, Ярославское шоссе, город Москва, 129337, Российская Федерация, kantardgi@yandex.ru

Афонюшкин Максим Сергеевич — аспирант, кафедра Гидравлики и гидротехнического строительства, Федеральное государственное бюджетное образовательное учреждение высшего образования «Национальный исследовательский Московский государственный строительный университет» (НИУ МГСУ), дом 26, Ярославское шоссе, город Москва, 129337, Российская Федерация, kanz@mgsu

DOI:10.22337/2587-9618-2024-20-4-43-56

METHOD FOR ANALYZING THE PROBABILITY OF STABILITY FAILURE OF A RC FRAME IN AN ACCIDENT SITUATION

Margarita A. Amelina, Sergei Y. Savin, Nataliya V. Fedorova

Moscow State University of Civil Engineering National Research University, Moscow, RUSSIA

Abstract: Despite the general principles on reliability for structures have been stated in the international standard ISO 2394, the implementation of these principles in the design and construction practice faces with difficulties. One of the current problems is probabilistic robustness checking for buildings and structures. This study focuses on the development of a probabilistic model to calculate the risk of failure of a reinforced concrete frame due to stability failure of its elements in a scenario of sudden removal of a structural component. The critical forces for the eccentrically compressed structural components of the frame are determined using the displacement method, considering the two-stage static-dynamic loading regime due to the sudden column collapse. The study takes into account the change in stiffness of frame elements due to cracking during loading. In addition, it proposes the probabilistic equigradient-based model for the failure of the frame elements after the sudden removal of a column. The mathematical formulation of this model is that if some value is a critical force associated with some parameters satisfying a given condition, then the extremum of that value can be found using an auxiliary Lagrangian function. To illustrate the application of the model, the paper provides an example of the calculation of the stability failure probability of a reinforced concrete frame structure under the considered loading regime. The calculated critical force values were compared with the experimental data for the reinforced concrete frame tested for sudden column removal.

Keywords: probability, stability, disproportionate collapse, reinforced concrete, frame, accidental action

МЕТОДИКА РАСЧЁТА ВЕРОЯТНОСТИ ПОТЕРИ УСТОЙЧИВОСТИ ЖЕЛЕЗОБЕТОННОЙ РАМЫ ПРИ ЕЕ СТРУКТУРНОЙ ПЕРЕСТРОЙКЕ

М.А. Амелина, С.Ю. Савин, Н.В. Федорова

Национальный исследовательский Московский государственный строительный университет, г. Москва, РОССИЯ

Аннотация: Несмотря на то, что общие принципы надежности конструкций изложены в международном стандарте ISO 2394, реализация этих принципов в практике проектирования и строительства сталкивается с трудностями. Одной из актуальных проблем является вероятностная оценка живучести зданий и сооружений. В настоящей статье предложена вероятностная модель расчета риска отказа железобетонной рамы из-за потери устойчивости ее элементов, вызванной особым воздействием – удалением одной из колонн. Определение критических сил во внецентренно сжатых колоннах рамы при рассматриваемом двухэтапном режиме нагружения рамы статической нагрузкой и динамическом догружении от внезапного особого воздействия выполнено методом перемещений. При этом учтено изменение жесткостей элементов рамы вследствие трещинообразования при нагружении конструкции. Вероятностная модель отказа элементов рамы после внезапного удаления одной из колонн построена с использованием принципа эквиградиентности, математическая формулировка которого состоит в том, что если некоторая величина – критическая сила связана с некоторыми параметрами, удовлетворяющими заданному условию, то экстремум этой величины может быть найден с помощью вспомогательной функции Лагранжа. Приведен пример определения вероятности потери устойчивости конструкции железобетонной рамы при рассмотренном режиме нагружения. Выполнено сопоставление расчетных и опытных значений критических сил при потере устойчивости рамы после внезапного удаления колонны.

Ключевые слова: вероятность, устойчивость, прогрессирующее обрушение, железобетон, каркас, особое воздействие

1. INTRODUCTION

As a result of constantly increasing natural and anthropogenic disasters, as well as significant deterioration of assets, the problem of structural safety of buildings and structures becomes one of the most important in the scientific research direction for structural engineers of many countries. A significant number of experimental and theoretical studies have been carried out to evaluate the structural robustness and effectiveness of solutions for the protection of structural systems against disproportionate collapse in case of accidental actions caused by the exhaustion of the load-bearing capacity of any structural component [1-3]. As a rule, the published researches consider the ultimate strain of the material as a criterion for the exhaustion of the bearing capacity at an accidental design action. The dynamic hardening of materials as a function of strain rate can also be considered according to diagrams and analytical expressions [1,2,3].

Current standards [4-7] require stability checks of slender components of reinforced concrete structures, where the deformation and failure are significantly influenced by geometric nonlinearity. Failure of such components may occur at forces less than the strength of the sections. In ACI 318 [4], a 5% reduction of the capacity of the component by the axial force is set as the ultimate limit state criterion in accidental design situation. EN [5-6] allows a slightly higher, up to 10%, reduction of the capacity of the component with respect to axial force, considering the second order nonlinear effects (buckling). SP63 and SP385 [8,9] also specify the calculation of reinforced concrete elements taking into account physical, geometrical and structural nonlinearity. These standards specify the strength of cross-sections and ultimate strains as capacity criteria for the structural components. In this case, the second-order effects are accounted through the buckling factor applied to the calculated value of the first-order bending moment. However, it should be noted, that the target values of the reliability index for stability failure and material failure of structural components are different. The second problem is the correct consideration of the stiffness of structures, since it significantly affects the failure load of slender components. Meanwhile, stiffness expressions in standards are semi-empirical and based on limited experimental data.

Thus, in addition to the robustness checks for the strength of structural components at accidental actions [10-15], the robustness check for stability failure criteria should be performed for frames with slender columns [16,17]. In the studies of buckling of elastoplastic structural components [17,18] and in the works [20,21] on buckling of reinforced concrete elements, the extremum of force – displacement diagram (null tangent stiffness) was adopted as the stability criterion. The work [20] points out that the calculation of reinforced concrete eccentrically compressed elements should consider both of physical and geometric nonlinearity. The authors provided specific recommendations for determining the stiffnesses of such elements in the presence of cracks in them. However, such studies have usually been limited to structural elements and do not take into account the phenomenon for framed structures, where structural components may experience unloading at buckling due to the reaction of the frame. At the same time, the supporting effect of the frame is of great importance as it provides load transfer in the hazardous event.

In this context, the energy-based criterion proposed by A.V. Aleksandrov and V.I. Travush [19] is promising to identify the most dangerous components of the structural system from the point of view of stability failure. According to this criterion, the shear force and bending moment in the end section of the structural element, which loses stability, perform the largest negative work. In a similar formulation, the problem of stability of reinforced concrete frames was solved in [22,23], where the stiffness parameters and the free length of the columns in the structures were varied.

There are relatively few studies that have applied the stability failure criterion to investigate the structural robustness of frames. For example, the studies [16,24] provide design models, stability failure criteria and algorithms for the stability analysis of reinforced concrete frames in column removal scenarios. In the study [25], an analytical model of an eccentrically compressed supper element was proposed to investigate the stability failure of W-shaped steel columns under accidental impact. In [26], the results of an experimental study of different types of stability loss of cold-deformed composite steel columns are presented. During the tests, all experimental specimens with cross-sectional imperfections exhausted the load-bearing capacity due to buckling.

Currently, there are also very few publications on the probabilistic robustness analysis of structural systems. We can mention the works of G.A. Geniev [27,28], who solved the reliability problem of reinforced concrete multi-span beams and obtained the minimum probability of their failure under an accidental action for given initial conditions.

As paper [29] noted, the reliability analysis requires probabilistic definitions of loads and strength of a structure. However, the standards and publications in this field do not contain such clear definitions for accidental design situations, which should be considered at robustness check. There is a lack of target reliability (or risk) values, partial factors or global resistance factor calibrated for conditions of accidental design situation. The fundamental postulate adopted in establishing acceptable (tolerable) risk is that the risks associated with the failure of structural systems of buildings designed and erected in accordance with current best practice are considered sufficiently small and acceptable to society. On the other hand, current best practices are reflected in standards [30,31] and structural design codes [32]. The correct application of these practices allows to create the safe and reliable structural systems. Taking into account the fact that the approaches for consequence assessment given in [29] have high level uncertainties, the modeling of collapse consequences in most cases is simplified by considering only human casualties [10,34]. Thus, in accordance with the model [34], the expected number of potential casualties N_j is calculated depending on the expected collapse area.

This study aimed at development of a probabilistic model for calculating the stability failure of a reinforced concrete frame at sudden removal of a column. Critical parameters of the frame structure are determined using an energy-based approach; meanwhile the probability of stability failure of the frame structural components under such an accidental action is determined using the equigradient method.

2. MODELS AND METHODS

The study examines probability of stability failure of the two-span scaled reinforced con-crete frame previously tested for sudden loss of the column in the paper [39] The frame is loaded with concentrated forces eccentrically applied at the upper joints of the structure. The columns of the second floor of the frame are of relatively large slenderness ratio that makes it vulnerable to stability failure. The frame dimensions, reinforcement scheme, and cross-sections are shown in Figure 1

The loading of the test frame involved two stages as shown in figure 2. At the first stage, constant static concentrated forces P_1 = 4.7 kN, P_2 = 26.2 kN, P_3 = 19.5 kN were applied with an eccentricity e = 10 mm to the upper joints of the frame that corresponds to normal operation conditions. The second stage involved an accidental action due to the sudden removal of the outermost column of the first floor simulating initial localized failure.

The frame has pinned restraints at the joints as shown in Figure 2 that corresponds to the experimental specimen. The stiffnesses and lengths of the beams and columns of the frame are also assumed to be the same as in the specimen tested in the study [37] in order to evaluate the developed approach comparing the calculation results with the experimental data.

The probability P_i of the stability failure of the frame components at the scenario of the sudden

removal of the outermost column of the first floor was evaluated in the following way.
Firstly, the critical force parameters have been determined for each column of the primary design scheme using the displacement method. The design scheme with accepted unknown displacements (rotation angles) is shown in Figure 3.

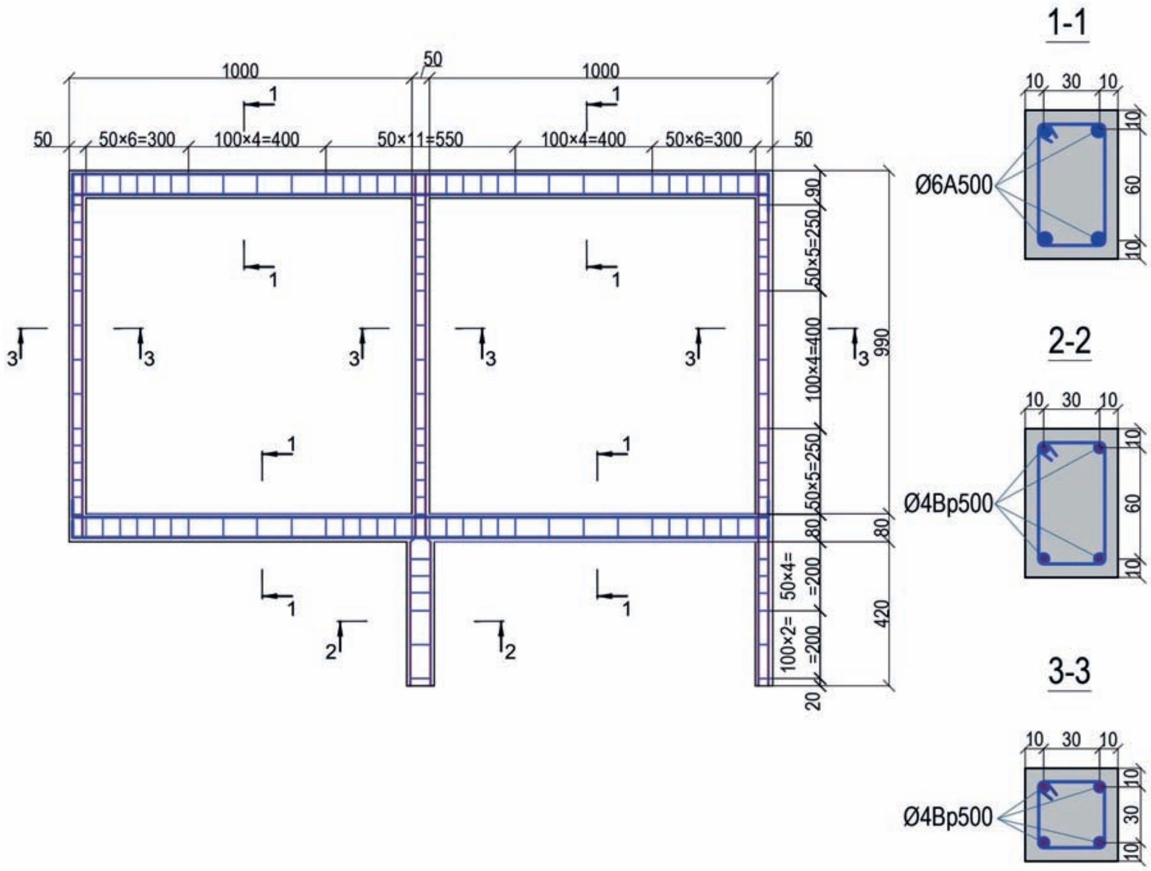

Figure 1. Design of the reinforced concrete frame and its reinforcement scheme

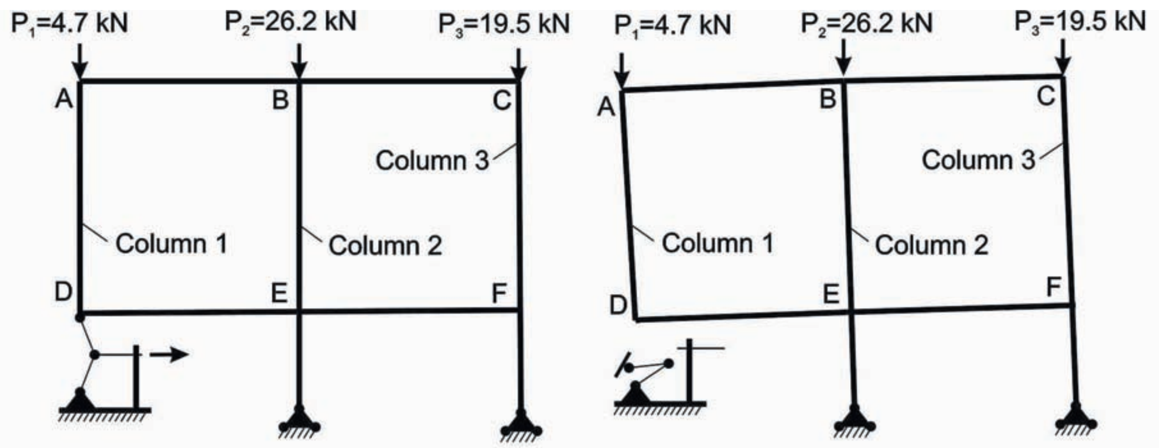

(a) (b)

Figure 2. Design scheme of the reinforced concrete frame at normal operation (a) and at sudden loss of the column (b)

According to the accepted geometrical dimensions of the frame and reinforcement scheme presented in Figure 1, the reduced linear stiffnesses of the structural components $i_n = B_{red,n}/l_n$ have been calculated to obtain the expressions for the force parameters $\nu_n = l\cdot(P_i/B_{red,i})^{0.5}$, where $B_{red,n}$ and l_n are the cross-section stiffness and component length (or height), P_i is the axial force acting in the i^{th} structural component.

During two-stage loading of the reinforced concrete frame, the stiffnesses of the column cross-sections change along the height due to cracking. As it is known, the accuracy of calculation of the stiffnesses significantly effect on the values of critical forces for compressed-bent components. Therefore, to achieve the correct result, the study employs a modified version of the stiffness calculation model, which accounts for deformation effect of F. Thomas – Vl.I. Kolchunov [35] at determination of the mean strains in steel rebars in the blocks between cracks. According to this model, the stiffness of an eccentrically compressed element with cracks is determined from the expression:

$$B_{red,i} = \frac{E_s \cdot A_s \cdot z \cdot h_0}{1.25 + \dfrac{\psi_b \cdot \mu \cdot \alpha}{\nu \cdot \xi}}, \tag{1}$$

where E_s, A_s are the elasticity modulus and cross-sectional area of tensile steel rebars; z is the leverage of the internal force pair in concrete and reinforcement; h_0 is the effective cross-section depth of the structural component; ξ is the relative compressive depth of a component cross-section; ν is the ratio of the secant modulus of concrete to the initial one; ψ_b is the factor accounting for irregularity of tensile concrete strains in the block between cracks; $\mu\cdot\alpha$ is the reinforcement ratio reduced with regard to concrete.

The design scheme of the frame according to the displacement method is shown in Figure 3. The stability equations for the frame are adopted according to the displacement method. The unknown parameters of these equations are the rotation angles of the frame joints Z_1, Z_2, Z_3, Z_4, Z_5, Z_6, the horizontal floor displacements Z_7, Z_8, and vertical displacement Z_9 of the joint above the column to be removed for modelling accidental action. The vertical displacement Z_9 is assumed to be zero before accidental action appears.

Then, the joint reactions r_{in} at unit displacements (rotations) should be obtained to construct the matrix of coefficients r for unknown displacements (rotations) matrix Z:

$$r \times Z = 0, \tag{2}$$

where

$$r = \begin{pmatrix} r_{11} & \dots & r_{1i} \\ \dots & \dots & \dots \\ r_{i1} & \dots & r_{ii} \end{pmatrix}. \tag{3}$$

In the general case of a robustness check of a structure, unknown vertical displacements are assigned at all axes where a hypothetical initial localized failure of a column is possible. Thus, the matrix of reactions of unit displacements (rotations) retains its form for any initial local failure scenario, which is modeled by equating the stiffness of the removed element to zero.

By assuming that the determinant of the matrix r equals zero, the solution of the characteristic equation in the Maple software gives the critical values of the force parameters ν_n.

Using these values and assuming that $Z_9 = 0$, we can calculate the critical forces $P_{cr,\mathrm{I},i}$ for each column of the primary design scheme of the frame. Similarly, the critical forces $P_{cr,\mathrm{II},i}$ can be calculated for the secondary design scheme, when the outermost column of the first floor is removed and $Z_9 \neq 0$. In this calculation, the dynamic effects in the structure at sudden column loss are replaced by the equivalent static force [36] applied in the joint above the removed component.

The sudden loss of a column usually results in a decrease of the critical force value for the modified structural system. In this case, the topology of the structural system may be the tool that allow ensuring the stability of the components under such an accidental action.

The considered approach for determining the critical force in physically and structurally nonlinear reinforced concrete frames allows us to perform a probabilistic assessment of the risk of frame stability failure under an accidental design situation, such as a hypothetical column loss.

To solve the problem of calculating the stability failure probability for structural components of the frame, we use the direct method of probabilistic analysis and the equigradient principle of G.A. Geniev [27]. The mathematical formulation of this principle is as follows. If a function P depends on parameters whose sum is constant, i.e., $q_1 + q_2 + ... + q_n = C =$ const, then the extremum of the function P on the given set of values q_i satisfies the equality:

$$\frac{\partial P}{\partial q_1} = \frac{\partial P}{\partial q_2} = ... = \frac{\partial P}{\partial q_n}. \quad (4)$$

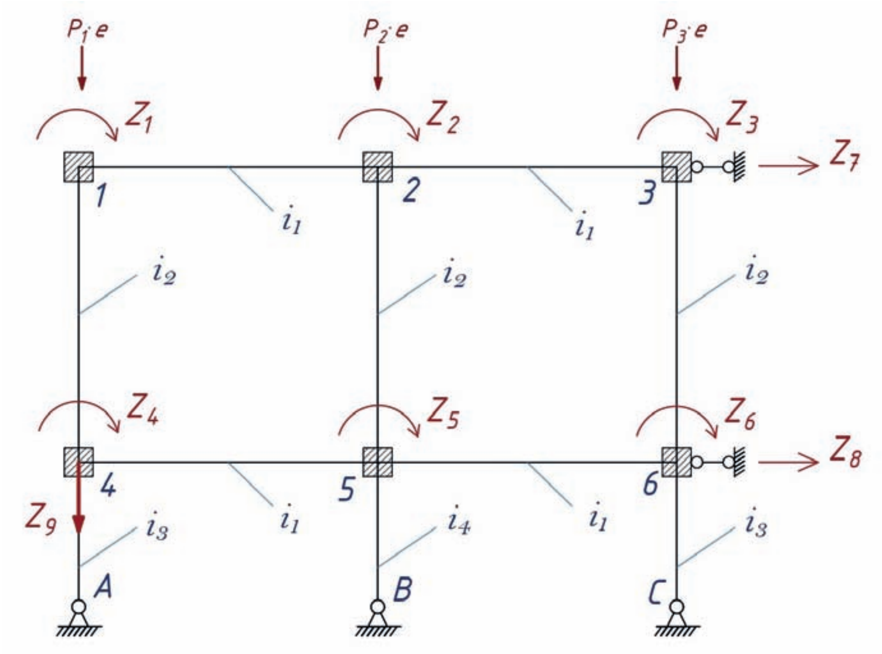

Figure 3. Design scheme of the displacement method for the primary design scheme of the frame

Assume that there is a relation between some parameters affecting on the stability of a structural element such as:

$$D = D\left(P, q_1, q_2, ..., q_n\right) = 0, \quad (5)$$

where $P = P_{cr}$ is the critical force related with the parameters q_1, q_2, ..., q_n, which satisfy the following condition:

$$q_1 + q_2 + ... + q_n = C = \text{const}. \quad (6)$$

Thus, the extremum of the function $P = P(q_1, q_2, ..., q_n)$ fulfilling condition (6) can be found using the auxiliary Lagrangian function:

$$L = P\left(q_1, q_2, ..., q_n\right) = \lambda \cdot \left(q_1 + q_2 + ... + q_n\right), \quad (7)$$

where λ is the Lagrange multiplier.

The extremum condition for this function is as follows:

$$\frac{\partial L}{\partial q_i} = 0. \quad (8)$$

Thus, we obtain the Lagrange multiplier:

$$-\lambda = \frac{\partial P}{\partial q_1} = \frac{\partial P}{\partial q_2} = ... = \frac{\partial P}{\partial q_n}. \tag{9}$$

The extremum of the critical force function P satisfies to the condition (4).

From this follows the conclusion: if some value of P depends on the parameters q_1, q_2, ..., q_n, which are related to each other by condition (6), then for the occurrence of the extremum of the function P it is sufficient to fulfill the criterion (4).

Let P_{s0i} is the initial load of the i^{th} structural element (i = 1, n) and $q_{0i} = v_{0i}$ is the value of the critical force parameter for the given frame before the column removal.

For this frame, the probability of non-destruction of the whole system P_{s0} can be found as follows:

$$P_{s0} = \prod_{i=1}^{n} P_{s0i}. \tag{10}$$

The sum of the values of critical force parameters before the column removal equals:

$$Q_0 = \sum_{i=1}^{n} v_{0i} = const. \tag{11}$$

The probability of non-destruction of i^{th} element of the frame, according to the method of direct mathematical analysis can be determined using the following relationship:

$$P_{s0i} = 1 - P_{f0i}, \tag{12}$$

where P_{f0i} is the probability of the i^{th} structural element stability failure.

The probability of the i^{th} element stability failure can be determined from the expression (13):

$$P_{f0i} = 0.5 - \Phi(U), \tag{13}$$

where $\Phi(U)$ is the Gauss probability integral:

$$\Phi(U) = \frac{1}{\sqrt{2 \cdot \pi}} \cdot \int_0^U e^{-\frac{x^2}{2}} dx, \tag{14}$$

For

$$U = \frac{\bar{R} - \bar{\Omega}}{\sqrt{s_R^2 + s_0^2}},$$

where $\bar{R}, \bar{\Omega}$ are mean values of critical load (capacity) and applied load; s_R and s_Ω are the standard deviations of the mean values, respectively.

The relationship between the probability P_{si} of non-destruction of the i^{th} element and the parameter v_i for a system of series-connected elements can be represented in the form:

$$P_{s0i} = 1 - a_i^{-\frac{v_i}{v_{0i}}}, \tag{15}$$

where

$$a_i = \left(1 - P_{0i}\right)^{-1} \tag{16}$$

According to the equigradient principle of G.A. Geniev, the solution of the problem is reduced to determining the conventional extremum of function (11) satisfying to condition (15) and constraint (12) at the number of compressed elements in the secondary design scheme of the frame n = 5:

$$f = \prod_{i=1}^{5} \left(1 - a_i^{-\frac{v_i}{v_{0i}}}\right) + \lambda \cdot \left(Q_0 - \sum_{i=1}^{5} v_i\right). \tag{17}$$

According to condition (4), it can be written:

$$\begin{cases} a_1^{-\frac{v_1}{v_{01}}} \cdot \frac{\ln a_1}{v_{01}} - \lambda = 0; \\ \qquad ... \\ a_5^{-\frac{v_5}{v_{05}}} \cdot \frac{\ln a_5}{v_{05}} - \lambda = 0. \end{cases} \tag{18}$$

By dividing expressions (18) to $P_{si} = 1 - a_i^{-\frac{v_i}{v_{0i}}}$, we obtain:

$$\frac{\ln a_1}{v_{01}} \cdot \frac{1 - P_{s1}}{P_{s1}} = \ldots = \frac{\ln a_5}{v_{05}} \cdot \frac{1 - P_{s5}}{P_{s5}} = A. \quad (19)$$

Using equality (19), the following relationships can be written:

$$\begin{aligned} &\frac{P_{f1}}{P_{s1}} : \frac{P_{f2}}{P_{s2}} : \frac{P_{f3}}{P_{s3}} : \frac{P_{f4}}{P_{s4}} : \frac{P_{f5}}{P_{s5}} = \\ &= \frac{\ln a_1}{v_{01}} : \frac{\ln a_2}{v_{02}} : \frac{\ln a_3}{v_{03}} : \frac{\ln a_4}{v_{04}} : \frac{\ln a_5}{v_{05}}. \end{aligned} \quad (20)$$

Thus, the expression for the critical values of v_i is as follows:

$$v_i = \frac{1}{\gamma_i} \cdot \ln\left(1 + \frac{\gamma_i}{A}\right), \quad (21)$$

where $\gamma_i = \dfrac{\ln a_i}{v_{0i}}$.

The value of the parameter A is derived taking into account relations (9), (20) and (21):

$$\begin{aligned} &\sum_{i=1}^{5} v_i = \sum_{i=1}^{5} \ln\left[\left(1 + \frac{\gamma_i}{A}\right)^{\frac{1}{\gamma_i}}\right] = \\ &= \ln \prod_{i=1}^{5} \left[\left(1 + \frac{\gamma_i}{A}\right)^{\frac{1}{\gamma_i}}\right] = Q_0. \end{aligned} \quad (22)$$

Accounting for the properties of logarithms, the value of the parameter A will be equal:

$$A = \exp\left[\frac{\ln\left(\prod_{i=1}^{n} \gamma_i^{\beta_i}\right) - Q_0}{\sum_{i=1}^{n} \beta_i}\right], \quad (23)$$

where $\beta_i = \dfrac{1}{\gamma_i}$.

Thus, if the critical values of v_i are obtained by formula (21), then we can find the extremal values of the function P, i.e., the critical forces. Thus, the non-destruction probability for the frame can be found using expression (12) for each structural component and then calculating by formula (10) for the frame. The obtained results should be compared with the target values of non-destruction probability for specified responsibility and operation condition of a facility. If the non-destruction probability is less than the target one the modification of the system should be carried out. Such a modification may be performed using the equigradient approach considered above. In this case, the non-destruction probability will be the target function, while the condition (6) for the total load or for the sum of the force parameters v_i remains relevant. The flow-chart of the stability failure (or non-destruction) probability is shown in figure 4.

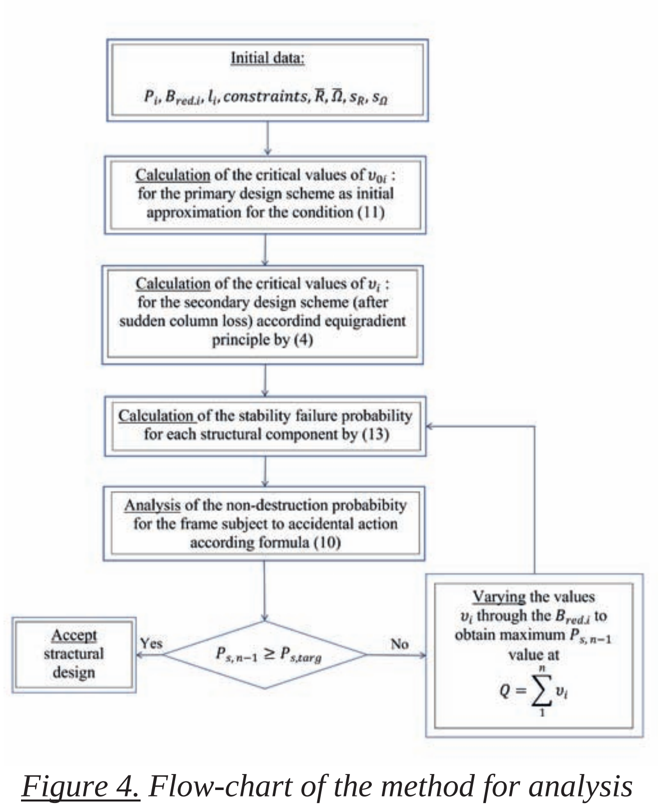

Figure 4. Flow-chart of the method for analysis of stability failure probability

3. RESULTS

Using the method in the previous section of this paper, the stability failure probabilities for the columns of the experimental reinforced concrete frame were calculated for the outermost column removal scenario. The initial data used in the analysis and the results are summarized in Table 1. The probability of non-destruction of the reinforced concrete frame under the accident scenario considered in the study was as follows: $P_{s0} = \prod_{i=1}^{n} P_{s0i} = 0.6936$ for mean values of the critical force $R = P_{cr}$ = 37.2kN and mean value of the axial force in the most vulnerable column $\Omega = N$ = 37.3 kN.

The obtained results are in agreement with the data of experimental studies and numerical modeling in LS-Dyna, as shown in Figure 5, which demonstrates the stability failure of column No. 2.

Table 1. Initial data and results of calculation of the probability of loss of stability of the experimental reinforced concrete frame elements

Column No.	Mean value of capacity (critical force) R, kN	Mean value of load Ω, kN	Standard deviation of capacity s_R, kN	Standard deviation of load s_Ω, kN	Probability of stability failure P_{fi}	Probability of non-destruction P_{si}
1	17.58	4.8	5.022	7.656	0.026	0.974
2	37.15	37.3	3.797	6.878	0.882	0.118
3	26.74	20.7	1.284	2.343	0.469	0.531
4	36.48	27,2	3.430	2.361	0.227	0.773
5	26.91	19.6	0.849	1.037	0.188	0.812

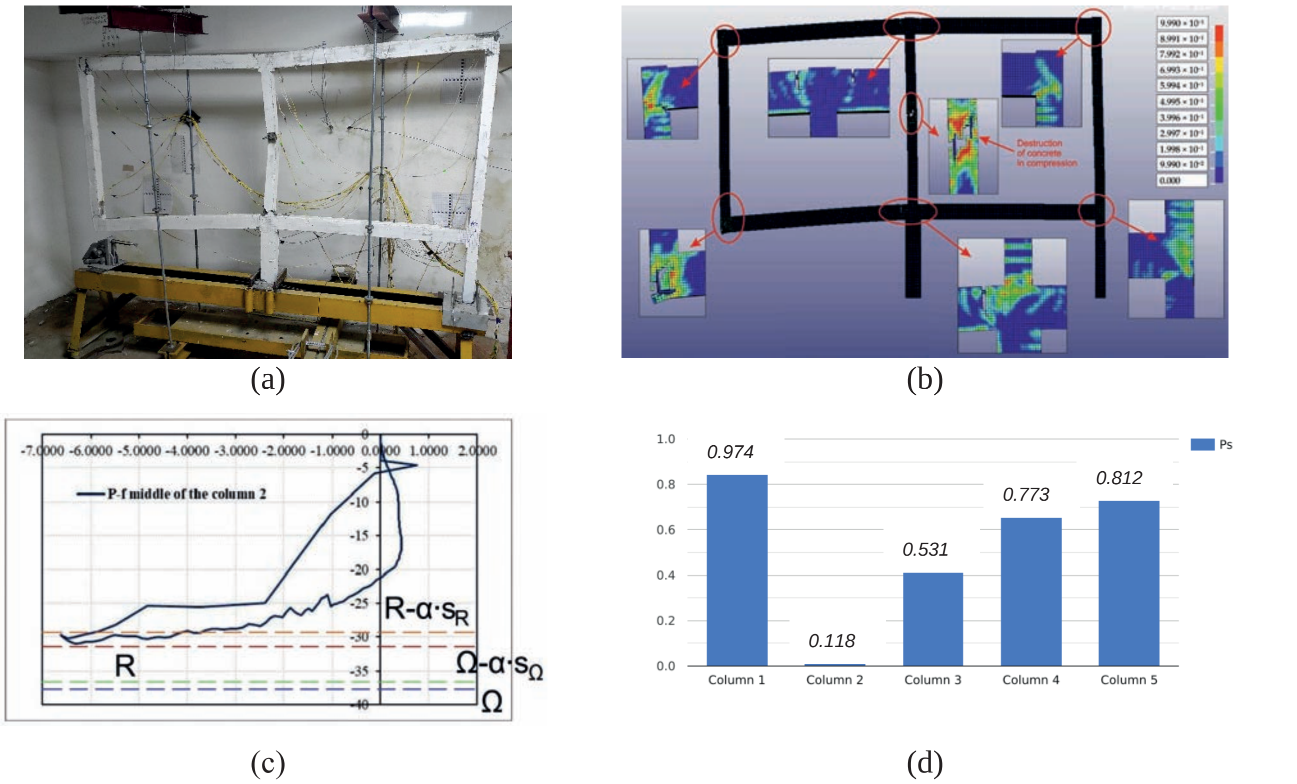

Figure 5. Results of the investigation of reinforced concrete frame stability under accidental impact: general view of the frame after test (a), results of modeling in LS-Dyna (b), force-displacement diagram for column No. 2 (c), distribution of probability of non-destruction for the columns (d)

4. CONCLUSIONS

1. A calculation model based on the equigradient principle is proposed to estimate the critical load and the probability of stability failure of reinforced concrete building frames in an accident situation due to the sudden loss of a column.
2. It has been shown that the results of analysis based on the proposed approach agree with the experimental data and the results of numerical modeling. The difference between the calculated mean value of the critical load and the value established experimentally is 5.9 %.
3. The equigradient method considered in the study can be applied to optimize structural design of building frames according to the criterion of minimizing the probability of stability failure at a fixed consumption of materials for the structural system.

5. ACKNOWLEDGEMENTS

This work was supported by the Russian Science Foundation grant No. 24-49-10010, https://rscf.ru//project/24-49-10010/

REFERENCES

1. **Amiri S., Saffari H., Mashhadi J.** Assessment of dynamic increase factor for progressive collapse analysis of RC structures. *Engineering Failure Analysis*. 2018. (84). Pp. 300–310.
2. **Tsai M.-H.** An Approximate Analytical Formulation for the Rise-Time Effect on Dynamic Structural Response Under Column Loss. International Journal of Structural Stability and Dynamics. 2018.vol 03 (18). pp. 1850038.
3. **Weng J., Tan K. H., Lee C. K.** Adaptive superelement modeling for progressive collapse analysis of reinforced concrete frames. *Engineering Structures. 2017.* (151). pp. 136–152.
4. **GOST 27751-2014.** Reliability of building structures and foundations. Basic provisions (Reissue, with Change No. 1) (in Russian)
5. **ASCE 76-23.** Standard for Mitigation of Disproportionate Collapse Potential in Buildings and Other Structures. - American Society of Civil Engineers. 2023.
6. **ACI 318-19.** Building Code Requirements for Structural Concrete and Commentary American Concrete Institute, 2019.
7. **STB ISO 2394-2007.** Reliability of building structures. General principles. Minsk: Gosstandart of the Republic of Belarus. 2007. - 69 p.
8. **SP 63.13330.2018.** Concrete and reinforced concrete structures. Basic provisions. (in Russian)
9. **SP 385.1325800.2018**. Protection of buildings and structures from progressive collapse. Design rules. Basic provisions. Moscow: Ministry of Construction of Russia, 2018. 33 p. (in Russian)
10. **Kolchunov V.I., Tur V.V.** Design directions of structural systems in special design situations. *Promyshlennoe i grazhdanskoe stroitel'stvo.* 2023. Vol. 7. pp. 5-15. (in Russian)
11. **Adam JM, Parisi F, Sagaseta J, Lu X.** Research and practice on progressive collapse and robustness of building structures in the 21st century. *Eng Struct* 2018; 173. Pp.122–49.
12. **Kiakojouri F, De Biagi V, Chiaia B, Sheidaii M.R.** Progressive collapse of framed building structures: Current knowledge and future prospects. **Eng Struct** 2020; 206:110061.
13. **Kiakojouri F., Zeinali E., Adam J.M., Biagi V.D.** Experimental studies on the progressive collapse of building structures: A review and discussion on dynamic column removal techniques. *Structures* 2023; 57:105059.
14. **Beck A. T., da Rosa Ribeiro L., Costa L. G., Stewart M. G.** Comparison of risk-based robustness indices in progressive col-

lapse analysis of building structures *Structures. Elsevier*, 2023. vol. 57. pp. 105295.
15. **Bassam A. Izzuddin, Miguel F. Pereira, Ulrike Kuhlmann, Lars Rölle, Ton Vrouwenvelder, Bernt J. Leira**. Application of Probabilistic Robustness Framework: Risk Assessment of Multi-Storey Buildings under Extreme Loading *Struct. Eng. Int.* 2012. Vol.22(1). Pp,79-85.
16. **Qiao H., Yang Y., Zhang J.** Progressive Collapse Analysis of Multistory Moment Frames with Varying Mechanisms. *Journal of Performance of Constructed Facilities.* 2018. Vol. 4 (32). pp. 04018043.
17. **Savin S.Y., Kolchunov V.I., Fedorova N.V.** Calculation of stability of reinforced concrete frames of buildings under special effects. *Promyshlennoe i grazhdanskoe stroitel'stvo*. 2023.vol.9. pp.12-21. (in Russian)
18. **Gemmerling A.V.** Calculation of rod systems, M.: Stroyizdat, 1974, 207 p. (in Russian)
19. **Aleksandrov A. V. V., Travush V. I., Matveev A. V.** About calculation of rod structures for stability. *Promyshlennoe i grazhdanskoe stroitel'stvo*. 2002. Vol. 3.Pp. 16-20. (in Russian)
20. **Golyshev A.B., Bachinsky V.Y., Polishchuk V.P.** Reinforced Concrete Structures. Resistance of Reinforced Concrete. vol.1. K.: Logos, 2001. 481 p. (in Russian)
21. **Tsai M.-H.** An Approximate Analytical Formulation for the Rise-Time Effect on Dynamic Structural Response Under Column Loss. *International Journal of Structural Stability and Dynamics.* 2018. Vol. 03 (18). Pp. 1850038.
22. **Kolchunov, V.I.; Prasolov, N.O.; Morgunov, M.V.** To an estimation of the survivability of the reinforced concrete frames at a loss of stability of the separate elements. *Stroitel'naya mekhanika inzhenernyh konstrukcij i sooruzhenij*. 2007.pp. 40-44. (in Russian)
23. **Kolchunov, V.I.; Morgunov, M.V.; Kozharinova, L.V.; Prasolov, N.O.** To the question of the algorithmicisation of the calculation problem of the reinforced concrete structures at the stability loss (in Russian) *Promyshlennoe i grazhdanskoe stroitel'stvo*. 2012.vol. 12. pp.77-79.
24. **Savin S Yu, Kolchunov V I, Korenkov P A.** Experimental research methodology for the deformation of RC frame under instantaneous loss of columnI OP Conf. Series: Materials Science and Engineering 962 (2020) 022054 doi:10.1088/1757-899X/962/2/022054
25. **Mehrdad Memari, A.M. ASCE; Hussam Mahmoud, M.** ASCE and Bruce Ellingwood, Dist.M. ASCE3 Stability of Steel Columns Subjected to Earthquake and Fire Loads J. Struct. Eng., 2018, 144(1): 04017173 DOI: 10.1061/ (ASCE ST.1943-541X.0001909.
26. **Francisco J. Meza, Jurgen Becque, Iman Hajirasouliha** Experimental study of cold-formed steel built-up columns, *Thin-Walled Structures,* doi.org/10.1016/j.tws.2019.106291.
27. **Geniev G.A**. About the principle of equigradient and its application to optimisation problems of stability of rod systems. 118. *Stroitel'naya mekhanika i raschet sooruzhenij.* 1979.-Vol.6.- Pp.. 8-13. (in Russian)
28. **Geniev G A, Kolchunov V I, Degtyar A N** Issues of optimisation of reliability characteristics of reinforced concrete multi-span beams from the position of minimum probability of their failure. Materials of the second international academic readings ‘New energy-saving architectural and structural solutions of residential and civil buildings’ - Orel, 2003 - Pp 163-166. (in Russian)
29. **Tamrazyan A.G**. Methodology of the analysis and estimation of the state reliability and prognostication of the service life of the reinforced concrete structures. *Zhelezobetonnye konstrukcii.* 2023. T. 1. Vol.1. Pp. 5-18. (in Russian)

30. **GOST R ISO 2394-2016.** Structures of construction. Basic principles of reliability. MoscowStandartinform.2016.- 61p.
31. **TCP EN 1991-1-7-2009.** Eurocode 1. Effects on structures. - Part 1-7. General impacts. Special effects. Minsk: Ministry of Architecture and Construction of the Republic of Belarus. 2010. - 66 p.
32. **CN 2.01.01-2022.** Fundamentals of design of building structures. Minsk. 2022. – 65 p.
33. **Tur V. V., Nadolskiy V. V**. Concept of building structures design on the basis of numerical resistance models. *Stroitel'stvo i rekonstrukciya*. 2022. Vol. 6. Pp. 78-90. (In. Russ.)
34. **Hingonrani R.** Acceptable life safety risks associated with the effects of gas explosions on reinforced concrete structures. Caminos, 2017.-227 pp.
35. **V.I. Kolchunov, S.S. Fedorov.** Determination of the level distance between cracks in reinforced concrete structures. *Stroitel'stvo i rekonstrukciya*. 2024. Vol. 4. - Pp. 14-28. (In. Russ.)
36. **Savin, S.; Kolchunov, V.; Fedorova, N.; Tuyen Vu, N.** Experimental and Numerical Investigations of RC Frame Stability Failure under a Corner Column Removal Scenario. *Buildings*. 2023, 13, 908. https://doi.org/10.3390/ buildings13040908.
37. **Thomas, F. G.** (1936). Cracking in reinforced concrete. The Structural Engineer, 1936.Vol.14, Pp. 298-320.

СПИСОК ЛИТЕРАТУРЫ

1. **Amiri S., Saffari H., Mashhadi J.** Assessment of dynamic increase factor for progressive collapse analysis of RC structures // Engineering Failure Analysis. 2018. (84). С. 300–310.
2. **Tsai M.-H.** An Approximate Analytical Formulation for the Rise-Time Effect on Dynamic Structural Response Under Column Loss // International Journal of Structural Stability and Dynamics. 2018. № 03 (18). С. 1850038.
3. **Weng J., Tan K. H., Lee C. K**. Adaptive superelement modeling for progressive collapse analysis of reinforced concrete frames // Engineering Structures. 2017. (151). С. 136–152.
4. **ГОСТ 27751-2014**. Надежность строительных конструкций и оснований. Основные положения (Переиздание, с Изменением N 1).
5. **ASCE 76-23.** Standard for Mitigation of Disproportionate Collapse Potential in Buildings and Other Structures. - American Society of Civil Engineers. 2023.
6. **ACI 318-19** Building Code Requirements for Structural Concrete and Commentary American Concrete Institute, 2019.
7. **СТБ ISO 2394-2007.** Надежность строительных конструкций. Общие принципы. Минск: Госстандарт Республики Беларусь. 2007. – 69 с.
8. **СП 63.13330.2018** Бетонные и железобетонные конструкции. Основные положения.
9. **СП 385.1325800.2018.** Защита зданий и сооружений от прогрессирующего обрушения. Правила проектирования. Основные положения. М.: Минстрой России, 2018. 33 с.
10. **Колчунов В.И., Тур В.В.** Направления проектирования конструктивных систем в особых расчетных ситуациях // Промышленное и гражданское строительство. 2023. № 7. С. 5-15.
11. **Adam JM, Parisi F, Sagaseta J, Lu X**. Research and practice on progressive collapse and robustness of building structures in the 21st century. Eng Struct 2018; 173:122–49.
12. **Kiakojouri F, De Biagi V, Chiaia B,** Sheidaii MR. Progressive collapse of framed building structures: Current knowledge and future prospects. Eng Struct 2020; 206:110061.
13. **Kiakojouri F., Zeinali E., Adam J.M., Biagi V.D**. Experimental studies on the

progressive collapse of building structures: A review and discussion on dynamic column removal techniques. Structures 2023; 57:105059.
14. **Beck A. T., da Rosa Ribeiro L., Costa L. G., Stewart M. G.** Comparison of risk-based robustness indices in progressive collapse analysis of building structures Structures. Elsevier, 2023. Т. 57. С. 105295.
15. **Bassam A. Izzuddin, Miguel F. Pereira, Ulrike Kuhlmann, Lars Rölle, Ton Vrouwenvelder, Bernt J. Leira**, Application of Probabilistic Robustness Framework: Risk Assessment of Multi-Storey Buildings under Extreme Loading Struct. Eng. Int. 2012. 22(1). 79-85.
16. Qiao H., Yang Y., Zhang J. Progressive Collapse Analysis of Multistory Moment Frames with Varying Mechanisms. Journal of Performance of Constructed Facilities. 2018. № 4 (32). С. 04018043.
17. **Савин С.Ю. Колчунов В.И., Федорова Н.В.** Расчет устойчивости железобетонных каркасов зданий при особых воздействиях //Промышленное и гражданское строительство. 2023.№9. С.12-21.
18. **Геммерлинг А.В**. Расчет стержневых систем, М.: Стройиздат, 1974, 207 с.
19. **Александров А. В., Травуш В. И., Матвеев А.** В. О расчете стержневых конструкций на устойчивость // Промышленное и гражданское строительство. 2002. No 3.С. 16—20.
20. **Голышев А.Б. Бачинский В.Я., Полищук В.П.** Железобетонные конструкции. Сопротивление железобетона. Т.1. К.: Логос, 2001. 481 с
21. **Tsai M.-H.** An Approximate Analytical Formulation for the Rise-Time Effect on Dynamic Structural Response Under Column Loss // International Journal of Structural Stability and Dynamics. 2018. № 03 (18). С. 1850038.
22. **Колчунов В.И.,Прасолов Н.О. Моргунов М.В.** К оценке живучести железобетонных рам при потере устойчивости отдельных элементов // Строительная механика инженрных конструкций и сооружений, 2007С. 40-44. .
23. **Колчунов, В.И., Моргунов М.В., Кожаринова Л.В., Прасолов Н.О**. К вопросу алгоритмизации задачи расчета железобетонных конструкций при потере устойчивости //Промышленное и гражданское строительство. 2012.№12. С.77-79.
24. **Savin S Yu, Kolchunov V I, Korenkov P A.** Experimental research methodology for the deformation of RC frame under instantaneous loss of columnI OP Conf. Series: Materials Science and Engineering 962 (2020) 022054 doi:10.1088/1757-899X/962/2/022054
25. **Mehrdad Memari, A.M. ASCE; Hussam Mahmoud, M.** ASCE and Bruce Ellingwood, Dist.M. ASCE3 Stability of Steel Columns Subjected to Earthquake and Fire Loads J. Struct. Eng., 2018, 144(1): 04017173 DOI: 10.1061/ (ASCE ST.1943-541X.0001909.
26. **Francisco J. Meza, Jurgen Becque, Iman Hajirasouliha** Experimental study of cold-formed steel built-up columns, Thin-Walled Structures, https://doi.org/10.1016/j.tws.2019.106291.
27. **Гениев Г.А.** О принципе эквиградиентности и применении его к оптимизационным задачам устойчивости стержневых систем. 118 //Строительная механика и расчет сооружений. -1979.-№6.- С. 8-13.
28. **Гениев Г А, Колчунов В И, Дегтярь А Н** Вопросы оптимизации характеристик надежности железобетонных многопролетных балок с позиции минимальной вероятности их отказа //Материалы вторых международных академических чтений «Новые энергосберегающие архитектурно-конструктивные решения жилых и гражданских зданий» -Орел, 2003 -С 163-166.
29. **Тамразян А.Г.** Методология анализа и оценки надежности состояния и прогнозирование срока службы железобетон-

ных конструкций // Железобетонные конструкции. 2023. Т. 1. № 1. С. 5–18.
30. **ГОСТ Р ИСО 2394—2016**. Конструкции строительные. Основные принципы надежности. МоскваСтандартинформ.2016.- 61с.
31. **ТКП EN 1991-1-7-2009.** Еврокод 1. Воздействия на конструкции. – Часть 1-7. Общие воздействия. Особые воздействия. Минск: Министерство архитектуры и строительства Республики Беларусь. 2010. – 66 с.
32. **СН 2.01.01-2022.** Основы проектирования строительных конструкций. Минск. 2022. – 65 с.
33. **Тур В. В., Надольский В. В.** Концепция проектирования строительных конструкций на основе численных моделей сопротивления //Строительство и реконструкция. – 2022. – №. 6. – С. 78-90.
34. **Hingonrani R.** Acceptable life safety risks associated with the effects of gas explosions on reinforced concrete structures: – Caminos, 2017.-227 p.p.
35. **Вл.И. Колчунов, С.С. Федоров.** Определение уровневого расстояния между трещинами в железобетонных конструкциях //Строительство и реконструкция. – 2024. – №. 4. – С. 14-28
36. **Savin, S.; Kolchunov, V.; Fedorova, N.; Tuyen Vu, N.** Experimental and Numerical Investigations of RC Frame Stability Failure under a Corner Column Removal Scenario. Buildings 2023, 13, 908. https://doi.org/10.3390/ buildings13040908.
37. **Thomas, F. G. (1936).** Cracking in reinforced concrete. The Structural Engineer, 1936.Vol.14, Pp. 298-320.

Margarita Andreevna Amelina - Post graduate student of the department of Reinforced Concrete and Masonry Structures. National Research Moscow State University of Civil Engineering, 26, Yaroslavskoe Shosse, Moscow, 129337, Russia, margo.dremova@mail.ru

Sergei Yurievich Savin — Candidate of Technical Sciences, Associate professor, Department of Reinforced Concrete and Masonry Structures, National Research Moscow State University of Civil Engineering, 26, Yaroslavskoe Shosse, Moscow, 129337, Russia, suwin@yandex.ru

Natalia Vitalievna Fedorova - Doctor of Technical Sciences, Professor, Head of the Department of Industrial and Civil Engineering, National Research Moscow State University of Civil Engineering, 26, Yaroslavskoye Shosse, Moscow, 129337, Russia, FedorovaNV@gic.mgsu.ru

Маргарита Андреевна Амелина - аспирант кафедры железобетонных и каменных конструкций. ФГБОУ ВО «Национальный исследовательский Московский государственный строительный университет» (НИУ МГСУ), д. 26, Ярославское шоссе, г. Москва, 129337, Россия, margo.dremova@mail.ru

Сергей Юрьевич Савин – кандидат технических наук, доцент кафедры железобетонных и каменных конструкций, ФГБОУ ВО «Национальный исследовательский Московский государственный строительный университет» (НИУ МГСУ), д. 26, Ярославское шоссе, г. Москва, 129337, Россия, suwin@yandex.ru

Наталия Витальевна Федорова — доктор технических наук, профессор, заведующий кафедрой Промышленного и гражданского строительства, Федеральное государственное бюджетное образовательное учреждение высшего образования «Национальный исследовательский Московский государственный строительный университет» (НИУ МГСУ), д. 26, Ярославское шоссе, г. Москва, 129337, Россия, FedorovaNV@gic.mgsu.ru

DOI:10.22337/2587-9618-2024-20-4-57-71

ENHANCING THE DAMPING BEHAVIOUR OF STEEL CRANE STRUCTURES BY INTRODUCING A CONCRETE CORE

Irina V. Shkoda [1,2], Olga I. Vediaikina [1], Daria A. Loshkaryova [1]

[1] Nizhny Novgorod State University of Architecture and Civil Engineering, Nizhny Novgorod, RUSSIA
[2] Mechanical Engineering Research Institute RAS, Branch of the Institute of Applied Physics RAS, Nizhny Novgorod, RUSSIA

Abstract: The potential use of steel tube confined concrete columns in crane structures is being explored as a means of enhancing damping during the movement of carrying and lifting machines. This is with a view to mitigating the impact of dynamic effects that may arise during operation. The results of experimental studies of tube confined concrete specimens for stability under central compression by static loading are given. This paper presents a methodology for dynamic tests of specimens, which is used to determine the damping ratio of vibrations and the inelastic resistance coefficient of composite materials. The results demonstrate that tube confined concrete specimens possess enhanced damping behaviour in comparison to steel and reinforced concrete structures. This observation suggests that they are an effective solution for load-bearing structures designed to support moving overhead cranes.

Keywords: crane structures, steel tube confined concrete, critical load, natural vibration frequency, damping ratio, inelastic resistance coefficient, damping

УЛУЧШЕНИЕ ДЕМПФИРУЮЩИХ ХАРАКТЕРИСТИК СТАЛЬНЫХ ПОДКРАНОВЫХ КОНСТРУКЦИЙ ПОСРЕДСТВОМ ИНТЕГРАЦИИ БЕТОННОГО СЕРДЕЧНИКА

И.В. Шкода [1,2], О.И. Ведяйкина [1], Д.А. Лошкарева [1]

[1] Нижегородский государственный архитектурно-строительный университет, г. Нижний Новгород, РОССИЯ
[2] Институт проблем машиностроения РАН – Филиал ФГБУН «Федеральный исследовательский центр Институт прикладной физики им. А.В. Гапонова-Грехова Российской академии наук, г. Нижний Новгород, РОССИЯ

Аннотация: Изучается перспектива применения трубобетонных колонн в подкрановых конструкциях с целью увеличения демпфирования во время движения подъемно-транспортных машин, подверженных динамическим воздействиям в процессе эксплуатации. Представлены результаты экспериментальных испытаний трубобетонных образцов на устойчивость под действием центрального сжатия статической нагрузки. Описана методика динамических испытаний образцов, на основе которой определены коэффициенты демпфирования колебаний и неупругого сопротивления. Полученные результаты показывают, что трубобетонные образцы обладают более высокими демпфирующими свойствами, чем стальные и железобетонные, что свидетельствует об их эффективности в качестве несущих конструкций, предназначенных для мостовых кранов.

Ключевые слова: подкрановые конструкции, трубобетон, критическая нагрузка, частота собственных колебаний, декремент затухания, коэффициент неупругого сопротивления, демпфирование

1. INTRODUCTION

Crane structures are an integral component of modern industrial plants, serving a crucial function in ensuring the safety and operational efficiency of these facilities. Fig. 1 illustrates the configuration of load-bearing and crane structures, with arrows indicating the potential movements of the crane trolley 1 along the overhead crane 2 and the girder itself along the crane rails 3 on crane girders 4. The columns 5 in crane systems may have various cross sections, including open sections such as I-beams or channels, as well as closed sections having rectangular, square and circular cross sections.

In the design of crane structures, it is essential to consider both static and dynamic loads in order to create a structure that can withstand the full range of forces acting on the crane during its operational lifetime. During operation, a number of factors can contribute to vibrations in crane structures. These include uneven load lifting, sudden changes in crane speed, wind effects, malfunctions in the control system, wear and tear of materials, and geometric imperfections in the structure. Additionally, vibration effects from surrounding machines can also play a role [1-3].

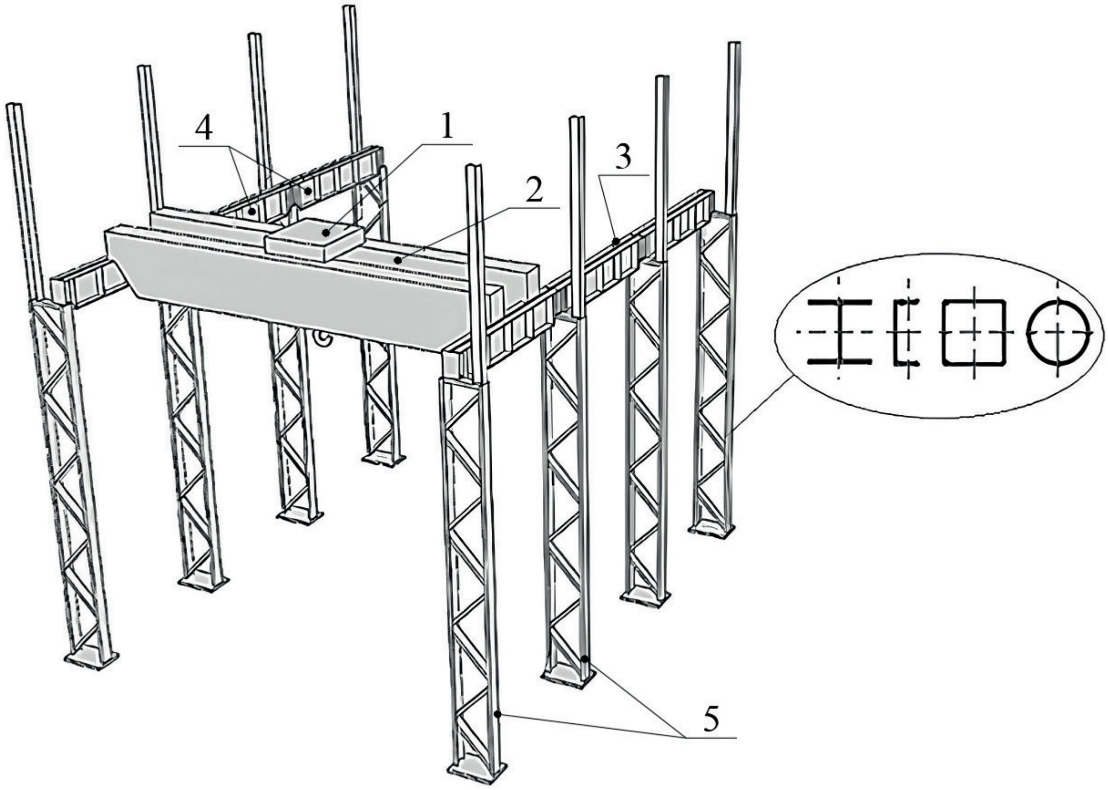

Figure 1. Configuration of load-bearing and crane structures:
1 – crane trolley; 2 – overhead crane (girder crane); 3 - crane rails; 4 - crane girders; 5 – columns

In order to ensure safe and reliable operation of the crane system, the vibrations occurring in the crane system must be damped. There are various technologies designed to reduce the amplitude of vibrations and increase the stability of the crane structure [4, 5]. These technologies include the use of damping devices, adaptive systems and advanced materials [6-9].

Hydraulic and pneumatic shock absorbers can be used to absorb vibrations [10, 11]. Adaptive systems, such as active shock absorbers or feedback systems, are able to modify their parameters in real time in response to changes in operating conditions.

Vibration protection systems consisting of flexible supports and materials with a high coefficient of internal friction play an important role in preventing vibrations. Similar systems are used in vehicles, industrial mechanisms, crane structures. Materials with increased damping include specialised elastomers, polymers with high damping capacity, active materials (e.g. piezoelectric components), vibration isolating foams, tube confined concrete, etc.

The use of steel tube confined concrete as a column material, combining the properties of concrete and steel, is a viable option when a closed-section profile is employed. This approach is widely used to create structures with increased resistance to vibrations. Concrete has a relatively high strength, fire resistance and durability, which makes it an excellent structural material. Concrete is also a good damping material. However, concrete is not an effective material for resisting cracking, which shortens the lifespan of concrete structures and requires regular maintenance. The use of a steel outer shell permits an enhanced resistance to cracking in concrete structures subjected to a combination of static loads and vibrations.

Steel tube confined concrete (STCC) is a complex structure, including a metal tube filled with concrete, which forms the inner core [12-17]. This combination exploits the distinctive characteristics of both materials, resulting in a notable reduction in steel and concrete usage, a decrease in the weight and volume of the structure, and a subsequent reduction in overall construction costs.

The shell tube, which serves the dual purpose of providing both longitudinal and transverse reinforcement, is capable of absorbing forces in all directions and at any angle [18]. The lateral pressure of the tube restrains the radial expansion of the concrete inside the tube due to the Poisson's ratio, which in turn prevents the development of micro-cracks. This significantly increases the bearing capacity of concrete, increasing its compressive strength by 50-80% [19], due to the triaxial state of stress [15]. In addition, the steel pipe is protected from loss of local secondary and general buckling.

A number of studies have been conducted by both Russian [12-14, 18-20] and foreign [21-32] authors on the subject of STCC structures, their deformation processes and the loss of stability that can occur. However, the effect of static compressive loading on the elastic-damping properties of STCC under forced vibrations has not been investigated in sufficient detail.

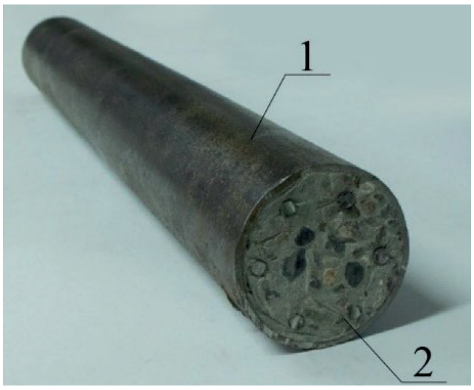

Figure 2. *General view of steel tube confined concrete: 1 - outer shell (steel tube); 2 - inner filler (concrete)*

This paper presents an experimental study to obtain data on the damping properties of STCC. The research findings establish the decrement and damping coefficients of vibrations, as well as the inelastic resistance coefficients of tube confined concrete.

2. STABILITY TESTS

2.1. Materials and methods

Centre compression stability tests were carried out to determine the critical compressive strength of the specimen. For this purpose, STCC specimens with a length of 700 mm and a diameter of 60 mm were fabricated. A tube made of 09G2S structural steel with 2 mm wall thickness was used as the outer shell, and concrete grade B17.5 was used as the filler.

All tests were conducted on a P-125 laboratory compression machine with a maximum compressive load of 1250 kN. Each specimen was put directly between the plates of the compression machine (Fig. 3a). To ensure that the end section rotates in the bending plane (loss of stability plane) 1, the specimens 2 were supported by an additional steel plate 3 and a cylindrical support hinge 6 with an axis perpendicular to the plane 1 that is under study. The use of a cylindrical hinge helps to define the bending plane (loss of stability) of a circular specimen.

By means of two deflection gauges 4, 5 placed in two perpendicular planes (one of which is the bending plane), the horizontal displacements Δ of the average cross-section of the rod were continuously recorded with an accuracy of 0.01 mm as the load P was increased. The readings recorded by the deflection gauge 5, installed to control the displacements from the stability loss plane, were close to zero, which confirms the validity of the experiment [34].

2.2. Experimental results

The test results are presented in Fig. 3b in compression diagrams, which were used to determine the values characterising the specimen stability loss. The critical load value corresponded to the load at which the values on the deflection gauge scale begin to decrease. In compression diagrams, this value is determined by the start of bending of the corresponding curves.

Table 1 shows the values of the destruction loads for the two tube confined concrete specimens tested.

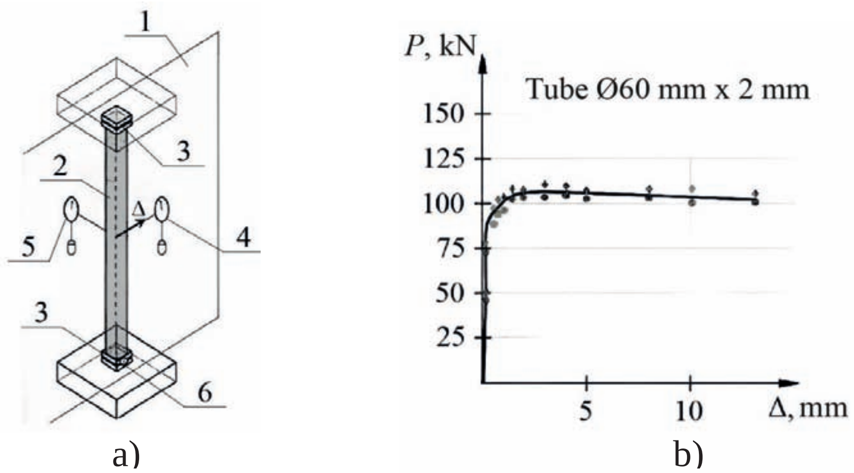

Figure 3. Specimens tested in center compression: a) experimental setup scheme; b) compression diagram

Table 1. Critical load values for the test specimens

Specimens mark	Specimen no.	Critical load, P_{cr}, kN	Average critical load, $P_{cr.\ avg}$, kN
STCC 60x2.700	1	105	108
	2	111	

3. DETERMINATION OF DYNAMIC CHARACTERISTICS OF TUBE CONFINED CONCRETE

3.1. Materials and methods

The dynamic characteristics of STCC were determined through experimental investigation, based on the findings of the study of natural vibrations of the STCC specimen that was subjected to impact. The tests were carried out at different values of axial compressive forces acting on the specimens.

The setup for dynamic testing of centrally compressed specimens is shown in *Fig. 4*. Specimen 1 was hinged at both ends between the load-bearing I-beam 2 and the foundation. A basket 3 with weights 4 of varying masses was suspended from the free end of the beam 2, with a hinge located in the wall recess.

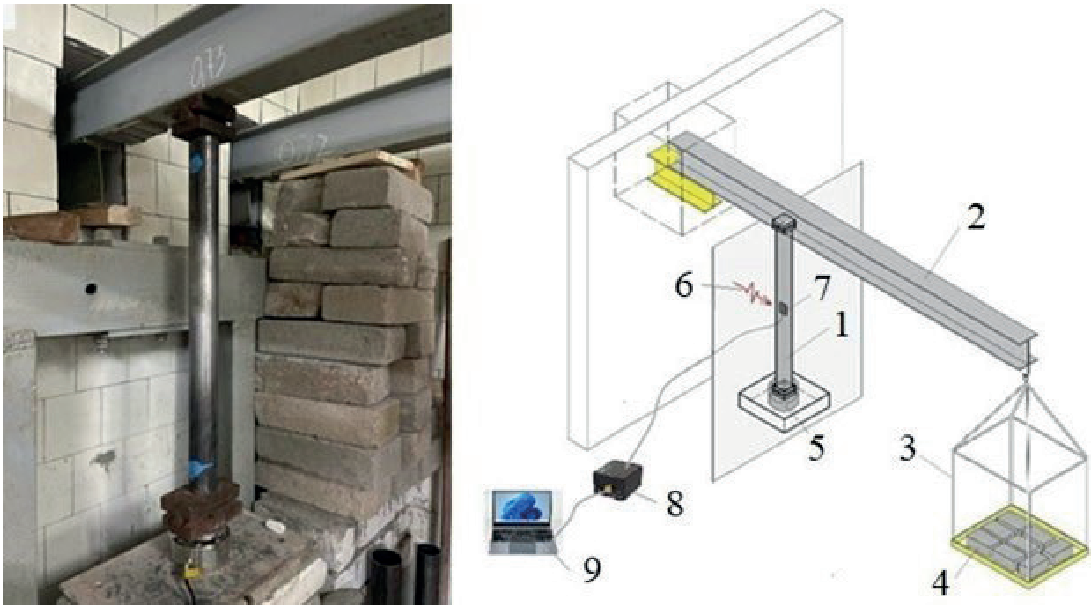

a) b)

Figure 4. Test setup for the study of free vibrations of centrally compressed specimens: a) general view; b) axonometric diagram

The actual load acting on the specimen (axial compressive force) includes the dead weight of the load basket and part of the gravity of the load I-beam applied to the specimen at its two-point bearing. This load was recorded using a strain gauge 5 installed under the lower support of the specimen (the values of the axial compressive force acting on the specimens during the tests are given in *Table 2*). The compressive force of the specimens did not exceed their load-bearing capacity determined by the stability tests.

Table 2. Compressive force of tube confined concrete specimens during testing

Number	Actual axial force on the specimen N_{act}, kN	Dimensionless axial force $N=N_{act}/N_{cr}$
1	1.3	0.011
2	6.8	0.057
3	12.8	0.108
4	18.7	0.157
5	24.6	0.207
6	30.6	0.257
7	36.5	0.307

The generation of transverse vibrations in the specimen was achieved at each stage of loading using a spring-loaded hammer 6. A triaxial accelerometer 7 of type TBA with a mass of approximately 50 g was used to record the vibrations (the insignificant mass of the accelerometer did not affect the accuracy of the measurements). The accelerometer was fixed in the mid-section of the specimen. The signal from the accelerometer was fed through the signal processing module 8 (matching amplifier and analogue-to-digital converter) to a personal computer 9 for registration and subsequent processing of the measurement results.

Free decreasing vibrations were generated in the specimen during a single impact. To illustrate the test results, *Figure 5* shows oscillograms of decreasing vibrations in the form of diagrams of the specimen mid-section displacement *A* over time *t*, obtained at two extreme values of axial compressive force N_1 = 6.8 kN (*Fig. 5a*) and N_6 = 36.5 kN (*Fig. 5b*).

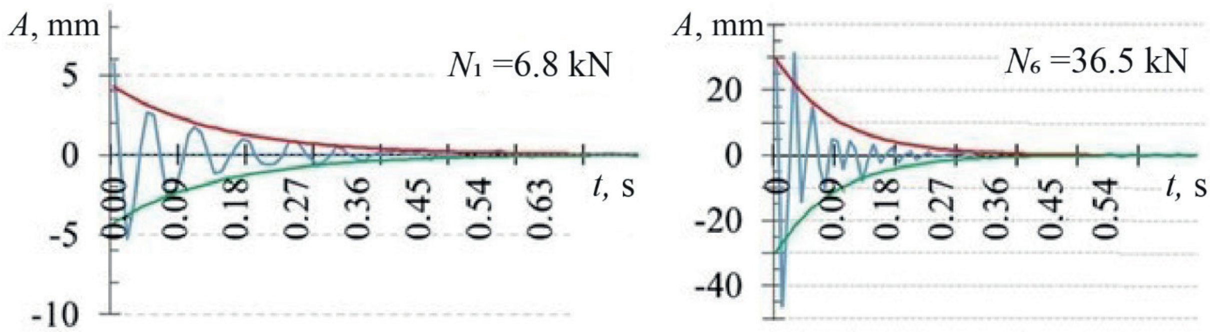

Figure 5. Graphs of bending vibrations of a tube confined concrete specimen loaded with axial compressive force N at impact: a) N_1 = 6.8 kN; b) N_6 = 36.5 kN

3.2. Experimental results

The analysis of the obtained oscillograms has demonstrated that these vibrations are highly analogous to those observed in linear systems with viscous friction, where the period of natural vibrations *T* is largely independent of the amplitude *A*. Moreover, the first natural frequency of bending vibrations of the STCC specimen $\omega = 2\pi/T$ increases with increasing axial compressive force *N* acting on the specimen (*Fig. 6*). The authors of [35-37] also observed a correlation between an increase in frequency and an increase in compressive stress. It is important to highlight that this behaviour in the compression of STCC differs from the established concepts regarding the behaviour of isotropic continuous media [38, 39]. This phenomenon may be attributed to the characteristics of the composite material and the specific interactions between the core and the shell of the STCC.

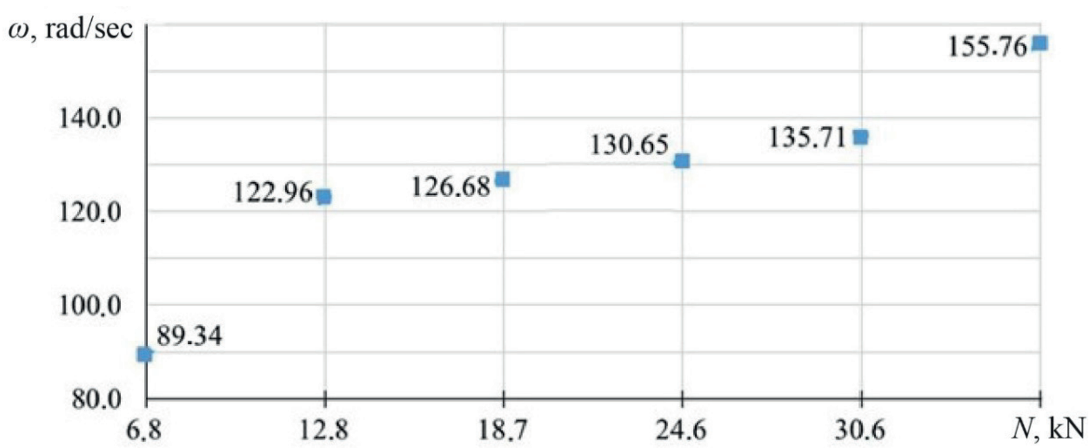

Figure 6. The values of the first natural frequency ω of bending vibrations of a tube confined concrete specimen depending on the axial compressive force N

These vibrations can be described with a reasonable degree of accuracy by the well-known law of free, decreasing vibrations of linear systems with viscous friction:

$$x(t) = A(t)e^{-\beta t}\cos(\omega t)\,, \qquad (1)$$

where $A(t)$ - amplitude of vibrations, m; β - logarithmic damping ratio, sec^{-1}; ω - circular oscillation frequency, rad/sec; t - time, sec.

According to the results presented in *Fig. 6*, we can see that an increase in the axial force leads to an increase in the natural frequency and, consequently, to an increase in the elastic properties of the structure. In the case of a linear hinged beam, the natural frequency of bending vibrations is determined by the following formula [40]:

$$\omega = \frac{\pi^2}{l^2}\sqrt{\frac{EJ}{\rho F}} = \frac{\pi^2}{l^2}\sqrt{\frac{EJ}{m_l}}\,, \qquad (2)$$

where E - average (reduced) elastic modulus of the STCC specimen material, N/m^2; J - moment of inertia of the specimen cross-section, m^4; ρ - reduced density, kg/m^3; F - cross-sectional area of the specimen, m^2; m_l - linear mass, kg/m; l - specimen length, m.

From equation (2), which is derived from the experimentally obtained value of the natural frequency of vibration, we can calculate the reduced coefficient, which accounts for the elasticity of the material and the influence of the axial compressive force N_{act} of the specimen.

$$E_N = \frac{\omega^2 m_l l^4}{\pi^4 J} \qquad (3)$$

In this instance, the alteration of the elastic properties of the structure as a consequence of the axial compressive force is accounted for by a conditional change in the value of the reduced E_N coefficient.

The proposed methodology was employed to calculate the values of the E_N coefficient for a distributed mass of the specimen, resulting in m_l = 0.01 t/m and $J = \pi D^4/64 = 6.36 \cdot 10^{-7}$ m^4. These values are presented in *Fig. 7*.

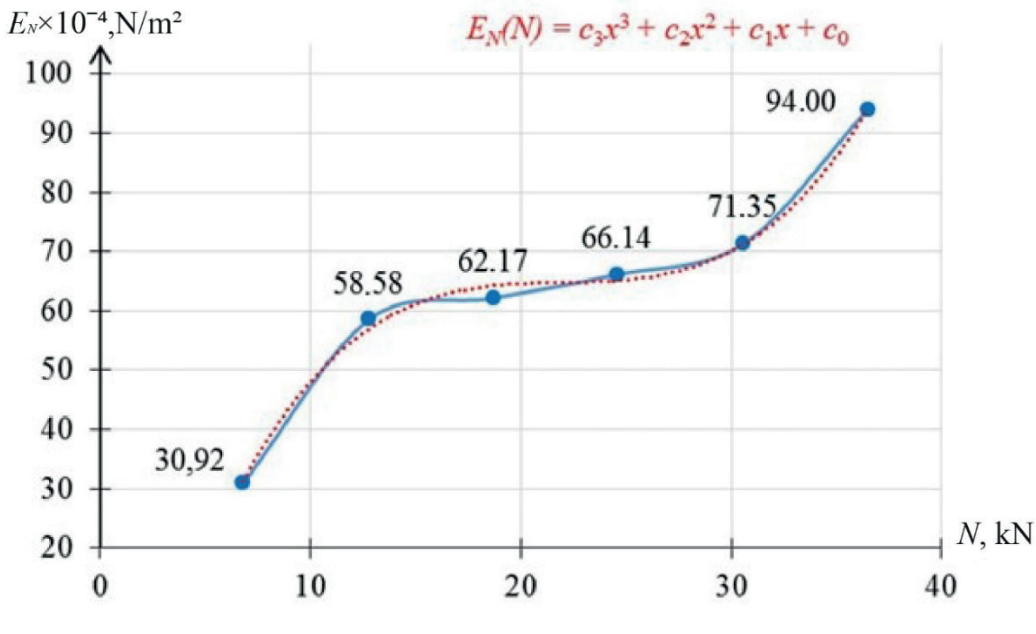

Figure 7. A graph of the reduced coefficient depending on the axial load with an approximating monotonic function $E_N(N)$

As illustrated in *Fig. 7*, the graph demonstrates that the value of the reduced coefficient rises in conjunction with an increase in the axial compression force. This outcome reflects the physical meaning of the coefficient, which is influenced by the axial compression force. Subsequent studies may use the obtained value to determine the frequency of natural vibrations of STCC structures produced from materials of other brands and with a section different from that under consideration.

Excluding the action of the axial force on the tested specimen, we obtain a reduced coefficient that fully reflects the elastic properties of the material and is in fact the average (reduced) modulus of elasticity E, which is confirmed by the results obtained in [32].

The logarithmic damping ratio included in the equation of motion (1) can be calculated as the average of several logarithmic damping ratios from the graphs shown in *Fig. 5*. In order to level local errors, instead of two neighbouring vibration amplitudes x_j, x_{j+1}, the ratio of vibration amplitudes x_j, x_{j+s} after several s periods was used in this work (*Fig. 8*). In the case under consideration, the logarithmic damping ratio β was determined on several n different sections of the oscillogram, offset one from another. Each section consisted of five periods, which explains the presence of the coefficient 0.2 in the equation. Then the average value of the logarithmic damping ratio $\bar{\beta}$ is calculated by the following formula:

$$\bar{\beta} = \frac{1}{n}\sum_{i=1}^{n}\left(\frac{0.2}{T} ln \frac{x_j}{x_{j+5}}\right)_j, \qquad (4)$$

where x_j, x_{j+5} are the peak values, at the boundaries of the time interval (t_j, t_{j+5}), m; n is the number of waveform sections taken to calculate damping ratio; T is the period, sec.

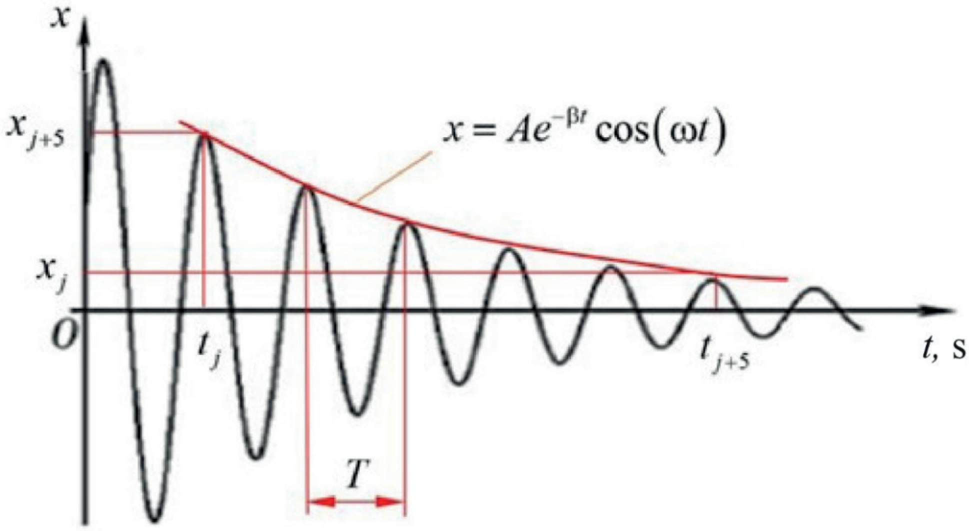

Figure 8. Determining the damping ratio

The processing of the obtained oscillograms yielded the following values for the logarithmic damping ratio of the STCC specimen under the two lowest and highest compressive forces: $\bar{\beta}$= 6.20 at N_1 = 6.8 kN and $\bar{\beta}_6$ = 10.21 at N_6 = 36.5 kN. Thus, it is found that the damping ratio depends on the axial compressive force of the STCC.

4. FORCED VIBRATIONS

In the context of forced vibrations, the damping behaviour of support structures are characterised by the inelastic resistance coefficient γ. This coefficient accounts for the dissipation of vibration energy due to internal friction within the material, with the resulting values determining the amplitudes of vibrations in near-resonant zones. This coefficient is a material constant and is directly related to the damping ratio and natural frequency of the system:

$$\gamma = \frac{2\bar{\beta}}{\omega} = \frac{\bar{\beta}T}{\pi} \tag{5}$$

The amplitude of forced vibrations is dependent upon the dynamic coefficient μ, which for linear systems with one degree of freedom is described by the following formula [35]:

$$\mu = \frac{1}{\sqrt{(1-\lambda^2)^2 + \gamma^2\lambda^2}}, \tag{6}$$

where $\lambda = \Omega/\omega$ is the ratio of the circular frequency Ω of the stimulus and the natural frequency of the system ω; γ is the coefficient of inelastic resistance of the material, taking into account the forces of internal friction.

The following values of the inelastic compressive force coefficient were obtained for the lowest and highest compressive forces (see *Table 3*).

Table 3. The value of the inelastic resistance coefficient

	Compression force	Damping ratio $\bar{\beta}$, sec^{-1}	Natural-vibration frequency ω, rad/sec	Coefficient of inelastic resistance γ, rad^{-1}
1	N_1=6.8 kN	6.20	89.34	0.139
2	N_6=36.5 kN	10.21	158.5	0.129

The calculated values for different values of compressive forces acting on the sample exceed the coefficient of inelastic behavior for concrete and reinforced concrete γ_{reinf} = 0.1 rad^{-1}, as well as for steel γ_{stl} = 0.12 rad^{-1}.

The obtained value of the inelastic resistance coefficient (γ_1=0.139 rad^{-1} and γ_6=0.129 rad^{-1}) differ by no more than 7%. At the same time, exceeding similar values for reinforced concrete by 30-40% results in a notable reduction in the dynamic coefficient at the resonant frequency (Fig. 9).

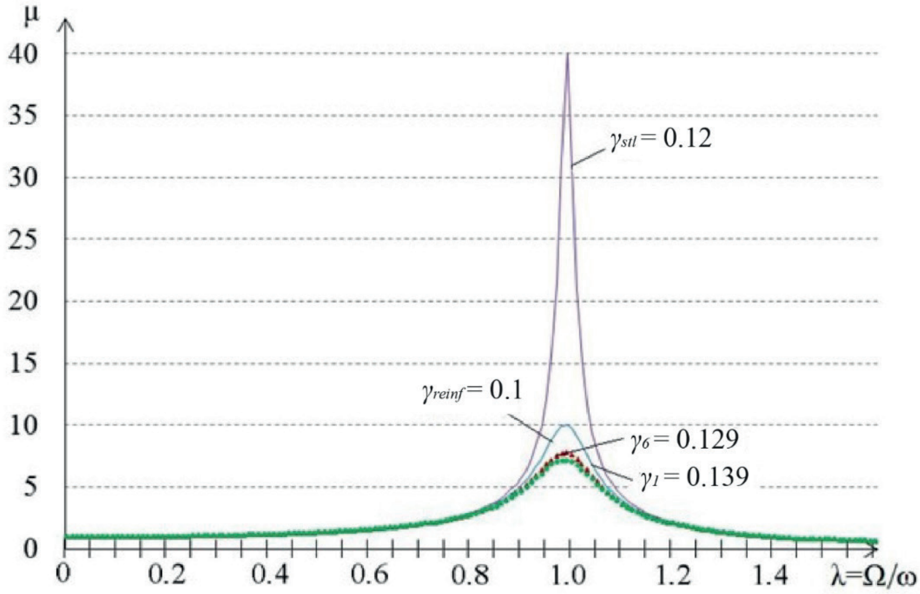

Fig. 9. Resonance curves of various materials: γ_{reinf} is the coefficient of inelastic resistance of reinforced concrete, γ_{stl} is the coefficient of inelastic resistance of steel, γ_1, γ_6 are the coefficients of inelastic resistance of tube confined concrete

5. CONCLUSIONS

In conclusion, the present work demonstrates the impact of axial compressive loads on the quantitative characteristics of elastic and damping behaviour in tube confined concrete. It was determined that internal stresses have no notable impact on the inelastic behaviour coefficient (≤7%) and, consequently, on the damping behaviour of the materials.

Additionally, tube confined concrete structures exhibit enhanced damping behaviour in comparison to steel and reinforced concrete structures. The damping parameters of tube confined concrete have been observed to exhibit characteristics that exceed the values of other materials by up to 40 per cent.

Due to its high strength and rigidity, tube confined concrete structures are able to withstand significant loads and ensure durability. Furthermore, their damping capacity helps to diminish vibrations under dynamic loads, which is of particular significance in various crane structures, motorway and railway bridges, and oil and gas platforms that are subjected to seismic and dynamic forces. The investigation of this subject matter has the potential to give rise to innovations and enhancements in the fabrication of tube confined concrete structures, which in turn could advance the development of engineering solutions that are more efficient and secure.

6. ACKNOWLEDGEMENTS

The work was conducted within the framework of the fundamental scientific research programme of the Institute of Applied Physics of the Russian Academy of Sciences (IAP RAS) for the period 2024-2026 (FFUF -2024-0031, no. R&D 1023032800130-3-2.3.2).

REFERENCES

1. **Potapov A.N., Zyambaev N.A.** Dinamicheskij raschet podkranovoj fermy pri konstruktivno nelinejnoj rabote ee elementov [Dynamic calculation of crane truss at structurally nonlinear operation of its elements]. Vestnik YuUrGU. Seriya «Stroitel'stvo i arhitektura». 2015. T. 15. № 3. P. 26–31.
2. **Musilek, J.** Horizontal Forces on Crane Runway Caused by Skewing of the Crane. IOP: Conference Series: Materials Science and Engineering. 2019. Vol. 471. Issue 5, 052001. DOI: 10.1088/1757-899X/471/5/052001.
3. **Musilek, J.** Dynamical Model for Determination of Horizontal Forces on Crane. Runway during Motion of the Crane. IOP Conference Series: Materials Science and Engineering. 2019. Vol. 603. Issue 5:052076. DOI: 10.1088/1757-899X/603/5/052076.
4. **Ahtulova L.N., Ahtulov A.L., Kirasirov O.M., Mashonskij V.A.** Vizual'noe modelirovanie dvuhbalochnogo mostovogo krana kak slozhnoj dinamicheskoj sistemy. [Visual modeling of double girder overhead travelling crane as a complex dynamic system]. Omsk Scientific vestnik. 2014. №1 (127). P. 147-152.
5. **Fedyaeva G. A., Kochevinov D. V., Lozbinev V.P., Lozbinev F.Yu.** Modelirovanie dinamiki elektromekhanicheskoj sistemy mostovogo krana [Modeling of dynamics of electromechanical system of overhead crane]. Vestnik Bryansk State Technical University. 2014. № 1 (41). P. 63-67.
6. **Korytov M.S., Shcherbakov V.S., Shershneva E.O.** Obosnovanie znachenij koefficientov regulyatorov gasheniya kolebanij gruza mostovogo krana [Justification of the values of coefficients of overhead crane load vibration damping regulators]. Vestnik SibADI. 2017. № 1(53). P. 12–19.
7. **Vib. J., Lee L., Huang P., Shih Y., et al.** Parallel neural network combined with sliding mode control in overhead crane control system. Control. 2014. № 20. P. 749–760.
8. **Kruglov S.P., Aksamentov D.N.** Metod adaptivnogo upravleniya mostovym kranom s pryamym otslezhivaniem peremeshcheniya gruza [Method of adaptive control of overhead crane with direct tracking of load

movement]. Mechatronics, automation, control. 2020. № 21(12). P. 682–688.
9. **Aksamentov D.N., Kruglov S.P., Kovyrshin S.V.** Ustanovka po issledovaniyu algoritmov uspokoeniya kolebanij gruza mostovogo krana [Installation on research of algorithms of oscillation calming of overhead crane load vibrations] Transportation infrastructure of the Siberian region. 2019. T. 2. P. 288–292.
10. **Sergei Repin, Roman Litvin, Victor Kuzmichev, Ivan Vorontsov.** Automotive shock absorbers' applicability for damping resonant oscillations in construction machines. Architecture and Engineering. 2021.Vol. 6. Issue 1. (2021). P. 81–87.
11. **Ramesh G, Jayabalan C, Selvam M, Palani S and Vijayakumar D.** Development of Pneumatic Shock Absorber by Variable Damping. International Journal of Engineering and Advanced Technology (IJEAT). 2019. Vol. 8. Issue 6. P. 1355-1360.
12. **Krishan A.L., Rimshin V.I., Rakhmanov V.A. et al.** Nesushchaya sposobnost' korotkih trubobetonnyh kolonn kruglogo secheniya [Bearing capacity of short round section tubular concrete columns]. Izvestia of higher educational institutions. Technology of textile industry. 2017. № 4 (370). P. 220-225.
13. **Vedernikova, A.A.** Chislennye issledovaniya trubobetonnyh elementov pri vnecentrennom szhati [Numerical Studies of Pipe Concrete Elements under Eccentric Compression]. Inzhenernyj vestnik Dona. 2022. № 11 (95). S.639-654.
14. **Khazov P.A.** Trekhosnoe napryazhennoe sostoyanie betona pri prodol'nom deformirovanii trubobetonnyh obrazcov [Triaxial stress state of concrete under longitudinal deformation of tube-concrete samples]. Problems of strength and plasticity. 2023. №3 (85). P. 312-322.
15. **Karpenko N.I., Korsun V.I., Karpenko S.N., Anushchenko A.M.** Kriterij prochnosti betona pri trekhosnom szhatii [Strength criterion of concrete under triaxial compression]. Volga Region Scientific Journal. 2022. №4 (64). P. 8-16.
16. SP 266.1325800.2016 Konstrukcii stalezhelezobetonnye. Pravila proektirovaniya (s Izmeneniem N 1, s Popravkoj) [Steel reinforced concrete structures. Design rules (with Change N 1, with Amendment)]. - M.: Ministry of Construction of Russia, 2016. 80 p.
17. **Faqi Liu, Yuyin Wang, Leroy Gardner, Amit H. Varma.** Experimental and numerical studies of reinforced concrete columns confined by circular steel tubes exposed to fire. Journal of Structural Engineering-ASCE. 2019. Vol. 145 (11): 04019130.
18. **Khazov P.A., Erofeev V.I., Lobov D.M., Pomazov A.P., Sitnikova A.K.** Experimental study of the calculated lengths and longitudinal bending coefficients of the composite pipe-concrete specimens [Eksperimental'noe issledovanie raschetnyh dlin i koefficientov prodol'nogo izgiba kompozitnyh trubobetonnyh obrazcov]. Volga Region Scientific Journal. 2022. №4 (64). P. 16-24.
19. **Khazov P.A., Erofeev V.I., Lobov D.M., Sitnikova A.K., Pomazov, A.P.** Experimental study of the strength of composite pipe-concrete specimens of small-sized sections [Eksperimental'noe issledovanie prochnosti kompozitnyh trubobetonnyh obrazcov malogabaritnyh sechenij]. Volga Region Scientific Journal. 2022. № 3 (63). P.36-43.
20. **Khazov P.A., Erofeev V.I., Nikitina E.A., Pomazov A.P.** Experimental and analytical models of longitudinal deformation in pipe-concrete specimens with small cross-sections. Structural Mechanics of Engineering Constructions and Buildings. 2023. Vol. 19. N. 4. P. 410-418. DOI: 10.22363/1815-5235-2023-19-4-410-418
21. **Morino S., Tsuba K.** Design and Construction of Concrete-Filled Steel Tube Column System in Japan. Earthquake and Engineering Seismology. 2005. No. 1. Vol. 4. P. 51-73.
22. **Wang J., Sun Q., Li J.** Experimental study on seismic behavior of high-strength circular concrete-filled thin-walled steel tubular columns. Engineering Structures. 2019. Vol. 182. P. 403-415.

23. **Prasanta K., Arun C.B., Konjengbam D.S.** Experimental investigation of partially confined concrete-filled steel tubular square columns under lateral cyclic loading. Journal of Constructional Steel Research. 2023. Vol. 201.
24. **Li P., Zhang T., Wang C.** Behavior of Concrete-Filled Steel Tube Columns Subjected to Axial Compression. Advances in Materials Science and Engineering. 2018. P. 1-15.
25. **Lu Y., Na Li, Li S., Liang H.** Behavior of steel fiber reinforced concrete-filled steel tube columns under axial compression. Construction and Building Materials. 2015. No 95. P. 74-85.
26. **Wang Z.B., Tao Z., Han L.H., Uy B., Lam D., Kang, W.H.** Strength, stiffness and ductility of concrete-filled steel columns under axial compression. Engineering Structures. 2017. Vol. 135. P. 209-221.
27. **Dai X.H., Lam D., Jamaluddin N.** Numerical analysis of slender elliptical concrete filled columns under axial compression. Thin-Walled Structures. 2014. No 77. P. 26–35.
28. **Xiaozhong, Li.** Numerical Study on the Axial Compressive Behavior of Steel-Tube-Confined Concrete-Filled Steel Tubes [Электронный ресурс]/ Li Xiaozhong, Sumei Zhang, Yu Tao, Bing Zhang. Experimental Tests and Numerical Analysis of Construction Materials. 2024. 17(1). 155. URL: https://DOI.org/10.3390/ma17010155.
29. **Hao, Dinh Phana.** Numerical analysis of compressive behavior of circular concrete filled steel tubular columns with high to ultra-high strength materials. Journal of Science and Technology in Civil Engineering (STCE) - HUCE. 2023. 17(2):83-98. DOI: 10.31814/stce.huce2023-17(2)-08.
30. **Singh, N. D.** Study and Buckling Analysis of Concrete Filled Steel Tubes Columns using ANSYS / N. D. Singh, Sh. Vaghmarey. International Research Journal of Engineering and Technology (IRJET). 2018. Vol. 05. Issue 12. P. 1259-1267.
31. **Xiong, Yongming & Ming, Yang & shi, heng.** Axial compression behavior of concrete-filled prefabricated aligned steel fiber UHPC tubes. Journal of Building Engineering. 2024. 10.1016/j.jobe.2024.109353.
32. **Fanghong, Wu & Xu, Lihua & Zeng, Yanqin & Yu, Min & Li, Ben.** Behavior of CA-UHPC filled circular steel tube stub columns under axial compression. Journal of Constructional Steel Research. 2023. 211. 108204. 10.1016/j.jcsr.2023.108204.
33. RSCIM: Testing machines. P-125. Mode of access: https://rscim.ru/produkciya/ispitatelnie-pressi/laboratornye-pressy-tipa-p/p-125
34. **Khazov, P.A.; Pomazov, A.P.** Strength and longitudinal bending of pipe-concrete rods under central compression (in Russian) [Prochnost' i prodol'nyj izgib trubobetonnyh sterzhnej pri central'nom szhatii]. Building mechanics and constructions. 2023. №2 (73). P. 77-86.
35. **Plyaskin A.S., Ustinov A.M., Plyaskin A.S.** Natural investigations of frequency characteristics of reinforced concrete columns of monolithic frame in the process of installation [Natural'nye issledovaniya chastotnyh harakteristik zhelezobetonnyh kolonn monolitnogo karkasa v processe montazha. Investments, construction, real estate. 2018. P. 421-425.
36. **Kopanica D.G., Kaparulin S.L., Plyaskin A.S., Ustinov A.M., Kalichkina A.S.** Natural studies of frequency characteristics of reinforced concrete columns of monolithic frame during assembly [Vzaimosvyaz' napryazhennogo sostoyaniya szhatoj kolonny i chastoty sobstvennyh kolebanij]. Investments, construction and real estate as a material basis for modernization and innovative development of the economy Materials of the Fifth All-Russian Scientific and Practical Conference with International Participation: In 2 parts. 2015. P. 294-300.
37. **Kopanica D.G., Kaparulin S.L., Plyaskin A.S.** Spectral analysis of physical condition of models of reinforced concrete columns subjected to axial compression [Spektral'nyj analiz fizicheskogo sostoyaniya modelej zhelezobetonnyh kolonn podverzhennyh osevomu szhatiyu]. Concrete and Reinforced Concrete - A Look into the Future Scientific Proceedings of

the III All-Russian (II International) Conference on Concrete and Reinforced Concrete: in 7 volumes. 2014. P. 179-182

38. **Khazov, P.A., Shkoda, I.V., Tyagunova, L.Yu.** Methodology for determining the dynamic parameters of the material at free vibrations [Metodika opredeleniya dinamicheskih parametrov materiala pri svobodnyh kolebaniyah]. Bulletin of Tomsk State University. 2023. Vol. 25. №6. C. 89-101.
39. **Biderman V.L.** Theory of mechanical vibrations: Textbook for universities [Teoriya mekhanicheskih kolebanij: Ucheb-nik dlya vuzov]. High School, 1980. 408 p.

СПИСОК ЛИТЕРАТУРЫ

1. **Потапов А.Н., Зямбаев Н.А.** Динамический расчет подкрановой фермы при конструктивно нелинейной работе ее элементов // Вестник ЮУрГУ. Серия «Строительство и архитектура». 2015. Т. 15, № 3, С. 26–31.
2. **Musilek, J.** Horizontal Forces on Crane Runway Caused by Skewing of the Crane. IOP: Conference Series: Materials Science and Engineering. 2019. Vol. 471. Issue 5, 052001. DOI: 10.1088/1757-899X/471/5/052001.
3. **Musilek, J.** Dynamical Model for Determination of Horizontal Forces on Crane // Runway during Motion of the Crane. IOP Conference Series: Materials Science and Engineering. 2019. Vol. 603. Issue 5:052076. DOI: 10.1088/1757-899X/603/5/052076.
4. **Ахтулова Л.Н., Ахтулов А.Л., Кирасиров О.М., Машонский В.А.** Визуальное моделирование двухбалочного мостового крана как сложной динамической системы // Омский научный вестник. 2014. №1 (127). С. 147-152.
5. **Федяева Г. А., Кочевинов Д. В., Лозбинев В.П., Лозбинев Ф.Ю.** Моделирование динамики электромеханической системы мостового крана // Вестник Брянского государственного технического университета. 2014. № 1 (41). С. 63-67.
6. **Корытов М.С., Щербаков В.С., Шершнева Е.О.** Обоснование значений коэффициентов регуляторов гашения колебаний груза мостового крана // Вестник СибАДИ. 2017. № 1(53). С. 12–19.
7. **Vib. J., Lee L., Huang P., Shih Y., et al.** Parallel neural network combined with sliding mode control in overhead crane control system // Control. 2014. № 20. P. 749–760.
8. **Круглов С.П., Аксаментов Д.Н.** Метод адаптивного управления мостовым краном с прямым отслеживанием перемещения груза // Мехатроника, автоматизация, управление. 2020. № 21(12). С. 682–688.
9. **Аксаментов Д.Н., Круглов С.П., Ковыршин С.В.** Установка по исследованию алгоритмов успокоения колебаний груза мостового крана // Транспортная инфраструктура Сибирского региона. 2019. Т. 2. С. 288–292.
10. **Sergei Repin, Roman Litvin, Victor Kuzmichev, Ivan Vorontsov.** Automotive shock absorbers' applicability for damping resonant oscillations in construction machines // Architecture and Engineering. 2021.Vol. 6. Issue 1. (2021). P. 81–87.
11. **Ramesh G, Jayabalan C, Selvam M, Palani S and Vijayakumar D.** Development of Pneumatic Shock Absorber by Variable Damping // International Journal of Engineering and Advanced Technology (IJEAT). 2019. Vol. 8. Issue 6. P. 1355-1360.
12. **Кришан А.Л., Римшин В.И., Рахманов В.А. и др.** Несущая способность коротких трубобетонных колонн круглого сечения // Известия высших учебных заведений. Технология текстильной промышленности. 2017. № 4 (370). С. 220-225.
13. **Ведерникова, А.А.** Численные исследования трубобетонных элементов при внецентренном сжатии // Инженерный вестник Дона.2022. № 11 (95). С.639-654.
14. **Хазов П.А.** Трехосное напряженное состояние бетона при продольном деформировании трубобетонных образцов //

Проблемы прочности и пластичности. 2023. №3 (85). С. 312-322.
15. **Карпенко Н.И., Корсун В.И., Карпенко С.Н., Анущенко А. М.** Критерий прочности бетона при трехосном сжатии // Приволжский научный журнал. 2022. №4 (64). С. 8-16.
16. СП 266.1325800.2016 Конструкции сталежелезобетонные. Правила проектирования (с Изменением N 1, с Поправкой). - М.: Минстрой России, 2016. 80 с.
17. **Faqi Liu, Yuyin Wang, Leroy Gardner, Amit H. Varma.** Experimental and numerical studies of reinforced concrete columns confined by circular steel tubes exposed to fire. Journal of Structural Engineering-ASCE. 2019. Vol. 145 (11): 04019130.
18. **Хазов П.А., Ерофеев В.И., Лобов Д.М., Помазов А.П., Ситникова А.К.** Экспериментальное исследование расчетных длин и коэффициентов продольного изгиба композитных трубобетонных образцов // Приволжский научный журнал. 2022. №4 (64). С. 16-24.
19. **Хазов П.А., Ерофеев В.И., Лобов Д.М., Ситникова А.К., Помазов А.П.** Экспериментальное исследование прочности композитных трубобетонных образцов малогабаритных сечений // Приволжский научный журнал. 2022. № 3 (63). С.36-43.
20. **Khazov P.A., Erofeev V.I., Nikitina E.A., Pomazov A.P.** Experimental and analytical models of longitudinal deformation in pipe-concrete specimens with small cross-sections // Structural Mechanics of Engineering Constructions and Buildings. 2023. Vol. 19. N. 4. P. 410-418. DOI: 10.22363/1815-5235-2023-19-4-410-418.
21. **Morino S., Tsuba K.** Design and Construction of Concrete-Filled Steel Tube Column System in Japan // Earthquake and Engineering Seismology. 2005. No. 1. Vol. 4. P. 51-73.
22. **Wang J., Sun Q., Li J.** Experimental study on seismic behavior of high-strength circular concrete-filled thin-walled steel tubular columns // Engineering Structures. 2019. Vol. 182. P. 403-415.
23. **Prasanta K., Arun C.B., Konjengbam D.S.** Experimental investigation of partially confined concrete-filled steel tubular square columns under lateral cyclic loading // Journal of Constructional Steel Research. 2023. Vol. 201.
24. **Li P., Zhang T., Wang C.** Behavior of Concrete-Filled Steel Tube Columns Subjected to Axial Compression // Advances in Materials Science and Engineering. 2018. P. 1-15.
25. **Lu Y., Na Li, Li S., Liang H.** Behavior of steel fiber reinforced concrete-filled steel tube columns under axial compression // Construction and Building Materials. 2015. No 95. P. 74-85.
26. **Wang Z.B., Tao Z., Han L.H., Uy B., Lam D., Kang, W.H.** Strength, stiffness and ductility of concrete-filled steel columns under axial compression // Engineering Structures. 2017. Vol. 135. P. 209-221.
27. **Dai X.H., Lam D., Jamaluddin N.** Numerical analysis of slender elliptical concrete filled columns under axial compression // Thin-Walled Structures. 2014. No 77. P. 26–35.
28. **Xiaozhong, Li.** Numerical Study on the Axial Compressive Behavior of Steel-Tube-Confined Concrete-Filled Steel Tubes [Электронный ресурс]/ Li Xiaozhong, Sumei Zhang, Yu Tao, Bing Zhang // Experimental Tests and Numerical Analysis of Construction Materials. 2024. 17(1). 155. Режим доступа: URL: https://DOI.org/10.3390/ma17010155.
29. **Hao, Dinh Phana.** Numerical analysis of compressive behavior of circular concrete filled steel tubular columns with high to ultra-high strength materials // Journal of Science and Technology in Civil Engineering (STCE) - HUCE. 2023. 17(2):83-98. DOI: 10.31814/stce.huce2023-17(2)-08.
30. **Singh, N.D.** Study and Buckling Analysis of Concrete Filled Steel Tubes Columns using ANSYS / N. D. Singh, Sh. Vaghmarey // International Research Journal of Engineering and Technology (IRJET). 2018. Vol. 05. Issue 12. P. 1259-1267.
31. **Xiong, Yongming & Ming, Yang & shi, heng.** Axial compression behavior of concrete-filled prefabricated aligned steel fiber

UHPC tubes // Journal of Building Engineering. 2024. 10.1016/j.jobe.2024.109353.
32. **Fanghong, Wu & Xu, Lihua & Zeng, Yanqin & Yu, Min & Li, Ben.** Behavior of CA-UHPC filled circular steel tube stub columns under axial compression // Journal of Constructional Steel Research. 2023. 211. 108204. 10.1016/j.jcsr.2023.108204.
33. РСЦИМ: Испытательные машины // П-125. Режим доступа: https://rscim.ru/produkciya/ispitatelnie-pressi/laboratornye-pressy-tipa-p/p-125
34. **Хазов П.А., Помазов А.П.** Прочность и продольный изгиб трубобетонных стержней при центральном сжатии // Строительная механика и конструкции. 2023. №2 (73). С. 77-86.
35. **Пляскин А.С., Устинов А.М., Пляскин А.С.** Натуральные исследования частотных характеристик железобетонных колонн монолитного каркаса в процессе монтажа // Инвестиции, строительство, недвижимость. 2018. С. 421-425.
36. **Копаница Д.Г., Капарулин С.Л., Пляскин А.С., Устинов А.М., Каличкина А.С.** Взаимосвязь напряженного состояния сжатой колонны и частоты собственных колебаний // Инвестиции, строительство и недвижимость как материальный базис модернизации и инновационного развития экономики Материалы Пятой Всероссийской научно-практической конференции с международным участием: в 2 частях. 2015. С. 294-300.
37. **Копаница Д.Г., Капарулин С.Л., Пляскин А.С.** Спектральный анализ физического состояния моделей железобетонных колонн подверженных осевому сжатию // Бетон и железобетон – взгляд в будущее Научные труды III Всероссийской (II Международной) конференции по бетону и железобетону: в 7 томах. 2014. С. 179-182
38. **Хазов П.А., Шкода И.В., Тягунова Л.Ю.** Методика определения динамических параметров материала при свободных колебаниях // Вестник Томского государственного университета. 2023. Т. 25. №6. С. 89-101.
39. **Бидерман В.Л.** Теория механических колебаний: Учебник для вузов // Высшая школа, 1980. 408 с.

Shkoda Irina Vasilevna, postgraduate student, Mechanical Engineering Research Institute RAS, Branch of the Institute of Applied Physics RAS, 85, Belinskogo str., Nizhny Novgorod, 603024, Russia; Senior teacher of the Department of Theory of Structures and Technical Mechanics, Nizhny Novgorod State University of Architecture and Civil Engineering, 65, Ilyinskaya str., Nizhny Novgorod, 603952, Russia, e-mail: ShkodaIrinaVasil@yandex.ru, тел. ORCID: 0000-0001-6759-0963.

Vediaikina Olga Ivanovna, Candidate of physical and mathematical sciences, Associate professor of the Department of general physics and theoretical mechanics, Nizhny Novgorod State University of Architecture and Civil Engineering, 65, Ilyinskaya str., Nizhny Novgorod, 603952, Russia, e-mail: razvnauki@rambler.ru. ORCID: 0009-0007-1686-2579.

Loshkaryova Daria Aleksandrovna, Candidate of pedagogical sciences, Associate professor of the Department of Theory of Foreign languages, Nizhny Novgorod State University of Architecture and Civil Engineering, 65, Ilyinskaya str., Nizhny Novgorod, 603952, Russia, e-mail: dariashokina@list.ru, ORCID: 0000-0001-8992-8726.

Шкода Ирина Васильевна, аспирант, Институт проблем машиностроения РАН – Филиал ФГБУН «Федеральный исследовательский центр Институт прикладной физики им. А.В. Гапонова-Грехова Российской академии наук, Адрес: д. 85, ул. Белинского, г. Нижний Новгород, 603024, Россия; старший преподаватель кафедры Теории сооружений и технической механики, Нижегородский государственный архитектурно-строительный университет (ННГАСУ), Адрес: д. 65, ул. Ильинская, г. Нижний Новгород, 603952, Россия, e-mail: ShkodaIrinaVasil@yandex.ru, ORCID: 0000-0001-6759-0963.

Ведяйкина Ольга Ивановна, кандидат физ.-мат. наук, доцент кафедры Общей физики и теоретической механики, Нижегородский государственный архитектурно-строительный университет (ННГАСУ), Адрес: д. 65, ул. Ильинская, г. Нижний Новгород, 603952, Россия, e-mail: razvnauki@rambler.ru, тел. ORCID: 0009-0007-1686-2579.

Лошкарева Дарья Александровна, кандидат пед. наук, доцент кафедры Иностранных языков, Нижегородский государственный архитектурно-строительный университет (ННГАСУ), Адрес: д. 65, ул. Ильинская, г. Нижний Новгород, 603952, Россия, e-mail: dariashokina@list.ru. ORCID: 0000-0001-8992-8726.

HYDROPHYSICAL PROPERTIES OF HEAVY-DUTY CONCRETE WITH A COMPLEX MODIFIER FOR HYDROMELIORATIVE CONSTRUCTION

Mariya B. Kaddo [1], Yulia S. Filimonova [2]

[1] National Research Moscow State University of Civil Engineering, Moscow, RUSSIA
[2] Moscow Polytechnic University, Moscow, RUSSIA

Abstract: Heavy concrete is widely used as the main structural material in irrigation and drainage construction, ensuring high reliability and safety of the complexes during operation. The main quality criteria for heavy concrete are their operational characteristics. The binder was Portland cement of class CEM I 42.5N. The dispersed composition, technological and strength characteristics of cement and cement stone obtained from it were determined using sieve analysis, pycnometric method, determination of bending and compressive strength in accordance with standard methods. Natural sand was used as a fine aggregate. Granite crushed stone was used as a coarse aggregate. Water was used to mix the concrete mixture. Melflux 5581 F superplasticizer was used as a plasticizing additive. Microsilica was used as an active mineral additive. Chopped basalt fiber was chosen for dispersed reinforcement of concrete stone. To determine the efficiency of water interaction with the matrix of the developed concrete and, as a consequence, the efficiency of diffusion processes inside the matrix, affecting the destruction of the concrete stone structure and possible moisture loss during irrigation, the porosity of concrete, its water absorption and water resistance were determined. Analysis of the obtained data shows that the introduction of a complex modifier together with basalt fiber reduced the water absorption index by 57.8% compared to the control. The water resistance of the modified concrete in composition 5 increased by 4 loading stages compared to control composition 1. Improvement of hydrophysical properties of modified concrete was established: water absorption decreased by 57.8%; water resistance grade increased by 4 loading stages in comparison with the control composition. After 600 cycles of frost resistance testing, the mass loss was 1.5-1.8%, the strength decrease was 9.1%-10.2%. The proposed modification with a complex additive together with basalt fiber allows obtaining high-quality heavy concrete with improved hydrophysical properties.

Keywords: heavy concrete, irrigation and drainage construction, complex additive, concrete modification

ГИДРОФИЗИЧЕСКИЕ СВОЙСТВА ТЯЖЕЛОГО БЕТОНА С КОМПЛЕКСНЫМ МОДИФИКАТОРОМ ДЛЯ ГИДРОМЕЛИОРАТИВНОГО СТРОИТЕЛЬСТВА

М.Б. Каддо [1], Ю.С. Филимонова [2]

[1] Национальный исследовательский Московский государственный строительный университет, г. Москва, РОССИЯ
[2] Московский политехнический университет, г. Москва, РОССИЯ

Аннотация: В качестве основного конструкционного материала при гидромелиоративном строительстве широко используется тяжелый бетон, обеспечивающего высокую надежность и безопасность комплексов при эксплуатации. Основными критериями качества тяжелых бетонов являются их эксплуатационные характеристики. Вяжущим являлся портландцемент класса ЦЕМ I 42,5Н. Дисперсный состав, технологические и прочностные характеристики цемента и получаемого из него цементного камня определяли с использованием ситового анализа, пикнометрического метода, определения прочности на изгиб и сжатие в соответствии со стандартными методиками. В качестве мелкого заполнителя использовали природный песок. В качестве крупного заполнителя использовали гранитный щебень. Для затворения бетонной смеси использовалась вода. В качестве пластифицирующей добавки использовался суперпластификатор Melflux 5581 F. В качестве водорастворимой полимерной добавки использовали «Полидон-А». В качестве активной минеральной добавки применялся микрокремнезём. Для дисперсного армирования бетонного камня было выбрано рубленное базальтовое волокно. Для определения эффективности взаимодействия воды с матрицей разработанного бетона и, как следствие, эффективности диффузионных процессов внутри матрицы, влияющих на разрушение структуры бетонного камня и возможной потери влаги при орошении, проводилось определение пористости бетона, его водопоглощение и водонепроницаемость. Анализ полученных данных показывает, что введение комплексного модификатора совместно с базальтовым волокном снизило показатель водопоглощения на 57,8% в сравнении с контрольным. Водонепроницаемость модифицированного бетона в 5 составе повысилась на 4 ступени нагружения в сравнении с контрольным составом 1. Выводы: установлено улучшение гидрофизических свойств модифицированного бетона: водопоглощение снизилось на 57,8%; марка по водонепроницаемости повысилась на 4 ступени нагружения в сравнении с контрольным составом. После 600 циклов испытания на морозостойкость потеря массы составила 1,5-1,8%, снижение прочности 9,1%-10,2%. Предлагаемое модифицирование комплексной добавкой совместно с базальтовым волокном, позволяет получить тяжелый бетон высокого качества с улучшенными гидрофизическими свойствами.

Ключевые слова: тяжелый бетон, гидромелиоративное строительство, комплексная добавка, модификация бетонов

INTRODUCTION

At present, in the Russian Federation, much attention is paid to the development and quality of irrigation and drainage construction, ensuring food security of the population, and especially to the quality of irrigation and drainage systems and the quality of the system's operation. Heavy concrete is widely used as the main structural material in irrigation and drainage construction, ensuring high reliability and safety of the systems during operation. The main quality criteria for heavy concrete are their performance characteristics: strength (up to 150 MPa and above), frost resistance (F1 = 1000), density (up to 2500 kg/m^3), water resistance (W20), corrosion resistance in aggressive environments. Research is also actively being conducted on modifying concrete, which allows for a given level of quality. Even a small number of modifying components allows for a radical change in the process of structure formation and the production of durable concrete with improved physical and mechanical characteristics [1-2]. Multicomponent modifiers on a chemical-mineral basis are used in hydraulic engineering; their application allows obtaining a dense durable structure [3-7]. To obtain concrete mixtures with optimal rheotechnological indicators and to improve the operational properties of hardened concrete, it is rational and promising to use chemical-mineral modifiers [8-10]. The most important achievements in the field of concrete science are studies that allow expanding the concepts of micro-, submicro- and nanolevels of structure formation processes and provide a significant increase in physical and mechanical characteristics, and above all, strength and durability. Scientifically substantiated patterns of hydration processes of cement clinker minerals and control of structure formation of cement stone and concrete have been obtained, developed and formulated [11-14]. Based on these provisions, effective methods for protecting concrete and reinforced concrete from corrosion and ways to increase its durability have been developed. Modification of concrete with chemical additives is the main direction of development of concrete technology, which is confirmed by scientific research and implemented in the practice of real enterprises. The main means of combating leaching corrosion in cement systems (washing out of calcium hydroxide) is the introduction of active mineral additives and the use of a dense matrix of cement stone. Such conclusions can be reached after studying the practical experience of the authors of scientific papers [15-17], which note that when leaching portlandite in an amount of 20-30% of the total content, the strength of the cement stone decreases by 35-50% or more. The key feature of the recommendations in these works is the use of silica-containing additives, in particular microsilica, which is a by-product containing more than 91% silicon oxide and is formed during the smelting of ferrosilicon, where dust particles of microsilica of 10-50 μm in size are retained on an electrostatic precipitator [18, 19]. Scientific interest is also aroused by the combined capabilities of amorphous silica and superplasticizer, which have an effect that improves the characteristics of the produced heavy concrete [20]. When using these two elements in production, the product gains additional compressive strength of up to 150 Mpa, and also becomes more waterproof and resistant to cracking. Thus, improving the quality of concrete for melioration and hydraulic engineering construction is a problematic issue and requires its development taking into account the technological paradigm being developed at the present stage, which provides for the use of a polydisperse binder in its composition together with a complex modifier.

METHODS

The work used the initial materials with the following characteristics. The binder was Portland cement of class CEM I 42.5N, manufactured by OOO Holcim (Rus) SM (Kolomna). The chemical and mineral composition of the cement was determined using X-ray phase and X-ray fluorescence analysis, the results of which are presented in Table 1.

Table 1. Chemical and mineral composition of Portland cement

<table>
<tr><td rowspan="2">Cement brand</td><td colspan="7">Chemical composition, wt.%</td></tr>
<tr><td>Na_2O</td><td>SO_3</td><td>MgO</td><td>Fe_2O_3</td><td>CaO</td><td>Al_2O_3</td><td>SiO_2</td></tr>
<tr><td rowspan="4">CEM I 42,5 N</td><td>0,83</td><td>0,6</td><td>0,88</td><td>3,9</td><td>64,1</td><td>5,89</td><td>23,8</td></tr>
<tr><td colspan="7">Content of crystalline phases in clinker, wt. %</td></tr>
<tr><td colspan="2">C_4AF ($4CaO·Al_2O_3·Fe_2O_3$)</td><td colspan="2">C_3A ($3CaO·Al_2O_3$)</td><td colspan="2">C_2S ($2CaO·SiO_2$)</td><td>C_3S ($3CaO·SiO_2$)</td></tr>
<tr><td colspan="2">11,46</td><td colspan="2">6,97</td><td colspan="2">11,5</td><td>60,92</td></tr>
</table>

The particle size distribution, process and strength characteristics of cement and cement stone obtained from it were determined using sieve analysis, pycnometric method, determination of bending and compressive strength in accordance with standard methods. To determine the mechanical strength, beam samples measuring 4×4 ×16 cm were made of cement-sand mortar with a water-cement ratio W/C=0.4. After production, the samples were kept in molds for 1 day in a bath with a hydraulic seal, which provided the following conditions: relative air humidity of at least 90% and an ambient temperature of (20±2) °C. After 24 hours, the samples were unmolded and then stored in a bath with water for 27 days, the temperature in which was controlled within (20±2) °C. Upon expiration of the storage period, the beam samples were removed from the bath with water and tested for strength no later than 30 minutes later. The results obtained are presented in Table 2. According to the test results, it was established that the cement meets the requirements of the standard for the standardized indicators: test for uniformity of volume change, the beginning of setting of the cement paste, compressive strength after 2 and 28 days.

Table 2. Results of determining the characteristics of Portland cement grade CEM I 42.5N

<table>
<tr><td>Indicator</td><td>Requirement GOST 31108-2020</td><td>Actual value</td></tr>
<tr><td>Residue on sieve 45 μm, %</td><td>-</td><td>3.1</td></tr>
<tr><td>Residue on sieve 80 μm, %</td><td>-</td><td>0.5</td></tr>
<tr><td>Normal density of cement paste, %</td><td>-</td><td>26.0</td></tr>
<tr><td>Test for uniformity of volume change (Le Chatelier Ring), expansion, mm</td><td>10</td><td>7</td></tr>
<tr><td>Specific surface (according to Blaine), cm^2/g</td><td>-</td><td>3500</td></tr>
<tr><td>Start of setting, min</td><td>not earlier than 60</td><td>175</td></tr>
<tr><td>End of setting, min</td><td>-</td><td>500</td></tr>
<tr><td>Presence of signs of false setting, yes/no</td><td>no</td><td>no</td></tr>
<tr><td>Average compressive strength at the age of 2 days, MPa</td><td>not less than 10</td><td>26.5</td></tr>
<tr><td rowspan="2">Average compressive strength at the age of 28 days, MPa</td><td>not less than 42,5</td><td rowspan="2">45.5</td></tr>
<tr><td>not more than 62,5</td></tr>
<tr><td>True density, kg/m^3</td><td>-</td><td>3150</td></tr>
<tr><td>Bulk density, kg/m^3</td><td>-</td><td>1250</td></tr>
</table>

Natural sand with a fineness modulus of 2.5 and particle sizes from 0.16 mm to 2.5 mm produced by Khromtsovsky Quarry LLC, located in the village of Khromtsovo, Ivanovo Region, was used as fine aggregate. Granite crushed stone produced by Bogaevsky Quarry LLC, Moscow Region, Ruzsky Urban District, was used as coarse aggregate. It meets the requirements for the content of plate-shaped and needle-shaped grains - 12.0%; dust, silt and clay particles - 0.93%; crushed stone grade for crushability - 1400; crushed stone grade for frost resistance - 300; bulk density - 1385 kg/m^3; specific effective activity of radionuclides (Aeff) - 90 Bq/kg; crushed stone grade for abrasion I-1. The maximum in the crushed stone size distribution was 20 mm. The aggregate under study belongs to the medium-grained type of crystalline structure.

Water was used to mix the concrete mixture. Water does not contain sulfates over 2700 mg/l (in terms of SO_4), all salts over 5000 mg/l, oil sludge and scale, the content of organic matter is less than 15 mg/l, pH 7.8, color is absent.

Melflux 5581 F superplasticizer additive by BASF Construction Additives (Germany) was used as a plasticizing additive, the consumption of which was 0.3% of the binder weight, recommended by the manufacturer.

Polydon-A additive by Orgpolimersintez LLC, St. Petersburg, was used as a water-soluble polymer additive, meeting the requirements of TU 9365-002-46270704-2001. The consumption of this additive was 0.2% of the binder weight.

"Polidon-A" is an aqueous solution of polyvinylpyrrolidone C_6H_9NO, with a density of about 1200 kg/m^3, a viscosity of 3000 to 6000 MPa s at 25 °C, and a melting point of 150-180 °C.

Microsilica grade MKU-95 was used as an active mineral additive. Microsilica was produced by OOO NTC EVEREST, Lipetsk.

The chemical composition of microsilica in terms of basic oxides was determined using X-ray phase analysis using a DRON-3 X-ray machine. The specified microsilica has a high content of amorphous and glassy silicon oxide (up to 95% SiO_2 by weight); the content of other oxides is low. The results of the analysis of the chemical composition of microsilica are presented in Table 3.

Table 3. Qualitative characteristics of microsilica grade MKU-95

Substance	Mass fraction, %
Silicon dioxide SiO_2	not less than 95.0
Phosphorus oxide P_2O_5	not more than 0.09
Magnesium oxide MgO	not more than 0.7
Aluminum oxide Al_2O_3	not more than 0.17
Iron oxide Fe_2O_3	not more than 0.1
Sulfuric anhydride SO_3	not more than 0.43
Calcium oxide CaO	not more than 0.25
Free alkalis Na_2O, K_2O	not more than 1.21
Water	not more than 0.3

Chopped basalt fiber manufactured in accordance with TU 5952-002-13307094-08 was selected for dispersed reinforcement of concrete stone. Unlike steel fiber, basalt fiber has a higher resistance to corrosion. Compared to polymer fibers, basalt fiber has a lower elastic modulus and is not subject to aging. The melting point of basalt fiber is 1450°C, the average length of a fiber section is 12.67 mm, the diameter of an elementary fiber is 16.19 μm, the relative elongation at break is 1.4-3.6%, the tensile strength Rt is 2.8-3.4 MPa·10^3, the true density of the fiber is 2.63 g/cm^3, the modulus of elasticity of the fiber is 100-130 MPa·10^3, and the resistance to alkalis and inorganic acids is high.

RESULTS AND DISCUSSION

When creating trays for irrigation canals in conditions of constant contact with water, concrete must be dense and have good hydrophysical properties: low rates of water absorption, capillary suction, water resistance and high rates of frost resistance and corrosion resistance. In the works [10-17] it is noted that the hydrophysical properties of concrete are improved with the use of modifiers, especially those that include ingredients with a hydrophobic-plasticizing effect of 15-30% or more. To determine the efficiency of water interaction with the matrix of the developed concrete and, as a consequence, the efficiency of diffusion processes inside the matrix, affecting the destruction of the structure of concrete stone and possible moisture loss during irrigation, the porosity of concrete, its water absorption and water resistance were determined. To determine water absorption, the method of successive saturation of samples with water to a constant mass was used in accordance with GOST 12730.3-2020. The cube samples used had a side of 100 mm and were made of concrete mixtures of the developed compositions. The samples hardened under normal conditions for 28 days. The series of samples for testing consisted of 3 cubes plus a control for each of the compositions. Water absorption of a series of samples of each composition was determined as the arithmetic mean of the water absorption values of each sample in the series. The porosity of samples of the developed compositions was determined by assessing the kinetics of water absorption using the discrete weighing method in accordance with GOST 12730.4-2020 "Concrete. Methods for determining porosity parameters." The cube samples had a side of 70 mm, the test series included two samples of each composition. The porosity value was calculated as the arithmetic mean. The water resistance of the developed concrete products was determined using the "wet spot" method in accordance with the requirements of GOST 12730.5-2018 [16]. To determine the water resistance, cylindrical samples with a diameter of 150 mm and a height of 150 mm were made from the developed compositions. According to GOST 24587-81 [17] and the technological conditions for the manufacture of trays, the largest filler size in them should not exceed 15 mm. The cylindrical samples also had a maximum filler size of 15 mm. Six samples of each composition were prepared in the series. Before testing, the samples were kept in a normal curing chamber under normal conditions for 24 hours before testing. Water resistance was determined using the Form + Test WE 6 MMZ installation (Germany). The samples were installed in the landing devices of the installation, the cuffs of which were pre-lubricated with waterproof grease. The water pressure was increased stepwise with subsequent holding (0.2 MPa for 1-5 minutes) and a duration of water exposure under pressure equal to 12 hours at each step. When a "wet spot" appeared, as well as other signs of water penetration into various places of the sample, the test was stopped. The value of the maximum water pressure, at which no water filtration was observed on at least four out of six samples, was taken as an indicator of the sample's water resistance. The first basic method was used to determine frost resistance. The test samples were a series of concrete cubes with an edge of 100 mm, six of which were taken as controls, and twelve had additives introduced into their composition in accordance with the developed experimental plan. The holding time of the samples was 24 hours with immersion to 1/3 of the sample height, 24 hours with immersion to 2/3 of the sample height, and 48 hours with complete immersion. The testing process was continued until the appearance of structural defects in the samples - cracks, chips and peeling, loss of mass and loss of strength of the samples by more than 5% of the required value [12, 14] The results of tests for water absorption and water resistance of concrete are presented in Table 4. Analysis of the obtained data shows that the introduction of a complex modifier together with basalt fiber (composition 6, PV + (0.3% Melflux + 0.2% Polydon-A + 15% MK) + 0.7% BV) reduced the water absorption index by - 57.8%; composition 2 PV + 0.3% Melflux reduced it by 37.8%); composition 3 PV + 0.2% Polydon-A reduced it by 48.9%; composition 4 PV + (0.3% Melflux + 0.2% Polydon-A reduced it by 53.3%. by 55.5% – 5 composition PV + (0.3% Melflux + 0.2% Polydon-A + 15% MK) compared to the control (composition 1). The water resistance of the modified concrete in composition 5 PV + (0.3% Melflux + 0.2% Polydon-A + 15% MK) increased by 4 loading stages compared to the control composition 1 (PC++ 0.3% Melflux). At the same time, the presence of basalt fiber PV + (0.3% Melflux + 0.2% Polydon-A + 15% MK) + 0.7% BV in composition 6 did not affect its water resistance.

Table 4. Results of water absorption and water resistance tests

Sample marking	Water absorption by weight, %	Water resistance, MPa	Concrete grade by water resistance
Composition 1 control factory PC + 0.3% Melflux	4.5	0.6	W6
Composition 2 PV + 0.3% + Melflux	2.8	0.8	W8
Composition 3 PV + 0.2% Polidon-A	2.3	1.0	W10
Composition 4 PV + (0.3% Melflux + 0.2% Polidon-A)	2.1	1.2	W12
Composition 5 PV + (0.3% Melflux + 0.2% Polidon-A + 15% MK)	2.0	1.4	W14
Composition 6 PV + (0.3% Melflux+ 0.2% Polidon-A + 15% MK) + 0.7% BV	1.9	1.4	W14

The results of tests under cyclic alternating freezing and thawing are shown in Table 5.

Table 5. Results of concrete tests under cyclic alternating freezing and thawing

Sample marking	Sample mass loss, %, after cycles						K_{mrz} after cycles					
	200	300	350	400	500	600	200	300	350	400	500	600
Composition 1 control factory PC + 0.3% Melflux	1.18	2.18	3.15	4.32	-	-	0.96	0.91	0.78	0.67	-	-
Composition 2 PV + 0.3% + Melflux	0.47	1.14	1.18	2.2	3.6	5.30	1.0	0.96	0.94	0.92	0.82	0.8
Composition 3 PV + 0.2% Polidon-A	0.32	1.09	1.56	2.0	3.2	4.82	1.02	0.98	0.95	0.94	0.86	0.85
Composition 4 PV + (0.3% Melflux + 0.2% Polidon-A)	0.23	0.98	1.6	1.9	2.9	3.89	1.03	1.01	0.97	0.96	0.94	0.88
Composition 5 PV + (0.3% Melflux + 0.2% Polidon-A + 15% MK)	0.12	0.94	1.2	1.4	1.6	1.80	1.04	1.02	0.98	0.94	0.92	0.91
Composition 6 PV + (0.3% Melflux+ 0.2% Polidon-A + 15% MK) + 0.7% BV	0.1	0.15	0.22	0.36	0.9	1.5	1.1	1.08	1.04	0.99	0.97	0.93

Note. K_{mrz} is the ratio of the strength index of a sample after testing its frost resistance to the strength of a sample of the material in a water-saturated state before determining frost resistance.

The results of tests with cyclic alternate freezing and thawing of cube samples made of concrete of different compositions, presented in Table 5, showed:

- maximum reduction in weight up to 6.32% and cube strength by 26% in control composition 1 (PC + 0.3% Melflux) after 400 cycles of alternate freezing and thawing tests, which exceeds the es-

tablished indicators of the requirements of GOST 10060-2012 (loss of weight and strength of concrete no more than 2% and 15%, respectively).
- high frost resistance characteristics of compositions containing the complex modifier PV + (0.3% Melflux + 0.2% Polydon-A + 15% MK). After 600 test cycles, the mass loss in compositions 5 and 6 was 1.8% and 1.5% with a decrease in strength of 10.2% and 9.1%, respectively, which confirms the sufficient margin of strength and frost resistance of the proposed modified concrete compositions.

CONCLUSION

Based on the presented research results, the following conclusion can be made:
1. An improvement in the hydrophysical properties of the modified concrete was established: water absorption decreased by 57.8%; the water resistance grade increased by 4 loading stages compared to the control composition. After 600 frost resistance test cycles, the mass loss was only 1.5-1.8% and the strength decreased by 9.1%-10.2%.
2. The proposed modification with a complex additive together with basalt fiber allows obtaining high-quality heavy concrete with improved hydrophysical properties: water absorption, water resistance and frost resistance, which makes it possible to recommend it for the production of building products and structures operating in harsh operating conditions.

REFERENCES

1. **Bazhenov Yu.M., Dem'yanova V.S., Kalashnikov V.I.** (2006) Modified high-quality concrete. *Moscow: Publ. Association of construction universities*, 368 p.
2. **Ur'ev N.B.** (1980) Highly concentrated dispersed systems. (Chemistry, Moscow,).
3. **Isaeva YU.V., Velichko E.G., Kasumov A.SH.** (2015) Structure optimization of ultra-light cement mortar with due regard for geometrical and physical and mechanical characteristics of components, *Construction Materials*, 8, 84-87. doi.org/10.31659/0585-430X-2015-728-8-84-88.
4. **Yakovlev G.I., Ginuchickaya YU.N., Kizinievich O., Kizinievich V., Gordina A.F.** (2016) Influence of dispersions of multilayer carbon nano-tubes on physical-mechanical characteristics and structure of building ceramics, *Construction Materials*. vol. 8. Pp. 20-29.
5. **Entin Z.B., Yudovich B.E.** Multicomponent cements. Scientific tract. // NIIcement, 1994. Issue 107. Pp. 3-76. doi.org/10.31659/0585-430X-2016-740-8-25-29.
6. **Velichko E.G., Shumilina Yu.S.** (2020) On the problem of formation of dispersed composition and properties of high-strength concrete. *Bulletin of MGSU*., vol. 15. Issue 2. Pp. 235-243. doi.org/10.22227/1997-0935.2020.2.235-243.
7. **Samchenko S.V., Egorov E.S.** (2021) Control of cement paste properties during its modification with pre-hydrated cement suspension. *Silicate engineering and technology*, vol. 28. No. 2. Pp. 54-58.
8. **Samchenko S.V., Abramov M.A., Egorov E.S.** (2020) Features of hydration and hardening of cement pastes with the addition of hydrated cement. *Silicate engineering and technology*, vol. 27. No. 1. P. 24- 28.
9. **Filimonova Yu.S., Velichko E.G.** (2021) Study of complex modification of heavy concrete. *Construction and reconstruction*. No. 4 (96). P. 107-109. doi.org/ 10.33979/2073-7416-2021-96-4-107-112.
10. **Soloviev V.I., Tkach E.V., Serova R.F., Tkach S.A., Toimbaeva B.M., Seidinova G.A**. (2014) Study of porosity of cement stone modified with complex organomineral modifiers. *Fundamental research*. No. 8-3. P. 590-595.
11. **Samchenko S.V., Kozlova I.V., Zemskova O.V., Dudareva M.O., Shubina E.S.** (2020) Comparative analysis of methods for modifying slag Portland cement with an ultradisperse component.

Silicate engineering and technology, vol. 27. No. 4. Pp. 113-120.
12. **Tkach E.V., Temirkanov R.I.** (2019) Cement concrete with improved physical and mechanical properties based on the use of activated microsilica // Innovations and Investments. No. 10. Pp. 289-292.
13. **Tkach E.V., Temirkanov R.I.** (2020) Improving the physical and mechanical properties of modified concrete based on the use of chemically activated microsilica with micro-reinforcing fiber. *Construction and Reconstruction*. No. 2 (88). pp. 123-135. (In Russian)
14. **Xu S.Q.** (2013) The Comprehensive Utilization of Fly Ash. *Applied Mechanics and Materials*, 459, 82-86. doi.org/ 10.4028/www.scientific.net/AMM.459.82.
15. **Feng N., Peng G.** (2006) High Performance Concrete with High Volume Fly Ash. *Key Engineering Materials*. 302-303, (470-478). doi.org/10.4028/www.scientific.net/KEM.302-303.470.
16. **Nai-Qian Feng, Gai-Fei Peng A.** (2006) Development of the Research on High Performance Concrete Incorporated with High Volume Fly Ash. *Key Engineering Materials*, 302-302, 26-34. doi.org/10.4028/www.scientific.net/KEM.302-303.26156.
17. Reiterman (2014) Comparative Investigations of Some Properties Related to Durability of Cement Concretes Containing Different Fly Ashes. *Advanced Materials Research*, 1054, 154-161. doi.org/10.4028/www.scientific.net/AMR.1054.154
18. **Kalashnikov V.I.** (2008) Non-metallic building materials industry and the future of concrete, *Construction Materials*, No. 3. P. 20-23.
19. **Suzdal'tsev O.V.** (2014) New high-performance concretes, New university. *Technical sciences*, 7-8 (29-30), 44-47.
20. **Melihov I.V.** (2009) Physicochemical Evolution of Solid, Binomial. Knowledge laboratory, Moscow.

СПИСОК ЛИТЕРАТУРЫ

1. **Баженов Ю.М., Демьянова В.С., Калашников В.И.** Модифицированные высококачественные бетоны. М.: Изд. Ассоциации строительных вузов. 2006. 368 с.
2. **Урьев Н.Б.** Высококонцентрированные дисперсные системы. (Chemistry, Moscow, 1980).
3. **Isaeva YU.V., Velichko E.G., Kasumov A.SH**. Structure optimization of ultra-light cement mortar with due regard for geometrical and physicaland mechanical characteristics of components, Construction Materials, 8, 84-87(2015) https://doi.org/10.31659/0585-430X-2015-728-8-84-88.
4. **Yakovlev G.I., Ginuchickaya YU.N., Kizinievich O., Kizinievich V., Gordina A.F.** Influence of dispersions of multilayer carbon nano-tubes on physical-mechanical characteristics and structure of building ceramics, Construction Materials. 2016. № 8. C. 20-29.
5. **Энтин З.Б., Юдович Б.Э.** Многокомпонентные цементы. Научн. тр. // НИИцемент, 1994. Вып 107. С. 3-76. https://doi.org/10.31659/0585-430X-2016-740-8-25-29.
6. **Величко Е.Г., Шумилина Ю.С.** К проблеме формирования дисперсного состава и свойств высокопрочного бетона// Вестник МГСУ. 2020. Т. 15. Вып. 2. С. 235-243. https://doi.org/10.22227/1997-0935.2020.2.235-243.
7. **Самченко С.В., Егоров Е.С**. Управление свойствами цементной пасты при ее модифицировании предварительно гидратированной цементной суспензией // Техника и технология силикатов. 2021. Т. 28. № 2. С. 54-58.
8. **Самченко С.В., Абрамов М.А., Егоров Е.С.** Особенности протекания гидратации и твердения цементных паст с добавкой гидратированного цемента //

Техника и технология силикатов. 2020. Т. 27. № 1. С. 24- 28.

9. **Филимонова Ю.С., Величко Е.Г.** Исследование комплексной модификации тяжелого бетона // Строительство и реконструкция. 2021. №4 (96). С.107-109 https://doi.org/10.33979/2073-7416-2021-96-4-107-112.
10. **Соловьев В.И., Ткач Е.В., Серова Р.Ф., Ткач С.А., Тоимбаева Б.М., Сейдинова Г.А.** Исследование пористости цементного камня, модифицированного комплексными органоминеральными модификаторами // Фундаментальные исследования. 2014. №8-3. С. 590-595.
11. **Самченко С.В., Козлова И.В., Земскова О.В., Дударева М.О., Шубина Е.С**. Сравнительный анализ способов модифицирования шлакопортландцемента ультрадисперсным компонентом // Техника и технология силикатов. 2020. Т. 27. № 4. С. 113-120.
12. **Ткач Е.В., Темирканов Р.И.** Цементный бетон с улучшенными физико-механическими свойствами на основе применения активированного микрокремнезема // Инновации и инвестиции. 2019. №10. С. 289-292.
13. **Ткач Е.В., Темирканов Р.И.** Улучшение физико-механических свойства модифицированного бетона на основе применения химически активированного микрокремнезема с микроармирующим волокном // Строительство и реконструкция. 2020. №2 (88). С. 123-135.
14. **Xu S.Q**. The Comprehensive Utilization of Fly Ash. Applied Mechanics and Materials, 459, 82-86(2013) https://doi.org /10.4028/www.scientific.net/AMM.459.82
15. **Feng N., Peng G.** High Performance Concrete with High Volume Fly Ash. Key Engineering Materials. 302-303, (470-478) 2006. https://doi.org/10.4028/www.scientifi c.net/KEM.302-303.470
16. **Nai-Qian Feng, Gai-Fei PengA** Development of the Research on High Performance Concrete Incorporated with High Volume Fly Ash. Key Engineering Materials. 302-302, 26-34(2006). https://doi.org/10.4028/www.scientific.net/ KEM.302-303.26156.
17. *Reiterman* Comparative Investigations of some Properties Related to Durability of Cement Concretes Containing Different Fly Ashes. Advanced Materials Research. 1054, 154-161(2014). https://doi.org/10.4028/www.scientific.net/ AMR.1054.154
18. **Калашников В.И.** Промышленность нерудных строительных материалов и будущее бетонов, Construction Materials. 2008. № 3. С. 20-23.
19. **Суздальцев О.В.** Новые высоко-эффективные бетоны, New university. Technical sciences, 7-8(29-30), 44-47(2014).
20. **Melihov I.V**. Physicochemical Evolution of Solid, (Binomial. Knowledge laboratory, Moscow, 2009).

Mariya Borisovna Kaddo - Candidate of Technical Sciences, Associate Professor, Associate Professor of the Department of Construction Materials Science, Federal State Budgetary Educational Institution of Higher Education "National Research Moscow State University of Civil Engineering", 26, Yaroslavskoye shosse, Moscow, 129337, Russia, kaddo.maria@yandex.ru

Yulia Sergeevna Filimonova - Candidate of Technical Sciences, Associate Professor of the Department of Industrial, Civil and Underground Construction of the Moscow Polytechnic University, 38, Bolshaya Semyonovskaya str., Moscow, 10702, Russia, JuliaS06@mail.ru

Мария Борисовна Каддо — кандидат технических наук, доцент, доцент кафедры «Строительное материаловедение», ФГБОУ ВО «Национальный исследовательский Московский государственный строительный университет», д. 26, Ярославское ш., г. Москва, 129337, Россия, kaddo.maria@yandex.ru

Юлия Сергеевна Филимонова — кандидат технических наук, доцент кафедры «Промышленное и гражданское строительство» ФГАОУ ВО «Московский политехнический университет», д. 38, ул. Б. Семеновская, г. Москва, 107023, Россия, JuliaS06@mail.ru

NUMERICAL MODELING OF RETAINING STRUCTURES MADE OF BLOCKS WITH SOIL INFILL

***Nikita Ya. Tsimbelman* [1], *Anatoly Yu. Mirnyy* [2], *Evgeny V. Fedorenko* [3], *Dmitry Yu. Ivannikov* [4], *Valentin N. Babkin* [4], *Igor V. Kuzovatkin* [5] *and* *Tatyana I. Chernova* [6]**

[1] Far Eastern Federal University, Vladivostok, RUSSIA
[2] Lomonosov Moscow State University, Moscow, RUSSIA
[3] NIP Informatica, Saint-Petersburg, RUSSIA
[4] KorBet LLC, Moscow, RUSSIA
[5] Far Eastern Federal University, Vladivostok, RUSSIA
[6] Branch FGBU "TSNIIP Russian Ministry of Construction" DalNIIS, Vladivostok, RUSSIA

Abstract: The relevance of the study is driven by the expanding use of numerical models in the design practice of retaining structures and the need for their verification. A promising design solution for retaining walls is a stepped structure, sequentially constructed from hollow-body box type blocks infilled with crushed stone. This solution has several features that require the adaptation of existing calculation methods.

A numerical model of a retaining structure made of thin-walled blocks infilled with soil has been developed based on the analysis of the interaction between the structure's components under load, taking into account the work of the foundation and surrounding soil. The SiO2D finite element modeling computer software was used as a modeling tool. The calculation results for the proposed numerical models are compared with corresponding results for analytical solutions. The parameter values of the main physico-mechanical properties of the numerical models were determined as a result of field and laboratory tests in accordance with standard methodologies considering the scale of the tests.

The features of the design solution and construction technology of retaining structures made of thin-walled reinforced concrete blocks infilled with crushed stone were examined. Numerical models of retaining structures made of soil-infilled blocks were constructed using the domestic software package SiO2D. Laboratory and field tests established the parameters of the numerical model of the retaining structure. The research demonstrates high values of the structural cohesion («interlocking») parameter c (up to 60 kPa), alongside a high internal friction angle value φ (up to 60°), ensuring high shear stability of the infilled blocks.

The study, using numerical models, proposes a calculation basis for retaining structures made of soil-infilled blocks forming a stepped construction, where the blocks are not rigidly connected but are held in their design position by the internal resistance forces of the soil against shear.

Keywords: retaining structures, new structures, calculation methods, numerical models, mechanical strength characteristics of crushed stone

ЧИСЛЕННОЕ МОДЕЛИРОВАНИЕ ПОДПОРНЫХ СООРУЖЕНИЙ ИЗ БЛОКОВ С ГРУНТОВЫМ НАПОЛНИТЕЛЕМ

***Н.Я. Цимбельман* [1], *А.Ю. Мирный* [2], *Е.В. Федоренко* [3], *Д.Ю. Иванников* [4], *В.Н. Бабкин* [4], *И.В. Кузоваткин* [5], *Т.И. Чернова* [6]**

[1] Дальневосточный Федеральный университет, г. Владивосток, РОССИЯ
[2] Московский государственный университет им. М.В. Ломоносова, г. Москва, РОССИЯ
[3] НИП Информатика, г. Санкт-Петербург, РОССИЯ
[4] ООО «КорБет», г. Москва, РОССИЯ
[5] Дальневосточный Федеральный университет, г. Владивосток, РОССИЯ
[6] Филиал ФГБУ «ЦНИИП Минстроя России» ДальНИИС, г. Владивосток, РОССИЯ

Аннотация: актуальность исследований обусловлена расширением области применения численных моделей в практике проектирования подпорных сооружений и необходимостью их верификации. Одним из перспективных конструктивных решений подпорных стен является ступенчатая конструкция, последовательно возводимая из пустотелых блоков-коробов с заполнением полостей щебнем. Решение обладает рядом особенностей, требующих адаптации существующих методов расчёта.
Численная модель подпорного сооружения из тонкостенных блоков, заполненных грунтом, разработана на основе анализа взаимодействия компонентов сооружения между собой под действием нагрузки с учетом работы основания и окружающего грунта. В качестве инструмента моделирования применена компьютерная программа конечно-элементного моделирования SiO2D. Результаты расчетов по предложенным численным моделям сопоставляются с соответствующими результатами аналитических решений. Значения параметров основных физико-механических характеристик численных моделей определены в результате полевых и лабораторных испытаний в соответствии с нормативными методиками с учётом масштаба испытаний.
Рассмотрены особенности конструктивного решения и технологии возведения подпорных сооружений, состоящих из тонкостенных железобетонных блоков, заполняемых щебнем. Построены численные модели подпорных сооружений из заполненных грунтом блоков с применением отечественного программного комплекса SiO2D. В результате лабораторных и полевых испытаний установлены параметры численной модели подпорного сооружения. Исследования демонстрируют высокие значения параметра структурного сцепления («зацепления») *c* (до 60 кПа), наряду с высоким значением угла внутреннего трения φ (до 60^0) обеспечивающего высокую устойчивость заполненных блоков на сдвиг.
В работе с применением численных моделей предложено расчетное обоснование подпорных сооружений, состоящих из заполненных грунтом блоков и составляющих ступенчатую конструкцию, в которой блоки не имеют между собой жёстких конструктивных связей, а удерживаются в проектном положении за счёт сил внутреннего сопротивления грунта сдвигу.

Ключевые слова: подпорные сооружения, новые конструкции, методы расчета, численные модели, прочностные характеристики щебня

INTRODUCTION

Numerical modeling of geotechnical systems is currently a relevant and routine task for design engineers [1, 2]. Modern finite element computer software packages, designed for mathematically describing system behavior, are typically verified by authoritative expert communities through a set of test solutions that possess a more rigorously established mathematical correctness [3, 4]. Such software packages serve largely as automated tools, allowing users to create models of system elements within the limits of their own ability, describe their interactions with each other and with the surrounding environment, based on their own understanding of the physical processes characteristic of the system. The methods for modeling system components in each program are implemented as a set of special user tools, enabling each component to be assigned a mathematical model that best corresponds to its actual performance [5, 6]. Therefore, despite the near-complete automation of calculations, system modeling remains a creative task, and the development of nearly any engineering model depends on the user's creative experience and preferences, rooted in their understanding of the actual behavior of the modeled system. As a result, research tasks aimed at justifying and developing methods for modeling complex engineering systems using mathematical tools, implemented as a set of tools in specific computer programs, remain highly relevant.

This is also true for systems that describe the interaction of retaining walls with surrounding soil and other components [7, 8]. Compared to analytical solutions, numerical models allow for more accurate reproduction of the configuration of the retaining structure within the computational model, the layering of soils, more precise positioning of applied loads, and the consideration of their distribution characteristics [9, 10]. The setup of the calculation allows for the description of the retaining structure's behavior, taking into account the stages of its construction and loading, as well as changes in loads over time and other factors.

Currently, combined solutions for retaining structures, where soil is used as a construction material, are becoming increasingly widespread [11]. This study investigates retaining walls composed of individual hollow-body box type blocks, stacked with an offset toward the slope and infilled with crushed stone (Fig. 1) [12, 13].
The use of retaining walls of this design began relatively recently in Japan [14], where initial studies on the stability of such structures under seismic loads were conducted [15].

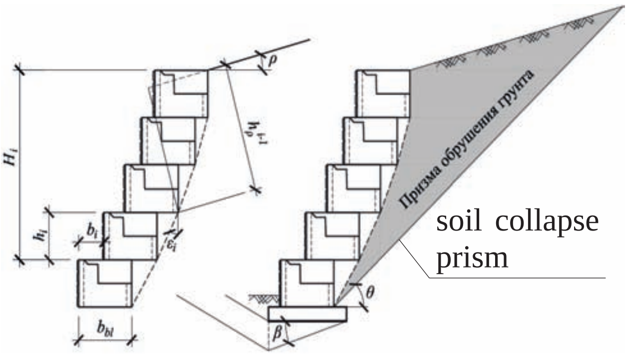

Figure 1. Cross-section of a retaining wall made of blocks infilled with crushed stone

The design offers several advantages, including high construction speed, cost-effectiveness, and aesthetic appeal. The main feature of the design, which affects its performance as part of a geotechnical system, is the absence of rigid structural connections between the blocks. The blocks are held in their design position by internal resistance to shear, generated by the weight of the infilled blocks and the shear resistance on the interfaces between the levels of the blocks.
The computational justification of this design and the potential expansion of its application scope require the substantiation of methods and techniques for numerical modeling. One of the criteria is the comparison of numerical modeling results with more mathematically rigorous analytical solutions, which should also be developed considering the design's specific features, including the perception of active soil pressure along the irregular profile of the retaining surface [16].

MATERIALS AND METHODS

The research is based on fundamental principles of structural mechanics, soil mechanics, elasticity and plasticity theory, as well as on methods of numerical modeling of spatial combined systems [17, 18]. When developing computational models of retaining walls made of soil-infilled blocks, the Coulomb-Mohr model was used by the authors to describe the properties of the granular medium [19].
In forming the computational models, modern achievements in applied mathematics and structural mechanics were utilized, particularly in the development of numerical methods for assessing the stress-strain state of calculated systems under static and dynamic loads. The SiO2D computational software was used as the primary modeling tool [20]. The main physical and mechanical properties of the computational models were determined through large-scale physical experiments and laboratory studies. The experiment planning adhered to the principles of similarity theory and dimensional analysis. The developed numerical models of retaining structures were verified by comparison with more rigorous mathematical solutions, feasible under specific computational conditions.

RESULTS OF THE RESEARCH

Provided below are the research results on the studied retaining structure, including the development of the computational model, results of numerical modeling, as well as the methodology and results of laboratory studies conducted to determine the parameters of the computational model.

Numerical Modeling in SiO2D
To enable a comparative analysis of the results from the analytical solution [16] with those obtained from numerical solutions, a calculation was performed for a retaining wall consisting of hollow-body reinforced concrete

blocks infilled with soil. The profile of the retaining structure, along with the indication of the soil's physical and mechanical properties, is shown in Fig. 2. The blocks are numbered from top to bottom.

In general, the analytical and numerical approaches can be considered comparable, although there are differences that can lead to significantly different results. The main distinction lies in the determination of active pressure. Analytical calculations typically assume wall movement and therefore use active pressure, with a coefficient Ka of approximately 0.2÷0.4.

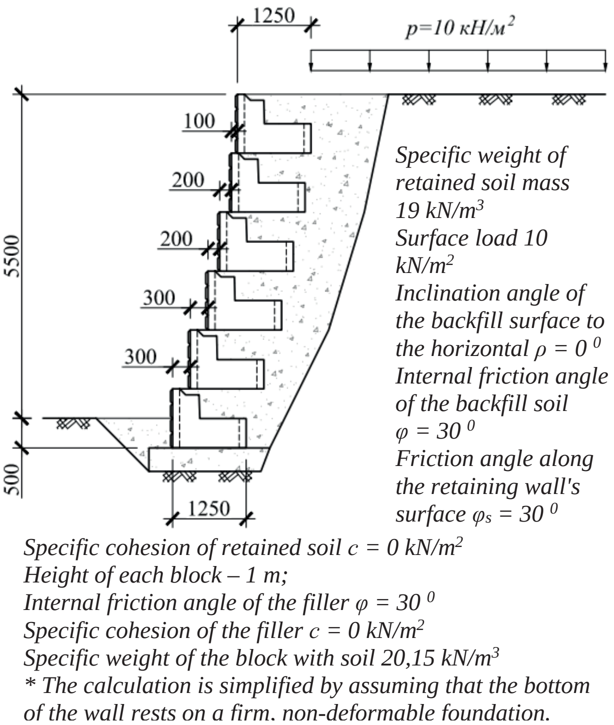

Figure 2. Profile of the retaining wall

Numerical modeling, through displacement calculations, allows for determining the degree of transition from at-rest pressure to active pressure. It should be noted that active pressure is lower than at-rest pressure (K0 is approximately 0.4÷0.6). A similar situation applies to passive pressure, where the transition from at-rest state to passive resistance must be determined, with the passive pressure coefficient being greater than the other two, being approximately 2÷6.

Another difference is the complexity of accounting for the existing slope with other strength characteristics. It is common to encounter situations where a retaining wall must be constructed in front of an existing slope. In this case, the slope, whether in its natural state or after partial cutting, must be stable, meaning that its contribution to active pressure follows different laws. The simplest way to account for such situations is to limit the volume of backfill when calculating active pressure. Sometimes, active pressure from backfill is combined with potential landslide pressure in the natural slope, but this is only possible if, given the specified safety factor, landslide pressure can take place.

Active Pressure) For comparing pressure values with analytical calculations, numerical modeling was performed using the finite element method in the SiO2D program. Figure 3a shows the results of horizontal displacements after the complete construction of the structure. The bottom block is fixed and has zero displacements, so maximum pressure is expected at this level not only due to the maximum soil height but also due to the use of the at-rest state lateral pressure coefficient K0. The top block has maximum displacement, and active pressure coefficient Ka is used in determining the pressure.

Initially, at-rest pressure was calculated by adding boundary conditions prohibiting displacements on the front face of each block. The pressure distributions are shown in Fig. 3b. The displacement constraints were then removed, and stress recalculation was performed. This resulted in the active pressure distributions shown in Fig. 3c.

In the studied scheme, the bottom block is assumed to be conditionally fixed, so its displacements can be considered zero. In this case, the pressure for this block will be calculated based on the at-rest lateral pressure coefficient (K0), and the pressure value will be significantly higher than the analytically calculated value based on the active pressure coefficient Ka. The average stress values on the vertical face of the block are presented in Table 1.

Table 1. Calculation results for block pressure according to FEM

Block №	Numerical pressure calculation		Analytical equivalent*, kPa
	by K0, kPa	by Ka, kPa	
1	13	5,5	12
2	36	19	20
3	52	20	25
4	65	22	34
5	68	19	35
6	66	66	43

**The analytical pressure equivalent is calculated for a rectangular pressure distribution*

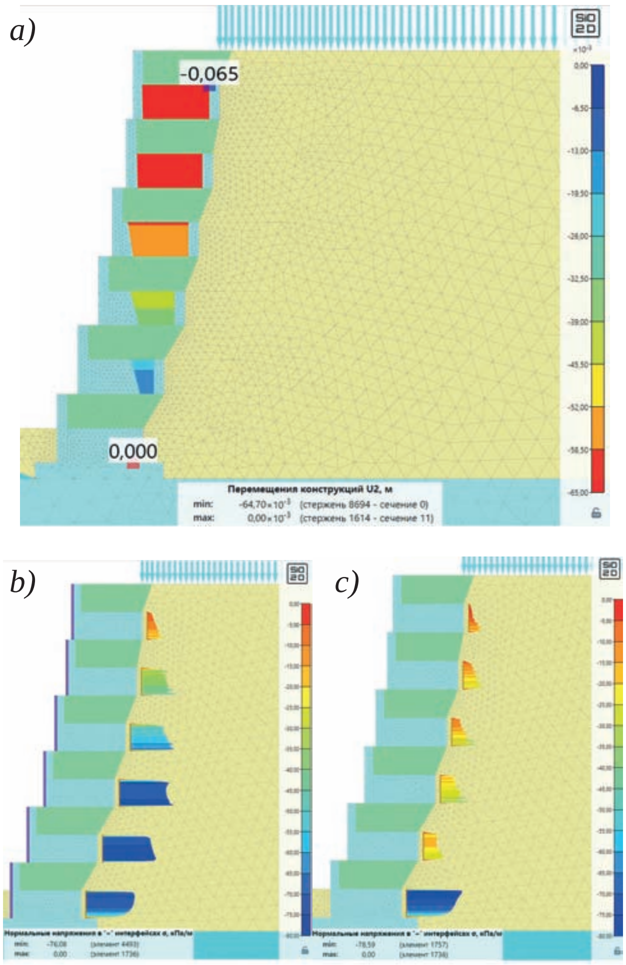

Figure 3. Stress distributions on the back face of the blocks: a – horizontal displacements of the blocks (min: -64,70×10^{-3} m (bar 8694 - section 0) max: 0,00×10^{-3} m (bar 1614 - section 11)); b – static pressure (normal stresses in '-' interfaces σ, kPa/m. min: -76,08 (element 4493) max: 0,00 (element 1736)); c – active pressure (normal stresses in '-' interfaces σ, kPa/m. min: -78,59 (element 1757) max: 0,00 (element 1736))

Conclusions: 1) The analytical calculation [16] takes into account the varying inclination of the back surface, considering each block level individually as a conditional monolith. Meanwhile, the numerical analysis can reveal several areas of shear deformations, forming local areas of active pressure within one global area;
2) In the analytical calculation, the distributed load is usually applied across the entire height of the wall, considering the coefficient of active lateral pressure. In the numerical calculation, the stresses are redistributed depending on the ultimate and pre-ultimate state of the finite element nodes;
3) The pressure distribution curve in the analytical calculation has a smooth shape, whereas in the numerical model, the shape depends on the mesh size of the finite elements;
4) In some cases, the uneven horizontal displacements of the front face of the modular retaining wall lead to different states of the soil behind it: part of the volume may be in a state of rest, part in a state of active pressure, and part in an intermediate state. This results in varying values of the lateral pressure coefficient depending on the state.

Determination of Numerical Model Parameters

A crucial task for successful numerical modeling was determining the actual values of the physico-mechanical properties of the soil material used to infill the blocks and voids between them – granite crushed stone with a particle size of 20-40 mm. Considering that the retaining walls are constructed using a unified technology, the parameters of the crushed stone had to be determined under conditions similar to those achieved in the field, corresponding to the desired compaction density. To achieve this, a series of tests on the soil material was conducted at the KorBet LLC testing site.

To ensure the crushed stone used met the supplier's declared specifications, a series of tests was conducted at the Petromodeling Lab LLC laboratory in accordance with GOST 8269.0-97 and GOST 8267-93 standards. The tests confirmed the compliance of the crushed stone with GOST 8267-93 and established its main physical characteristics.

The actual compaction density was determined by placing crushed stone in an air-dry state into the cavity of a KBP 100/200 block, positioned on a horizontal concrete foundation, with layer-by-layer compaction using a hand-operated vibrating tamper. After the cavity was filled, the horizontal alignment of the infill surface was checked, and excess crushed stone was removed. The crushed stone was then extracted from the cavity and weighed. This compaction and weighing process was repeated three times, resulting in obtaining the mass value of crushed stone filling the cavity of the KBP block with the selected compaction method. The cavity volume was measured by filling it with liquid and was determined to be 0.506±0.01 m³.

Based on the obtained crushed stone mass (M) and the known cavity volume (V), the average density of the crushed stone skeleton (ρ) was calculated as 1815±72.5 kg/m^3. This value was used as the target density for subsequent laboratory determination of shear resistance parameters.

The determination of shear resistance parameters was carried out in the Petromodeling Lab LLC laboratory using mobile shear units MSU-1 in accordance with GOST 20276.4-2020 and GOST 12248.1-2020 standards. The tests were conducted on disturbed structure samples with a diameter of 256 mm and a height of 195-200 mm [21]. The samples were formed directly in the shear carriage rings by filling them with compaction. The target density was specified as the previously obtained value of 1.82 g/cm^3. However, under laboratory conditions, this density could not be achieved, and the actual density range of the samples during testing was 1.48-1.66 g/cm^3.

The tests were conducted without water saturation, in a drained mode. The range of vertical stresses applied during the tests was 25-300 kPa, with a step of 25 kPa. The vertical stress was applied in one step and maintained until the displacement of the stamp stabilized to 0.1 mm/30 min. Then, a stepwise application of shear load was performed with holding until stabilization, in accordance with GOST 20276.4-2020 (0.1 mm/1 min). The shear load step was 5 kPa. A total of 12 tests were conducted. After completing the entire series of tests, some of the results were rejected based on the actual achieved density of the samples. The Coulomb-Mohr envelope constructed in the «σ – τ» coordinates is shown in Fig. 4.

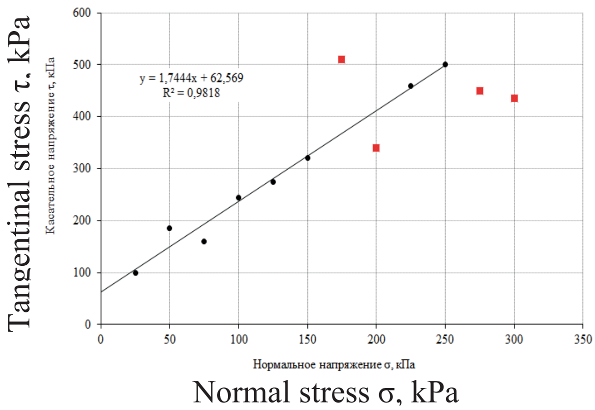

Figure 4. Coulomb-Mohr envelope constructed in «σ – τ» coordinates. Points excluded from consideration due to deviations in sample density are marked in red

As a result of processing in accordance with the requirements of Sections 7.6 – 7.12 of GOST 20522-2012, the normative and calculated values of shear resistance parameters were obtained. The average density of the samples was 1.6 g/cm^3, which is 12% below the target value. It is worth noting that within the investigated range of normal stresses, no deviations from linearity were observed in the Coulomb-Mohr envelope, allowing for the continued use of the Coulomb-Mohr strength theory in further modeling without switching to more complex nonlinear theories (such as the Hoek-Brown failure criterion).

It is also noteworthy that even at a density lower than that achieved in field conditions, this type of crushed stone exhibits significant interlocking (cohesion was 63 kPa). It is reasonable to assume that at the actual density in the mass, this crushed stone will have even higher cohesion values. The minimum pressure at the base from a single infilled block is 18 kPa, making lower normal pressure values in the retaining wall structure technically impossible. This allows us to disregard changes in cohesion in the low-stress region.

Considering the mono-fraction composition of the crushed stone used and the high compaction density, the dilatancy angle was determined to improve calculation accuracy. The determination was carried out during single-plane shear tests by additionally measuring vertical deformation. As a result, dependencies of vertical displacement of the stamp on the horizontal displacement of the shear carriage were obtained.

Table 2. Final table of physical and physico-mechanical properties of crushed stone

№	Parameter		Symbol	Unit	Value
1	Bulk density	norm.	ρ_{min}	g/cm^3	1,47
2	Density after compaction	norm.	ρ	g/cm^3	1,82± 0,07
3	Particle density	norm.	ρ_s	g/cm^3	2,69
4	Moisture content in air-dry state	norm.	W	%	0,1
5	Internal friction angle	norm.	$\varphi_н$	°	60,2
6		α = 0,95	φ_I		57,3
7		α = 0,85	φ_{II}		58,3
8	Specific cohesion	norm.	$c_н$	kPa	62,6
9		α = 0,95	c_I		55,9
10		α = 0,85	c_{II}		58,1
11	Dilatancy angle	norm.	ψ	°	7,9

The dilatancy angle was determined using the formula proposed by Bolton (1986) [22], based on the assumption of equality between the relative vertical deformation and the relative shear deformation. The range for determining the dilatancy angle was the section of maximum graph rise, which in most cases corresponded to the sample's hardening stage during shear. Table 2 presents the obtained values of the physico-mechanical properties sufficient for numerical modeling.

CONCLUSION

The main results obtained from the research are summarized by the authors in the following conclusions:

1) Stepped retaining structures made of box type blocks infilled with crushed stone are a promising design solution suitable for reinforcing soil slopes in civil, industrial, transportation, and hydrotechnical construction. However, due to the design’s structural features (primarily the absence of rigid connections between the blocks), this solution requires the development of traditional analytical calculation methods, as well as the justification for the creation of numerical calculation models;

2) For modular retaining walls, the use of numerical calculation methods is preferable due to the advantages of the finite element method. The "structure-soil" system is multiply statically indeterminate, and the soil's lateral pressure distribution under the same external load scheme will differ. Numerical calculations allow to identify a single stress state from a multitude of likely and permissible possibilities, determined by the set parameters of all system elements;

3) During a series of tests conducted in accordance with standard methodologies, the actual values of the physico-mechanical properties of the soil material used to fill the blocks and the spaces between them were determined. Normative and calculated shear resistance parameters were obtained. It was found that within the studied range of normal stresses, the Coulomb-Mohr envelope is linear. This allows the justified use of Coulomb-Mohr strength theory when model-

ing the considered retaining walls without resorting to more complex nonlinear theories, which require a larger number of parameters.

ACKNOWLEDGEMENTS

The research is conducted within the framework of cooperation agreements between Far Eastern Federal University (Vladivostok, Russia), the «Lomonosov» Cluster at M.V. Lomonosov Moscow State University (Moscow, Russia) and Branch FGBU “TSNIIP Russian Ministry of Construction” DalNIIS (Vladivostok, Russia) with financial and organizational support from KorBet LLC (Moscow, Russia). The authors express their sincere gratitude to Ya.I. Kotyk, A.Yu. Voronov, S.V. Vavrenyuk, Yu.V. Novak, A.D. Sokolov, and V.G. Reshetnikov for their valuable advice and productive cooperation, as well as K.A. Sokolov for editing and preparing the article for publication.

REFERENCES

1. **Travush V.I., Akimov P.A., Belostockij A.M., Sidorov V.N., Monastyrev P.V., Evdokimcev O.V., Mamontov A.A., Mamontov S.A.** (2023) Ob osnovnyh itogah vos'mogo mezhdunarodnogo simpoziuma «Aktual'nye problemy komp'yuternogo modelirovaniya konstrukcij i sooruzhenij» [About main results of the eighth international symposium "Actual problems of computer modeling in civil engineering"]. *Ekspert: teoriya i praktika*, no 3, pp. 27–39.doi:10.51608/26867818_2023_3_27.
2. **Belostockij A.M.** (2014) Sovremennaya metodologiya chislennogo modelirovaniya nagruzok i vozdejstvij, napryazhenno-deformirovannogo sostoyaniya i ustojchivosti vysotnyh zdanij i kompleksov [Modern methodology of numerical modeling of loads and impacts, stress-strain state, and stability of high-rise buildings and complexes]. *Vysotnye zdaniya*, no 1, pp. 94–97.
3. **Belostockij A.M., Dubinskij S.I., Aul A.A.** (2010) Verifikaciya programmnyh kompleksov dlya resheniya naukoyomkih zadach stroitel'nogo profilya (v sisteme RAASN). Opyt i perspektivy [Experience of program packages verification for civil engineering scientific problems]. *Vestnik MGSU*, no 4, pp. 185–189.
4. **Ter-Martirosyan A.Z., Sidorov V.V., Ermoshina L.Yu.** (2018) Opredelenie i verifikaciya parametrov modeli slabogo grunta s uchetom polzuchesti [Determination and verification of parameters of the soft soil model with account for creep]. Vestnik MGSU, vol. 13, no 6, pp. 697–708.doi:10.22227/1997–0935.2018.6.697-708.
5. **Brinkgreve R.B.J., Engin E.** (2013) Validation of geotechnical finite element analysis. Proceeding of the *18th International Conference on Soil Mechanics and Geotechnical Engineering, Paris, France. 2-6 September*, pp. 677–682.
6. **Sharafutdinov R.F.** (2023) Validation metrics for non-linear soil models using laboratory and in-situ tests. *Magazine of Civil Engineering*, no 122, Article No. 12205.
7. **Guan X., Madabhushi G.S.P.** (2020) Numerical Modelling of Structures Adjacent to Retaining Walls Subjected to Earthquake Loading. *Geosciences*, vol. 10, no 12, 486.
8. **Mustafa R.** (2024) Numerical modeling of gravity retaining wall using EPS geofoam under seismic condition. *Asian J Civ Eng*, vol. 25, no 3, pp. 2541–2552.
9. **Mangushev R., Nikitina N., Le Trung H., Tereshchenko I.** (2021) Analytical and numerical methods for determining the carrying capacity of a pile barett on weak soils in deep pits. *International Journal for Computational Civil and Structural Engineering*, vol. 17, no 3, pp. 94–101.
10. **Behr F., Dolzmann G., Hackl K. et al.** (2023) Analytical and numerical relaxation results for models in soil mechanics. *Con-*

tinuum Mech. Thermodyn., no 35, pp. 2019–2041.
11. **Muñoz-Medina B., Ordóñez J., Romana M.G., Lara-Galera A.** (2021) Typology Selection of Retaining Walls Based on Multicriteria Decision-Making Methods. *Appl. Sci*,, no 11, 1457.
12. **Tsimbelman N.Ya., Kuzovatkin I.V., Kotyk Ya.I., Ivannikov D.Yu., Babkin V.N.** (2022) Metodika raschyota i praktika primeneniya podpornyh sten iz blokov s gruntovym napolnitelem [Calculation method and application practice of retaining walls of blocks with ground filler]. *Dorogi i Mosty*, no 48, pp. 167–180.
13. **Tsimbelman N.Ya, Chernova T.I., Ivannikov D.Yu., Kuzovatkin I.V., Babkin V.N**. (2024) Primenenie zapolnennyh gruntom blokov pri reshenii zadach beregoukrepleniya [Application of soil-filled blocks in solving problems of shore protection]. *Gidrotehnicheskoye stroitel'stvo*, no 4, pp. 23–29.
14. Civil Engineering Research Centre (2014) *Construction technology inspection report. Building materials/ products/ technologies, road maintenance technologies. Construction and technical inspection act № 0327. Angled retaining wall with contact capability "Box retaining wall"*, Japan.
15. Civil Engineering Research Centre (2016) *Construction method "Box type retaining wall". Engineering manual*, Japan.
16. **Tsimbelman N.Ya., Kuzovatkin I.V., Chernova T.I., Kotik Ya.I., Ivannikov D.Iu., Babkin V.N.** (2023) Retaining walls made of infilled blocks in civil engineering. Proceedings of the *17th Asian Regional Conference on Soil Mechanics and Geotechnical Engineering 17th ARC, Astana, Kazakhstan, 14-18 August*, pp. 2600-2605.
17. **Iovlev G.A., Piscunov N.S., Bahvalov E.D., Ochkurov V.I.** (2022) Metody optimizacii parametrov nelinejnyh gruntovyh modelej dlya inzhenerno-geologicheskih uslovij Sankt-Peterburga [Optimizing nonlinear soil body models for geotechnical conditions of Saint-Petersburg]. *Gornyj informacionno-analiticheskij byulleten'*, no 7, pp. 148–163.doi: 10.25018/0236_1493_2022_7_0_148.
18. **Chauhan V.B., Dasaka S.M.** (2023) Numerical evaluation of the relief shelves for lateral thrust reduction on wall under at-rest condition. *Transportation Infrastructure Geotechnology*, no 11, pp. 359–380.
19. **Pereira P., Pacheco M., Lima B.** (2021) Numerical analysis of soft soil improved with stone column technique. *REM - International Engineering Journal*, no 74, pp. 319–327.
20. **Fedorenko E.V.** (2024) *Geotechnical features of SiO 2D v2024.0.2 program (a new Russian program for geotechnical calculations)*, Conference: geotechnical software. Public file.
21. **Ivanov V.I., Kurinov M.B., Men'shikov V.A., Shirokov V.N.** (2010) Features of performing in situ direct shear tests of soils using the MSU-1 machine. Proceedings of the *Sergeev's readings, Moscow, Russia, 23-24 March*, pp. 330–333.
22. **Bolton M.D.** (1986) The strength and dilatancy of sands. *Geotechnique*, vol. 36, no 1, pp. 65–78.

СПИСОК ЛИТЕРАТУРЫ

1. **Травуш В.И, Акимов П.А., Белостоцкий А.М., Сидоров В.Н., Монастырев П.В., Евдокимцев О.В., Мамонтов А.А., Мамонтов С.А.** Об основных итогах восьмого международного симпозиума «Актуальные проблемы компьютерного моделирования конструкций и сооружений» // Эксперт: теория и практика, 2023, № 3 (22). С. 27-39.
2. **Белостоцкий А.М.** Современная методология численного моделирования нагрузок и воздействий, напряженно-деформированного состояния и устойчивости высотных зданий и комплексов // Высотные здания, 2014. №1. С. 94-97.

3. **Белостоцкий А.М., Дубинский С.И., Аул А.А.** Верификация программных комплексов для решения наукоёмких задач строительного профиля (в системе РААСН). Опыт и перспективы // Вестник МГСУ, 2010. №4. С. 185-189.
4. **Тер-Мартиросян А.З., Сидоров В.В., Ермошина Л.Ю.** Определение и верификация параметров модели слабого грунта с учетом ползучести // Вестник МГСУ, 2018. Т. 13. Вып. 6 (117). С. 697–708.
5. **Brinkgreve, R.B.J., Engin, E.** Validation of geotechnical finite element analysis // Proceeding of the 18th International Conference on Soil Mechanics and Geotechnical Engineering. Paris, France, 2013, pp. 677–682.
6. **Sharafutdinov, R.F.** Validation metrics for non-linear soil models using laboratory and in-situ tests // Magazine of Civil Engineering, 2023, № 122(6). Article No. 12205.
7. **Xiaoyu Guan, Gopal S.P. Madabhushi** Numerical Modelling of Structures Adjacent to Retaining Walls Subjected to Earthquake Loading // Geosciences 2020, No 10(12), 486.
8. **Mustafa R.** Numerical modeling of gravity retaining wall using EPS geofoam under seismic condition // Asian J Civ Eng, 2024, No. 25, pp. 2541–2552.
9. **Mangushev, R., Nikitina, N., Le Trung, H., Tereshchenko, I.** Analytical and numerical methods for determining the carrying capacity of a pile barett on weak soils in deep pits // International Journal for Computational Civil and Structural Engineering, 2021, No. 17(3), pp. 94-101.
10. **Behr, F., Dolzmann, G., Hackl, K. et al.** Analytical and numerical relaxation results for models in soil mechanics // Continuum Mech. Thermodyn., 2023, No. 35, pp. 2019-2041.
11. **Muñoz-Medina B., Ordóñez J., Romana M.G., Lara-Galera A.** Typology Selection of Retaining Walls Based on Multicriteria Decision-Making Methods // Appl. Sci., 2021, No. 11, p.1457.
12. **Цимбельман Н.Я., Кузоваткин И.В., Котык Я.И., Иванников Д.Ю., Бабкин В.Н.** Методика расчёта и практика применения подпорных стен из блоков с грунтовым наполнителем // Дороги и мосты, 2022. № 48. С. 167-180.
13. **Цимбельман Н.Я., Чернова Т.И., Иванников Д.Ю., Кузоваткин И.В., Бабкин В.Н.** Применение заполненных грунтом блоков при решении задач берегоукрепления // Гидротехническое строительство, 2024. № 4. С. 23-29.
14. Civil Engineering Research Centre (2014) *Construction technology inspection report. Building materials/ products/ technologies, road maintenance technologies. Construction and technical inspection act № 0327. Angled retaining wall with contact capability "Box retaining wall"*, Japan.
15. Civil Engineering Research Centre (2016) *Construction method "Box type retaining wall". Engineering manual*, Japan.
16. **Tsimbelman N.Ya., Kuzovatkin I.V., Chernova T.I., Kotik Ya.I., Ivannikov D.Iu., Babkin V.N.** Retaining walls made of infilled blocks in civil engineering // Proceedings of the 17th Asian Regional Conference on Soil Mechanics and Geotechnical Engineering 17th ARC, Astana, Kazakhstan, 2023, pp. 2600-2605.
17. **Иовлев Г.А., Пискунов Н.С., Бахвалов Е.Д., Очкуров В.И.** Методы оптимизации параметров нелинейных грунтовых моделей для инженерно-геологических условий Санкт-Петербурга // Горный информационно-аналитический бюллетень, 2022. № 7. С. 148–163.
18. **Chauhan, V.B., Dasaka, S.M.** Numerical evaluation of the relief shelves for lateral thrust reduction on wall under at-rest condition // Transportation Infrastructure Geotechnology, 2023, No. 11, pp. 359–380.
19. **Pereira P., Pacheco M., Lima B.** Numerical analysis of soft soil improved with stone column technique // REM - International

Engineering Journal, 2021, no 74, pp. 319–327.

20. **Федоренко Е.В.** Геотехнические особенности программы SiO 2D v2024.0.2 (a new Russian program for geotechnical calculations) // Conference: geotechnical software. Public file. 2024.
21. **Иванов В.И., Куринов М.Б., Меньшиков В.А., Широков В.Н.** Особенности выполнения полевых испытаний грунтов на срез с использованием установки МСУ-1// Сергеевские чтения, выпуск 12, 2010. С.330-333.
22. **Bolton M.D.** The strength and dilatancy of sands // Geotechnique, 1986, no. 1. (36), pp. 65–78.

Nikita Yakovlevich Tsimbelman - Doctor of Technical Sciences, Professor & Director of Geoinformation Technologies Department of Polytechnic Institute (School), Far Eastern Federal University (FEFU), room E918, FEFU Campus, p. Ajax 10, Vladivostok, 690922, Fr. Russian, tsimbelman.nya@dvfu.ru;

Anatoly Yuryevich Mirnyy - Candidate of Technical Sciences, Associate Professor of Lomonosov Moscow State University, Leninskie Gory, GSP-1, Moscow, 119991, Russia, mirnyyAY@mail.ru;

Evgeny Vladimirovich Fedorenko - Candidate of Technical Sciences, Associate Professor, NIP Informatica, 24, 4K, Fuchika str., Saint-Petersburg, 192102, Russia, eugeniy.fedorenko@nipinfor.ru;

Dmitry Yuryevich Ivannikov - Chief Designer, KorBet LLC, 1, Ramensky Boulevard, Moscow, 119607, Russia, d.ivannikov@korbetstroy.ru;

Valentin Nikolaevich Babkin - Managing Director, KorBet LLC, 1, Ramensky Boulevard, Moscow, 119607, Russia, info@korbetstroy.ru;

Igor Valerievich Kuzovatkin - Assistant of Geoinformation Technologies Department of Polytechnic Institute (School), Far Eastern Federal University (FEFU), room E906, FEFU Campus, p. Ajax 10, Vladivostok, 690922, Fr. Russian, kuzovatkin_iv@dvfu.ru;

Tatyana Igorevna Chernova - Senior Lecturer of Geoinformation Technologies Department of Polytechnic Institute (School), Far Eastern Federal University (FEFU), room E915, FEFU Campus, p. Ajax 10, Vladivostok, 690922, Fr. Russian, chernova.ti@dvfu.ru.

Никита Яковлевич Цимбельман – доктор технических наук, профессор и директор департамента геоинформационных технологий Политехнического института (Школы) Дальневосточного Федерального университета (ДВФУ), к. E918, Кампус ДВФУ, п. Аякс, 10, о. Русский, г. Владивосток, 690922, Россия, tsimbelman.nya@dvfu.ru;

Анатолий Юрьевич Мирный – кандидат технических наук, доцент Московского государственного университета им. М.В. Ломоносова, Ленинские горы, ГСП-1, г. Москва, 119991, Россия, mirnyyAY@mail.ru;

Евгений Владимирович Федоренко – кандидат технических наук, доцент, НИП Информатика, 24, 4К, ул. Фучика, г. Санкт-Петербург, 192102, Россия, eugeniy.fedorenko@nipinfor.ru;

Дмитрий Юрьевич Иванников – главный конструктор, ООО «КорБет», 1, Раменский бульвар, г. Москва, 119607, Россия, d.ivannikov@korbetstroy.ru;

Валентин Николаевич Бабкин – генеральный директор, ООО «КорБет», 1, Раменский бульвар, г. Москва, 119607, Россия, info@korbetstroy.ru;

Игорь Валерьевич Кузоваткин – ассистент департамента геоинформационных технологий Политехнического института (Школы) Дальневосточного Федерального университета (ДВФУ), к. E906, Кампус ДВФУ, п. Аякс, 10, о. Русский, г. Владивосток, 690922, Россия, kuzovatkin_iv@dvfu.ru;

Татьяна Игоревна Чернова – старший преподаватель департамента геоинформационных технологий Политехнического института (Школы) Дальневосточного Федерального университета (ДВФУ), к. E915, Кампус ДВФУ, п. Аякс, 10, о. Русский, г. Владивосток, 690922, Россия, chernova.ti@dvfu.ru.

INVESTIGATING THE CRACK PROPAGATION RESISTANCE OF NANO CONCRETE THROUGH FRACTURE MECHANICS

Kalpesh Laljibhai Kapadiya [1], Dr. Sanjay Joshi [1], Dr. Ajaysinh Vaghelas [1], Parag Rameshbhai Savsani [2]

[1] Department of Civil Engineering, R. K. University, Rajkot, Gujarat, INDIA
[2] Department of Civil Engineering, Dr. Subhash University, Junagadh, Gujarat, INDIA

Abstract. In the concrete treatments, small cracks are beginning developing inside. As a result of temperature and stress variations during extraction, the fragments will enlarge and unite to form some noticeable cracks. Concrete constructions may suddenly shatter as a result of cracks spreading. The study focuses consideration of the inspiration of additives on the properties of fracture in high-performance concrete with additives (HPCA) as a foundation for the effective application of building structures. Compared to traditional concrete, HPCA has better mechanical qualities and durability. The highly responsive nanoparticles significantly improved concrete performance. Portland cement has been replaced with nanoparticles at different percentages of weight to create HPCA mixtures. The impact of nano silica (nS) and nano alumina (nA) on the appearance of fracture and crack extension resistance of HPC during the process of entire fracture will be assessed in this research. Based on the softening laws and outcomes of the bending test of three-point of concrete material along with grooves, the resistance of crack extension of HPCA was determined. The crack mouth opening displacement versus load relationship curves (P-CMOD) represent the ultimate result. Compressive strength and additional mechanical properties have been determined within the model. Ultimately, the P-CMOD curves are used to analyse and compute the fracture parameters and features of HPCA utilizing nano particles.

Keywords: Concrete, Nano-particles, Fracture, Characterizations, Durability, Mechanics

ИССЛЕДОВАНИЕ СОПРОТИВЛЕНИЯ РАСПРОСТРАНЕНИЮ ТРЕЩИН В НАНОМОДИФИЦИРОВАННОМ БЕТОНЕ НА ОСНОВЕ МЕХАНИКИ РАЗРУШЕНИЯ

Калпеш Лалджибхай Кападия [1], Санджай Джоши [1], Аджайсинх Вагелас [1], Параг Рамешбхай Савсани [2]

[1] Кафедра гражданского строительства, Университет Р. К., Раджкот, Гуджарат, ИНДИЯ
[2] Факультет гражданского строительства, Университет доктора Субхаша, Джунагадх, Гуджарат, ИНДИЯ

Аннотация. В процессе обработки бетона в нем могут появляться небольшие трещины. В результате колебаний температуры и напряжения при прекращении обработки микротрещины увеличиваются и объединяются, образуя заметные трещины. В результате распространения трещин бетонные конструкции могут внезапно разрушиться. Данное исследование посвящено рассмотрению влияния добавок на параметры разрушения высокопрочного бетона с добавками (HPCA) как основы для эффективного применения в строительных конструкциях. По сравнению с традиционным бетоном, HPCA обладает лучшими механическими свойствами и долговечностью. Высокочувствительные наночастицы значительно улучшили характеристики бетона. Для создания смесей HPCA портландцемент был заменен наночастицами в различных весовых процентах. В данном исследовании было оценено влияние нанокремнезема (nS) и наноглинозема (nA) на появление трещин и сопротивление раскрытию трещин в HPC в процессе полного разрушения. На основе законов разупрочнения и результатов испытания на трехточечный изгиб бетонного образца с вырезом было определено сопротивление расширению трещин в HPCA. Получены кривые зависимости смещения устья трещины от нагрузки (P-CMOD). В рамках модели были определены прочность на сжатие и дополнительные механические характеристики. Кривые P-CMOD использованы для анализа и расчета параметров разрушения и характеристик высокопрочного наномодифицированного бетона (HPCA).

Ключевые слова: Бетон, наночастицы, разрушение, характеристики, долговечность, механика

1. INTRODUCTION

Concrete is the greatest frequently employed construction substantial and heterogeneous composite material made of cement, water, sand, and stones. When concrete is moistened and mixed with various fluids while in use, a lot of microcracks are created. Microcracks will continually form, enlarge, and penetrate when under load. The internal microcracks in concrete ultimately broaden and seep through, causing the material to fracture. Three stages can be observed in the propagation of concrete cracks under uniaxial compression: unstable crack growth, stable crack growth, and crack initiation. The advancement of concrete crack propagation research has important implications for damage-warning techniques and safety evaluations in numerous construction structures.

Inserting nanoparticles to high-performance concrete greatly enhance the material's durability and mechanical qualities. Compared to silica fume materials in micro-meter sizes, HPC has used silica material in the size of nano-meter is seen as a novel development. Ultrafine silica particles have a size of nano-meters aid in launching reactions of pozzolanic, uneven $Ca(OH)_2$ elements has been rejected and result in gel product of pozzolan at the performance has high. According to (Lam et al. 2020) [8], the mechanical characterizations like strength of compression, flexural, modulus of elasticity and deformation stress of HPC with NS has been improved. The impression of nano-silica on the properties of fracture in concrete was highlighted by recent studies utilizing NS in HPC (Khaloo et al. 2016; Zhang et al. 2017; Vivek et al. 2021) [7,20,19], but no particular experiments were conducted for evaluation.

Most of the structures of concrete was affected by the areas of fracture mechanics Mindess (2002) [12]. Concrete that contains silica fume have better fracture properties than usual ones (Ricardo and Marta, 2006). A new approach of measuring the fracture using artificial failure surfaces of concrete were performed and analysed by (Mechtcherine and Müller, 2021) [10] The transition of interface zone of quality between aggregate and mortar is enhanced by silica fume, which also improves the C-S-H structure and uniformity. When silica fume is used, fracture energy, fracture toughness, and length characteristics all grow more, and the brittleness of HPC tends to diminish. The properties of fracture are very crucial for the endurance and safety structures of HPC represented by (Zhang et al. 2017) [20]. The quality of fracture in concrete's are impacted when pore structures in HPC are improved through the use of chemical and mineral admixtures. These results are increasing the mortar-aggregate density transition zone of interface. The consistency performance of mortar will be enhanced by silica ultrafine particles, which also increase the cohesiveness between aggregate and cement particles and greatly improve the concrete's fracture characteristics.

The microstructure and fracture behaviour of concrete will both be enhanced by the presence of ultrafine particles. Because of the high strength properties of HPC concrete, brittle fracture occurs more often and often passes through the coarse aggregate rather than along the aggregate boundary as it would in regular concrete. The mechanical properties of normal concrete have low compared to HPC. The slope curve's downward (after the apex) steepens for HPC. This demonstrates that HPC is more prone than regular concrete to sustain unexpected deterioration.

The main focus of the essay is centered on figuring out HPCA's mode I fracture characteristics and parameters. To ascertain the fracture parameters of HPCA, a unique testing procedure in accordance with RILEM was used, which involved regulating the open displacement of the crack mouth. In accordance of IS method as per 10262-2019 for M40 grade guidelines, the five mixed proportions of HPC with contents of 0.5%, 1%, 1.5%, 2%, and 2.5 % were computed for the component design to be used in the experiments. It was determined how the nA and nS contents affected the HPC's fracture properties. The fracture mechanics approach was applied to assess the experimental findings and determine the properties of HPCA beams' resistance to crack extension.

2. RELATED WORKS

Van Mier, Jan GM (2012) [18] asserts that ultrafine particles will dramatically alter how concrete behaves during the fracturing process. The deformation of stress curve illustrates an improvement in ductility, particularly as the curves' post-peak slope gradually declines. The inclusion of ultrafine NS particles helps to bridge broken surfaces, which explains why the toughness has improved. The fracture quality has minimum of normal concrete compared with silica fume of concrete (Einsfeld et al. 2006) [4]. The administration of silica fume optimizes the standardization and structure of C-S-H gels, as well as the functionality of the ITZ as a of mortar and aggregate. When utilizing silica fume, the characteristics of toughness, length, and fracture energy are increased. HPC brittleness tends to diminish. Concrete's fracture characteristics are impacted when the ITZ of mortar and aggregate is made denser by chemical and mineral admixtures in HPC (Zhang et al. 2014) [21].

Additionally, some research employing HPC with ultrafine nano particles asserted, when hardened the mortar performance and consistency has been continuously improved. Increasing the cohesiveness between the aggregates and cement particles also considerably increases the fracture toughness of concrete (Chithra et al. 2016) [3]. Concrete's microstructure and fracturing behaviour are greatly improved by ultrafine particles. (Quercia et al. 2013) [13] indicated that the inclusion of fine material significantly alters the way that concrete fractures. The enhanced ductility of the ultrafine concrete component is indicated by the load-deformation curve. In comparison to the concrete without fine particles, slope curve of post-peak is lower Bianchi (2014) [2]. Bridging surfaces are broken at maximum in the ultrafine particles’ presence accounts for an improved toughness. To comprehend the connection between ultrafine particles and the behaviour of concrete cracks, some empirical research has also been carried out. Overall, the findings indicate that the ultrafine mineral composition appears to have an impact property of concrete fracture (Zhang et al. 2017).

(Torabian Isfahani et al. 2016) [17] investigated the impact of varying nanosilica dosages on the compressive strength and durability of concrete with different water/binder ratios. They evaluated concrete properties by measuring water sorptivity, apparent chloride diffusion coefficient, electrical resistivity, and carbonation coefficient. Results indicated that compressive strength improved significantly for a water/binder ratio of 0.65 with the addition of nanosilica, while no significant change was observed for a ratio of 0.5. Water sorptivity decreased with increased nanosilica only for a water/binder ratio of 0.55. A 0.5% nanosilica addition reduced the chloride diffusion coefficient for water/binder ratios of 0.65 and 0.55, but higher dosages did not yield further improvements. Electrical resistivity increased with 0.5% nanosilica across all ratios and with 1.5% only for a water/binder ratio of 0.5. Carbonation coefficient changes were minimal, with some adverse effects noted for a ratio of 0.65. Microstructural analysis through techniques such as X-ray diffraction and scanning electron microscopy provided additional insights, showing that nanosilica's effectiveness was more pronounced in lower strength mixes.

(Mahender et al. 2017) [9]explored using waste plastics and rubber as partial replacements in concrete, with incremental 5% substitutions in both fine and coarse aggregates. Concrete cubes and cylinders were tested at 7 and 28 days and compared with specimens containing 0% waste materials. The study found that incorporating waste plastics and rubber was effective for constructing rigid pavements, sewers, tennis courts, and walkways, resulting in a reduction in the overall pavement thickness.

Despite advancements in concrete technology, the investigation of crack propagation resistance in nano concrete using fracture mechanics remains underexplored. Existing research primarily focuses on the general mechanical properties and durability of nano concrete, often neglecting a detailed analysis of its fracture behavior. Current studies do not sufficiently address how nanoscale additives influence crack initiation, growth, and propagation under various stress conditions. There is a lack of comprehensive understanding of the interaction between nano materials and concrete matrix at the microstructural level concerning crack resistance. This gap highlights the need for targeted research that employs fracture mechanics principles to evaluate the effectiveness of nano additives in enhancing the crack propagation resistance of concrete, which could lead to more resilient and long-lasting construction materials.

3. MATERIALS AND METHOD

3.1 Materials

The Portland cement contains aggregates of coarse basalt with 12.5 mm D_{max}, superplasticizer, nano-silica, nano-alumina and fine aggregates with a module 2.7 mm. The Adnano technologies NS product has a surface area of 200 ± 25 m^2/g and diameters of 5-50 nm, was used for the research. Nano alumina (nA) and nano silica (nS) particles were utilized as additives in concrete beams.

3.2 Mix Proportion

An IS method as per 10262-2019 for M40 grade method is used to design the compressive strength of HPCA for 49 MPa (Sivasankaran et al. 2019) [16]. Mixtures with 0.5%, 1%, 1.5%, 2%, and 2.5% nano particles ratios were made for the experimental test. The ratio has chosen and modified combinations in accordance with the recommendations Fédération-internationale-du-béton (2008) [5]. A mixture of the percentage of HPC with additives as depicted in Table 1.

Table 1. Different proportion of additives

Mix Mode (nA and nS)	0.5%	1%	1.5%	2%	2.5%
Cement (kg)	543.31	540.5	534.8	530.9	525.7
Fine Aggregate (kg)	673.2	672.4	671.6	670.8	669.8
Coarse Aggregate (kg)	1049.75	1049.75	1049.75	1049.75	1049.75
Nano-Alumina	0.5	1	1.5	2	2.5
Nano-silica	0.5	1	1.5	2	2.5
Superplasticizer	5.32	6.42	7.51	8.21	9.25
Water	154.67	154.67	154.67	154.67	154.67
Water/Binder	0.27	0.27	0.27	0.27	0.27

3.3 Preparation of sample

Before mixing, material components including cement, fine and coarse aggregate, and superplasticizer are ready for measurement. To make sure that the additives are distributed equally throughout the mixture, they are specifically combined with half of the water needed and vigorously agitated. Following material preparation, the specimen mixing process is carried out in accordance with the protocol depicted in Figure 1.

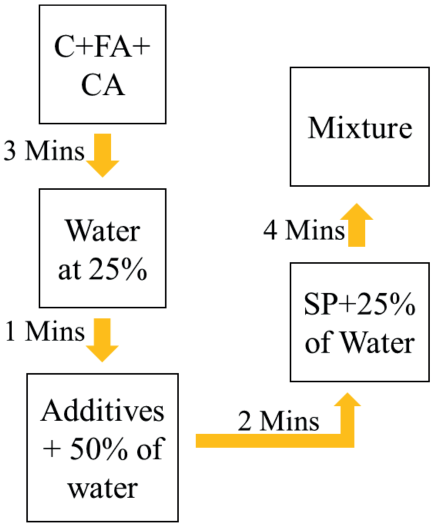

Figure 1. HPCA preparation procedure

As seen in Figure_2, the concrete design with notch has been created. Table 2 represents the different sizes of beam used for this research work.

Table 2. Different size of beams

Dimensions	Length (L) mm	Width (B) mm	Depth (D) mm	Notch Size (a) mm
Small	151.62	57	57	11.4
Medium	303.24	57	114	22.8
Large	606.48	57	228	45.6
Ratio of a/d 0.2				

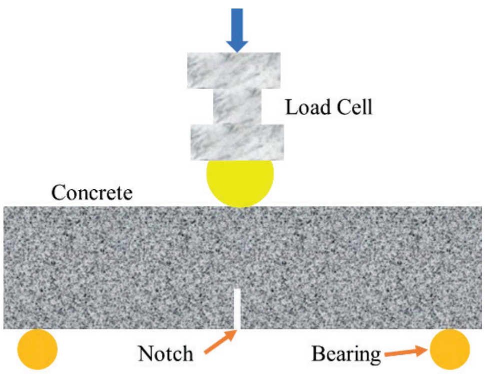

Figure 2. Specimen used for fracture test

3.4 Experimental Methods

To ascertain the concrete's fracture parameters, conduct an experiment using notch with bending beam of 3-point apparatus. A test procedure has illustrated in Figure_3. The fracture test uses specimen displacement as opposed to load control, establishing it separate from the stronger test and other mechanical evaluations. The Control experiment machine is used to perform all three-point bending experiments in a closed-loop setting. In Figure_3 represented the linear variable differential transformer (LVDT) has measured the outcome of load and beam displacement and crack mouth open displacement (CMOD) as determined using extensometer were the parameters measured during the experiment.

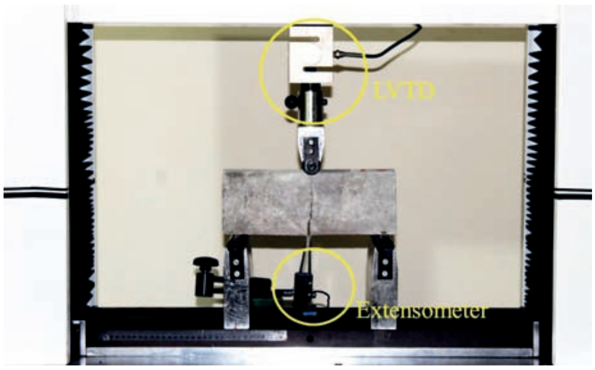

Figure 3. 3-Point bending test of HPCA specimen

According to FMC's recommendations Recommendation, RILEM Draft (1985) [15], studies must be carried out to ensure that the mid-span displacement increases at rate of consistent is 0.2 mm/min. Nonetheless, the analysis suggests that this condition could be modified slightly. An experimental test was carried out CMOD control rather than mid-span displacement control.

3.4.1 Test of Determining Fracture Energy

The deflection of beam is monitored using linear variable differential transformer (LVDT) located at center of the concrete beam. The maximum load was attained 30 seconds after the loading began selection of velocity loading. A rate of loading chosen is 0.25 mm/min. Next, a curve of load-deflection (F-δ) was drawn, and under the curve area was represented by the energy symbol "W_0." The following expression can be used to determine the GF (N-m) (AlKhatib et al. 2020; Rakesh et al. 2021) [1,14].

$$G_F = W_0 + mg\,\frac{\delta_0}{A} \quad (1)$$

where W_0 = load-deflection area curve (N-m)
m = beam of mass between the supports (kg)
g = gravity acceleration
δ_0 = beam deflection at final stage (m)
A = beam cross sectional area exclusive notch (m^2).

3.4.2 Test for Determining K^S_{IC}

The test procedure represented by (Jenq et al. 1985) [6] was utilized to determine K^S_{IC}, and it involved a closed-loop testing apparatus with crack mouth opening displacement (CMOD) control. The clip gauge was used to monitor the CMOD. Throughout the test, the applied load and the CMOD were continually recorded. There were two loading and unloading steps in the test protocol. The applied load was manually lowered (also known as unloading) once the load passed the maximum load and was roughly 95% of the peak load. The first process involved loading until the peak load was attained. Reloading was used when the applied load was lowered to zero. About a minute was needed to complete each loading and unloading cycle. For the test, a single loading-unloading cycle was needed. The following formula is used to determine the K^S_{IC}.

$$K^S_{IC} = \frac{3SP_{max}}{2bd^2} + \pi\alpha_c\, F(\alpha) \quad (2)$$

where P_{max} = Load at maximum (N)
S = beam length
b = width of beam
d = depth of beam
α_c = crack length at critical effective.

4. RESULTS AND DISCUSSION

4.1 Consequence of additives in HPCA deflection-load and CMOD-load curves

As seen in Figure 4 represented the variation of outcome CMOD-P slope equivalent to the concrete specimens of beam cured for 28 days utilizing ratios of 0.5%, 1%, 1.5%, 2%, and 2.5 % of nA and nS. The HPC with additives P-CMOD curve has a high slope once it reaches the peak (Pmax). A tiny CMOD causes the force value to drop off rapidly. The P-CMOD curve significantly changes when additives are added to concrete at ratios of 2% and 2.5%, particularly when 2.5% of additives are added. The conducted experiment test of beam has elasticity limit still, the curves often grow in the same way at first, but as the curve approaches its peak, a difference begins to become evident.
The P-CMOD curve with a reduced additive percentage Once concrete reaches its peak (Pmax), it slopes significantly; at very tiny CMOD values, the force value rapidly drops. There is a noticeable shift in the P-CMOD curve that results from adding chemicals to the concrete at 2% and 2.5%. Since the stages of beginning the reached elastic limit of the concrete. Figure_ 4 illustrates how the curves of all the samples tend to develop uniformly. The top of the curve for concrete containing additives (2.5%) is higher than that of regular concrete, and variation of slope in HPCA beam curve peak is high. These can readily realize tensile strength of the concrete is higher when additives are used than when they are ignored.

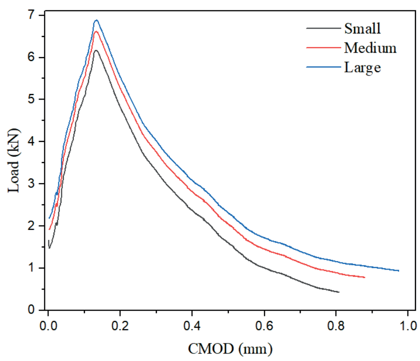

Figure 4. P-CMOD curve of HPCA specimen thickness

The HPCA (2.5%) curve has a lower slope in the period of post-peak than slope of HPCA (0.5%). When comparing similar results in CMOD, the outcome of the load has decreased

growth of slower CMOD as represented in Figure_4. Specimens with additives continued to have a higher load valuation than specimens with a lower percentage of additives.
In comparison to control samples (0.5%), beam samples with 2.5% additives showed an increase in crack mouth open displacement, or Pmax (CMOD), of 107.14%. The displacement of fractures increased to a maximum of 10% when the CMOD of beam samples with 2.5% additives was achieved maximum compared to sample of control (0.5%). According to the CMOD results, the hardness of concrete is considerably increased by the addition of small amounts of additional particles.

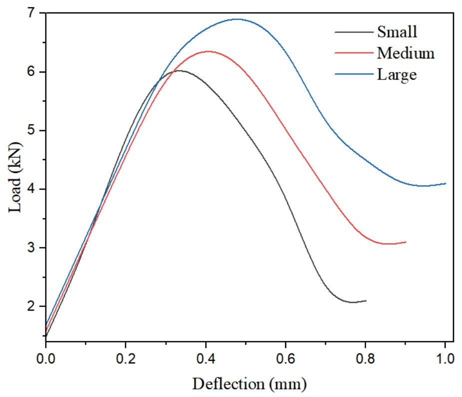

Figure 5. Load deflection curve of HPCA specimen

Figure 5 displays that the HPCA specimen slope of deflection load outcome with different concentration of additives. The load declines more slowly, the slope has been lengthens represented as phase of nonlinear, and slope of P-δ is thicker for the concrete that uses additives. Based on Figure 5, it is evident that the highest length of position (δ_{max}) test of bending at three points conducted on prepared specimens increases when samples utilizing NS are compared from 0.5% to 1.5% of the control sample (0.5%).
Consider the resulting change in the slope of deflection and load relationship length of the center is depicted in Figure_5, which also demonstrates how the horizontal axis of the graph and slope of deflection and load under the area alter in proportion of additives. An area under the P-δ curve is computed using the integral technique. According to the findings, horizontal axis rose by 7.69%, respectively, at 2.5% additives ratios.

4.2 Influence of additives on the energy of fracture (GF)

The energy of fracture has observed the increases, when the concentration of additives increased from 0.5% to 2.5% is depicted in Figure 6. The fracture energy (GF) produced from the test of bending at three-point is computed using deflection-load slope relationship. The average of six specimens' results is used in the computation. Figure_6 illustrates that specimens with a larger percentage of additives had fracture energy that increased by 78% when the additives ratio was 2.5%, respectively, when compared to concrete specimens with varied percentages of additives.
At 28 days old, the fracture toughness was assessed. Comparing the macro fracture toughness of the additive-added samples (2.5%) to that of the control samples (0.5%), it is shown that the additive-added samples (2.5%) have the best strengthening effect. Adding 2.5% of additives greatly increases the macro fracture toughness. Consequently, it is advised to use 2.5% of additives to enhance fracture characteristics for significant buildings that are vulnerable to frost attack at a relatively young age.

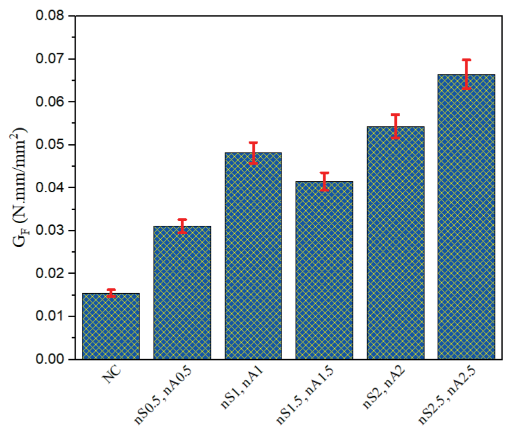

Figure 6. Fracture energy of HPCA specimen.

4.3 Mechanical Properties

After the day of 28, the strength of compression was observed for different concentration of additive mixes taken into consideration during the study's initial phase (Figure_7). The mixtures' 28-day compressive strengths varied from 40 to 53 MPa. As was noted, mixture 2.5% produced the highest compressive strength. Results for compressive strength were often much greater than those for concrete strength at high (i.e., around 53 MPa) or standard concrete (i.e., around 39 MPa).

To the concrete, additives concentration starts with 0% to 2.5% by adding of weight of cement. According to reports, additives enhanced both the concrete's early age strength and compressive strength (AlKhatib et. al., 2020). It was determined that 2.5% of nA and nS concentration provided the best crushing strength (Rakesh et. al., 2021). This study examined an impact of additives as nS and nA on different strength of concretes. nA and nS were substituted in different proportions by cement weight:0.5,1,1.5,2, and 2.5%. The prepared concrete with different concentration of additives (2.5%) has been achieved maximum strength of compression compared to control concrete (0.5%), and the concentration of 0.55 water to cement has been increased by 70%. Compared to lower strength concrete, greater strength concrete was less affected by nS and nA (Mendes et al. 2019) [11].

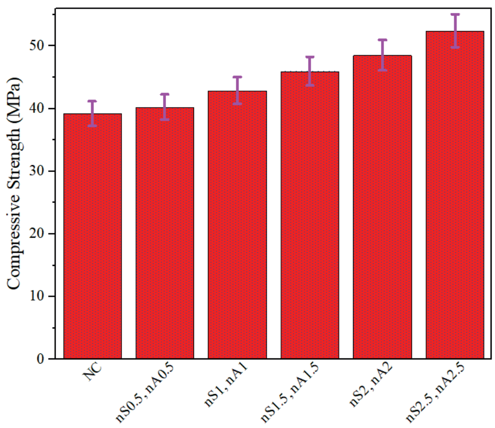

Figure 7. Compressive strength of HPCA specimen

It is evident from the data that 0.5% mixtures were able to reach the minimum compressive strength of 40 MPa. Additionally, mixture 2.5% yielded the best compressive strength of 53 MPa. It's interesting to note that the compressive strength of the combinations slightly worsened when more additives were added.

4.5 Splitting Tensile strength

When concretes containing nA and nS were tested in the first stage of the experiment, the strength of tensile splitting concrete was 0.5%, however a greater value was observed for specimens with a nominal weight percentage of 2.5. For the stronger concrete, the additions increased the tensile strength by 2.5%, whereas for the weaker HPCA concrete, the improvement was only 0.5%. The strength improvement for concretes containing higher weight percentages of additives was 2.1% for 0.5wt% and 4.5% for 2.5wt%. 2.1% and 4.5%, respectively, were the increases in tensile strength for tougher concrete (2.5%).

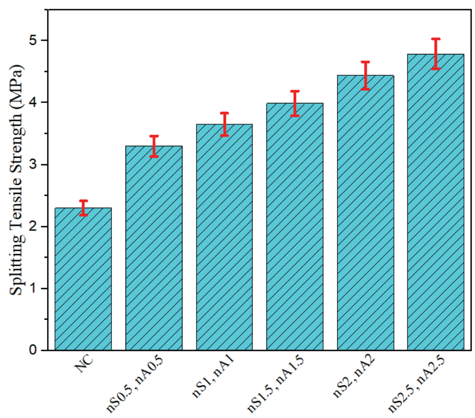

Figure 8. Splitting tensile strength of HPCA specimen

4.6 Stress Intensity Factor

With a notch beam in a three-point bend test, the critical stress intensity factor (K^S_{IC}) was experimentally calculated using a closed-loop testing apparatus under the CMOD control. Plots of load-CMOD curves from testing were made. Equation (2) was applied to calculate the

K^S_{IC}. Tests were conducted on concrete specimens at 14 and 56 days. The results are summarized in Figure_8. It demonstrates how the GF and the related tendency of the concrete's K^S_{IC} are comparable.

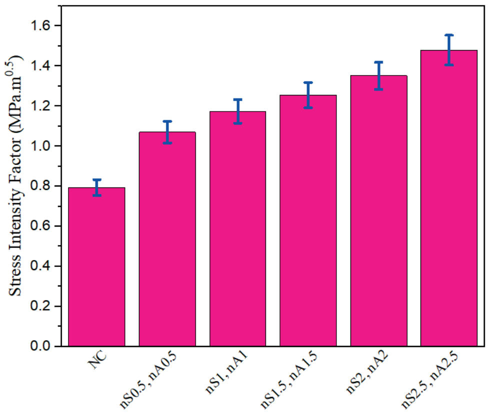

Figure 9. Stress intensity factor of HPCA specimen

The K^S_{IC} values of HPCA (2.5%) are lower than those of the reference concrete (0.5%) at a young age (14 days), but they rise over 0.5% after 56 days. According to this, the extra pozzolanic reaction of additives with Ca $(OH)_2$ in concrete is said to become active between the 14 and 56-day mark, increasing the HPCA's K^S_{IC}. Furthermore, it is shown that for different ages, the concrete with a higher additive level (2.5%) had a lower KSIC value than the concrete with a lower additive content (0.5%). Conversely, concrete that has been mixed with finer additions may have higher K^S_{IC} values. Figure_9 shows that, for a range of ages, an increase in the slag's fineness level causes the K^S_{IC} value of concrete to rise. Put otherwise, the combination containing finer slag (2.5%) has a higher K^S_{IC} value (2.5%) compared to the 0.5% K^S_{IC} value for the same additive replacement ratio (0.5%). Furthermore, for the various ratio of 0.5%, the K^S_{IC} of 2.5% > 2% > 0.5%. The achievement is attributable to the finer additives (2.5%) particle's larger surface area, which promotes a more active pozzolanic process and elevates strength and fracture toughness.

5. CONCLUSION

From the experimental setup of bending test of three point at the different concentration of additives in concrete, the outcomes revealed that the parameters of fracture and properties of HPCA in mode I form were determined. Through experimentation and analysis, the fracture parameters and features of HPCA were established. The outcome of the HPCA has been represented by CMOD-load, deflection and load slope, energy of fracture (GF) and strength of compression. Findings demonstrate that the substantial impact of different concentration of nA and nS on HPC parameters of fracture and features. When it comes to use, the additives ratio of 2.5% is ideal. The enhanced ductility of the HPCA is demonstrated by the fracture energy and distinctive mechanical characteristics.

When 2.5% of HPCA is used, the crack resistance will be stronger than when 0.5% of the control type is used. The mechanical characteristics of HPCA have been reached at 2.5% and 0.5% of additives, respectively, at 53 MPa and 40 MPa. Because of their better filling effect, finer additives (2.5%) have a positive impact on concrete's fracture energy (GF) even at young ages (14 days). The GF value of concrete increases or its fracture toughness is improved with an increase in the fineness level of the added additives. Similar to the fracture energy, the stress intensity factor (K^S_{IC}) critical of HPCA (2.5%) has a comparable tendency.

Though this study investigates the crack propagation resistance of nano concrete through fracture mechanics, offering valuable insights into its performance. However, several limitations must be acknowledged. Firstly, the experimental scope was restricted to a specific range of nano-materials and concrete compositions. The influence of varying types and concentrations of nano-additives on crack propagation was not exhaustively explored. Additionally, the study focused on static loading conditions; dynamic or cyclic loading scenarios were not considered, which could significantly impact crack behavior in real-world applications.

Future research should address these limitations by expanding the range of nano-materials and concrete mixtures studied. Investigating the effects of different loading conditions, including dynamic and cyclic loads, would provide a more comprehensive understanding of crack resistance in practical applications. Additionally, incorporating long-term durability studies to assess how environmental factors affect crack propagation could offer deeper insights into the long-term performance of nano concrete. Advanced modeling techniques and larger-scale experiments could further enhance the reliability of predictions and guide the development of more resilient nano concrete formulations. Such efforts will contribute to optimizing nano concrete for diverse structural applications and improving overall construction practices.

DECLARATIONS:

ETHICS APPROVAL

No ethics approval is required.

HUMAN AND ANIMAL ETHICS

Not Applicable.

DECLARATION OF INTERESTS

The authors declare that they have no known competing financial interests or personal relationships that could have appeared to influence the work reported in this paper.

DATA AVAILABILITY STATEMENT

All the data is collected from the simulation reports of the software and tools used by the authors. Authors are working on implementing the same using real world data with appropriate permissions.

FUNDING

This research did not receive any specific grant from funding agencies in the public, commercial, or not-for-profit sectors.

CONFLICTS OF INTEREST

The authors declare that we have no conflict of interest

COMPETING INTERESTS

The authors declare that we have no competing interest.

INFORMED CONSENT

Not Applicable.

CONSENT FOR PUBLICATION

Not Applicable

ACKNOWLEDGMENTS

The authors would like to thank the Deanship of R. K. University for supporting this work.

REFERENCES

1. **AlKhatib, Anas, Mohammed Maslehuddin, and Salah Uthman Al-Dulaijan.** "Development of high performance concrete using industrial waste materials and nano-silica." *Journal of Materials Research and Technology* 9, no. 3 (2020): 6696-6711.
2. **Bianchi, G. Quercia.** "Application of nano-silica in concrete." (2014).
3. **Chithra, Sankar, SRR Senthil Kumar, and K. Chinnaraju**. "The effect of Colloidal Nano-silica on workability, mechanical and durability properties of High Performance Concrete with Copper slag as partial fine aggregate." *Construction and Building Materials* 113 (2016): 794-804.
4. **Einsfeld, Ricardo A., and Marta SL Velasco.** "Fracture parameters for high-performance concrete." *Cement and Concrete Research* 36, no. 3 (2006): 576-583.
5. Fédération-internationale-du-béton, T. G. "Constitutive modelling of high

strength/high performance concrete." *Bulletin (Fédération internationale du béton) Lausanne, Switzerland* (2008): 125.

6. **Jenq, Yeoushang, and Surendra P. Shah.** "Two parameter fracture model for concrete." *Journal of engineering mechanics* 111, no. 10 (1985): 1227-1241.
7. **Khaloo, Alireza, Mohammad Hossein Mobini, and Payam Hosseini**. "Influence of different types of nano-SiO2 particles on properties of high-performance concrete." *Construction and Building Materials* 113 (2016): 188-201.
8. **Lam, Thanh Quang Khai, Thi My Dung Do, V. T. Ngo, and Trong Chuc Nguyen**. "Increased plasticity of nano concrete with steel fibers." *Magazine of civil engineering* 1 (93) (2020): 27-34.
9. **Mahender, Billa, and R. Ashok.** "Effect of Nano Silica on the Compressive Strength of Concrete." *International Journal of Professional Engineering Studies* 8, no. 2 (2017): 222-226.
10. **Mechtcherine, V., and H. S. Müller.** "Fracture behaviour of high-performance concrete." In *Finite Elements in Civil Engineering Applications*, pp. 35-43. CRC Press, 2021.
11. **Mendes, Thiago Melanda, and Wellington L. Repette**. "Effect of nano-silica on Portland cement matrix." *Revista IBRACON de Estruturas e Materiais* 12 (2019): 1383-1389.
12. **Mindess, S.** "Applications of Fracture Mechanics to Concrete: Where Do We Go From Here?." *Special Publication* 206 (2002): 475-486.
13. **Quercia, G., A. Lazaro, J. W. Geus, and H. J. H. Brouwers.** "Characterization of morphology and texture of several amorphous nano-silica particles used in concrete." *Cement and Concrete Composites* 44 (2013): 77-92.
14. **Rakesh, Pawan Kumar, Apurbba Kumar Sharma, and Inderdeep Singh**. *Advances in Engineering Design*. Singapore: Springer Singapore, 2021.
15. Recommendation, RILEM Draft. "Determination of the fracture energy of mortar and concrete by means of three-point bend tests on notched beames." Materials and structures 18, no. 106 (1985): 285-290.
16. **Sivasankaran, Usha, Seetha Raman, and S. Nallusamy.** "Experimental analysis of mechanical properties on concrete with nano silica additive." *Journal of nano research* 57 (2019): 93-104.
17. **Torabian Isfahani, Forood, Elena Redaelli, Federica Lollini, Weiwen Li, and Luca Bertolini.** "Effects of nanosilica on compressive strength and durability properties of concrete with different water to binder ratios." *Advances in Materials Science and Engineering* 2016, no. 1 (2016): 8453567.
18. **Van Mier, Jan GM.** *Concrete fracture: a multiscale approach*. CRC press, 2012.
19. **Vivek, D., K. S. Elango, R. Saravanakumar, B. Mohamed Rafek, P. Ragavendra, S. Kaviarasan, and E. Raguram.** "Effect of nano-silica in high performance concrete." *Materials Today: Proceedings* 37 (2021): 1226-1229.
20. **Zhang, Peng, Jinyi Wan, Kejin Wang, and Qingfu Li.** "Influence of nano-SiO2 on properties of fresh and hardened high performance concrete: A state-of-the-art review." *Construction and Building Materials* 148 (2017): 648-658.
21. **Zhang, Peng, Ya-Nan Zhao, Qing-Fu Li, Tian-Hang Zhang, and Peng Wang.** "Mechanical properties of fly ash concrete composite reinforced with nano-SiO 2 and steel fibre." *Current science* (2014): 1529-1537.

СПИСОК ЛИТЕРАТУРЫ

1. **AlKhatib, Anas, Mohammed Maslehuddin, and Salah Uthman Al-**

Dulaijan. "Development of high performance concrete using industrial waste materials and nano-silica." *Journal of Materials Research and Technology* 9, no. 3 (2020): 6696-6711.
2. **Bianchi, G. Quercia.** "Application of nano-silica in concrete." (2014).
3. **Chithra, Sankar, SRR Senthil Kumar, and K. Chinnaraju**. "The effect of Colloidal Nano-silica on workability, mechanical and durability properties of High Performance Concrete with Copper slag as partial fine aggregate." *Construction and Building Materials* 113 (2016): 794-804.
4. **Einsfeld, Ricardo A., and Marta SL Velasco.** "Fracture parameters for high-performance concrete." *Cement and Concrete Research* 36, no. 3 (2006): 576-583.
5. Fédération-internationale-du-béton, T. G. "Constitutive modelling of high strength/high performance concrete." *Bulletin (Fédération internationale du béton) Lausanne, Switzerland* (2008): 125.
6. **Jenq, Yeoushang, and Surendra P. Shah.** "Two parameter fracture model for concrete." *Journal of engineering mechanics* 111, no. 10 (1985): 1227-1241.
7. **Khaloo, Alireza, Mohammad Hossein Mobini, and Payam Hosseini**. "Influence of different types of nano-SiO2 particles on properties of high-performance concrete." *Construction and Building Materials* 113 (2016): 188-201.
8. **Lam, Thanh Quang Khai, Thi My Dung Do, V. T. Ngo, and Trong Chuc Nguyen**. "Increased plasticity of nano concrete with steel fibers." *Magazine of civil engineering* 1 (93) (2020): 27-34.
9. **Mahender, Billa, and R. Ashok.** "Effect of Nano Silica on the Compressive Strength of Concrete." *International Journal of Professional Engineering Studies* 8, no. 2 (2017): 222-226.
10. **Mechtcherine, V., and H. S. Müller.** "Fracture behaviour of high-performance concrete." In *Finite Elements in Civil Engineering Applications*, pp. 35-43. CRC Press, 2021.
11. **Mendes, Thiago Melanda, and Wellington L. Repette**. "Effect of nano-silica on Portland cement matrix." *Revista IBRACON de Estruturas e Materiais* 12 (2019): 1383-1389.
12. **Mindess, S.** "Applications of Fracture Mechanics to Concrete: Where Do We Go From Here?." *Special Publication* 206 (2002): 475-486.
13. **Quercia, G., A. Lazaro, J. W. Geus, and H. J. H. Brouwers.** "Characterization of morphology and texture of several amorphous nano-silica particles used in concrete." *Cement and Concrete Composites* 44 (2013): 77-92.
14. **Rakesh, Pawan Kumar, Apurbba Kumar Sharma, and Inderdeep Singh**. *Advances in Engineering Design*. Singapore: Springer Singapore, 2021.
15. Recommendation, RILEM Draft. "Determination of the fracture energy of mortar and concrete by means of three-point bend tests on notched beames." Materials and structures 18, no. 106 (1985): 285-290.
16. **Sivasankaran, Usha, Seetha Raman, and S. Nallusamy.** "Experimental analysis of mechanical properties on concrete with nano silica additive." *Journal of nano research* 57 (2019): 93-104.
17. **Torabian Isfahani, Forood, Elena Redaelli, Federica Lollini, Weiwen Li, and Luca Bertolini.** "Effects of nanosilica on compressive strength and durability properties of concrete with different water to binder ratios." *Advances in Materials Science and Engineering* 2016, no. 1 (2016): 8453567.
18. **Van Mier, Jan GM.** *Concrete fracture: a multiscale approach*. CRC press, 2012.
19. **Vivek, D., K. S. Elango, R. Saravanakumar, B. Mohamed Rafek, P.**

Ragavendra, S. Kaviarasan, and E. Raguram. "Effect of nano-silica in high performance concrete." *Materials Today: Proceedings* 37 (2021): 1226-1229.

20. **Zhang, Peng, Jinyi Wan, Kejin Wang, and Qingfu Li.** "Influence of nano-SiO2 on properties of fresh and hardened high performance concrete: A state-of-the-art review." *Construction and Building Materials* 148 (2017): 648-658.
21. **Zhang, Peng, Ya-Nan Zhao, Qing-Fu Li, Tian-Hang Zhang, and Peng Wang.** "Mechanical properties of fly ash concrete composite reinforced with nano-SiO 2 and steel fibre." *Current science* (2014): 1529-1537.

Kalpesh Laljibhai Kapadiya – Research Scholar, Department of Civil Engineering, R. K. University, Rajkot, Gujarat, India, kalpeshlaljibhaikapadiya55@gmail.com

Dr. Sanjay Joshi – 2Professor, Department of Civil Engineering, R. K. University, Rajkot, Gujarat, India, sanjayjoshi9837@gmail.com

Dr. Ajaysinh Vaghelas – Assistant Professor, Department of Civil Engineering, R. K. University, Rajkot, Gujarat, India, ajaysinhvaghelas585@gmail.com

Parag Rameshbhai Savsani – Assistant Professor, Department of Civil Engineering, Dr. Subhash University, Junagadh, Gujarat, India, paragrameshbhaisavsani2@gmail.com

Калпеш Лалджибхай Кападия – Научный сотрудник, факультет гражданского строительства, Университет Р.К., Раджкот, Гуджарат, Индия, kalpeshlaljibhaikapadiya55@gmail.com

Санджай Джоши – Профессор, кафедра гражданского строительства, Университет Р. К., Раджкот, Гуджарат, Индия, sanjayjoshi9837@gmail.com

Аджайсинх Вагелас – Профессор, кафедра гражданского строительства, Университет Р. К., Раджкот, Гуджарат, Индия, ajaysinhvaghelas585@gmail.com

Параг Рамешбхай Савсани – Доцент, факультет гражданского строительства, Университет доктора Субхаша, Джунагадх, Гуджарат, Индия, paragrameshbhaisavsani2@gmail.com

DOI:10.22337/2587-9618-2024-20-4-105-118

THE STIFFNESS OF STEEL-PLATE COMPOSITE STRUCTURES FOR SHORT-TERM LOADS

Vladimir I. Travush [1], Denis V. Konin [2], Alexey S. Krylov [2], Mikhail A. Desyatkin [3], Andrey N. Ivaschenko [3]

[1] Gorproject, Moscow, RUSSIA
[2] JSC Research Center of Construction TSNIISK named after V.A. Koucherenko, Moscow, RUSSIA
[3] Inforsproekt, Moscow, RUSSIA

Abstract: The features of the behavior of steel-plate composite walls for static short-term loads are considered. Based on the analysis of modern technical and regulatory documentation, the rationale for the chosen research topic is given. A review of the literature is performed, and the features of development are noted. Description and features of the experimental structures are presented. Analytical and numerical calculations of structures for central compression have been performed. A description of the calculation complex is presented; a description of numerical models, features of their construction and calculation are given. Calculation results are presented – features of changes in structural rigidity during load application. The general types of experimental models tested for central compression are presented, and the destruction pattern is shown. The analysis of the experimental data obtained and their comparison with analytical and numerical calculations are performed. An assessment of the features of modeling steel-plate composite structures in software complexes is given.

Keywords: concrete, steel, reinforced concrete, composite steel and concrete structure, steel-plate reinforcement, steel-plate composite (SC) walls, adhesion, stud

ЖЕСТКОСТЬ СТАЛЕЖЕЛЕЗОБЕТОННЫХ КОНСТРУКЦИЙ С ЛИСТОВЫМ АРМИРОВАНИЕМ ПРИ ДЕЙСТВИИ КРАТКОВРЕМЕННЫХ НАГРУЗОК

В.И. Травуш [1], Д.В. Конин [2], А.С. Крылов [2], А.Н. Иващенко [3], М.А. Десяткин [3]

[1] ЗАО «ГОРПРОЕКТ», г. Москва, РОССИЯ
[2] Центральный научно-исследовательский институт строительных конструкций (ЦНИИСК) имени В.А. Кучеренко АО «НИЦ «Строительство», г. Москва, РОССИЯ
[3] ООО «Инфорспроект», г. Москва, РОССИЯ

Аннотация: Рассмотрены особенности работы сталежелезобетонных конструкций с листовым армированием при воздействии кратковременных нагрузок. Дано обоснование выбранной темы исследования на основе анализа современной технической и нормативной документации. Выполнен обзор литературы, отмечены особенности развития вопроса. Представлено подробное описание и особенности исследуемых конструкций. Выполнены аналитические и численные расчеты конструкций на центральное сжатие. Представлено описание расчетного комплекса; дано описание численных моделей, особенности их построения и расчета, приведены результаты расчетов – характер изменения жесткости конструкций в процессе приложения нагрузки. Представлены общие виды экспериментальных моделей, испытанных на центральное сжатие, приведена картина разрушения. Выполнен анализ полученных экспериментальных данных, их сравнение с аналитическими и численными расчетами. Дана оценка особенностей моделирования сталежелезобетонных конструкций с листовым армированием в программных комплексах.

Ключевые слова: бетон, сталь, железобетон, сталежелезобетонная конструкция, листовое армирование, композитные стены с листовым армированием, сцепление, анкерное устройство

INTRODUCTION

It is essential to properly determine longitudinal deformations and stiffnesses of the elements in the walls of high-rise buildings, where the elements are subjected to significant compression forces under the action of long-term and short-term loads. The influence of longitudinal deformations in multi-storey and high-rise buildings can affect the drift of the frame cells, which should have deformations no greater than those specified in SP 20.13330 and clause 8.2.4.16 of SP 267.1325800 “High rise buildings and complexes. Design rules” which allow displacements of 1/300 of the height of this building.

Cell drift is calculated by the formula $f_1/h_s + f_2/l$, where f_1 and f_2 are the horizontal and vertical displacement, respectively, and h_s and l are the height of the cell and its span (Figure E.3 in SP 20.13330 "Loads and actions"). Since there is no experimentally and theoretically substantiated methodology for calculating the stiffness of steel-reinforced concrete (composite) structures with sheet reinforcement, as well as the actual experience of building construction using such systems, it is practically impossible to reliably determine the values of controlled vertical and horizontal deformations of the entire building frame and its individual elements that are permissible for a particular structure.

The papers [1, 2] present the results of tests of eccentrically compressed steel-reinforced concrete elements with a percentage of longitudinal reinforcement from 3 to 20, made with concrete of compressive strength class up to B90 and fiber concretes. These articles, as well as in [3], provide the results of tests and calculations for the first group of limit states in detail. The paper [4] analyzes domestic and foreign experience in studying the performance of steel-reinforced concrete structures in eccentric compression. The issues of structural performance in compression are also considered in [5, 6].

Extensive studies of steel-reinforced concrete structures with sheet reinforcement have been carried out by foreign authors in Japan [7, 8], South Korea [9...14] and China [15...17]. In these studies, a comprehensive assessment of the performance of structures with sheet reinforcement was performed, as well as experimental and theoretical results and design recommendations were given.

There is an important description of the features of modeling and calculation of the considered structures in the software complexes [18] in addition to the available experimental and theoretical information on the operation of structures, discussed above. In calculations of the frames of unique buildings and structures involving steel-reinforced concrete components, certified software packages that implement the finite element method are used. Composite columns and walls, as a rule, are modeled by beam and shell finite elements of reduced stiffness, less often - by solid finite elements for separate nodes. The capability of such an approach requires a certain justification, which is presented in this paper based on the experimental study of R&D “Experimental and numerical studies for the development of recommendations for the calculation, design, construction and erection of steel-reinforced concrete structures with external sheet reinforcement...”. The results of studies devoted to the assessment of stiffness and deformability of high-strength concrete [19, 20] were taken into account when analyzing the obtained data.

The presented experimental and theoretical data were obtained for structures with the percentage of reinforcement - 2.5...5.0 % and are correct provided that the design requirements for sheet reinforcement and stad-bolts are met.

METHODS

Large-scale tests of steel-reinforced concrete structures for central and eccentric compression have been carried out in the laboratories of the V.A. Kucherenko Central Research Institute of Steel and Concrete Structures. Detailed test results are given in [1, 2].

The paper [21] presents a methodology for calculating the strength of steel reinforced concrete compressed-bending elements (columns) using a nonlinear deformation model, which corresponds to the modern norms for the calculation of reinforced concrete structures - SP 63.13330. The limit state of the structure is determined by reaching the limit longitudinal deformations of concrete, reinforcement and rigid reinforcing steel. The limiting value of longitudinal strains of concrete $\varepsilon_{b,ult}$ is taken depending on the ratio of concrete edge strains $\varepsilon_1$and ε_2 by linear interpolation from -0.002 at $\varepsilon_1/\varepsilon_2 = 1$ to -0.0035 at $\varepsilon_1/\varepsilon_2 \leq 0$ (where ε_2 is the concrete strain at the most compressed edge with the minus sign). In this case, the resistance of the tensile concrete is not taken into account in the calculation. The limit value of the strain of the core steel and tensile reinforcement is assumed to be 0.025.

In current standards for the calculation of steel structures SP 16.13330 “Steel Structures”, a generalized diagram of steel deformation under load action is given for various steels. Figure 1 a, b shows the dependences “stress-relative strain” for steels from C255 to C550 in accordance with the characterisitic parameters. The ultimate strain of the steel should be taken corresponding to the end of the yield point. For steels with yield point from 255 to 550 MPa, the value of ultimate strain will vary from 0.017 to 0.047 respectively. From the above, it is obvious that it is incorrect to take the ultimate strain as 0.025 (as for rebar), irrespective of the yield strength of the steel. Since for steels C235, C245, C255 this value will correspond to the steel performance in the self-strengthening section (above the yield strength), and for steels C355 and above - will not be fully utilized plastic properties of steel.

For proper accounting of concrete strains in steel-reinforced concrete structures, it is possible to adopt several variants of diagrams of its work under load. In modern standards it is allowed to use two- and three-line diagrams (clauses 6.1.19...6.1.21 in SP 63.13330), as well as curvilinear diagram of concrete deformation (Appendix D in SP 63.13330), which is developed on the basis of the studies summarized in the monograph by Academician N.I. Karpenko [22...24]. Also, Prof. G.V. Murashkin and co-authors developed and presented in [25, 26] an exponential variant of the concrete deformation diagram. In addition to the above mentioned, it is possible to use the curvilinear diagram given in the European Union standards (Eurocode 2). In this paper, we will limit ourselves to the consideration of the three-linear (Figure 1 c) and curvilinear (Figure 1 d) diagrams, since by now they are reflected in the normative documents (SP 266.1325800.2014 “Composite steel and concrete structures. Design rules”, SP 63.13330.2018 ”Concrete and reinforced concrete structures. General provisions"), implemented in finite element software systems, tested by a large amount of experimental data and many years of experience in the design and operation of real buildings and structures.

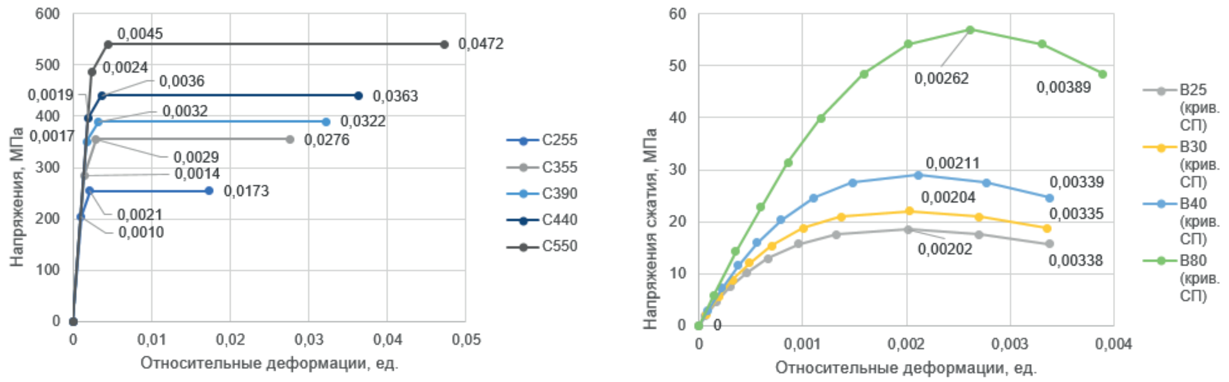

a) *b)*

<u>Figure 1.</u> Deformation diagrams of steel and concrete: a - for steel, b - curvilinear for concrete

The theoretical stiffness of a structure subjected to compression is calculated as follows: the reduction coefficients of reinforcement and sheet steel to concrete are calculated, and then the area of the reduced cross-section A_{red} is determined.

$$\alpha_{st} = \frac{E_{st}}{E_b}, \alpha_s = \frac{E_s}{E_b}, \tag{1}$$

$$A_{red} = A_b + A_{st}\alpha_{st} + A_s\alpha_s \tag{2}$$

where A_b, A_{st}, A_s are the areas of concrete, sheet and bar reinforcement, respectively.
The longitudinal stiffness of the reduced section D_a is calculated by the formula:

$$D_a = E_b A_{red} \tag{3}$$

Calculations using the above formulas allow us to estimate the value of shortening in compression and compare it with the corresponding results of numerical modeling and experimental data.

To verify the solution of the problem, the results of central compression tests of steel reinforced concrete columns with sheet reinforcement are considered. The models are prisms of 600 mm height, the cross-section is square of 150x150 mm. The material of sheet reinforcement is C345 steel. Concrete of the models has different compressive strength of class B100, B60, B30. Concrete mix of class B30, B60 is made on basalt crushed stone with increased deformation characteristics (relative to the normative indicators). Concrete of compressive strength class B100 has an increased modulus of elasticity - not less than 50 GPa. Longitudinal reinforcement is A500C class, transverse reinforcement is A500C class.
To ensure that the sheet reinforcement cooperates with concrete, the installation of restraints in the form of bolts with a spacing of 40 mm is provided. A general view of the steel core and the location of the restraints is shown in Figure 2. Characteristics of the tested models are given in Table 1.

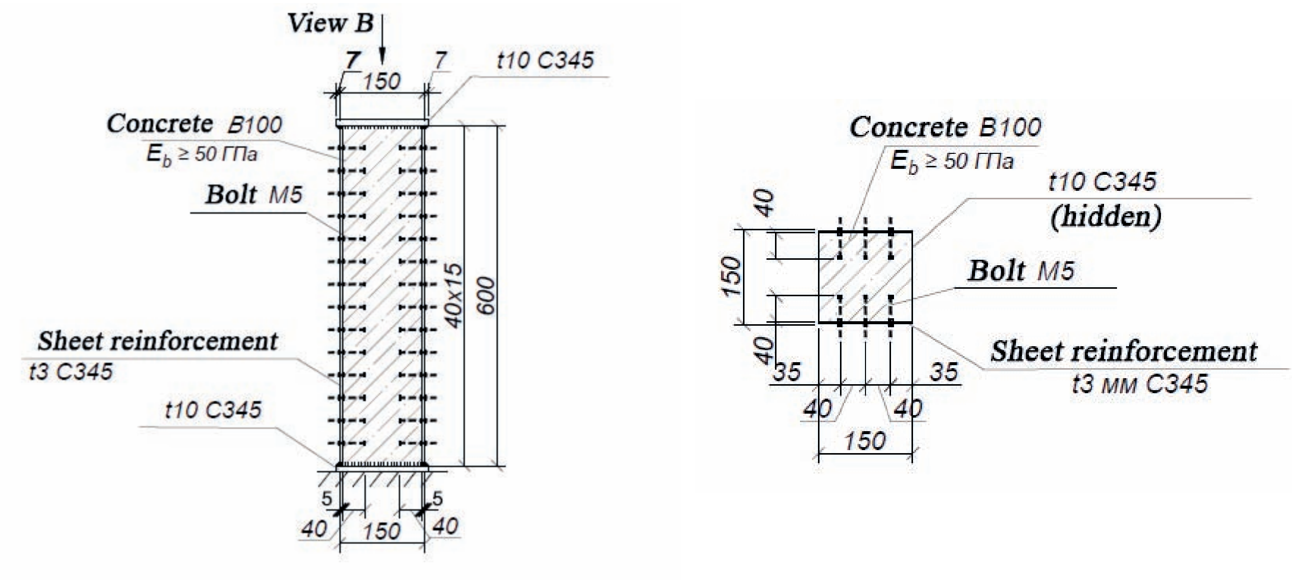

a) General view b) cross-section

Figure 2. General view of the tested experimental models

Table 1. Characteristics of the experimental models

No	Quantity, pcs	Scheme	μ, % reinforcement ratio	Steel class of sheets	Concrete compressive strength class	h, cm	b, cm	L, cm
1	3	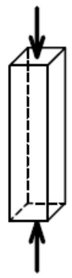	4,67	C345	B30	15	15	60
2	3		4,67	C345	B60	15	15	60
3	3		4,67	C345	B100 ($E_b \geq$ 50 GPa)	15	15	60

Note:
μ is the reinforcement ratio, equal to the ratio of the area of steel in the cross-section to the area of concrete; h,b are the dimensions of the cross-section of the concrete part, L is the length of the model, along the axis of which the external load is transferred.

The tests were carried out on a calibrated hydraulic press MAN1000 (Germany), simulating axial load up to 1000 tf (10 MN) in V.A. Kucherenko Central Research Institute for Structural Engineering. Loading was carried out according to GOST 8829-2018 “Prefabricated construction concrete and reinforced concrete products. Load testing methods. Rules for assessment of strength, rigidity and crack resistance” in stages of not more than 10% of the failure load. “Central” compression of the model was ensured by centering the column model relative to the markings on the press tabletops, as well as by controlling the readings of sensors at the first stages of loading. If a significant difference in deformations was revealed, the model was additionally leveled relative to the press table. During testing of models under stepwise application of compressive load, the magnitude of applied load, vertical absolute shortening of models (by means of displacement sensors) were recorded at each step. The presented models were tested within the framework of R&D “Experimental and numerical studies for the development of recommendations on calculation, design, construction and erection of steel-reinforced concrete structures with external sheet reinforcement...”. It is important to note that in order to confirm the correctness of the calculation of the total stiffness of the steel-reinforced concrete element, it is necessary to accurately measure its longitudinal deformations at all stages of loading. In this case, it is necessary to exclude random factors of non-uniform load transfer, non-uniform load absorption by steel and concrete. Therefore, to investigate the stiffness, we analyzed models that are equipped with accurate strain gauges with the possibility of averaging values over the cross section, as well as those tested under “accurate” central compression with spherical press table supports to exclude “clamping” of individual fibers of the structure.

Numerical modeling by the finite element method was performed in the ATENA software package for models similar in size and material properties, taking into account the nonlinear performance of materials: a curvilinear diagram for concrete and a three-linear diagram for steel. The number of steps and mesh size for each model was also selected individually. The minimum number of loading steps was at least 20 and the mesh size was about 20 mm. The Fracture-Plastic Constitutive Model (CC3DCementitious2) material model, which is based on the combination of the tensile fracture model with the compressive fracture model of the material, was used to describe the performance of the concrete. The characteristics of the FE models fully replicated the experimental specimens and were consistent with the data shown in Figure 2 and Table 1. Structures with contact interaction between steel and concrete were also modeled. It was found that for models with small or zero eccentricities, the presence of finite contact interaction at the steel-concrete joint has little or no effect on the longitudinal strain results. The general view of numerical models and some results of calculations for models made of high-strength concrete are shown in Figures 3, 4. The general view and characteristic failure of the experimental models are shown in Figure 5.

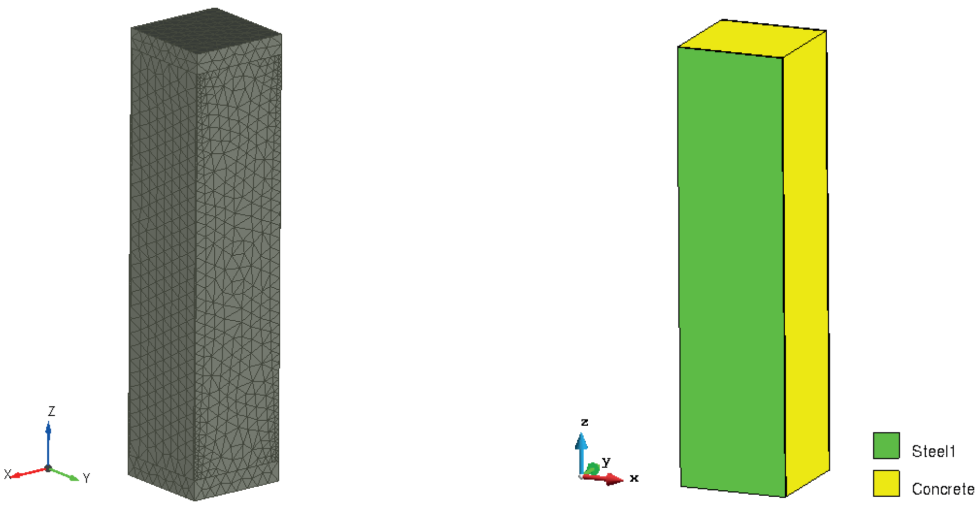

Figure 3. General view of numerical models

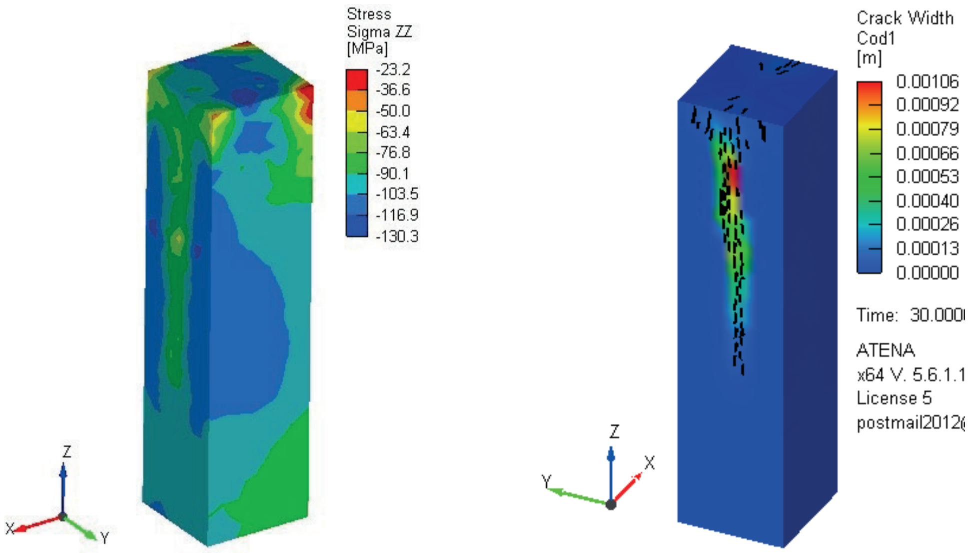

a) stresses in concrete models along Z axis, MPa

b) deformed structure with cracks, crack opening width, m

Figure 4. Calculation results

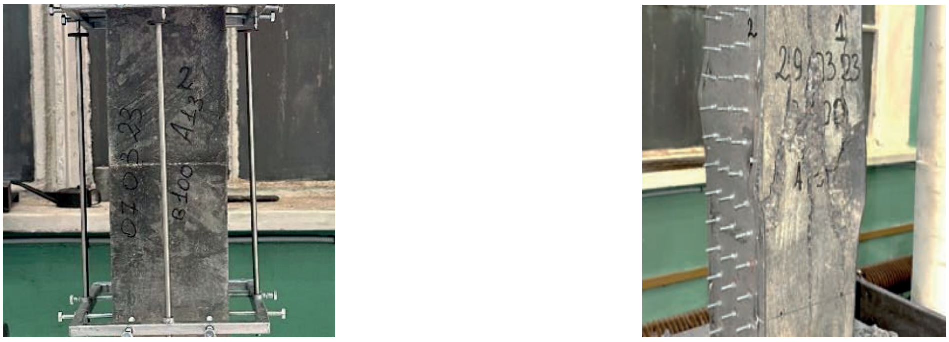

a) general view of the model *b) characteristic failure*

Figure 5. General view and characteristic failure of the model made of high-strength concrete

3 RESULTS AND ANALYSIS

The results of comparison of theoretical, numerical calculations and experimental data for the changes in longitudinal stiffness of centrally compressed structures are shown in Figure 6. The stiffness of the structures was determined taking into account the short-term action of loads according to SP 63.13330, the concrete deformation modulus was assumed to be E_{b1}=0.85E_b. Comparison of models was performed in dimensionless coordinate by force, as it is required to compare theoretical calculation, in which characteristic values of strength and deformation properties of materials are utilized. The experimental data, in which values of actual failure loads are overestimated in relation to characteristic values. That is, one of the coordinates of the graphs was the value N/N_u, where N is the current compressive load during tests or calculations, and N_u is the ultimate design compressive load, which is calculated by the formula:

$$N_u = R_b A_b + R_y A_{st} + R_s A_s \ , \qquad (6)$$

where $R_b, R_y,\ R_s$ are the design values of concrete compressive strength, steel strength, design strength of reinforcement, respectively.

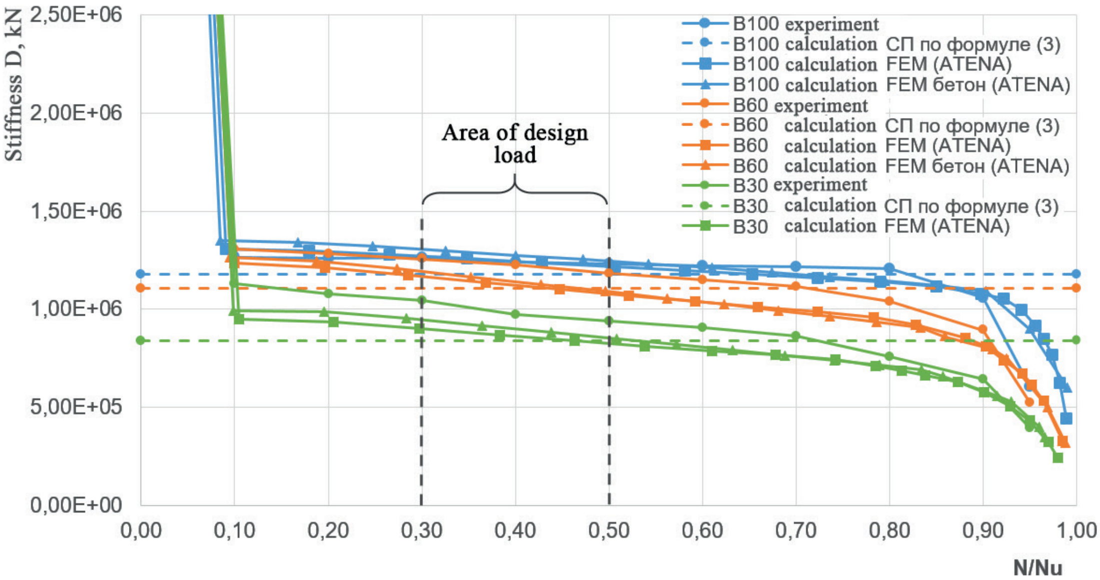

Figure 6. Changes in column stiffness during loading (for all types of specimens and concrete classes)

Figure 6 clearly shows the trend of stiffness drop as the structure approaches failure, and at the last stage of loading the stiffness tends to zero. It can also be noted that the stiffness drops as the compressive strength class of concrete decreases, which can be explained by a similar decrease in the elastic modulus of the material. A significant drop in stiffness for all the studied specimens was observed at loads above 80% of the failure load. Moreover, for low-strength concrete, stiffness starts to decrease somewhat earlier than for high-strength concrete as it approaches failure. Experimental data coincide well with numerical calculations. For high-strength concrete, the difference in stiffnesses is within 1.5%. Comparison of experimental and calculated data for the studied specimens is given in Table 2. The calculated characteristic stiffnesses of the structures (dashed lines in Figure 6) have a satisfactory coincidence with the stiffnesses obtained experimentally and numerically, and the characterisric stiffness curves are slightly underestimated. This can be explained by the use of non-standard concrete with moduli of elasticity different from the characteristic ones.

Table 2. Comparison of experimental and calculated data for the studied specimens

Parameter	Experiment	Numerical calculation	Difference, %
Prisms, concrete B100			
Stiffness at design loads	1229381,4	1220861,9	0,69
Reduced stiffness at design loads	1229381,4	1244345,7	1,2
Prisms, concrete B60			
Stiffness at design loads	1184924,8	1079326,9	9,7
Reduced stiffness at design loads	1184924,8	1090418,4	8,6
Prisms, concrete B30			
Stiffness at design loads	938902,3	826346,6	13,6
Reduced stiffness at design loads	938902,3	854559,3	9,8

To illustrate the possibility of using the approach implemented in SP63.13330 and SP 266.1325800 to determine the stiffness, where the characteristics of the cross-section of the element are introduced into the calculation, a computational comparison was performed. A structure completely similar to the experimental model was modeled, including concrete and steel cladding sheets on both sides. The calculations were performed in the solid formulation using the finite element method, taking into account the nonlinear performance of materials. A similar calculation was also performed for the structure with reduced concrete performance. Comparing the results of the calculation for the actual structure and the structure with the reduced characteristics, a complete match was obtained (see Figure 9).

Having a good confirmation of the possibility to use in the calculations of real steel and reinforced concrete structures with sheet reinforcement the reduced cross-sectional characteristics, the calculation of a section of a real structure the wall of the stiffening core with a thickness of 2 m, made of high-strength concrete of compressive strength class B100 was performed. The calculation was also performed in two variants: for the actual element, taking into account the presence of sheet and bar reinforcement, studs and stad bolts, and for the equivalent cross-section reduced to concrete. The general view of the numerical models and individual calculation results are shown in Figures 7, 8. Calculation results as a comparison of graphs of change in longitudinal stiffness of structures in dimensionless coordinates by load are presented in Figure 9.

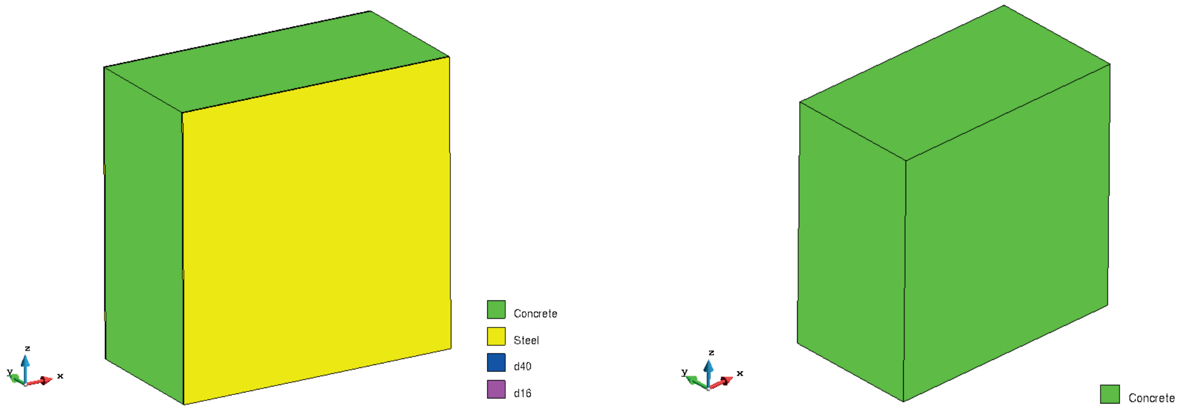

a) model similar to the physical structures *b) specified model*

Figure 7. General view of numerical models

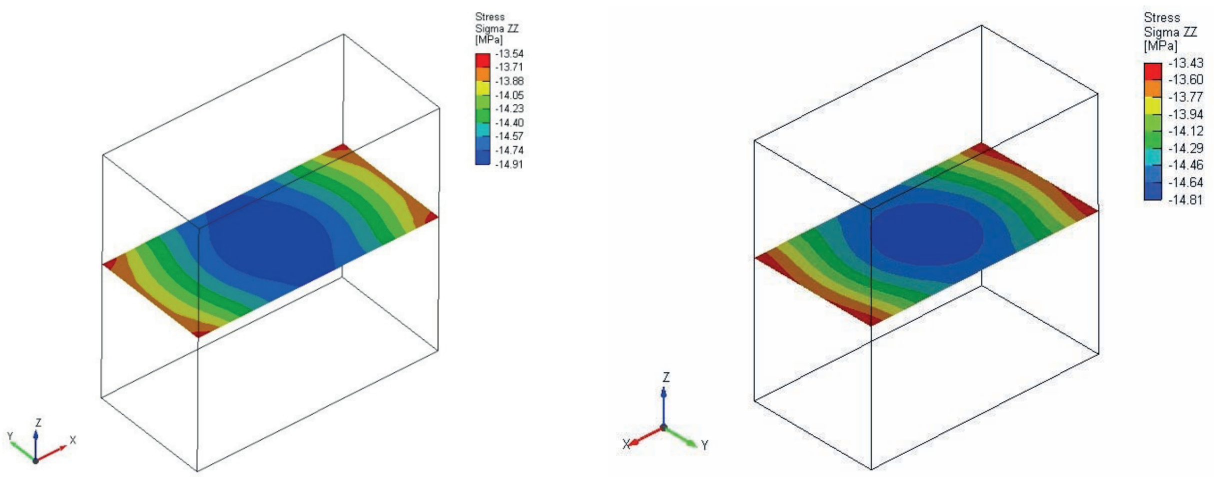

a) stresses in concrete models along Z axis, MPa *b) stresses in concrete models along Z axis, MPa*

Figure 8. Results of calculations

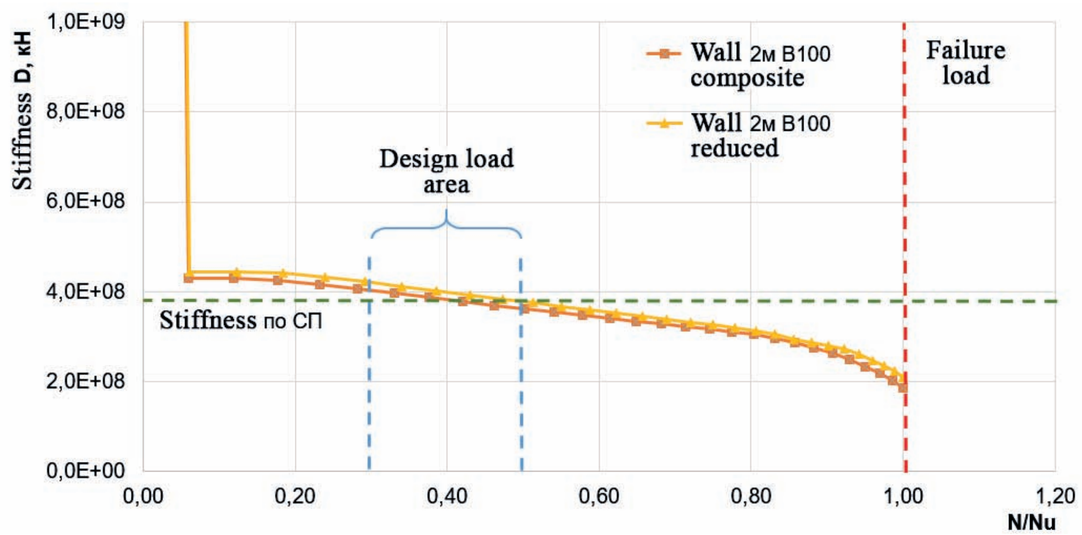

Figure 9. Variation of stiffness of steel-reinforced concrete wall with sheet reinforcement during loading process

Analysis of the obtained results, presented in Figure 12, has shown a good convergence of the calculated data with a difference of 5%. The insignificant difference can be explained by the presence of the volumetric stress state when the material performs in a complex massive structure. Summarizing the performed experimental, theoretical and numerical studies, it is possible to note the validity of the existing normative calculation methods in relation to the considered steel-reinforced concrete structures with sheet reinforcement. Performing complex calculation schemes with a large number of finite elements, it is possible to recommend the introduction of the reduced stiffness characteristics of structures into the calculation. As it was shown above, such an assumption does not introduce a significant error when analyzing the calculation results.

CONCLUSIONS

1. The peculiarities of stiffness changes in structures with sheet reinforcement under short-term loads have been evaluated. The presented experimental and theoretical data are obtained for structures with the percentage of reinforcement - 2.5...5.0 % and are valid under the condition of compliance with the design requirements for sheet reinforcement and stud-bolts..
2. A comparison has been made of “experiment - FE model - formulaic calculation” for the tested models and “verified FE model of a real wall from a building structure with nonlinear materials - FE model with reduced to concrete characteristics” for a real designed wall. The comparison results show that the numerical and experimental models have almost the same load-stiffness diagrams. The difference of stiffness values obtained by formula (3) for high-strength concrete according to the experimental and FE models is not more than 8% in the load range of 0.4-0.5 N/Nu (which corresponds to the design load range).
3. Good agreement of the experimental data with the results of numerical and theoretical calculations is ensured, among other things, due to the uniform inclusion in the operation of the sheet reinforcement located at the opposite edges of the cross-section, by installing a sufficient number of flexible stops (stad-bolts) and compliance with the structural requirements in the design of experimental models.
4. The use of reduced cross-sectional characteristics in the stress region, which corresponds to the design stresses, gives the same deformation results as those obtained by solid FE calculations with nonlinear material characteristics.
5. The possibility of simplified modeling of steel-reinforced concrete structures with sheet reinforcement (only concrete section with the given characteristics) in the general calculation of the building without compromising the accuracy of the deformation calculation of the whole structure is confirmed.

REFERENCES

1. **Travush V.I.** Experimental Investigations of Steel-Reinforced Concrete Structures Operating in Eccentric Compression [Text]. - Travush V.I., Konin D.V., Rozhkova L.S., Krylov A.S., Kaprielov S.S., Chilin I.A., Fimkin A.I. - Academia. Architecture and Construction. 2016. № 3. - Pp. 127-135.
2. **Travush V.I.** Determination of the shear bearing capacity of the contact surface “steel-concrete” in steel-reinforced concrete structures for concrete of different compressive strength and fiber concrete [Text]. - Travush V.I., Kaprielov S.S., Konin D.V., Krylov A.S., Kashevarova G.G., Chilin I.A. - Building and Reconstruction. - 2016, №4 (66). - Pp. 45-55.
3. **Travush V.I.** Calculation of a steel reinforced concrete column of a high-rise building for oblique off-centered

compression [Text]. - Desyatkin M.A., Konin D.V., Martirosyan A.S., Travush V.I. - Housing construction. - 2015. № 5. - Pp. 92-95.

4. **Travush V.I.** Domestic and foreign experience of research of steel-reinforced concrete structures operation on off-center compression [Text]. - Travush V.I., Rozhkova L.S., Krylov A.S. - Building and reconstruction. - 2016, №5. - C. 31-44.
5. **Arleninov P.D.** Deformation and stability of compressed and eccentrically compressed rod reinforced concrete elements with account of creep and cracking [Text]. - Candidate's thesis, JSC "SIC 'Construction' (A.A. Gvozdev Research Institute of Reinforced Concrete). - 2016. - 143 p.
6. **Krylov S.B.** Critical force for reinforced concrete rod elements [Text]. - Academia. Architecture and Construction. - 2012. №2. - pp. 136-138.
7. **Takeuchi M., Narikawa M., Matsuo I., Hara, K. and Usami S**. (1998) Study on a Concrete Filled Structure for Nuclear Power Plants. *Nuclear Engineering and Design*, vol. 179, no 2, pp. 209–223.
8. **Takeuchi M., Fujita F., Funakoshi A., Shohara R., Akira S. and Matsumoto R.** (1999) Experimental Study on Steel Plate Reinforced Concrete Structure, Part 2: Response of SC Members Subjected to Out-of-Plane Load (Outline of the Experimental Program and the Results). *Proceedings of the Annual Conference of Architectural Institute of Japan, (in Japanese)*, pp. 1.037–1.038.
9. **Moon I.H., Kim S.M., Kim W.B. and Kim W.K.** (2007) The Use of Steel Plate Concrete for Structural Module of NPP Structures, Journal of the Korean Society of Steel Construction (in Korean), vol. 19, no. 2, pp 740–745.
10. **Moon I.H., Kim T.Y. and You S.T.** (2008) Nuclear Power Plant Structure and SC Structure Design, Journal of the Korean Society of Steel Construction (in Korean), vol. 20, no. 2, pp. 14–23.
11. **Kim W.B. and Kim W.K.** (2008) Status and Background in Developing SC Structure Specifications for Nuclear Power Plants, Journal of the Korean Society of Steel Construction (in Korean), vol. 20, no. 2, pp. 9–13.
12. **Lee U.W., Kim K.K., Mun T.Y. and Sun W.S.** (2008) Nuclear Power Plant Construction and SC Structures, Journal of the Korean Society of Steel Construction (in Korean), vol. 20, no. 2.
13. **Lee S.J., Choi B.J. and Kim T.K**. (2009) An Experimental Study on the Behavior of Steel Plate Concrete Wall with Vertical Ribs, Journal of the Korean Society of Steel Construction (in Korean), vol. 21, no. 3, pp. 277–287.
14. **Hong S., Kim W., Lee K., Hong N.K. and Lee D.** (2009) Out-of-Plane Shear Strength of Steel Plate Concrete Walls Dependent on Bond Behavior, Transactions of the 20th International Conference on Structural Mechanics in Reactor Technology, SMiRT-20, Div-6: Paper 1,855, Espoo, Finland, IASMIRT, North Carolina State University, Raleigh, NC, pp. 1–10.
15. **Song X., Chu M., Ge H. and Wang H.** (2014) A Failure Criterion for Steel-Concrete Composite Walls. Sustainable Development of Critical Infrastructure, ASCE, pp. 324–331.
16. **Leng Y.-B., Song X.-B., Chu M. and Ge H.-H.** (2015) Experimental Study and Theoretical Analysis of Resistance of Steel-Concrete-Steel Sandwich Beams. Journal of Structural Engineering, ASCE, vol. 141, no. 2.
17. **Leng Y.-B., Song X.-B. and Wang H.-L.** (2015) Failure Mechanism and Shear Strength of Steel-Concrete-Steel Sandwich Deep Beams, Journal of Constructional Steel Research, vol. 106, pp. 89–98.
18. **Arleninov, P.D.** Analysis of different methods of calculation schemes creation at computer modeling of load-bearing

structures // BST: Bulletin of Building Technology. - №5(969). - 2015 - Pp.58-59.
19. **Bezgodov, I.** Relationship between strength and deformation characteristics of high-strength self-compacting concrete / Bezgodov, I., Kaprielov, S., & Sheynfeld, A. // International Journal for Computational Civil and Structural Engineering. – 2022. №18(2), pp. 175–183.
20. **Kaprielov, S.** Control of heavy concrete characteristics affecting structural stiffness / Kaprielov, S., Sheinfeld, A., Selyutin, N. // International Journal for Computational Civil and Structural Engineering. – 2022. №18(1), pp. 24–39.
21. **Mukhamediev T.A.** Calculation of strength of steel-reinforced concrete columns using deformation model [Text]. - Mukhamediev T.A., Starchikova O.I. - Concrete and Reinforced Concrete. - 2006. №4. - Pp. 18-21.
22. **Karpenko N.I.** General models of reinforced concrete mechanics [Text]. - Karpenko N.I. - M.: Stroyizdat. - 1996.- 416 p.
23. **Karpenko N.I.** About diagrammatic methodology of calculation of deformations of rod elements and its particular cases [Text]. - Karpenko N.I., Karpenko S.N. - Concrete and reinforced concrete. - 2012. №6. - Pp. 20-27.
24. **Karpenko N.I.** Analysis and improvement of curvilinear concrete deformation diagrams for calculation of reinforced concrete structures by deformation model [Text]. - Karpenko N.I., Sokolov B.S., Radaykin O.V. - Industrial and civil construction. - 2013. №1. - Pp.28-30
25. **Murashkin G.V.** Modeling of a concrete deformation diagram and a scheme of a stress-strain state [Text]. - Murashkin G.V., Murashkin V.G. - Herald of higher educational institutions. Construction. - 1997. №10. - Pp. 4-6.
26. **Mordovskiy S.S.** Stress state of experimental specimens under off-center loading [Text]. - Mordovskiy S.S., Murashkin V.G. - Modern problems of science and education. - 2012. № 4. - URL: http://science-education.ru/ru/article/view?id=6794 (date of reference: 01.03.2018).

СПИСОК ЛИТЕРАТУРЫ

1. **Травуш В.И**. Экспериментальные исследования сталежелезобетонных конструкций, работающих на внецентренное сжатие [Текст]. - Травуш В.И., Конин Д.В., Рожкова Л.С., Крылов А.С., Каприелов С.С., Чилин И.А., Фимкин А.И. - Academia. Архитектура и строительство. 2016. № 3. - С. 127-135.
2. **Травуш В.И.** Определение несущей способности на сдвиг контактной поверхности «сталь-бетон» в сталежелезобетонных конструкциях для бетонов различной прочности на сжатие и фибробетона [Текст]. - Травуш В.И., Каприелов С.С., Конин Д.В., Крылов А.С., Кашеварова Г.Г., Чилин И.А. – Строительство и реконструкция. – 2016, №4 (66). – С. 45-55.
3. **Травуш В.И.** Расчет сталежелезобетонной колонны высотного дома на косое внецентренное сжатие [Текст]. - Десяткин М.А., Конин Д.В., Мартиросян А.С., Травуш В.И. - Жилищное строительство. - 2015. № 5. - С. 92-95.
4. **Травуш В.И**. Отечественный и зарубежный опыт исследований работы сталежелезобетонных конструкций на внецентренное сжатие [Текст]. – Травуш В.И., Рожкова Л.С., Крылов А.С. – Строительство и реконструкция. – 2016, №5. – С. 31-44.
5. **Арленинов П.Д.** Деформирование и устойчивость сжатых и внецентренно сжатых стержневых железобетонных элементов с учетом ползучести и трещинообразования [Текст]. – Кандидатская диссертация, АО «НИЦ

«Строительство» (НИИЖБ им. А.А. Гвоздева). – 2016. – 143 с.
6. **Крылов С.Б.** Критическая сила для железобетонных стержневых элементов [Текст]. – Academia. Архитектура и строительство. – 2012. №2. – С. 136-138.
7. **Takeuchi M., Narikawa M., Matsuo I., Hara, K. and Usami S.** (1998) Study on a Concrete Filled Structure for Nuclear Power Plants. *Nuclear Engineering and Design*, vol. 179, no 2, pp. 209–223.
8. **Takeuchi M., Fujita F., Funakoshi A., Shohara R., Akira S. and Matsumoto R**. (1999) Experimental Study on Steel Plate Reinforced Concrete Structure, Part 2: Response of SC Members Subjected to Out-of-Plane Load (Outline of the Experimental Program and the Results). *Proceedings of the Annual Conference of Architectural Institute of Japan, (in Japanese)*, pp. 1.037–1.038.
9. **Moon I.H., Kim S.M., Kim W.B. and Kim W.K.** (2007) The Use of Steel Plate Concrete for Structural Module of NPP Structures, Journal of the Korean Society of Steel Construction (in Korean), vol. 19, no. 2, pp 740–745.
10. **Moon I.H., Kim T.Y. and You S.T**. (2008) Nuclear Power Plant Structure and SC Structure Design, Journal of the Korean Society of Steel Construction (in Korean), vol. 20, no. 2, pp. 14–23.
11. **Kim W.B. and Kim W.K**. (2008) Status and Background in Developing SC Structure Specifications for Nuclear Power Plants, Journal of the Korean Society of Steel Construction (in Korean), vol. 20, no. 2, pp. 9–13.
12. **Lee U.W., Kim K.K., Mun T.Y. and Sun W.S.** (2008) Nuclear Power Plant Construction and SC Structures, Journal of the Korean Society of Steel Construction (in Korean), vol. 20, no. 2.
13. **Lee S.J., Choi B.J. and Kim T.K.** (2009) An Experimental Study on the Behavior of Steel Plate Concrete Wall with Vertical Ribs, Journal of the Korean Society of Steel Construction (in Korean), vol. 21, no. 3, pp. 277–287.
14. **Hong S., Kim W., Lee K., Hong N.K. and Lee D**. (2009) Out-of-Plane Shear Strength of Steel Plate Concrete Walls Dependent on Bond Behavior, Transactions of the 20th International Conference on Structural Mechanics in Reactor Technology, SMiRT-20, Div-6: Paper 1,855, Espoo, Finland, IASMIRT, North Carolina State University, Raleigh, NC, pp. 1–10.
15. **Song X., Chu M., Ge H. and Wang H.** (2014) A Failure Criterion for Steel-Concrete Composite Walls. Sustainable Development of Critical Infrastructure, ASCE, pp. 324–331.
16. **Leng Y.-B., Song X.-B., Chu M. and Ge H.-H.** (2015) Experimental Study and Theoretical Analysis of Resistance of Steel-Concrete-Steel Sandwich Beams. Journal of Structural Engineering, ASCE, vol. 141, no. 2.
17. **Leng Y.-B., Song X.-B. and Wang H.-L**. (2015) Failure Mechanism and Shear Strength of Steel-Concrete-Steel Sandwich Deep Beams, Journal of Constructional Steel Research, vol. 106, pp. 89–98.
18. **Арленинов П.Д.** Анализ различных методик создания расчетных схем при компьютерном моделировании несущих конструкций // БСТ: Бюллетень строительной техники. - №5(969). – 2015 - С.58-59.
19. **Bezgodov, I.** Relationship between strength and deformation characteristics of high-strength self-compacting concrete / Bezgodov, I., Kaprielov, S., & Sheynfeld, A. // International Journal for Computational Civil and Structural Engineering. – 2022. №18(2), pp. 175–183.
20. **Kaprielov, S.** Control of heavy concrete characteristics affecting structural stiffness / Kaprielov, S., Sheinfeld, A., Selyutin, N. // International Journal for Computational Civil and Structural Engineering. – 2022. №18(1), pp. 24–39.
21. **Мухамедиев Т.А.** Расчет прочности сталежелезобетонных колонн с

использованием деформационной модели [Текст]. - Мухамедиев Т.А., Старчикова О.И. – Бетон и железобетон. – 2006. №4. – С. 18-21.

22. **Карпенко Н.И.** Общие модели механики железобетона [Текст]. – Карпенко Н.И. – М.: Стройиздат. – 1996.- 416 с.
23. **Карпенко Н.И.** О диаграммной методике расчета деформаций стержневых элементов и ее частных случаях [Текст]. – Карпенко Н.И., Карпенко С.Н. – Бетон и железобетон. – 2012. №6. – С. 20-27.
24. **Карпенко Н.И**. Анализ и совершенствование криволинейных диаграмм деформирования бетона для расчета железобетонных конструкций по деформационной модели [Текст]. – Карпенко Н.И., Соколов Б.С., Радайкин О.В. – Промышленное и гражданское строительство. – 2013. №1. – С.28-30
25. **Мурашкин Г.В.** Моделирование диаграммы деформирования бетона и схемы напряженно-деформированного состояния [Текст]. – Мурашкин Г.В., Мурашкин В.Г. – Известия высших учебных заведений. Строительство. – 1997. №10. – С. 4-6.
26. **Мордовский С.С.** Напряжённое состояние экспериментальных образцов при внецентренном нагружении [Текст]. - Мордовский С.С., Мурашкин В.Г. – Современные проблемы науки и образования. – 2012. № 4. - URL: http://science-education.ru/ru/article/view?id=6794 (дата обращения: 01.03.2018).

Travush V.I., GORPROJECT, Moscow. Doctor of technical Sciences, Professor. Chief designer, Deputy General Director on scientific work. Vice-President of Russian Academy of Architecture and Construction Sciences, 105064, Nizhnyi Susal’nyi lane 5/5A, Moscow, Russia, e-mail: travush@mail.ru

Desyatkin M.A, Chief Structural Engineer LLC "Inforsproekt", 115280, 19, Leninskaya Sloboda str., Moscow, Russia, e-mail: mdesyatkin@mail.ru

Ivashchenko A.N, Chief Structural Engineer LLC "Inforsproekt", 115280, 19, Leninskaya Sloboda str., Moscow, Russia, e-mail: a.ivaschenko@inforceproject.ru

Konin D.V., Candidate of Technical Sciences, Deputy Director for Scientific Work, Chief manager of Laboratory of High-rise Buildings and Structures of the Department of Metal Structures, Research Institute of Building Constructions (TSNIISK) Named After V. A. Koucherenko JSC Research center of Construction,109428, 6, 2nd Institutskaya str., Moscow, Russia, e-mail: konden@inbox.ru

Krylov A.S., Candidate of Technical Sciences, Leading Researcher of Laboratory of High-rise Buildings and Structures, Research Institute of Building Constructions (TSNIISK) Named After V. A. Koucherenko JSC Research center of Construction, 109428, 6, 2nd Institutskaya str., Moscow, Russia, e-mail: kryl07@mail.ru

Травуш Владимир Ильич, ЗАО «ГОРПРОЕКТ», г. Москва, Доктор технических наук, профессор. Главный конструктор, заместитель генерального директора по научной работе. Вице-президент РААСН, 105064, Москва, Нижний Сусальный переулок, д. 5, стр. 5А, e-mail: travush@mail.ru

Десяткин Михаил Александрович, главный конструктор ООО "Инфорспроект", 115280, Москва,ул. Ленинская Слобода, д. 19, e-mail: mdesyatkin@mail.ru

Андрей Николаевич Иващенко, технический директор ООО "Инфорспроект", 115280, Москва,ул. Ленинская Слобода, д. 19, e-mail: a.ivaschenko@inforceproject.ru

Денис Владимирович Конин, кандидат технических наук, заместитель Директора по научной работе, заведующий лабораторией Высотных зданий и сооружений отдела металлических конструкций, ЦНИИСК им. В.А. Кучеренко АО "НИЦ "Строительство", Москва, 2-я Институтская улица, д.6, e-mail: konden@inbox.ru

Крылов Алексей Сергеевич, кандидат технических наук, ведущий научный сотрудник лаборатории Высотных зданий и сооружений, ЦНИИСК им. В.А. Кучеренко АО "НИЦ "Строительство", Москва, 2-я Институтская улица, д.6, e-mail: kryl07@mail.ru

DESIGN AND EXPERIMENTAL STUDIES OF STRENGTHENING OF BACKWATER TYPE HYDRAULIC STRUCTURES WITH COMPOSITE MATERIALS

Oleg D. Rubin, Dmitry V. Kozlov, Anton S. Antonov, Amer Almasri, Zhang Junhao

National Research Moscow State University of Civil Engineering, Moscow, RUSSIA

Abstract: During long-term operation of hydraulic structures of sluices, retaining walls, abutments, there are non-design settlements, tilts, displacements, opening of inter-block construction joints, corrosion of working reinforcement, change in strength characteristics of concrete, which leads to a decrease in operational properties and bearing capacity. The analysis of scientific and technical documentation is presented, the results of surveys are analysed, a spatial mathematical model based on the finite element method is developed. The computational research of the stress-strain state of sluices is carried out, including taking into account the reinforcement with prestressed basalt-composite reinforcement. The scheme of reinforcement of sluice walls has been justified by calculation. In experimental researches the complex problem on definition of strength, deflections, width of opening of inter-block construction joints, deformations of steel and prestressed basalt-composite reinforcement of reinforced concrete structures including those exposed to water environment was solved. The conducted design and experimental studies substantiate the use of prestressed basalt-composite reinforcement as an effective method of reinforcement of retaining structures, increasing their load-bearing capacity and maintaining deflections, width of opening of interlock construction joints, deformations of steel and prestressed basalt-composite reinforcement within the limits allowed by normative documents.

Keywords: sluice walls, design and experimental studies, inter-bay construction joints, cracks, reinforcement, prestressing, basalt-composite reinforcement, transverse reinforcement, bearing capacity

РАСЧЕТНО-ЭКСПЕРИМЕНТАЛЬНЫЕ ИССЛЕДОВАНИЯ УСИЛЕНИЯ ГИДРОТЕХНИЧЕСКИХ СООРУЖЕНИЙ ПОДПОРНОГО ТИПА КОМПОЗИТНЫМИ МАТЕРИАЛАМИ

О.Д. Рубин, Д.В. Козлов, А.С. Антонов, Амер Алмасри, Чжан Цзюньхао

Национальный исследовательский Московский государственный строительный университет, Москва, РОССИЯ

Аннотация: При длительной эксплуатации гидротехнических сооружений шлюзов, подпорных стен, устоев возникают не проектные осадки, крены, перемещения, раскрытие межблочных строительных швов, коррозия рабочей арматуры, изменение прочностных характеристик бетона, что приводит к снижению эксплуатационных свойств и несущей способности. Представлен анализ научно-технической документации, проанализированы результаты обследований, разработана пространственная математическая модель на основе метода конечных элементов. Проведены расчетные исследования напряженно-деформированного состояния шлюзов, в том числе с учетом усиления предварительно напряженной базальтокомпозитной арматурой. Обоснована расчетным путем схема усиления стен шлюзов. В экспериментальных исследованиях решалась комплексная задача по определению прочности, прогибов, ширины раскрытия межблочных строительных швов, деформаций стальной и предварительно напряженной базальтокомпозитной арматуры усиления железобетонных конструкций, в том числе подвергшихся воздействию водной среды. Проведенные расчетно-экспериментальные исследования обосновывают применение предварительно напряженной базальтокомпозитной арматуры в качестве эффективного способа усиления сооружений подпорного типа, повышая их несущую способность и сохраняя прогибы, ширину раскрытия межблочных строительных швов, деформации стальной и предварительно напряженной базальтокомпозитной арматуры в допускаемых нормативными документами пределах.

Ключевые слова: стены шлюзов, расчетные и экспериментальные исследования, межблочные строительные швы, трещины, усиление, предварительное напряжение, базальтокомпозитная арматура, поперечное армирование, несущая способность

INTRODUCTION

The methodology of computational-experimental studies of strengthening with pre-stressed basalt composite reinforcement (BCR) of sluice chamber walls taking into account the actual data on the operational condition is based on finite element models of the system "structures - surrounding soil mass - base" and data of experimental studies [1-14].

Bending studies of reinforced concrete beams with basalt reinforcement (BFRP) [1] indicate that the use of BFRP is an effective way to repair and strengthen structures that have changed their performance characteristics over a period of long-term operation. BFRP repair systems provide a cost-effective alternative to conventional repair systems and materials. It is noted that BFRP reinforcement has high tensile strength and a lower modulus of elasticity than steel reinforcement. The advantages of BFRP over steel reinforcement are also noted.

It is noted that BFRP is an ideal choice for use in buildings and structures operating in water environments, including marine environments; BFRP increases the service life of reinforced concrete structures, resulting in long-term safe operation of structures.

The paper [2] presents the results of experiments in bending of prestressed beams reinforced with BFRP, including the evaluation of prestress losses. Five beams were fabricated, of which three were reinforced with 6 mm diameter BFRP prestressed to 20%, 30% and 40% of the ultimate prestress level. The prestress losses were monitored using strain gauges on the reinforcement bars. In addition, two control beams were reinforced with tensile BFRP and steel bars of the same cross-sectional area, respectively. The dimensions of all specimens were 125x200x1900 mm.

Based on the results of experiments with beams tested in bending to failure, the following conclusions are presented:

– prestressing more than 30% (of the ultimate tensile strength of the bars) of the BFRP-reinforced beams improved the performance of the beams to a level exceeding that of the steel bar-reinforced specimens;

– the ultimate deflections of prestressed beams are recorded lower compared to unstressed beams with BFRP;

– the crack opening at different values of prestressing of reinforcement bars was measured.

It should be noted that the conducted studies do not contain data on strengthening of the beams with external reinforcement system.

The aim of the research [3] was to study the flexural strength of beams reinforced with NSM (near surface mounted) technology using basalt-composite reinforcement (BFRP), and to evaluate the effectiveness of the strengthening. In addition, the near surface mounted prestressing technology (PNSM), which to some extent combines two well-known technologies "external prestressing" and "NSM", was considered.

The variables considered in this study were:

– strengthening effect (not strengthened and strengthened);

– type of composite reinforcement (BFRP and GFRP);

– strengthening method (NSM and PNSM);

– initial prestress level (30% and 50% of the ultimate tensile strength of BFRP bars);

– position of the NSM composite reinforcement (bottom and side).

The test results demonstrated the effectiveness of using BFRP beams for NSM and PNSM strengthening of RC beams. In addition, BFRP reinforcement provided an additional advantage over GFRP reinforcement for PNSM strengthening due to its higher tensile and deformation strength.

In the article [4] the options of basalt composite reinforcement (BFRP) application for strengthening of RC-beams were considered and according to the research results the conclusion was made: since BFRP have much lower bending stiffness than traditional steel reinforcement, it is necessary to use BFRP prestressing to maintain beam deflections within acceptable values.

This paper focuses on the evaluation of the failure and shear behaviour of concrete beams reinforced with prestressed BFRP in the absence of reinforcement clamps. Both experimental and numerical results (ANSYS) are presented in the paper. All tested beams showed identical failure mechanics: bending and shear. As it follows from the article, the experimental results and results obtained by numerical modelling in ANSYS are in reasonably good agreement. Thus, the research results are very useful for the development of strengthening systems for serviceable reinforced concrete structures.

In [5] the results of experimental studies of concrete beams with prestressed reinforcement are presented.

The experimental results were analysed, computational nonlinear models were created in ANSYS and a fairly good agreement between experiments and calculations was obtained in terms of the nature of fracture and numerical values of the failure load, as well as in terms of stress distribution.

The article [6] analyses the results of tests of concrete beams with prestressed basalt composite reinforcement, including those with and without external clamps. It is noted that the use of concrete beams with steel reinforcement is problematic when exposed to water and saline environments, as well as chemicals due to intensive corrosion, and therefore the use of BFRP reinforcement is necessary. In order to prevent intensive cracking in the beams it is necessary to pre-stress the BFRP reinforcement. Experiments were carried out on two beams with shear failure. The other two beams were shear reinforced with external steel clamps and collapsed in bending due to yielding of the reinforcement. In summary, it is noted that the distribution of shear force and bending moment along the length of the beam must be considered in the design of beams in order to create structures of the required strength.

It is noted in [7] that BFRP reinforcement is a new environmentally friendly construction material. In this study, the performance of concrete beams reinforced with BFRP reinforcement was evaluated. Full-scale tests were conducted on eight large-scale specimens of concrete beams reinforced with either BFRP reinforcement or steel reinforcement. The test data were analysed to evaluate the shear and flexural performance of concrete beams reinforced with BFRP reinforcement. It was found that at low reinforcement ratio, beams reinforced with BFRP reinforcement exhibited more flexural and shear cracks than similar beams reinforced with steel reinforcement. Cracking moments were found to be 30-50% higher for specimens reinforced with steel reinforcement compared to specimens reinforced with BFRP. The study also showed that shear failure can be determined by the design of reinforced concrete beams reinforced with BFRP reinforcement and containing BFRP clamps.

The paper [8] investigates the shear strengthening of flat slabs using carbon fibre reinforced polymer (CFRP) sheets. Fifteen reinforced concrete slab specimens were tested. Thirteen of them were reinforced with CFRP sheets and two specimens were left as control specimens. Four reinforced specimens were tested by cyclic vertical loading. The width of the CFRP sheets varied from specimen to specimen. The CFRP sheets were placed on the tensile side of the plates in two perpendicular directions. The vertical load was applied using a hydraulic jack. No rupture of the CFRP sheets was observed in all specimens. The test results showed that the use of CFRP sheets in addition to steel reinforcing bars as flexural reinforcement improves the pushover shear strength of the slabs. This improvement can be significant for slabs made of high-strength concrete with low steel reinforcement ratio. However, under cyclic vertical loading, the improvement in pushover shear strength due to FRP reinforcement is reduced. For strengthened slabs, the equivalent reinforcement coefficient should be used to account for the effect of both steel and FRP reinforcement on the flexural resistance.

The research [9] presents a method of mounting reinforcement near the surface (NSM), which is one of the promising methods currently used for strengthening of reinforced concrete structures. In the NSM method, carbon fibre reinforced polymer (CFRP) bars are placed in pre-cut grooves and attached to concrete with epoxy adhesive. In this paper, corroded beams repaired by NSM technique using CFRP rods are investigated. The failure mode of the repaired beam is studied by experimental and numerical modelling results. Experimental results and numerical simulation results with a two-dimensional finite element model using FEMIX software were obtained on five 3 m long beams: three corroded beams that had been subjected to natural corrosion for 25 years and two control beams without corrosion. Two beams, one corroded and one control beam (A1CL3-R and A1T-R), were flexural strengthened using the NSM method with a single 6 mm diameter CFRP rod and then tested in three-point bending until failure. The ultimate strength, yield strength and failure modes were analysed. Experimental results showed that the NSM method increased the overall strength and yield strength of the control and corroded beams, despite the non-classical failure mode with delamination of the concrete cover in the corroded beam due to corrosion damage. The results of the numerical simulations in FEMIX were in agreement with the experimental results. Comparisons were made between the experimental results and the numerical simulation results obtained using ABAQUS software to investigate the specific failure mode of the corroded beam that occurred as a result of concrete cover separation.

In [10], an innovative hybrid reinforcement is investigated to improve the strength of reinforced concrete flexural elements. The main objective of this study is to evaluate the effectiveness of hybrid fibre reinforced polymer (FRP) strengthening in the overall evaluation of the flexural behaviour of reinforced concrete (RC) elements. Eight full-scale square RC elements were moulded and strengthened with FRP using a variety of techniques including near surface mounted (NSM) FRP carbon laminates only, externally bonded (EB) carbon fibre reinforcement only and hybrid strengthening using a combination of NSM carbon fibre reinforcement and EB carbon fibre fabric. A three-dimensional non-linear finite element (FE) based model is developed to simulate the behaviour of RC beams with and without FRP reinforcement. Experimental results showed that the hybrid FRP strengthening is able to increase the strength by 175% compared to the control RC specimens. RC beams strengthened by NSM method alone increased the maximum strength by 111%.

Paper [11] presents a study of lightweight, non-corrosive basalt composite reinforcement bars (BCR) made of continuous basalt filaments, epoxy and polyester resins by pultrusion. It is a rod with a continuous spiral ribbing formed by basalt filament for better bonding with concrete. The advantages of BCR reinforcement compared to steel reinforcement are presented:

– BCR is more than twice as strong in tension (to prevent cracking in concrete) as steel reinforcement;
– BCR is not susceptible to corrosion, which is inherent to steel reinforcement;
– BCR is 89 % lighter than steel reinforcement (significantly faster fabrication, installation and handling of BCR);
– BCR has the same coefficient of thermal expansion as concrete;
– basalt fibres do not absorb or transmit moisture and therefore do not create water penetration pathways that cause concrete failure;
– BCR is not a conductor of electricity, which prevents electrolysis in marine environments;
– BCR does not create magnetic fields when exposed to electromagnetic energy;
– BCR operating temperature range from -70 °C to +100 °C, which is an important parameter for operation also in fire-resistant rooms.

Thus, the use of basalt-composite reinforcement increases the service life of reinforced concrete structures, which is relevant in the creation of long-term operating structures, which include the structures of hydroelectric power plants.

In the article [12] it is noted that nowadays the method of strengthening of reinforced concrete structures of long-term operating hydraulic structures by the system of external reinforcement based on carbon fibre fabrics is being applied. At the same time, the specified method of strengthening is applicable for structures, to the tensile zone of which there is an access.

In headwalls, abutments, sluice walls and other hydraulic structures on the side of the tensile face there is a soil backfill for practically their entire height, which essentially excludes the use of external strengthening.

The application of prestressed basalt-compact reinforcement for strengthening of operating reinforced concrete structures with installation and caulking in drilled boreholes seems to be effective. Experiments of reinforced concrete fragments reinforced with BCR have shown an increase in strength up to 1.55 times. Practical recommendations on the placement of prestressed BCR in structural sections based on experimental and design studies are presented.

The research [13] is experimental and theoretical and is aimed at developing a methodology for numerical modelling and calculation of reinforced concrete structures of operating hydraulic structures strengthened with prestressed basalt-composite reinforcement.

Vertical inter-bay construction joints, normal and inclined cracks, steel and basalt-compact reinforcement were reproduced in spatial finite element models. Comparison of experimental values of stresses in the compressed zone of concrete structures, tensile stresses in prestressed BCR and in steel reinforcement, width of opening of inter-bay joints and cracks with calculations confirms the operability and reliability of the developed method of modelling and calculation of reinforced concrete structures of operating hydraulic structures strengthened with prestressed BCR.

The paper [14] analyses the results of inspection of sluice wall structures, develops a spatial model based on the finite element method, and performs calculations to determine the stress-strain state, including strengthening with prestressed basalt-compact reinforcement. As a result of the calculations, the occurrence of cracks and opening of horizontal construction joints were confirmed. At the same time, taking into account the corrosion of reinforcement in the area of construction joints established by inspections, tensile stresses occur in it, reaching the design resistance of A-II class reinforcement.

During the repair of sluice walls the anchorage of "new" concrete with "old" concrete was investigated and found to be insufficient in terms of anchorage length. It is noted that repair of sluice walls from the side of the front face plays mainly the role of preservation of concrete of the main mass and restoration of concrete parameters in the compressed zone (from the side of the front face), while the work of the wall structure as a whole and first of all from the side of the back surface (from the side of soil backfill) is unsecured. Justification of application of prestressed BCR for strengthening of sluice walls with placement at the faces and back surfaces of the walls with reduction of tensile stresses by 40 % in the steel rear reinforcement installed during the construction period is given, thus reducing the width of crack opening along the construction joints, providing extension of service life of the structure as a whole.

Thus, researches [1-14], aimed at substantiation of the technology of strengthening of operating reinforced concrete structures by means of application of perspective composite materials, require further development and improvement in relation to various reinforced concrete structures having high safety requirements.

METHODS

Strengthening of structures based on the use of prestressed BCR allows to increase the load-bearing capacity of structures. The choice of BCR is justified by the following:

– The cost of BCR is comparable in value to steel reinforcement;
– BCR has 2.5-3 times higher tensile strength compared to steel reinforcement with equal diameter;
– BCR is resistant to the alkaline environment of concrete;
– BCR weight compared to steel reinforcement is 4-4.5 times less with the same diameter;

– BCR corrosion resistance (does not corrode in water, moisture saturated and aggressive environments).

Also of note is the use of an integrated strengthening method: BCR and composite external reinforcement with carbon tapes.

Corrosion of steel reinforcement is inevitable in reinforced concrete structures during operation of hydraulic structures. Therefore, the use of BCR reinforcement seems reasonable in solving this problem when strengthening structures.

Application of the finite element method is widely spread for establishing the actual condition of stress-strain state of hydraulic structures (HS). With the modern development of computational technology, it is possible to solve nonlinear problems and determine by calculation the actual location and opening of cracks and inter-bay construction joints in structures.

RESULTS AND DISCUSSION

Initial data for design and experimental studies of sluice walls on the example of Pavlovsk and Gorodets sluices (Russia):

1. The Pavlovsk sluice is a single lift, single-line sluice made of monolithic reinforced concrete. Overall dimensions of the sluice chamber: length - 120.0 m; width - 15.0 m; wall height - 39.5 m.

The sluice chamber consists of 4 sections.

A distinctive feature of the condition of the walls of the sluice chamber before the overhaul in 2022 - 2023 was the presence of horizontal cracks on the face of the lower wall, which represent the exit of secondary inclined cracks (Fig. 1), wedged out of the horizontal inter-bay construction joints in the direction of the face side due to the lack of transverse (horizontal) reinforcement in the wall. There were also voids in the concrete going deep into the wall mass along the path of inclined cracks (Fig. 2).

2. Composition of navigable structures of the Gorodets hydro-scheme: two lines of single-chamber reinforced concrete sluices. Overall dimensions of the sluices' chambers: length - 290.0 m; width - 30.0 m; wall height - 14.0 m. Each sluice chamber consists of 12 sections.

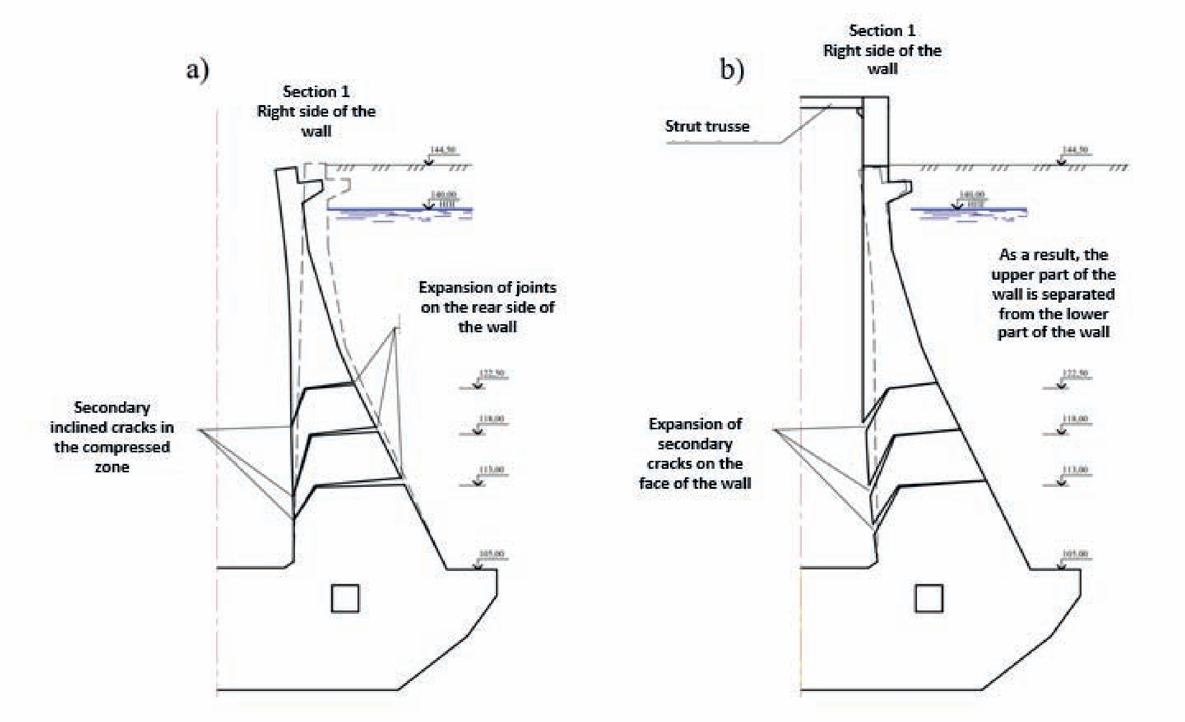

Figure 1. Nature of formation and opening of secondary inclined cracks

Inspections carried out prior to the overhaul (2017-2018) of the sluice chamber walls revealed the presence of multidirectional cracks and, primarily, outcrops on the faces of secondary inclined cracks (Fig. 3) formed from inter-bay construction joints, as well as voids extending deep into the concrete mass of the walls (Fig. 4) along the path of inclined cracks.

Figure 2. View of the right wall of section No.1 with a sloping crack extending to the face, with voids, exposed reinforcement and water leaks (before overhaul)

DESIGN CASE

Based on the analysis of various load combinations during operation and overhaul of sluice chambers, as well as on the analysis of design materials and the results of earlier studies, the design case corresponding to the most unfavourable state of loading of sluice chamber walls is accepted:

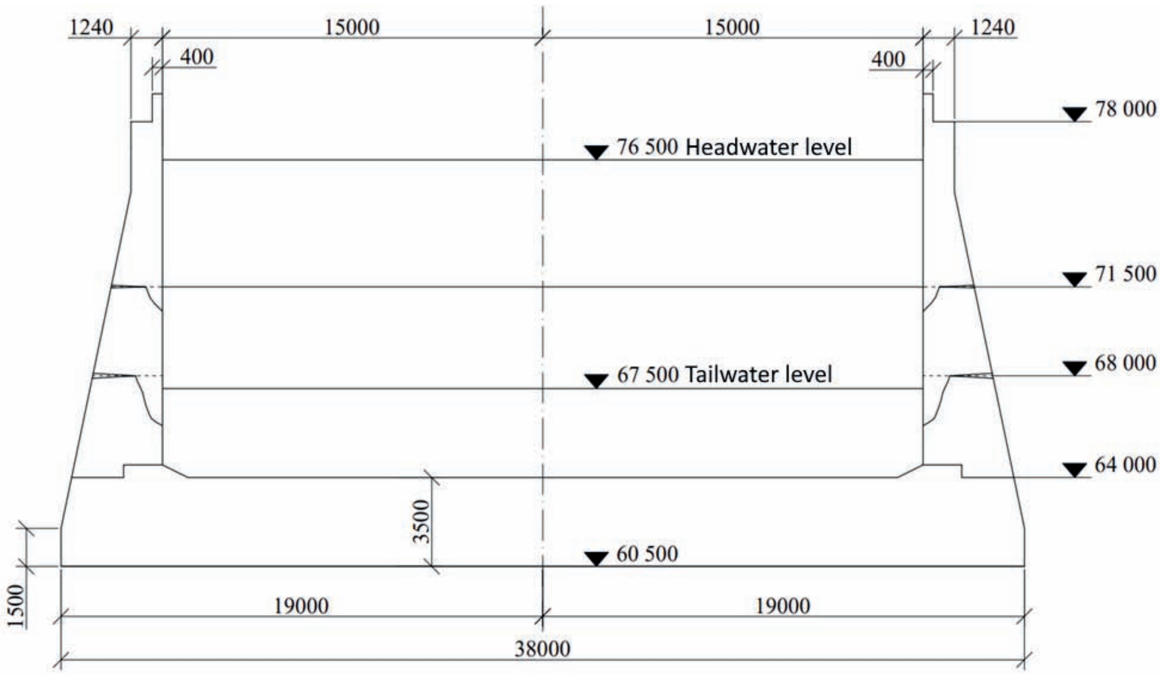

Figure 3. Section of the sluice chamber. Dimensions are given in mm, marks in m

<u>Figure 4.</u> View of a wall with sloping cracks extending to the face, with voids, exposed reinforcement and water leaks (before overhaul)

1. In the case of a drained chamber, the load from the ground pressure on the rear edge of the wall is the highest and the groundwater level is the highest (in the case of rapid emptying of the chamber, when the water level in the ground behind the wall does not have time to drop).
2. The impact of winter temperatures is taken into account.

METHODOLOGY OF COMPUTATIONAL MODELLING AND EXPERIMENTAL STUDIES OF REINFORCED CONCRETE STRUCTURES

The present method provides finite element modelling of sluice structures as part of the system "structure - backfill - base" in a spatial setting, as the sluice chambers and heads, as well as their backfill interact with each other.
Experience in numerical modelling of HS reinforced concrete structures with construction joints has been taken into account in the development of the methodology.
Finite element models take into account the structural features of the structures, including the actual placement of reinforcement. Horizontal and vertical contact construction joints are modelled, taking into account the strength reduction under the combined action of shear with tension or compression compared to a continuous monolithic structure. Breach of bond between reinforcement and concrete in the zones of opened horizontal construction joints and cracks is modelled.
Special approaches are used for modelling cracking of construction joints and monolithic concrete, as well as cracking of face concrete. In this case, the conditions for crack formation are the action of tensile stresses exceeding the tensile strength of concrete and the strength of joints in a complex stress state, i.e. the combined action of shear forces with tensile (or compressive) forces in the plane of construction joints.
In the calculation model, horizontal and vertical construction joints caused by interruptions in the concreting of the walls and repair of the concrete face were specified. In the areas of construction joints, the disruption of bonding of the working reinforcement in the concrete of the sluice walls during the construction period was taken into account.
Due to cracking of the face concrete, a reduced strain modulus is taken into account in the calculation models.
Also, the calculation models take into account the corrosion deterioration of the working reinforcement of the back surface of the wall as a result of a long period of operation.
The model of the system "structure - backfill - base" reproduced a fragment of the sluice base massif, massifs of soils of the backfill of the slots behind the outer walls of the chambers and the backfill of the inter-sluice space (between the inner neighbouring walls of the two lines of sluices).
Loads are modelled in accordance with the accepted design scheme (i.e. in accordance with

the accepted levels of soil, groundwater, water in the chambers, etc.), as well as taking into account physical and mechanical properties of materials of structures, base soils and backfills. The main and auxiliary software were used for calculation studies allow obtaining loads on sluice structures from soil and water taking into account the current state of soil mechanics theory (reflecting the peculiarities of soil pressure as active, reactive, passive, at rest, etc.).

Temperature effects were reproduced in the models "structure - backfill - base" in accordance with average monthly and average annual temperature values for the area of hydraulic structures on the basis of normative documents. The thermophysical properties of the areas of the "structure - backfill - base" system were also taken into account.

The problem of temperature distribution inside the computational domain was solved in one of the modules of the computational software system. Initial design temperature values were set on the contour of the computational domain and then, taking into account the thermophysical properties of the elements of the domain, the temperature values inside the domain were calculated.

In accordance with the obtained temperature distribution in each finite element into which the computational domain is divided, the main problem of determining the deformed and then the stress state of the structure was solved.

One of the most important features of the approach of modelling structures, which distinguishes it from traditional approaches to ordinary engineering calculations to be used in design, is that it allows various damages, defects and other deviations from the assumptions adopted in design to be taken into account by incorporating them into the finite element models being developed and adjusted.

In the experimental studies, a complex problem was solved to determine the strength, deflections, opening width of inter-bay construction joints, deformations of metal and prestressed basalt composite reinforcement (BCR) of strengthened reinforced concrete structure.

Phasing of the work:

– experimental studies of low-reinforced RC models (analogues of hydraulic structures, for example, sluice walls, retaining walls, hydroelectric power plant piers) with operational cracks (including inter-bay construction joints) reinforced with metal reinforcement and BCR strengthening;

– experimental studies under static loading of reinforced concrete models strengthened with transverse reinforcement in the zone of inter-bay construction joints (in the zone of joint action of bending moments and transverse forces);

– experimental research of reinforced concrete models strengthened with composite straps in the zone of joint action of excessive moments and transverse forces, under the action of static loading, and repeated research after holding for 60 days in a water environment.

Reinforced concrete models (2020) are used:

1) concrete of class B30-B35;
2) metal reinforcement A400;
3) basalt-composite reinforcement ($R_{f\mu}$=800 MPa and $E_{f\mu}$=50 000 MPa);
4) *Carbon Wrap Tape* with a surface density of (900±30) g/m^2 and *Carbon Wrap Resin* epoxy two-component binder.

Computational studies of the Pavlovsk sluice walls taking into account the formation and opening of cracks along the inter-bay construction joints revealed the trajectories of inclined secondary cracks (Fig. 1.a). For example, tensile (horizontal) stresses of 4.2 MPa were obtained in the right wall of section No.1 in the joint zone at 118.00 m and 4.9 MPa in the left wall, which is significantly higher than the tensile strength of the wall concrete.

The obtained values of tensile stresses confirm the formation of secondary inclined cracks wedging out of the inter-bay construction joints, with the exit to the face of the walls. The calculations also show that the stresses in the transverse (horizontal) reinforcement in the zones of secondary inclined cracks significantly exceed the resistance of transverse reinforcement of A-I class ($R_{sw} = 175\,MPa$). These results indicate an insignificant amount of transverse reinforcement installed solely for constructional (off-design) purposes. The stresses in the longitudinal (vertical) reinforcement at the back surface were obtained as 304 MPa, which exceeds the resistance of A-I class reinforcement ($R_s = 225\,MPa$).

In 2022 - 2023, in order to carry out overhaul of the walls face, strut trusses were installed in the upper part of the walls (Fig. 1. b). In this case, the stresses in the transverse (horizontal) reinforcement in the zones of secondary cracks decreased and did not exceed the resistance of transverse reinforcement of A-I class ($R_{sw} = 175$ MPa), and the stresses in the longitudinal (vertical) reinforcement at the back surface reached 384 MPa, which exceeds the resistance of reinforcement of A-I class ($R_s = 225$ MPa). The stresses in the longitudinal (vertical) reinforcement at the face exceed tensile stresses of 97 MPa.

It should be noted that in this variant with strut trusses, the opening of secondary inclined cracks on the face side was confirmed by inspection results (Fig. 2).

Thus, the calculations of the Pavlovsk sluice walls showed the necessity of their strengthening not only of the face (new concrete and reinforcement, reinforced concrete columns), but also the necessity of reinforcement of the wall structure as a whole through the application of additional prestressed reinforcement.

The computational studies showed (Table. 1) that the maximum displacement of the top of the walls inside the Gorodets sluice chambers, taking into account the corrosion of metal reinforcement of the back surface, was 38.9 mm (1/360 of the wall height) at a stress in the tensile reinforcement of the back surface of the walls - 23.0 MPa, which is close enough (82 %) to the design resistance for the reinforcement of class A-II (280 MPa), the compression stress in the concrete of the main mass increases up to 7.67 MPa, which exceeds the design compressive resistance for the concrete of class B10 (6 MPa).

In the course of computational studies, cracking in the walls along the contact surfaces of horizontal construction inter-bay joints in the concrete of the main massif was revealed. The presence of tensile stresses in the concreting blocks under the inter-bay joints has been established. In accordance with the provisions of [17] in the structures of the walls of the sluice chambers require horizontal transverse reinforcement in the areas of horizontal inter-bay joints, which was confirmed by calculations.

It should be noted that the face concrete of the sluice walls was replaced with B22.5 concrete in 2017 - 2018 as part of a major overhaul.

It follows from the analysis of the survey results, overhaul measures and a set of calculations that the reconstruction of the face of the Gorodets sluice chamber walls contributed to the preservation of the concrete of the main massif and restoration of the concrete parameters of the compressed zone, while the performance of the structure as a whole and, first of all, on the side of the back tensile surface is insufficiently ensured.

As a result of calculations, it is obtained that the application of prestressed BCR gives the following results:

– installation at the face reduces by 36 % the tensile stresses in the rear metal reinforcement, which is subject to corrosion as a result of prolonged operation;

– installation at the back surface makes it possible to reduce by 42 % the tensile stresses in the rear metal reinforcement, which is subject to corrosion as a result of prolonged operation; reduce the opening width of horizontal construction joints, thus extending the service life of the structure as a whole.

Table 1. Summary table with the results of calculations

Type of stress	Both sluice chambers drained	Corrosion deterioration of metal back reinforcement in the opening areas of horizontal construction joints is taken into account	Prestressed BCR at the face is taken into account	Prestressed BCR at the back surface is taken into account
Horizontal displacements of the top of the walls towards the inside of the chamber, mm	31,9	38,9	32,7	31,5
Verticals compressive stresses in the concrete of the main mass, MPa	-4,82	-7,67	-5,49	-5,29
Tensile stresses in the rear metal reinforcement, MPa	164,0	230,0	168,5	161,5

EXPERIMENTAL RESULTS

In 2020, reinforced concrete beam-type models with vertical inter-bay construction joints and with design dimensions: length - 2000 mm, height - 300 mm, width - 150 mm were manufactured and tested for static loading.
In addition to reinforcing the beams with metal reinforcement, pre-stressed BCR was installed.
In the present research (2024), experiments were carried out on the same experimental beams B1 (with the placement of prestressed BCR in the tensile zone) and B2 (with the placement of prestressed BCR in the compressed zone) in order to obtain new data on the strength, deflections, opening widths of the inter-bay construction joints, stresses in the metal reinforcement and in the BCR after 4 years of prestressing the beams through the application of BCR.
The test type and characteristics of the experimental beams B1 and B2 are presented below. Experimental beams B1 and B2 were fabricated in 2020 with steel reinforcement in two steps (block concreting) for inter-bay construction joints. They had a channel for BCR installation with subsequent prestressing of BCR "on concrete", caulking of the channel and with subsequent release of BCR "on beam concrete" after the channel concrete had gained strength.
BCR in beams B1 and B2 was subjected to prestressing for the value: 0.45×800=360 MPa (accepted: coefficient 0.45 regarding [15]; $R_{f,n}$=800 MPa; BCR tensile strength regarding [16]) with subsequent concreting of channels in the beams.

Type of testing of test beams

All beams have basic longitudinal reinforcement of 2Ø12 steel reinforcement of class A400 in the tensile zone; longitudinal reinforcement coefficient μs=0,0056, also all beams have 2 vertical inter-bay construction joints.

1) B1 beam (Phase 1): 2020 г

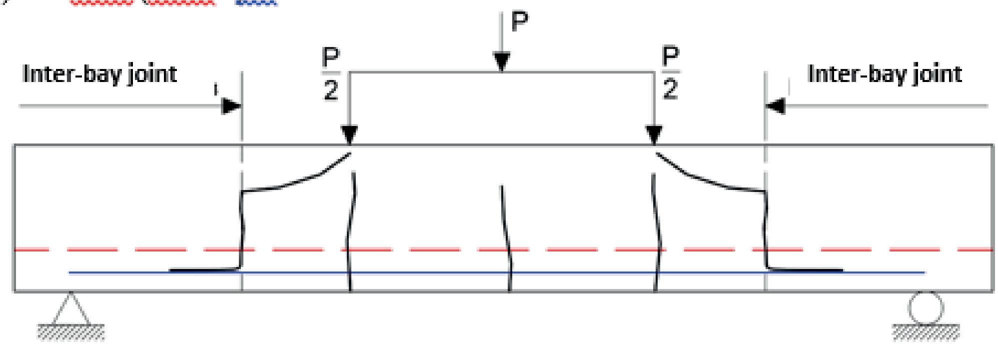

Availability of Ø32 channel in the tensile zone of the beam for subsequent installation of 1Ø12 BCR.

2) B1 beam (Phase 2): 2020 г

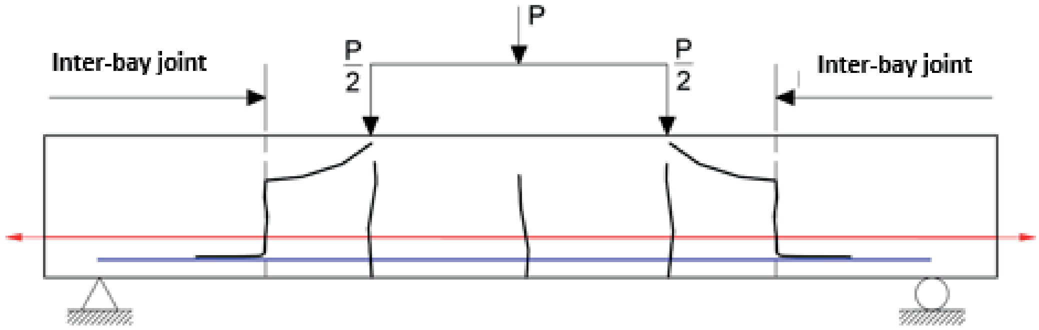

Prestressed BCR 1Ø12 with monolithic channel in the tensile zone of the beam, μf=0.0033 (beam B1, stage 1).

3) Beam B1 (Phase 3): 2024 г

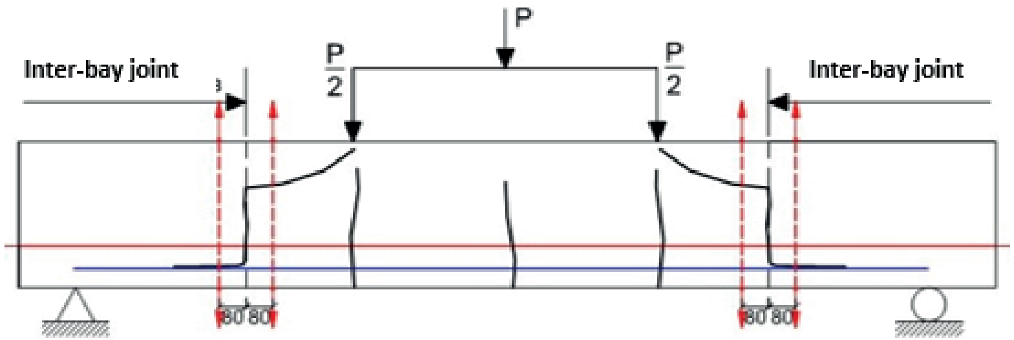

Prestressed Ø12 transverse reinforcement installed on both sides of the inter-bay construction joints (beam B1, stage 2).

1) B1 beam (Phase 1): 2020 г

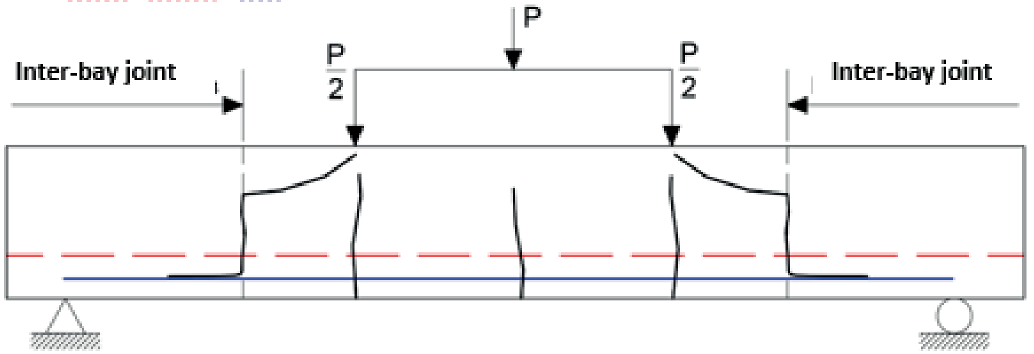

Availability of Ø32 channel in the tensile zone of the beam for subsequent installation of 1Ø12 BCR.

2) B1 beam (Phase 2): 2020 г

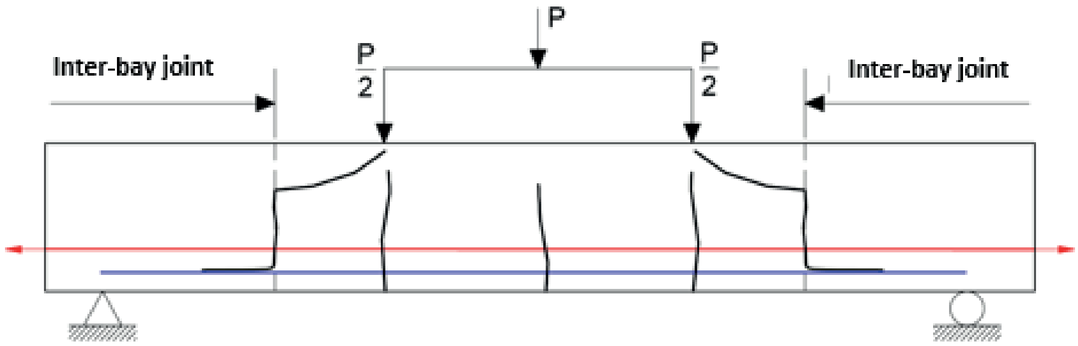

Prestressed BCR 1Ø12 with monolithic channel in the tensile zone of the beam, μf=0.0033 (beam B1, stage 1).

3) Beam B1 (Phase 3): 2024 г

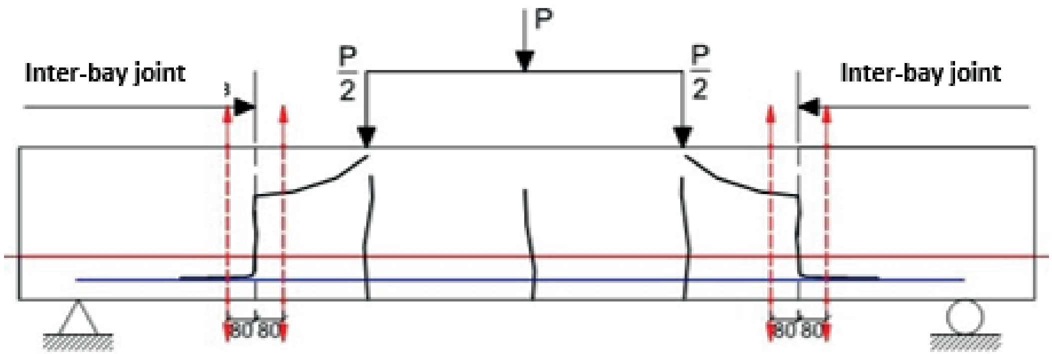

Prestressed Ø12 transverse reinforcement installed on both sides of the inter-bay construction joints (beam B1, stage 2).

4) B2 beam (Phase 3): 2024 г

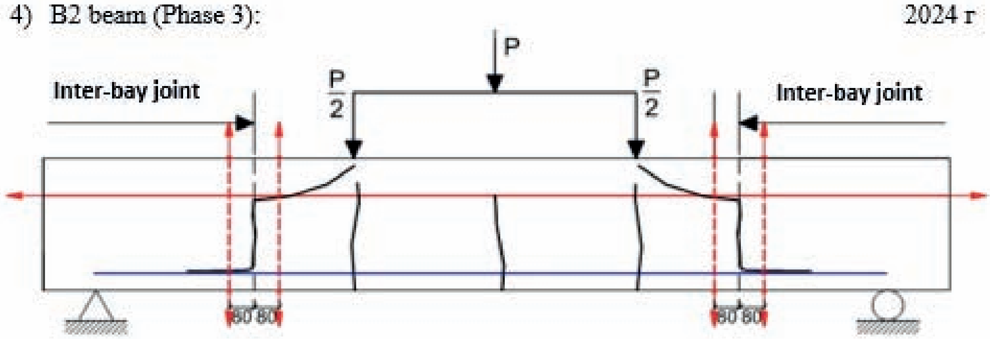

Prestressed Ø12 transverse reinforcement installed on both sides of the inter-bay construction joints (beam B2, stage 2).

5) Beam B2 (Phase 4 and Phase 5): 2024 г

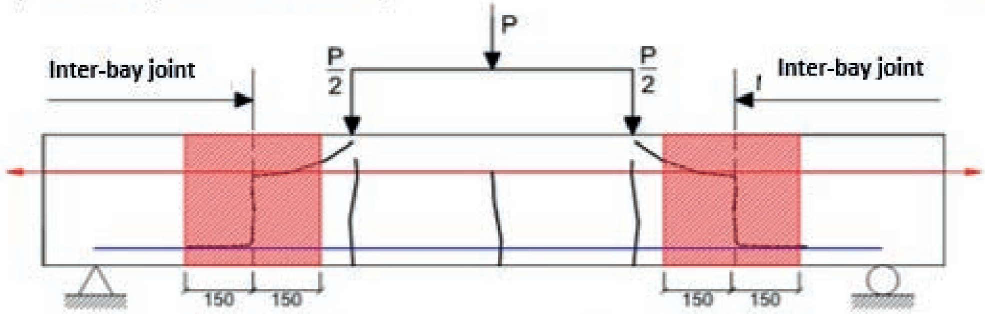

Composite carbon fabric installed in the shear span after removal of prestressed transverse reinforcement (beam B2, stage 2)

It should be noted that Ø12 transverse prestressed reinforcement was installed in 2024 in beams B1 (stage 3) and B2 (stage 3) on both sides in relation to the inter-bay construction joint; CarbonWrap Tape-900/300 composite fabric in a single layer was bonded in 2024 in the span between the support and the P/2 force application point after removal of the transverse prestressed reinforcement (beams B1 (stage 4) and B2 (stage 4)).

The design of the experimental beams is shown in Figure 5.

It should be noted:

1) During testing, the experimental beams were supported on movable (roller) and fixed (knife) supports located at a distance of 150 mm from the ends.

2) The load was applied vertically in steps by a hydraulic jack and transmitted through a horizontal crosshead at two points 320 mm from the centre of the beam, with a force spacing (the 'pure bending' zone) of 640 mm and a force-support spacing ('shear span') of 540 mm (Figure 5).

Experimental beams were equipped with instrumentation to measure: deflections; opening width of inter-bay construction joints; deformations of steel reinforcement and BCR. For this purpose, strain gauges with a base of 20-50 mm and clock-type indicators were used.

The following main results were obtained in the process of experimental research.

In the experimental beams B1 (stage 1) and B2 (stage 1) in 2020 the following character of cracking was recorded: after opening of vertical inter-bay construction joints there was formation (wedging out) of inclined cracks in the direction to the applied forces P/2 (at the distance $X_j = 0{,}24 \times h_j - 0{,}34 h_j$ from the upper compressed face of the beams) at P = 44.2 kN and 39.0 kN, respectively.

Under the action of a load close to the destructive load, cracks were formed along the longitudinal working reinforcement in the direction "from the inter-bay joint to the supports" (violation of the bond between the reinforcement and concrete in the tensile zone of the beams). A system of vertical normal cracks was formed at the section between the forces in the "pure bending" zone (Fig. 6).

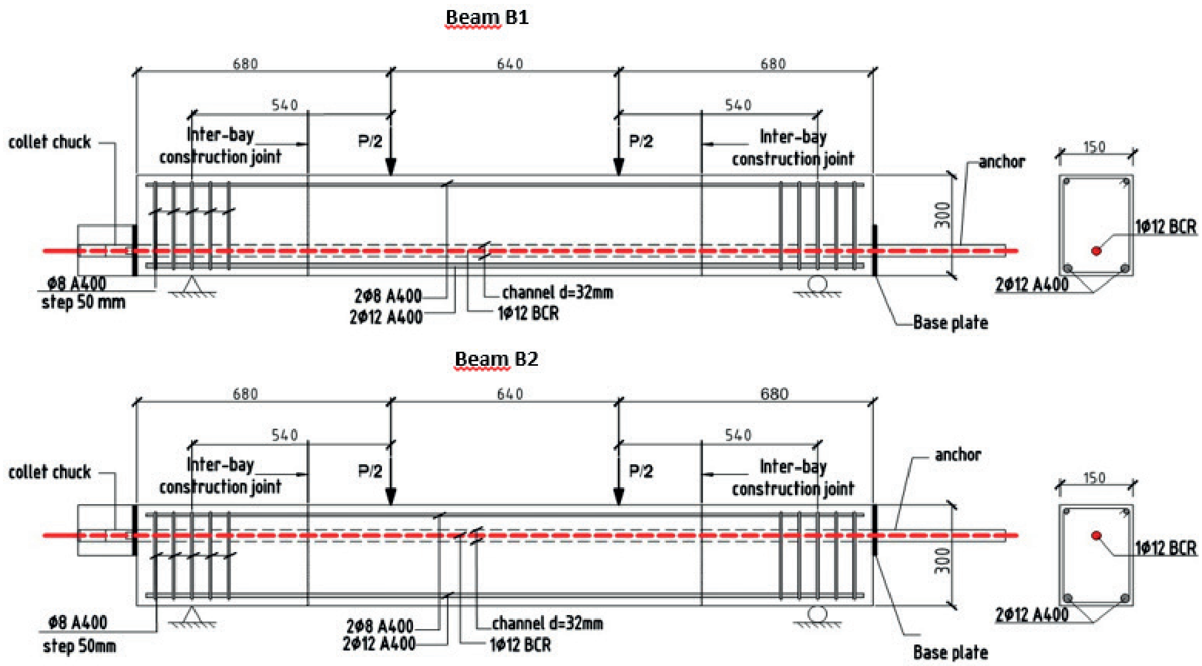

Figure 5. Design of experimental beams B1 and B2

Analyses of the beam test results showed:

1) The force corresponding to the failure of not strengthened prestressed BCR beams B1 (Stage 1) and B2 (Stage 1), having working longitudinal steel reinforcement 2Ø12 class A400 in the tensile zone of the beams, in the presence of two inter-bay construction joints, is 46.8 kN and 41.6 kN, respectively. At the same time, in beam B1 (Stage 1) the Ø32 channel for BCR placement is located in the tensile zone and in beam B2 (Stage 1) in the compressed zone, which explains the difference in the magnitude of the failure force. Both the above-mentioned beams failed brittle by an inclined crack formed (wedged) in their inter-bay construction joint from the combined action of bending moment and shear force.

2) The tests of beams B1 (Stage 2) and B2 (Stage 2) with prestressed BCR installed in the tensile and compression zone, respectively, showed that their load carrying capacity increased to 67.6 kN and 55.12 kN, respectively.

3) Further experiments of beams B1 (Stage 3) and B2 (Stage 3) with prestressed transverse reinforcement up to 50 MPa on both sides of the inter-bay construction joints showed an increase in load carrying capacity up to 83.2 kN with no signs of brittle failure.

4) Further, in the shear span (after removal of transverse reinforcement) of beam B1 (Stage 4), composite fabric was bonded in one layer. The bearing capacity of the beam increased to 142.5 kN with no signs of brittle failure.

After conditioning beam B1 for 60 days in an water environment, the load carrying capacity was maintained at 150 kN with no signs of brittle fracture.

5) In beam B2 (stage 4) after removal of transverse reinforcement, composite fabric was bonded in one layer. The load-bearing capacity of the beam increased to 124.8 kN, while the metal working reinforcement in the tensile zone of the beam was found to yield.

After conditioning beam B2 (stage 5) for 60 days in a water environment, when the load carrying capacity reached 124.8 kN, there were signs of beam failure.

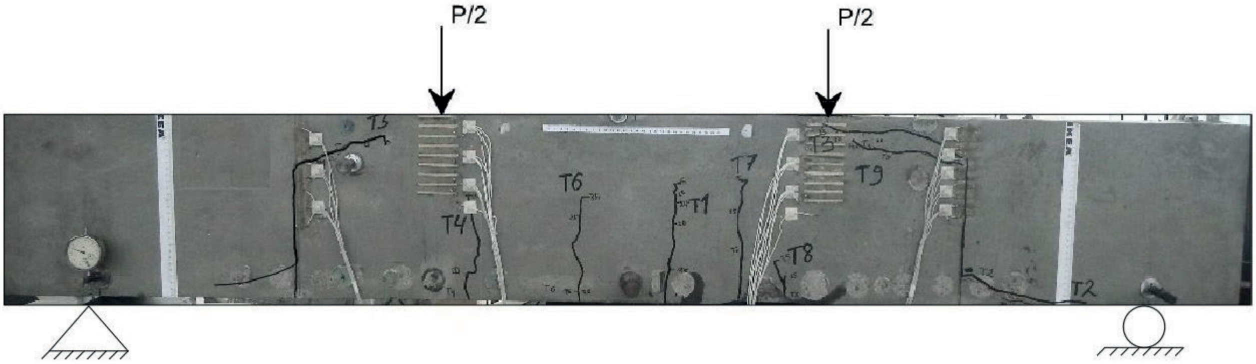

Figure 6. Cracking behavior in test beams (2020)

From the analysis of beam test results in terms of deflections, opening width of inter-bay construction joints, deformations of steel and basalt-composite reinforcement it follows:

1) The deflections of beam B1 (stages 1, 2, 3, 4, 5) as it is strengthened from the variant of longitudinal prestressed BCR - location in the tensile zone of the beam (stage 2) - to external transverse reinforcement with composite fabric after exposure in aqueous environment (stage 5) are lower by a factor of 1.32, with deflections of B1 (stage 4) lower than B1 (stage 5) by a factor of 1.14 as a result of the effect of the aqueous environment (Figure 7).

The deflections of beam B2 (stages 1, 2, 3, 4, 5) as it is strengthened from the variant of longitudinal prestressed BCR - located in the compressed zone of the beam (stage 2) - to the external transverse reinforcement with composite fabric are almost the same at P=55.12 kN, with the deflections of B2 (stage 4) lower than B2 (stage 5) by a factor of 1.65, which is the result of the water environment (Fig.8).

It should be noted that the pattern of variation of deflections of B1 and B2 (Figs. 7 and 8) by a smaller magnitude is preferred for B1 with the location of prestressed BCR in the tensile zone when strengthening by transverse reinforcement with composite fabric.

2) The opening width of the inter-bay construction joints in beam B1 (stage 2) (prestressed BCR located in the tensile zone of the beam) was recorded 1.21 times smaller than that in beam B2 (stage 2) (prestressed BCR located in the compressed zone of the beam) at P=55.12 kN (Figures 9 and 10).

As beams B1 and B2 are strengthened to the options of external transverse reinforcement with composite fabric (stages 4 and 5), the opening width of the inter-bay construction joints varies within 10%, while comparison with the normative document [17] shows that the permissible values are not exceeded $a_{cr.i}$ (Fig. 8 and 9). It is noted that in the research variant B2 (stage 5) in comparison with B2 (stage 4) the width of opening of inter-bay construction joints is on average 1.23 times higher (Fig. 9).

3) Strengthening of beams B1 and B2 (steps 3) with external prestressed transverse reinforcement resulted in increased deformations of steel reinforcement (Figures 11 and 12). 3) Strengthening of beams B1 and B2 (steps 4) with external transverse reinforcement with composite fabric reduced the deformations of the steel reinforcement, while

the deformations of the steel reinforcement almost doubled (steps 5) after the beams were aged in a water environment. Comparison ε_{si} in the study of beams B1 and B2: stages 1, 2, 3 with stages 4, 5 indicates that the option of strengthening by external reinforcement with composite fabric is preferable (Figs. 11 and 12).
It should be noted that the maximum tensile strains of steel reinforcement at maximum loads in the range of 83.2-150.0 kN were recorded in the range of $(160\text{-}220)\times10^{-5}$, which corresponds to average stresses of 380 MPa close to the yield strength.
4) The tensile strains of the prestressed BCR located in beam B1 (Fig. 12) in the tensile zone showed smaller values (about 2 times) in the strengthening option of external transverse reinforcement with composite fabric (steps 4 and 5).
In inter-bay construction joints, the character of the maximum values of tensile strains of steel reinforcement and prestressed BCR are quite similar (Figs. 11 and 13), indicating their joint operation in the structures.
5) Deformations of prestressed BCR located in beam B2 (Fig.14) in the compressed zone showed compression at all strengthening variants in the range of 20÷75 MPa.

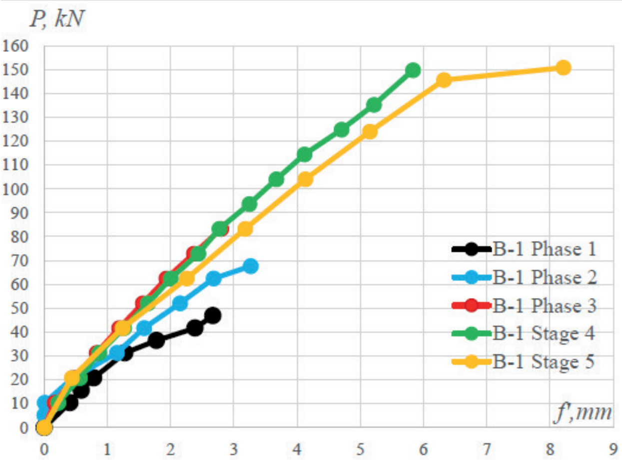

Figure 7. *Deflection diagram of beam B1*

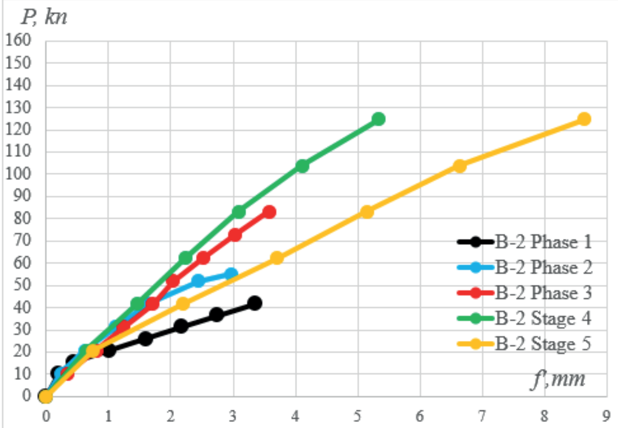

Figure 8. *Deflection diagram of beam B2*

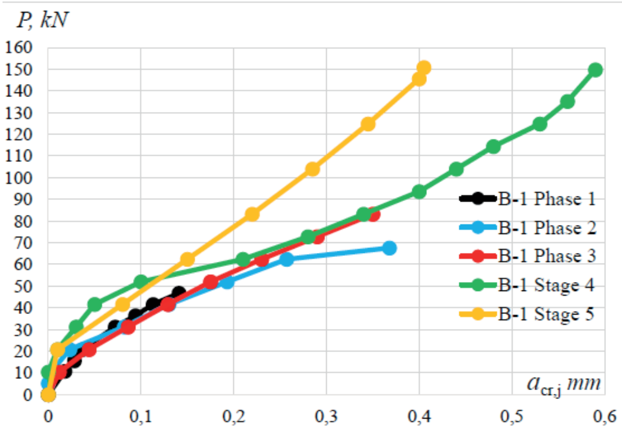

Figure 9. *Diagram of opening widths of inter-bay construction joints in beam B1*

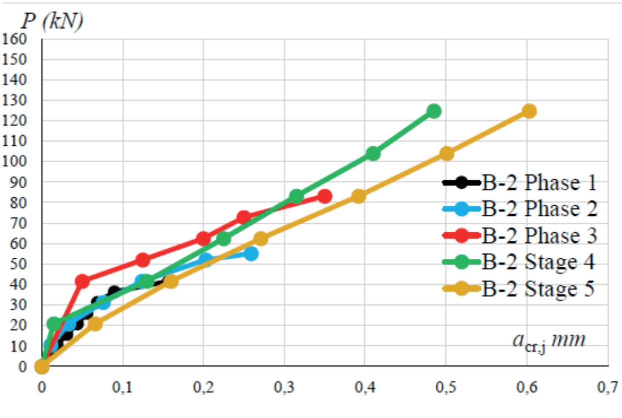

Figure 10. *Diagram of opening widths of inter-bay construction joints in beam B2*

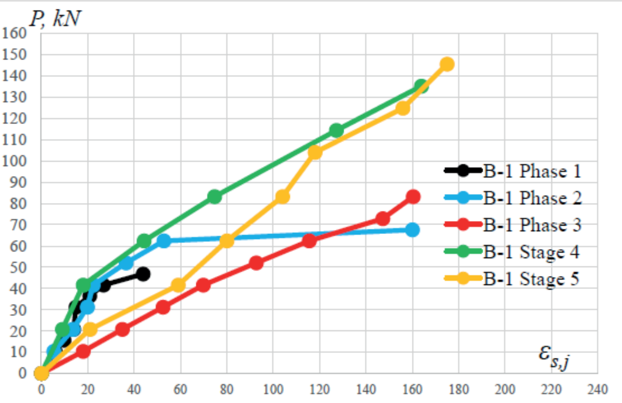

Figure 11. *Deformation diagram of steel reinforcement in the joints of beam B1*

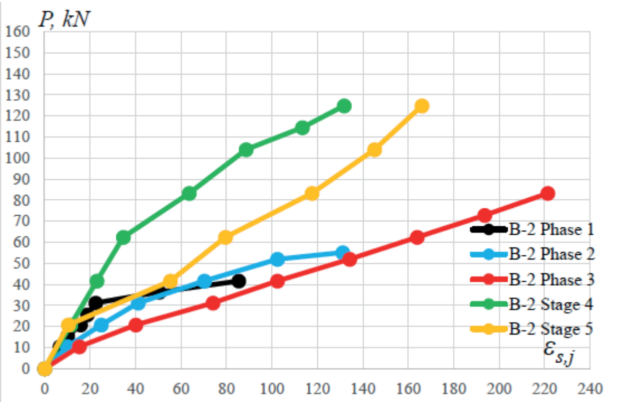

Figure 12. *Deformation diagram of steel reinforcement in the joints of beam B2*

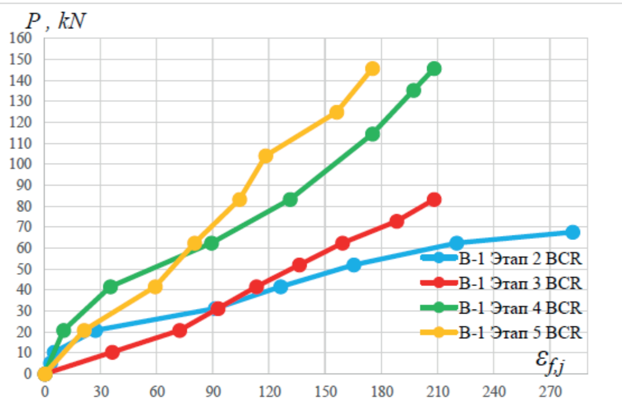

Figure 13. *Deformation diagram of prestressed BCR in beam B1*

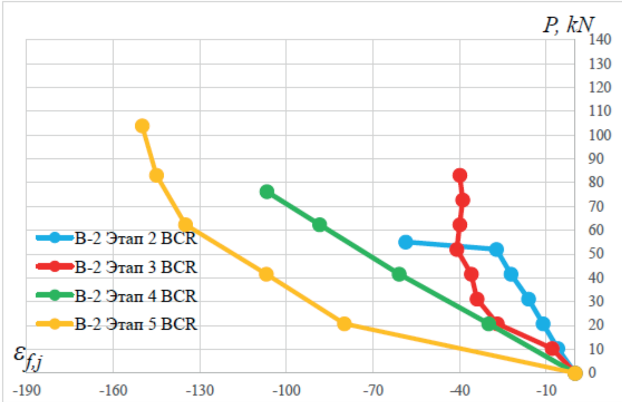

Figure 14. *Deformation diagram of prestressed BCR in beam B2*

CONCLUSION

1) Experimental studies of low-reinforced concrete beams with cracking (2020) on strengthening with prestressed basalt composite reinforcement and external transverse reinforcement (2024) showed positive results, primarily in that the 4-year conditioning of the beams in prestressed condition (BCR) showed their serviceability and confirmed the stabilisation of prestress losses [18].

2) The bearing capacity of beams B1 and B2 increased 1.4 - 2.5 times as they were strengthened from the variant of prestressed basalt-composite longitudinal reinforcement to the variant of external transverse reinforcement, including with holding for 60 days in aqueous environment.

3) The deflections of beams, the opening width of inter-bay construction joints, the deformations of steel reinforcement and prestressed basalt-composite reinforcement decrease with the application of various above-mentioned strengthening options. At the same time, the numerical indicators of all values are within the limits allowed by the normative documents [15, 16, 17].

4) The fact that in the variant of strengthening with prestressed basalt-composite longitudinal reinforcement located in the compressed zone of the reinforced concrete structure, the load-bearing capacity, deflections, width of opening

of inter-bay construction joints, deformations and stresses in steel longitudinal reinforcement and in BCR are within the limits allowed by the normative documents was very positive.

It follows that in hydraulic structures and structures of hydroelectric power plants, where it is not possible to determine by engineering method the location of the compressed or stretched zone, as well as under the action of seismic impact, the results of research carried out by the authors of the article reasonably allow to achieve a positive effect.

ACKNOWLEDGEMENTS

This section is optional. It indicates the sources of funding (projects, grants, government programs, etc.) on the basis of which the research was conducted and the article was written. It is also appropriate to thank scientists, other persons who contributed to the research and preparation of the article, laboratories, institutes, universities, academies of sciences, etc., who provided support (intellectual, material) during the research and/or writing of the article.

REFERENCES

1 **Elamathi E., Priyanka R., Sangeehta V.** Flexural Study on Basalt Rebar Reinforced Concrete Beams // 08 (1), s.l.: Journal of Engineering, January 2018, pp. 01-05.

2 **Pavlovic A., Donchev T.** Pretensioned BFRP reinforced concrete beams: Flexural behaviour and estimation of initial prestress losses // 289, s.l.: MATEC Web of Conferences. Concrete Solutions, 2019, pp. 1-5.

3 **Hesham Sokairge, Fareed Elgabbas, Hany Elshafie**. Structural behaviour of RC beams strengthened with prestressed near surface mounted technique using basalt FRP bars // January 2022. Engineering Structures 250(9): pp. 113489-113489.

4 **Eythor Thorhallsson, Todor Zhelyazov, Andri Gunnarsson, Jonas Thor Snaebjornsson**. Concrete beams reinforced with prestressed basalt bars. Concrete // Innovation and Design, fib Symposium, Copenhagen May 18-20, 2015.

5 **Andri Gunnarsson, Eythor Rafn Thorhallsson, Jonas Thor Snaebjornsson**. Simulation of Experimental Research of Concrete Beams Prestressed with BFRP Tendons // Nordic Concrete Research Symposium. Reykjavik, Iceland. August 2014.

6 **Eythor Thorhallsson, Sindri Hlifar Gudmundsson**. Test of prestressed basalt FRP concrete beams with and without external stirrups // Proceedings of Fib symposium Engineering a Concrete future: Technology, modelling & Construction. At: Tel Aviv. Israel. 2013.

7 **Duic J., Kenno S., Das S.** Performance of concrete beams reinforced with basalt fibre composite rebar // Construction and Building Materials. 2018. Vol. 176. Pp. 470-481. DOI: 10.1016/j.conbuildmat.2018.04.208.

8 **Esfahani M.R., Kianoush M.R., Moradi A.R.** Punching shear strength of interior slab-column connections strengthened with carbon fibre reinforced polymer sheets // Engineering Structures. 2009. Vol. 31. Issue 7. Pp. 1535-1542. DOI: 10.1016/j.engstruct.2009.02.021.

9 **Almassri B., Mahmoud F.A., Francois R.** Behaviour of corroded reinforced concrete beams repaired with nsm cfrp rods, experimental and finite element study // Composites Part B: Engineering. 2016. Vol. 92. Pp. 1-25. DOI: 10.1016/j.compositesb.2015.01.022.

10 **Chellapandian M., Prakash S.S., Sharma A.** Experimental and finite element studies on the flexural behaviour of reinforced concrete elements strengthened with hybrid FRP technique // Composite Structures. 2019. Vol. 208. Pp.

466-478. DOI: 10.1016/j.compstruct.2018.10.028.

11 **Subramanian N.** Sustainability of RCC Structures using Basalt Composite Rebars // The Masterbuilder. September 2010.

12 **Rubin, O.D.; Lisichkin, S.E.; Zyuzina, O.V. (2021)** Prochnost' maloarmirovannykh zhelezobetonnykh konstruktsiy s mezhblochnymi stroitel'nymi shvami, usilennykh predvaritel'nykh ispytaniy bazal'tokompozitnoy armaturoy [Strength of the low-reinforced reinforced concrete structures with the inter-bay construction joints strengthened by the prestressed basalt-composite reinforcement] // Prirodoobustroystvo. No.1. pp. 53-62. DOI: 10.26897/1997-6011-2021-1-53-62.

13 **Bellendir, E.N.; Rubin, O.D.; Lisichkin, S.E.; Baklykov, I.V.** (2021) Metodika rascheta i rascheta zhelezobetonnykh konstruktsiy, poluchayemykh GTS, usilennykh predvaritel'nykh ispytaniy bazal'tokompozitnoy armatury [Modelling and calculation methods for reinforced concrete structures of operating hydro structures strengthened by prestressed basalt-composite reinforcement] // Prirodoobustroystvo. No.5. pp. 59-67. DOI: 10.26897/1997-6011-2021-5-59-67.

14 **Rubin, O.D.; Bellendir, E.N.; Baklykov, I.V.; Zyuzina, O.V.; Shaitanov, M.V.** (2022) Metodika raschetnykh issledovaniy usilivayet predvaritel'nuyu ostanovku bazal'tokompozitnoy armatury stenok kamer shlyuzov s uchetom fakticheskikh dannykh ob ikh ekspluatatsionnom sostoyanii [Methodology of calculation studies of the strengthening by the pre-stressed basalt-composite reinforcement of the sluice chamber walls taking into account the actual data on their operational condition] // Construction: Science and Education. vol. 12. (3). Art. 2. DOI: 10.22227/2305-5502.2022.3.2.

15 **Code of Practice SP 63.13330.2018**. Concrete and reinforced concrete structures. Basic statements. Updated edition of SNiP 52-01-2003. M., 2019. 126 p.

16 **Code of Practice SP 295.1325800.2017**. Concrete structures reinforced with polymer composite reinforcement. Design rules. M., Standardinform, 2017. 55 p.

17 **Code of Practice SP 41.13330.2012**. Concrete and reinforced concrete structures of hydraulic structures. Updated edition of SNiP 2.06.08-87. M., 2012. 67 p.

18 **Bellendir E.N., Rubin O.D., Lisichkin S.E., Zyuzina O.V.** Experimental Study Into Prestress Losses of Basalt Composite Reinforcement Used in the Composition of Concrete Elements. Power Technology and Engineering, 2021, 54(5) - pp. 605-608.

СПИСОК ЛИТЕРАТУРЫ

1 **Elamathi E., Priyanka R., Sangeehta V.** Flexural Study on Basalt Rebar Reinforced Concrete Beams // 08 (1), s.l.: Journal of Engineering, January 2018, pp. 01-05.

2 **Pavlovic A., Donchev T.** Pretensioned BFRP reinforced concrete beams: Flexural behavior and estimation of initial prestress losses // 289, s.l.: MATEC Web of Conferences. Concrete Solutions, 2019, pp. 1-5.

3 **Hesham Sokairge, Fareed Elgabbas, Hany Elshafie**. Structural behavior of RC beams strengthened with prestressed near surface mounted technique using basalt FRP bars // January 2022. Engineering Structures 250(9): pp. 113489-113489.

4 **Eythor Thorhallsson, Todor Zhelyazov, Andri Gunnarsson, Jonas Thor Snaebjornsson**. Concrete beams reinforced with prestressed basalt bars // Concrete – Innovation and Design, fib Symposium, Copenhagen May 18-20, 2015.

5 **Andri Gunnarsson, Eythor Rafn Thorhallsson, Jonas Thor Snaebjornsson**. Simulation of Experimental Research of Concrete Beams Prestressed with BFRP Tendons // Nordic Concrete Research Symposium. Reykjavik, Iceland. August 2014.
6 **Eythor Thorhallsson, Sindri Hlifar Gudmundsson.** Test of prestressed basalt FRP concrete beams with and without external stirrups // Proceedings of Fib symposium Engineering a Concrete future: Technology, modelling & Construction. At: Tel Aviv. Israel. 2013.
7 **Duic J., Kenno S., Das S.** Performance of concrete beams reinforced with basalt fibre composite rebar // Construction and Building Materials. 2018. Vol. 176. Pp. 470-481. DOI: 10.1016/j.conbuildmat.2018.04.208.
8 **Esfahani M.R., Kianoush M.R., Moradi A.R.** Punching shear strength of interior slab-column connections strengthened with carbon fiber reinforced polymer sheets // Engineering Structures. 2009. Vol. 31. Issue 7. Pp. 1535-1542. DOI: 10.1016/j.engstruct.2009.02.021.
9 **Almassri B., Mahmoud F.A., Francois R.** Behavior of corroded reinforced concrete beams repaired with nsm cfrp rods, experimental and finite element study // Composites Part B: Engineering. 2016. Vol. 92. Pp. 1-25. DOI: 10.1016/j.compositesb.2015.01.022.
10 **Chellapandian M., Prakash S.S., Sharma A.** Experimental and finite element studies on the flexural behavior of reinforced concrete elements strengthened with hybrid FRP technique // Composite Structures. 2019. Vol. 208. Pp. 466-478. DOI: 10.1016/j.compstruct.2018.10.028.
11 **Subramanian N.** Sustainability of RCC Structures using Basalt Composite Rebars // The Masterbuilder. September 2010.
12 **Рубин О.Д., Лисичкин С.Е., Зюзина О.В.** Прочность малоармированных железобетонных конструкций с межблочными строительными швами, усиленных предварительно напряженной базальтокомпозитной арматурой // Природообустройство. 2021. №1. С. 53-62. DOI: 10.26897/1997-6011-2021-1-53-62.
13 **Беллендир Е.Н., Рубин О.Д., Лисичкин С.Е., Баклыков И.В.** Методика моделирования и расчета железобетонных конструкций эксплуатируемых ГТС, усиленных предварительно напряженной базальтокомпозитной арматурой// Природообустройство. 2021. №5. С. 59-67. DOI: 10.26897/1997-6011-2021-5-59-67.
14 **Рубин О.Д., Беллендир Е.Н., Баклыков И.В., Зюзина О.В., Шайтанов М.В.** Методика расчетных исследований усиления предварительно напряженной базальтокомпозитной арматурой стен камер шлюзов с учетом фактических данных об их эксплуатационном состоянии // Строительство: наука и образование. 2022. Т. 12. Вып. 3., Ст. 2. DOI: 10.22227/2305-5502.2022.3.2.
15 СП 63.13330.2018. Бетонные и железобетонные конструкции. Основные положения. Актуализированная редакция СНиП 52-01-2003. М., 2019. 126 с.
16 СП 295.1325800.2017. Конструкции бетонные, армированные полимерной композитной арматурой. Правила проектирования. М., Стандартинформ, 2017. 55 с.
17 СП 41.13330.2012. Бетонные и железобетонные конструкции гидротехнических сооружений. Актуализированная редакция СНиП 2.06.08-87. М., 2012. 67 с.
18 **Bellendir E.N., Rubin O.D., Lisichkin S.E., Zyuzina O.V.** Experimental Study Into Prestress Losses of Basalt Composite Reinforcement Used in the Composition of Concrete Elements. Power Technology and Engineering, 2021, 54(5) – pp. 605-608.

Rubin Oleg, doctor of science, Department of hydraulics and hydraulic engineering, Institute of hydraulic engineering and power plant construction, Moscow State University of Civil Engineering (National Research University), associate professor, 26, Yaroslavskoye Shosse, Moscow, 129337, rubinod@niies.ru

Kozlov Dmitry, doctor of science, Department of hydraulics and hydraulic engineering, Institute of hydraulic engineering and power plant construction, Moscow State University of Civil Engineering (National Research University), head of department, 26, Yaroslavskoye Shosse, Moscow, 129337, kozlovdv@mail.ru

Antonov Anton, PhD, Department of hydraulics and hydraulic engineering, Institute of hydraulic engineering and power plant construction, Moscow State University of Civil Engineering (National Research University), associate professor, 26, Yaroslavskoye Shosse, Moscow, 129337, antonov.an.s@yandex.ru

Amer Almasri, postgraduate student Department of hydraulics and hydraulic engineering, Institute of hydraulic engineering and power plant construction, Moscow State University of Civil Engineering (National Research University), 26, Yaroslavskoye Shosse, Moscow, 129337, Ameralmasri3522@gmail.com

Zhang Junhao, postgraduate student Department of hydraulics and hydraulic engineering, Institute of hydraulic engineering and power plant construction, Moscow State University of Civil Engineering (National Research University), 26, Yaroslavskoye Shosse, Moscow, 129337, weiw0951@gmail.com

Рубин Олег Дмитриевич, доктор технических наук, доцент кафедры гидравлики и гидротехнического строительства, Национальный исследовательский Московский государственный строительный университет, 26, Ярославское шоссе, Москва,129337, rubinod@niies.ru

Козлов Дмитрий Вячеславович — доктор технических наук, профессор, заведующий кафедрой гидравлики и гидротехнического строительства, Национальный исследовательский Московский государственный строительный университет, 26, Ярославское шоссе, Москва, 129337, kozlovdv@mail.ru

Антонов Антон Сергеевич, кандидат технических наук, доцент кафедры гидравлики и гидротехнического строительства, Национальный исследовательский Московский государственный строительный университет, 26, Ярославское шоссе, Москва, 129337, antonov.an.s@yandex.ru

Амер Алмасри, аспирант кафедры гидравлики и гидротехнического строительства, Национальный исследовательский Московский государственный строительный университет, 26, Ярославское шоссе, Москва,129337, Ameralmasri3522@gmail.com

Чжан Цзюньхао, аспирант кафедры гидравлики и гидротехнического строительства, Национальный исследовательский Московский государственный строительный университет, 26, Ярославское шоссе, Москва,129337, weiw0951@gmail.com

DOI:10.22337/2587-9618-2024-20-4-141-149

A FINITE ELEMENT MODEL FOR CALCULATING A NON-THIN ORTHOTROPIC CYLINDRICAL SHELL, TAKING INTO ACCOUNT THE INDUCED INHOMOGENEITY

Alexander A. Treshchev, Dmitry O. Besstrashnov
Tula State University, Tula, RUSSIA

Annotation. The formulation of a model for the deformation and strength calculation of an open cylindrical shell of circular shape rigidly pinched along contour planes formed by generators is considered. The ratios of the geometric parameters of the shell differ significantly from thin-walled structures, to which traditional technical hypotheses could be applied. The formulation of a mathematical model defining the stress-strain states of a thick-walled structure was carried out within the framework of a nonlinear three-dimensional theory. The peculiarity of the developed model was that orthotropic composites were adopted as the structural materials of the shell, the deformation and strength properties of which manifest themselves in different ways in accordance with the types of stress states being realized. The manifestation of such mechanical properties of materials is interpreted as induced heterogeneity, which significantly complicates the methodology for calculating spatial structures. Due to the specified features of the research object, isoparametric finite elements of a three-dimensional tetrahedral shape, the nodes of which had three degrees of freedom, were used to develop a computational model. In order to adequately account for the stiffness properties of orthotropic composites exhibiting induced heterogeneity, the basis of the determining relationships for them was the deformation potential formulated in the normalized stress tensor space associated with the main axes of orthotropy of materials. Due to the nonlinearity of the problem under consideration, the process of solving it was based on the method of variable elasticity parameters. As a result of the implementation of the computational model, comprehensive information was obtained on the stresses, deformations and displacements of the shell, the main of which are presented in the text of the article with the addition of their analysis.

Keywords: finite element method, open cylindrical shell, structural orthotropy, induced inhomogeneity, dependence of stiffness on the type of stress state

КОНЕЧНО-ЭЛЕМЕНТНАЯ МОДЕЛЬ РАСЧЕТА НЕТОНКОЙ ОРТОТРОПНОЙ ЦИЛИНДРИЧЕСКОЙ ОБОЛОЧКИ С УЧЕТОМ НАВОДИМОЙ НЕОДНОРОДНОСТИ

А.А. Трещев, Д.О. Бесстрашнов
Тульский государственный университет, г. Тула, РОССИЯ

Аннотация. Рассмотрена формулировка модели деформационно-прочностного расчета незамкнутой цилиндрической оболочки кругового очертания, жестко защемленной по контурным плоскостям, сформированным образующими. Соотношения геометрических параметров оболочки существенно отличаются от тонкостенных конструкций, которым могли быть применены традиционные технические гипотезы. Формулировка математической модели, определяющей напряженно-деформированные состояния толстостенной конструкции, была осуществлена в рамках нелинейной трехмерной теории. Особенностью разработанной модели явилось то, что в качестве конструкционных материалов оболочки были приняты ортотропные композиты, деформационные и прочностные свойства которых проявляются по-разному в соответствии с реализуемыми видами напряженных состояний. Проявление подобных механических свойств материалов трактуется как наведенная неоднородность, что существенно усложняет методику расчета пространственных конструкций. Ввиду указанных особенностей объекта исследований для разработки расчетной модели были приняты изопараметрические конечные элементы объемной тетраэдрической формы, узлы которой имели три степени свободы. Для адекватного учета жесткостных свойств ортотропных композитов, проявляющих наведенную неоднородность, основой определяющих соотношений для них был принят потенциал деформаций, сформулированный в нормированном тензорном пространстве напряжений, связанном с главными осями ортотропии материалов. Ввиду нелинейности рассматриваемой задачи процесс ее решения строился по методу переменных параметров упругости. В результате реализации расчетной модели получена исчерпывающая информация о возникающих напряжениях, деформациях и перемещениях оболочки, основные из которых представлены в тексте статьи с добавлением их анализа.

Ключевые слова: метод конечных элементов, незамкнутая цилиндрическая оболочка, структурная ортотропия, наведенная неоднородность, зависимость жесткости от вида напряженного состояния

1. INTRODUCTION

Modern technology and construction use all new structural materials, among which composites have become widespread. Their peculiarity often lies in the presence not only of structural orthotropy, but also in the manifestation of deformation anisotropy, such as the dependence of deformation and strength properties on the kind of stress state. These materials are widely used in the manufacture of spatial structures, the elements of which cannot be classified as thin-walled. In particular, this applies to cylindrical shells of various configurations and other curved structures. Calculations for the strength and deformability of similar structures should be based on reliable calculation models based on the specifics of the mechanical properties of these composites and be adequate to the real picture of the loading processes and geometry of structures. It is obvious that the accuracy of the calculation methods used depends on the reliability of the determining ratios, which do not contradict established and approved mechanical deformation experiments of the studied composites. Obviously, the dependences of strain and stress tensors arising from the potential proposed in the works can serve as the most reliable equations of state [1 – 3]. In the same works and in monographs [4, 5], a detailed analysis of the serious shortcomings of widely known models published by many authors [6 – 14] is presented and, therefore, their assessment is not given here.

2. EQUATIONS OF STATE FOR ORTHOTROPIC MATERIALS EXHIBITING INHOMOGENEITY DURING DEFORMATION

As a result of the use of the author's technique of the normalized tensor stress space associated with the main axes of the structure of materials, the deformation potential of an orthotropic substance sensitive to the kind of stress state was postulated in [2, 3]:

$$\begin{gathered} W = 0,5(A_{1111} + B_{1111}\alpha_{11})\sigma_{11}^2 + 0,5(A_{2222} + \\ +B_{2222}\alpha_{22})\sigma_{22}^2 + 0,5(A_{3333} + B_{3333}\alpha_{33})\sigma_{33}^2 + \\ +[A_{1122} + B_{1122}(\alpha_{11} + \alpha_{22})]\sigma_{11}\sigma_{22} + [A_{2233} + \\ +B_{2233}(\alpha_{22} + \alpha_{33})]\sigma_{22}\sigma_{33} + [A_{3311} + \\ +B_{3311}(\alpha_{33} + \alpha_{11})]\sigma_{33}\sigma_{11} + 0,5(A_{1212}\tau_{12}^2 + \\ +A_{2323}\tau_{23}^2 + A_{3131}\tau_{31}^2), \end{gathered} \tag{1}$$

where $\alpha_{ij} = \sigma_{ij} / S$ – stresses in the normalized space of the tensor associated with the main axes of the orthotropy of the material; $S = \sqrt{\sigma_{ij}\sigma_{ij}}$ – the norm of the tensor stress space; $\alpha_{ij}\alpha_{ij} = 1$ – tensor space normalization condition; material parameters A_{ijkm}, B_{ijkm} are determined after identification of the equations of state arising from the potential (1) using the results of mechanical tests performed; (i, j, k, m= 1, 2, 3).

Having differentiated the potential (1) according to the Castigliano rules, we establish the equations of connection between the tensors of the second rank of the deformed and stressed states for orthotropic structures acquiring deformation anisotropy:

$$e_{ij} = C_{ijkm}\sigma_{km}, \quad i, j, k, m = 1, 2, 3, \qquad (2)$$

where $C_{1111} = (A_{1111} + B_{1111}\alpha_{11}) +$
$+0,5[B_{1111}\alpha_{11}(1-\alpha_{11}^2) - B_{2222}\alpha_{22}^3 -$
$-B_{2222}\alpha_{22}^3 - B_{3333}\alpha_{33}^3 - A_{1212}\alpha_{12}^3 - A_{2323}\alpha_{23}^3 -$
$-A_{1313}\alpha_{13}^3] + B_{1122}\alpha_{22}(1-\alpha_{11}^2 - \alpha_{11}\alpha_{22}) +$
$+B_{1133}\alpha_{33}(1-\alpha_{11}^2 - \alpha_{11}\alpha_{33}) -$
$-B_{2233}\alpha_{22}\alpha_{33}(\alpha_{22} + \alpha_{33});$
$C_{1122} = A_{1122} + B_{1122}(\alpha_{11} + \alpha_{22});$
$C_{1133} = A_{1133} + B_{1133}(\alpha_{11} + \alpha_{33});$
$C_{2222} = (A_{2222} + B_{2222}\alpha_{22}) +$
$+0,5[B_{2222}\alpha_{22}(1-\alpha_{22}^2) - B_{1111}\alpha_{11}^3 - B_{3333}\alpha_{33}^3 -$
$-A_{1212}\alpha_{12}^3 - A_{2323}\alpha_{23}^3 - A_{1313}\alpha_{13}^3] +$
$+B_{1122}\alpha_{11}(1-\alpha_{22}^2 - \alpha_{11}\alpha_{22}) +$
$+B_{2233}\alpha_{33}(1-\alpha_{22}^2 - \alpha_{22}\alpha_{33}) -$
$-B_{1133}\alpha_{11}\alpha_{33}(\alpha_{11} + \alpha_{33});$
$C_{2233} = A_{2233} + B_{2233}(\alpha_{22} + \alpha_{33});$
$C_{3333} = (A_{3333} + B_{3333}\alpha_{33}) +$
$+0,5[B_{3333}\alpha_{33}(1-\alpha_{33}^2) - B_{1111}\alpha_{11}^3 -$
$-B_{2222}\alpha_{22}^3 - A_{1212}\alpha_{12}^3 - A_{2323}\alpha_{23}^3 - A_{1313}\alpha_{13}^3] +$
$+B_{1133}\alpha_{11}(1-\alpha_{33}^2 - \alpha_{11}\alpha_{33}) +$
$B_{2233}\alpha_{22}(1-\alpha_{33}^2 - \alpha_{22}\alpha_{33}) -$
$-B_{1122}\alpha_{11}\alpha_{22}(\alpha_{11} + \alpha_{22});$
$C_{1212} = 0,5\{A_{1212} - (B_{1111}\alpha_{11}^3 + B_{2222}\alpha_{22}^3 +$
$+B_{3333}\alpha_{33}^3) - 2[B_{1122}\alpha_{11}\alpha_{22}(\alpha_{11} + \alpha_{22}) +$
$+B_{2233}\alpha_{22}\alpha_{33}(\alpha_{22} + \alpha_{33}) + B_{1133}\alpha_{11}\alpha_{33}(\alpha_{11} + \alpha_{33})]\};$
$C_{2323} = 0,5\{A_{2323} - (B_{1111}\alpha_{11}^3 + B_{2222}\alpha_{22}^3 +$
$+B_{3333}\alpha_{33}^3) - 2[B_{1122}\alpha_{11}\alpha_{22}(\alpha_{11} + \alpha_{22}) +$
$+B_{2233}\alpha_{22}\alpha_{33}(\alpha_{22} + \alpha_{33}) + B_{1133}\alpha_{11}\alpha_{33}(\alpha_{11} + \alpha_{33})]\};$
$C_{1313} = 0,5\{A_{1313} - (B_{1111}\alpha_{11}^3 + B_{2222}\alpha_{22}^3 +$
$+B_{3333}\alpha_{33}^3) - 2[B_{1122}\alpha_{11}\alpha_{22}(\alpha_{11} + \alpha_{22}) +$
$+B_{2233}\alpha_{22}\alpha_{33}(\alpha_{22} + \alpha_{33}) + B_{1133}\alpha_{11}\alpha_{33}(\alpha_{11} + \alpha_{33})]\};$

$C_{1212} = C_{2121}$, $C_{2323} = C_{3232}$, $C_{1313} = C_{3131}$, the other components of the tensor C_{ijij}, characterizing the malleability of the material are identically equal to zero

As a result of the analysis of experimental data on the proportional loading of standard samples made of orthotropic composites of various classes, the identification of equations of state (2) was carried out in [2, 3, 5]. In this case, the constants of the compliance tensor (2) were calculated using technically measured parameters established during tensile testing, compression of standards cut along the main axes of orthotropy and in shear experiments in the main planes of materials:

$$A_{kkkk} = (1/E_k^+ + 1/E_k^-)/2;$$
$$B_{kkkk} = (1/E_k^+ - 1/E_k^-)/2;$$
$$A_{iijj} = -(\nu_{ij}^+/E_j^+ + \nu_{ij}^-/E_j^-)/2;$$
$$B_{iijj} = -(\nu_{ij}^+/E_j^+ - \nu_{ij}^-/E_j^-)/2;$$
$$A_{ijij} = 1/G_{ij}; \quad \nu_{ij}^+/E_j^+ = \nu_{ji}^+/E_i^+;$$
$$\nu_{ij}^-/E_j^- = \nu_{ij}^-/E_i^-; \quad i, j, k = 1, 2, 3, \qquad (3)$$

where $E_k^{\pm}$, $\nu_{ij}^{\pm}$ – elastic modulus and transverse strain coefficients calculated as a result of processing data from experiments conducted in the directions of the main axes of orthotropy using the least squares method (a positive sign corresponds to tensile experiments, and a negative sign corresponds to compression); G_{ij} – shear modules in the main orthogonal planes of orthotropy.

Along with the identification of the model (1) – (3), in the same works [2, 3, 5], the boundaries of possible potential constants were determined in accordance with Drucker's postulate and the proof of the theorems of the existence and uniqueness of solutions to boundary value problems. These procedures confirmed the inviolability of energy conservation [2, 3, 5]. Particular values of the mechanical characteristics of orthotropic materials with acquired heterogeneity are available in well–known publications [1 – 13, 15].

3. PROBLEM STATEMENT AND SHELL CALCULATION

Using the physical and mathematical correctness of potential dependencies (1) – (3), they can be used as the basis for a finite element model for calculating the stress-strain state of thick-walled cylindrical shells. Considering that it is supposed to investigate shells that do not meet the criteria of thin ones, three-dimensional finite elements of isoparametric interpretation were used in the form of a tetrahedron having three degrees of freedom at the node. The mathematical apparatus of these finite elements is fully developed in [16, 17]. The presented article is based on the transformation of only the stiffness matrix of the specified elements, into which the equations of state (2) were embedded, previously converted into the matrix form of the stress-strain relationship:

$$\{\sigma\} = [P]\{e\} \tag{4}$$

where $\{\sigma\}$ and $\{e\}$ – six-dimensional stress and strain vectors composed of components of the corresponding tensors (2); $[P]$ – a rigid matrix in size 6×6, the inverse of the material's compliance matrix, consisting of tensor components C_{ijij} (2), depending on the type of stress state, $[P]=[C]^{-1}$.

A short, unclosed cylindrical shell of circular shape with rigid clamping along the reference planes was selected for analysis. The breakdown of the shell into finite elements is shown in Fig. 1, and the calculation scheme is shown in Fig. 2. In the process of sampling the shell continuum, the convergence of the FE model was checked, which is shown in Fig. 3.

The developed FE model was used not only taking into account the equations of state (2), (4) introduced, but also calculations were carried out on its basis with embedded determining ratios of widespread theories of deformation of different resistant orthotropic materials. In order to compare the results of shell calculations, the equations proposed in the works of such authors as R.M.Jones – D.A.R.Nelson [8, 9, 11, 12] and S.A.Ambartsumyan [14] were used. In addition, to estimate the error given by the generalized Hooke's law formulated for orthotropic materials [18], if it is used as physical dependencies of deformation mechanics, it was also used in calculations. At the same time, the average characteristics obtained from experiments on uniaxial tension and compression in the main axes of orthotropy were taken as elastic modulus and transverse deformation coefficients. To calculate the shell, a composite material based on graphite of the ATJ-S brand, widely used in technology, was adopted. A complete set of stiffness parameters characterizing its properties is given in [11]. As a result of the calculations, complete information was obtained on the distribution of shell SSC parameters. Here we will focus on the analysis of individual parameters, which are presented in Fig. 4 – 8.

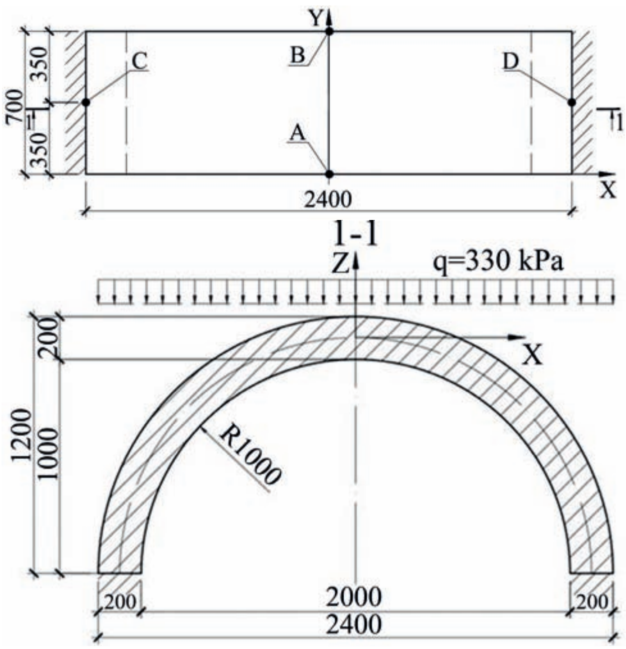

Figure 1. The design scheme of the cylindrical shell

Figure 2. Discretization of the shell on the FE

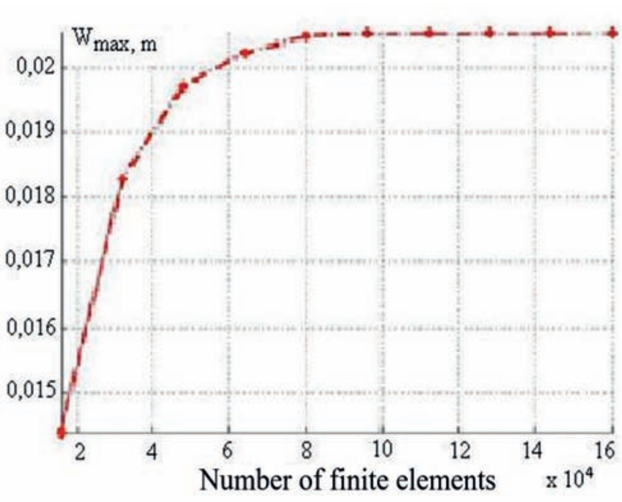

Figure 3. Convergence of the FE model with respect to maximum deflections

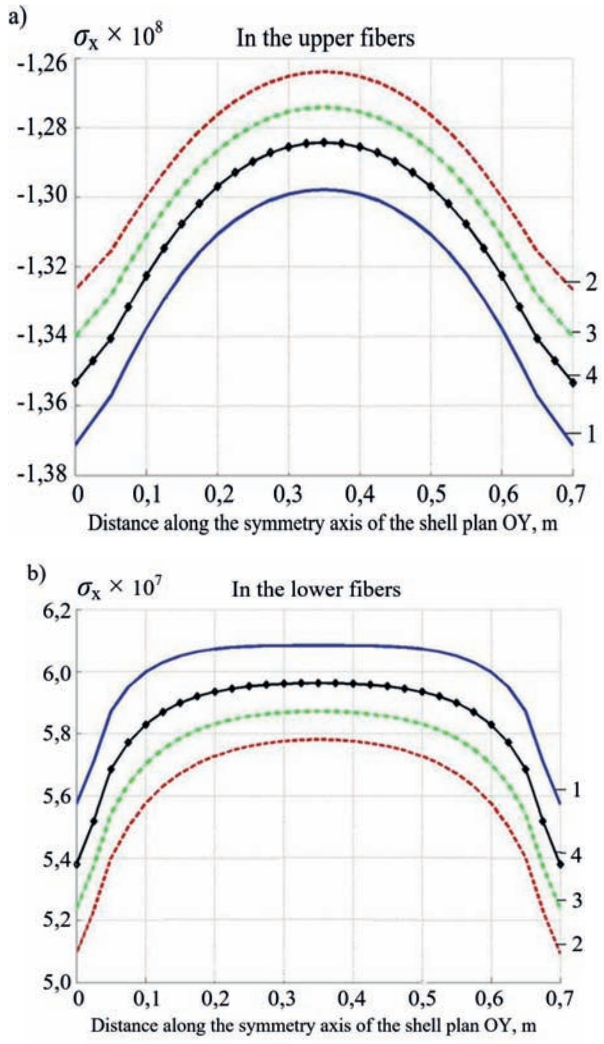

Figure 4. Normal stress distribution σ_x along the line A-B, Pa: in the upper fibers (a); in the lower fibers (b)

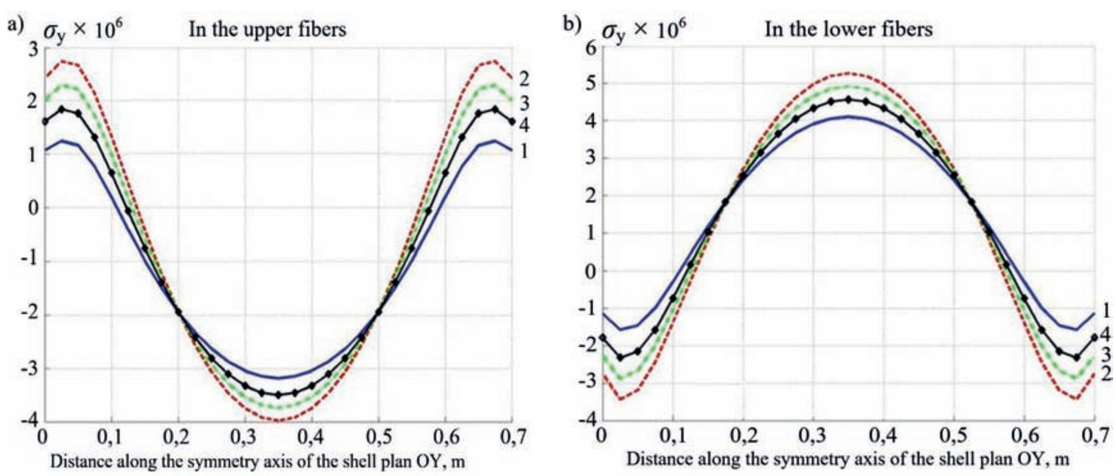

Figure 5. Normal stress distribution σ_y along the line A-B, Pa: in the upper fibers (a); in the lower fibers (b)

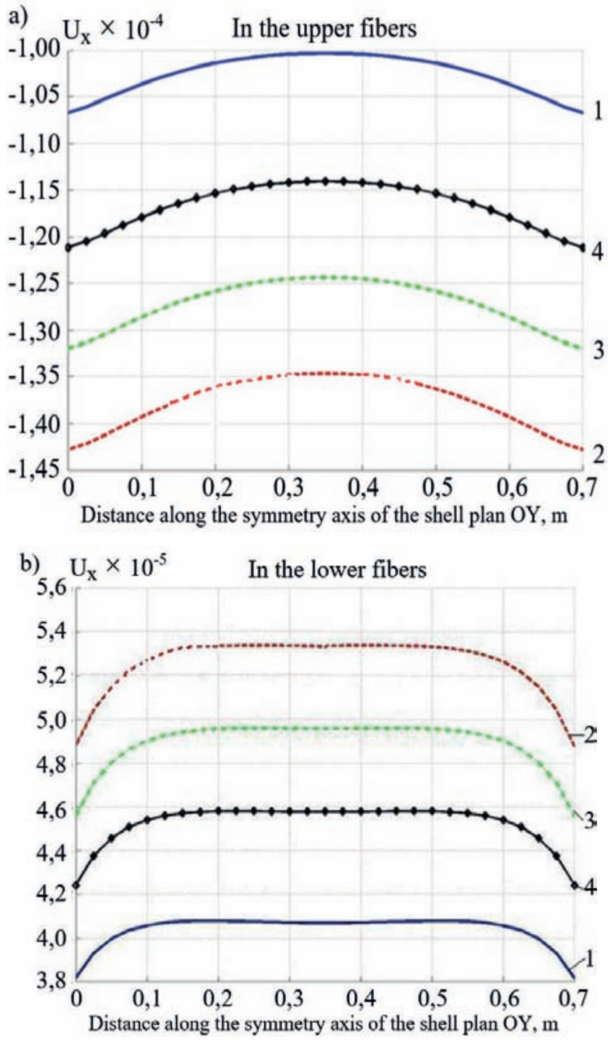

<u>Figure 6.</u> Distribution of displacements U_X along the line A-B, m: in the upper fibers (a); in the lower fibers (b)

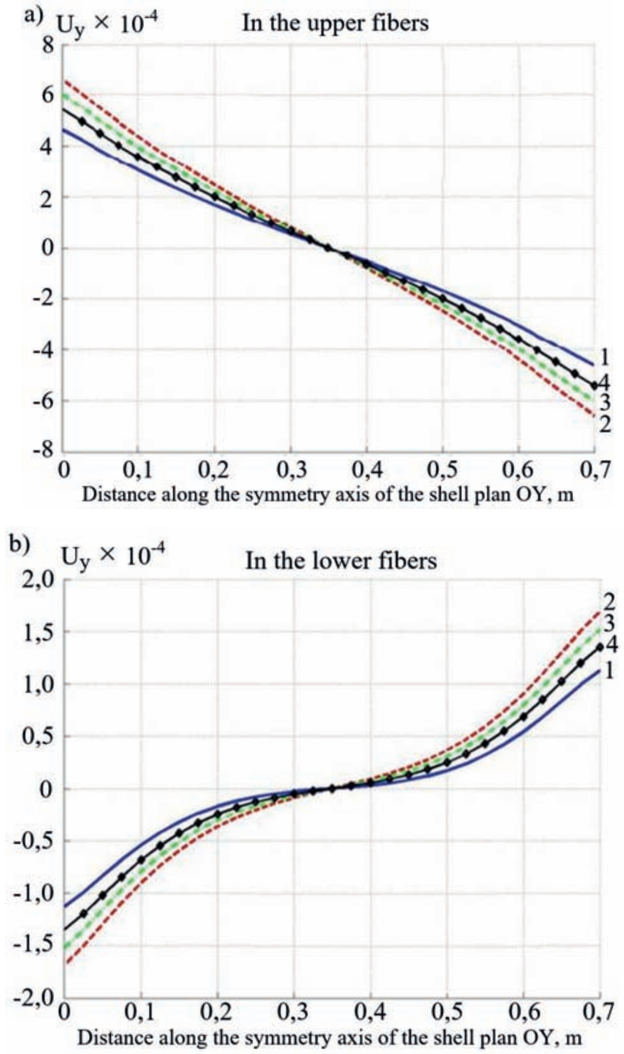

<u>Figure 7.</u> Distribution of displacements U_Y along the line A-B, m: in the upper fibers (a); in the lower fibers (b)

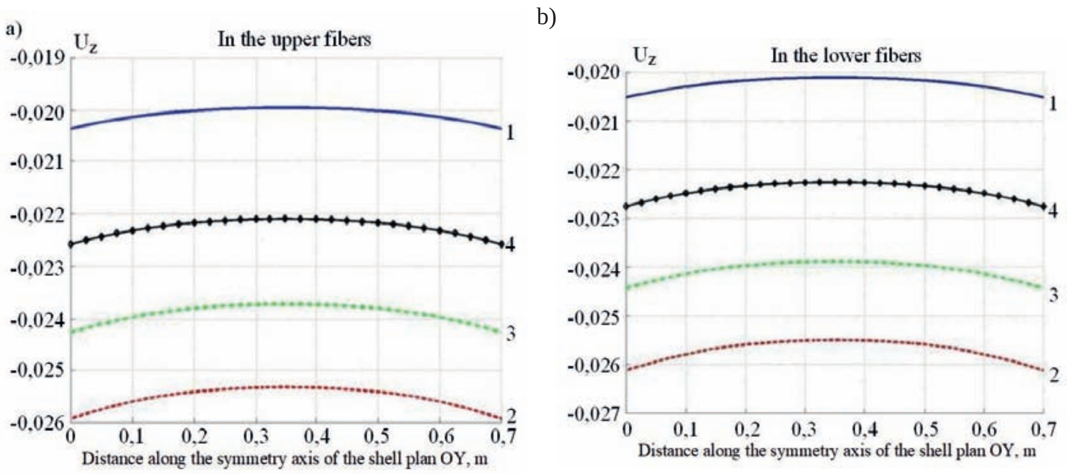

<u>Figure 8.</u> Distribution of displacements U_Z along the line A-B, m: in the upper fibers (a); in the lower fibers (b)

In Fig. 4 – 8 the introduced digital designations of the graphs of changes in the calculated values, refer to solutions obtained on the basis of various models of constitutive relations: 1 – author's model; 2 – model based on the classical theory of deformation of orthotropic materials using the generalized Hooke’s law [18] and using the medium mechanical characteristics of the material; 3 – model by S.A. Ambartsumyan [14]; 4 – model by R.M.Jones – D.A.R.Nelson [8, 9, 11, 12].

4. ANALYSIS OF THE RESULTS OBTAINED

Analyzing the results of calculations of cylindrical shells with structural orthotropy and made of ATJ-S composite, which are presented in Fig. 4 – 8, important theoretical features can be noted. These features are concluded in the fact that traditional mathematical models, which are based on the generalized Hooke’s law, which does not take into account the dependence of the rigidity properties of the material on the kind of stress state, lead to serious errors in determining stresses up to 58% – 78%. In this case, errors in determining the points of the cylindrical shell can reach 35%. If the R.M.Jones – D.A.R.Nelson model is used for shell calculations [8, 9, 11, 12], then the results will differ from the theoretical data using the generalized Hooke’s law somewhat less and reach 16–36% and 18%, respectively. An explanation for this may be the not entirely correct consideration of the effect of a complex stress state on the change in the components of the compliance tensors, which are used by models [8, 9, 11, 12] and [14] in comparison with equations obtained using normalized tensor stress spaces [1 – 5].

5. CONCLUSION

The results of the calculations performed and the analysis of the results obtained demonstrate and confirm the fact that the design of elements of spatial structures with a curvilinear outline such as cylindrical shells made of graphite-based composite materials should be carried out most carefully. In this case, it is imperative to take into account the peculiarities of the mechanical behavior of such composites. In addition, when performing calculations of stresses and strains of shells, special attention should be paid to the selection of mathematical models of constitutive relations that do not conflict with known experimental data and are most adequate to the latter when changing complex kinds of stress states.

REFERENCES

1. **Treshchev A.A.** Potential dependence between deformations and stresses for orthotropic physically nonlinear materials / A.A.Treshchev // Fundamental and applied problems of engineering and technology. – 2017. – No. 4-1 (324). – pp. 71–74.
2. **Treshchev A.A.** Variant of the deformation model of orthotropic composite materials / A.A. Treshchev, Yu.A. Zavyalova, M.A. Lapshina // Expert: Theory and Practice (Scientific and Practical Journal). – Tolyatti: ANO “Institute of Forensic Construction and Technical Expertise” – 2020. – No. 3(6). – P. 62 – 68.
3. **Treschev A.A.** Defining equations of deformation of materials with double anisotropy / A.A. Treschev, Yu.A. Zavyalova, M.A. Lapshina, A.E. Gvozdev, O.V. Kuzovleva, E.S. Krupitsyn // Chebyshevskiisbornik. – 2021. – Vol. 22. – No. 4. – pp. 369 – 383.
4. **Treshchev A.A.** Theory of deformation and strength of materials with initial and induced sensitivity to the kind of stress state. Defining relations / A.A. Treshchev. – M.; Tula: RAASN; Tula State University, 2016. – 326 p.
5. **Treschev** A.A. Theory of deformation and strength of different resistant materials / A.A.Treschev. – Tula: Publisher Name TulSU. – 2020. – 359 p.
6. **Schmueser D.W.** Nonlinear Stress-Strain and Strength Response of Axisymmetric Bimodulus Composite Material Shells /

D.W.Schmueser // AIAA Journal. – 1983. – Vol. 21. – №12. – pp. 1742 – 1747.
7. **Reddy L.N.** On the Behavior of Plates Laminated of Bimodulus Composite Materials / L.N.Reddy, C.W.Bert // ZAMM. – 1982. – Vol. 62. – № 6. – pp. 213 – 219.
8. **Jones R.M.** A Nonsymmetric Compliance Matrix Approach to Nonlinear Multimodulus Ortotropic Materials / R.M.Jones // AIAA Journal. – 1977. – Vol. 15. – № 10. – pp. 1436 – 1443.
9. **Jones R.M.** Modeling Nonlinear Deformation of Carbon-Carbon Composite Material / R.M.Jones // AIAA Journal. – 1980. – Vol. 18. – № 8. – pp. 995 – 1001.
10. **Rose A.V.** Three-reinforced woven materials / A.V. Rose, I.G. Zhigun, M.N. Dushin // Polymer mechanics. – 1970. – No. 3. – pp. 471–476.
11. **Jones R.M.** Theoretical-experimental correlation of material models for non-linear deformation of graphite / R.M.Jones, D.A.R.Nelson // AIAA Journal. – 1976. – Vol. 14 – №10. – pp. 1427–1435.
12. **Jones R.M.** Stress-Strain Relations for Materials with Different Moduli in Tension and Compression / R.M.Jones // AIAA Journal. – 1977. – Vol. 15. – №1. – pp. 16–25.
13. **Zolochevsky A.A.** Calculation of anisotropic shells from different modulus materials under non-axisymmetric loading / A.A. Zolochevsky, V.N. Kuznetsov // Dynamics and strength of heavy machines. – Dnepropetrovsk: DSU, 1989. – pp. 84–92.
14. **Ambartsumian S.A.** Basic equations and of the ratio of the heterogeneous theory of elasticity of an anisotropic body / S.A.Ambartsumian // News USSR Academy of Sciences. Solid State Mechanics. – 1969. – No. 3. – pp. 51 – 61.
15. **Kayumov R.A.** Identification of mechanical characteristics of fiber-reinforced composites / R.A. Kayumov, S.A. Lukankin, V.N. Paimushin, S.A. Kholmogorov // Scientific Notes of the Kazan University. Physical and mathematical sciences. – 2015. – Vol. 157. – Book 4. – pp. 112 – 132.
16. **Treshchev A.A.** Theory of deformation of spatial reinforced concrete structures / A.A. Treshchev, V.G. Telichko. – M.; Tula: RAASN; Tula State University, 2019. – 386 p.
17. **Treshchev A.A.** Finite element model for calculating spatial structures made of materials with complex properties / A.A. Treshchev, V.G. Telichko, A.N. Tsarev, P.Yu. Khodorovich // Izvestia of Tula State University. Technical science. – Tula: Tula State University Publishing House, 2012. – Issue. 10. − pp. 106 – 114.
18. **Green A.** Large elastic deformations and nonlinear mechanics of a continuous medium / A.Green, J.Adkins. – Moskow: Publisher Name Mir. – 1976. – 416 p.

СПИСОК ЛИТЕРАТУРЫ

1. **Трещев А.А.** Потенциальная зависимость между деформациями и напряжениями для ортотропных физически нелинейных материалов / А.А.Трещев // Фундаментальные и прикладные проблемы техники и технологии. – Орел: ОГУ. – 2017. – № 4-1 (324). – С. 71 – 74.
2. **Трещев А.А.** Вариант модели деформирования ортотропных композитных материалов / А.А.Трещев, Ю.А.Завьялова, М.А.Лапшина // Эксперт: Теория и практика (Научно-практический журнал). – Тольятти: АНО «Институт судебной строительно-технической экспертизы» – 2020. – №3(6). – С. 62 – 68.
3. **Treschev A.A.** Defining equations of deformation of materials with double anisotropy / A.A.Treschev, Yu.A.Zavyalova, M.A.Lapshina, A.E.Gvozdev, O.V.Kuzovleva, E.S.Krupitsyn // Chebyshevskiisbornik. – 2021. – Vol. 22. – No. 4. – pp. 369 – 383.
4. **Трещев А.А.** Теория деформирования и прочности материалов с изначальной и наведенной чувствительностью к виду напряженного состояния. Определяющие соотношения / А.А.Трещев. – М.; Тула: РААСН; ТулГУ, 2016. –326с.

5. **Трещев А.А.** Теория деформирования и прочности разносопротивляющихся материалов / А.А.Трещев. – Тула: ТулГУ, 2020. – 359 с.
6. **Schmueser D.W.** Nonlinear Stress-Strain and Strength Response of Axisymmetric Bimodulus Composite Material Shells / D.W.Schmueser // AIAA Journal. – 1983. – Vol. 21. – №12. – pp. 1742 – 1747.
7. **Reddy L.N.** On the Behavior of Plates Laminated of Bimodulus Composite Materials / L.N.Reddy, C.W.Bert // ZAMM. – 1982. – Vol. 62. – № 6. – pp. 213 – 219.
8. **Jones R.M.** A Nonsymmetric Compliance Matrix Approach to Nonlinear Multimodulus Ortotropic Materials / R.M.Jones // AIAA Journal. – 1977. – Vol. 15. – № 10. – pp. 1436 – 1443.
9. **Jones R.M.** Modeling Nonlinear Deformation of Carbon-Carbon Composite Material / R.M.Jones // AIAA Journal. – 1980. – Vol. 18. – № 8. – pp. 995 – 1001.
10. **Розе А.В.** Трехармированные тканые материалы / А.В.Розе, И.Г.Жигун, М.Н.Душин // Механика полимеров. – 1970. – №3. – с. 471–476.
11. **Jones R.M.** Theoretical-experimental correlation of material models for non-linear deformation of graphite / R.M.Jones, D.A.R.Nelson // AIAA Journal. – 1976. – Vol. 14 – №10. – pp. 1427–1435.
12. **Jones R.M.** Stress-Strain Relations for Materials with Different Moduli in Tension and Compression / R.M.Jones // AIAA Journal. – 1977. – Vol. 15. – №1. – pp. 16–25.
13. **Золочевский А.А.** Расчет анизотропных оболочек из разномодульных материалов при неосесимметричном нагружении / А.А.Золочевский, В.Н.Кузнецов // Динамика и прочность тяжелых машин. – Днепропетровск: ДГУ, 1989. – С. 84–92.
14. **Амбарцумян С.А.** Основные уравнения и соотношения разномодульной теории упругости анизотропного тела / С.А.Амбарцумян // Изв. АН СССР. МТТ, 1969. − № 3. − С. 51 − 61.
15. **Каюмов Р.А.** Идентификация механических характеристик армированных волокнами композитов / Р.А. Каюмов, С.А. Луканкин, В.Н. Паймушин, С.А. Холмогоров // Ученые записки Казанского университета. Физико-математические науки. – 2015. – Т. 157. – Кн. 4. – С. 112–132.
16. **Трещев А.А.** Теория деформирования пространственных железобетонных конструкций / А.А.Трещев, В.Г.Теличко. – М.; Тула: РААСН; ТулГУ, 2019. – 386 с.
17. **Трещев А.А.** Конечно-элементная модель расчета пространственных конструкций из материалов с усложненными свойствами / А.А.Трещев, В.Г.Теличко, А.Н.Царев, П.Ю.Ходорович // Известия ТулГУ. Технические науки. – Тула: Изд-во ТулГУ, 2012. – Вып. 10. − С. 106-114.
18. **Green A.** Large elastic deformations and nonlinear mechanics of a continuous medium / A.Green, J.Adkins. – Moskow: Publisher Name Mir. – 1976. – 416 p.

Aleksander Anatolyevich Treshchev, Doctor of Technical Sciences, Professor, Head of the Department of Construction, Building Materials and Structures, Tula State University, Corresponding Member of RAACS; 300012, Russia, Tula, Lenin Avenue. 92. E-mail: taa58@yandex.ru.

Dmitry Olegovych Besstrashnov, graduate student of the department «Construction, building materials and structures» of Tula State University; 300012, Russia, Tula, Lenin Avenue. 92. *E-mail: mr.d-best@yandex.ru*

Александр Анатольевич Трещев, доктор технический наук, профессор, заведующий кафедрой «Строительство, строительные материалы и конструкции» Тульского государственного университета, член-корреспондент РААСН; 300012, г. Тула, Проспект Ленина, 92, E-mail: taa58@yandex.ru.

Дмитрий Олегович Бесстрашнов, аспирант кафедры «Строительство, строительные материалы и конструкции» Тульского государственного университета; 300012, г. Тула, Проспект Ленина, 92. E-mail: mr.d-best@yandex.ru

DOI:10.22337/2587-9618-2024-20-4-150-159

ESTIMATION OF ELECTRICITY CONSUMPTION FOR WATER TRANSPORTATION IN PRESSURE PIPELINES AFTER THEIR REPAIR

Vladimir A. Orlov, Sergey P. Zotkin, Dmitry V. Podolyan, Dmitry A. Petersburgsky
National Research Moscow State University of Civil Engineering, Moscow, RUSSIA

Abstract. The issues of using pipes made of different materials in water supply systems and the current situation with the technical condition of pressure pipeline transport are considered. It is noted that in order to ensure the standard service life of pipelines, it is necessary to carry out high-quality repair and restoration work using trenchless technologies and modern building materials, which include polymer pipes and flexible hoses. The object of research is a section of a dilapidated steel pipeline network of a certain thickness, diameter, depth and groundwater level above the tray. For the renovation of the pipeline, internal protective coatings are used, applied by dragging new pre-compressed polymer pipes and flexible polymer sleeves based on fiberglass. A description of trenchless technologies is presented, as well as automated programs that implement the tasks of determining the technological parameters (wall thickness of a polymer pipe and a polymer sleeve), hydraulic calculation of pressure losses depending on the degree of roughness of the pipeline walls, the inner diameter of a new two-layer pipe structure when passing a certain water flow, as well as the amount of electricity consumed for water transportation when appropriate wall thicknesses of protective coatings.

Keywords: pipelines, reconstruction, protective coatings, energy consumption

ОЦЕНКА ПОТРЕБЛЕНИЯ ЭЛЕКТРОЭНЕРГИИ НА ТРАНСПОРТИРОВКУ ВОДЫ В НАПОРНЫХ ТРУБОПРОВОДАХ ПОСЛЕ ИХ РЕМОНТА

В.А. Орлов, С.П. Зоткин, Д.В. Подолян, Д.А. Петербургский
Национальный исследовательский Московский государственный строительный университет (НИУ МГСУ), г. Москва, РОССИЯ

Аннотация. Рассмотрены вопросы использования в системах водоснабжения труб из разных материалов и сложившуюся ситуацию с техническим состоянием напорного трубопроводного транспорта. Отмечено, что для обеспечения нормативного срока службы трубопроводов необходимо качественное проведение ремонтно-восстановительных работ с использованием бестраншейных технологий и современных строительных материалов, к которым относятся полимерные трубы и гибкие рукава. Объектом исследований является участок ветхой трубопроводной сети из стали определенной дины, диаметра, глубины залегания и уровня грунтовых вод над лотком. Для реновации трубопровода используются внутренние защитные покрытия, наносимые путем протаскивания в трубопровод новых предварительно сжатых полимерных труб и гибких полимерных рукавов на основе стекловолокна. Представлено описание бестраншейных технологий, а также автоматизированных программ, реализующих поставленные задачи определения технологических параметров санации (толщины стенки полимерной трубы и полимерного рукава), гидравлического расчета потерь напора в зависимости от степени шероховатости стенок трубопровода, внутреннего диаметра новой двухслойной трубной конструкции при пропуске определенного расхода воды, а также величины затрачиваемой электроэнергии на транспортировку воды при соответствующих вариантах толщины стенок защитных покрытий.

Ключевые слова: трубопроводы, реконструкция, защитные покрытия, энергозатраты

INTRODUCTION

In cities and towns of Russia, steel and cast-iron pipelines have become the most widespread in pressure pipeline transport systems [1]. However, over the past 30 years, both in Russia and abroad, polymer pipes have become a serious competitor to steel, cast iron and reinforced concrete pipes [2]. In particular, in the Russian Federation, they account for 86.5% of newly built water supply networks after 2010, excluding data for Moscow and St. Petersburg. In addition, polymer pipes and flexible hoses made of polymer materials have firmly become one of the most promising building materials for the renovation of pipelines made of various materials [3]. Despite the clear progress in terms of the widespread use of pipes made of such traditional materials as steel, cast iron and others for both construction and trenchless repair of pipelines, their actual service life is below the standard values. Statistics show that, in general, in all settlements of the Russian Federation, there is an excess of the standard service life of water supply networks up to 40.8%. This circumstance is a consequence of the early appearance of various kinds of defects and, as a result, an increase in the amount of leaks of transported water [4, 5]. At the same time, it should be noted that the pace of renovation of existing domestic pipeline water supply networks, where modern trenchless technologies are used, sometimes leaves much to be desired, since they amount to about 2 and at best 4% per year of the length of the networks with a need of about 7-8%, which would allow in the coming years to fully restore the required condition and efficient operation pipeline networks [6]. To ensure the standard service life of pipelines, it is necessary to carry out high-quality repair and restoration work using modern materials, which include polymer pipes and hoses. An equally important component of the task of effective reconstruction of pressure pipeline transport is the reduction of energy costs for transporting water through a two-layer pipeline after construction work [7-9].

Foreign researchers note that a significant role in energy consumption in water distribution systems is given to their hydraulic indicators and the effective management of hydrophore stations (i.e. pumping stations with several parallel installed pumps), when modeling (by correlation) between the amount of water supplied and electricity is necessary [10, 11].

Also, a certain role in energy consumption is given to the temperature factor, in particular, the temperature of the surrounding natural environment (i.e., the soil where the pipeline is laid and transported water) [12], as well as increasing the capacity of the restored pipeline network based on the changing parameters of its operation [13-15].

The circumstances listed above are a significant argument when making the final decision on choosing the appropriate trenchless renovation method, since operating costs for electricity can affect the payback period of restoration work [16].

The essence of the method of stretching a new polymer pipeline into an old one is that the outer diameter of the polymer pipe slightly exceeds the inner diameter of the steel pipeline being restored. Due to the preheating of the polymer pipeline in a special installation and subsequent compression in a conical matrix, its diameter decreases and the walls thicken at the same time. After cooling for several hours, the polymer pipeline increases in diameter to values equal to the inner diameter of the old pipeline, i.e. it fits snugly in the inner surface, forming a two-layer pipe structure [17, 18].

In turn, the essence of the method of applying a flexible polymer sleeve based on fiberglass consists in its inversion in an old pipeline (steam or water pressure) and subsequent polymerization of organic resin previously applied to the inner surface of the sleeve billet, forming a durable two-layer pipe structure [19].

Figure 1 shows an illustration of the process of heating, compressing and dragging a polymer pipeline into an old one, and Figure 2 shows as a sample one of the possible schemes for applying a flexible polymer sleeve using an inversion drum.

METHODS AND MATERIALS

The study consists of two stages, where, at the first stage, the analysis of design options for restoration work on a dilapidated steel pipeline is carried out using the technology of stretching pre-compressed polymer pipes into it, and at the second stage flexible polymer hoses are considered as the object of research. Polymer pipes with different SDR values (the ratio of diameter to wall thickness of the pipe), as well as different wall thicknesses of polymer hoses, depending on their modulus of elasticity and a number of conditions for laying the old pipeline (diameter, length, depth and groundwater level), are subject to analysis for the most effective use in terms of saving electricity during water transportation. The research method is the analysis of automated calculations to determine the complex parameters of a polymer pipeline after operations for its compression and straightening in an old pipeline, taking into account the transformation of hydraulic and energy parameters of a two-layer pipeline structure [20, 21].

Automated programs were used as information retrieval systems [22-24].

The initial information for carrying out the entire complex of necessary technological, hydraulic and energy calculations using the above-mentioned automated programs is the following:

-the inner diameter of the old steel pipeline to be renovated d: 400 mm (outer 426 mm);

-length of the pipeline l: 4500 m;

-depth of the pipeline H: 3.0 m;

-groundwater level h: 2.5 m of water column;

-flow rate of transported water Q: 0.134 m3/s;

-efficiency of the pumping unit ηp: 0.9;

-outer diameter of the polymer pipe dp: 450 mm;.

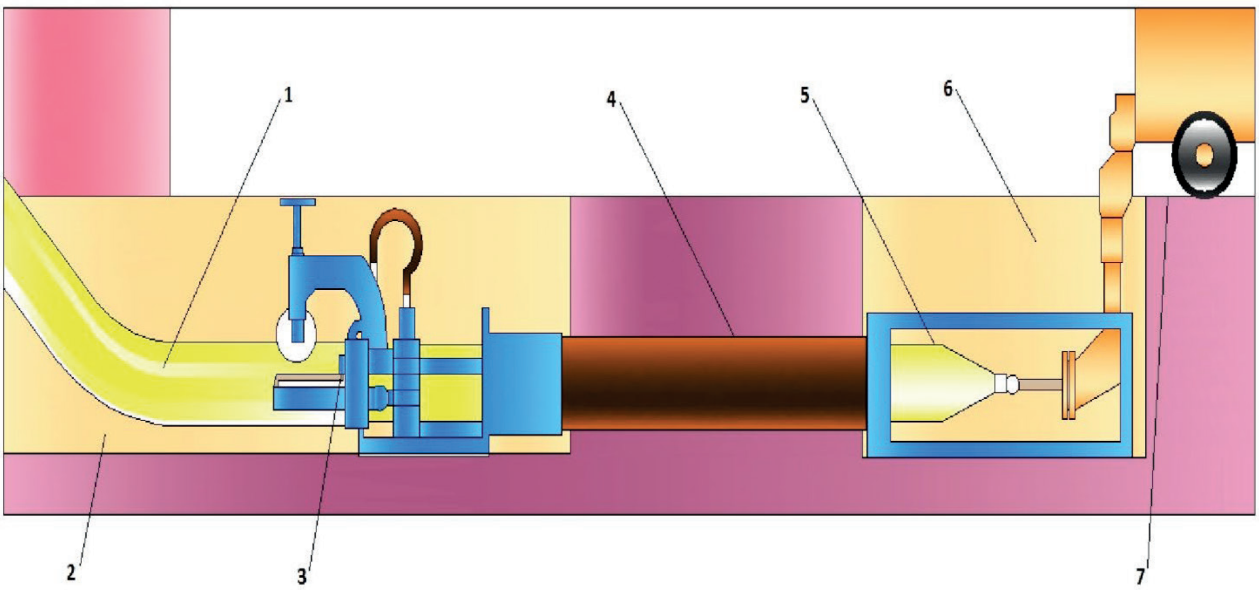

Figure 1. An illustration of the operations of preheating, compressing and dragging a polymer pipe into an old pipeline

1-polymer pipe subject to thermomechanical compression, 2- starting well, 3- device for stretching a pipeline with a furnace chamber and a narrowing matrix, 4- section of the pipeline being restored, 5- deformed polymer pipeline, 6- finishing well, 7- site for installing equipment for the implementation of the process

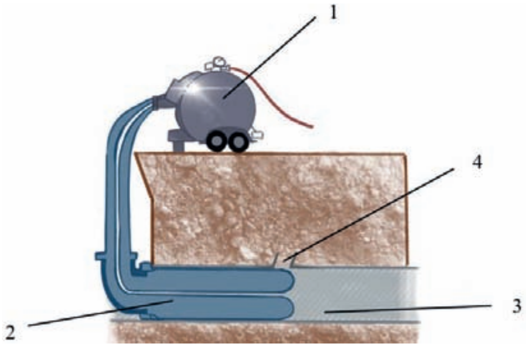

Figure 2. Inversion of a flexible polymer sleeve using a special drum
1- inversion drum; 2- polymer sleeve; 3- repair site; 4- pipeline defect

RESULTS

The calculation of energy consumption savings during water transportation through a pipeline for two alternative repair options is performed according to formulas (1) and (2), which are basic in the algorithms of the above-mentioned automated programs [25].

$$\Delta E_{1m}=[9.81\cdot Q^3(A_s - A_n)\cdot 24\cdot 365]/\eta_p \qquad (1)$$

where Δ E is the amount of savings in electricity consumed, kW·h/year; Q is the consumption of transported water, m^3/s; A_s and A_p are, accordingly, the resistivity coefficients of the old and restored pipeline using the technology of dragging a polymer pipe or a flexible polymer sleeve; η_p is the efficiency of the pumping unit; *l* is the length of the pipeline, *m*; 24 is the number of hours of pump operation per day, *h*; 365 –the number of days in a year

$$A_s = 0{,}0017 d_s^{-5{,}1359} \qquad (2)$$

where d_s is the inner diameter of the old pipeline, *m*; d_n is the inner diameter of the new two–layer pipeline structure, *m*

For the reconstruction option of the old pipeline using a polymer pipe with a wide range of *SDR* values, the resistivity coefficients of the A_n are calculated using the formula (3), and for a polymer sleeve A_n based on fiberglass for the base array of the considered values of the elastic modulus *S* (N/mm^2) according to the formula (4):

$$A_n = 0{,}0004 d_n^{-5{,}7276} \qquad (3)$$
$$A_n = 0{,}0007 d_n^{-5{,}2791} \qquad (4)$$

The above formulas for the dependence of resistivity on the diameter $An=f(d)$ were obtained experimentally on experimental hydraulic stands in the laboratory of the National Research University MGSU, where pipes made of various materials [17].

The results of the automated calculation of technological, hydraulic and energy parameters in the implementation of renovation technology by dragging a polyethylene pipe into an old pipeline are presented in Table 1.

Table 1. Summary data of the automated calculation when using a polymer pipe with an outer diameter of 450 mm for renovation

Calculated values for different SDR	SDR 17	SDR 21	SDR 26	SDR 33	SDR 41	SDR 50
The wall thickness of the polymer pipe after compression and straightening operations in the old pipeline, mm	27.09	21.64	17.5	13.95	11.09	9.04
The inner diameter of the double-layer pipeline after renovation, mm	345.81	356.71	365.0	372.11	377.81	381.91
Pressure losses along the entire length of the pipeline before renovation, m of water column	15.698					

Pressure losses along the entire length of the pipeline after renovation, m of water column	14.152	11.847	10.386	9.301	8.524	8.041
Average annual energy savings after renovation, kW·h/year	21987.7	54749.4	75521.1	9955.4	101992.0	109250.0

According to Table 1, with an increase in the SDR values, there is a pronounced tendency to change the inner diameter of a two-layer pipe structure due to a decrease in the wall thickness of the polymer pipe. Also, with an increase in SDR, there is a significant reduction in pressure losses along the entire length of the pipeline. At the same time, the average annual energy savings increases with an increase in SDR due to an increase in the diameter of the two-layer pipe structure after renovation. The observed effect in terms of energy savings is also achieved due to the lower hydraulic resistances of the polymer pipe compared to steel.

For the case of use during the renovation of a polymer sleeve, calculated data on wall thicknesses, elastic modulus values and internal diameters of a two-layer pipe structure are presented in Table 2.

Table 2. Summary data of the automated calculation when using a polymer sleeve for renovation

The values of the elastic modulus S, N/mm2	3500	4000	4500	5000	5500	6000	7000	8000
The thickness of the polymer sleeve in the old pipeline, mm	4.8	4.7	4.5	4.4	4.3	4.2	4.1	4.0
The inner diameter of the double-layer pipeline after renovation, mm	390.4	390.6	391.0	391.2	391.4	391.6	391.8	392.0
Average annual energy savings after renovation, kW·h/year	90578.4	90919.1	91476.7	91754.2	92013.7	92306.5	92581.3	92855.2

According to Table 2, the thickness of the polymer sleeve at elastic modulus values in a wide range (3500-8000 N/mm2) does not undergo significant changes, which practically does not affect the amount of annual energy savings calculated by formula (1).

Comparing the calculated data presented in tables (1) and (2), it can be stated that the most advantageous reconstruction option in terms of saving electricity during water transportation is the use of trenchless technology of pre-compression of a polymer pipe and its dragging into an old pipeline in the SDR values 33-50 range. However, in the range of SDR values 17-26, the polymer pipe as a protective coating is significantly inferior to the polymer sleeve in terms of achieving an energy-saving effect.

In order to analyze the possible expansion of the effective range of SDR values of polymer pipes during the renovation period, an automated calculation was performed, provided that a polyethylene pipe with a smaller outer diameter, i.e. 400 mm instead of 450 mm, is used to drag into the old pipeline. The calculation results are presented in Table 3.

Table 3. Summary data of the automated calculation when using a polymer pipe with an outer diameter of 400 mm for renovation

Calculated values for different SDR	SDR 17	SDR 21	SDR 26	SDR 33	SDR 41	SDR 50
The wall thickness of the polymer pipe after compression and straightening operations in the old pipeline, mm	23.7	19.0	15.4	12.3	9.8	8.0

The inner diameter of the double-layer pipeline after renovation, mm	352.6	362.0	369.2	375.4	380.4	384.0
Pressure losses along the entire length of the pipeline before renovation, m of water column	15.698					
Pressure losses along the entire length of the pipeline after renovation, m of water column	12.661	10.89	9.728	8.843	8.198	7.767
Average annual energy savings after renovation, kW·h/year	43182.4	63361.6	84876.0	97458.3	106633.7	112754.6

An analysis of the data in Table 3 shows that in this case, there is also an advantage of the steel pipeline repair method by dragging a polymer pipe compared to a polymer sleeve in the same SDR ranges, i.e. 33-50. However, the average annual energy savings when replacing a pipe with a smaller outer diameter increases, for example, for SDR 50 by 3.21% (112754.6×100/109250).

Thus, it can be stated that when choosing the technology of trenchless reconstruction of dilapidated pressure pipelines, the required standard standards in terms of their strength can also include the amount of energy saving, characterizing it as an additional significant argument for making a final decision. Using automated calculations, it is possible to identify the most effective use case for a particular technology for the appropriate renovation of old pipelines of certain diameters and lengths, depths of occurrence, costs of transported water and other parameters. Such a methodological approach using automated information retrieval systems for estimating electricity consumption, as well as carrying out estimated calculations of the cost of repair and restoration work, make it possible to choose the optimal option for trenchless renovation of pressure pipelines, taking into account their initial technological parameters and the nature of defects.

CONCLUSIONS

1. An analysis of the use of alternative trenchless technologies for the renovation of dilapidated pressure pipelines, including accompanying algorithms and automated programs for calculating technological, hydraulic and energy parameters, is presented.
2. A methodological approach to the automated selection of the optimal option for the renovation of old pipelines with polymer pipes and flexible polymer sleeves is recommended and implemented, which allows us to identify a range of wall thicknesses of protective coatings of pipelines and their diameters, which save energy costs for water transportation.

REFERENCES

1. **Shuvalov M.V., Tarakanov D.I.** The use of pipes made of various materials for the installation of water supply networks // Urban planning and architecture. 2023. Vol. 13, No 152. pp. 53-59. DOI: 10.17673/Vestnik.2023.01.07
2. Using pipes from various materials for sewage network: theoretical analysis. Tarakanov D.I. IOP Conference Series: Materials Science and Engineering. International Conference on Civil, Architectural and Environmental Sciences and Technologies, CAEST 2019. 2020. P. 012103
3. **Zakharov Yu.S., Orlov V.A.** Repair and restoration of gravity drainage networks. Publishing house ASV. 2023. 265 p.
4. Plastic pipes and their use in rainwater drainage systems. Tarakanov D.I. IOP Conference Series: Earth and Environmental Science. «International Science and Technology Conference «Earth Science», ISTC Earth Science 2022. Chapter 4» 2022. P. 052032.

5. **Khramenkov S.V.** Strategy of modernization of the water supply network.-M: Stroyizdat. 2005. 398 p.
6. **Khramenkov S.V.** Time to manage water.-M.: JSC Moscow textbooks and cartolithography. 2012. 279 p.
7. **Leznov B.S.** Energy saving and adjustable drive in pumping and blower installations.-M.: Energoatomizdat. 2006. 359 p.
8. **Houghtalen R., Osman A., Akan A., Hwang N.** Fundamentals of Hydraulic Engineering Systems, 5th edition. Pearson. 2016. 528 p.
9. **Gonzalez-Velazquez J.L**. Fatique Fracture //Fractography and Failure Analysis, Springer. Cham. 2018. P. 71-95
10. **Grigoras G. Istrate M.** Energy consumption estimation in water distribution systems using fuzzy techniques. Environmental Engineering and Management Journal. 2008. Vol. 9. Nr. 2, ISSN: 1843-3707
11. **Gilda Gavrilaş, Mihai Gavrilas, Ovidiu Ivanov** /Electricity load prediction for water supply systems // Environmental Engineering and Management Journal, July/August 2008, Vol. 7, Nr. 4, ISSN: 1843 – 3707 p.
12. **Mihai Toderaşc, Vlad Iordache, Cristian Petcu, Horia Petran** Real time monitoring of indoor environment quality and energy consumption in a residential building //Environmental Engineering and Management Journal. July 2019, Vol. 18, No. 7, 1391-1620
13. **Heber Pimentel Gomes, Pedro Augusto Silva Sabino de Farias, Saulo de Tarso Marques Bezerra, Sabrina da Silva** Efficiency indicator for assessment of water distribution networks carrying capacity //Environmental Engineering and Management Journal. May 2020, Vol. 19, No. 5, 747-753
14. **Mihai Toderaşc, Vlad Iordache, Cristian Petcu, Horia Petran** Real time monitoring of indoor environment quality and energy consumption in a residential building //Environmental Engineering and Management Journal. July 2019, Vol. 18, No. 7, 1391-1620
15. **Chupin R.V., Melekhov E.S.** Justification of the parameters of developing water supply and sanitation systems based on their electronic models // IOP Conference Series: Materials Science and Engineering, 2020. DOI: 10.1088/1757-899X/880/1/012050
16. **Simanovich V.M., Ermolaev E.E.** Features of determining costs as part of the consolidated estimate of the cost of construction. A practical guide.Moscow: Stroyinformizdat, 2010. 269 p.
17. **Yudina A.F., Kobelev E.A.** Innovative technologies for trenchless laying of new and repair of old engineering networks // Bulletin of Civil Engineers, 2017. No.3(62). pp. 101-108.
18. **Terekhov L.D., Prodous O.A., Fedorchuk A.V.** The use of PE100 polyethylene pipes for trenchless repair of pressure pipelines. Bulletin of the Irkutsk State Technical University. 2014. No. 2. pp. 144-148
19. **Khramenkov S.V., Primin O.G.** Reconstruction of pipeline systems. Publishing house ASV. 2008. 215 p.
20. **Prodous O.A., Yakubchik P.P.** Hydraulic calculation of pipelines made of polymer materials taking into account the parameters of the roughness of the inner surface. Water supply and sanitary equipment. 2020. № 11. From 55-60
21. **Prodous O.A**. Forecasting pressure losses in pipelines made of various polymer materials. Water supply and sanitary equipment. 2018. No. 11. pp. 60-64
22. **Orlov V.A., Zotkin S.P., Zotkina I.A., Khrenov K.E.** Calculation of the parameters of pipelines restored by pre-compressed polymer pipes. Certificate of state registration of the computer program No. 2014612753 dated 03/06/2014,
23. **Orlov V.A., Zotkin S.P., Pelipenko A.A.** Calculation of the wall thickness of a

flexible polymer sleeve during pipeline renovation. Certificate of state registration of the computer program No. 2017615864 dated 30.05.2017

24. **Orlov V.A., Zotkin S.P., Inshakova M.A.** Calculation of electricity consumption during water transportation through pressure pipelines. Certificate of state registration of the computer program No. 2021613107 dated 03/02/2021
25. **Orlov V.A.** Trenchless technologies and energy saving. – M.: Publishing House of the DIA. (2021). 124 p.

СПИСОК ЛИТЕРАТУРЫ

1. **Шувалов М.В., Тараканов Д.И.** Применение труб из различных материалов для устройства водопроводных сетей // Градостроительство и архитектура. 2023. Т. 13, No 152. С. 53-59. DOI: 10.17673/Vestnik.2023.01.07
2. Using pipes from various materials for sewage network: theoretical analysis. Tarakanov D.I. IOP Conference Series: Materials Science and Engineering. International Conference on Civil, Architectural and Environmental Sciences and Technologies, CAEST 2019. 2020. P. 012103
3. **Захаров Ю.С., Орлов В.А.** Ремонт и восстановление самотечных водоотводящих сетей. Издательство АСВ. 2023. 265 с.
4. Plastic pipes and their use in rainwater drainage systems. Tarakanov D.I. IOP Conference Series: Earth and Environmental Science. «International Science and Technology Conference «Earth Science», ISTC Earth Science 2022. Chapter 4» 2022. P. 052032.
5. **Храменков С.В.** Стратегия модернизации водопроводной сети. - М: Стройиздат. 2005. 398 с.
6. **Храменков С.В.** Время управлять водой.-М.: ОАО Московские учебники и картолитография. 2012. 279 с.
7. **Лезнов Б.С.** Энергосбережение и регулируемый привод в насосных и воздуходувных установках.-М.: Энергоатомиздат. 2006. 359 с.
8. **Houghtalen R., Osman A., Akan A., Hwang N.** Fundamentals of Hydraulic Engineering Systems, 5th edition. Pearson. 2016. 528 p.
9. **Gonzalez-Velazquez J.L.** Fatique Fracture //Fractography and Failure Analysis, Springer. Cham. 2018. P. 71-95
10. **Grigoras G. Istrate M**. Energy consumption estimation in water distribution systems using fuzzy techniques. Environmental Engineering and Management Journal. 2008. Vol. 9. Nr. 2, ISSN: 1843-3707
11. **Gilda Gavrilaş, Mihai Gavrilas, Ovidiu Ivanov** /Electricity load prediction for water supply systems // Environmental Engineering and Management Journal, July/August 2008, Vol. 7, Nr. 4, ISSN: 1843 – 3707 p.
12. **Mihai Toderaşc, Vlad Iordache, Cristian Petcu, Horia Petran** Real time monitoring of indoor environment quality and energy consumption in a residential building //Environmental Engineering and Management Journal. July 2019, Vol. 18, No. 7, 1391-1620
13. **Heber Pimentel Gomes, Pedro Augusto Silva Sabino de Farias, Saulo de Tarso Marques Bezerra, Sabrina da Silva** Efficiency indicator for assessment of water distribution networks carrying capacity //Environmental Engineering and Management Journal. May 2020, Vol. 19, No. 5, 747-753
14. **Mihai Toderaşc, Vlad Iordache, Cristian Petcu, Horia Petran** Real time monitoring of indoor environment quality and energy consumption in a residential building //Environmental Engineering and

Management Journal. July 2019, Vol. 18, No. 7, 1391-1620
15. **Chupin R.V., Melekhov E.S.** Justification of the parameters of developing water supply and sanitation systems based on their electronic models // IOP Conference Series: Materials Science and Engineering, 2020. DOI: 10.1088/1757-899X/880/1/012050
16. **Симанович В.М., Ермолаев Е.Е.** Особенности определения затрат в составе сводного сметного расчета стоимости строительства. Практическое пособие.-М: Стройинформиздат, 2010. 269 с.
17. **Юдина А.Ф., Кобелев Е.А.** Инновационные технологии бестраншейной прокладки новых и ремонта старых инженерных сетей // Вестник гражданских инженеров, 2017. №3(62). С. 101–108.
18. **Терехов Л.Д., Продоус О.А., Федорчук А.В.** Применение полиэтиленовых труб ПЭ100 для бестраншейного ремонта напорных трубопроводов. Вестник Иркутского Государственного Технического Университета. 2014. № 2. С. 144-148
19. **Храменков С.В., Примин О.Г**. Реконструкция трубопроводных систем. Издательство АСВ. 2008. 215 с.
20. **Продоус О.А., Якубчик П.П**. Гидравлический расчет трубопроводов из полимерных материалов с учетом параметров шероховатости внутренней поверхности. Водоснабжение и санитарная техника. 2020. № 11. С 55-60
21. **Продоус О.А.** Прогнозирование потерь напора в трубопроводах из разных полимерных материалов. Водоснабжение и санитарная техника. 2018. № 11. С. 60-64
22. **Орлов В.А., Зоткин С.П., Зоткина И.А., Хренов К.Е.** Расчет параметров работы трубопроводов, восстанавливаемых предварительно сжатыми полимерными трубами. Свидетельство о государственной регистрации программы на ЭВМ № 2014612753 от 06.03.2014,
23. **Орлов В.А., Зоткин С.П., Пелипенко А.А.** Расчет толщины стенки гибкого полимерного рукава при реновации трубопроводов. Свидетельство о государственной регистрации программы для ЭВМ № 2017615864 от 30.05.2017
24. **Орлов В.А., Зоткин С.П., Иншакова М.А.** Расчет потребления электроэнергии при транспортировке воды по напорным трубопроводам. Свидетельство о государственной регистрации программы для ЭВМ № 2021613107 от 02.03.2021
25. **Орлов В.А.** Бестраншейные технологии и энергосбережение. – М.: Издательство АСВ. (2021). 124 с

Orlov Vladimir A., Professor, Doctor of Technical Sciences; National Research Moscow State Construction University (NIU MSCU), Russia, 129337, Moscow, 26 Yaroslavskoe Shosse, E-mail: OrlovVA@mgsu.ru.

Орлов Владимир Александрович, профессор, доктор технических наук; Федеральное государственное бюджетное образовательное учреждение высшего образования «Национальный исследовательский Московский государственный строительный университет» (НИУ МГСУ), Россия, 129337, Москва, Ярославское шоссе, 26; E-mail: OrlovVA@mgsu.ru.

Zotkin Sergey P., Professor, Candidate of Technical Sciences; Russia, National Research Moscow State Construction University (NIU MSCU), Russia, 129337, Moscow, 26 Yaroslavskoe Shosse; E-mail: ZotkinSP@mgsu.ru.

Зоткин Сергей Петрович, профессор, кандидат технических наук; Россия, Федеральное государственное бюджетное образовательное учреждение высшего образования «Национальный исследовательский Московский государственный строительный университет» (НИУ МГСУ), 129337, Москва, Ярославское шоссе, 26; E-mail: ZotkinSP@mgsu.ru.

Podolyan Dmitry V., PhD student; National Research Moscow State Construction University (NIU MSCU), Russia, 129337, Moscow, 26 Yaroslavskoe Shosse; E-mail: dim.p-2010@yandex.ru.

Подолян Дмитрий Владимирович, аспирант; Федеральное государственное бюджетное образовательное учреждение высшего образования «Национальный исследовательский Московский государственный строительный университет» (НИУ МГСУ), Россия, 129337, Москва, Ярославское шоссе, 26; E-mail: dim.p-2010@yandex.ru

Petersburgsky Dmitry A., PhD student; National Research Moscow State Construction University (NIU MSCU), Russia, 129337, Moscow, 26 Yaroslavskoe Shosse. E-mail: piter.rus@inbox.ru

Петербургский Дмитрий Александрович, аспирант; Федеральное государственное бюджетное образовательное учреждение высшего образования «Национальный исследовательский Московский государственный строительный университет» (НИУ МГСУ), 129337, Россия, г. Москва, пр. Мира, 26, piter.rus@inbox.ru

DOI:10.22337/2587-9618-2024-20-4-160-171

NUMERICAL INVESTIGATION ON FLEXURAL PERFORMANCE OF BUILT-UP STEEL BEAMS WITH DIFFERENT WEB OPENINGS

***Hussein Talab Nhabih* [1]*, Mohammad R.K.M. Al-Badkubi* [2]*, Marwa Marza Salman* [3]**

[1] Department of Civil Engineering, Faculty of Engineering, Babylon University, Babylon, IRAQ
[2] Department of building and construction technology, Islamic University,Najaf, IRAQ
[3] Department of Ceramic and Building Material, Faculty of Materials Engineering, Babylon University, Babylon, IRAQ

Abstract. Recently, the usage of Structural Steel Beams with Opening in the Web has spread extensively in all over the world, in various types of buildings such as high-rise buildings and industrial buildings. There are several advantages in using openings in beams. There for, an analytical investigation was carried out on fourSteel Beams with Opening (SBWO) models by using a powerful nonlinear simulation software ABAQUS. The initiative was to study the overall flexural behaviour of (SBWO's) and to establish the maximum load carrying capacity, and deflection. Only vertical loads have been considered in the (SBWO's) performance investigation. The Built-Up sections were tested up to failure. The simulated models were considered to be under simply supported condition at their edges and a uniform distributed load were applied over the upper flange of the beam along all beam's length. The flexural behaviour of beams with different opening shapes were tested and compared. The test results proved to be very useful in selecting the opening shape.

Keywords*:* Finite Element Modeling, Abaqus Computer Program, Flexural Behavior, Built-Up Section, Steel Beam, Web Opening

ЧИСЛЕННОЕ ИССЛЕДОВАНИЕ ИЗГИБА СОСТАВНЫХ СТАЛЬНЫХ БАЛОК С ОТВЕРСТИЯМИ РАЗЛИЧНОЙ ФОРМЫ В СТЕНКЕ

Хусейн Талаб Набих* [1]*, Мохаммад Р.К.М. Аль-Бадкуби* [2]*,
***Марва Марза Салман* [3]**

[1] Кафедра гражданского строительства, инженерный факультет, Вавилонский университет, Вавилон, ИРАК
[2] Кафедра строительства и строительных технологий, Исламский университет, Наджаф, ИРАК
[3] Кафедра керамики и строительных материалов, факультет материаловедения, Вавилонский университет, Вавилон, ИРАК

Аннотация. В последнее время использование стальных балок с отверстиями в стенке получило широкое распространение во всем мире, в различных типах зданий, таких как высотные и промышленные здания. Использование отверстий в стенках балок имеет ряд преимуществ. Поэтому было проведено численное исследование четырех моделей стальных балок с отверстиями (SBWO) с помощью программного обеспечения для нелинейного моделирования ABAQUS. Целью исследования было изучение общего сопротивления изгибу балок (SBWO) и определение максимальной несущей способности, а также прогиба. При исследовании характеристик (SBWO) учитывались только вертикальные нагрузки. Нагружение выполнялось вплоть до разрушения. Рассматривались свободно опертые по краям балки. К верхней полке балки по всей ее длине прикладывалась равномерно распределенная нагрузка. Были исследования и сравнение результатов для балок с различными формами отверстий. Полученные результаты исследований могут быть использованы при выборе формы отверстий в стальных двутавровых балках.

Ключевые слова: Конечно-элементное моделирование, компьютерная программа Abaqus, изгиб, составное сечение, стальная балка, отверстие в стенке

I. INTRODUCTION

From about eight decades, a large number of investigations have made by structural engineers looking for an untraditional methods to decrease the charge of steel constructions as much as possible. From designing point of view the maximum potential structural steel strength properties cannot always be achievable due to existence of other design factor such as serviceability. This factor usually accounts in the design process by taking the maximum permissible deflection to be the design factor. Therefore, numerous innovative ways have been suggested to increase the steel member's stiffness without increasing the required weight of steel, significantly.
Thus, steel beams with web opening also known as castellated or cellular beams have been used widely. One of the major benefits of using the openings in the beam in construction is the incorporation of services, such as electric cables as well as ventilation and hydraulic pipes, through the designed section depth of the beams, as shown in Fig.1.
The strength of structural members with web opening has been stated that may have large reduction. This statements were made by researchers like Bower (1968) [2], Lawson (1987) [3], and Darwin (1990) [4].

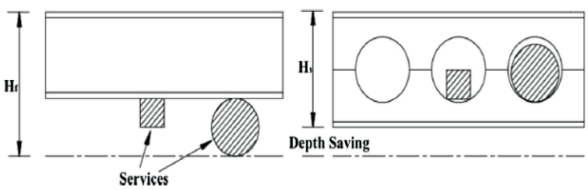

Figure 1. Reduction of beam height by utilizing holes for insertion service combinations [1]

However, the present specifications and design procedure codes for such beams are also difficult to use or inadequate (SCI P355 2011) [5]. This can be because the complexity in understanding and analyzing the performance of steel beams with web openings, and too difficulties to simplify design procedures. Thus, more extensive researches and investigations are needed in order to achieve sufficient information for understanding the behavior of beams with web opening to develop a much simpler design method. There are some analytical and experimental investigations have been made in the past to study SBWOs behavior. Redwood (1969) [6] suggested that by using modified dimensions equivalent rectangular opening, most of the design rules can be applied for steel beams with circular web openings. However, the ultimate strength of steel beams are substantially underestimated as a result of the simplistic approach. Chan and Redwood (1974) [7] used the curved beam analysis and the theory of elasticity to examine stress distribution in elastic range for beams having big circular shape web openings. The investigations made by Olander (1953) [8] and Sahmel (1969) [9] were used to develop a design method at the Steel Building Institute in 1990 in order to find the ultimate strength of steel beams having several circular shape web openings using an explicit approach. Later on in 1998, the method incorporated in Euro code 3 (EN1993-1-3)[10] after minor modification. However, this method also has been recommended to use for steel beams with separate circular shape web openings using a dissimilar set of approximate design methods. Laboratory tests and Numerical investigation on steel beams with circular and rectangular openings have been approved by Thevendran and Shanmugan (1991) [11]. They constructed cantilever and simply supported beams models made from a plexi glass sheet. For computing the critical buckling load for this type of beams the energy technique was proposed. Lawson and Chung (2001) [12] made an theoretical investigation on steel beams having circular and rectangular openings using a large web opening composite beams design method and presented in Euro code 4. Two suggestions were made by Chung et al. (2001) [13] first a practical design method against Vierendeel mechanism for circular web opening steel beams, second the perforated section empirical shear–moment interaction curve. An empirical design method was industrialized by Chung et al. (2003) [14]using generalized moment–shear interaction curve for steel beam with various shapes and sizes web openings. Tsavdaridic and D'Mello (2011) [15] made a study on the web post buckling effective 'strut' action and guess the final vertical shear load strength of web posts using an empirical formula obtained from the particular shapes of web opening. In order to achieve a simplified approach to develop a reliable prediction for moment modification factor K_{LB} in cellular beams an investigation was made by Sweedan (2011) [16]. An experimental investigation was made by Saka and Erdal (2013) [17] and they observed different types of failure modes including post buckling of the web, Vierendeel bending, web buckling and lateral torsional buckling. A through finite element method was performed by Panedpojaman and Thepchatri (2013) [18] and a modified coefficient function were suggested after analyzing 408 nonlinear finite element model fore liable deflection prediction of cellular beams. A numerical and experimental study was made by Boissonnade et al. (2014) [19] and a design procedure for lateral torsional buckling in cellular beam was suggested. Samadhan and Laxmikant (2015) [1] performed an experimental and parametric study on simply supported steel beams with web opening subjected to vertical loading. Iman Satyarno et al. (2017) [20], perform an analysis on castellated steel beam by full scaled rectangular opening shape in which some of the specimens were partially encased in reinforced mortar and some of them without encasing. Made Sukrawa (2017) [21], made a finite element study on reinforced steel beam with large opening in the web subjected to axial forces. Tareq Almusallam et al. (2018), perform an experimental and numerical investigation on behavior of FRP-strengthened RC beams having large rectangular shape web openings in flexural zones. Morkhade et al. (2019) [23], made an effort on study the effect of opening in the web on the ultimate strength of steel beam by trapezoidal corrugated shape web in which it can increase the share capacity without providing the transverse stiffeners.

There are numerous benefits of using SBWOs, some of them can be listed as:

- Incorporation of services within the structural height of the beams.
- Reduction of overall dead weight of the structure which allows smaller foundation sizes.
- Reducing overall costs due to reduction of material consumption.
- Longer spans between columns than traditional structures.

II. SAMPLES DESCRIPTION

This study signifies an analytical study on flexural performance of built-up section steel beams with different web opening which consists tests on four steel beam models up to failure using a nonlinear simulation software Abaqus to find the better opening type which gives better performance during the application of loading.

In general the test results give an overall understanding of the behavior of these beams. The failure type which controls the behavior of these beams is flexural failure in the section. In the present investigation the load–deflection behavior, the ultimate load-carrying capacity and the failure modes are to be considered. Fig. 2 & 3 illustrated the specification details of the test specimens. These details also listed in Table 1.

As it is shown in Fig.2a-d, for all steel beam specimens the parameters such as beam overall dimensions and total number of the openings and beam's depth were kept constant in order to investigate only the influence of opening shape on the flexural behavior of the steel beams with web opening exclusively. From practical point of view manufacturing circular web opening is the easiest comparing to other shapes because of the drilling, measuring and residual stresses. Thus, the steel beam having circular shape web opening is used to select other opening shapes dimensions and spacing. As shown in the Fig. 2a, 3the diameter of the circular opening is selected so that the opening be large enough to see the effect of the opening on flexural behavior more clearly, and the spacing between the circular openings is calculated according to the design of openings from BS 5950 part-I (2000) [24] which considers to take opening spacing to its diameter ratio (S/D_o = 1.08–1.5). Also, the web openings considered to start from 250 mm from the ends of the beam. This distance is selected in order to increase the stiffness of the beam at support zone and also not too far from the support so that the opening is spread in all beam's length and practically be possible to use any length for the beam and do not need special manufacturing for different beam's length. Furthermore, to investigate the influence of the opening shape exclusively the dimensions of the other web opening shapes are selected so that the area of the shape remain almost equal to the area of the circular shape. For dissimilar opening shapes for example rectangular, triangular, and hexagonal shape, in order to minimize the high stress concentration which occurs in the opening shape corners, a 5 mm in radius fillet is provided in those regions. As shown in Fig. 2c the spacing between the openings is not large enough to place the triangles with same orientation, so to maintain the opening numbers and spacing the nearby triangle for each opening is flipped upside down.

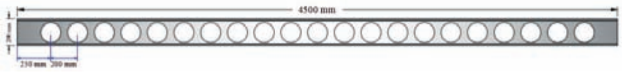

a) Steel beam with circular web opening (SBCWO).

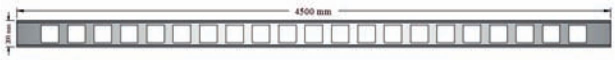

b) Steel beam with square web opening (SBSWO).

c) Steel beam with triangular web opening (SBTWO).

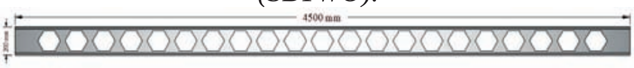

d) Steel beam with hexagonal web opening (SBHWO).

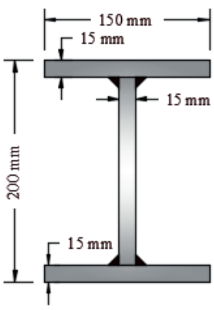

Figure 2. Schematic representation of tested specimens

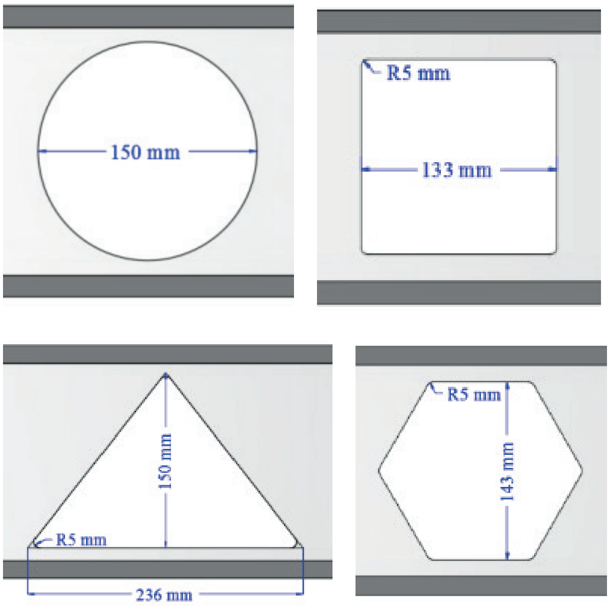

Figure 3. Opening details

Table 1. Samples Identification

No.	Beam Symbol	Length (mm)	Opening Shape	Flange Width (mm)
1	SBCWO	4500	Circular	150
2	SBSWO	4500	Square	150
3	SBTWO	4500	Triangular	150
4	SBHWO	4500	Hexagonal	150

III. FINITE ELEMENT MODELLING OF THE SPECIMENS

The simulated SBWO models have been used to guess ultimate strength capacity and flexural behavior of the samples during the loading time and at the final stage of loading which considered to be the model rupture failure using finite element simulation technique. Thus, a 3-D model with limited finite elements is developed by using a powerful simulation software Abaqus (6.14-4), which can simulate the material properties as well as geometric nonlinearity in beam samples.

Building the models is the starting step in the finite element analysis method. In this step, the overall structure of the model is formed after that the model divided in to finite elements, each element connected with others at their nodes. It is necessary to define the element type, material properties and overall geometry of the model to build an accurate finite element model. Furthermore, the accuracy and cogency of the adapted sample is verified by comparing the test results to those given by an experimental study made by Samadhan (2015) [1].

A. Modelling of Built-Up Steel Beam with Web Opening

1) Steel Beam Sketch

In order to establish valid and reliable simulated models of the steel beam with web opening the steel beam parts are drew and their characteristics are carefully designated. First, the structure of steel beam is formed after selecting the 3D space modeling, solid extrusion shape, and deformable type, as shown in Fig.4.The beam's cross section dimensions and its length have been simulated according to the specimen identification table shown previously. The simulation of the openings for other types of openings are also done by selecting the 3D space modeling, solid extrusion shape, and deformable type, as shown in Fig.5.

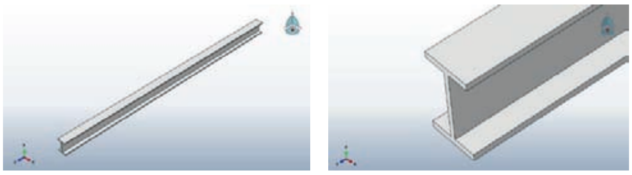

Figure 4. Modelling of solid steel beam part

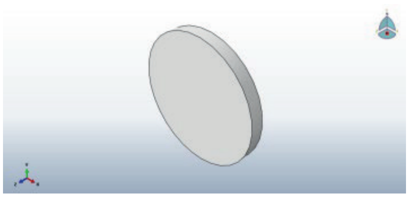

Figure 5. Modelling of solid opening shape part

Finally to achieve the steel beam with web opening models, the solid opening shape part is subtracted from the solid steel beam part. Then, a new complete steel beam with web opening part is created as shown in Fig.6.

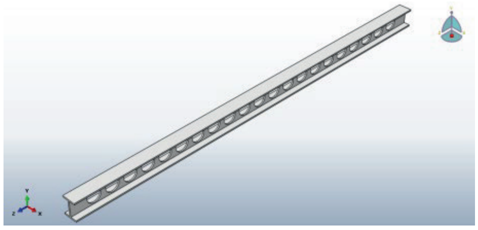

Figure 6. Complete steel beam with web opening model

2) Element Type Selection

In the presented study the element type which adopted to represent the steel beams was a 10-noded 3D stress quadratic tetrahedron elements (C3D10M) which has six degree of freedom at each node. Fig. 7 show the adapted element for steel beams.

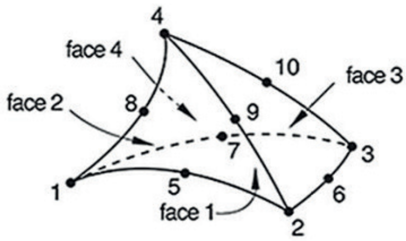

Figure 7. 10-node quadratic tetrahedron element (C3D10M) [25]

The selection of the model mesh density was done in such a way so that each element has the same length of 25mm length. Thus, the total number of element in the beam width are 6 elements and in the length 180 element. Fig. 8 demonstrations the meshed shape of the steel beam.

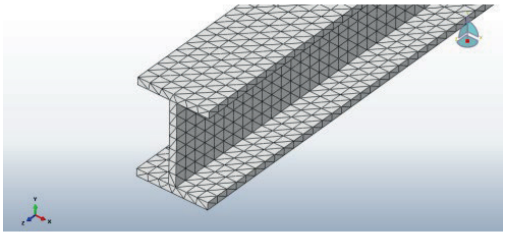

Figure 8. Meshed shape of steel beam model

3) Material Mechanical Properties

The steel material properties in this study taken similar to steel properties in experimental study made by Samadhan (2015) [1], which obtained from tensile test made on a coupons cut of a steel plate. The experiment results such as modulus of elasticity, ultimate stress, and yield stress, are given in Table 2.

Table 2. Properties of Steel Material

f_y (MPa)	f_u (MPa)	E_s (MPa)	υ
350	490	200,000	0.3

A simplified stress–strain curve shown in Fig. 9 is adapted for modelling the steel material mechanical properties along by the von Misses yield criterion having the isotropic hardening law. The adapted properties simulation shown to be adequate in simulating steel material properties due to test results. Also, in here the effect of large deformation have been considered.

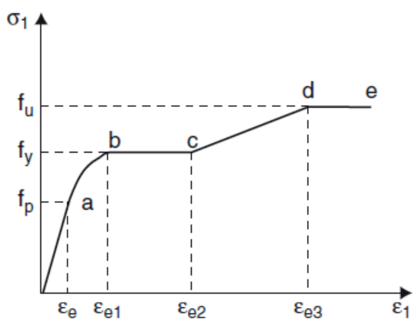

Figure 9. Stress-strain curve for steel [26]

4) Models Boundary Conditions

To make sure of obtaining a unique results in analyzing the deformation and maximum load capacity in the simulated steel beams with web opening the selection of the models end boundary conditions are necessary. In the present research work the steel beams are considered to be simply supported beams. In order to achieve this condition in the simulated models two additional solid extrudes are used at the bottom face of the steel beams. The solid extrudes considered to have rectangular shape with dimensions of (100, 150, 50 mm) in width, length and thickness, respectively. The extrudes considered to be made from hard steel with (f_y = 600 MPa and f_u = 900 MPa), this type of steel is used to ensure that the extrudes will not deform under the ultimate load for the steel beams. The solid extrudes are placed at a distance of 150 mm from the two edges of the steel beams. The left support considered to be hinged support and the right one considered to be roller support. The type of support can be determined by selecting the restricted transition direction. To ensure the nodal action of the supports the center line on the bottom face of the solid extrude are selected to be the line of supports. Fig.10 shows the solid extrude simulation and modelling of the support line location.

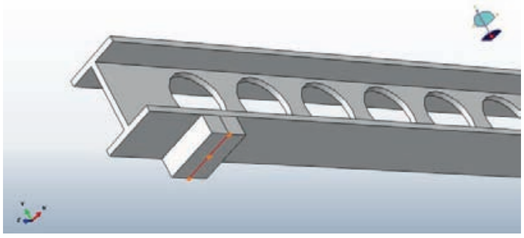

Figure 10. Solid extrude simulation and modelling of the support line location

5) Loading Mechanism

To simulate the applied load on the beam specimen the mechanical pressure type was selected to act on top face of the steel beams as shown in Fig. 11.

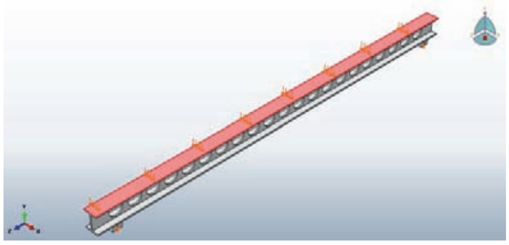

Figure 11. Modelling of loading pressure on top face of the steel beam sample

The applied pressure is distributed evenly at all surface area and increases linearly up to failure of the specimen.

IV. PARAMETRIC STUDY

A parametric study was made after making sure of the accuracy of the used finite element modeling predicting the ultimate load capacity, to investigate the shape of the opening influence on the flexural behavior of steel beams with web openings.

For simulating the other steel beams models with other types opening shapes, similar procedure which was used to simulate the steel beam with circular shape opening in the web model is used. But, with slight difference due to different shapes of the openings. Fig.12 illustrates the other steel beams modeled in Abaqus.

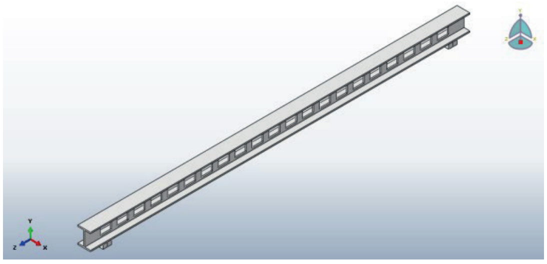

a) Steel Beam with Square Web Opening (SBSWO)

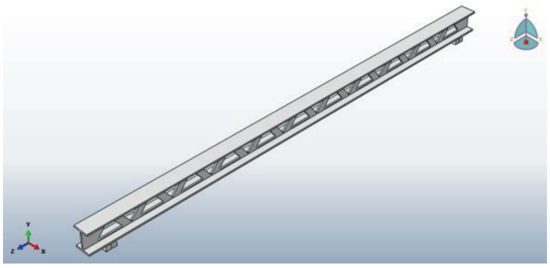

b) Steel Beam with Triangular Web Opening (SBTWO)

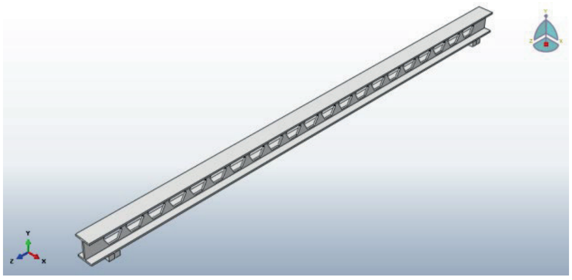

c) Steel Beam with Hexagonal Web Opening (SBHWO)

Figure 12. Representation of other steel beams modelled in Abaqus

V. RESULTS AND DISCUSSION

As it was mentioned previously the analysis concerns around the effect of the shape of the openings on the flexural behavior of the steel beams. Fig. 13 shows the applied load and mid-span deflection curve for the different types of the openings considered in the investigation.

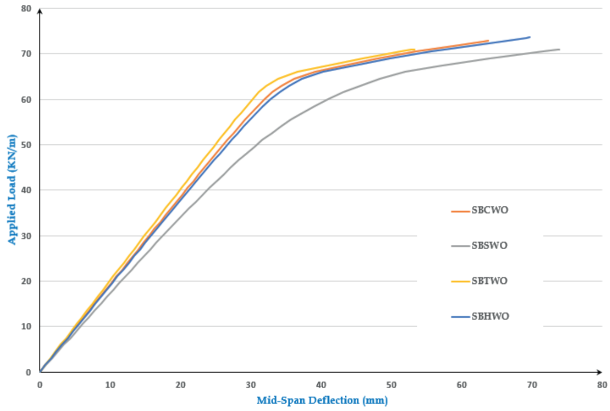

Figure 13. Comparison of load-deflection curves between different types of opening shape

By seeing the load-deflection curves shown in Fig. 13, it can be see that the stiffness of the steel beams with triangular and square web opening are greater and smaller than the stiffness of the other shapes, respectively. For all beams the plastic range of the curves starts from almost (30 mm) mid-span deflection at this point the amount of the applied load on the steel beams are (59.42 KN/m), (56.77KN/m), (55.68 KN/m) and (49 KN/m), for (SBTWO), (SBCWO), (SBHWO) and (SBSWO), respectively. Though, despite of the maximum load carrying capacities and maximum deflections are not in the same order, but in this study it was assumed that any strength of a beam after a mid-span deflection more than (30 mm) (almost after elastic range) is not considered safe strength since the deflection would be so large that it can be considered as failed beam. Thus, in this investigation the steel beam with triangular web opening considered to have the best performance in flexural resistance under the applied load. However, the maximum load carrying capacity and corresponding maximum mid span deflection for every tested beam in this analysis is illustrated in Table 3.

Table 3. FEM Test Results

No.	Beam Symbol	W (KN/m) at Δ = 30 mm	W_{max} (KN/m)	Δ_{max} (mm)
1	SBCWO	56.77	72.9	63.82
2	SBSWO	49	70.92	73.89
3	SBTWO	59.42	70.98	53.3
4	SBHWO	55.68	73.61	69.73

VI. SPECIMENS STRESS DISTRIBUTION AND DEFORMED SHAPE

The following figures, Fig.14, illustrates the stress distribution and deformed shape of the analytically tested samples with different types of web openings by subjecting the distributed load on samples top surface in F.E. analysis models.

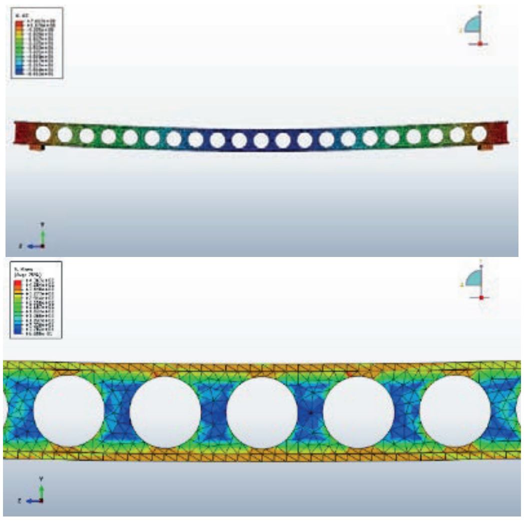

a) The deformed shape and stress distribution for FEM tested specimen (SBCWO)

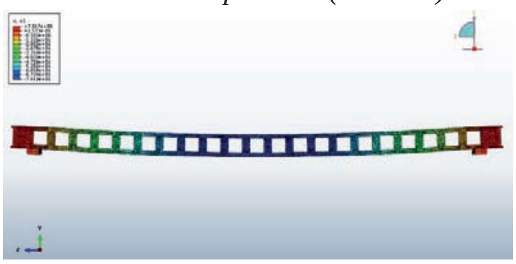

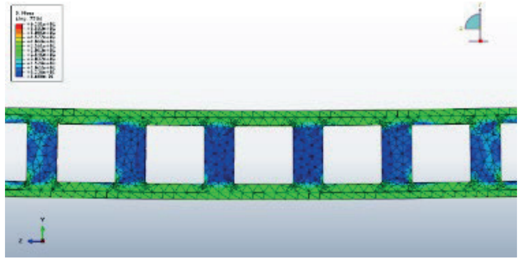

b) The deformed shape and stress distribution for FEM tested specimen (SBSWO).

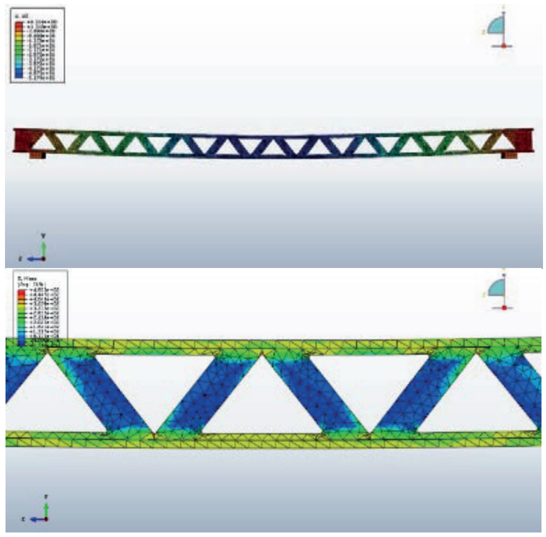

c) The deformed shape and stress distribution for FEM tested specimen (SBTWO)

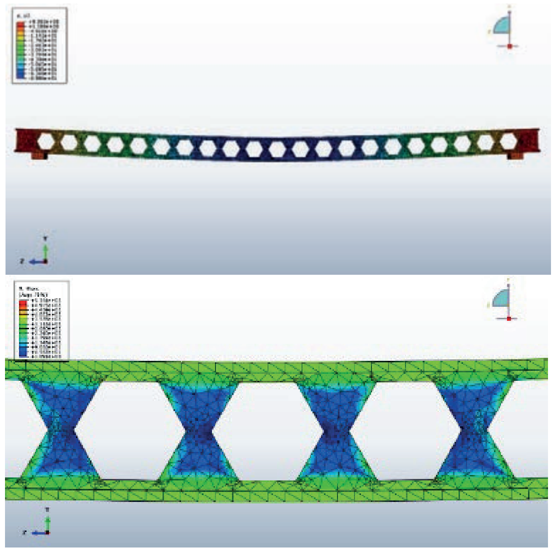

d) The deformed shape and stress distribution for FEM tested specimen (SBHWO)

Figure 14. The deformed shape and stress distribution of the tested steel beams with web openings

Form the figure above it can be observed that the stress distribution will be more concentrated at the regions between the openings and it reduces by increasing the width of this region.

VII. CONCLUSIONS

The chief aim of this work was to examine the flexural behavior of steel beam with different types of opening in the web by using a nonlinear simulation software (Abaqus). Thus, some model tests are established on SBWOs. The subsequent results and conclusions are complete in accordance of the obtained simulated SBWO models test results:

1) Test results of the analysis demonstrations that the load carrying capacity and the stiffness of the steel beam with triangular web opening is greater than the other three shapes which are circular, square and hexagonal at the elastic region by (4.66%, 21.26%, 6.71%) respectively.

2) The ultimate load at which the specimen fails will causes very large amount of deflection, thus the applied load which causes 30 mm deflection was the control value of the comparisons.

3) The circular web opening shows almost similar response to flexural stress as the hexagonal opening, this may be due to the shape of the hexagonal geometry which has more internal angles and make it to be more like a circle shape.

4) Furthermore, the square web opening has the least strength and stiffness due to large flexural stress concentration around its corners. Also, the deformations in the rectangular opening sample is greater than other test samples.

REFERENCES

1. **Samadhan G**. Morkhade1, and Laxmikant M. Gupta1 (2015), *"An experimental and parametric study on steel beams with web openings"*, Int J Adv Struct Eng, Vol. 7, P.P. 249–260.
2. **Bower J.E.** (1968), *"Design of beam with web openings"*, J Struct Div 94, Vol. 3, P.P.783–807.
3. **Lawson R.M.** (1987), *"Design for openings in the webs of composite beams"*, CIRIA Special Publication and SCI Publication 068. CIRIA/Steel Construction Institute, London.
4. **Darwin D.** (1990), *"Steel and composite beams with web openings"*, Steel design guide series no. 2. AISC, Chicago.
5. Design of composite beams with large web openings. SCI P355 (2011).
6. **Redwood R.G.** (1969), *"The strength of steel beams with unreinforced web holes"*, Civil Eng. Public Works Rev 64(755): P.P.559–562
7. **Chan P.W., Redwood R.G.** (1974), *"Stresses in beams with circular eccentric web holes"*, J Struct Div 100(ST1): P.P.231–248
8. **Olander H.C.** (1953), *"A method of calculating stress in rigid frame corners"*, J Struct Div Proc. ASCE
9. **Sahmel P.** (1969), *"Konstruktive Ausbildung und Näherungsbenechaung geschewisster Biegeträger und Torsionsst äbe mit grossen stegausnehmungen"* [The design, construction and approximate analysis of weld beams and torsion members having large web openings]. Schweissen und Schneiden 21(3): P.P.116–122
10. European committee for standardization. EN 1993-1-3, Euro code 3 (EC3) (1998) Design of steel structures—part 1.1: general rules and rules for buildings; 1992, and amendment A2 of Euro code 3: Annex N ‘Openings in webs’. British Standards Institution.
11. **Thevendran V., Shanmugam N.E.** (1991), *"Lateral buckling of doublysymmetric beams containing openings"*, J Eng Mech 117(7): P.P.1427–1441
12. **Lawson R.M., Chung K.F.** (2001), *"Simplified design of composite beamswith large web openings to Euro code 4"*, J Constr Steel Res 57: P.P.135–163

13. **Chung K.F., Liu T.C.H., Ko A.C.H.** (2001), *"Investigation on Vierendeelmechanism in steel beams with circular web openings"*, J Constr Steel Res 57: P.P. 467–490
14. **Chung K.F., Liu T.C.H., Ko A.C.H.** (2003), *"Steel beams with large webopenings of various shapes and sizes: an empirical designmethod using a generalized moment–shear interaction curve"*,J Constr Steel Res 59: P.P.1177–1200
15. **Tsavdaridis K.D., D'Mello C.** (2011), *"Web buckling study of thebehaviour and strength of perforated steel beams withdifferent novel web opening shapes"*, J Constr Steel Res 67: P.P.1605–1620
16. **Sweedan A.M.I.** (2011),*"Elastic lateral stability of I-shaped cellular steel beams"*, J Constr Steel Res 67: P.P.151–163
17. **Saka M.P., Erdal F**. (2013),*"Ultimate load carrying capacity of optimally designed steel cellular beams"*, J Constr Steel Res 80: P.P.355–368
18. **Panedpojaman P., Thepchatri T.** (2013), *"Finite element investigation ondeflection of cellular beams with various configuration"*, Int JSteel Struct 13: P.P.487–494
19. **Boissonnade N., Nseir J., Lo M., Somja H.** (2014), *"Design of cellularbeams against lateral torsional buckling"*, Proc Inst Civil EngStruct Build 167:436–444
20. **Iman Satyarno, Djoko Sulistyo, Dina Heldita, A.** Talodaci Corte Real De Oliviera (2017), *"Full height rectangular opening castellated steel beam partially encased in reinforced mortar"*, Procedia Engineering 171: P.P. 176 – 184
21. **Made Sukrawa** (2017), *"Finite element modelling of reinforced large-opening on the web of steel beam considering axial forces"*, AIP Conference Proceedings 1903, 020018, P.P. 1-9
22. **Tarek Almusallam, Yousef Al Salloum, Hussein Elsanadedy, Abdulhafiz Alshenawy and Rizwan Iqbal** (2018), *"Behavior of FRP-Strengthened RC Beams with Large Rectangular Web Openings in Flexure Zones: Experimental and Numerical Study"*, Int J Concr Struct Mater 12:47, P.P. 1-28
23. **Morkhade, S.G., Baswaraj, S.M. & Nayak, C.B.** (2019), *"Comparative study of effect of web opening on the strength capacities of steel beam with trapezoidally corrugated web"*, Asian J Civ Eng 20, P.P.1089-1099
24. BS 5950: Part 1 (2000),*"Structural use of steelwork in building"*, BritishStandards Institution, London: Code of practice for design.Rolled and welded sections
25. Abaqus (6.14-4), *"Analysis User's Manual"*, U.S.A. (2014).
26. **Mohammad R.K.M. Al-badkubi** (2019), *"Finite Element Study on Ultimate Shear Capacity of Voided Reinforced Concrete Beams"*, 2nd International Conference on Engineering Technology and their Applications 2019-IICET2019- Islamic University, Alnajaf-Iraq, P.P. 19-24

СПИСОК ЛИТЕРАТУРЫ

1. **Samadhan G**. Morkhade1, and Laxmikant M. Gupta1 (2015), *"An experimental and parametric study on steel beams with web openings"*, Int J Adv Struct Eng, Vol. 7, P.P. 249–260.
2. **Bower J.E.** (1968), *"Design of beam with web openings"*, J Struct Div 94, Vol. 3, P.P.783–807.
3. **Lawson R.M.** (1987), *"Design for openings in the webs of composite beams"*, CIRIA Special Publication and SCI Publication 068. CIRIA/Steel Construction Institute, London.
4. **Darwin D.** (1990), *"Steel and composite beams with web openings"*, Steel design guide series no. 2. AISC, Chicago.
5. Design of composite beams with large web openings. SCI P355 (2011).

6. **Redwood R.G.** (1969), *"The strength of steel beams with unreinforced web holes"*, Civil Eng. Public Works Rev 64(755): P.P.559–562
7. **Chan P.W., Redwood R.G.** (1974), *"Stresses in beams with circular eccentric web holes"*, J Struct Div 100(ST1): P.P.231–248
8. **Olander H.C.** (1953), *"A method of calculating stress in rigid frame corners"*, J Struct Div Proc. ASCE
9. **Sahmel P.** (1969), *"Konstruktive Ausbildung und Näherungsbenechaung geschewisster Biegeträger und Torsionsst äbe mit grossen stegausnehmungen"* [The design, construction and approximate analysis of weld beams and torsion members having large web openings]. Schweissen und Schneiden 21(3): P.P.116–122
10. European committee for standardization. EN 1993-1-3, Euro code 3 (EC3) (1998) Design of steel structures—part 1.1: general rules and rules for buildings; 1992, and amendment A2 of Euro code 3: Annex N 'Openings in webs'. British Standards Institution.
11. **Thevendran V., Shanmugam N.E.** (1991), *"Lateral buckling of doublysymmetric beams containing openings"*, J Eng Mech 117(7): P.P.1427–1441
12. **Lawson R.M., Chung K.F.** (2001), *"Simplified design of composite beamswith large web openings to Euro code 4"*, J Constr Steel Res 57: P.P.135–163
13. **Chung K.F., Liu T.C.H., Ko A.C.H.** (2001), *"Investigation on Vierendeelmechanism in steel beams with circular web openings"*, J Constr Steel Res 57: P.P. 467–490
14. **Chung K.F., Liu T.C.H., Ko A.C.H.** (2003), *"Steel beams with large webopenings of various shapes and sizes: an empirical designmethod using a generalized moment–shear interaction curve"*,J Constr Steel Res 59: P.P.1177–1200
15. **Tsavdaridis K.D., D'Mello C.** (2011), *"Web buckling study of thebehaviour and strength of perforated steel beams withdifferent novel web opening shapes"*, J Constr Steel Res 67: P.P.1605–1620
16. **Sweedan A.M.I.** (2011),*"Elastic lateral stability of I-shaped cellular steel beams"*, J Constr Steel Res 67: P.P.151–163
17. **Saka M.P., Erdal F**. (2013),*"Ultimate load carrying capacity of optimally designed steel cellular beams"*, J Constr Steel Res 80: P.P.355–368
18. **Panedpojaman P., Thepchatri T.** (2013), *"Finite element investigation ondeflection of cellular beams with various configuration"*, Int JSteel Struct 13: P.P.487–494
19. **Boissonnade N., Nseir J., Lo M., Somja H.** (2014), *"Design of cellularbeams against lateral torsional buckling"*, Proc Inst Civil EngStruct Build 167:436–444
20. **Iman Satyarno, Djoko Sulistyo, Dina Heldita, A.** Talodaci Corte Real De Oliviera (2017), *"Full height rectangular opening castellated steel beam partially encased in reinforced mortar"*, Procedia Engineering 171: P.P. 176 – 184
21. **Made Sukrawa** (2017), *"Finite element modelling of reinforced large-opening on the web of steel beam considering axial forces"*, AIP Conference Proceedings 1903, 020018, P.P. 1-9
22. **Tarek Almusallam, Yousef Al Salloum, Hussein Elsanadedy, Abdulhafiz Alshenawy and Rizwan Iqbal** (2018), *"Behavior of FRP-Strengthened RC Beams with Large Rectangular Web Openings in Flexure Zones: Experimental and Numerical Study"*, Int J Concr Struct Mater 12:47, P.P. 1-28
23. **Morkhade, S.G., Baswaraj, S.M. & Nayak, C.B.** (2019), *"Comparative study of effect of web opening on the strength capacities of steel beam with trapezoidally corrugated web"*, Asian J Civ Eng 20, P.P.1089-1099

24. BS 5950: Part 1 (2000),*"Structural use of steelwork in building"*, BritishStandards Institution, London: Code of practice for design.Rolled and welded sections
25. Abaqus (6.14-4), *"Analysis User's Manual"*, U.S.A. (2014).
26. **Mohammad R.K.M. Al-badkubi** (2019), *"Finite Element Study on Ultimate Shear Capacity of Voided Reinforced Concrete Beams"*, 2nd International Conference on Engineering Technology and their Applications 2019-IICET2019- Islamic University, Alnajaf-Iraq, P.P. 19-24

Hussein Talab Nhabih, Department of Civil Engineering, Faculty of Engineering, Babylon University, Babylon, Iraq. E-mail: eng.hussein.t@uobabylon.edu.iq

Mohammad R.K.M. Al-Badkubi, Department of building and construction technology, Islamic University,Najaf, Iraq. E-mail: Mohammad.R.Albadkub@iunajaf.edu.iq

Marwa Marza Salman, Department of Ceramic and Building Material, Faculty of Materials Engineering, Babylon University, Babylon, Iraq. E-mail: mat.marwa.marza@uobabylon.edu.iq

Хусейн Талаб Набих, кафедра гражданского строительства, инженерный факультет, Вавилонский университет, Вавилон, Ирак. Эл. почта: eng.hussein.t@uobabylon.edu.iq

Мохаммад Р.К.М. Аль-Бадкуби, кафедра строительства и строительных технологий, Исламский университет, Наджаф, Ирак. Эл. почта: Mohammad.R.Albadkub@iunajaf.edu.iq

Марва Марза Салман, кафедра керамики и строительных материалов, факультет материаловедения, Вавилонский университет, Вавилон, Ирак. Эл. почта: mat.marwa.marza@uobabylon.edu.iq

THE RESEARCH OF AN IMPACT IN STRENGTH CHARACTERISTICS OF OIL-CONTAMINATED SANDY SOILS

Rashid A. Mangushev*, *Alina V. Kvashuk, Alexandra V. Vagurina, Ilya D. Kulyashov

Saint Petersburg State University of Architecture and Civil Engineering, Saint Petersburg, RUSSIA

Abstract: A review of existing studies by domestic and foreign authors on changes in the angle of internal friction of sandy soils contaminated with oil products is provided. The main experimentally confirmed results of studies of the angle of internal friction of sandy soils interacting with oil products are outlined. Laboratory tests were conducted to determine the strength characteristics of sandy soils contaminated with oil products using the in-plane shear method. Coarse, medium and fine sands contaminated with A-95 gasoline, diesel fuel, and heavy oil at a concentration of 0-12% by dry soil weight were used as test samples. A methodology for conducting laboratory tests using the in-plane shear method for sands contaminated with oil products is described and tested. The degree of influence of viscosity and oil product concentration factors on the value of the angle of internal friction of sands of different sizes was determined and mathematically substantiated using regression multifactorial analysis. The sensitivity analysis of the adopted regression equation with six degrees of freedom is performed. The scope of application of the proposed function is designated. It is shown that the use of polynomials of the second kind in linear regressions leads to a significant complication of the model associated with the impossibility of explicitly identifying individual influence coefficients without additional calculation of partial derivatives to compile the function gradient with its subsequent analysis.

A decrease in the angle of internal friction of coarse, medium and fine sandy soils regardless of the type of oil product and its concentration has been laboratory confirmed. A graph of the dependence of the angle of internal friction of sands of different sizes on the concentration of oil products is presented. It has been statistically substantiated that the greatest influence on the angle of internal friction of sandy soils contaminated with oil products is exerted by concentration, to a lesser extent - the type (viscosity) of oil products.

Keywords: sandy soil, oil products, in-plane shear, angle of internal friction, regression analysis, concentration

УСТАНОВЛЕНИЕ ВЛИЯНИЯ ЗАГРЯЗНЕНИЯ ПЕСЧАНЫХ ГРУНТОВ НЕФТЕПРОДУКТАМИ НА ИЗМЕНЕНИЕ ИХ ПРОЧНОСТНЫХ ХАРАКТЕРИСТИК

Р.А. Мангушев, А.В. Квашук, А.В. Вагурина, И.Д. Куляшов

Санкт-Петербургский государственный архитектурно-строительный университет, г. Санкт-Петербург, РОССИЯ

Аннотация: Выполнен обзор существующих исследований отечественных и зарубежных авторов об изменении угла внутреннего трения песчаных грунтов при загрязнении нефтепродуктами. Обозначены основные экспериментально подтвержденные результаты исследований угла внутреннего трения песчаных грунтов при взаимодействии с нефтепродуктами.

Проведены лабораторные испытания по определению прочностных характеристик песчаных грунтов, загрязненных нефтепродуктами, методом одноплоскостного среза. В качестве испытуемых образцов применялись пески крупный, средней крупности и мелкий, загрязненные бензином А-95, дизельным топливом, тяжелой нефтью в концентрации 0-12% по массе сухого грунта. Описана и апробирована методика проведения лабораторных испытаний методом одноплоскостного среза для песков, загрязненных нефтепродуктами. Посредством регрессионного многофакторного анализа определена и математически обоснована степень влияния факторов вязкости и концентрации нефтепродукта на величину угла внутреннего трения песков различной крупности. Проведен анализ чувствительности принятого уравнения регрессии с шестью степенями свободы. Обозначена область применения предложенной функции. Показано, что

использование полиномов второго рода в линейных регрессиях ведёт к значительному усложнению модели, связанному с невозможностью явного выделения отдельных коэффициентов влияния без дополнительного вычисления частных производных для составления градиента функции с его последующим анализом.
Лабораторно подтверждено снижение угла внутреннего трения песчаных грунтов крупных, средней крупности и мелких вне зависимости от вида нефтепродукта и его концентрации. Представлен график зависимости угла внутреннего трения песков различной крупности от концентрации нефтепродуктов. Статистически обосновано, что наибольшее влияние на угол внутреннего трения песчаных грунтов, загрязненных нефтепродуктами, оказывает концентрация, в меньшей степени – вид (вязкость) нефтепродуктов.

Ключевые слова: песчаный грунт, нефтепродукты, одноплоскостной срез, угол внутреннего трения, регрессионный анализ, концентрация

1. INTRODUCTION

According to the Ministry of Energy, the number of accidents accompanied by oil product spills (hereinafter - OP) exceeded 17000 in 2019 in the territory of the Russian Federation [1], [2]. Oil spills are accompanied by infiltration into the soil mass, resulting in changes in the physical and mechanical characteristics of soils [3].
Mechanical properties are the most important in the design and construction of bases and foundations, since they form the stress-strain state of the soil along with the acting loads on the base. It is known that the strength of sandy soils is ensured by friction forces arising at the contact points of mineral particles.
According to studies [4-8], contamination of sandy soils with oil products is accompanied by the formation of oily envelope around mineral particles, resulting in the effect of “slipping” of sand particles relative to each other. Hence, the angle of internal friction is reduced.
Thus, in the studies of C. Shin, J.B. Lee, B.M. Das [9] as an object of investigation were considered medium coarse sands with relative density of 50% and 75% samples, contaminated with oil in concentration from 0% to 4.5% by weight of dry sand. Single plane shear tests were conducted at a vertical pressure of 40 kPa. As a result of the experiment, the angle of internal friction decreased significantly at oil concentration C = 1.3%, with further increase in concentration, the decrease in the angle of internal friction continued, but was insignificant (Fig.1). Decrease of the angle of internal friction is also noted in [10-13].
The opposite result was reached by Z. N. Rasheed, F. R. Ahmed, H. M. Jassim in the research [14], where the object was coarse sand contaminated with gasoline and kerosene. According to the results obtained, the angle of internal friction increased by 3-8° as the.

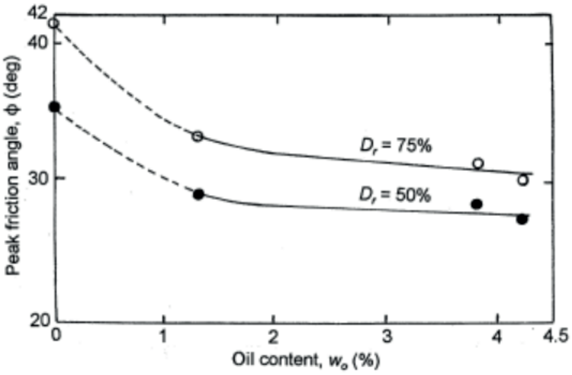

Figure 1. Graph of relationship between the peack angle of internal friction of medium-sized sand and oil concentration [9]

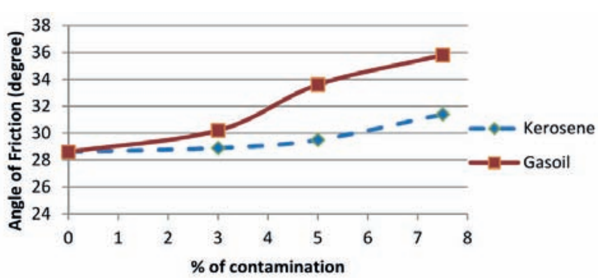

Figure 2. Graph of relationship between the angle of internal friction of coarse sands and the concentration of gasoline and kerosene [14]

At the same time, the results of the study [15] indicate that there is no obvious law of change in the angle of internal friction with increasing oil products concentration.

Taking into account the contradictions in the results of domestic and foreign authors, the aim of the study is to substantiate the degree of influence of variable parameters such as sand coarseness, type (viscosity) and concentration of oil products on the degree of change in the angle of internal friction of sandy soils contaminated with oil products, as well as to establish their regression dependencies.

Objectives of the study:

1. Determine the nature and degree of change in the angle of internal friction of sands of different coarseness at contamination of oil products (heavy oil, diesel fuel, gasoline A-95) in different concentrations (0,2,6,12%) by mass of dry soil.
2. By means of regression multi-factor analysis, using the results of laboratory tests, to identify the degree of influence of sand size, type of oil products and its concentration on the change in the angle of internal friction.

2. LABORATORY TEST PROCEDURE

Tests for determining the angle of internal friction were carried out by the method of single-plane-bone shearing on monofractional samples of sand of different sizes (coarse, medium and fine), contaminated with gasoline A-95, diesel fuel and heavy oil at a concentration of C = 0, 2, 6, 12% by weight of dry soil.

Concentration of oil products and humidity in the tested samples were set so that complete filling of pores with pore fluid (oil products + water) was ensured. Thus, the maximum and minimum oil products concentrations were provided at minimum and maximum soil moisture, respectively.

The volumes of oil products (1) and water (2) added to the test samples were calculated according to the expressions:

$$V_{нп} = C \cdot V_s \cdot \frac{\rho_s}{\rho_{нп}}, \qquad (1)$$

$$V_w = V_s \cdot \left(e - C \frac{\rho_s}{\rho_{нп}} \right), \qquad (2)$$

where C is the concentration of oil products; V_s is the volume of soil particulate, cm^3; ρ_s is the soil particulate density, g/cm^3; $\rho_{нп}$ is the oil products density, g/cm^3, e is the porosityfactor.

Figure 3. Sandy soil sample contaminated with diesel fuel after the single plane shear test

2.1. Results of Laboratory Tests (Input Data for Regression Analysis)

Coarse sand:

The angle of internal friction of coarse sand decreases from 9% to 19% for heavy oil contamination, from 6% to 11% for A-95 gasoline contamination, and from 8% to 14% for diesel contamination compared to clean sand.

Medium coarse sand:

The angle of internal friction of medium coarse sand decreases from 8% to 19% for heavy oil contamination, from 5% to 8% for A-95 gasoline contamination, and from 5% to 14% for diesel fuel contamination compared to clean sand.

Fine sand:

The angle of internal friction of fine sand decreases from 14% to 22% when polluted with heavy oil, from 7% to 17% when polluted with gasoline A-95, from 13% to 19% when polluted with diesel fuel in comparison with clean sand.

It is worth noting the similar character of decrease in the angle of internal friction for sands of different sizes when polluted with all considered oil products: the maximum decrease at a concentration not exceeding 6%, with further increase in concentration the angle of internal friction insignificantly decreases.

The results of laboratory tests of sandy soils contaminated with oi products are presented in Fig. 4. Numerical values of the angle of internal friction are summarized in Table 1.

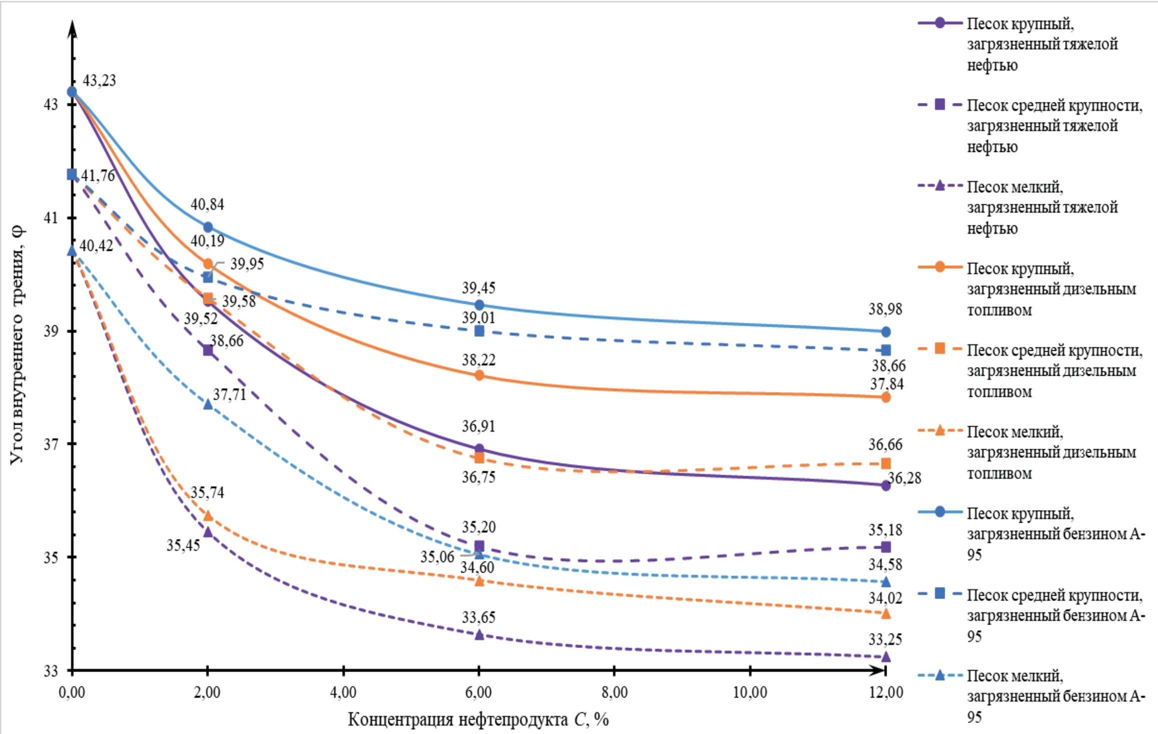

Figure 4. Graph of the relationship between the angle of internal friction and oil products concentration for sands of different sizes at different types of pollutant oil products

Table 1. Values of the angle of internal friction of sands of different coarseness depending on the type and concentration of oil products

	Coarse sand				**Medium coarse sand**				**Fine sand**			
The pore space is filled with heavy oil and water												
C, %	0,00	2,00	6,00	12,00	0,00	2,00	6,00	12,00	0,00	2,00	6,00	12,00
φ,°	43,23 (0%)	39,52 (9%↓)	36,91 (17%↓)	36,28 (19%↓)	41,76 (0%)	38,66 (8%↓)	35,2 (19%↓)	35,18 (19%↓)	40,42 (0%)	35,45 (14%↓)	33,65 (20%↓)	33,25 (22%↓)
The pore space is filled with A-95 gasoline and water												
C, %	0,00	2,00	6,00	12,00	0,00	2,00	6,00	12,00	0,00	2,00	6,00	12,00
φ,°	43,23 (0%)	40,84 (6%↓)	39,45 (10%↓)	38,98 (11%↓)	41,76 (0%)	39,95 (5%↓)	39,01 (7%↓)	38,66 (8%↓)	40,42 (0%)	37,71 (7%↓)	35,06 (15%↓)	34,58 (17%↓)
The pore space is filled with diesel fuel and water												
C, %	0,00	2,00	6,00	12,00	0,00	2,00	6,00	12,00	0,00	2,00	6,00	12,00
φ,°	43,23 (0%)	40,19 (8%↓)	38,22 (13%↓)	37,84 (14%↓)	41,76 (0%)	39,58 (5%↓)	36,75 (14%↓)	36,66 (14%↓)	40,42 (0%)	35,74 (13%↓)	34,6 (17%↓)	34,02 (19%↓)

Note: *n*%↓ is the decrease in the angle of internal friction of sandy soil contaminated with oil products, compared to clean sand, expressed in percentage.

3. METHOD OF STATISTICAL ANALYSIS

3.1. Solving regression equation with number of degrees of freedom m=5

The multiple linear regression model can be generally expressed as:

$$y = \sum_{i=1}^{k} x_i \cdot \beta_i + \varepsilon = x_1 \cdot \beta_1 + x_2 \cdot \beta_2 + \ldots + x_k \cdot \beta_k + \varepsilon, \quad (3)$$

where $x_1; x_2; \ldots; x_k$ – are the factors influencing the value of the function (predictors);
$\beta_1; \beta_2; \ldots; \beta_k$ – model parameters (influence coefficients);
ε – is the random unpredictable error.
To determine the degree of influence of each factor on the intensity of change in the angle of internal friction of sands contaminated with oil products, a multiple linear regression model will be written for the case under consideration:

$$y = \beta_1 \cdot x_1 + \beta_2 \cdot x_2 + \beta_3 \cdot \Delta_к + \beta_4 \cdot \Delta_с + \beta_5 \cdot \Delta_м + \varepsilon, \quad (4)$$

where:
Factor 1: $x_1 = C \in [0;12], \%$ – independent variable of **oil products concentration** by mass of dry soil, in the range from 0 to 12 %;
Factor 2: $x_2 = \kappa \in [0,596; 49,702]$ – independent variable of **coventional viscosities of oil products**, calculated as $\kappa = \frac{\eta_{загрязнитель}}{\eta_{вода}}$. Since the conventional viscosity of water $\kappa = 1,000$ and kinematic viscosity of water $\eta \approx 1 \cdot 10^{-6} \frac{м^2}{с}$, then in the equations with the conventional viscosity η it is possible to perform substitution for the kinematic viscosity with a change of their corresponding coefficients by a factor of 10^6 (Table 2).
Factors 3-5: $\Delta_к; \Delta_с; \Delta_м \in \{0;1\}$ – discrete independent variables indicators **of sand size** (dummy variables): $\Delta_к$ – coarse sand; $\Delta_с$ – medium sand; $\Delta_м$ – fine sand, where 1 indicates the presence of sand of a given size in the test, and 0 indicates the absence.

Table 2. Physical properties of pore fluids

Pore fluid	Water	Gasoline A-95	Diesel fuel	Heavy oil
Density $\rho, \frac{кг}{м^3}$	1000,0	737,8	837,8	898,4
Kinematic viscosity $\eta \cdot 10^{-6}, \frac{м^2}{с}$	1,006	0,600	3,452	50,000
Conventional viscosity κ	1,000	0,596	3,431	49,702

Since the tests were carried out on monofractional sand samples, the indicators for coarse, medium coarse and fine sands are as follows:

$$\begin{cases} \Delta_к = 1 \rightarrow \Delta_с = \Delta_м = 0 \\ \Delta_с = 1 \rightarrow \Delta_к = \Delta_м = 0 \\ \Delta_м = 1 \rightarrow \Delta_к = \Delta_с = 0 \end{cases}; \quad (5)$$

$\beta_1; \beta_2; \beta_3; \beta_4; \beta_5$ – model parameters (influence coefficients), which take into account the change in the angle of internal friction when changing the values of predictors.
The initial data for the multifactor regression analysis are presented in Table 3.
Assume $y = \varphi^\circ$, where φ° – is the angle of internal friction according to the results of laboratory tests. Then the equation of multiple linear regression can be represented as:

$$\tilde{\varphi} = \beta_1 \cdot C + \beta_2 \cdot \kappa + \beta_3 \cdot \Delta_к + \beta_4 \cdot \Delta_с + \beta_5 \cdot \Delta_м,$$

or

$$\tilde{y} = \beta_1 \cdot x_1 + \beta_2 \cdot x_2 + \beta_3 \cdot \Delta_к + \beta_4 \cdot \Delta_с + \beta_5 \cdot \Delta_м \quad (6)$$

Table 3. Initial data for regression analysis and list of accepted factors

No	$\varphi°$ based on the results laboratory tests	factor 1	factor 2	factor 3	factor 4	factor 5
	y	x_1	x_2	$\Delta_{к}$	$\Delta_{с}$	$\Delta_{м}$
The sand is coarse. The pore space is filled with heavy oil and water						
1	43,23	0	1,000	1	0	0
2	39,52	2	49,702	1	0	0
3	36,91	6	49,702	1	0	0
4	36,28	12	49,702	1	0	0
Medium-sized sand. The pore space is filled with heavy oil and water						
5	41,76	0	1,000	0	1	0
6	38,66	2	49,702	0	1	0
7	35,20	6	49,702	0	1	0
8	35,18	12	49,702	0	1	0
The sand is fine. The pore space is filled with heavy oil and water						
9	40,42	0	1,000	0	0	1
10	35,45	2	49,702	0	0	1
11	33,65	6	49,702	0	0	1
12	33,25	12	49,702	0	0	1
The sand is coarse. The pore space is filled with gasoline A-95 and water						
13	40,84	2	0,596	1	0	0
14	39,45	6	0,596	1	0	0
15	38,98	12	0,596	1	0	0
Medium coarse sand. The pore space is filled with gasoline A-95 and water						
16	39,95	2	0,596	0	1	0
17	39,01	6	0,596	0	1	0
18	38,66	12	0,596	0	1	0
The sand is fine. The pore space is filled with gasoline A-95 and water						
19	37,71	2	0,596	0	0	1
20	35,06	6	0,596	0	0	1
21	34,58	12	0,596	0	0	1
The sand is coarse. The pore space is filled with diesel fuel and water						
22	40,19	2	3,431	1	0	0
23	38,22	6	3,431	1	0	0
24	37,84	12	3,431	1	0	0
Medium coarse sand. The pore space is filled with diesel fuel and water						
25	39,58	2	3,431	0	1	0
26	36,75	6	3,431	0	1	0
27	36,66	12	3,431	0	1	0
The sand is fine. The pore space is filled with diesel fuel and water						
28	35,74	2	3,431	0	0	1
29	34,60	6	3,431	0	0	1
30	34,02	12	3,431	0	0	1

Using the least squares method we determine the values of influence coefficients: $\beta_1 = -0,309$, $\beta_2 = -0,041$, $\beta_3 = 41,633$, $\beta_4 = 40,664$, $\beta_5 = 37,971$.

Substituting the influence coefficients into the multiple linear regression equation, we obtain:

$$\tilde{y} = -0,309 \cdot x_1 - 0,041 \cdot x_2 + 41,633 \cdot \Delta_{к} + 40,664 \cdot \Delta_{с} + 37,971 \cdot \Delta_{м}, \qquad (7)$$

Comparison of the results of laboratory results of internal friction angle with the predicted values is presented in Table 4.

Table 4. Comparison of values of the results of laboratory measurement of the angle of internal friction with predicted values

No	$\varphi°$ based on the results of laboratory tests	Predicted value $\varphi°$ at the calculated influence coefficients	Total error	Relative error
	y	$\tilde{y}$	$\varepsilon = \tilde{y} - y$	$\xi = \frac{\tilde{y}_i - y_i}{y_i} \cdot 100\%$
The sand is coarse. The pore space is filled with heavy oil and water				
1	43,23	41,59	-1,64	-3,79
2	39,52	38,97	-0,55	-1,40
3	36,91	37,73	0,82	2,22
4	36,28	35,88	-0,40	-1,10
Medium-sized sand. The pore space is filled with heavy oil and water				
5	41,76	40,62	-1,14	-2,72
6	38,66	38,00	-0,66	-1,71
7	35,20	36,76	1,56	4,44
8	35,18	34,91	-0,28	-0,78

The sand is fine. The pore space is filled with heavy oil and water				
9	40,42	37,93	-2,49	-6,17
10	35,45	35,31	-0,15	-0,42
11	33,65	34,07	0,42	1,26
12	33,25	32,22	-1,03	-3,11
The sand is coarse. The pore space is filled with gasoline A-95 and water				
13	40,84	40,99	0,15	0,38
14	39,45	39,75	0,30	0,76
15	38,98	37,90	-1,08	-2,78
Medium coarse sand. The pore space is filled with gasoline A-95 and water				
16	39,95	40,02	0,07	0,19
17	39,01	38,78	-0,22	-0,57
18	38,66	36,93	-1,73	-4,48
The sand is fine. The pore space is filled with gasoline A-95 and water				
19	37,71	37,33	-0,38	-1,02
20	35,06	36,09	1,03	2,94
21	34,58	34,24	-0,34	-0,99
The sand is coarse. The pore space is filled with diesel fuel and water				
22	40,19	40,99	0,80	2,00
23	38,22	39,75	1,53	4,01
24	37,84	37,90	0,06	0,16
Medium coarse sand. The pore space is filled with diesel fuel and water				
25	39,58	39,90	0,32	0,81
26	36,75	38,67	1,91	5,21
27	36,66	36,81	0,15	0,42
The sand is fine. The pore space is filled with diesel fuel and water				
28	35,74	37,21	1,47	4,11
29	34,60	35,97	1,38	3,99
30	34,02	34,12	0,10	0,30

Thus, the executed model has the following characteristics:

1) *Coefficient of determination:*

$$R^2 = \frac{\sum_{i=1}^{n}\left(\tilde{y}_i - \overline{y}\right)^2}{\sum_{i=1}^{n}\left(y_i - \overline{y}\right)^2} = \frac{161,20}{192,73} \approx 0,833, \quad (8)$$

High R^2 indicates a small share of unexplained variance and, therefore, a high level of fit of the linear regression model to the laboratory data.

2) *Fisher's criterion:*

$$F = \frac{MSR}{MSE} = \frac{R^2}{1-R^2} \cdot \frac{n-m}{m} = \frac{0,833}{1-0,833} \cdot \frac{30-5}{5} \approx 24,94, \quad (9)$$

where $MSR = \frac{SSR}{m} -$ is the *Mean Square Regression*;

$MSE = \frac{SSE}{n-m} -$ is the *Mean Square Error*;

$SSR = SST \cdot R^2 = \sum_{i=1}^{n}\left(\tilde{y}_i - \overline{y}\right)^2 -$ is the *Sum of Squares for Regression*;

$SST = \frac{SSE}{1-R^2} = \sum_{i=1}^{n}\left(y_i - \overline{y}\right)^2 -$ is the *Total Sum of Squares*;

$SSE = \sum_{i=1}^{n}\left(y_i - \tilde{y}_i\right)^2 -$ is the *Sum of Squares for Error*;

$n = 30 -$ is the total number of observations in the sample;

$m = 5 -$ is the number of parameters in the model;

$R^2 = 1 - \frac{SSE}{SST} = 0,833 -$ coefficient of determination (*R-squared*).

Comparing the obtained value of Fisher's criterion with the tabulated value, we obtain the following results:

$$F_{табл}\left(\alpha; k_1 = m; k_2 = n-m\right) = F_{табл}\left(0,05; 5; 25\right) \approx 2,60$$
$$F = 24,94 > F_{табл} = 2,60, \quad (10)$$

Therefore, the regression equation is statistically significant.

3) *P-value* is determined using the Fisher distribution function. The level of significance obtained from the p-value is $2,1 \cdot 10^{-9}$, that confirms the high statistical significance of the model against the null hypothesis, according to which all additional parameters are equal to zero and do not improve the explanatory power of the model.

Thus, we can reject the null hypothesis and conclude that the included parameters are significant.

4) *Average approximation error index*

$$\overline{A} = \frac{1}{n} \cdot \sum_{i=1}^{n}\left|\frac{y_i - \tilde{y}_i}{y_i}\right| \cdot 100\% \approx 2,14\%, \quad (11)$$

indicates that, on average, the predicted values of the angle of internal friction deviate from the laboratory values by 2.14 %, which indicates a high accuracy of the equation.

Conclusion: the proposed regression equation with the number of degrees of freedom has a high level of explained variance and the level of statistical significance. However, according to Table 5, the coefficient of influence $\beta_4 = 40,664$ has *p*-value = 0,06719 $> \alpha = 0,05$, which is not statistically significant. In order to ensure statistical significance of all influence coefficients, we perform the regression analysis again, increasing the number of degrees of freedom to $m = 6$.

3.2. Solving regression equation with number of degrees of freedom m=6

In the course of calculations of different variants of mathematical description of graphs of relationships between the angle of internal friction and concentration for different sands and oil products in the regression analysis, the variable x_1 is represented in the form of a polynomial of degree 2, in connection with which the equation will have an additional degree of freedom:

$$y = \beta_1 \cdot x_1 + \beta_2 \cdot x_1^2 + \beta_3 \cdot x_2 + \beta_4 \cdot \Delta_к + \beta_5 \cdot \Delta_с + \beta_6 \cdot \Delta_м + \varepsilon, \quad (12)$$

Table 5. Regression analysis of model parameters (influence coefficients)

Predictor	Values of the influence coefficients, β_i	Standard error	t-statistics	*p*-value	Confidence intervals	
					low 95%	Top 95%
x_1	$\beta_1 = -0,309$	0,0475	-6,51	$8,0 \cdot 10^{-7}$	-0,407	-0,211
x_2	$\beta_2 = -0,041$	0,0094	-4,38	0,00019	-0,061	-0,022
$\Delta_к$	$\beta_3 = 41,633$	0,4710	88,39	$9,9 \cdot 10^{-33}$	40,663	42,603
$\Delta_с$	$\beta_4 = 40,664$	21,2901	1,91	0,06719	39,650	41,589
$\Delta_м$	$\beta_5 = 37,971$	5,2519	7,23	$1,4 \cdot 10^{-7}$	36,957	39,044

The initial data for the regression analysis and the list of accepted factors taking into account the additional degree of freedom of the regression equation are presented in Table 6.

Table 6. Initial data for regression analysis and the list of accepted factors taking into account the additional degree of freedom of the regression equation

No	$\varphi°$ based on the results of laboratory tests	factor 1	factor 2	factor 3	factor 4	factor 5	factor 6
	y	x_1	x_1^2	x_2	$\Delta_к$	$\Delta_с$	$\Delta_м$
The sand is coarse. The pore space is filled with heavy oil and water							
1	43,23	0	0	1,000	1	0	0
2	39,52	2	4	49,702	1	0	0
3	36,91	6	36	49,702	1	0	0
4	36,28	12	144	49,702	1	0	0
Medium coarse sand. The pore space is filled with heavy oil and water							
5	41,76	0	0	1,000	0	1	0
6	38,66	2	4	49,702	0	1	0
7	35,20	6	36	49,702	0	1	0
8	35,18	12	144	49,702	0	1	0
The sand is fine. The pore space is filled with heavy oil and water							
9	40,42	0	0	1,000	0	0	1
10	35,45	2	4	49,702	0	0	1
11	33,65	6	36	49,702	0	0	1
12	33,25	12	144	49,702	0	0	1
The sand is coarse. The pore space is filled with gasoline A-95 and water							
13	40,84	2	4	0,596	1	0	0
14	39,45	6	36	0,596	1	0	0
15	38,98	12	144	0,596	1	0	0

Sand of medium coarseness. The pore space is filled with gasoline A-95 and water							
16	39,95	2	4	0,596	0	1	0
17	39,01	6	36	0,596	0	1	0
18	38,66	12	144	0,596	0	1	0
The sand is fine. The pore space is filled with gasoline A-95 and water							
19	37,71	2	4	0,596	0	0	1
20	35,06	6	36	0,596	0	0	1
21	34,58	12	144	0,596	0	0	1
The sand is coarse. The pore space is filled with diesel fuel and water							
22	40,19	2	4	3,431	1	0	0
23	38,22	6	36	3,431	1	0	0
24	37,84	12	144	3,431	1	0	0
Medium coarse sand. The pore space is filled with diesel fuel and water							
25	39,58	2	4	3,431	0	1	0
26	36,75	6	36	3,431	0	1	0
27	36,66	12	144	3,431	0	1	0
The sand is fine. The pore space is filled with diesel fuel and water							
28	35,74	2	4	3,431	0	0	1
29	34,60	6	36	3,431	0	0	1
30	34,02	12	144	3,431	0	0	1

A comparison of the results of laboratory determination of the angle of internal friction with the predicted values within the regression analysis is presented in Table 7.

Table 7. Comparison of values of the results of laboratory determination of the angle of internal friction with the predicted values within the regression analysis

No	$\varphi°$ based on the results of laboratory tests	Predicted value $\varphi°$ at the calculated influence coefficients	Total error	Relative error
	y	$\tilde{y}$	$\varepsilon = \tilde{y} - y$	$\xi = \frac{\tilde{y}_i - y_i}{y_i} \cdot 100\%$
The sand is coarse. The pore space is filled with heavy oil and water				
1	43,23	42,95	-0,28	-0,65
2	39,52	39,25	-0,27	-0,69
3	36,91	36,78	-0,13	-0,35
4	36,28	36,57	0,29	0,80
Medium coarse sand. The pore space is filled with heavy oil and water				
5	41,76	41,97	0,21	0,51
6	38,66	38,28	-0,38	-0,99
7	35,20	35,81	0,61	1,74
8	35,18	35,59	0,41	1,17
The sand is fine. The pore space is filled with heavy oil and water				
9	40,42	39,28	-1,14	-2,83
10	35,45	35,58	0,13	0,36
11	33,65	33,12	-0,53	-1,57
12	33,25	32,90	-0,35	-1,05
The sand is coarse. The pore space is filled with gasoline A-95 and water				
13	40,84	41,03	0,20	0,48
14	39,45	38,57	-0,89	-2,24
15	38,98	38,35	-0,63	-1,62
Sand of medium coarseness. The pore space is filled with gasoline A-95 and water				
16	39,95	40,06	0,11	0,28
17	39,01	37,60	-1,41	-3,62
18	38,66	37,38	-1,28	-3,31
The sand is fine. The pore space is filled with gasoline A-95 and water				
19	37,71	37,37	-0,34	-0,91
20	35,06	34,90	-0,16	-0,45
21	34,58	34,69	0,11	0,31
The sand is coarse. The pore space is filled with diesel fuel and water				
22	40,19	41,03	0,85	2,11
23	38,22	38,57	0,35	0,91
24	37,84	38,35	0,51	1,36
Medium coarse sand. The pore space is filled with diesel fuel and water				
25	39,58	39,96	0,37	0,94
26	36,75	37,49	0,74	2,01
27	36,66	37,28	0,62	1,68
The sand is fine. The pore space is filled with diesel fuel and water				
28	35,74	37,26	1,52	4,26
29	34,60	34,80	0,20	0,59
30	34,02	34,58	0,56	1,66

The obtained coefficients at variables have high statistical significance (Table 8). Substituting the influence coefficients into the expression for multiple linear regression we obtain:

$$\tilde{y} = -1,08 \cdot x_1 + 0,058 \cdot x_1^2 - 0,036 \cdot x_2 + \\ +42,984 \cdot \Delta_{\kappa} + 42,01 \cdot \Delta_{c} + 39,317 \cdot \Delta_{M}, \quad (13)$$

The addition of a degree of freedom resulted in a change in characteristics:

1. *coefficient of determination:*

$$R^2 = \frac{\sum_{i=1}^{n}\left(\tilde{y}_i - \overline{y}\right)^2}{\sum_{i=1}^{n}\left(y_i - \overline{y}\right)^2} = \frac{180,15}{192,74} \approx 0,935, \quad (14)$$

2. *Fisher's criterion*:

$$F = \frac{R^2}{1-R^2}\cdot\frac{n-m}{m} = \frac{0,935}{1-0,935}\cdot\frac{30-6}{6} \approx 57,23$$

$$F \approx 57,23 > F_{табл}\left(0,05;6;24\right) \approx 2,51, \quad (15)$$

3. *p-value* $= 4,6\cdot 10^{-13}$,

4. *average percentage of approximation error:*

$$\overline{A} = \frac{1}{n}\cdot\sum_{i=1}^{n}\left|\frac{y_i - \tilde{y}_i}{y_i}\right|\cdot 100\% \approx 1,38\%, \quad (16)$$

Conclusion: since the coefficient of determination and Fisher's criterion have increased, and the p-value and average percentage of approximation error decreased in comparison with similar ones at $m=5$, it can be concluded that the function at $m=6$ has higher statistical significance than the equation with $m=5$ degrees of freedom of re-regression.

Table 8. *Estimation of regression coefficients (regression analysis of model parameters)*

Predictor	Values of influence coefficients, β_i	Standard error	t-statistics	*p*-value	Confidence intervals	
					low 95%	top 95%
x_1	$\beta_1 = -1,080$	0,1301	-8,30	$1,6\cdot10^{-8}$	-1,349	-0,812
x_1^2	$\beta_2 = 0,058$	0,0095	6,10	$2,7\cdot10^{-6}$	0,038	0,078
x_2	$\beta_3 = -0,036$	0,0061	-6,00	$3,4\cdot10^{-6}$	-0,049	-0,024
$\Delta_к$	$\beta_4 = 42,984$	0,3738	114,99	$2,0\cdot10^{-34}$	42,212	43,755
$\Delta_с$	$\beta_5 = 42,010$	0,3745	112,19	$3,6\cdot10^{-34}$	41,237	42,783
$\Delta_м$	$\beta_6 = 39,317$	0,3745	105,00	$1,8\cdot10^{-33}$	38,544	40,090

3.3 Comparison of the proposed linear multiple regressions with different regression degrees of freedom m=5 and m=6 by Fisher's criterion

The quality of models with m=5 and m=6 was compared using F-test (Fisher's exact test). The results are presented in Table 9.

Table 9. *Comparison of regression equations with m=5 and m=6 (F-test)*

Null hypothesis (H0)	Alternative hypothesis (H1)
Parameter $\beta_2\cdot x_1^2$, added to the regression equation compared to the equation with m=5, **insignificantly** improves the predictive ability of the model.	The regression equation with m=6 degrees of freedom **significantly** improves the predictive power compared to the equation with m=5
Fisher's criterion value $F \approx 10,30$	
p-value = 0,00376 < α = 0,05	

Conclusion: since p-values $0,00376 < \alpha = 0,05$, null hypothesis (H0) deviates and the addition of the summand $\beta_2\cdot x_1^2$ into the equation statistically significantly improves the regression equation in comparison with the model with the number of degrees of freedom $m=5$. Thus, to identify the degree of influence of the given factors on the angle of internal friction of sandy soils at oil products pollution, we take the regression equation with the number of degrees of freedom $m=6$.

3.4. Verification of error variance by the Goldfeld-Quandt method for the adopted regression equation with m=6 degrees of freedom

To check the homogeneity of the random error variance of the regression model, we will perform the Goldfeld-Quandt test. We introduce the null hypothesis (H0) about homoscedasticity of the model and the alternative hypothesis (H1) about heteroscedasticity of the model. For the calculation, we order and divide the existing sample of trials $n=30$ into 2 groups: $N_1=\{1;...;10\}$ and $N_2=\{21;...;30\}$, excluding $N=\{11;...;20\}$ of the central observations. We determine the sum of squares of regression errors for group 1 $ESS_1 \approx 0,537$ and for group 2 - $ESS_2 \approx 0,475$. Thus, the Fisher criterion is determined and compared with the tabulated value in the form:

$$F=\frac{ESS_1/m}{ESS_2/m}=\frac{ESS_1}{ESS_2}=\frac{0,537}{0,475}\approx 1,13$$

$$F=1,13<F_{табл}\left(0,05;6;4\right)\approx 6,16, \qquad (17)$$

Since the calculated value F is less than $F_{табл}$, the null hypothesis (H0) of homoscedasticity is accepted, which, in turn, indicates a constant error variance.

We accept the final regression equation that satisfies the main tests with a 95% confidence level:

$$\tilde{y}=-1,08\cdot x_1+0,058\cdot x_1^2-0,036\cdot x_2+$$
$$+42,984\cdot\Delta_к+42,01\cdot\Delta_с+39,317\cdot\Delta_м,$$

or

$$\tilde{\varphi}=-1,08\cdot C+0,058\cdot C^2-0,036\cdot\kappa+$$
$$+42,984\cdot\Delta_к+42,01\cdot\Delta_с+39,317\cdot\Delta_м, \qquad (18)$$

The graphical representation of the regression model with the experimental points obtained through laboratory experiments is presented in Fig. 5.

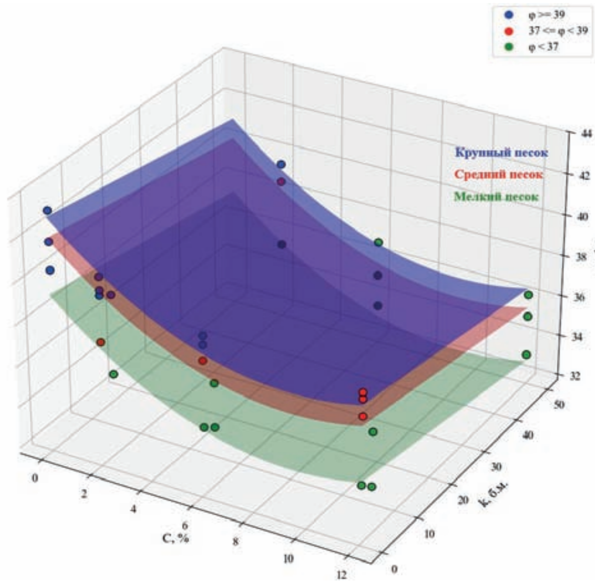

Figure 5. Graphical representation of the regression model with experimental points obtained through laboratory tests

3.5. Sensitivity analysis of the adopted regression equation with the number of degrees of freedom m=6

To analyze the sensitivity of the function, we calculate the gradient, which shows how changes in individual variables affect the function in order to determine which variables are most critical for changing the values of the function:

$$\nabla\tilde{y}=\left(\frac{\partial\tilde{y}}{\partial x_1};\frac{\partial\tilde{y}}{\partial x_2};\frac{\partial\tilde{y}}{\partial\Delta_к};\frac{\partial\tilde{y}}{\partial\Delta_с};\frac{\partial\tilde{y}}{\partial\Delta_м}\right), \qquad (19)$$

$$\nabla\tilde{y}\left(x_1;x_2;\Delta_к;\Delta_с;\Delta_м\right)=$$
$$=\left[-1,08+0,116\cdot x_1;-0,036;42,984;42,01;39,317\right], \qquad (20)$$

It should be noted that the value of the partial derivative $\frac{\partial\tilde{y}}{\partial x_1}=-1,08+0,116\cdot x_1$ depends on x_1. The initial sensitivity value is -1.08 and changes by 0.116 for each unit change in x_1. Since the dummy variables $(\beta_4,\beta_5,\beta_6)$ indicate only the reference point, they cannot be taken into account to analyze the degree of change in the angle of internal friction. The obtained dependence gives an extremum at the point

$x_1 = \frac{1,08}{0,116} \approx 9,3\%$. This feature of the model is associated with a sharp drop in the angle of internal friction at low oil products concentrations. For example, for a point with a low oil products concentration $x_1 = 2\%$, the change in the angle of internal friction $\Delta\tilde{y}$ with a change in concentration by $\Delta x_1 = 1\%$ will be calculated as the scalar product of a vector consisting of partial derivatives of functions for each parameter (function gradient $\nabla\tilde{y}$) and a vector containing changes in the variables under consideration (vector of changes ΔX):

$$\Delta\tilde{y} \approx \nabla\tilde{y} \cdot \Delta X = \nabla\tilde{y} \cdot (\Delta x_1; \Delta x_2; 0; 0; 0) = \\ = (-0,848; -0,036; 42,984; 42,01; 39,317) \cdot \\ \cdot (1; 0; 0; 0; 0), \quad (21)$$

$$\Delta\tilde{y} \approx (-0,848 \cdot 1) + (-0,036 \cdot 0) + (42,984 \cdot \\ \cdot 0) + (42,01 \cdot 0) + (39,317 \cdot 0) = -0,848 \approx -1$$

Such a value $\Delta\tilde{y}$, indicates a decrease in the angle of internal friction of approximately 1 degree. However, in the region of oil products concentrations from about 8 to 10%, the change in the angle of internal friction will be smaller than in the region of small concentrations from 0 to 4%. As the conditional viscosity of the NP changes, the angle of internal friction will change linearly by -0.036 for each unit change in conditional viscosity: if the viscosity increases by 10 units, the angle of internal friction will change by an insignificant -0.36 degrees.

3.6. Assumptions and scope of the adopted function

1. The equation is valid in the range of concentrations $C = x_1 \in (0;12]\%$.

2. The presence of oil products in soil pores implies a non-zero concentration.

3. The equation is valid if the dummy values fulfill the following condition: $\Delta_i = 1$, then $\forall\Delta_{j\neq i} = 0$.

4. CONCLUSIONS:

The influence of the considered factors on the intensity of the decrease of the angle of internal friction is expressed by the values of derivatives: at any point within the given interval $(0;12]$ % for concentration and constant for viscosity $\frac{\partial\tilde{y}}{\partial x_2} = \beta_2 = -0,036$. The highest value of the derivative corresponds to the concentration of the oil product, the lowest value corresponds to the viscosity, thus, the concentration of the oil product has the greatest influence on the angle of internal friction of sandy soil, and the viscosity has the least influence.

Dispersity (coarseness) had no effect on the reduction of the angle of internal friction for oil product contamination because sand coarseness was set as a fictitious parameter indicating only the initial values of the angle of internal friction, i.e. $\varphi(C = 0)$. Consequently, the granulometric composition cannot be considered as a factor influencing the change in the angle of internal friction of sandy soils contaminated with oil products.

REFERENCES

1. **Kvashuk A.V.** The effect of sandy soil contamination with petroleum products on the soil`s physical properties// Vestnik grazhdanskih inzhenerov. – 2023. – № 1(96). – p. 57-66. – DOI 10.23968/1999-5571-2023-20-1-57-66. – EDN EGNVSV.
2. **Kvashuk A.V.** The effect of sandy soil contamination with petroleum products on the soil`s physical properties// Vestnik grazhdanskih inzhenerov. – 2023. – № 1(96). – p. 57-66. – DOI 10.23968/1999-5571-2023-20-1-57-66. – EDN EGNVSV.
3. **Dashko R.E., Lange I.Yu**. Negative consequences of contamination of the underground environment with petroleum hydrocarbons: transformation of soils and structural materials // Housing construction. 2014. No. 10. P. 56-59.

4. **Korolev V.A.** Cleaning and restoration of the geological environment / Textbook for universities - M .: SamPrint, 2019 - 430 p.
5. **Rajab M. Abousnina*, Allan Manalo, Weena Lokuge, Jim Shiau** « Oil contaminated sand: An emerging and sustainable construction material» Procedia Engineering 118 (2015) 1119–1126
6. **Hamid Rajabi, Mohammad Sharifipour**, «Geotechnical properties of hydrocarbon-contaminated soils: a comprehensive review» Springer-Verlag GmbH Germany, part of Springer Nature 2018
7. **Dashko R.E., Lange I.U.** Geotechnical analysis of long-term stability of oil reservoirs on water-saturated sandy-clayey soils. Industrial and Civil Engineering.2016. No. 3. p. 48-54.
8. **Kvashuk A.V.** 2024.On the issue of changing the filtration properties of sandy soils when interacting with petroleum products//Vestnik grazhdanskih inzhenerov. – 2024. - № 2(103). – С. 62-73. – DOI 10.23968/1999-5571-2024-21-2-62-73.
9. **E.C. SHIN, J.B. LEE, B.M. DAS.** Bearing capacity of a model scale footing on crude oil-contaminated sand. Geotechnical and Geological Engineering 17: 123–132, 1999
10. **Al-Sanad H.A., Eid W.K, Ismael N.F.** Geotechnical properties of oil contaminated Kuwaiti sand. J Geotech Eng. ASCE №121 (5),1995: p. 407–412.
11. **Amirhossein Mohammadi, Taghi Ebadi, Mehrdad Ahmadi.** Effect of Bentonite Addition on Geotechnical Properties of Oil-Contaminated Sandy Soil. Journal of Civil Engineering and Construction 2018;7(4):153-162
12. **Dashko R.E., Lange I.U.,** 2017. Engineering-geological aspects of the negative consequences of contamination of dispersive soils with petroleum products. Zapiski Gornogo instituta. 2017. T. 228. p. 624-630, DOI/10.25515/PMI.2017
13. **Al-Adili Aqil, Yali Kawtar, Shakir Ali**. Study of the influence of oil contamination of sandy and gypsum-containing soils on strength // OFMG, No. 4-217.- p.30-35.
14. **Z. N. Rasheed, F. R. Ahmed, H. M. Jassim**. Effect of crude oil products on the geotechnical properties of soil. WIT Transactions on Ecology and The Environment, Vol 186, © 2014 WIT Press www.witpress.com, ISSN 1743-3541 (online) doi:10.2495/ESUS140301
15. **Osovetsky B.M., Kachenov V.I., Rastegaev A.V., Afanasyev R.A., Pikulev D.A.** Patterns of changes in the strength properties of sands contaminated with diesel fuel // Geological and Mineralogical Sciences. 2014, No. 9, pp. 1769-1774.

СПИСОК ЛИТЕРАТУРЫ

1. **Квашук, А.В.** Влияние загрязнения песчаного грунта нефтепродуктами на его физические свойства / А.В. Квашук // Вестник гражданских инженеров. – 2023. – № 1(96). – С. 57-66. – DOI 10.23968/1999-5571-2023-20-1-57-66. – EDN EGNVSV.
2. **Квашук, А.В.** Изменение механических свойств песчаных грунтов при их загрязнении нефтепродуктами. Вестник гражданских инженеров, № 3(98), с. 33-43, DOI:10.23968/1999-5571-2023-20-3-33-43.
3. **Дашко Р. Э., Ланге И. Ю.** Негативные последствия контаминации подземной среды нефтяными углеводородами: преобразование грунтов и конструкционных материалов // Жилищное строительство. 2014. № 10. С. 56-59.
4. **Королев В.А.** Очистка и восстановление геологической среды / Учебное пособие для вузов - М.: СамПринт, 2019 – 430 с
5. **Rajab M. Abousnina*, Allan Manalo, Weena Lokuge, Jim Shiau** « Oil contaminated sand: An emerging and sustainable construction material» Procedia Engineering 118 (2015) 1119 – 1126
6. **Hamid Rajabi, Mohammad Sharifipour**, «Geotechnical properties of hydrocarbon-contaminated soils: a comprehensive review» Springer-Verlag GmbH Germany, part of Springer Nature 2018

7. **Дашко, Р.Э.** Прогнозирование изменения несущей способности песчано-глинистых грунтов в процессе их контаминации нефтепродуктами / Р.Э. Дашко, И.Ю. Ланге // Записки Горного института. – 2015. – Т. 211. – С. 16-21. – EDN TQMGNX.
8. **Квашук, А.В.** К вопросу изменения фильтрационных свойств песчаных грунтов при взаимодействии с нефтепродуктами / А.В. Квашук // Вестник гражданских инженеров. – 2024. - № 2(103). – С. 62-73. – DOI 10.23968/1999-5571-2024-21-2-62-73.
9. **E.C. SHIN, J.B. LEE, B.M. DAS**. Bearing capacity of a model scale footing on crude oil-contaminated sand. Geotechnical and Geological Engineering 17: 123–132, 1999
10. **Al-Sanad H.A., Eid W.K, Ismael N.F.** Geotechnical properties of oil contaminated Kuwaiti sand. J Geotech Eng. ASCE №121 (5),1995: p. 407–412.
11. **Amirhossein Mohammadi, Taghi Ebadi, Mehrdad Ahmadi.** Effect of Bentonite Addition on Geotechnical Properties of Oil-Contaminated Sandy Soil. Journal of Civil Engineering and Construction 2018;7(4):153-162
12. **Дашко Р.Э.** Инженерно-геологические аспекты негативных последствий контаминации дисперсных грунтов нефтепродуктами / Р.Э.Дашко, И.Ю.Ланге // Записки Горного института. 2017. Т. 228. С. 624-630. DOI: 10.25515/PMI.2017
13. **Аль-Адили Акиль, Йали Кавтар, Шакир Али.** Исследование влияния загрязнения нефтью песчаного и гипсосодержащего грунтов на прочность// ОФМГ, №4-217.- С.30-35.
14. **Z. N. Rasheed, F. R. Ahmed, H. M. Jassim.** Effect of crude oil products on the geotechnical properties of soil. WIT Transactions on Ecology and The Environment, Vol 186, © 2014 WIT Press www.witpress.com, ISSN 1743-3541 (on-line) doi:10.2495/ESUS140301
15. **Осовецкий Б. М., Каченов В.И., Растегаев А.В., Афанасьев Р. А., Пикулев Д.А.** Закономерности изменения прочностных свойств песков, загрязненных дизельным топливом // Геолого-минералогические науки. 2014, №9, С.1769-1774.

Rashid Abdullovich Mangushev – Corresponding Member of the Russian Academy of Architecture and Civil Engineering, Doc-tor of Engineering Sciences, Professor of the Department of Geotechnics at the Saint Petersburg State University of Architecture and Civil Engineering. 4. 2-ya Krasnoarmeyskaya Street, Saint Petersburg, 190005, Russia. e-mail: ramangushev@yandex.ru

Alina Vitalievna Kvashuk – postgraduate student, research fellow of the Department of Geotechnics at the Saint Petersburg State University of Architecture and Civil Engineering. 4. 2-ya Krasnoarmeyskaya Street, Saint Petersburg, 190005, Russia. e-mail: alina_kvashuk@mail.ru

Alexandra Viktorovna Vagurina – Senior Laboratory Assistant of the Department of Geotechnics of the Saint Petersburg State University of Architecture and Civil Engineering. 4. 2-ya Krasnoarmeyskaya Street, Saint Petersburg, 190005, Russia. e-mail: alexandra.vagurina@yandex.ru

Ilya Dmitrievich Kulyashov – Student of the Saint Petersburg State University of Architecture and Civil Engineering. 4. 2-ya Krasnoarmeyskaya Street, Saint Petersburg, 190005, Russia. e-mail: teleshpak@mail.ru

Рашид Абдуллович Мангушев – чл.-корр. РААСН, д.т.н., профессор кафедры геотехники Санкт-Петербургского госу-дарственного архитектурно-строительного университета. д.4. 2-я Красноармейская улица, г. Санкт-Петербург, 190005, Россия. e-mail: ramangushev@yandex.ru

Алина Витальевна Квашук – аспирант, научный сотрудник кафедры геотехники Санкт-Петербургского государственного архитектурно-строительного университета. д.4. 2-я Красноармейская улица, г. Санкт-Петербург, 190005, Россия. e-mail: alina_kvashuk@mail.ru

Александра Викторовна Вагурина – старший лаборант кафедры геотехники Санкт-Петербургского государственного архитектурно-строительного университета. д.4. 2-я Красноармейская улица, г. Санкт-Петербург, 190005, Россия. e-mail: alexandra.vagurina@yandex.ru

Илья Дмитриевич Куляшов – студент Санкт-Петербургского государственного архитектурно-строительного универси-тета. д.4. 2-я Красноармейская улица, г. Санкт-Петербург, 190005, Россия. e-mail: teleshpak@mail.ru

TO THE MATHEMATICAL ESTIMATION OF THE STRAIN SENSORS ERROR

Nelly N. Rogacheva, Vladimir N. Sidorov, Yulia G. Zheglova
National Research Moscow State University of Civil Engineering, Moscow, RUSSIA

Abstract: The work is devoted to the mathematical analysis of the error of the theory of strain sensors. In the theory of deformation sensors, it is assumed that the sensor, due to its geometric and mechanical characteristics, does not make changes (or makes minor changes) to the stress-strain state (SSS) of the tested structure. To numerically estimate the sensor error, an exact solution of the dynamic contact problem of the sensor and the elastic half-space is obtained. For the analytical solution of the problem, the method used by Lamb to determine the dynamic stress-strain state of an elastic half-space under the action of concentrated forces applied to its surface is generalized. A numerical solution of this problem has been performed for sensors and elastic half-space made of various materials. Practical recommendations are formulated. A numerical solution of this problem has been performed

Keywords: stress-strain state, strain sensor, contact problem, Lamb problem, error estimation

К МАТЕМАТИЧЕСКОЙ ОЦЕНКЕ ПОГРЕШНОСТИ ДАТЧИКОВ ДЕФОРМАЦИЙ

Н.Н. Рогачева, В.Н. Сидоров, Ю.Г. Жеглова
Национальный исследовательский Московский государственный строительный университет, г. Москва, РОССИЯ

Аннотация: Работа посвящена математическому анализу погрешности теории датчиков деформаций. В теории датчиков деформаций предполагается, что датчик в силу своих геометрических и механических характеристик не вносит изменений (или вносит незначительные изменения) в напряженно-деформированное состояние (НДС) испытуемой конструкции. Для численной оценки погрешности датчика получено точное решение динамической контактной задачи датчика и упругого полупространства. Для аналитического решения этой задачи обобщен метод, который использовал Лэмб для определения динамического напряженно-деформированного состояния упругого полупространства под действием сосредоточенных сил, приложенных к его поверхности. Выполнено численное решение этой задачи для датчиков и упругого полупространства из различных материалов. Сформулированы практические рекомендации.

Ключевые слова: напряженно-деформированное состояние, датчик деформации, контактная задача, задача Лэмба, оценка погрешности

INTRODUCTION

The history of the emergence and use of strain sensors begins in the middle of the 19th century with the invention by Professor Thomson (known as Lord Kelvin) of the first sensor for measuring elongation (compression) strains [1] on the surface of the structure under study. To ensure reliable operation of the structure, as a rule, the analytical or numerical calculation of the structure should be supplemented and verified with experimental studies of its stress-strain state (SSS). If the results of the calculation and experiments differ slightly, then the calculation is correct. In particularly difficult cases, when it is impossible to obtain a sufficiently accurate solution to the problem, the role of the experiment is irreplaceable. The main role in BIM technology in construction, as well as in monitoring the responsible for unique buildings and structures, is played by long-term experimental observation of the state of the structure. This is why it is very important to estimate the error of experiments.

The measurement error of strain sensors analysis is a complex problem, since it is necessary to estimate both the error of the theory of sensors and the error of experimental measurements.

We will consider the error of the theory of strain sensors using the example of the most common sensor of Lord Kelvin. The obtained conclusions are also suitable for new types of piezoelectric sensors [2-3].

Lord Kelvin was the first to notice that the deformation of a conductor is accompanied by a change in its electrical resistance. By measuring the change in resistance, its deformation can be detected. The first strain sensor, Lord Kelvin's strain sensor, is based on this fact. The change in resistance is extremely small, but it can be amplified and measured using additional equipment.

The theory of the piezoelectric sensor was constructed and confirmed by experiments in [2]. Thin-walled elements made of pre-polarized ceramics with a strong piezoelectric effect were used as the sensor. The front surfaces of the piezoelectric element were covered with electrodes. The piezoelectric sensor was glued to the surface of the deformed body and deformed together with it. The operation of the sensor is based on the use of the direct piezoelectric effect. The direct piezoelectric effect is as follows: when the piezoelectric element is mechanically loaded, an electric charge appears on its electrodes. For a material with a strong piezoelectric effect, a significant part of the mechanical energy of the deformed piezoelectric element is converted into electrical energy. Tangential deformations were calculated based on the measured difference in electrical potentials on the electrodes.

The error of the sensor theory is the error of the contact problem of the sensor and the structure under study. It should be noted that insufficient attention is paid to the estimation of the error of the main hypotheses of the theory of deformation sensors in research. As a rule, research is devoted to sensor calibration, experimental measurement errors, errors in the description of material properties, etc. [4-11]. In the paper, we will evaluate the validity of the sensor theory.

Each sensor measures one integral characteristic. For example, the integral characteristic of the Kelvin sensor is the change in resistance. The change in the cross-sectional area of the conductor is used to calculate the change in the resistance of the conductor and its deformation.

For a piezoelectric sensor, the integral characteristic is the difference in electric potential on its electrodes. Based on this measured value of the difference in electric potential, the corresponding component of the strain tensor at the point of the test object is calculated.

APPROXIMATE DETERMINATION OF THE SSS OF A STRAIN SENSOR

The contact problem of a sensor and a body under study is a complex mathematical problem. For simplicity of research, we will assume that we measure the elongation or compression strain at a point on the surface of an elastic half-space using a sensor. Figure 1 shows the sensor and the elastic half-space related to the Cartesian coordinate system. It is assumed that the sensor has a length $2l$, a thickness τ and is infinite in the direction x_2. We will investigate the deformation of e_1 in the direction x_1. To simplify the problem, we will assume that our solution does not depend on x_2.

We will assume that the elastic half-space performs harmonic oscillations under the action of a load changing according to the law $e^{-i\omega t}$, where i is an imaginary unit, t is time, ω is the circular frequency of oscillations. Since the oscillations are harmonic, all equations can be written relative to the amplitude values of the sought quantities. Note that the solution to the contact problem does not depend on the coordinate x_2.

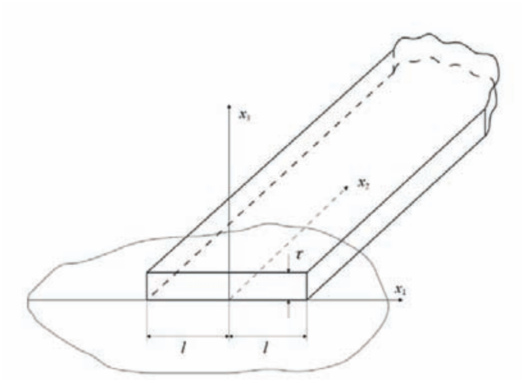

Figure 1. Schematic representation of the sensor on the surface of the elastic half-space

To solve our problem, we will use the iteration method. Describing the zero approximation of the solution to the problem, we assume that the sensor satisfies all the conditions of its applicability for measuring deformations:
-in the contact area of the sensor and the structure under study, the conditions of ideal contact are met;
-on the part of the body surface where the sensor is located, there is no surface load;
-the sensor is made of a material that slightly changes the stress-strain state of the body being studied in the area of its contact with the sensor;
-the characteristic length of the deformation pattern in the elastic half-space is greater than the width of the active element (this means that the variability of the sensor's SSS along the coordinate x_1 is small), which allows us to assume that the elongation (compression) deformation along the coordinate x_1 does not change.
In all sensor theories, it is assumed that the sensor does not introduce disturbance into the SSS of the test object, therefore, as a zero approximation of the iterative process, it is natural to assume that within the sensor, the elongation (compression) deformation in the direction of the axis does not depend on the variable x_1.

As a zero approximation of the contact problem, we assume that the longitudinal deformation of the half-space and the sensor are equal and are constant in the contact region. In this case, the contact condition for stresses is not satisfied. Then, at the next step of the iteration process, we will fulfill the contact condition for stress - we will remove the discrepancy that appeared at the previous step.
The equations describing the zero approximation of the sensor's SSS relative to the amplitude values have the following form (below are written only those equations that will be used for the zero approximation of solving the formulated contact problem):
Equation of motion

$$\frac{\partial \sigma_{11}}{\partial x_1} + \frac{\partial \sigma_{13}}{\partial x_3} + \rho\omega^2 u_1 = 0 \qquad (1)$$

Hooke's Law

$$\sigma_{11} = Ee_1 \qquad (2)$$

Geometric equation relating deformation to displacement

$$e_1 = \frac{\partial u_1}{\partial x_1} \qquad (3)$$

In equations (1)-(3) σ_{11}, σ_{13} are stresses, e_1 are the component of the strain tensor in the direction x_1, and u_1 is the component of the displacement vector in the direction x_1.
Let us transform these equations.
Since, according to the assumptions made, the strain component e_1 does not depend on the variable x_1, then

$$e_1 = const \qquad (4)$$

By virtue of relation (2) the stress component also does not depend on the variable x_1.

$$\sigma_{11} = const \tag{5}$$

Taking into account (5), the equation of motion (1) becomes simpler and can be written as

$$\frac{d\sigma_{13}}{dx_3} + \rho\omega^2 x_1 e_1 = 0 \tag{6}$$

We integrate equation (4) and find that the displacement is an odd function x_1 and changes along the coordinate x_1 according to a linear law

$$u_1 = x_1 e_1 \tag{7}$$

From the accepted assumption of the absence of surface load on the outer surface of the sensor it follows

$$\sigma_{13}\big|_{x_3=\tau} = 0 \tag{8}$$

Integrating the equation of motion (6) with respect to the variable x_3 and satisfying condition (8), we obtain

$$\sigma_{13}\big|_{x_3=0} = x_1 \tau\rho\omega^2 e_1 \tag{9}$$

For further use, the stress σ_{13} should be continued as a periodic function of x_1 over the interval $[-L,+L]$, $L \geq 2l$ as follows:

$$\sigma_{13}(x_1) = \tau\rho\omega^2 e_1 \begin{cases} 2l - x_1 & l \leq x_1 \leq 2l \\ x_1 & -l \leq x_1 \leq l \\ -(2l + x_1) & -2l \leq x_1 \leq -l \end{cases}$$

$$\sigma_{13}(x_1) = \frac{4l\tau\rho\omega^2 e_1}{\pi^2} \sum_{n=0}^{N} (-1)^n \frac{1}{(2n+1)^2} \sin\frac{(2n+1)}{2l} x_1 \tag{10}$$

The function $\sigma_{13}(x_1)$ is chosen so that the function $F(x_1)$ is continuous in the interval $[-L,+L]$. In addition, the integral $\int_{-L}^{+L} F(x_1)dx$ must be equal to zero. Note that the function can be continued $[-L,+L]$ in any way that ensures rapid convergence of the solution.

The conditions of ideal contact of two deformable bodies are that at all points of the contact area of the bodies the displacements and stresses of both bodies are equal. In this particular case, instead of equality of displacements, equality of deformations can be used.

In the zero approximation of the iteration method, it was assumed that the deformations of the sensor and the half-space are equal. At the same time, on the contact surface, as shown by formula (9), the condition of ideal contact for stress σ_{13} is not satisfied. We will remove this discrepancy under contact conditions at the first step of the iteration process. To do this, we will calculate the elastic half-space loaded with surface load (9) in the region $-l \leq x_1 \leq l$. After performing the first step of the iteration process, a discrepancy in the equality of deformations in the contact region will appear. It is this value - the value of the maximum deformation of the half-space surface that serves in the contact region, serves as an estimate of the sensor error.

PROBLEM FOR AN ELASTIC HALF-SPACE

The complete system of equations describing an elastic half-space SSS $(x_3 \leq 0)$ includes equilibrium equations, geometric ratios relating deformations to displacements, and equations of state (Hooke's law).

Since analogous to the Lamb problem is considered, the equations are taken in the traditional form in terms of displacements. To solve the problem, the Lamb method is used, described in papers [12, 13] for the case of concentrated forces applied at a point on the surface of an elastic body. In this paper, the Lamb method is generalized to the case of a distributed surface load. This generalized Lamb method was previously used in [14] to solve the dynamic contact problem of an actuator and an elastic half-space.

Following Lamb, the equilibrium equations are written as

$$\begin{aligned}(\lambda+\mu)\frac{\partial\theta}{\partial x_1}+\mu\nabla^2 u_1+\rho\omega^2 u_1=0\\(\lambda+\mu)\frac{\partial\theta}{\partial x_3}+\mu\nabla^2 u_3+\rho\omega^2 u_3=0\end{aligned}\tag{11}$$

where ∇^2 is the Laplace operator, θ is the volumetric deformation, λ and μ are the Lame coefficients:

$$\nabla^2=\frac{\partial^2}{\partial x_1^2}+\frac{\partial^2}{\partial x_3^2},\quad \theta=\frac{\partial u_1}{\partial x_1}+\frac{\partial u_3}{\partial x_3}\tag{12}$$

$$\lambda=\frac{\nu E}{(1+\nu)(1-2\nu)},\quad \mu=\frac{E}{2(1+\nu)}\tag{13}$$

Stress-strain formulas with Lame coefficients are written as

$$\begin{aligned}\sigma_1&=\lambda(e_1+e_3)+2\mu e_1\\\sigma_3&=\lambda(e_1+e_3)+2\mu e_3\\\sigma_{13}&=\mu e_{13}\end{aligned}\tag{14}$$

Here e_1, e_3, e_{13} the components of the deformation

$$e_1=\frac{\partial u_1}{\partial x_1},\ e_3=\frac{\partial u_3}{\partial x_3},\ e_{13}=\frac{\partial u_1}{\partial x_3}+\frac{\partial u_3}{\partial x_1}\tag{15}$$

The functions φ and ψ associated with movements are introduced in the usual way:

$$u_1=\frac{\partial\varphi}{\partial x_1}+\frac{\partial\psi}{\partial x_3},\quad u_1=\frac{\partial\varphi}{\partial x_3}-\frac{\partial\psi}{\partial x_1}\tag{16}$$

The equilibrium equations and formulas for stresses through functions φ and ψ can be written as follows:

$$\left(\nabla^2+h^2\right)\varphi=0\ ,\ \left(\nabla^2+k^2\right)\psi=0\tag{17}$$

$$\begin{aligned}\sigma_1&=\mu\left(-k^2\varphi-2\frac{\partial^2\varphi}{\partial x_3^2}+2\frac{\partial^2\psi}{\partial x_1\partial x_3}\right)\\\sigma_3&=\mu\left(-k^2\varphi-2\frac{\partial^2\varphi}{\partial x_1^2}+2\frac{\partial^2\psi}{\partial x_1\partial x_3}\right)\\\sigma_{13}&=\mu\left(-k^2\psi-2\frac{\partial^2\psi}{\partial x_1^2}+2\frac{\partial^2\psi}{\partial x_1\partial x_3}\right)\end{aligned}\tag{18}$$

$$\begin{aligned}h^2=\frac{\omega^2}{c_L^2},\quad k^2=\frac{\omega^2}{c_T^2},\\c_L=\sqrt{\frac{\lambda+2\mu}{\rho}},\quad c_T=\sqrt{\frac{\mu}{\rho}}\end{aligned}\tag{19}$$

Here, c_L and c_T are the phase velocities of longitudinal and transverse waves, h and k are the wave numbers of longitudinal and transverse waves, respectively.

To solve the problem, the integral Fourier transform of a variable x_1 is used

$$\begin{aligned}\varphi^*&=\frac{1}{2\pi}\int_{-\infty}^{+\infty}\varphi e^{-i\xi x_1}dx_1\\\psi^*&=\frac{1}{2\pi}\int_{-\infty}^{+\infty}\psi e^{-i\xi x_1}dx_1\end{aligned}\tag{20}$$

Since the axis x_3 is directed from the elastic half-space surface (Figure 1), the solution in the elastic half-space should decrease with x_3 decreasing, so the solution is taken as

$$\varphi^*=Ae^{\alpha x_3},\quad \psi^*=Be^{\beta x_3}\tag{21}$$

where α, β are positive real values, which ensures the attenuation of the stress-strain state of an elastic body when moving away from the source of vibrations deep into the body. The values α, β can be found as a result of substituting (21) into equations (7), transformed taking into account the formulas (20)

$$\alpha = \sqrt{\xi^2 - h^2}\,, \qquad \beta = \sqrt{\xi^2 - k^2} \qquad (22)$$

Equations (16), (19) as a result of applying the Fourier transform will take the form

$$\begin{aligned} u_1^* &= i\xi A e^{\alpha x_3} + \beta B e^{\beta x_3} \\ u_3^* &= \alpha A e^{\alpha x_3} - i\xi\beta e^{\beta x_3} \end{aligned} \qquad (23)$$

$$\begin{aligned} \sigma_3^* &= \mu\left(\left(2\xi^2 - k^2\right)Ae^{\alpha x_3} - 2i\xi\beta Be^{\beta x_3}\right) \\ \sigma_{13}^* &= \mu\left(\left(2\xi^2 - k^2\right)e^{\beta x_3}B - 2i\xi\alpha Ae^{\alpha x_3}\right) \end{aligned} \qquad (24)$$

Arbitrary integration constants A and B are found from the contact conditions of the sensor and the elastic half - space on the plane $x_3 = 0$.

The problem for an elastic half-space is solved using the integral Fourier transform. The integral stress σ_{31} conversion takes into account the equality of these stresses to the corresponding sensor stresses in the contact area and their equality to zero on the rest of the elastic body surface. A similar method is used in hydroacoustics to solve the problem of vibrations of a pivotally supported cylindrical shell immersed in an infinite liquid.

The first step of the iterative process is to solve the problem for a half-space when only a tangential load $\sigma_{31} = \sin px_1$ acts in the contact area on the surface of the half-space.

AUXILIARY PROBLEM FOR AN ELASTIC HALF-SPACE

The following stresses are set on the surface $x_3 = 0$ of an elastic body

$$\begin{gathered} \sigma_{33}\Big|_{x_3=0} = 0\,,\ \sigma_{13}\Big|_{x_3=0} = X_{13}\,, \\ X_{13} = \sin px_1\,,\ (\left|x_1\right| \le l)\,, \qquad (25) \\ \sigma_{33}\Big|_{x_3=0} = 0\,,\ \sigma_{13}\Big|_{x_3=0} = 0\,,\ (\left|x_1\right| > l)\,, \end{gathered}$$

With boundary conditions (25), N+1 auxiliary problems should be solved, in which $p=p_n=(2n+1)/2l$, $n=0,1,2,...N$. Then we write σ_{13} as a sum

$$\sigma_{13} = \sum_{n=0}^{N} C_n \sigma_{13} p_n x_1$$

with unknown constants c_n. The unknown constants c_n are determined by equating the sensor stress σ_{13} to the half-space stress σ_{13} in the contact area.

Using the Fourier transform (10), (11), (6), (9) reduces the conditions (25) to formulas

$$\sigma_3^*\Big|_{x_3=0} = 0\,, \qquad \sigma_{13}^*\Big|_{x_3=0} = X_{13}^*\,, \qquad (26)$$

$$X_{13}^* = \frac{1}{4\pi}\left(\frac{e^{i(p+\xi)l} - e^{-i(p+\xi)l}}{p+\xi} - \frac{e^{i(p-\xi)l} - e^{-i(p-\xi)l}}{p-\xi}\right)$$

As a result of the Fourier transform, the conditions on the surface of the half- space $x_3 = 0$ will be written as

$$\begin{aligned} &(2\xi^2 - k^2)A - 2i\xi\beta B = 0, \\ &2i\xi\alpha A + (2\xi^2 - k^2)B = \frac{X_{13}^*}{\mu} \end{aligned} \qquad (27)$$

where

$$A = \frac{2i\xi\beta}{F(\xi)}\frac{X_{13}^*}{\mu}\,, \quad B = \frac{2\xi^2 - k^2}{F(\xi)}\frac{X_{13}^*}{\mu} \qquad (28)$$

To estimate the error of the sensor, the main interest is the displacement u_1 and the deformation e_1 on the surface of the half-space $x_3 = 0$, so we will write only the formula for u_1^*

$$u_1^* = \frac{\beta X_{13}^*}{\mu F(\xi)}(-2\xi^2 e^{\alpha x_3} + (2\xi^2 - k^2)e^{\beta x_3}) \qquad (29)$$

$$u_1 = \frac{1}{\mu}\int_{-\infty}^{+\infty}(-2\xi^2 e^{\alpha x_3} + (2\xi^2 - k^2)e^{\beta x_3})\frac{\beta X_{13}^*}{F(\xi)}e^{i\xi x_1}d\xi \qquad (30)$$

Integrals (29) in the contact area $|x_1| \le l$ can be transformed to a form convenient for calculations

$$u_1^{(n)} = -\frac{i}{2\mu} H_2^{(n)} e^{-i\kappa x_1} - \frac{i}{2\mu} P_2^{(n)} e^{-ipx_1} - \\ -\frac{i}{2\pi\mu} e^{-ikx_1} \int_0^\infty S_1 e^{-\eta x_1} d\eta - \frac{2i}{\pi\mu} e^{-ihx_1} \int_0^\infty S_2 e^{-\eta x_1} d\eta \quad (31)$$

here

$$H_2^{(n)} = -k^2 \beta_\kappa \frac{Z_1(-\kappa)}{F^{'}(\kappa)}, \quad P_2^{(n)} = \frac{-k^2 \beta_P}{F(p)} \quad (32)$$

$$S_1^{(n)} = [4\varsigma^2 \Phi(\varsigma) - F(\varsigma) - F_1(\varsigma)] \frac{\beta\Phi(\varsigma)}{2F_2(\varsigma)} Z_1(\varsigma)\Big|_{\varsigma=-k+i\eta}$$

$$S_2^{(n)} = [F_1(\varsigma) - F(\varsigma) - 4\Phi(\varsigma)\alpha\beta] \frac{\varsigma^2\beta}{4F_2(\varsigma)} Z_1(\varsigma)\Big|_{\varsigma=-h+i\eta}$$

$$Z_1(\varsigma) = \frac{e^{i(p+\varsigma)l}}{p+\varsigma} + \frac{e^{i(p-\varsigma)l}}{p-\varsigma}$$

NUMERICAL EXAMPLES OF CALCULATIONS FOR ESTIMATING THE ERROR OF THE STRAIN SENSOR

According to the general theory of deformation sensors, the elongation along the axis of the sensor is a constant value and is equal to the elongation on the surface of the half-space in the area of contact with the sensor. Then the movement of u_1 along the sensor changes linearly. The error of these assumptions is determined by calculating the displacement corrections u_1 found at the first step of the iterative process.

The sequence of calculations is as follows:

- calculate by formulas (31), (32) the displacement corrections u_1 as a function of the variable x_1 for problems with boundary conditions (25), where $p=p_n=(2n+1)/2l$, $n=0,1,2,...N$, - summarize the found corrections for n.

The results of the calculation are summarized in tables.

In all tables, the first column shows the values of the longitudinal displacements u_1 as a linear function of the variable x_1 obtained by the sensor as a result of the widely used assumption that the sensor does not change the SSS of the studied design. Columns 2-4 show the corrections for displacements obtained as a result of solving the contact problem. The sensor readings are correct if the corrections are significantly less than the displacement values in the first column. If the corrections are larger or of the same order as the movements written out in the first column, then this means that the sensor gives completely incorrect results.

Let us denote by $u_1^{(b)}$ the longitudinal displacement determined according to the accepted hypothesis that the sensor does not introduce disturbance into the stress-strain state of the structure under study. Let us denote by $u_1^{(c)}$ the corrections to $u_1^{(b)}$, obtained as a result of solving the contact problem.

<u>Table 1.</u> Values of displacements u_1 (first column) and corrections to them (columns 2-4) as functions of the variable x_1 and the circular frequency ω for a half-space made of steel and a sensor made of copper (sensor τ =0.002 m, l=0.02 m)

$u_1^{(b)}$	ω=1000	ω=10000	ω=100000
	$u_1^{(c)}$		
0.002	$5.5\cdot10^{-7}$	$6.2\cdot10^{-8}$	$10\cdot10^{-7}$
0.004	$1.3\cdot10^{-6}$	$3.3\cdot10^{-7}$	$1.6\cdot10^{-7}$
0.006	$2.2\cdot10^{-6}$	$1.1\cdot10^{-6}$	$2.9\cdot10^{-6}$
0.008	$3.1\cdot10^{-6}$	$2.0\cdot10^{-6}$	$6.6\cdot10^{-6}$
0.01	$4.1\cdot10^{-6}$	$3.0\cdot10^{-6}$	$1.1\cdot10^{-5}$
0.012	$5.0\cdot10^{-6}$	$4.1\cdot10^{-6}$	$1.6\cdot10^{-5}$
0.014	$5.8\cdot10^{-6}$	$5.1\cdot10^{-6}$	$2.0\cdot10^{-5}$
0.016	$6.5\cdot10^{-6}$	$6.1\cdot10^{-6}$	$2.5\cdot10^{-5}$
0.018	$7.2\cdot10^{-6}$	$7.0\cdot10^{-6}$	$2.9\cdot10^{-5}$
0.02	$7.7\cdot10^{-6}$	$7.8\cdot10^{-6}$	$3.4\cdot10^{-5}$

It can be seen from the table that the corrections are small, the error in the theory of strain sensors is less than 0.001%. It means that the main hypothesis according to which the sensor introduces a small disturbance in the SSS of the studied structure is correct.

Table 2. Values of displacements u_1 (first column) and corrections to them (columns 2-4) as functions of the variable x_1 and the circular frequency ω for a half-space made of reinforced concrete and a sensor made of copper (sensor τ =0.002 m, l=0.02 m)

$u_1^{(b)}$	ω=50	ω=100	ω=500
	$u_1^{(c)}$		
0.002	0.0128	0.0075	-0.0253
0.004	0.0325	0.0240	-0.0244
0.006	0.0572	0.0470	-0.0041
0.008	0.0847	0.0740	0.0296
0.01	0.1129	0.1025	0.0715
0.012	0.1399	0.1304	0.1176
0.014	0.1646	0.1563	0.1653
0.016	0.1865	0.1797	0.2128
0.018	0.2058	0.2004	0.2593
0.02	0.2227	0.2190	0.3047

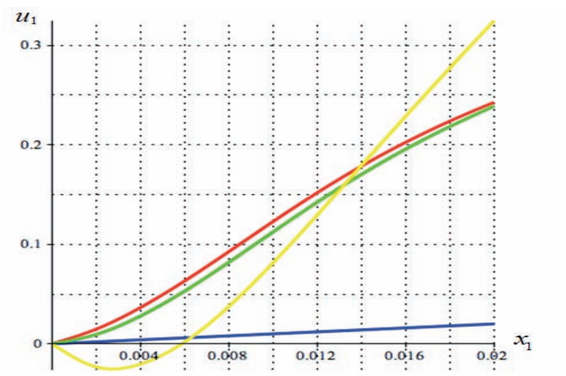

Figure 2. Displacement u_1 as a function of the variable x_1 in accordance with Table 2

The blue line on the Figure 2 corresponds to the displacement $u_1^{(b)}$ of Table 2 (column 1), the green line corresponds to the displacement $u_1^{(b)}$ taking into account the correction $u_1^{(c)}$ at ω=50 (Table 2, column 2), the red line - taking $u_1^{(b)}$ into account the correction $u_1^{(c)}$ at ω=100 (Table 2, column 3), the yellow line - $u_1^{(b)}$ taking into account the correction $u_1^{(c)}$ at ω=500 (Table 2, column 4).

The Figure 2 shows that in this case the sensor measurements are incorrect. The corrections $u_1^{(c)}$ are significantly greater than $u_1^{(b)}$.

Table 3. Values of displacements u_1 (first column) and corrections to them (columns 2-4) as functions of the variable x_1 and the circular frequency ω for a half-space made of reinforced concrete and a sensor made of constantan (sensor τ =0.0001 m, l=0.02 m)

$u_1^{(b)}$	ω=50	ω=100	ω=500
	$u_1^{(c)}$		
0.002	0.0010	0.0006	0.0019
0.004	0.0024	0.0018	0.0018
0.006	0.0043	0.0035	0.0003
0.008	0.0063	0.0055	0.0022
0.01	0.0084	0.0076	0.0053
0.012	0.0104	0.0097	0.0088
0.014	0.0123	0.0117	0.0123
0.016	0.0139	0.0134	0.0159
0.018	0.0154	0.0150	0.0194
0.02	0.0166	0.0163	0.0227

Tables 2, 3 show that the strain sensor introduces a large disturbance in the SSS of the studied structure, and gives incorrect values of deformations.

Table 4. Values of displacements u_1 (first column) and corrections to them (columns 2-4) as functions of the variable x_1 and the circular frequency ω for a half-space made of reinforced concrete and a sensor made of piezo film (sensor τ =0.0001 m, l=0.02 m)

$u_1^{(b)}$	ω=50	ω=100	ω=500
	$u_1^{(c)}$		
0.002	$2.9 \cdot 10^{-6}$	$1.7 \cdot 10^{-6}$	$-5.7 \cdot 10^{-6}$
0.004	$7.3 \cdot 10^{-6}$	$5.4 \cdot 10^{-6}$	$-5.5 \cdot 10^{-6}$
0.006	$1.3 \cdot 10^{-5}$	$1.1 \cdot 10^{-5}$	$9.2 \cdot 10^{-7}$
0.008	$1.9 \cdot 10^{-5}$	$1.7 \cdot 10^{-5}$	$6.6 \cdot 10^{-6}$
0.01	$2.5 \cdot 10^{-5}$	$2.3 \cdot 10^{-5}$	$1.6 \cdot 10^{-5}$

0.012	$3.1 \cdot 10^{-5}$	$2.9 \cdot 10^{-5}$	$2.6 \cdot 10^{-5}$
0.014	$3.7 \cdot 10^{-5}$	$3.5 \cdot 10^{-5}$	$3.7 \cdot 10^{-5}$
0.016	$4.2 \cdot 10^{-5}$	$4.0 \cdot 10^{-5}$	$4.8 \cdot 10^{-5}$
0.018	$4.6 \cdot 10^{-5}$	$4.5 \cdot 10^{-5}$	$5.8 \cdot 10^{-5}$
0.02	$5.0 \cdot 10^{-5}$	$4.9 \cdot 10^{-5}$	$6.8 \cdot 10^{-5}$

The results of the calculation in Table 4 show that the piezoelectric film deformation sensor causes a small disturbance in the SSS of the structure under study, and can be used to measure deformations in reinforced concrete structures.

CONCLUSION

The paper presents a relatively simple method for estimating the error of the theory of strain sensors.

It is shown by numerical examples that sensors made of materials with large elastic modules, used for structures made of materials with significantly smaller elastic modules, give incorrect measurements of deformations. This is confirmed by calculations performed for reinforced concrete structures. The calculation results allow us to recommend piezoelectric film sensors. Even more accurate measurements of deformations in reinforced concrete structures can be obtained using layered piezo film sensors [15]. Effective coefficients of this sensor must be obtained using the homogenization method [16]. Such a sensor has a smaller modulus of elasticity and a higher efficiency than a single-layer sensor.

Using the proposed method, it is possible to develop recomendations, which will specify the types of sensors for structures made of different materials that guarantee sufficiently correct measurements of deformations.

ACKNOWLEDGEMENTS

The research was funded by the National Research Moscow State University of Civil Engineering (grant for fundamental and applied scientific research, project No. 23-392/130).

REFERENCES

1. **Tomson W. (Lord Kelvin).** On the electrodynamic qualities of metals. Proc. R. Soc. London, 1856, no. 146, pp. 649–751.
2. **Infimovskaya A.A., Rogacheva N.N., Chernyshev G.N.** Use of thin piezoceramic gauges to measure dynamic deformations. Izv. Academy of Sciences of the USSR. MTT, 1989, Vol, 24, no. 2, pp.157-162.
3. **Rogacheva N., Sidorov V., Zheglova Yu.** Piezoelectric Sensor of Small Dynamic Bending Strains, Buildings 2024, Issue 14, Vol. 2447, doi:10.3390/buildings14082447.
4. **Li Y. Sharif-Khodaei Z.** Accuracy of Distributed Strain Sensing with Single-Mode Fibre in Composite Laminates under Thermal and Vibration Loads. Structural Control and Health Monitoring, 2023, no. 2, pp. 1-13, doi: 10.1155/2023/9269987.
5. **Calderon P., Glisic B.** Influence of mechanical and geometrical properties of embedded long-gauge strain sensors on the accuracy of strain measurement. IOP publishing Meas. Sci. Technol, 2012, Vol. 23, 065604, doi: 10.1088/0957-0233/23/6/065604.
6. **Zhao Y., Mengzhen L.** A theoretical strain transfer model analysis of the substrate-bonded FBG sensor considering the influence of groove. Journal of Instrumentation, Engineering, 2024, doi: 10.1088/1748-0221/19/09/p09005.
7. **Han D., Liu G., Xi Y., Zhao Y.** Theoretical analysis on the measurement accuracy of embedded strain sensor in asphalt pavement dynamic response monitoring based on FEM. Structural Control and Health Monitoring, 2022, Vol. 29, doi: 10.1002/stc.3140.
8. **Xinghao H. et al.** High-stretchability and low-hysteresis strain sensors using origami-inspired 3D mesostructures. Sci. Adv.,

2023, Vol. 9, 9799, doi: 10.1126/sciadv.adh9799.
9. **Aidong Q. et al.** Stretchable and calibratable graphene sensors for accurate strain measurement. Materials Advances, 2020, no. 1, pp. 235-243, doi: 10.1039/D0MA00032A.
10. **Shipunov G.S., Baranov M.A., Nikiforov A.S., Khabibrakhmanova F.R.** Comparison of mechanical strain measurement accuracy of fiberoptic sensor and smart-lay. Materials Physics and Mechanics, 2022, Vol. 48, no. 3, pp. 342-354, doi: 10.18149/MPM.4832022_5.
11. **Baldassarre A., Ocampo J., Martinez M., Rans C.** Accuracy of strain measurement systems on a non-isotropic material and its uncertainty on finite element analysis. Journal of Strain Analysis for Engineering Design, 2020, Vol. 56, Issue 2, pp. 76-95, doi: 10.1177/0309324720924580.
12. **Lamb H.**, Dynamic Theory of Sound, 2d edn, Edward Arnold (Publishers) Ltd., London, 1931, 307 p.
13. **Love A.E.H.**, Some Problems of Geodynamics, Cambridge University Press, Cambridge, UK, 1911.
14. **Kochetkov I.D., Rogacheva N.N.** Contact interaction of a piezoelectric actuator and elastic half-space. Journal of Applied Mathematics and Mechanics, 2005, Vol. 69, pp. 792-804.
15. **Rogacheva N.N.** Multilayered dynamic strain gauge using of piezoelectric PVDF films. MATEC Web of Conferences, 2017 Vol. 117, doi: 10.1051/matecconf/20 1711700146.
16. **Bensoussan A., Lions J.L., Papanicolaou G.** Asymptotic Analysis for Periodic Structures. American Mathematical Society, 2011, 392 p.

СПИСОК ЛИТЕРАТУРЫ

1. **Tomson W. (Lord Kelvin).** On the electrodynamic qualities of metals // Proc. R. Soc. London. 1856. № 146. pp. 649–751.
2. **Инфимовская А.А., Рогачева Н.Н., Чернышев Г.Н.** Использование тонких пьезокерамических датчиков для измерения динамических деформаций // Изв. Академия наук СССР. МТТ. 1989. Т. 24. вып. 2. с. 157-162.
3. **Rogacheva N., Sidorov V., Zheglova Yu.** Piezoelectric Sensor of Small Dynamic Bending Strains // Buildings. 2024. Issue 14. Vol. 2447, doi: 10.3390/buildings14082447.
4. **Li Y. Sharif-Khodaei Z.** Accuracy of Distributed Strain Sensing with Single-Mode Fibre in Composite Laminates under Thermal and Vibration Loads // Structural Control and Health Monitoring. 2023. № 2. pp. 1-13, doi: 10.1155/2023/9269987.
5. **Calderon P., Glisic B.** Influence of mechanical and geometrical properties of embedded long-gauge strain sensors on the accuracy of strain measurement // IOP publishing Meas. Sci. Technol. 2012. Vol. 23. 065604, doi: 10.1088/0957-0233/23/6/065604.
6. **Zhao Y., Mengzhen L.** A theoretical strain transfer model analysis of the substrate-bonded FBG sensor considering the influence of groove // Journal of Instrumentation, Engineering. 2024, doi: 10.1088/1748-0221/19/09/p09005.
7. **Han D., Liu G., Xi Y., Zhao Y.** Theoretical analysis on the measurement accuracy of embedded strain sensor in asphalt pavement dynamic response monitoring based on FEM // Structural Control and Health Monitoring. 2022. Vol. 29, doi: 10.1002/stc.3140.
8. **Xinghao H. et al.** High-stretchability and low-hysteresis strain sensors using origami-inspired 3D mesostructures // Sci. Adv. 2023. Vol. 9. 9799. doi: 10.1126/sciadv.adh9799.
9. **Aidong Q. et al.** Stretchable and calibratable graphene sensors for accurate strain measurement // Materials Advances.

2020. № 1. pp. 235-243, doi: 10.1039/D0MA00032A.
10. **Shipunov G.S., Baranov M.A., Nikiforov A.S., Khabibrakhmanova F.R.** Comparison of mechanical strain measurement accuracy of fiberoptic sensor and smart-lay // Materials Physics and Mechanics. 2022. Vol. 48. № 3. pp. 342-354, doi: 10.18149/MPM.4832022_5.
11. **Baldassarre A., Ocampo J., Martinez M., Rans C.** Accuracy of strain measurement systems on a non-isotropic material and its uncertainty on finite element analysis // Journal of Strain Analysis for Engineering Design. 2020. Vol. 56. Issue 2. pp. 76-95, doi: 10.1177/0309324720924580.
12. **Lamb H.**, Dynamic Theory of Sound, 2d edn, Edward Arnold (Publishers) Ltd. London. 1931. 307 p.
13. **Love A.E.H.**, Some Problems of Geodynamics, Cambridge University Press, Cambridge. UK. 1911.
14. **Kochetkov I.D., Rogacheva N.N.** Contact interaction of a piezoelectric actuator and elastic half-space // Journal of Applied Mathematics and Mechanics. 2005. Vol. 69. pp. 792-804.
15. **Rogacheva N.N.** Multilayered dynamic strain gauge using of piezoelectric PVDF films // MATEC Web of Conferences. 2017. Vol. 117, doi: 10.1051/matecconf/20 1711700146.
16. **Bensoussan A., Lions J.L., Papanicolaou G.** Asymptotic Analysis for Periodic Structures. American Mathematical Society. 2011. 392 p.

Rogacheva Nelly Nikolaevna — Doctor of Physical and Mathematical Sciences, Associate Professor of the Department of Computer Science and Applied Mathematics of the National Research Moscow State University of Civil Engineering; 129337, Russia, Moscow, Yaroslavskoe shosse, 26. E-mail: Rogachevann@mgsu.ru.

Sidorov Vladimir Nikolaevich — Doctor of Technical Sciences, Professor, Academician of the Russian Academy of Sciences, Head of the Department of Computer Science and Applied Mathematics of the National Research Moscow State University of Civil Engineering; 129337, Russia, Moscow, Yaroslavskoe shosse, 26. E-mail: Sidorovvn@mgsu.ru

Zheglova Yulia Germanovna — Candidate of Technical Sciences, Associate Professor of the Department of Information Systems, Technologies and Automation in Construction of the National Research Moscow State University of Civil Engineering; 129337, Russia, Moscow, Yaroslavskoe shosse, 26. E-mail: Jeglovayug@mgsu.ru

Рогачева Нэлля Николаевна — д.ф.-м.н., доцент кафедры Информатики и прикладной математики Национального исследовательского Московского государственного строительного университета; 129337, Россия, г. Москва, Ярославское шоссе, д. 26. E-mail: Rogachevann@mgsu.ru

Сидоров Владимир Николаевич — д.т.н., профессор, академик РААСН, заведующий кафедрой Информатики и прикладной математики Национального исследовательского Московского государственного строительного университета; 129337, Россия, г. Москва, Ярославское шоссе, д. 26. E-mail: Sidorovvn@mgsu.ru

Жеглова Юлия Германовна — к.т.н., доцент кафедры Информационных систем, технологий и автоматизации в строительстве Национального исследовательского Московского государственного строительного университета; 129337, Россия, г. Москва, Ярославское шоссе, д. 26. E-mail: Jeglovayug@mgsu.ru

RATING THE LIMITING SHIFT OF A STORY AS A CRITERIA FOR A SPECIAL LIMITING STATE

Oleg V. Mkrtychev, Ekaterina M. Lokhova, Timur A. Tagirov

National Research Moscow State University of Civil Engineering, Moscow, RUSSIA

Abstract: The article presents a verification of one of the existing seismic resistance criteria found in domestic and international standards. The study examines the limit value of relative displacement of the first-floor column in a reinforced concrete building under seismic loading using two different material models in a nonlinear dynamic framework. The article introduces a modeling approach that allows for the assessment of the seismic resistance of reinforced concrete buildings and structures in a nonlinear dynamic framework. The objective of the work is to verify the standardized limit drift value for a specific structural scheme when modeling the column with volumetric elements including direct reinforcement.

Two different material models, implemented in the LS-DYNA software, were used in the column modeling. The first material model is the Karagozian & Case (K&C) Concrete model. This material model represents a three-invariant model with multiple strength and yield surfaces. The model's input parameters include various factors, including empirical ones, such as yield strength, ultimate strength, and residual strength, which are key parameters for the damage accumulation function. The second material model is the Continuous Surface Cap Model, represented by a closed surface (a cap model with a continuous yield surface). This model also accounts for damage accumulation and the degradation of stiffness and strength under cyclic loading.

The results include isocontours of the damage accumulation function in concrete, isocontours of strain and stress intensities in concrete and reinforcement at various time steps, as well as graphs of the damage accumulation functions. The findings confirm the accuracy of the numerically determined limit displacement value and identify which material model most precisely represents the failure mechanisms of concrete, thus indicating its suitability for further in-depth research.

Keywords: seismic resistance, accumulation of damage, calculation in nonlinear dynamic setting, material models, criteria for seismic resistance

НОРМИРОВАНИЕ ПРЕДЕЛЬНОГО СДВИГА ЭТАЖА КАК КРИТЕРИЯ ОСОБОГО ПРЕДЕЛЬНОГО СОСТОЯНИЯ

О.В. Мкртычев, Е.М. Лохова, Т.А. Тагиров

Национальный исследовательский Московский государственный строительный университет, г. Москва, РОССИЯ

Аннотация: В статье представлена верификация одного из существующих в отечественной и зарубежной нормативной документации критерия сейсмостойкости. Рассматривается предельное относительное перемещение колонны первого этажа железобетонного здания при сейсмическом воздействии. Верификация производится с использованием двух различных моделей материалов в нелинейной динамической постановке. В статье приведен подход моделирования, позволяющий производить оценку сейсмостойкости конструкции железобетонных зданий и сооружений в нелинейной динамической постановке. Целью работы является верификация нормируемого предельного значение перекоса для конкретной конструктивной схемы при моделировании колонны объемными элементами с непосредственным армированием.

При моделировании колонны были использованы две различные модели материалов, реализованные в программном комплексе LS-DYNA. Первая модель материала - Karagozian & Case (K&C) Concrete. Данная модель материала представляет трехинвариантную модель с множественными поверхностями прочностями и текучести. Исходными параметрами модели являются различные параметры, в том числе и эмпирические, в частности предел текучести, предельная прочность и остаточная прочность, которые являются определяющими параметрами для функции накопления повреждений. Вторая модель материала - Continuous Surface Cap Model представлена замкнутой поверхностью (шатровая модель с непрерывной

предельной поверхностью). Данная модель также учитывает накопление повреждений и деградацию жесткости и прочности при циклических нагрузках.
В качестве результатов представлены изополя функции накопления повреждений в бетоне, изополя интенсивности деформаций и напряжений в бетоне и арматуре в различные моменты времени, а также графики функций накопления повреждений. Результаты исследований свидетельствуют об обоснованности численного значения предельного перемещения, а также позволяют сделать вывод о том, какая из моделей материала наиболее точно описывает характер разрушения бетона и может быть использована для дальнейших исследований.

Ключевые слова: сейсмостойкость, накопление повреждений, расчеты в нелинейной динамической постановке, модели материалов, критерии сейсмостойкости

INTRODUCTION

Existing domestic and international seismic design standards commonly utilize maximum allowable relative displacement, or inter-story drift, as one of the criteria for assessing seismic resilience. The maximum displacement can be taken equal to h/150 (h – floor height). [1] However, this criterion has yet to be substantiated through rigorous nonlinear dynamic analysis. [2,3] The article presents a detailed examination of this specific limit state criterion, including an analysis of the seismic resistance of first-floor columns in a reinforced concrete structure. The study employs two distinct material models within a nonlinear dynamic framework, implemented using the LS-DYNA software package.
The primary objective of this study is to verify the standardized allowable drift criterion for a specific structural configuration. This is achieved by modeling the column with volumetric elements and detailed reinforcement, utilizing material models that incorporate effects of degradation and damage accumulation.

Methods

The study examines a first-floor column (Figure 1). The concrete used is of strength class B25, with a column height of 6 meters and a cross-section of 400x400 mm. The longitudinal reinforcement consists of four rebars with a diameter of 28 mm (A500C). The transverse(shear) reinforcement is provided by hoops by 10 mm diameter ties (A500C) in the central part of the column and 14 mm diameter ties (A500C) at the ends, spaced 200 mm apart. The concrete was modeled using solid elements, while the reinforcement bars were modeled using beam elements.
The finite element mesh size for both the reinforcement and concrete was set at 12.5 mm in all directions. Column base is fixed in three linear directions. The top of the column is subjected to a forced horizontal displacement of 2 cm along the X-axis (varying sinusoidally), along with a vertical load of 3 tons applied at each node. The model consists of 248521 finite elements. Several material models were used: Piecewise Linear Isotropic Plasticity for the reinforcement, and both the Continuous Surface Cap Model and the Karagozian & Case (K&C) Concrete model for the concrete.

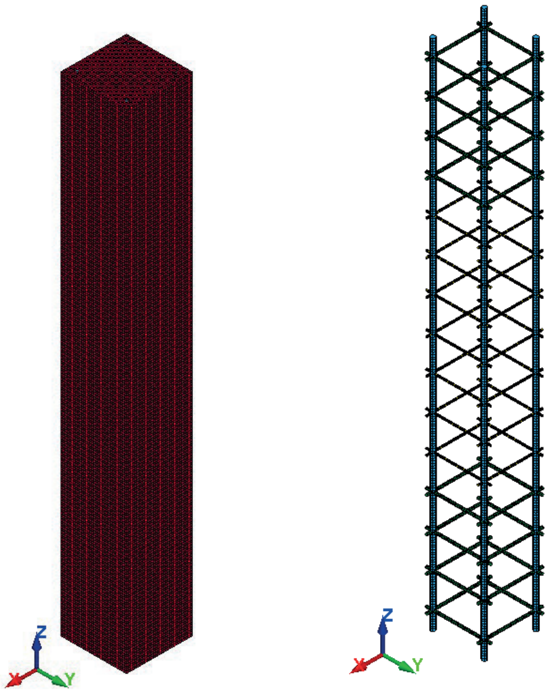

Figure 1. Finite element model used

Considered mathematical models of materials are presented below.

KARAGOZIAN & CASE (K&C) CONCRETE MAT072R3

This material model is primarily designed for simulating the dynamic responses of reinforced concrete structures. It accounts for various concrete properties such as hardening, softening, strain rate effects, compaction, and shear dilatancy. The model is a three-invariant formulation featuring multiple yield and strength surfaces. The initial parameters of the model are various parameters, including empirical ones. In particular, the yield strength, ultimate strength and residual strength of the material, determined as functions of damage accumulation during compression and tension.

The model decomposes the stress into hydrostatic pressure and deviatoric stress components:

$$\sigma_{ij} = s_{ij} + \frac{1}{3}\sigma_{ii}\delta_{ij}, \tag{1}$$

where:

σ_{ij} - is the stress tensor:

s_{ij} - is the deviatoric stress tensor;

σ_{ij} - is the hydrostatic pressure.

Hydrostatic pressure is related to the material's volumetric strain, while deviatoric stress is associated with its shear resistance. The deviatoric stress is usually expressed through the second invariant of the deviatoric stress tensor:

$$J_2 = \frac{1}{2}s_{ij}s_{ji} = \frac{s_1^2 + s_2^2 + s_3^2}{2} = \frac{1}{2}\sigma' : \sigma' \tag{2}$$

The model features three independent strength surfaces: the maximum strength surface, the yield surface, and the residual strength surface, as illustrated in Figure 2.

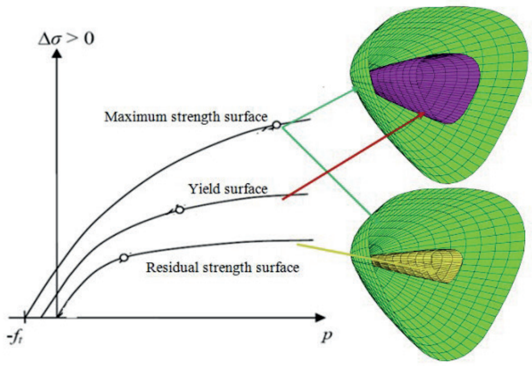

Figure 2. Strength surfaces for the Karagozian and Case concrete model (KCC) material model [4]

The general expression for the strength surfaces can be written as:

$$\Delta\sigma = \sqrt{3J_2} = f(p, J_2), \tag{3}$$

where: $\Delta\sigma$ - is the difference between the principal stresses; p -is the hydrostatic pressure.

Typically, equation (3) refers to the compressive meridian. The whole failure curve can be obtained through rotation of the compressive meridian around the hydrostatic pressure axis by multiplying Θ_L [5] (4-5):

$$\Theta_L = \frac{r}{r_c} = $$

$$= \frac{2(1-\psi^2)\cos\theta_L + (2\psi-1)\sqrt{4(1-\psi^2)\cos^2\theta_L + 5\psi^2 - 4\psi}}{4(1-\psi^2)\cos^2\theta_L + (1-2\psi)^2}$$

$$\Delta\sigma = r_3\Theta_L \cdot \sqrt{3J_2} = f(p, J_2, J_3); \tag{4}$$

$$\theta = \cos^{-1}\left(\frac{3\sqrt{3}}{2}\frac{J_3}{J_2^{3/2}}\right)/3$$

$$\psi = \begin{cases} \frac{1}{2} & \text{if } p \le 0 \\ \frac{1}{2} + \frac{3f_t}{2f_c'} & \text{if } p = \frac{f_c'}{3} \\ \dfrac{\alpha f_c'}{a_0 m + \dfrac{2\alpha f_c'}{3a_1 m + 2a_2 m\alpha f_c'}} & \text{if } p = \frac{2\alpha f_c'}{3}, \alpha \approx 1.15 \\ 0.753 & \text{if } p = 3f_c' \\ 1.000 & \text{if } p \ge 8.45 f_c' \end{cases} \tag{5}$$

where:

ψ - is the ratio between the tensile and compressive meridians. This ratio is a function of pressure and can be calculated using the Malvar method [5].

f_c' - is the compressive strength;

f_t' - is the tensile strength.

At the initial increase in hydrostatic pressure, deviatoric stresses remain within the elastic range until the yield surface is reached. Deviatoric stresses can continue to evolve until the ultimate strength surface is attained, at which point the material begins to fail. Following the onset of failure, the material progressively loses its load-bearing capacity and eventually reaches the residual strength surface. The equations for these three surfaces are provided in the following equations [4]:

Yield surface:

$$\Delta\sigma_y = a_{0y} + \frac{p}{a_{1y} + a_{2y} p}. \tag{6}$$

Maximum strength surface:

$$\Delta\sigma_m = a_0 + \frac{p}{a_1 + a_2 p}. \tag{7}$$

Residual strength surface:

$$\Delta\sigma_r = \frac{p}{a_{1f} + a_{2f} p}. \tag{8}$$

The parameters a_0, a_1 ,a_2 a_{1f} ,a_{2f} ,a_{0y} ,a_{1y} ,a_{2y}, used for these three surfaces, can be determined based on the results of experimental tests, such as triaxial compression, biaxial compression, or uniaxial tension/compression.[5]

After reaching the initial yield surface but before attaining the ultimate strength surface, the current surface can be obtained through linear interpolation between the yield surface and the ultimate strength surface.

Once the maximum strength surface is reached, ongoing failure is interpolated between the maximum strength surface and the residual strength surface. The dynamic form of the failure surface is implemented by interpolating between pairs of fixed strength surfaces based on the damage parameter λ. The evolution of this parameter is defined as a function of the plastic strain rate tensor $\hat{\dot{\varepsilon}}^p$:

$$\dot{\lambda} = h(p)\hat{\dot{\varepsilon}}^p; \tag{9}$$

$$\hat{\dot{\varepsilon}}^p = \sqrt{\left(\dot{\varepsilon}^p : \dot{\varepsilon}^p\right)\frac{2}{3}}. \tag{10}$$

The function $h(p)$ describes the dependency between pressure and the rate of change of damage accumulation.

$$h(p) = \begin{cases} \left[1 + \dfrac{p}{(r_f f_t)}\right]^{-b_1} / r_f & , p \geq 0; \\ \left[1 + \dfrac{p}{(r_f f_t)}\right]^{-b_2} / r_f & , p < 0. \end{cases} \tag{11}$$

where :

r_f - is the Dynamic Increase Factor(DIF).

b_1, b_2 – are experimentally determined parameters.

The concrete model also uses the parameter η for interpolation between different strength surfaces. This parameter varies from zero to one, depending on the accumulated effective plastic strain. Specifically:

1. As λ begins to increase, η increases from 0 to 1.
2. When λ reaches the value λ_m (plastic strain at maximum strength) η becomes 1.
3. η then decreases back to 0 as λ continues to increase (1<λ<2). indicating softening and progressive failure. The material continues to degrade after reaching its maximum strength.

The parameter η aids in modeling the transition between the ultimate strength surface, the yield surface, and the residual strength surface, depending on the degree of material damage.

Theoretically, each of the three strength surfaces is described by equations, with nine parameters calibrated based on experimental data. Howev-

er, due to limited data, it may be impossible to calibrate the parameters across the entire range of pressures. As a result of this scarcity of experimental data, several assumptions have been incorporated into the model when using the strength surfaces.[6]
Firstly, experimental data for calibrating the ultimate strength surface at pressures below $f_c'/3$, are likely unavailable, as damage does not occur within this range. Consequently, in the model implementation, the ultimate strength surface is predefined as:

$$\hat{\sigma}_m = \begin{cases} a_{0m} + \dfrac{p}{a_{1m} + a_{2m} p} & p \geq \dfrac{f_c'}{3} \\ \dfrac{3}{2\psi}(p + f_t) & 0 \leq p \leq \dfrac{f_c'}{3} \text{ or } \lambda \leq \lambda_m \\ & -f_t \leq p \leq 0 \\ 3\left(\dfrac{p}{\eta} + f_t\right) & p \leq 0 \text{ and } \lambda > \lambda_m \end{cases} \tag{12}$$

Similarly, the yield surface cannot be calibrated for pressures between 0 and 0 и $f_{yc}'/3$(f_{yc}' — is the yield limit), as yielding does not occur within this pressure range. Therefore, the yield surface is modified as follows:

$$\hat{\sigma}_y = \begin{cases} a_{0y} + \dfrac{p}{a_{1y} + a_{2y} p} & p \geq \dfrac{f_{yc}'}{3} \\ 1.35 f_t + 3p\left(1 - \dfrac{1.35 f_t}{f_{yc}'}\right) & 0 \leq p \leq \dfrac{f_{yc}'}{3} \\ 1.35(p + f_t) & p \leq 0 \end{cases} \quad ((13)$$

The residual strength surface (Figure 2) models the transition from brittle to ductile behavior in concrete as lateral pressure increases. At very high lateral pressures, the concrete may exhibit strain-hardening behavior. The model accounts for this by defining the residual surface so that, at high pressures, it equals or exceeds the ultimate strength surface.

CONTINUOUS SURFACE CAP MODEL

This model also incorporates damage accumulation, with the damage accumulation function accounting for both the reduction in material strength and the degradation of the elastic modulus. [7]

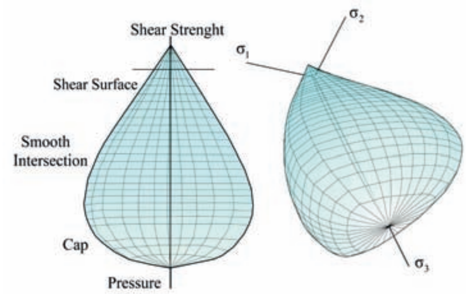

Figure 3. Continuous surface cap model CSCM

The damage accumulation is mathematically expressed as follows:

$$\sigma_{ij}^d = (1 - d)\sigma_{ij}^{vp}. \tag{14}$$

Here d – is a scalar damage parameter that transforms the undamaged stress tensor, denoted as σ^{vp}, into the damaged stress tensor, denoted as σ^d. The damage parameter d varies from 0 (indicating no damage) to 1 (indicating complete loss of strength). The effect of this parameter also includes the proportional reduction of both the bulk modulus and the shear modulus simultaneously.[8]
Brittle damage accumulates under tension. The accumulation of brittle damage depends on the maximum principal strain ε_{max}:

$$\tau_b = \sqrt{E\varepsilon_{max}^2}. \tag{15}$$

where τ_b - is an energy-type parameter. Brittle damage initiates when τ_b exceeds the initial threshold r_{0b}.
Plastic damage accumulates under compressive loading and is dependent on the components of the total strain ε_{ij}:

$$\tau_d = \sqrt{\frac{1}{2}\sigma_{ij}\varepsilon_{ij}}\ , \qquad (16)$$

where τ_d - is an energy-based parameter. Plastic damage begins to accumulate when τ_d exceeds the initial threshold r_{0d}.

RESULTS AND DISCUSSION

The key results are summarized as follows:
Fig. 4 shows the calculation scheme with isofields of the damage accumulation function, and also highlights the fragment for which the results will be presented.

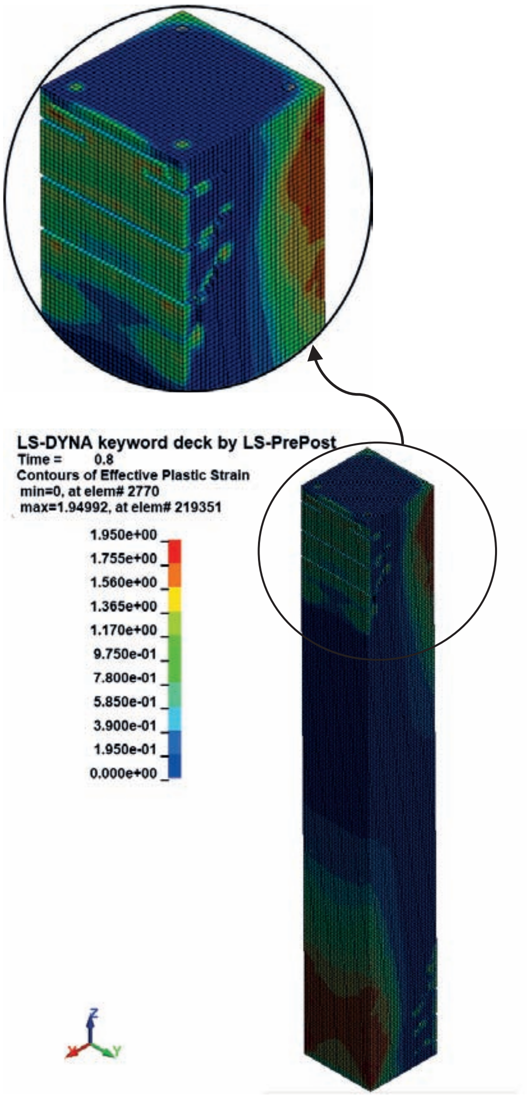

Figure 4. Calculation scheme with isofields of the damage accumulation function (t=0,8 s)

Figure 5 shows a group of finite elements for which the graphs of damage accumulation functions are given. (For Karagozian & Case (K&C) Concrete model - in Figure 6, for Continuous Surface Cap Model - in Figure 7)

Figure 5. The area under consideration

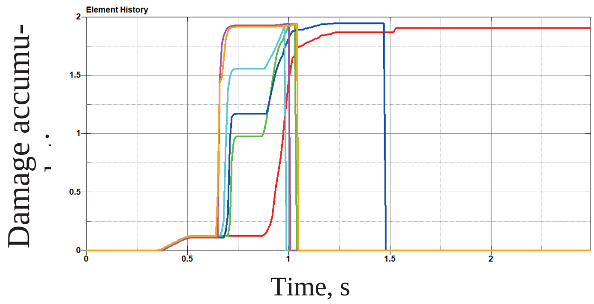

Figure 6. Damage accumulation function in concrete element

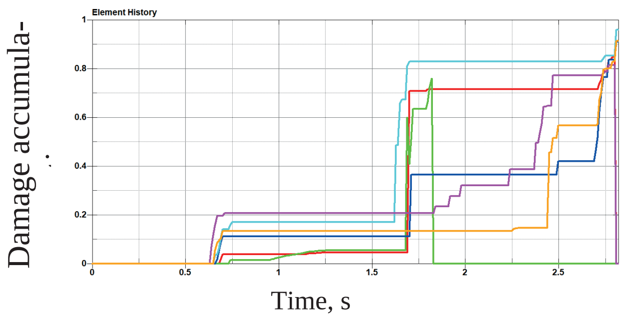

Figure 7. Damage accumulation function in concrete element

Figures 8-11 depict the isopleths of stress intensity in concrete at different time steps. Figures 12-15 depict the isopleths of stress intensity in reinforcement at different time steps.
Figures 16-19 depict the isopleths of strain intensity in concrete at different time steps. Figures 20-23 depict the isopleths of strain intensity in reinforcement at different time steps.

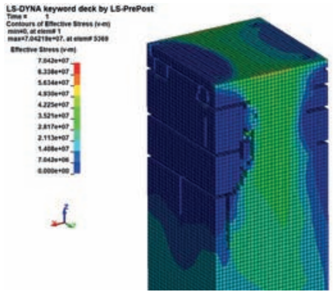

Figure 8. Stress intensity in concrete (t=1,0 s), Pa
(Karagozian & Case (K&C) Concrete model)

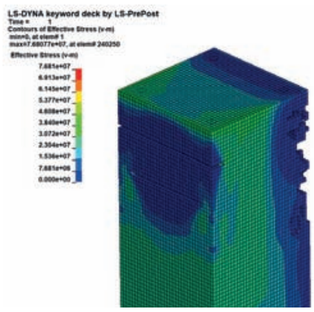

Figure 9. Stress intensity in concrete (t=1,0 s), Pa
(Continuous Surface Cap Model)

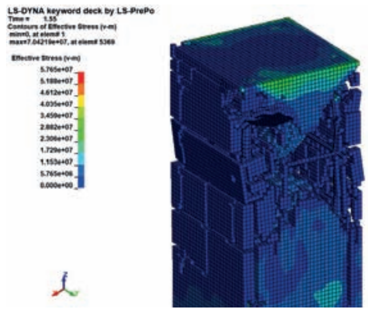

Figure 10. Stress intensity in concrete (t=1,55 s), Pa
(Karagozian & Case (K&C) Concrete model)

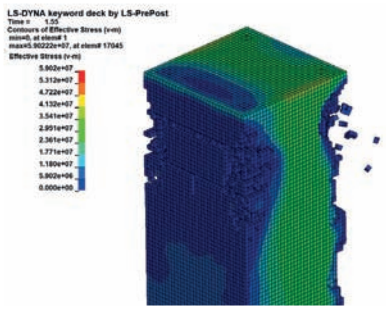

Figure 11. Stress intensity in concrete (t=1,55 s), Pa
(Continuous Surface Cap Model)

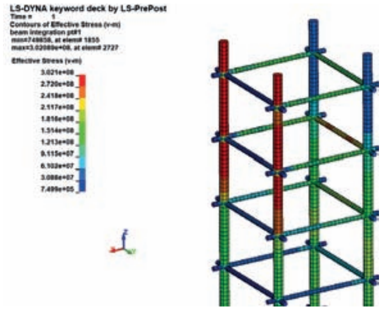

Figure 12. Stress intensity in in reinforcement (t=1,0 s), Pa
(Karagozian & Case (K&C) Concrete model)

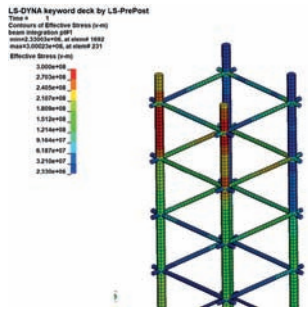

Figure 13. Stress intensity in in reinforcement (t=1,0 s), Pa
(Continuous Surface Cap Model)

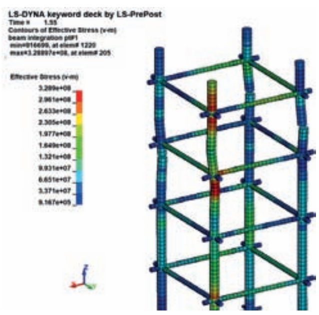

Figure 14. Stress intensity in reinforcement (t=1,55 s), Pa
(Karagozian & Case (K&C) Concrete model)

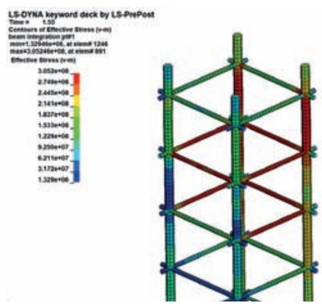

Figure 15. Stress intensity in reinforcement (t=1,55 s), Pa
(Continuous Surface Cap Model)

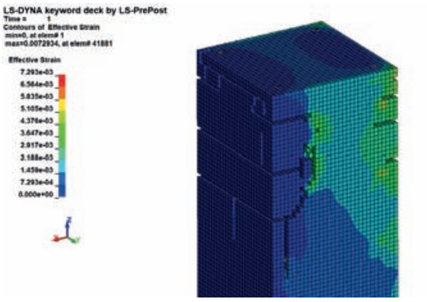

Figure 16. Intensity of deformations in concrete (t=1,0 s)
(Karagozian & Case (K&C) Concrete model)

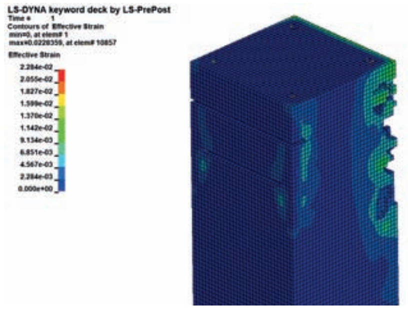

Figure 17. Intensity of deformations in concrete (t=1,0 s)
(Continuous Surface Cap Model)

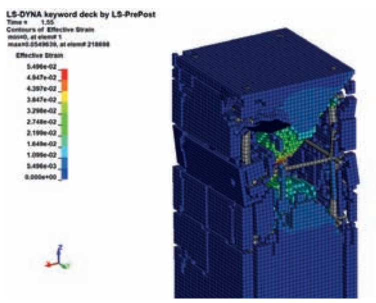

Figure 18. Intensity of deformations in concrete (t=1,55 s)
(Karagozian & Case (K&C) Concrete model)

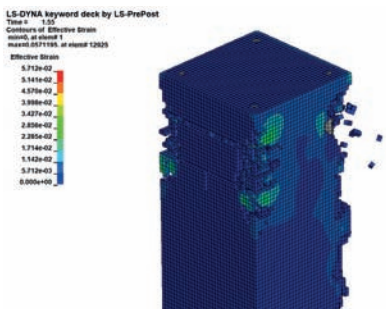

Figure 19. Intensity of deformations in concrete (t=1,55 s)
(Continuous Surface Cap Model)

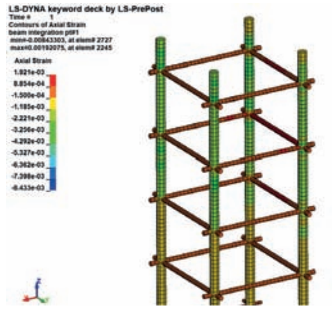

Figure 20. Intensity of deformations in reinforcement (t=1,0 s)
(Karagozian & Case (K&C) Concrete model)

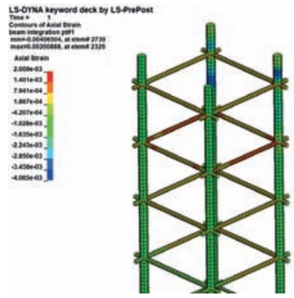

Figure 21. Intensity of deformations in reinforcement (t=1,0 s)
(Continuous Surface Cap Model)

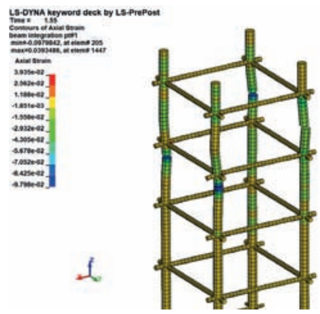

Figure 22. Intensity of deformations in reinforcement (t=1,55 s)
(Karagozian & Case (K&C) Concrete model)

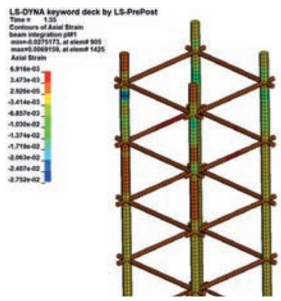

Figure 23. Intensity of deformations in reinforcement (t=1,55 s)
(Continuous Surface Cap Model)

Figures 24-28 present the isopleths of the damage accumulation function at various time intervals.

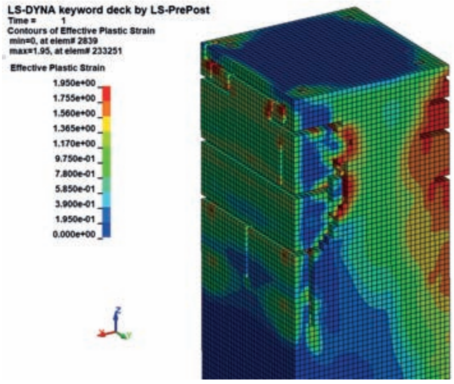

<u>Figure 24.</u> Damage accumulation function in concrete (t=1 s)
(Karagozian & Case (K&C) Concrete model)

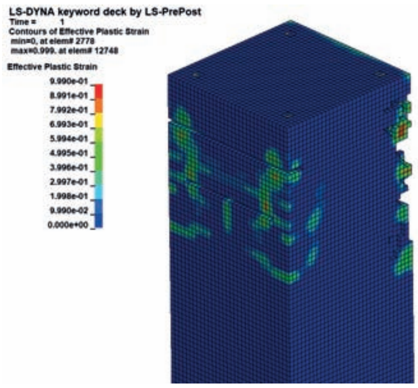

<u>Figure 25.</u> Damage accumulation function in concrete (t=1 s)
(Continuous Surface Cap Model)

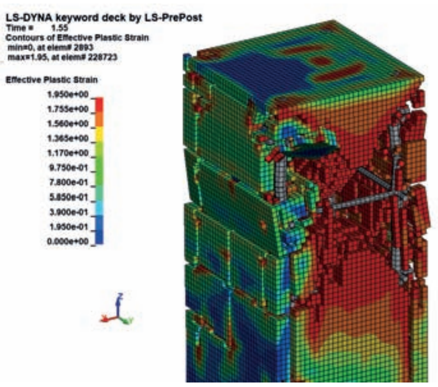

<u>Figure 26.</u> Damage accumulation function in concrete (t=1.55 s)
(Karagozian & Case (K&C) Concrete model)

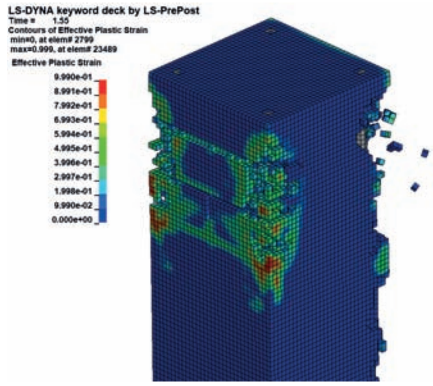

<u>Figure 27.</u> Damage accumulation function in concrete (t=1.55 s)
(Continuous Surface Cap Model)

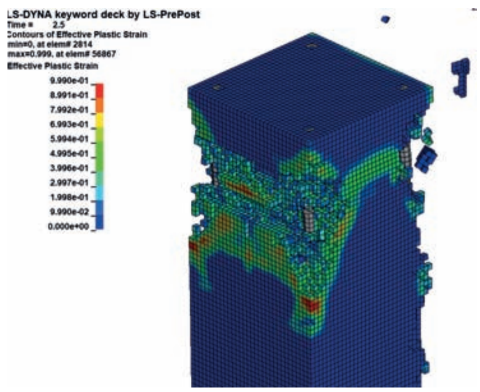

<u>Figure 28.</u> Damage accumulation function in concrete (t=2.60 s)
(Continuous Surface Cap Model)

CONCLUSION

1. The research results indicate the adequacy and validity of the limit value for the inter-story drift for this structural scheme, which is numerically set at 2 cm.
2. The approach to modeling proposed in this study enables the evaluation of the seismic resistance of reinforced concrete buildings and structures in a nonlinear dynamic framework. This approach accounts for the degradation of strength and softening of the structural system, as well as the accumulation of damage under cyclic loading.
3. Based on the results of the study, it can be concluded that the Karagozian & Case (K&C) Concrete material model more adequately de-

scribes the nature of concrete destruction and can be utilized in further research.

ACKNOWLEDGEMENTS

The research was funded by the National Research Moscow State University of Civil Engineering (grant for fundamental and applied scientific research, project No. 32-392/130.

REFERENCES

1. NEHRP recommended provisions for seismic regulations For new buildings and other structures (2004) *Building Seismic Safety Council for the Federal Emergency Management Agency*.
2. **Mkrtychev O.V., Lokhova E.M.** (2024) Proektirovanie sejsmostojkih zdanij. Normy novogo pokoleniya [Design of earthquake-resistant buildings. New generation standards]. Zhilishchnoe Stroitel'stvo [Housing Construction]. 2023. No. 4, pp. 42–46. DOI: https://doi.org/10.31659/0044-4472-2024-4-42-46.
3. **Dorozhinsky V.B.** (2022) Nelinejnye metody raschetov pri provedenii nauchno-tekhnicheskogo soprovozhdeniya [Nonlinear calculation methods for scientific and technical support] Promyshlennoe i grazhdanskoe stroitel'stvo. No. 10, pp. 32–36 DOI: 10.33622/0869-7019.2022.10.32-36.
4. **Jun Wu, Liang Li, Xiuli Du and Xuemei Liu** (2017) Numerical Study on the Asphalt Concrete Structurefor Blast and Impact Load Using the Karagozian and Case Concrete Model, *Advanced Asphalt Materials and Paving Technologies*, vol. 7, no. 202.
5. **Malvar L. J., Crawford J. E., Wesevich, J. W., and Simons, D.** (1997) A plasticity concrete material model for DYNA3D. *Int. J. Impact*, 19(9–10), pp. 847–873.
6. **Youcai Wu and John E. Crawford** (2015) Numerical modeling of concrete using a partially associative plasticity model, *American Society of Civil Engineers*, vol.141, no.12. DOI: 10.1061/(ASCE)EM.1943-7889.0000952
7. **Nemecek J., Padevet P., Bittnar Z.** Effect of stirrups on behavior of normal and high strength concrete columns]. *Acta Polytechnica*, 2004, vol. 44(5-6), pp. 158-164.
8. **Murray Y.D.** Users manual for LS-DYNA. Concrete material model 159-HRT-05-062. 2007. 77 p.

СПИСОК ЛИТЕРАТУРЫ

1. NEHRP recommended provisions for seismic regulations For new buildings and other struc-tures (2004) Building Seismic Safety Council for the Federal Emergency Management Agen-cy.
2. **Мкртычев О.В., Лохова Е.М.** Проектирование сейсмостойких зданий. Нормы нового поколения // Жилищное строительство. 2024. No 4. С. 42–46. DOI: https://doi.org/10.31659/0044-4472-2024-4-42-46.
3. **Дорожинский В.Б.** Нелинейные методы расчетов при проведении научно-технического сопровождения // Промышленное и гражданское строительство. 2022. № 10. С. 32–36. DOI: 10.33622/0869-7019.2022.10.32-36.
4. **Jun Wu, Liang Li, Xiuli Du and Xuemei Liu** (2017) Numerical Study on the Asphalt Concrete Structurefor Blast and Impact Load Using the Karagozian and Case Concrete Model, *Advanced Asphalt Materials and Paving Technologies*, vol. 7, no. 202.
5. **Malvar L. J., Crawford J. E., Wesevich, J. W., and Simons, D**. (1997) A plasticity concrete material model for DYNA3D. *Int. J. Impact*, 19(9–10), pp. 847–873.
6. **Youcai Wu and John E. Crawford** (2015) Numerical modeling of concrete using a partially associative plasticity model, *American Society of Civil Engineers*, vol.141, no.12. DOI: 10.1061/(ASCE)EM.1943-7889.0000952

7. **Nemecek J., Padevet P., Bittnar Z.** Effect of stirrups on behavior of normal and high strength concrete columns]. Acta Polytechnica, 2004, vol. 44(5-6), pp. 158-164.

8. **Murray Y.D.** Users manual for LS-DYNA. Concrete material model 159-HRT-05-062. 2007. 77 p.

Mkrtychev Oleg Vartanovich, D.Sc., Professor, Head of the Department of Strength of Materials, Federal State Budget Educational Institution of Higher Education «Moscow State University of Civil Engineering (National Research University) (MSUCE), 26, Yaroslavskoe shosse, Central Federal District, Moscow, 129337, Russia, e-mail: mkrtychev@yandex.ru

Lokhova Ekaterina Mikhailovna, Senior Lecturer, Department of Strength of Materials, Federal State Budget Educational Institution of Higher Education «Moscow State University of Civil Engineering (National Research University) (MSUCE), 26, Yaroslavskoe shosse, Central Federal District, Moscow, 129337, Russia, e-mail: elm97@mail.ru

Tagirov Timur Alikhanovich, postgraduate student of the Department of Strength of Materials, engineer of the Research Center , Federal State Budget Educational Institution of Higher Education «Moscow State University of Civil Engineering (National Research University) (MSUCE), 26, Yaroslavskoe shosse, Central Federal District, Moscow, 129337, Russia, e-mail: tagirovv_timur@mail.ru

Мкртычев Олег Вартанович, д.т.н, профессор, заведующий кафедрой «Сопротивление материалов», Федеральное государственное бюджетное образовательное учреждение высшего образования «Национальный исследовательский Московский государственный строительный университет» (НИУ МГСУ), д.26, Ярославское шоссе, Центральный федеральный округ, г. Москва, 129337, Россия. Эл. почта: mkrtychev@yandex.ru

Лохова Екатерина Михайловна, старший преподаватель кафедры «Сопротивление материалов», Федеральное государственное бюджетное образовательное учреждение высшего образования «Национальный исследовательский Московский государственный строительный университет» (НИУ МГСУ), д.26, Ярославское шоссе, Центральный федеральный округ, г. Москва, 129337, Россия. Эл. почта: elm97@mail.ru

Тагиров Тимур Алиханович, аспирант кафедры «Сопротивление материалов», инженер НИЦ «Надежность и сейсмостойкость сооружений», Федеральное государственное бюджетное образовательное учреждение высшего образования «Национальный исследовательский Московский государственный строительный университет» (НИУ МГСУ), д.26, Ярославское шоссе, Центральный федеральный округ, г. Москва, 129337, Россия. Эл. почта: tagirovv_timur@mail.ru

ANALYSIS OF VIBRATIONS OF AN ELASTIC PLATE ON A VISCOELASTIC BASE VIA THE FRACTIONAL DERIVATIVE KELVIN-VOIGT MODEL

Marina V. Shitikova, Anastasiya S. Kornilova
National Research Moscow State University of Civil Engineering, Moscow, RUSSIA

Abstract: In the present paper, free and forced vibrations of an elastic Kirchhoff-Love plate on a viscoelastic foundation of the Fuss-Winkler type are studied, the damping properties of which are described using the Kelvin-Voigt model with a fractional derivative. The integral Laplace transform method with further expansion of the sought functions into a series of eigenfunctions of the problem is used as the method for solving the problem of non-stationary vibrations of linear elastic plates on a viscoelastic foundation. The solution is obtained as the sum of two terms, one of which controls the drift of the equilibrium position of the system and is determined by the quasi-static creep processes occurring in the system, and the other term describes the damping of oscillations around the equilibrium position and is determined by the inertia and energy dissipation of the system.

Keywords: free and forced vibrations of an elastic plate, viscoelastic Fuss-Winkler-type foundation, Kelvin-Voigt model with fractional derivative, Riemann-Liouville fractional derivative, Laplace integral transform

АНАЛИЗ КОЛЕБАНИЙ УПРУГОЙ ПЛАСТИНКИ НА ВЯЗКОУПРУГОМ ОСНОВАНИИ С ПОМОЩЬЮ МОДЕЛИ КЕЛЬВИНА-ФОЙГТА С ДРОБНОЙ ПРОИЗВОДНОЙ

М.В. Шитикова, А.С. Корнилова
Национальный исследовательский Московский государственный строительный университет,
г. Москва, РОССИЯ

Аннотация: Исследованы свободные и вынужденные колебания упругой пластины Кирхгофа-Лява на вязкоупругом основании типа Фусса-Винклера, демпфирующие свойства которого описываются при помощи модели Кельвина-Фойгта с дробной производной. В качестве метода решения использован метод интегрального преобразования Лапласа с дальнейшим разложением искомых функций в ряд по собственным функциям задачи. Решение получено в виде суммы двух слагаемых, одно из которых управляет дрейфом положения равновесия системы и определяется квазистатическими процессами ползучести, происходящими в системе, а другое слагаемое описывает затухание колебания вокруг положения равновесия и определяется инерцией и диссипацией энергии системы.

Ключевые слова: свободные и вынужденные колебания упругой пластинки,
вязкоупругое основание типа Фусса-Винклера, модель Кельвина-Фойгта с дробной производной,
дробная производная Римана-Лиувилля, интегральное преобразование Лапласа

INTRODUCTION

The analysis of plate vibrations on a viscoelastic base is an important area of structural mechanics, since plates are used as structural elements in the construction of buildings and structures. The effect of the base response on the dynamic behavior of the slabs is of common interest to structural engineers.

At present, there is an increased interest in the analysis of plates and beams resting on a viscoelastic base under the influence of various types of dynamic loads [1]. Viscoelastic base models of the Fuss-Winkler type with fractional derivatives have become widespread [2], since fractional calculus plays an important role in dynamic problems of structural mechanics [3-6].

Modeling the vibrations of elastic plates on a viscoelastic base is an important and urgent task not only from a theoretical point of view. Due to the wide application of elastic plates in various fields of science and technology, including mechanics, construction and acoustics, the study and modeling of vibrations of elastic plates on a viscoelastic base, damping features of which are described by the fractional derivative Kelvin-Voigt model [7,8], is of great practical importance, since it makes it possible to adequately describe the dynamic reaction of the "plate + viscoelastic base" system with the fewest parameters. At the same time, the order of the fractional derivative is an additional structural parameter, the variation of which from zero to one corresponds to the change in the level of viscoelasticity and allows for a more flexible description and analysis of the hereditary behavior of systems with long-term memory.

Thus, the study of the dynamics of plates on a viscoelastic base using models with fractional derivatives is a significant area in mechanics of materials and structural mechanics, covering both theoretical and practical aspects. In recent years, researchers have focused on the use of fractional derivatives in models of viscoelastic properties of different structural elements, what makes it possible to describe the complex behavior of plates under loads more correctly [3-5, 9].

For example, Rossikhin and Shitikova [10] were among the first to study the dynamic response of an elastic rectangular plate oscillating in a viscous medium, the damping properties of which are described by the Kelvin-Voigt model with fractional derivatives. Vibrations of the plate were described by three linear differential equations with respect to in-plane and out-of-plane displacements of the plate. Laplace method of integral transformations was used as a method of solution.

The analysis of the dynamic behavior of viscoelastic thin Kirchhoff-Love plates under impact was carried out for circular and rectangular plates, respectively, in [11] and [12,13]. A modified Hertzian law was used, in which the modulus of elasticity was replaced by a viscoelastic operator of the fractional order.

Quasi-static analysis of an elastic rectangular plate lying on a viscoelastic Winkler base, the properties of which are described by the Kelvin-Voigt model or a standard linear rigid body with fractional derivatives, was carried out by the Laplace transform method in [14] and [15], respectively.

Free and forced linear oscillations of plates on a viscoelastic Winkler base under the action of a moving harmonic force and a harmonic force whose position does not change over time are considered in [16]. The damping properties of the foundation were described by a standard linear solid model with fractional derivatives. Numerical studies of the amplitude-frequency characteristics of the system were carried out. The results demonstrate how the oscillation parameters change under different types of loads and how the viscoelastic properties of the foundation affect the dynamic behavior of the system.

In this paper, the forced linear oscillations of the system "elastic plate + viscoelastic base of the Fuss-Winkler type" are investigated, the damping properties of which are described by the fractional derivative Kelvin–Voigt model, under the influence of a concentrated harmonic load, using the approach proposed in [10]. It is based on the assumption that each mode of oscillation possesses its own damping coefficient and retardation time, what makes it possible to obtain a solution in a form convenient for engineering applications.

PROBLEM FORMULATION

Let us consider the oscillations of a linearly elastic rectangular plate with sides a and b along the x- and y-axes, respectively, lying on the base (Fig. 1).

The dynamic behavior of a Kirchhoff-Love plate on a viscoelastic base under the action of an external transverse load $q = q(x, y, t)$ is described by the following differential equation:

$$D\nabla^2\nabla^2 w + \rho h\ddot{w} = q - F_1, \qquad (1)$$

where $w = w(x, y, t)$ is the transverse displacement (deflection of the plate), $D = Eh^3/12(1-\nu^2)$ is the cylindrical stiffness of the plate, E is the Young's modulus of the plate, h is its thickness, ρ is the density of the plate material, $\nabla^2\nabla^2$ is the biharmonic operator, $q = F\delta(x - x_0)(y - y_0)\cos\Omega_F t$ is the external harmonic load, F and Ω_F is its amplitude and frequency, $\delta(x - x_0)(y - y_0)$ is the Dirac delta function, and F_1 is the reaction of the viscoelastic base.
Let us assume that damping properties of the viscoelastic base are described by the Fuss-Winkler model:

$$F_1 = \tilde{\lambda} w, \qquad (2)$$

where $\tilde{\lambda}$ is the compliance operator of the viscoelastic base, the damping properties of which are modeled using the Kelvin-Voigt operator of the fractional order [2]:

$$\tilde{\lambda} = \lambda_0(1 + \tau^\gamma D^\gamma), \qquad (3)$$

and λ_0 is the coefficient of compliance of the base, τ is the retardation time,

$$D^\gamma u = \frac{d}{dt}\int_0^t \frac{u(t-t')dt'}{\Gamma(1-\gamma)t'^{\gamma}}, \quad 0 < \gamma \le 1 \qquad (4)$$

- fractional derivative of Riemann-Liouville [17], Γ(1-γ) is a gamma function, γ is the order of a fractional derivative, which is a parameter of the fractionality of the underlying viscoelastic medium.

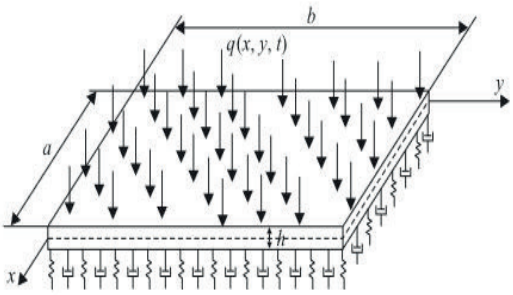

Figure 1. Elastic plate on a viscoelastic base

The boundary conditions for a plate hinged along the contour are as follows:

$$x = 0 \text{ and } a, \quad w = \frac{\partial^2 w}{\partial x^2} = 0$$

$$y = 0 \text{ and } b, \quad w = \frac{\partial^2 w}{\partial y^2} = 0.$$

Let us represent the dynamic deflection of the plate as an eigenfunction expansion of the problem: $W_{mn}(x, y)$:

$$w(x, y, t) = \sum_{m=1}^{\infty}\sum_{n=1}^{\infty} W_{mn}(x, y)x_{mn}(t), \quad (5)$$

where $x_{mn}(t)$ are generalized displacements that depend only on time, and

$$W_{mn}(x, y) = \sin\frac{m\pi x}{a}\sin\frac{n\pi y}{b},$$

are eigenfunctions that satisfy boundary conditions.
When deriving differential equations, we will take into account the filtering property of the delta function:

$$\iint \delta(x - x_0)(y - y_0)\, f(x, y)dxdy = f(x_0, y_0) \qquad (6)$$

Substituting the proposed solution (5) into the system of equations (1) and (2), taking the relation (3) into account, multiplying each of the obtained equations by $W_{mn}(x, y)$, and integrating the length and width of the plate with due account for the orthogonality properties of eigenfunctions, we obtain the following system of differential equations with respect to generalized displacements $x_{mn}(t)$:

$$\ddot{x}_{mn} + \Omega_{mn}^2 x_{mn} + \frac{\lambda_0}{\rho h}(1 + \tau^\gamma D^\gamma)x_{mn} = P_{mn}(t) \quad (7)$$

where $\Omega_{mn}^2 = \frac{Eh^2}{12\rho(1-\nu^2)}\nabla^2 W_{mn}(x, y)$ are the squares of the natural frequencies of oscillations of the elastic plate, and

$$P_{mn}(t)=\frac{\int_0^a\int_0^b q(x,y,t)W_{mn}(x,y)dxdy}{\rho h\int_0^a\int_0^b [W_{mn}(x,y)]^2dxdy}=\frac{\int_0^a\int_0^b (F\cos\Omega_F t)\delta(x-x_0)(y-y_0)\sin\frac{m\pi x}{a}\sin\frac{n\pi y}{b}dxdy}{\rho h\int_0^a\int_0^b \sin^2\frac{m\pi x}{a}\sin^2\frac{n\pi y}{b}dxdy}=$$
$$=\frac{4F\cos\Omega_F t\sin\frac{m\pi x_0}{a}\sin\frac{n\pi y_0}{b}}{\rho hab}.$$

Let us introduce dimensionless values:

$$x^*_{mn}=\frac{(ab)^{1/2}}{h^2}x_{mn},\ \ t^*=\frac{\pi^2h}{ab}\sqrt{\frac{E}{12\rho(1-\nu^2)}}\,t,\quad x^*=\frac{x}{a},\ \ y^*=\frac{y}{b}.$$

Equation (7) could then be rewritten in a dimensionless form as

$$\ddot{x}^*_{mn}+\omega^{*2}_{mn}x^*_{mn}+\lambda_0{}^*\tau^\gamma{}_{mn}\ D^\gamma x^*_{mn}-$$
$$-4F^*\sin\pi m x_0{}^*\sin\pi n y_0{}^*\cos\Omega_F{}^*t^*=0, \qquad (8)$$

where is $\Omega^*_{mn}=\frac{\zeta^2m^2+n^2}{\zeta}$, $\zeta=\frac{b}{a}$,
$\lambda_0{}^*=\frac{12a^2b^2(1-\nu^2)}{h^3\pi^4E}\lambda_0$, $F^*=\frac{12(ab)^{\frac{3}{2}}(1-\nu^2)}{E\cdot h^5\pi^4}F$,
$\Omega_F{}^*=\frac{ab}{\pi^2h}\sqrt{\frac{12\rho(1-\nu^2)}{E}}\Omega_F$, $\omega^{*2}_{mn}=\Omega^{*2}_{mn}+$
$+\lambda_0{}^*$ are squares of the dimensionless natural frequencies of oscillations of the "plate + base" system.

Equations (8) for each fixed pair of values of m and n in the Laplace domain are reduced to equation (9) (here and below * for dimensionless quantities are omitted for ease of presentation):

$$p^2\overline{x}_{mn}+\omega^2_{mn}\overline{x}_{mn}+\lambda_0p^\gamma\tau^\gamma\overline{x}_{mn}=\overline{P}_{mn}, \qquad (9)$$

where p is the Laplace variable, $\overline{P}_{mn}=\beta\frac{p}{p^2+\Omega_F}$, $\beta=4F\sin\pi m x_0\sin\pi n y_0$.

Equation (9) coincides with an accuracy of coefficients with the equation of forced oscillations of a single-mass mechanical system in a viscoelastic medium, the damping properties of which are described by the fractional derivative Kelvin-Voigt model. The solution of a similar equation for the case of free oscillations of the Kelvin-Voigt oscillator was obtained in [18]. Using the solution method proposed in [18] to equation (9) and then applying the inverse Laplace transformation, it is possible to find the dynamic deflection of the plate in the form of the expansion (5).

METHOD OF SOLUTION

Analysis of the characteristic equation

The characteristic equation for the system of equations (8) has the form:

$$f_{mn}(p)=p^2+\lambda_0\tau^\gamma{}_{mn}\,p^\gamma+\omega^2_{mn}. \qquad (10)$$

Let us introduce the substitution of variables in the characteristic equation (10) using the formulas:

$$p=p^*\,\omega_{mn},\quad \tau_{mn}=\tau^*\,\omega^{-1}{}_{mn}.$$

As a result, we will get

$$f^*(p^*)=p^{*2}+\frac{\lambda_0}{\omega^2_{mn}}p^{*\gamma}\tau^{*\gamma}+1=0\,, \qquad (11)$$

whence at $\tau^*=0$ it follows that $p_0=\pm i$.
Substituting $p^*=r^*e^{i\psi^*}$ in equation (11) and separating the real and imaginary parts yield

$$r^{*2}\cos2\psi^*+\frac{\lambda_0}{\omega^2_{mn}}\tau^{*\gamma}r^{*\gamma}\cos\gamma\psi^*+1=0,$$
$$r^{*2}\sin2\psi^*+\frac{\lambda_0}{\omega^2_{mn}}\tau^{*\gamma}r^{*\gamma}\sin\gamma\psi^*=0. \qquad (12)$$

To calculate the roots of the system of equations (12) at $\frac{\pi}{2}<\psi^*<\pi$, following [18], let us introduce new variables $x_1=r^{*2}$ and $x_2=\frac{\lambda_0}{\omega^2_{mn}}\tau^{*\gamma}r^{*\gamma}$. Then, for each fixed angle $\frac{\pi}{2}<\psi^*<\pi\gamma$ at given λ_0 and ω^2_{mn}, we arrive at a set of two linear equations with two unknowns x_1 and x_2:

$$x_1\cos2\psi^*+x_2\cos\gamma\psi^*+1=0,$$
$$x_1\sin2\psi^*+x_2\sin\gamma\psi^*=0, \qquad (13)$$

the solution of which has the form

$$x_1 = \frac{\sin\gamma\psi^*}{\sin(2-\gamma)\,\psi^*},$$
$$x_2 = -\frac{\sin 2\psi^*}{\sin(2-\gamma)\,\psi^*}. \qquad (14)$$

This allows one to calculate the values $r^* = {x_1}^{1/2}$, $\frac{\lambda_0}{\omega_{mn}^2}\tau^{*\gamma} = x_2\, r^{*-\gamma}$, which together with one selected value of ψ^*, governs the root of the characteristic equation. Substituting $-\psi^*$ instead of ψ^* results in its complex-conjugate root.

Thus, equation (11) for each fixed value $\frac{\lambda_0}{\omega_{mn}^2}\tau^{*\gamma}$ has two complex-conjugate roots $p^* = -\delta^* \pm \omega^*$ in the plane with the negative real semi-axis cut out $-\pi < \psi^* \leq \pi$.

The behavior of roots in the complex plane $-\pi < \psi^* \leq \frac{\pi}{2}$ as function of the parameter $\tau^{*\gamma}$ at $\omega_{mn}^2 = 1$ and given λ_0 is shown in Figure 2 (dashed lines indicate asymptotes for selected γ). Figure 2 shows that when the parameter $\tau^{*\gamma}$ changes from 0 to ∞, the root curves p^* leave the points $\pm i$ and grow monotonically and unlimitedly, while rapidly approaching the corresponding asymptotes coming out of the origin at the angle $\psi^* = \frac{\pi}{2-\gamma}$.

Having determined the roots of the basic equation (11), we could find all roots of the characteristic equation (10) using the formulas:

$$p_{mn} = \omega_{mn}\, r^* e^{i\psi^*}, \quad \tau_{mn} = \tau^*\, \omega^{-1}{}_{mn} \qquad (15)$$

The values of the roots of the characteristic equation (10) are presented in Table 1 at $\gamma = 0.25$, $\zeta = 1$, $1 \leq m, n \leq 6$, for the initial retardation time $\tau^* = 1$, which corresponds to the main roots $p^* = -0.4013 \pm 2.2368i$.

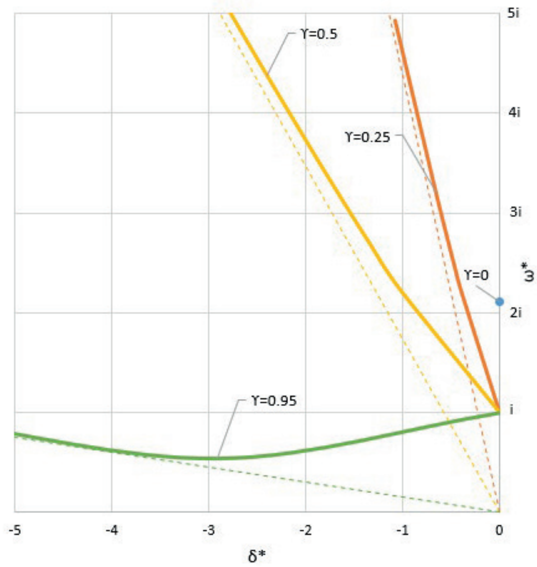

Figure 2. Behavior of the roots of the basic equation (11) of the plate+base system based on model (3)

Construction of the solution

Let us reduce equation (9) to the form:

$$(p^2 + \lambda_0 p^\gamma \tau^\gamma + \omega_{mn}^2)\, \overline{x}_{mn} = \overline{P}_{mn}. \qquad (16)$$

or

$$\overline{x}_{mn} = \overline{P}_{mn}\; f^{-1}{}_{mn}(p), \qquad (17)$$

where $f_{mn}(p)$ is defined by formula (10).

Equation (17) shows that functions $\overline{x}_{mn}$ on the complex plane are multivalued functions with branch points $p = 0$ и $p = -\infty$, which have poles at values $p = p_k$ that turn the denominator (17) into zero, that is, they are the roots of the characteristic equation (10).

For multivalued functions that have branch points, the Mellin-Fourier inversion formula

$$x_{mn}(t) = \frac{1}{2\pi i}\int_{c-i\infty}^{c+i\infty} \overline{x}_{mn}(p)\; e^{pt} dp \qquad (18)$$

is valid only for the first sheet of the Riemann surface, that is, when $-\pi < \arg p < \pi$. Therefore, the integration path should be selected as shown in Figure 3.

Table 1. Values of the roots of the characteristic equation (10)

m	n	Ω_{mn}	ω_{mn}	τ_{mn}	r_{mn}
1	1	2	2.730	0.366	6.204
1	2	5	5.334	0.187	12.122
2	1	5	5.334	0.187	12.122
2	2	8	8.213	0.122	18.664
1	3	10	10.171	0.098	23.114
3	1	10	10.171	0.098	23.114
2	3	13	13.132	0.076	29.843
3	2	13	13.132	0.076	29.843
3	3	18	18.096	0.055	41.123
1	4	17	17.101	0.058	38.863
4	1	17	17.101	0.058	38.863
2	4	20	20.086	0.050	45.646
4	2	20	20.086	0.050	45.646
3	4	25	25.069	0.040	56.970
4	3	25	25.069	0.040	56.970
4	4	32	32.054	0.031	72.843
1	5	26	26.066	0.038	59.236
5	1	26	26.066	0.038	59.236
2	5	29	29.059	0.034	66.038
5	2	29	29.059	0.034	66.038
3	5	34	34.051	0.029	77.381
5	3	34	34.051	0.029	77.381
4	5	41	41.042	0.024	93.269
5	4	41	41.042	0.024	93.269
5	5	50	50.035	0.020	113.704
1	6	37	37.047	0.027	84.189
6	1	37	37.047	0.027	84.189
2	6	40	40.043	0.025	90.999
6	2	40	40.043	0.025	90.999
3	6	45	45.038	0.022	102.350
6	3	45	45.038	0.022	102.350
4	6	52	52.033	0.019	118.246
6	4	52	52.033	0.019	118.246
5	6	61	61.028	0.016	138.688
6	5	61	61.028	0.016	138.688
6	6	72	72.024	0.014	163.675

According to Jordan's lemma, the curvilinear integral taken by arcs C_R tends to zero at $R \to \infty$, and the integral calculated by c_ρ, also tends to zero at $\rho \to 0$.

Using the main theorem of the residue theory, the solution of equation (18) can be written as

$$x_{mn}(t) = x_{mn}^{drift}(t) + x_{mn}^{vibr}(t), \tag{19}$$

$$x_{mn}^{drift}(t) = \frac{1}{2\pi i}\int_0^\infty \left[\bar{x}_{mn}(s\, e^{-i\pi}) - \bar{x}_{mn}(s\, e^{i\pi})\right] \times e^{-st} ds, \tag{20}$$

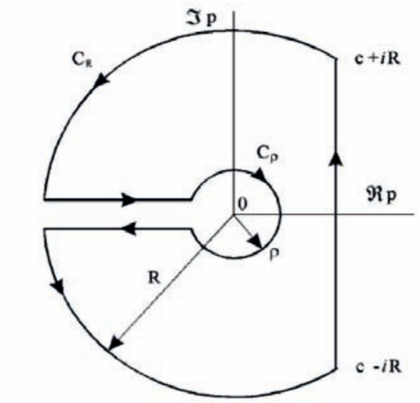

Figure 3. A contour used to compute the complex integral of inversion in the Laplace method

$$x_{mn}^{vibr}(t) = \sum_k res[\bar{x}_{mn}(p_k)\, e^{p_k t}], \quad (21)$$

where the summation is carried out over all isolated special points (poles).

In other words, the solution (19) is represented as the sum of two terms, the first of which (20) determines the displacement of the equilibrium position of the system and is determined by the quasi-static creep processes occurring in the system, and the second term (21) describes the damped oscillations around the equilibrium position and is determined by the inertia of the system and the dissipation of energy [10].

Analysis of elastic plate vibrations

A) *in the case of free oscillations*

To obtain a solution in the case of free oscillations of the plate, it is sufficient to put $\bar{P}_{mn} = 0$ for all *m* and *n* in (17).

Knowing the roots of the characteristic equation (10) and substituting the relation (17) in (19) – (21), we get $x_{mn}^{drift}(t)$, $x_{mn}^{vibr}(t)$ and $x_{mn}(t)$:

$$x_{mn}^{drift}(t) = \frac{1}{\pi}\int_0^\infty \chi_{mn}(s)\, e^{-st} ds \qquad (22)$$

$$x_{mn}^{vibr}(t) = d_{mn} e^{-\delta_{mn}} \sin(\omega_{mn} t - \varphi_{mn}), (23)$$

where

$$\chi_{mn}(s) = \frac{\lambda_0 \tau_{mn}^\gamma s^\gamma \sin\gamma\pi}{s^4 + \omega_{mn}^4 + 2s^2\omega_{mn}^2 + \lambda_0{}^2 \tau_{mn}^{2\gamma} s^{2\gamma} + 2\lambda_0 \tau_{mn}^\gamma s^\gamma (s^2 + \omega_{mn}^2)\cos\gamma\pi},$$

$$d_{mn} = \frac{2}{\sqrt{4r^2{}_{mn} + \lambda_0{}^2 \gamma^2 \tau^{2\gamma}{}_{mn} r_{mn}{}^{2(\gamma-1)} + 4\lambda_0 \gamma \tau^\gamma{}_{mn} r^\gamma{}_{mn} \cos(2-\gamma)\,\psi_{mn}}},$$

$$\tan\varphi_{mn} = -\frac{2r_{mn}\cos\psi_{mn} + \lambda_0\gamma\tau^\gamma{}_{mn} r_{mn}{}^{\gamma-1}\cos(1-\gamma)\psi_{mn}}{2r_{mn}\sin\psi_{mn} - \lambda_0\gamma\tau^\gamma{}_{mn} r_{mn}{}^{\gamma-1}\sin(1-\gamma)\psi_{mn}}.$$

Then the solution for generalized movements will take the form:

$$x_{mn}(t) = d_{mn} e^{-\delta_{mn} t} \sin(\omega_{mn} t - \varphi_{mn}) + \\ + \frac{1}{\pi}\int_0^\infty \chi_{mn}(s)\, e^{-st} ds. \quad (24)$$

B) *in the case of forced oscillations*

To obtain a solution for the forced oscillations of the plate, let us reduce equation (9) to the form:

$$(p^2 + \lambda_0 p^\gamma \tau^\gamma + \omega_{mn}^2)\bar{x}_{mn} = \\ \frac{p}{p^2+\Omega_F} 4F \sin\pi m x_0 \sin\pi n y_0 \qquad (25)$$

When an external harmonic load is applied to the plate, the expressions for $x_{mn}^{drift}(t)$, $x_{mn}^{vibr}(t)$ and $x_{mn}(t)$ take the form:

$$x_{mn}^{drift}(t) = \frac{\beta}{\pi}\int_0^\infty \frac{\lambda_0 \tau_{mn}^\gamma s^{\gamma+1}\,(\sin(\gamma+1)\pi + \Omega_F \sin(\gamma-1)\pi)}{(s+\Omega_F)^2\,((s+\omega_{mn}^2)^2 + \lambda_0{}^2 s^{2\gamma} \tau_{mn}^{2\gamma} + 2(s+\omega_{mn}^2)\lambda_0 \tau_{mn}^\gamma s^\gamma \cos\gamma\pi} e^{-st} ds, \qquad (26)$$

$$x_{mn}^{vibr}(t) = 2d_{mn}\beta e^{-\delta_{mn}t}\sin(\omega_{mn}t - \varphi_{mn}), \tag{27}$$

$$x_{mn}(t) = 2d_{mn}\beta e^{-\delta_{mn}t}\sin(\omega_{mn}t - \varphi_{mn}) + \frac{\beta}{\pi}\int_0^\infty \chi_{mn}(s)\, e^{-st}ds, \tag{28}$$

where $$\tan\varphi_{mn} = -\frac{4r^4{}_{mn}\cos2\psi_{mn} + 2\gamma\chi r_{mn}{}^{2+\gamma}\cos\gamma\psi_{mn} + 4r^2{}_{mn}\Omega_F + 2\Omega_F\gamma\chi r^\gamma{}_{mn}\cos(2-\gamma)\psi_{mn}}{4r^4{}_{mn}\sin2\psi_{mn} + 2\gamma\chi r_{mn}{}^{2+\gamma}\sin\gamma\psi_{mn} + 2\Omega_F\gamma\chi r^\gamma{}_{mn}\sin(2-\gamma)\psi_{mn}},$$

$$d_{mn} = \frac{\sqrt{\begin{gathered}4r^8{}_{mn} + \gamma^2\chi^2 r_{mn}{}^{2(\gamma+1)} + 4\gamma\chi r_{mn}{}^{2+\gamma}\left(r^4{}_{mn} + \Omega_F{}^2\right)\cos(2-\gamma)\psi_{mn} + \\ +\Omega_F{}^2(4r^4{}_{mn} + \gamma^2\chi^2 r_{mn}{}^{2\gamma}) + \Omega_F(8r^6{}_{mn}\cos2\psi_{mn} + 2\gamma^2\chi^2 r_{mn}{}^{2(\gamma+1)}\times \\ \times\cos(1-\gamma)2\psi_{mn} + 4\gamma\chi r_{mn}{}^{4+\gamma}\cos\gamma\psi_{mn}\end{gathered}}}{\begin{gathered}(r^4{}_{mn} + \Omega_F{}^2 + 2\Omega_F r^2{}_{mn}\cos2\psi_{mn})(4r^2{}_{mn} + \gamma^2\chi^2 r_{mn}{}^{2(\gamma-1)} + \\ +4\gamma\chi r_{mn}{}^\gamma\cos(2-\gamma)\psi_{mn})\end{gathered}},$$

$$\chi_{mn}(s) = \int_0^\infty \frac{\lambda_0\tau_{mn}^\gamma s^{\gamma+1}(\sin(\gamma+1)\pi + \Omega_F\cdot\sin(\gamma-1)\pi)}{(s+\Omega_F)^2\left((s+\omega_{mn}^2)^2 + \lambda_0{}^2 s^{2\gamma}\tau_{mn}^{2\gamma} + 2(s+\omega_{mn}^2)\lambda_0\tau_{mn}^\gamma s^\gamma\cdot\cos\gamma\pi\right)} e^{-st}ds.$$

Substituting the generalized displacements $x_{mn}(t)$ determined by equations (24) and (28) in relation (5), it is possible to obtain the desired displacements of an elastic plate lying on a viscoelastic base using the Kelvin-Voigt model with a fractional derivative under free oscillations and under the influence of harmonic loading, respectively.

NUMERICAL EXAMPLE

All calculations were performed in the MathCad program for mathematical and engineering calculations.

For numerical calculations, the following characteristics were taken for the plate and the base: $E = 32500$ MPa for concrete B30, $\lambda_0^* = 3.454$ for the base from hard loam, the material of the plate is concrete B30, $\rho = 2430\ \frac{kg}{m^3}$, dimensions in the plan $a = 6$ m, $b = 6$ m, and height $h = 0.2$ m, Poisson's ratio $\nu = 0.25$; $\gamma = 0,\ 0.25,\ 0.5,\ 0.95$.

The external load varies according to the law $q = 10\delta(x - x_0)(y - y_0)\cos10t$ and is applied in the center of the plate, where $F = 10$, $\Omega_F = 10$, $x_0 = \frac{1}{2}, y_0 = \frac{1}{2}$.

Dynamic displacements $w(x, y, t)$ are shown in Figure 4 for the center of the plate $x = \frac{1}{2}, y = \frac{1}{2}$, considering 9 terms of the series, since for the middle of the plate with even modes, the eigenfunctions $W_{mn}(x, y)$ are zeroed. Figure 5 shows the deflection $w(x, y, t)$ at free vibrations for the point of the plate with coordinates $x = \frac{1}{3}, y = \frac{1}{3}$, with due account for 36 terms of the series.

Displacements $w(x, y, t)$ under force driven vibration s are shown in Figure 6 for the point of the plate with coordinates $x = \frac{1}{2}, y = \frac{1}{2}$ considering 9 terms of the series.

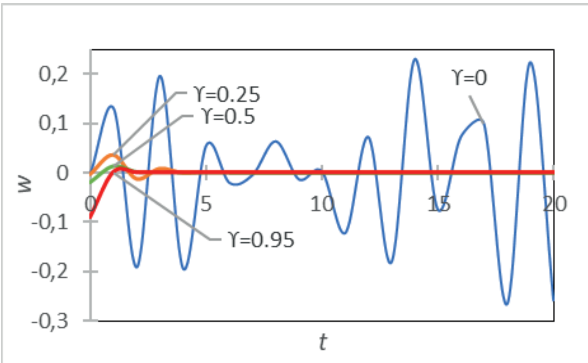

Figure 4. The time dependence of dimensionless displacements at free oscillations for a point of a plate with coordinates $x = \frac{1}{2}, y = \frac{1}{2}$

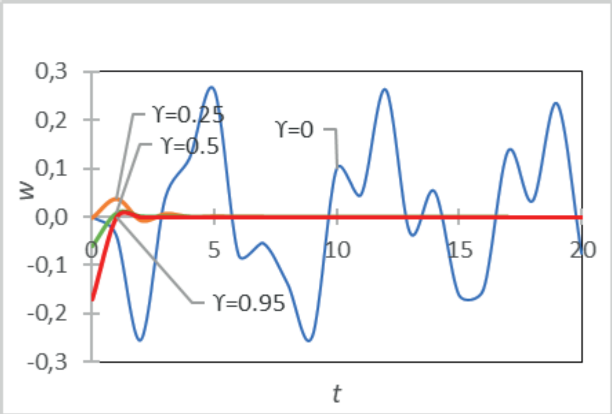

Figure 5. The time dependence of dimensionless displacements for free oscillations for a point of a plate with coordinates $x = \frac{1}{3}, y = \frac{1}{3}$

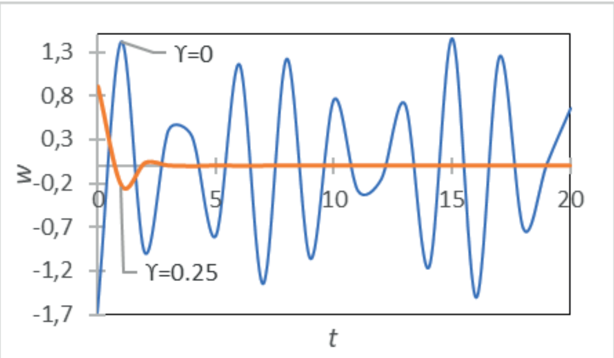

Figure 6. The time dependence of dimensionless displacements for forced oscillations for a point of a plate with coordinates $x = \frac{1}{2}, y = \frac{1}{2}$

CONCLUSION

This article presents an original method for solving the problem of non-stationary oscillations of linear elastic plates on a viscoelastic base, the properties of which are described by fractional derivatives.

The solution algorithm is based on the use of the integral Laplace transform with further decomposition of the desired functions into a series according to the eigenfunctions of the problem. However, in contrast to the traditional approach, when the rationalization of a characteristic equation with fractional powers is carried out during the transition from the frequency domain to the time domain, here the non-rationalized characteristic equation is solved by the method proposed in [10].

As a result of this approach, the solution is obtained as a sum of two terms, one of which controls the drift of the equilibrium position of the system and is determined by quasi-static creep processes occurring in the system, and the other term describes the attenuation of oscillation around the equilibrium position and is determined by the inertia and dissipation of the energy of the system [10, 18].

Modeling the vibrations of an elastic plate lying on a viscoelastic base using the fractional derivative Kelvin-Voigt model allows one to take the viscoelastic characteristics of the base into account and to obtain more accurate results. The findings of the research show that the oscillations depend on the parameters of the model and the foundation, which can be used to optimize the design of various devices and systems.

REFERENCES

1. **Younesian D., Hosseinkhani A., Askari H., Esmailzadeh E.** Elastic and viscoelastic foundations: a review on linear and nonlinear vibration modeling and applications // Nonlinear Dynamics, 2019, Vol. 97, pp. 853–895.
2. **Shitikova M.V., Krusser A.I.** Application of fractional calculus for modeling the dynamic behavior of structures under moving loads: a review // Radiophysics and Quantum Electronics, 2024, Vol. 67, № 5.
3. **Rossikhin Yu.A., Shitikova M.V.** Application of fractional calculus for dynamic problems of solid mechanics: Novel trends and recent results // Applied Mechanics Reviews, 2010, Vol. 63, № 1, Article ID 010801.
4. **Rossikhin Yu.A., Shitikova M.V.** Fractional calculus in structural mechanics / Handbook of Fractional Calculus with Applications. Vol. 7, Applications in

Engineering, Life and Social Sciences, Part A (edited by D. Baleanu and A.M. Lopes), Berlin: De Gruyter, 2019, pp. 159-192.

5. **Rossikhin Yu.A., Shitikova M.V.** Fractional calculus models in dynamic problems of viscoelasticity / Handbook of Fractional Calculus with Applications. Vol. 7, Applications in Engineering, Life and Social Sciences, Part A (edited by D. Baleanu and A.M. Lopes), Berlin: De Gruyter, 2019, pp. 139-158.
6. **Atanacković T.M., Pilipović S., Stanković B. Zorica D.** Fractional Calculus with Applications in Mechanics: Wave Propagation, Impact and Variational Principles. London: Wiley, 2014.
7. **Shitikova M.V.** Fractional operator viscoelastic models in dynamic problems of mechanics of solids: a review // Mechanics of Solids, 2022, Vol. 57, pp. 1–33.
8. **Shitikova M.V., Krusser A.I.** Models of viscoelastic materials: a review on historical development and formulation // Advanced Structured Materials, 2022, Vol. 175, P. 285-326.
9. **Krusser A.I., Shitikova M.V.** Numerical analysis of nonlinear vibrations of a plate on a viscoelastic foundation under the action of a moving oscillating load based on models with fractional derivatives // Journal of Samara State Technical University, Series Physical and Mathematical Sciences, 2022, Vol. 26, № 4, pp. 694-714.
10. **Rossikhin Yu.A., Shitikova M.V.** Analysis of damped vibrations of linear viscoelastic plates with damping modeled with fractional derivatives // Signal Processing, 2006, Vol. 86, № 10, pp. 2703-2711.
11. **Ingman D., Suzdalnitsky J.** Response of viscoelastic plate to impact // ASME Journal of Vibration and Acoustics, 2008, Vol. 130, PaperID 011010.
12. **Shitikova M.V.** Impact response of a viscoelastic plate made of a material with negative Poisson's ratio // Mechanics of Advanced Materials and Structures, 2023, Vol. 30, № 5, pp. 982-994.
13. **Teimouiri H., Faal R.T., Milani A.S.** Impact response of fractionally damped rectangular plates made of viscoelastic composite materials // Applied Mathematical Modelling, 2025, Vol. 137, PaperID 115678.
14. **Zhu H., Liu L., Ye X**. Response of a loaded rectangular plate on fractional derivative viscoelastic foundation // Journal of Basic Science and Engineering, 2011, Vol. 19, № 2, pp. 271-278.
15. **Zhang C., Zhu H., Shi B., Liu L.** Theoretical investigation of interaction between a rectangular plate and fractional viscoelastic foundation // Journal of Rock Mechanics and Geotechnical Engineering, 2014, Vol. 6, № 4, pp. 373-379.
16. **Song P., Wei P., Zhou X.** Vibration of rectangular plate on fractional order viscoelastic foundation subjected to standing and moving loads // Mechanics of Time-Dependent Materials, 2023, Vol. 28, № 2, pp. 541-561.
17. **Samko S., Kilbas A., Marichev O**. Fractional Integrals and Derivatives. Theory and Applications. Switzerland: Gordon and Breach Science Publishers, 1993.
18. **Rossikhin Yu.A., Shitikova M.V.**, Application of fractional derivatives to the analysis of damped vibrations of viscoelastic single mass systems // Acta Mechanica, 1997, Vol. 120, pp. 109–125.

СПИСОК ЛИТЕРАТУРЫ

1. **Younesian D., Hosseinkhani A., Askari H., Esmailzadeh E.** Elastic and viscoelastic foundations: a review on linear and nonlinear vibration modeling and applications // Nonlinear Dynamics, 2019, Vol. 97, pp. 853–895.
2. **Шитикова М.В., Круссер А.И.** Применение дробного исчисления при

моделировании динамического поведения конструкций под воздействием подвижных нагрузок: обзор // Известия вузов. Радиофизика, 2024, Т. 67, № 5. С. 439-456.
3. **Rossikhin Yu.A., Shitikova M.V**. Application of fractional calculus for dynamic problems of solid mechanics: Novel trends and recent results // Applied Mechanics Reviews, 2010, Vol. 63, № 1, Article ID 010801.
4. **Rossikhin Yu.A., Shitikova M.V.** Fractional calculus in structural mechanics / Handbook of Fractional Calculus with Applications. Vol. 7, Applications in Engineering, Life and Social Sciences, Part A (edited by D. Baleanu and A.M. Lopes), Berlin: De Gruyter, 2019, pp. 159-192.
5. **Rossikhin Yu.A., Shitikova M.V.** Fractional calculus models in dynamic problems of viscoelasticity / Handbook of Fractional Calculus with Applications. Vol. 7, Applications in Engineering, Life and Social Sciences, Part A (edited by D. Baleanu and A.M. Lopes), Berlin: De Gruyter, 2019, pp. 139-158.
6. **Atanacković T.M., Pilipović S., Stanković B. Zorica D.** Fractional Calculus with Applications in Mechanics: Wave Propagation, Impact and Variational Principles. London: Wiley, 2014.
7. **Шитикова М.В.** Обзор вязкоупругих моделей с операторами дробного порядка, используемых в динамических задачах механики твердого тела // Известия РАН. Механика твердого тела. 2022. № 1. С. 3-40.
8. **Shitikova M.V., Krusser A.I.** Models of viscoelastic materials: a review on historical development and formulation // Advanced Structured Materials, 2022, Vol. 175, P. 285-326.
9. **Круссер А.И., Шитикова М.В.** Численный анализ нелинейных колебаний пластины на вязкоупругом основании под действием подвижной осциллирующей нагрузки на основе моделей с дробными производными // Вестник Самарского государственного технического университета. Серия Физико-математические науки, 2022, Т. 26, № 4, С. 694-714.
10. **Rossikhin Yu.A., Shitikova M.V.** Analysis of damped vibrations of linear viscoelastic plates with damping modeled with fractional derivatives // Signal Processing, 2006, Vol. 86, № 10, pp. 2703-2711.
11. **Ingman D., Suzdalnitsky J.** Response of viscoelastic plate to impact // ASME Journal of Vibration and Acoustics, 2008, Vol. 130, PaperID 011010.
12. **Shitikova M.V.** Impact response of a viscoelastic plate made of a material with negative Poisson’s ratio // Mechanics of Advanced Materials and Structures, 2023, Vol. 30, № 5, pp. 982-994.
13. **Teimouiri H., Faal R.T., Milani A.S.** Impact response of fractionally damped rectangular plates made of viscoelastic composite materials // Applied Mathematical Modelling, 2025, Vol. 137, PaperID 115678.
14. **Zhu H., Liu L., Ye X**. Response of a loaded rectangular plate on fractional derivative viscoelastic foundation // Journal of Basic Science and Engineering, 2011, Vol. 19, № 2, pp. 271-278.
15. **Zhang C., Zhu H., Shi B., Liu L.** Theoretical investigation of interaction between a rectangular plate and fractional viscoelastic foundation // Journal of Rock Mechanics and Geotechnical Engineering, 2014, Vol. 6, № 4, pp. 373-379.
16. **Song P., Wei P., Zhou X.** Vibration of rectangular plate on fractional order viscoelastic foundation subjected to standing and moving loads // Mechanics of Time-Dependent Materials, 2023, Vol. 28, № 2, pp. 541-561.
17. **Самко, С.Г., Килбас, А.А., Маричев, О.И.** Интегралы и производные дробного порядка и некоторые их приложения. Минск: Наука и техника, 1987. 688 с.

18. **Rossikhin Yu.A., Shitikova M.V.**, Application of fractional derivatives to the analysis of damped vibrations of viscoelastic single mass systems // Acta Mechanica, 1997, Vol. 120, pp. 109–125.

Marina V. Shitikova, Prof., Dr.Sc., Head of the Department of High Mathematics, Moscow State University of Civil Engineering; Yaroslavskoe shosse 26, Moscow, 129337, Russia; E-mail: mvs@cchgeu.ru; ORCID: 0000-0003-2186-1881.

Шитикова Марина Вячеславовна, профессор, доктор физико-математических наук; заведующая кафедрой Высшей математики, Научный исследовательский Московский государственный строительный университет; 129337, Россия, г. Москва, Ярославское шоссе, д. 26, E-mail: mvs@cchgeu.ru; ORCID: 0000-0003-2186-1881.

Anastasiya S. Kornilova, Senior Lecturer of the Department of Structural and Theoretical Mechanics, Moscow State University of Civil Engineering, Moscow; Yaroslavskoe shosse 26, Moscow, 129337, Russia; E-mail: zkstasy@gmail.com; ORCID: 0000-0002-0250-4910.

Корнилова Анастасия Сергеевна, старший преподаватель кафедры Строительной и теоретической механики, Научный исследовательский Московский государственный строительный университет; E-mail: zkstasy@gmail.com; ORCID: 0000-0002-0250-4910.

EXPERIMENTAL SUBSTANTIATION OF CONSTANTS IN THE MATHEMATICAL MODEL OF CONCRETE IN STRUCTURES MADE BY 3D PRINTING TECHNOLOGY

Oleg V. Kabantsev, Alexey V. Karlin

National Research University Moscow State Construction University of Civil Engineering, Moscow, RUSSIA

Abstract*:* The paper presents the results of the study of concrete fracture mechanisms in structures made by 3D printing technology using the layer-by-layer extrusion method. It is established that concrete fractures in such structures occur by fundamentally different mechanisms - cohesion and adhesion fracture mechanisms. The type of fracture mechanism is determined by the load direction relative to the direction of concrete extrusion layers. The compressive strength of concrete and the corresponding basic constant (compressive strength of concrete - R_b) is determined, in general, by the cohesive fracture mechanism. But when loaded parallel to the extrusion layers, the influence of the adhesion mechanism of fracture on the overall value of the key constant of the concrete model has been established. Fracture of concrete in structures made by 3D-printing technology by layer-by-layer extrusion is determined by the direction of loading relative to the direction of concrete extrusion layers. Under loading perpendicular to the extrusion layers (direction of tensile stresses is parallel to the extrusion layers), failure occurs by cohesive mechanism. The value of concrete tensile strength (R_{bt}) corresponding to the cohesive fracture mechanism can be used as a key constant of the mathematical model of concrete. When loading parallel to the extrusion layers (direction of tensile stresses is perpendicular to the extrusion layers), the failure occurs by the adhesion mechanism. As a key constant of the mathematical model of concrete can be used the value of adhesive strength of interaction of layers (R_{adh}), corresponding to the adhesive mechanism of fracture. The presented experimentally substantiated key constants of the mathematical model of concrete provide adaptation of such a model for concrete in structures made by layer-by-layer extrusion.

Keywords: 3D Concrete Printing (3DCP), Mechanical Properties, Anisotropy, Orthotropic Material, Stress-Strain Diagram, Mechanisms of destruction

ЭКСПЕРИМЕНТАЛЬНОЕ ОБОСНОВАНИЕ КОНСТАНТ МАТЕМАТИЧЕСКОЙ МОДЕЛИ БЕТОНА В КОНСТРУКЦИЯХ, ВЫПОЛНЕННЫХ ПО ТЕХНОЛОГИИ 3D-ПЕЧАТИ

О.В. Кабанцев, А.В. Карлин

Национальный исследовательский Московский государственный строительный университет, г. Москва, РОССИЯ

Аннотация: В статье представлены результаты исследования механизмов разрушения бетона в конструкциях, выполненных по технологии 3D-печати методом послойной экструзии. Установлено, что разрушения бетона в таких конструкциях происходят по принципиально различным механизмам – когезионный и адгезионный механизмы разрушения. Вид механизма разрушения определяется направлением нагрузки относительно направления слоев экструзии бетона. Прочность бетона на сжатие и соответствующая базовая константа (прочность бетона на сжатие – R_b) определяется, в целом, когезионным механизмом разрушения. Но при нагружении параллельно слоям экструзии установлено влияние адгезионного механизма разрушения на общую величину ключевой константы модели бетона. Разрушение бетона в конструкциях, выполненных по технологии 3D-печати методом послойной экструзии, определяется направлением нагружения относительно направления слоев экструзии бетона. При нагружении перпендикулярно слоям экструзии (направление растягивающих напряжений параллельно слоям экструзии) разрушение происходит по когезионному механизму. В качестве ключевой константы математической модели бетона может быть использована величина прочности бетона на растяжение (R_{bt}), соответствующая когезионному механизму разрушения. При нагружении параллельно слоям экструзии (направление растягивающих напряжений перпендикулярно слоям экструзии) разрушение происходит по адгезионному механизму. В качестве ключевой константы математической модели бетона может быть использована величина адгезионной прочности взаимодействия слоев (R_{adh}), соответствующая адгезионному механизму разрушения. Представленные экспериментально обоснованные ключевые константы математической модели бетона обеспечивают адаптацию такой модели для бетона в конструкциях, изготовленных методом послойной экструзии.

Ключевые слова: технология 3D-печати бетоном (3DCP), механические характеристики, анизотропия механических характеристик, ортотропная модель бетона, диаграмма «напряжения-деформации, механизмы разрушения

1. INTRODUCTION

3D Concrete Printing (3DCP - 3D Concrete Printing) is one of the most promising technological trends, which is part of a vast group of additive technologies, providing increased efficiency of work on the construction of building structures. Additive technologies provide the implementation of the principles of digital approach to construction: on the basis of a 3-dimensional digital model of structures of the bearing system of the building a program of the printer is created. Under the control of such a program the printer layer by layer forms structures using 3D concrete printing technology. The technology of 3D concrete printing provides the possibility of transition to mass construction of houses according to individual designs developed in digital technologies. Thus, 3DCP technology is a modern industrial approach with the production of the necessary structure directly at the place of its further use. In this case, the known limitations on the diversity of architectural appearance of construction objects are removed, which is ensured by the use of individual digital projects of houses built using standard standard standard technology. Construction production based on digital principles realizes the task of digital transformation of the construction industry as a whole and ensures the growth of labor productivity in construction [1-4].

The obvious prospects of 3DCP-technology application in the construction industry are recognized in many countries. Saudi Arabia has adopted a program for the construction of housing with the mass application of 3DCP technology [5]. In the UK, the National Additive Manufacturing Strategy program [6] evaluated the possibility of creating marketable products in the volume of the country's GDP up to 1 billion dollars and creating up to 15,000 jobs in the construction industry. A group of industrial ministries in the People's Republic of China has developed an initiative [7-8] to support industrialized construction methods, including 3DCP technologies, as the main direction for the development of the construction industry.

The possibility of practical realization of 3DCP technology is provided by the achievements of construction science in several main directions: the development of methods and technologies of layer-by-layer structure formation with various effective extrusion mechanisms [9-13]; the development of new types of concrete mixtures with specified characteristics that allow layer-by-layer formation of a structure that retains its shape until the moment of strength gain [14-16]. At present, two directions of realization of the method of 3D printing with concrete using the technology of layer-by-layer horizontal extrusion are actively developing: Direct Digital Fabrication of Concrete (DDFC) / Direct Digital Fabrication of Concrete Structures/ and Digital Fabrication of Formworks (DFF) / Digital Fabrication of Formwork/.

The DDFC direction allows, on the basis of the general technological process of 3D printing with concrete, to realize the production of concrete structures of various shapes in conditions of limited possibilities of using reinforcement elements. The DDFC direction can be very effective in the production of small-scale and individual structures, in the operational modes of which there are no significant tensile or shear forces. Such limitations are determined by the current state of 3D concrete printing technology, in the framework of which the installation of reinforcing elements in the body of the structure to absorb tensile forces is quite complicated, and the technology of installation of reinforcing elements is a foreign (in relation to the 3DCP concrete technology) process. The actual practice of DDFC direction implementation shows that the installation of reinforcement elements into the body of a structure is possible with human intervention in the highly mechanized technology of 3D printing with concrete or in the conditions of using additional equipment [17].

The currently known problems in the field of practical application of 3D concrete printing technology are not critical for manufacturing building structures using the new innovative technology. The characteristics of masonry structures are quite similar, as masonry made of piece materials (bricks, large-sized artificial stones) on masonry mortar is a layered structure with minimal opportunities for installing interlayer reinforcement. But the characteristics of masonry do not prevent the widespread use of masonry structures in construction.

The most significant factor that ensures the wide application of a particular technology in the construction industry, including 3D concrete printing technology, is the availability of methods that allow you to justify the strength, reliability and level of deformability of designed structures by calculation. Such calculation methods are based on a scientifically substantiated model of the material forming the structure and realizing strength properties as part of this structure. The latter circumstance is very important, as the model should correctly reflect the realization of mechanical characteristics of the material, which are formed not only in the frames of local volumes of such material, but also in the conditions of interaction of local volumes in the total volume of the structure. Such local volumes of the material can be formed due to the peculiarities of the manufacturing technology of the structure.

The analysis of 3DCP technology shows that the structure obtained by layer-by-layer extrusion of concrete has significant differences from the traditional technology of manufacturing structures by monolithic concreting technology. The traditional technology of manufacturing of reinforced concrete structures, which includes the procedure of concrete mixture compaction, provides the formation of a sufficiently homogeneous concrete body of the structure with minimal amounts of leaks. The most important quality control procedures in the traditional monolithic concreting technology is the control of concrete mixture homogeneity. Concrete homogeneity ensures the realization of interaction of concrete mixture particles throughout the entire volume of the structure. According to [18], concrete obtained by conventional technology is a composite material consisting of binder particles, aggregate particles of different size and transition zone of interaction between particles, modeled by a set of elastic bonds. In general, the model of interaction of concrete particles in a structure made by traditional technology with concrete compaction procedures is presented in Fig. 2. The homogeneity of the concrete mixture makes it possible to use the characteristics of concrete strength and deformability corresponding to the model of a homogeneous deformable body in the design justification.

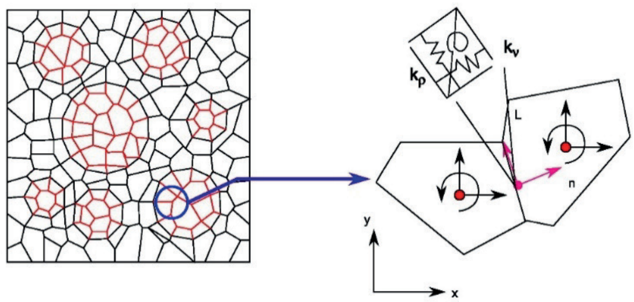

Figure 1. Principle model of interaction of concrete particles in a structure made with the procedure of concrete mixture compaction (by [18])

Contrary to concrete in a structure made by traditional technology with concrete compaction throughout the entire volume of the structure, concrete in a structure made by 3D-printed concrete by layer-by-layer horizontal extrusion has natural zones of concrete layers of a given thickness, each of which is produced separately from other layers with a gap in the time of production. In this way, a layered structure of concrete is technologically formed, and each layer has a mechanism of contact interaction with other layers. Since freshly placed concrete has adhesive properties due to the presence of binder, the interaction of layers is realized by adhesive mechanism (Fig. 2).

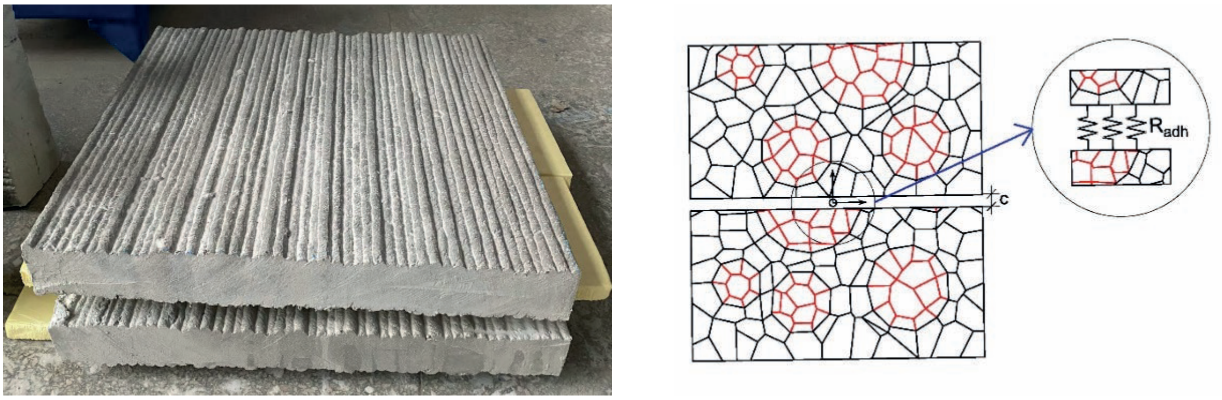

(a) *(b)*

Figure 2. Principle model of interaction of local elements of the structure made layer-by-layer by 3DCP technology; a - appearance of the structure at single-row concrete extrusion; b - model of interaction of local elements of the structure; c - zone of contact interaction of local elements of the structure

Differences in the structure of concrete in structures made by the technology of traditional forming of the monolithic concrete body of the structure in comparison with structures made by 3DCP technology have been investigated by many authors, but, in general, this direction is at the initial stage of development.

In [19] the issues of concrete mixes formulation peculiarities suitable for 3DCP method of structural fabrication are investigated. In [20] the influence of 3DCP-technology on changes in the mechanical characteristics of concrete under compression conditions is studied. The issues of variability of mechanical characteristics of concrete in structures made using the 3DCP method are considered in [21-23].

A number of studies have investigated the manifestation of anisotropy properties in concrete, the volume of which is made using 3DCP technology by layer-by-layer extrusion. The results of such studies confirm: concrete in a structure made by 3D printing technology realizes a pronounced anisotropy effect. In [24] the results of the study of the influence of 3DCP-method on the formation of the anisotropy effect of concrete strength characteristics are presented. The results of the study show that the average axial compressive strength of the samples drilled from the massif made by 3D printing technology is 15-27% lower than that of the samples drilled from the massif made by the traditional technology of monolithic concreting. The data on the measured densities of different zones of concrete of the array made by 3D-printing technology are also given. It is shown that 3DCP technology forms the concrete body of the structure with a significantly lower compaction relative to the same indicator of concrete of structures made using traditional technology. In [25], the influence of the layered structure and imperfections in the geometry of the structure, determined by the peculiarities of 3DCP technology, which influence the premature failure of the structure in the manufacturing process, was investigated. In [26, 27], the mechanical properties of concrete at an early age are investigated, which allows predicting the behavior of the structure in the mode of fabrication using 3D printing technology. In [28], a method of modeling concrete deformation in the process of structure fabrication is proposed. The standard method of modeling of the construction with additional functions of activation of layers of the manufactured structure was used, which allows to correct the geometry of the model. In [29] it is noted: in structures made by 3DCP technology, in the process of extrusion in the layer of concrete can be formed zones of looseness, and in some cases - breaks in the body of the concrete layer, which has a negative impact on the cohesion (monolithicity) of the concrete in the structure.

In [30, 31] it was established: the layered structure of concrete in structures made by 3DCP technology with layer-by-layer extrusion of concrete forms a special type of concrete, the mechanical characteristics of which have a pronounced anisotropy, which is a fundamental difference from traditional cast-in-place concrete with compaction of the mixture in the formwork (the mechanical characteristics of traditional concrete are recognized as isotropic).

The reason for the anisotropy of mechanical properties of 3DCP concretes according to [32, 33] is the weak bonds of extruded concrete layers. It is quite obvious that the direction of bond failure between the layers corresponds to the extrusion trajectory of the layers, and this, in turn, determines the anisotropy of the me-mechanical properties of concrete. Studies [34] have established that the anisotropy of 3DCP concrete properties can be correlated with mutually orthogonal directions: properties in the direction perpendicular to the extrusion layers and properties in the direction of the extrusion layers.

Thus, the fact of a significant difference between the mechanical characteristics of concrete in structures with the traditional technology of monolithic concreting with compaction of the mixture over the volume of the structure and the similar characteristics of concrete in structures made with the technology of 3D printing by layer-by-layer extrusion can be considered established and substantiated by scientific research.

However, it should be emphasized that neither academic reviews on the topic of 3DCP technology nor open publications provide information on the development/adaptation of a mathematical model of 3DCP-concretes, which would take into account the pronounced anisotropic properties of such concretes. Also there is no information about works on correction or improvement of methods of calculation of constructions made by 3DCP technology. The analysis of few published works on the subject of calculation analysis of structures made by 3D printing technology by layer extrusion method shows that traditional concrete models are used with minimal refinements of traditional constants values. Thus, [35] provides only a list of issues that need to be taken into account when calculating the strength of structures made by 3DCP technology, as well as directions for optimizing concrete structures made by layer-by-layer extrusion technology. In [36], a model of concrete structures made by 3DCP technology is proposed in the form of a brittle-plastic material model. The model uses the well-known orthotropic smeared crack model for tension (fracture) and a plasticity-based model for compression (plastic behavior). This material model is extended to take into account the temporal variability of its parameters. The interaction of layers was modeled by weaker (relative to concrete) interface elements. However, the failure of layered materials occurs by significantly different mechanisms (adhesion and cohesion), which must be taken into account in the layered material model. A similar approach was used in [37, 38], where the interaction of layers was modeled by special interfacial elements. For the conditions of the time interval corresponding to the fabrication of the structures, results close to the experimental results were obtained. For the conditions of concrete with design strength, the results of numerical studies have significant differences from the results of physical experiments, which indicates the need to improve the mathematical model of concrete as a layered material.

Thus, the analysis of open publications on the results of studies of mechanical characteristics of 3DCP-concretes made by the technology of layer-by-layer extrusion shows: mechanical characteristics of 3DCP-concretes have pronounced anisotropic properties, which determines the fundamental differences of such concretes from traditional cast concrete. It is obvious that anisotropy of mechanical properties is determined by various factors. The factor of looseness of the layered material, which was not subjected to compaction throughout the entire volume of structures, is an objective consequence of the technology of layer-by-layer extrusion. However, the most significant factor affecting the manifestation of anisotropic properties of concrete in structures made by 3DCP technology is the factor of layer interaction in a multilayer structure, which requires an experimental study to determine the mechanism of layer interaction and the mechanism of destruction of interlayer interaction. The results of the study will allow us to substantiate the characteristic characteristics of the key constants of the mathematical model of concrete in structures made by layer-by-layer extrusion using 3DCP technology.

2. MATERIALS AND METHODS

Concrete in structures made by traditional technology with concrete placement in the formwork of the structure and concrete compaction throughout the volume, which provides an acceptable level of uniformity of the material, is described by a well-known mathematical model, which is approved by the International Federation for Structural Concrete (FIB) and is used in the normative documents of many countries, computing systems, for example, [39], and is given in many publications.

In a generally accepted form, the model of traditional cast-in-place concrete for uniaxial compression-tension conditions is described in the stress-strain axes (“σ-ε”) is shown in Fig. 3.

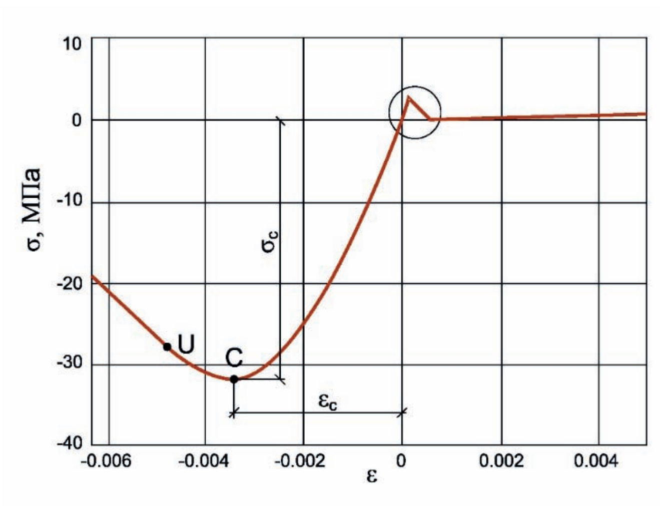

(a)

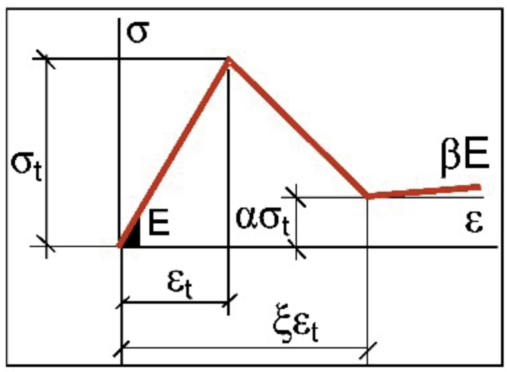

(b)

Figure 3. Diagrams “ σ-ε ” for concrete at traditional technology of structural performance: a - full diagram; b - fragment of the diagram for tensile conditions

The diagram is represented by the following ratios:

$$\sigma(\varepsilon)=\begin{cases} E\varepsilon, 0\le\varepsilon\le\varepsilon_t, \\ \alpha\sigma_t+\dfrac{(1-\alpha)E}{1-\xi}(\varepsilon-\xi\varepsilon_t), \varepsilon_t\le\varepsilon\le\xi\varepsilon_t, \xi>1, \\ \alpha\sigma_t+\beta E(\varepsilon-\xi\varepsilon_t), \varepsilon>\xi\varepsilon_t, \\ \dfrac{\frac{E}{E_r}\varepsilon_r\ \sigma_c}{1+A\varepsilon_r\ +B\varepsilon_r^2+C\varepsilon_r^3}, \varepsilon_r\le\varepsilon<0, \end{cases} \tag{1}$$

where the point C(ε_c, σ_c) corresponds to the compressive strength; the point U(ε_u, σ_u) is the limit point, and (according to FIB experts' recommendations) σ_u = 0,85ε_c; ε_u = 1,41ε_c. The other parameters correspond to [40]:

$$\begin{gathered} E_r=\frac{\sigma_c}{\varepsilon_c}, \varepsilon_r=\frac{\varepsilon}{\varepsilon_c}, E_u=\frac{\sigma_u}{\varepsilon_u}, p=\frac{\varepsilon_u}{\varepsilon_c}, \\ A=\frac{\frac{E}{E_u}+(p^3-2p^2)\frac{E}{E_r}-(2p^3-3p^2+1)}{p(p^2-2p+1)}, \\ B=2\frac{E}{E_r}-3-2A, C=2-\frac{E}{E_r}+A. \end{gathered} \tag{2}$$

The descending sections of the diagram simulate the strength reduction during crack formation and opening. The parameter ξ determines the length of the descending section of the diagram, while the parameters α and β determine the residual strength of concrete and secondary strengthening.

The diagram shown in Fig. 3, is based on well known mechanisms of deformation and fracture of concrete under uniaxial stress state, uses natural characteristics of strength and deformability of concrete and allows correct modeling of concrete performance in a structure made by traditional technology with the formation of a monolithic structure of concrete in the structure.

The deformation theory of plasticity of concrete, which is widely used in mathematical modeling of concrete, is based on the following provisions:

- elastic volume change:

$$\Theta = 3K\sigma, \tag{3}$$

where $\Theta = \sigma_x + \sigma_y + \sigma_z$; $\sigma = (\sigma_1 + \sigma_2 + \sigma_3)/3$; $K = (1 - 2\nu)/E$; Θ – volume expansion; σ – average pressure; E – initial strain modulus; ν – Poisson's ratio;

- stress and strain deviators are proportional to:

$$\mathbf{D}_\sigma = 2G'(\mathbf{D}_\varepsilon - \mathbf{D}_\varepsilon^A), \tag{4}$$

where $\mathbf{D}_\sigma$, $\mathbf{D}_\varepsilon$ - stress and strain deviators; $\mathbf{D}_\varepsilon^A$ – residual strain deviator; G’ = σ_e / (3 ε_e) – shear modulus; σ_e, ε_e – reduced stresses and strains;

- elastic relief:

$$\mathbf{D}_\sigma = \mathbf{2}G'\mathbf{D}_\varepsilon^P - \mathbf{2}G(\mathbf{D}_\varepsilon - \mathbf{D}_\varepsilon^A), \tag{5}$$

where индекс P – plot point σ_e – ε_e (Fig. 4), corresponding to the beginning of unloading; $G = E / (2(1 + \nu))$ – elastic shear modulus.

In the framework of the deformation theory of plasticity of concrete, let us consider the case shown in Fig. 4, when the deformation process starts in the tensile zone of concrete and active loading is carried out along the *OP* trajectory (described in detail in [41, 42]).

According to [41, 42], at the loading step, at each subsequent time instant the reduced strain exceeds its value at the previous time instant:

$\varepsilon_e^{i+1} > \varepsilon_e^{i}$, where i is the conditional number of the moment (step) of the analysis. If the analysis at the considered step demonstrates $\varepsilon_e > \varepsilon_e^P$, the loading process continues. In the case where $\varepsilon_e \leq \varepsilon_e^P$, elastic unloading occurs, which corresponds to equation (5).

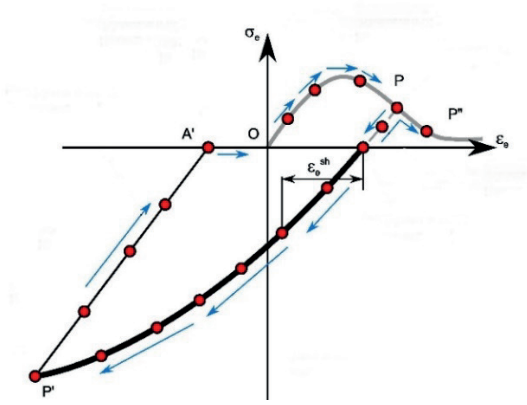

Figure 4. Unsymmetrical "σ-ε" diagram for concrete

The analysis of the considered situation shows that the mathematical model of concrete, developed for the traditional technology of manufacturing of structures, corresponds to the conditions of realization of the elastic unloading phase in the mode of tensile stresses. The realization of the elastic unloading phase is ensured by the homogeneous structure of concrete throughout the entire volume of the structure under cohesion failure conditions.

The cohesive mechanism of tensile fracture adopted in the traditional mathematical model of concrete is substantiated by numerous experimental studies and corresponds to a key constant in the form of concrete tensile strength (R_{bt}). A number of methods for modeling the process of crack development in monolithic concrete, including the method of distributed ("smeared") cracks, have been developed based on the use of this constant (R_{bt}).

The 3DCP technology of layer-by-layer horizontal concrete extrusion has fundamental differences from the traditional technology, which is that the volume of concrete in the structure is formed layer by layer. The concrete structure made by the method of layer-by-layer concrete extrusion consists of concrete layers formed during the passage of the extrusion head of the 3D printer, and contact zones of such layers (Fig. 5). The concrete of the layers is heterogeneous (Fig. 5b): the main part of the layer volume (estimated up to 80%) has a structure close to the traditional concrete structure; the volume of concrete forming the outer part of the layer (estimated up to 20%) has a more loose structure with increased porosity, which is confirmed by studies [21]. The interaction of concrete layers is determined by the mechanism of adhesion of layers with a certain level of adhesion strength (R_{adh}), which is determined by the composition of concrete mixtures including binders, such as cement. In general, at the micro level, the assumed scheme of interaction of structural elements (layers) is presented in Fig. 5c, which requires experimental confirmation.

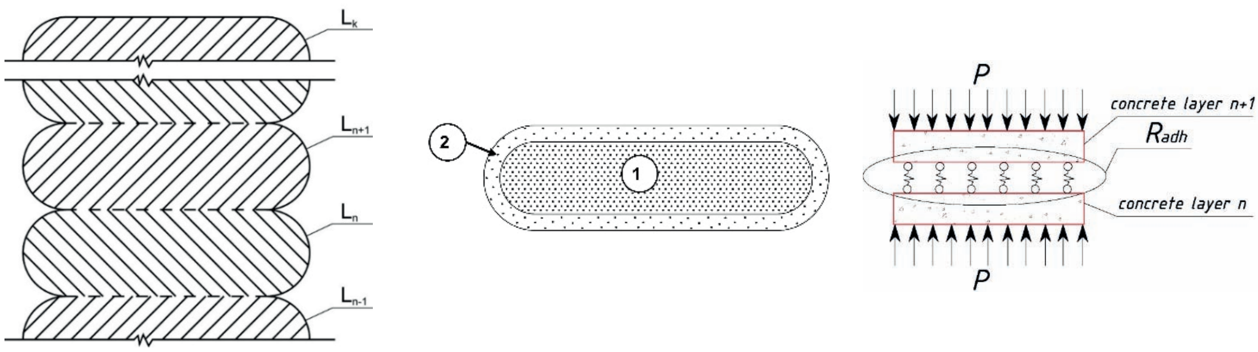

(a) (b) (c)

Figure 5. Peculiarities of the structure of the concrete structure made by the technology of layer-by-layer extrusion of concrete: a) - scheme of layers of the structure (L_i - layers of concrete); b) - scheme of the layer structure (1 - central area of the layer; 2 - outer area of the layer); c) - assumed scheme of interaction of the layers of the structure

Taking into account these features of concrete structure in the structure made by layer-by-layer extrusion by 3DCP-method, the model of concrete of such a structure, including basic constants based on cohesive fracture mechanism, should be adapted to the fabrication technology on the basis of taking into account the actual characteristics and fracture mechanisms that are realized by concrete. Thus, to substantiate the parameters of the adapted model of concrete, correctly reflecting the specific features and influence of the manufacturing technology, it is necessary to perform experimental studies to determine the mechanisms of fracture and mechanical characteristics of concrete in the structure made by the method of layer-by-layer horizontal concrete ex-trusion.

For experimental studies of concrete compressive strength (R_b), fragments of the structure made by layer-by-layer extrusion by 3DCP method (Fig. 6a) and control specimens made by traditional technology (Fig. 6b) were made.

Fragments of the structure for 3DCP-concrete samples were made by layer-by-layer extrusion using a 3D printer with an extrusion head, which provides the formation of a layer of concrete with a width of 50 mm and a thickness of 20 mm. The structure for making 3DCP-concrete specimens is a rectangular slab of 200x200 mm size with a thickness of 100 mm (Fig. 6a). Multilayer 3D printing was applied in the fabrication of the fragments. For 3DCP-concrete samples, a special mixture for 3D printing produced by the building materials industry of the Russian Federation was used. Control samples were made of this mixture using the traditional technology, including concrete compaction in the formwork.

Cylinder specimens with a diameter of 70 mm (Fig. 6c) were selected from the fragments of structures for testing. From the fragments of the structure made by layer-by-layer extrusion using the 3DCP method, cylinder specimens were selected by drilling parallel and perpendicular to the layers of extrusion.

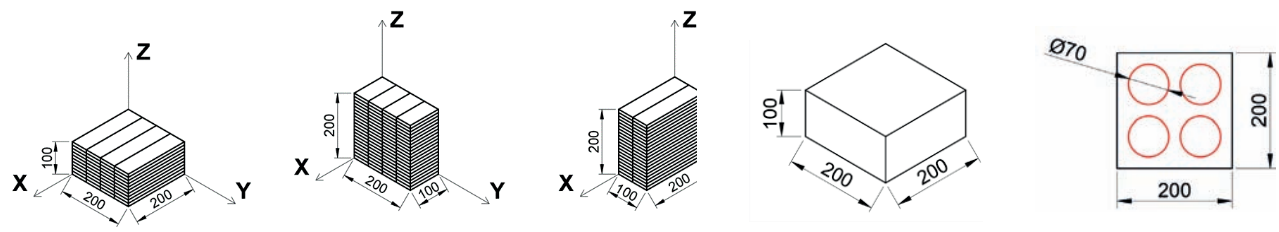

(a) (b) (c)

Figure 6. Geometric dimensions of concrete fragments for determining the compressive strength of concrete (R_b) a - samples made of fragments by the method of layer-by-layer horizontal extrusion of concrete; b - samples made by the traditional technology with compaction of concrete mixture; c - scheme of drilling out cylinder samples from concrete fragments for determining the compressive strength of concrete (R_b)

Compression testing of the specimens was performed according to the method recommended by FIB on a laboratory press machine MEGA 6-3000-100 (Form+Test, Germany) with a maximum compression force of 3000 kN. The loading of the specimen was carried out at a constant rate of 0.6 MPa/s.

For testing, the specimen ends were machined to obtain a plane perpendicular to the longitudinal axis of the specimens. Before the tests the specimens were prepared to standard humidity (55%). The tests were carried out within 30-36 days after fabrication of fragments for 3DCP-concrete specimens and control specimens.

The values of compressive strength were determined by loading the specimen-cylinders with compressive loads in the press equipment (Fig. 7).

(a) *(b)*

<u>Figure 7.</u> *Test of cylinder specimens for determining the compressive strength of concrete (R_b) a - test with loading perpendicular to the extrusion layers; b - test with loading parallel to the extrusion layers*

For experimental investigations of concrete tensile strength (R_{bt}), beam specimens of two types of sizes (*bxhxl*) were fabricated (Fig. 8) using 3DCP technology: 100x100x400 mm (series 1); 150x150x600 mm (series 2). The control beam specimens with similar dimensions were manufactured using conventional technology with concrete mix compaction.
3DCP-concrete specimens were produced by layer-by-layer extrusion using a 3D printer with an extrusion head, which ensures the formation of a layer of concrete with a width of 50 mm and thickness of 20 mm. Multilayer 3D-printing was used in the fabrication of the fragments. For 3DCP-concrete samples a special mixture for 3D-printing, produced by the building materials industry of the Russian Federation, was used. Control samples were made of this mixture according to the traditional technology, including concrete compaction in the formwork.

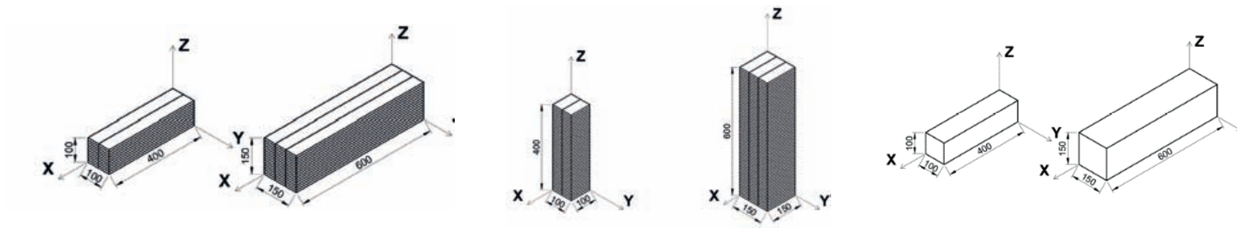

(a) *(b)* *(c)*

<u>Figure 8.</u> *Geometric dimensions of concrete fragments for determining the tensile strength of concrete (R_{bt}), made fragments by layer-by-layer horizontal extrusion of concrete: a) - specimens for flexural tensile tests under loading perpendicular to the layers of the seal; b) - specimens for flexural tensile tests under loading parallel to the layers of the seal; c - control specimens made by traditional technology*

Flexural tensile testing of specimens was performed according to the method recommended by FIB on a laboratory press machine MEGA 6-3000-100 (Form+Test, Germany) with a maximum force of 100 kN. The loading of the specimen was carried out at a constant rate of 0.05 MPa/s.
Tensile strength (R_{bt}) testing of concrete specimens was performed on the press with loading at two points (Fig. 9).

(a) (b) (c)

Figure 9. Testing of concrete tensile strength (R_{bt}) specimens (a) specimens for flexural tensile tests when loaded perpendicular to the extrusion layers; (b) - specimens for flexural tensile tests when loaded parallel to the extrusion layers; (c) tests of control specimens

3. RESULTS AND DISCUSSION

The results of the concrete compressive strength (R_b) tests are presented in Table 1.

Table 1. Results of concrete compressive strength studies (R_b)

№	Type of characterization	Cylinder specimens made by 3DCP method in compression along the X-axis (parallel to the extrusion layers) / % of control values	Cylinder specimens made by 3DCP method in compression along the Y-axis (perpendicular to the extrusion layers) / % of control values	Control samples
1	Average value	17,0 / 68,8%	19,7/ 79,8%	24,7
2	RMS deviation	1,2	1,8	-
3	Coefficient of variation (%)	7,1	9,26	-

The analysis of the results of concrete compressive strength (R_b) studies demonstrates failures by traditional cohesive mechanisms. At the same time, the reduction of concrete strength characteristics by ≈20-30%, which is determined by the presence of the outer area of the concrete layer with higher porosity compared to the central area of the layer. To the greatest extent, the influence of the outer region of the concrete layer is realized when the specimen is loaded parallel to the extrusion layers: the tangential stresses destroying the specimen form cracks confined to the contact areas of the layers. The interaction of concrete layers is determined by a complex mechanism, including, among others, the adhesive interaction of layers subjected to tensile tangential stresses. It should be taken into account that the value of adhesive strength (R_{adh}) is significantly lower than the concrete tensile strength (R_{bt}), which corresponds to the cohesive failure mechanism. The combination of dissimilar fracture mechanisms (adhesive and cohesive) leads to a 31.2% decrease in the concrete compressive strength (R_b) when the specimen is loaded parallel to the extrusion layers in relation to the control specimens made of monolithic concrete.

The values of the coefficients of variation of the compression test results of the specimens indicate insignificant deviations from the average values of the test results, which correctly reflects the peculiarities of the structure of 3DCP-concretes for compression conditions.

The results of the concrete tensile strength (R_{bt}) tests are presented in Table 2.

Table 2. Results of tensile strength of concrete specimens (R_{bt})

№	Type of characteristic	Specimens for flexural tensile tests when loaded perpendicular to the extrusion layers / % of control specimen		Samples for flexural tensile tests when loaded parallel to the extrusion layers / % of reference sample		Beam test specimens for bending tensile tests	
		100×100×400 mm	150×150×600 mm	100×100×400 mm	150×150×600 mm	100×100×400 mm	150×150×600 mm
1	Average value	2,23 / 69,25	2,08 / 78,49	0,19 / 5,90	0,22 / 8,30	3.22	2,65
2	RMS deviation	0,32	0,25	0,12	0,11	0,22	0,29
3	Coefficient of variation (%)	14,45	11,89	-	53,16	6,70	10,88

The analysis of the results of concrete tensile strength (R_{bt}) studies demonstrates a pronounced anisotropy of the concrete structure material made by the technology of layer-by-layer extrusion.

Under the action of external loads perpendicular to the layers of extrusion (direction of tensile stresses is parallel to the extrusion layers), the destruction of samples by cohesive mechanism is observed. The reduction of concrete strength characteristics by ≈20-30% was recorded. The magnitude of strength reduction depends on the size of experimental samples and is determined by the presence of the outer area of the concrete layer with higher porosity in comparison with the central area of the layer and, accordingly, the reduced strength of the concrete of the outer area. The presence of the concrete area with reduced density leads to a decrease in the resistance of the compression zone of the experimental specimen, which determines the reduction of the failure load level and, consequently, to a decrease in the tensile strength of concrete (R_{bt}).

At action of external loads parallel to layers of extrusion (direction of tensile stresses is perpendicular to the extrusion layers) the destruction of samples on adhesive mechanism is observed - destruction occurs on planes of contact of layers without presence of damages of a surface of concrete of layers in a zone of the destroyed contact. At the same time, a multiple (≈90-95%) decrease in the tensile strength of the specimen was recorded.

Such a significant reduction of mechanical characteristics is determined by a fundamentally different structure of concrete in the structure: concrete has a pronounced layered structure. The layers of the structure are made with a break in time and (in the absence of special structural measures) interact by the mechanism of adhesion. Under the conditions of tensile stresses per-perpendicular to the layers of extrusion, destruction is realized by the weakest mechanism of mutual interaction of concrete elements of the structure - by the mechanism of destruction of adhesive interaction of layers with adhesive strength (R_{adh}), the value of which is many times lower than the tensile strength of concrete (R_{bt}), corresponding to monolithic compacted concrete.

An important feature of the fracture mechanism of adhesive interaction is its brittle character: the unloading phase is practically absent, fracture occurs within a short time. For detailed studies of the unloading phase with adhesive fracture mechanism, it is necessary to perform additional studies.

The values of the coefficients of variation of the tensile test results indicate acceptable deviations from the average values of the test results when loading perpendicular to the extrusion layers. For loading conditions along the extrusion layers, the values of variation coefficients show high heterogeneity of the results, which corresponds to the high variability of the key indicator of monolithicity of the tested structure - adhesion strength of contact interaction between the layers (R_{adh}). The analysis of experimental results shows that the tests demonstrate fundamental differences in the mechanical characteristics of 3DCP-concretes from the analogous parameters of traditional cast-in-place concrete.

Thus, when external loads are applied perpendicularly to the extrusion layers (direction of tensile stresses is parallel to the extrusion layers), the specimen fracture is realized by the mechanism of cohesive failure of concrete of extrusion layers with reduced tensile strength (R_{bt}). When external loads are applied parallel to the extrusion layers (direction of tensile stresses is perpendicular to the extrusion layers), the specimen fracture is realized by the mechanism of adhesive interaction failure of layers with adhesive strength (R_{adh}). Such different fracture mechanisms determine a pronounced anisotropy of the material of the concrete structure made by the technology of layer-by-layer extrusion. The presence of different fracture mechanisms should be taken into account in the mathematical model of concrete: for the conditions of loading parallel to the extrusion layers, the value of adhesive strength (R_{adh}) should be used as a key constant of the model.

The analysis of the experimental results shows that in compression mode the deformation of the samples qualitatively coincides with the known diagrams of concrete deformations of structures made by traditional technology. The diagrams of deformation diagrams of concrete structures made by 3D-printing technology are similar to the traditional diagrams of concrete deformation. As a key constant of the mathematical model of concrete can be used the value of concrete compressive strength (R_b), corresponding to the cohesive failure mechanism, but corrected on the basis of experimental studies, corresponding to the type of construction made by 3D-printing technology. Differences are observed only in the value of ultimate compression stresses (σ_c) corresponding to the point C(ε_c,σ_c) and some difference in the value of ε_c. To determine more precisely the differences in the limit values of relative strains (ε_c), it is necessary to conduct additional studies. In view of the above, it seems reasonable to adopt the scheme of the diagram "σ-ε" in the compression mode of concrete structures made by 3D-printing technology similar to the scheme of deformation of concrete structures made by traditional technology (the proposals are presented in Fig. 10).

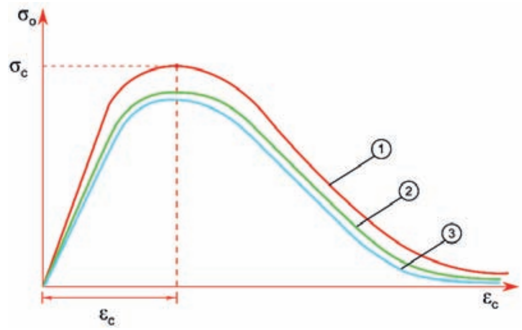

Figure 10. Fragment of the diagram of the "σ-ε" diagram for concrete in compression mode: 1 - concrete in structures made by traditional technology; 2 - concrete in structures made by 3D-printing technology (compression perpendicular to the printing layers); 3 - concrete in structures made by 3D-printing technology (compression parallel to the printing layers)

The analysis of experimental results shows that the deformation of specimens in the tensile mode has significant differences.

When the specimens are loaded perpendicularly to the extrusion layers (direction of tensile stresses is parallel to the extrusion layers), the deformation of the specimens coincides qualitatively with the known diagrams of concrete diagrams of structures made by traditional technology. The coincidence of deformation diagrams is determined by the same cohesive failure mechanisms. As a key constant of the mathematical model of concrete can be used the value of concrete tensile strength (R_{bt}), corresponding to the cohesive fracture mechanism, but corrected on the basis of experimental studies, corresponding to the type of structure made by 3D printing technology. The diagrams of concrete deformation diagrams of the 3D-printed structure are similar to the traditional concrete deformation diagrams. Differences are observed only in the value of ultimate compressive stresses (σ_0) and some difference in the value of ultimate relative strains (ε_t). For more precise determination of differences in the limit values of relative strains (ε_t) it is necessary to carry out additional studies. In view of the above, it is reasonable to consider the scheme of the σ-ε diagram in the tensile mode of concrete structures made by 3D-printing technology under loading perpendicular to the extrusion layers to be similar to the scheme of deformation of concrete structures made by traditional technology (the proposals are presented in Fig. 11, line 2).

When the specimens are loaded parallel to the extrusion layers (direction of tensile stresses is perpendicular to the extrusion layers), the deformation of the specimens has a prin- tially different character. This is determined by adhesive mechanisms of specimen fracture with the destruction of adhesive interaction between the layers. As a key constant of the mathematical model of concrete should be used the value of adhesion strength of contact interaction of layers (R_{adh}), corresponding to the adhesion failure mechanism Adhesion strength (R_{adh}) is many times lower than the tensile strength of concrete (R_{bt}), which limits the tensile strength of the specimen to the value of adhesion strength. The adhesive failure is brittle in nature (Fig. 12, line 3) and the angle of inclination of the unloading line to the vertical (α) tends to 0. The value of the limit value of relative strain in the adhesive fracture mechanism ($\varepsilon_{t,adh}$) is significantly lower than the analogous value for concrete in structures made by conventional technology (ε_t). To determine the exact values of α and $\varepsilon_{t,adh}$ it is necessary to perform additional studies.

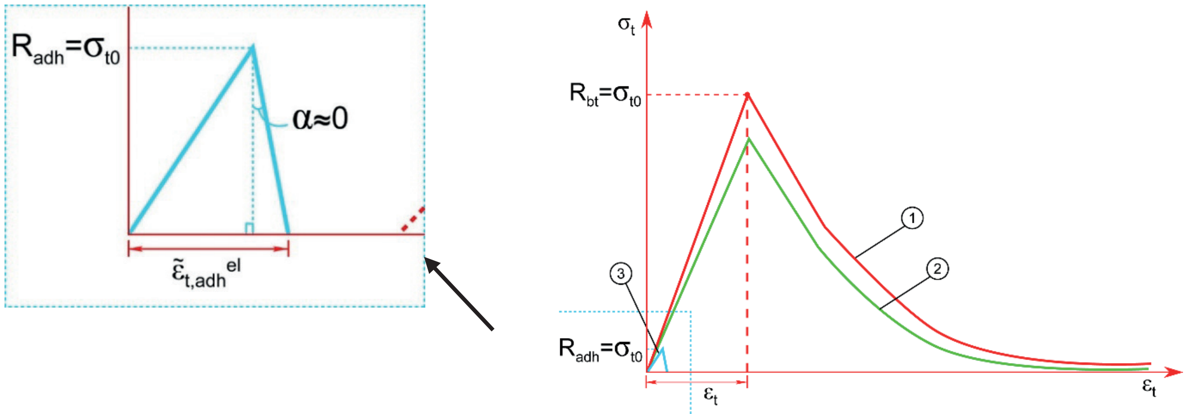

Figure 11. Fragment of the diagram of σ-ε diagram for concrete in the tensile mode: 1 - concrete in structures made by traditional technology; 2 - concrete in structures made by 3D-printing technology (stretching along the printing layers); 3 - concrete in structures made by 3D-printing technology (stretching perpendicular to the printing layers)

The presented stress-strain dependence (“σ-ε”) for 3DCP-concretes has prin- cipal differences from similar dependences for traditional cast-in-place concretes. First, the “σ-ε” dependence shows a pronounced anisotropy: the stress limits have significant differences for different directions (along the seal layers/perpendicular to the seal layers). Secondly, the mode of unloading is also fundamentally different: when tensile along the print layers, the concrete demonstrates a smooth mode of fracture, close to the fracture patterns of monolithic concrete made by traditional technologies. When stretching perpendicular to the seal layers, the unloading corresponds to the brittle fracture mechanism.

It should be emphasized that the currently used engineering methods of calculation of concrete and reinforced concrete structures, as well as methods of physically nonlinear calculation cannot realize such significant differences in mechanical characteristics in different directions of concrete in the structure. Traditional mathematical models of concrete, based on isotropic properties of concrete and cohesive failure mechanisms, do not allow to justify by calculation the level of bearing capacity and reliability of structures made of 3DCP-concrete, which essentially restrains the development of promising innovative technology. Consequently, the existing calculation methods need to be finalized and improved (on the basis of an adapted mathematical model of concrete for the conditions of structural fabrication by layer-by-layer extrusion, taking into account fundamentally different failure mechanisms), which will allow the use of such methods for calculations of structures made by 3D printing technology.

4. CONCLUSIONS

The analysis of the performed research allows us to formulate conclusions:
1. The structure of concrete in structures made by the method of layer-by-layer horizontal extrusion of concrete (3DCP) has a layered piecewise homogeneous structure, which forms fundamental differences from the structure of concrete in structures made by the traditional technology of cast-in-place concrete with compaction over the volume of the structure.
2. The results of experimental studies of concrete samples in structures made by the 3DCP method testify to the pronounced anisotropy of concrete properties of such a structure. In a simplified form (with limitations determined by the technology of layer-by-layer extrusion), it is acceptable to define concrete in structures made by the 3DCP method as a piecewise homogeneous layered orthotropic material having different values of mechanical characteristics along mutually orthogonal axes.
3. The results of the research substantiate that fractures in compression mode of concrete structures made by the 3DCP method occur by complex mechanisms. Under loading perpendicular to the extrusion layers, failure occurs by cohesive mechanism. When loading parallel to the extrusion layers, fracture is determined by a complex mechanism, including, among others, adhesive interaction of layers subjected to tensile tangential stresses. As a key constant of the mathematical model of concrete can be used the value of concrete compressive strength (R_b), corresponding to the cohesive mechanism of fracture, but corrected on the basis of experimental studies corresponding to the type of structure made by 3D printing technology. The scheme of "stress-strain" diagram ("σ-ε") in the compression mode of concrete of structures made by 3DCP method can be accepted as similar to the scheme of deformation of concrete of structures made by traditional technology.
4. The results of the research substantiate that tensile failure of concrete structures made by the 3DCP method under loading perpendicular to the extrusion layers (direction of tensile stresses is parallel to the extrusion layers) occurs by the cohesive mechanism. As a key constant of the mathematical model of concrete can be used the value of concrete tensile strength (R_{bt}), corresponding to the cohesive mechanism of failure, but corrected on the basis of experimental studies corresponding to the type of construction made by 3D printing technology. The stress-strain diagram ("σ-ε") in the tensile mode under loading perpendicular to the extrusion layers can be assumed to be similar to the deformation diagram of concrete structures made by traditional technology.
5. The results of the research substantiate that the fracture in the tensile mode under loading parallel to the extrusion layers (direction of tensile stresses is perpendicular to the extrusion layers) occurs by the adhesion mechanism. The value of adhesion strength of layer interaction (R_{adh}), corresponding to the adhesive mechanism of fracture, can be used as a key constant of the mathematical model of concrete. The stress-strain diagram ("σ-ε") in the tensile mode under loading parallel to the extrusion layers in the ascending section can be approximated by a straight line with a constraint determined by the value of the adhesion strength (R_{adh}). The adhesive failure has a brittle character and the angle of inclination of the unloading line to the vertical (α) tends to 0.

6. The presented experimentally substantiated key constants of the mathematical model of concrete provide adaptation of such a model for concrete in structures made by layer-by-layer extrusion. The proposed adapted mathematical model and new types of key constants serve as a basis for the development of engineering methods of calculation of structural elements made of 3DCP-concrete, as well as for the development of numerical methods of calculation of structures made of 3DCP-concrete in the finite element formulation taking into account the physical nonlinearity and anisotropy of the structural material. The creation of methods for the calculation of 3DCP-concrete structures will allow to remove restrictions on the mass application of 3DCP technology in the construction of buildings and structures.

FUNDING

The research was funded by the National Research Moscow State University of Civil Engineering (grant for fundamental and applied scientific research, project No. 25-392/130).

REFERENCES

1. **Hou, S.; Duan, Z.; Xiao, J.; Ye, J.** A Review of 3D Printed Concrete: Performance Requirements, Testing Measurements and Mix Design. Constr Build Mater 2021, 273, 121745, doi:10.1016/j.conbuildmat.2020.121745.
2. **Wangler, T.; Roussel, N.; Bos, F.P.; Salet, T.A.M.; Flatt, R.J.** Digital Concrete: A Review. Cem Concr Res 2019, 123, 105780, doi:10.1016/j.cemconres.2019.105780.
3. **Lu, B.; Weng, Y.; Li, M.; Qian, Y.; Leong, K.F.; Tan, M.J.; Qian, S.** A Systematical Review of 3D Printable Cementitious Materials. Constr Build Mater 2019, 207, 477–490, doi:10.1016/j.conbuildmat.2019.02.144.
4. **Lim, S.; Buswell, R.A.; Le, T.T.; Austin, S.A.; Gibb, A.G.F.; Thorpe, T.** Developments in Construction-Scale Additive Manufacturing Processes. Autom Constr 2012, 21, 262–268, doi:10.1016/j.autcon.2011.06.010.
5. A. News. https://www.arabnews.com/node/1554891/saudi-arabia. Accessed 2021/09/28.
6. **R. Laubier, M. Wunder, S. Witthoft, C.** Rothballer. https://www.bcg.com/publications/2018/will-3d-printing-remodel-construction-industry. Accessed 2021/10/28.
7. http://www.mohurd.gov.cn/index.html. Accessed 2021/8/31.
8. **G. Ma, L. Wang,** A critical review of preparation design and workability measurement of concrete material for largescale 3D printing, Front. Struct. Civ. Eng. 6 (2017) 1–19.
9. **Bos, F.; Wolfs, R.; Ahmed, Z.; Salet, T.** Additive Manufacturing of Concrete in Construction: Potentials and Challenges of 3D Concrete Printing. Virtual Phys Prototyp 2016, 11, 209–225, doi:10.1080/17452759.2016.1209.
10. **Tay, Y.W.D.; Panda, B.; Paul, S.C.; Noor Mohamed, N.A.; Tan, M.J.; Leong, K.F.** 3D Printing Trends in Building and Construction Industry: A Review. Virtual Phys Prototyp 2017, 12, 261–276, doi:10.1080/17452759.2017.1326724.
11. **Paul, S.C.; van Zijl, G.P.A.G.; Tan, M.J.; Gibson, I**. A Review of 3D Concrete Printing Systems and Materials Properties: Current Status and Future Research Prospects. Rapid Prototyp J 2018, 24, 784–798, doi:10.1108/RPJ-09-2016-0154.
12. **Paolini, A.; Kollmannsberger, S.; Rank, E.** Additive Manufacturing in Construction: A Review on Processes, Applications, and Digital Planning Methods. Addit Manuf 2019, 30, 100894, doi:10.1016/j.addma.2019.100894.
13. **Mohan, M.K.; Rahul, A.V.; De Schutter, G.; Van Tittelboom, K.** Extrusion-Based

Concrete 3D Printing from a Material Perspective: A State-of-the-Art Review. Cem Concr Compos 2021, 115, 103855, doi:10.1016/j.cemconcomp.2020.103855.

14. **A. Perrot, A. Pierre, V.N. Nerella, R.J.M. Wolfs, E. Keita, S.A.O. Nair, N. Neithalath, N. Roussel, V. Mechtcherine,** From analytical methods to numerical simulations: a process engineering toolbox for 3D concrete printing, Cem. Concr. Compos. 122 (2021), 104164.
15. **S. Ketel, G. Falzone, B. Wang, N. Washburn, G. Sant**, A printability index for linking slurry rheology to the geometrical attributes of 3D-printed components, Cem. Concr. Compos. 101 (2019) 32–43.
16. **F. Bos, J. Dirrenberger, L. Ferrara, E. Kreiger, W.R.L. Silva, V. Mechtcherine, C. Menna, M. Pradena, A.U. Rehmann, D. Weger, R.J.M. Wolfs, Y. Zhang,** The realities of additively manufactured concrete structures in practice, Cem. Concr. Res. (2022), https://doi.org/10.1016/j.cemconres.2022.106746.
17. **C. Menna, M. Pradena, A.U. Rehmann, D. Weger, R.J.M. Wolfs, Y. Zhang**, The realities of additively manufactured concrete structures in practice, Cem. Concr. Res. (2022), https://doi.org/10.1016/j.cemconres.2022.106746.
18. **Wang L. C.** Meso-scale numerical modeling of the mechanical behavior of reinforced concrete members. IACSIT International Journal of Engineering and Technology. 5, 6, 2013. P. 680 – 684.DOI: 10.7763/IJET.2013.V5.641.
19. **Rahul, A.V.; Santhanam, M.; Meena, H.; Ghani, Z.** Mechanical Characterization of 3D Printable Concrete. Constr Build Mater 2019, 227, 116710, doi:10.1016/j.conbuildmat.2019.116710.
20. **Aramburu, A.; Calderon-Uriszar-Aldaca, I.; Puente, I.** 3D Printing Effect on the Compressive Strength of Concrete Structures. Constr Build Mater 2022, 354, 129108, doi:10.1016/j.conbuildmat.2022.129108.
21. **Feng, P.; Meng, X.; Chen, J.-F.; Ye, L.** Mechanical Properties of Structures 3D Printed with Cementitious Powders. Constr Build Mater 2015, 93, 486–497, doi:10.1016/j.conbuildmat.2015.05.132.
22. **Wolfs, R.J.M.; Bos, F.P.; Salet, T.A.M.** Hardened Properties of 3D Printed Concrete: The Influence of Process Parameters on Interlayer Adhesion. Cem Concr Res 2019, 119, 132–140, doi:10.1016/j.cemconres.2019.02.017.
23. **Le, T.T.; Austin, S.A.; Lim, S.; Buswell, R.A.; Law, R.; Gibb, A.G.F.; Thorpe, T**. Hardened Properties of High-Performance Printing Concrete. Cem Concr Res 2012, 42, 558–566, doi:10.1016/j.cemconres.2011.12.003.
24. **Adamtsevich, A.O.; Pustovgar, A.P.** Additive Manufacturing in Construction: The Research of the Anisotropy Concrete Strength Effect. Stroitel'nye Materialy 2022, 18–24, doi:10.31659/0585-430X-2022-806-9-18-24.
25. **Wolfs, R.J.M.; Suiker, A.S.J.** Structural Failure during Extrusion-Based 3D Printing Processes. The International Journal of Advanced Manufacturing Technology 2019, 104, 565–584, doi:10.1007/s00170-019-03844-6.
26. **Wolfs, R.J.M.; Bos, F.P.; Salet, T.A.M**. Early Age Mechanical Behaviour of 3D Printed Concrete: Numerical Modelling and Experimental Testing. Cem Concr Res 2018, 106, 103–116, doi:10.1016/j.cemconres.2018.02.001.
27. **Wolfs, R.J.M.; Bos, F.P.; Salet, T.A.M.** Triaxial Compression Testing on Early Age Concrete for Numerical Analysis of 3D Concrete Printing. Cem Concr Compos 2019, 104, 103344, doi:10.1016/j.cemconcomp.2019.103344.
28. **Červenka J; Jendele L; Vaitová M.** Simulation of Digitally Printed Concrete Structures Using 3D Extrusion. In

Proceedings of the NAFEMS World Congress; Quebec City, 2019.
29. **Ahmed, G.H.; Askandar, N.H.; Jumaa, G.B.** A Review of Largescale 3DCP: Material Characteristics, Mix Design, Printing Process, and Reinforcement Strategies. Structures 2022, 43, 508–532, doi:10.1016/j.istruc.2022.06.068.
30. **Zhang, Y.; Zhang, Y.; She, W.; Yang, L.; Liu, G.; Yang, Y.** Rheological and Harden Properties of the High-Thixotropy 3D Printing Concrete. Constr Build Mater 2019, 201, 278–285, doi:10.1016/j.conbuildmat.2018.12.061.
31. **Panda, B.; Paul, S.C.; Hui, L.J.; Tay, Y.W.D.; Tan, M.J.** Additive Manufacturing of Geopolymer for Sustainable Built Environment. J Clean Prod 2017, 167, 281–288, doi:10.1016/j.jclepro.2017.08.165.
32. **Tay, Y.W.D.; Ting, G.H.A.; Qian, Y.; Panda, B.; He, L.; Tan, M.J.** Time Gap Effect on Bond Strength of 3D-Printed Concrete. Virtual Phys Prototyp 2019, 14, 104–113, doi:10.1080/17452759.2018.1500420.
33. **Torrado, A.R.; Roberson, D.A.** Failure Analysis and Anisotropy Evaluation of 3D-Printed Tensile Test Specimens of Different Geometries and Print Raster Patterns. Journal of Failure Analysis and Prevention 2016, 16, 154–164, doi:10.1007/s11668-016-0067-4.
34. **Heras Murcia, D.; Genedy, M.; Reda Taha, M.M.** Examining the Significance of Infill Printing Pattern on the Anisotropy of 3D Printed Concrete. Constr Build Mater 2020, 262, 120559, doi:10.1016/j.conbuildmat.2020.12055.
35. **Chengcheng Li, Jinxian Qi**. Structural Analysis of 3D Printing Model. Advances in Computer Science Reseach, Volum 75, 7th International Conference on Mechatronics, Computer and Education Informationization (MCEI 2017), pp 289-293.
36. **Rymes J., Cervenka J., Jendele L**. / Material Modelling And Simulation Of 3D Concrete Printing Process / 11th International Conference on Fracture Mechanics of Concrete and Concrete Structures, pp 1 – 8.DOI: 10.21012/FC11.092346.
37. **Cervenka J., Rymes J., Jendele L.** / Integrating 3D Modelling and Non-linear Numerical Simulations in Concrete Additive Manufacturing / Concrete Structures / Volume 67. pp 247.
38. **Jendele L., Rymes J., Cervenka J.** Optimizing Digital 3D Printing of Concrete Structures / RILEM Bookseries, Volume 48, pp. 59–72, 2024. DOI: 10.1007/978-3-031-53389-1_6.
39. ABAQUS Inc ABAQUS Analysis User's Manual Version 6.6 Available online: https://classes.engineering.wustl.edu/2009/spring/mase5513/abaqus/docs/v6.6/books/usb/default.htm (accessed on 14 October 2024).
40. **Bathe, K.-J.; Walczak, J.; Welch, A.; Mistry, N.** Nonlinear Analysis of Concrete Structures. *Comput Struct* 1989, *32*, 563–590, doi:10.1016/0045-7949(89)90347-7.
41. **Fialko, S.; Karpilowskyi, V**. Spatial Thin-Walled Reinforced Concrete Structures Taking into Account Physical Nonlinearity in SCAD Software. Rod Finite Element.; December 3 2019.
42. **Fialko, S.; Perelmuter, A.; Perelmuter, A.** Inelastic Analysis of Reinforced Concrete Structures in SCAD. International Journal for Computational Civil and Structural Engineering 2019, 15, 54–60, doi:10.22337/2587-9618-2019-15-1-54-60.

СПИСОК ЛИТЕРАТУРЫ

1. **Hou, S.; Duan, Z.; Xiao, J.; Ye, J.** A Review of 3D Printed Concrete: Performance Requirements, Testing Measurements and Mix Design. Constr

Build Mater 2021, 273, 121745, doi:10.1016/j.conbuildmat.2020.121745.

2. **Wangler, T.; Roussel, N.; Bos, F.P.; Salet, T.A.M.; Flatt, R.J.** Digital Concrete: A Review. Cem Concr Res 2019, 123, 105780, doi:10.1016/j.cemconres.2019.105780.
3. **Lu, B.; Weng, Y.; Li, M.; Qian, Y.; Leong, K.F.; Tan, M.J.; Qian, S.** A Systematical Review of 3D Printable Cementitious Materials. Constr Build Mater 2019, 207, 477–490, doi:10.1016/j.conbuildmat.2019.02.144.
4. **Lim, S.; Buswell, R.A.; Le, T.T.; Austin, S.A.; Gibb, A.G.F.; Thorpe, T.** Developments in Construction-Scale Additive Manufacturing Processes. Autom Constr 2012, 21, 262–268, doi:10.1016/j.autcon.2011.06.010.
5. A. News. https://www.arabnews.com/node/1554891/saudi-arabia. Accessed 2021/09/28.
6. **R. Laubier, M. Wunder, S. Witthoft, C.** Rothballer. https://www.bcg.com/publications/2018/will-3d-printing-remodel-construction-industry. Accessed 2021/10/28.
7. http://www.mohurd.gov.cn/index.html. Accessed 2021/8/31.
8. **G. Ma, L. Wang,** A critical review of preparation design and workability measurement of concrete material for largescale 3D printing, Front. Struct. Civ. Eng. 6 (2017) 1–19.
9. **Bos, F.; Wolfs, R.; Ahmed, Z.; Salet, T.** Additive Manufacturing of Concrete in Construction: Potentials and Challenges of 3D Concrete Printing. Virtual Phys Prototyp 2016, 11, 209–225, doi:10.1080/17452759.2016.1209.
10. **Tay, Y.W.D.; Panda, B.; Paul, S.C.; Noor Mohamed, N.A.; Tan, M.J.; Leong, K.F.** 3D Printing Trends in Building and Construction Industry: A Review. Virtual Phys Prototyp 2017, 12, 261–276, doi:10.1080/17452759.2017.1326724.
11. **Paul, S.C.; van Zijl, G.P.A.G.; Tan, M.J.; Gibson, I**. A Review of 3D Concrete Printing Systems and Materials Properties: Current Status and Future Research Prospects. Rapid Prototyp J 2018, 24, 784–798, doi:10.1108/RPJ-09-2016-0154.
12. **Paolini, A.; Kollmannsberger, S.; Rank, E.** Additive Manufacturing in Construction: A Review on Processes, Applications, and Digital Planning Methods. Addit Manuf 2019, 30, 100894, doi:10.1016/j.addma.2019.100894.
13. **Mohan, M.K.; Rahul, A.V.; De Schutter, G.; Van Tittelboom, K.** Extrusion-Based Concrete 3D Printing from a Material Perspective: A State-of-the-Art Review. Cem Concr Compos 2021, 115, 103855, doi:10.1016/j.cemconcomp.2020.103855.
14. **A. Perrot, A. Pierre, V.N. Nerella, R.J.M. Wolfs, E. Keita, S.A.O. Nair, N. Neithalath, N. Roussel, V. Mechtcherine,** From analytical methods to numerical simulations: a process engineering toolbox for 3D concrete printing, Cem. Concr. Compos. 122 (2021), 104164.
15. **S. Ketel, G. Falzone, B. Wang, N. Washburn, G. Sant**, A printability index for linking slurry rheology to the geometrical attributes of 3D-printed components, Cem. Concr. Compos. 101 (2019) 32–43.
16. **F. Bos, J. Dirrenberger, L. Ferrara, E. Kreiger, W.R.L. Silva, V. Mechtcherine, C. Menna, M. Pradena, A.U. Rehmann, D. Weger, R.J.M. Wolfs, Y. Zhang,** The realities of additively manufactured concrete structures in practice, Cem. Concr. Res. (2022), https://doi.org/10.1016/j.cemconres.2022.106746.
17. **C. Menna, M. Pradena, A.U. Rehmann, D. Weger, R.J.M. Wolfs, Y. Zhang**, The realities of additively manufactured concrete structures in practice, Cem. Concr. Res. (2022), https://doi.org/10.1016/j.cemconres.2022.106746.

18. **Wang L. C.** Meso-scale numerical modeling of the mechanical behavior of reinforced concrete members. IACSIT International Journal of Engineering and Technology. 5, 6, 2013. P. 680 – 684.DOI: 10.7763/IJET.2013.V5.641.
19. **Rahul, A.V.; Santhanam, M.; Meena, H.; Ghani, Z.** Mechanical Characterization of 3D Printable Concrete. Constr Build Mater 2019, 227, 116710, doi:10.1016/j.conbuildmat.2019.116710.
20. **Aramburu, A.; Calderon-Uriszar-Aldaca, I.; Puente, I.** 3D Printing Effect on the Compressive Strength of Concrete Structures. Constr Build Mater 2022, 354, 129108, doi:10.1016/j.conbuildmat.2022.129108.
21. **Feng, P.; Meng, X.; Chen, J.-F.; Ye, L.** Mechanical Properties of Structures 3D Printed with Cementitious Powders. Constr Build Mater 2015, 93, 486–497, doi:10.1016/j.conbuildmat.2015.05.132.
22. **Wolfs, R.J.M.; Bos, F.P.; Salet, T.A.M.** Hardened Properties of 3D Printed Concrete: The Influence of Process Parameters on Interlayer Adhesion. Cem Concr Res 2019, 119, 132–140, doi:10.1016/j.cemconres.2019.02.017.
23. **Le, T.T.; Austin, S.A.; Lim, S.; Buswell, R.A.; Law, R.; Gibb, A.G.F.; Thorpe, T**. Hardened Properties of High-Performance Printing Concrete. Cem Concr Res 2012, 42, 558–566, doi:10.1016/j.cemconres.2011.12.003.
24. **Adamtsevich, A.O.; Pustovgar, A.P.** Additive Manufacturing in Construction: The Research of the Anisotropy Concrete Strength Effect. Stroitel’nye Materialy 2022, 18–24, doi:10.31659/0585-430X-2022-806-9-18-24.
25. **Wolfs, R.J.M.; Suiker, A.S.J.** Structural Failure during Extrusion-Based 3D Printing Processes. The International Journal of Advanced Manufacturing Technology 2019, 104, 565–584, doi:10.1007/s00170-019-03844-6.
26. **Wolfs, R.J.M.; Bos, F.P.; Salet, T.A.M**. Early Age Mechanical Behaviour of 3D Printed Concrete: Numerical Modelling and Experimental Testing. Cem Concr Res 2018, 106, 103–116, doi:10.1016/j.cemconres.2018.02.001.
27. **Wolfs, R.J.M.; Bos, F.P.; Salet, T.A.M.** Triaxial Compression Testing on Early Age Concrete for Numerical Analysis of 3D Concrete Printing. Cem Concr Compos 2019, 104, 103344, doi:10.1016/j.cemconcomp.2019.103344.
28. **Červenka J; Jendele L; Vaitová M.** Simulation of Digitally Printed Concrete Structures Using 3D Extrusion. In Proceedings of the NAFEMS World Congress; Quebec City, 2019.
29. **Ahmed, G.H.; Askandar, N.H.; Jumaa, G.B.** A Review of Largescale 3DCP: Material Characteristics, Mix Design, Printing Process, and Reinforcement Strategies. Structures 2022, 43, 508–532, doi:10.1016/j.istruc.2022.06.068.
30. **Zhang, Y.; Zhang, Y.; She, W.; Yang, L.; Liu, G.; Yang, Y.** Rheological and Harden Properties of the High-Thixotropy 3D Printing Concrete. Constr Build Mater 2019, 201, 278–285, doi:10.1016/j.conbuildmat.2018.12.061.
31. **Panda, B.; Paul, S.C.; Hui, L.J.; Tay, Y.W.D.; Tan, M.J.** Additive Manufacturing of Geopolymer for Sustainable Built Environment. J Clean Prod 2017, 167, 281–288, doi:10.1016/j.jclepro.2017.08.165.
32. **Tay, Y.W.D.; Ting, G.H.A.; Qian, Y.; Panda, B.; He, L.; Tan, M.J.** Time Gap Effect on Bond Strength of 3D-Printed Concrete. Virtual Phys Prototyp 2019, 14, 104–113, doi:10.1080/17452759.2018.1500420.
33. **Torrado, A.R.; Roberson, D.A.** Failure Analysis and Anisotropy Evaluation of 3D-Printed Tensile Test Specimens of Different Geometries and Print Raster Patterns. Journal of Failure Analysis and Prevention

2016, 16, 154–164, doi:10.1007/s11668-016-0067-4.

34. **Heras Murcia, D.; Genedy, M.; Reda Taha, M.M.** Examining the Significance of Infill Printing Pattern on the Anisotropy of 3D Printed Concrete. Constr Build Mater 2020, 262, 120559, doi:10.1016/j.conbuildmat.2020.12055.
35. **Chengcheng Li, Jinxian Qi**. Structural Analysis of 3D Printing Model. Advances in Computer Science Reseach, Volum 75, 7th International Conference on Mechatronics, Computer and Education Informationization (MCEI 2017), pp 289-293.
36. **Rymes J., Cervenka J., Jendele L**. / Material Modelling And Simulation Of 3D Concrete Printing Process / 11th International Conference on Fracture Mechanics of Concrete and Concrete Structures, pp 1 – 8.DOI: 10.21012/FC11.092346.
37. **Cervenka J., Rymes J., Jendele L.** / Integrating 3D Modelling and Non-linear Numerical Simulations in Concrete Additive Manufacturing / Concrete Structures / Volume 67. pp 247.
38. **Jendele L., Rymes J., Cervenka J.** Optimizing Digital 3D Printing of Concrete Structures / RILEM Bookseries, Volume 48, pp. 59–72, 2024. DOI: 10.1007/978-3-031-53389-1_6.
39. ABAQUS Inc ABAQUS Analysis User's Manual Version 6.6 Available online: https://classes.engineering.wustl.edu/2009/spring/mase5513/abaqus/docs/v6.6/books/usb/default.htm (accessed on 14 October 2024).
40. **Bathe, K.-J.; Walczak, J.; Welch, A.; Mistry, N.** Nonlinear Analysis of Concrete Structures. *Comput Struct* 1989, *32*, 563–590, doi:10.1016/0045-7949(89)90347-7.
41. **Fialko, S.; Karpilowskyi, V**. Spatial Thin-Walled Reinforced Concrete Structures Taking into Account Physical Nonlinearity in SCAD Software. Rod Finite Element.; December 3 2019.
42. **Fialko, S.; Perelmuter, A.; Perelmuter, A.** Inelastic Analysis of Reinforced Concrete Structures in SCAD. International Journal for Computational Civil and Structural Engineering 2019, 15, 54–60, doi:10.22337/2587-9618-2019-15-1-54-60.

Oleg Vasilievich Kabantsev, Doctor of Engineering Sciences, Professor, Director, Department of Research and Technology Projects, Federal State Budget Educational Institution of Higher Education "Moscow State University of Civil Engineering (National Research University)" (MGSU), 26 Yaroslavskoye Shosse, Moscow, 129337, Russia

Alexey Vladimirovich Karlin, engineer,Federal State Budget Educational Institution of Higher Education "Mos-cow State University of Civil Engineering (National Research University)" (MGSU), 26 Yaroslavskoye Shosse, Moscow, 129337, Russia, akarlinmgsu@yandex.ru

Олег Васильевич Кабанцев, д.т.н., профессор, директор Дирекции научно-технических проектов, Федеральное государственное бюджетное образовательное учреждение высшего образования «Национальный исследовательский Московский государственный строительный университет» (НИУ МГСУ), д. 26, Ярославское шоссе, Москва, 129337, Россия, ovk531@gmail.com

Карлин Алексей Владимирович, инженер, Федеральное государственное бюджетное образовательное учреждение высшего образования «Национальный исследовательский Московский государственный строительный университет» (НИУ МГСУ), д. 26, Ярославское шоссе, Москва, 129337, Россия, akarlinmgsu@yandex.ru

DOI:10.22337/2587-9618-2024-20-4-241-252

EARTHQAUKE OF BUILDINGS AND STRUCTURES: REGULATORY "MUST-DO" OR SCIENTIFICALLY SUBSTANTIATED RESULTS

Alexander M. Belostotsky, Alexander I. Nagibovich, Pavel I. Novikov, Vladislav V. Vershinin

National Research Moscow State University of Civil Engineering, Moscow, RUSSIA

Abstract: Within the present article the problem of selection and substantiation of "compensating measures" to provide earthquake resistance of buildings and structures which have deviations from structural regulatory requirements is considered. The authors proposed and tested a theoretical approach to substantiation of earthquake resistance of buildings and structures as opposed to unreasonable utilization of seismic isolation devices. The proposed approach is demonstrated through validation of seismic resistance of the Choreographic Academy building located in Sevastopol city with the use of a numerical (finite element) analysis performed in a physically nonlinear dynamic formulation, taking into account the structural solution compensating extra factor.

Keywords: mathematical modeling, numerical methods, finite element method, earthquake resistance, seismic protection, stress-strain state, structural solutions compensating factor, scientific and technical support

СЕЙСМОСТОЙКОСТЬ ЗДАНИЙ И СООРУЖЕНИЙ: НОРМАТИВНАЯ "ОБЯЗАЛОВКА" ИЛИ НАУЧНО-ОБОСНОВАННЫЕ РЕЗУЛЬТАТЫ

А.М. Белостоцкий, А.И. Нагибович, П.И. Новиков, В.В. Вершинин

Национальный исследовательский Московский государственный строительный университет, г. Москва, РОССИЯ

Аннотация: в статье представлена проблема выбора и обоснования «компенсирующих мероприятий» для обеспечения сейсмостойкости зданий и сооружений с отступлениями от нормативных конструктивных требований. Авторами предложен и апробирован расчетный подход к обоснованию сейсмостойкости зданий и сооружений в противовес необоснованному применению сейсмоизолирующих устройств. Предложенный подход демонстрируется на примере обоснования сейсмостойкости здания Хореографической академии в г. Севастополь с реализацией численного (конечно-элементного) моделирования в физически-нелинейной динамической постановке с учетом дополнительного компенсирующего коэффициента конструктивных решений.

Ключевые слова: математическое моделирование, численные методы, метод конечных элементов, сейсмостойкость, сейсмозащита, напряженно-деформированное состояние, компенсирующий коэффициент конструктивных решений, научно-техническое сопровождение

PROBLEM RELEVANCE

For unique buildings, structures and complexes with bold modern architecture, designed and constructed in earthquake-prone regions, it is a common issue of compelled deviations from structural requirements prescribed by current building codes [9]. In such cases certain compensating measures are usually designed.

One of the ways to decrease seismic forces is to construct a specific seismic protection system. There is a view that installation of seismic isolation devices (seismic isolation pads, dampers, etc.) by itself is enough to provide sufficient earthquake resistance. Such design solutions are often proposed without any theoretical substantiation. Evidently, installation of seismic isolation and (or) damping devices will change the eigen spectrum of a structure, but, without a sophisticated theoretical analysis, it is impossible to determine whether corresponding changes of the structure dynamic response will provide its better earthquake resistance or not.

An alternative proposed and tested on several unique structures by the authors [2] is to use the following measures as compensating ones:

- *Detailed accounting of loads and excitations*, in particular their actual areas of application, seismological parameters, potential earthquake focuses, possible earthquakes and their spectra. Design response spectra and ground acceleration histories are developed basing onto seismic microzonation of a construction site.
- *Structural solutions extra factor* $\boldsymbol{K_2}$ *is taken into account* during design earthquake analysis and maximum considered earthquake analysis when there are deviations from the requirements of SP 14.13330 [9].
- *Sophisticated theoretical substantiation of structural safety parameters for special load combinations including the seismic loading.* A theoretical substantiation of structural safety is prescribed by SP 14.13330 [9] which requires to account of current standards. Among design parameters are: a location of the construction site, a structure type according to its function, a structure risk category (K_0), a design level of structural damage during an earthquake (K_1), energy dissipation factor (K_ψ), and structural solutions factor (K_2). Also, the following factors altering the stress-strain state of the structural system shall be taken into consideration: foundation bed stiffness, soil-structure interaction, three-dimensional response of the structural system, orientation of the structure relative to the seismic sources, heterogeneous damping in structural elements, and, where necessary, nonlinear properties of structural materials, large deformations and large strains of structural elements and their erection sequence.
- *Scientific and technical support during design and construction* with eventual determination of actual earthquake resistance of a structure using its dynamic characteristics obtained from thorough microseismic-based investigations.

The mentioned issues can be illustrated by a representative example of the Choreographic Academy located in Sevastopol city.

BUILDING DESCRIPTION

The construction site of the educational facility is located in the coastal zone with significant difference of local topography. The building has a planform of open rectangle (114.8×104.9 m) and is divided into six dynamically independent blocks with various number of stories (up to 8 stories), functions and architecture. The general view of the Choreographic Academy is shown in Fig. . The structural system of the Academy is classified as wall-frame with stiffness cores. The cast-in-place reinforced concrete frame is formed by vertical bearing elements – columns, walls, and stiffness cores (staircase and elevator blocks) – and horizontal floor slabs.

All connections of structural elements are rigid. The foundation is made of cast-in-place reinforced concrete and underlain by natural bed.

The construction site is located in the earthquake-prone region. According to the map OSR-2015-A and SP 14.13330 [9], the seismic intensity at the construction site is 8 grade with a mean return period of 500 years and the probability of 0.90 for the seismic intensity to stay within its nominal value within a 50-years period (risk level “A”). The construction site is classified as Category II based on the seismic behavior of foundation soils.

a) Architectural rendering

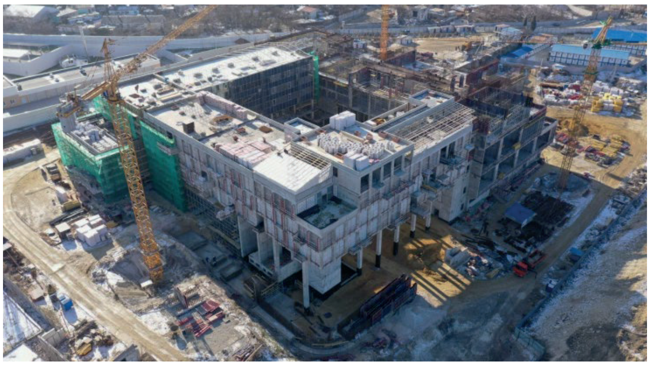

б) Construction stage

Figure 1. *The general view of the Choreographic Academy*

DEVIATIONS FROM THE REGULATORY REQUIREMENTS

The most critical deviation from the requirements of SP 14.13330 [9] refers to *the limit height (number of stories)* of the building. In such cases when the limit number of stories is exceeded due to functional requirements, it is prescribed to utilize a specific seismic protection system. Also, there are deviations concerning the shape of expansion joints as compared to the required one in the cases when separated blocks have significantly different stiffness and (or) mass, foundation type, layout of walls, diaphragms, bracing, stiffness cores and columns.

COMPENSATING MEASURES

Initially, at the behest of "seismic marketers", to reduce seismic forces, it was decided to design and construct a special seismic pad beneath the foundation slabs of the building blocks. Also, the building frame was intended to be provided with damping system.

The interesting point is that the Choreographic Academy building locates in the immediate proximity to a unique structure – the Opera and Ballet Theater (Sevastopol city, Fig. 2) which earthquake resistance in the absence of any seismic protection system was successfully substantiated by NIC StaDyO JSC [2]. The results of an elaborated dynamic analysis of the Opera and Ballet Theater building validated the earthquake resistance of the designed structural system without any seismic protection system, which has arisen certain questions concerning necessity of "enforced" measures to provide earthquake resistance of the Choreographic Academy.

The authors proposed an alternative – utilization of "compensating measures" that do not require mandatory seismic isolation. The proposed approach is based onto real (not "fake") complex scientific and technical support including sophisticated theoretical analysis of major structural safety parameters, performed independently of the design analysis.

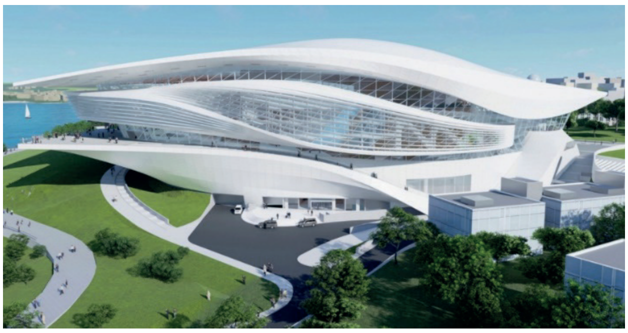

Figure 2. *Architecture rendering of the Opera and Ballet Theater in Sevastopol city*

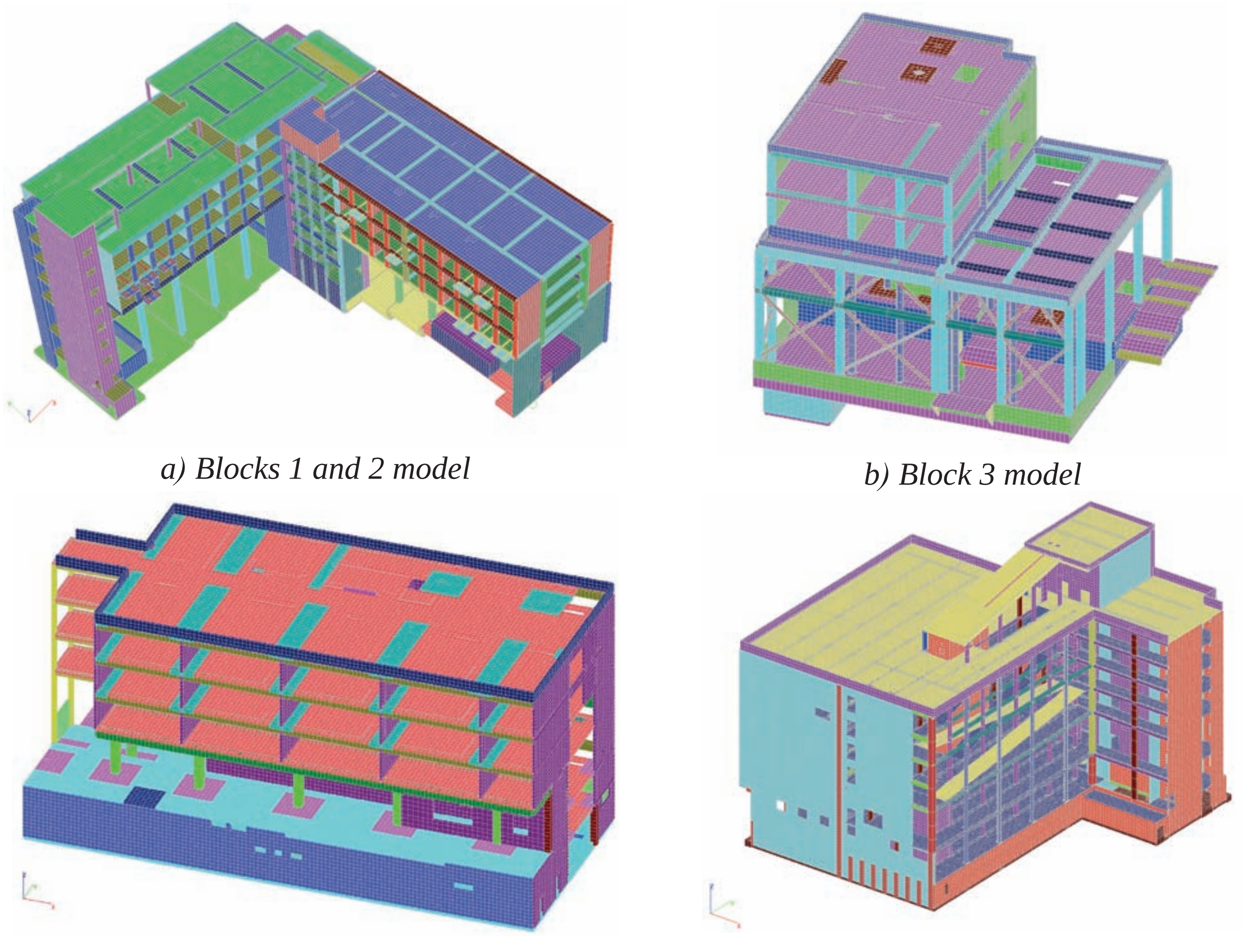

a) Blocks 1 and 2 model

b) Block 3 model

c) Block 4 model

d) Block 6 model

Figure 3. Mathematical (finite element) models of the Choreographic Academy blocks

STRUCTURAL MODELING

Three-dimensional finite element structural models of the Choreographic Academy blocks were constructed in SCAD Office 21.1 software using shell type and beam type finite elements. Reinforced concrete columns, beams and bracing were modeled with beam type finite elements, while reinforced concrete foundation slabs, floors, bearing walls were meshed with triangular and quadrilateral shell type finite elements of constant thickness. Foundation bed elastic properties required for the static analysis were determined using KROSS software. Mathematical models of blocks having joint foundation were assembled together, and the full model was analyzed.

Design earthquake effects were determined through modal response spectrum analysis. Three directions of a seismic ground motion were considered: along X and Y horizontal axes and along Z vertical axis. The corresponding response spectra ignoring K_0, K_1, K_ψ, K_2 factors are shown in Fig. 4.

Dead and live gravitational loads were considered according to Table 5.1 of SP 14.13330 [**9**].

Requirements of SP 13.13330 [**9**] concerning the minimum value of a combined modal mass participation were fulfilled as well.

Due to the deviations from the requirements of SP 14.13330 [9] (caused by the challenging construction site conditions and functional requirements) design earthquake effects were calculated using structural solutions extra factor K_2 = 1.2. Adopted values of seismic load factors K_0, K_1, K_ψ, K_2 are given in Table 1.

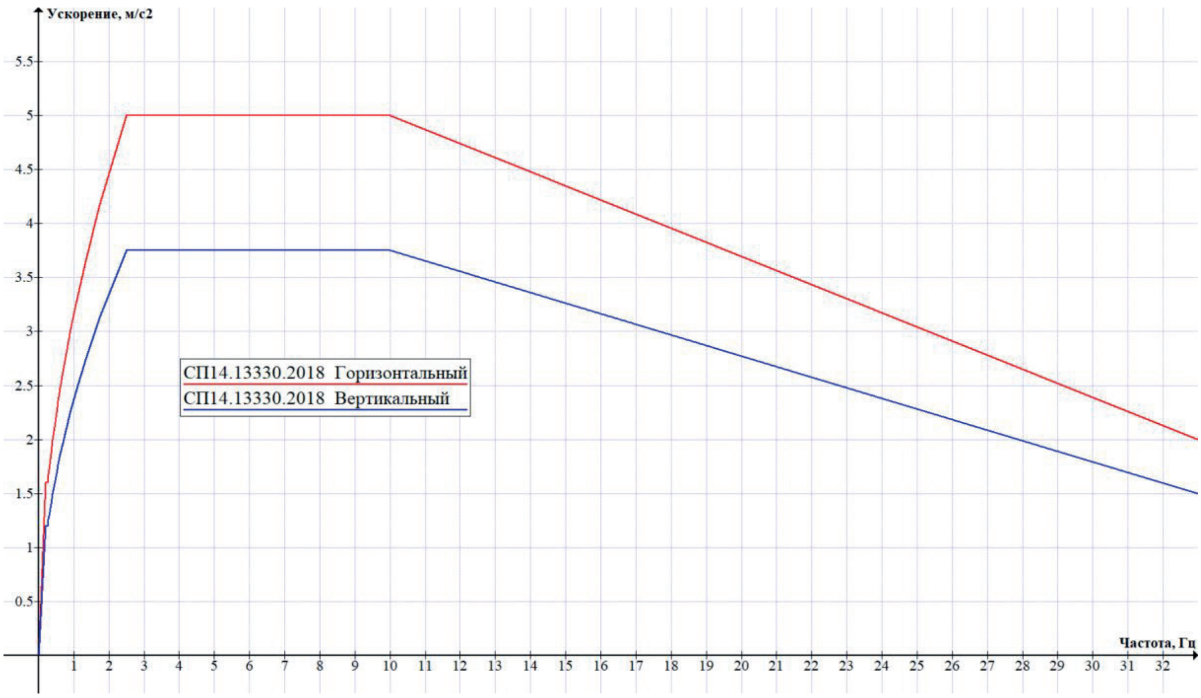

Figure 4. Spectral response acceleration (ignoring K_0, K_1, K_ψ, K_2 factors) for horizontal (colored in red) and vertical (colored in blue) components of the design earthquake according to SP 14.13330.2018

Table 1. Adopted values of seismic load factors

No.	Factor	Design earthquake	Maximum considered earthquake
1	K_0	1,1	1,5
2	K_1	0,3	1,0
3	K_ψ	1,0	1,0
4	K_2	**1,2**	**1,2**

Maximum considered earthquake effects were calculated through nonlinear dynamic analysis with seismic excitation applied in the form of the ground acceleration history having three independent components. To integrate the equations of motion over time, the implicit Newmark scheme was used with a time increment set equal to 0.005 s. Damping in the structural model was defined as the Rayleigh one corresponding to 5% of the critical damping. Within the nonlinear dynamic analysis, reinforcement and concrete of vertical bearing elements were modeled taking their physically nonlinear properties defined as bilinear stress-strain curves into account. Horizontal structural elements were modeled as elastic ones.

The analysis was performed in two stages. At the first stage, dead and live loads were statically applied and retained in the further analysis. At the second stage, a ground displacement history having three independent components and time duration of 25 s came into action. An example of ground displacement history and corresponding ground acceleration history having three independent components and used in calculations are shown in Fig. 5.

Reinforcement of concrete structural elements was defined in the mathematical model according to design drawings (see, for instance, Fig. 6).

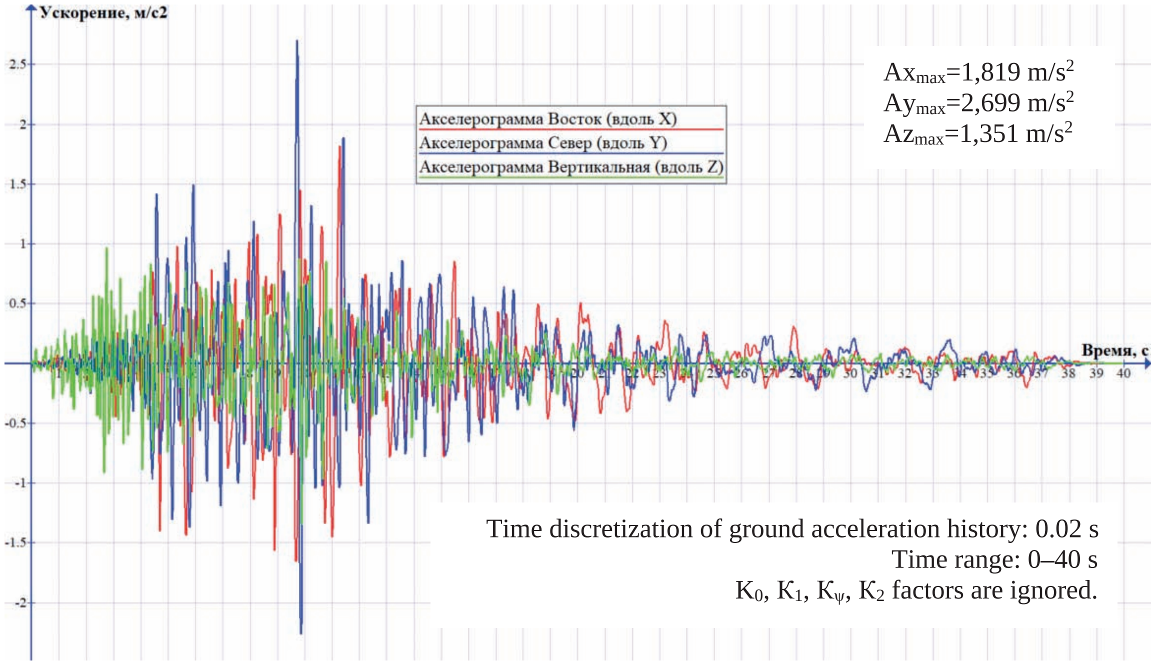

a) Ground acceleration history [m/s^2]

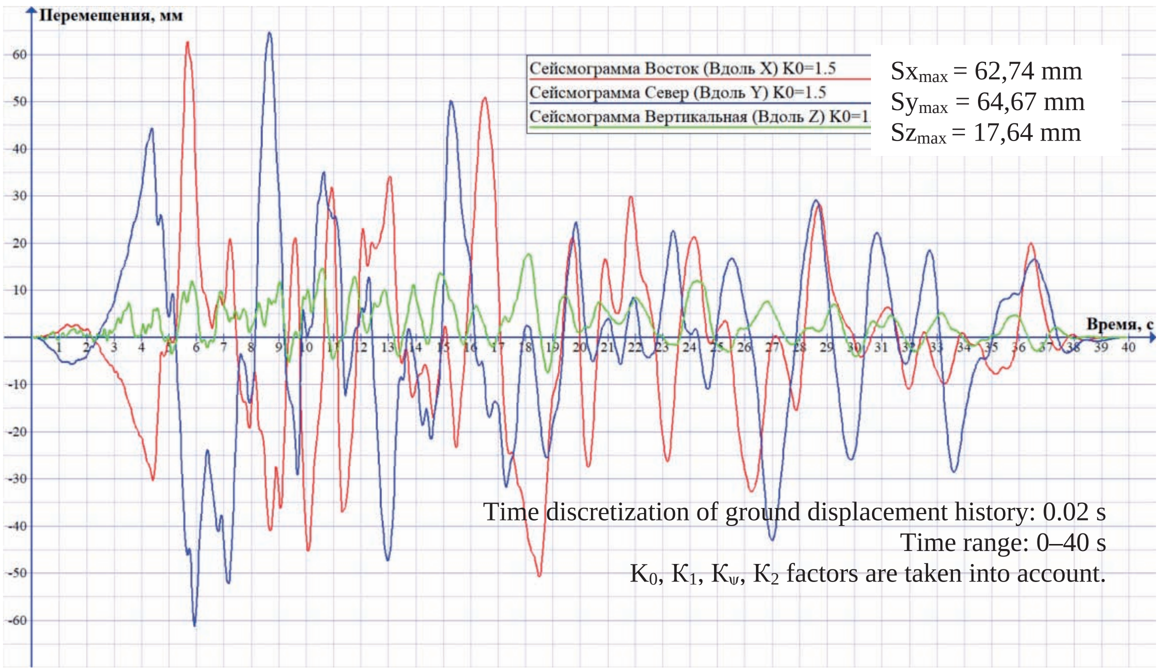

b) Ground displacement history [mm]

Figure 5. Ground acceleration (Ax, Ay, Az) and displacement (Sx, Sy, Sz) histories

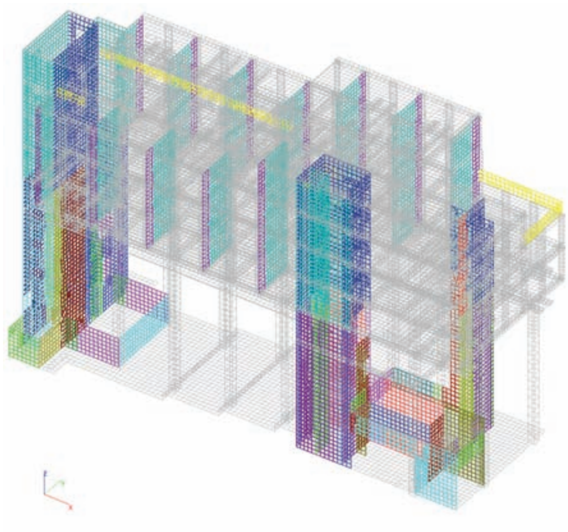

	S_1	S_2	S_3	S_4	W_x	W_y
	d16/200	d16/200	d16/200	d16/200	d10/300	d10/300
	d16/200	d16/200	d12/200	d12/200	d10/300	d10/300
	d16/200	d16/200	d16/200	d16/200	d10/300	d10/300
	d16/200	d16/200	d16/100	d16/100	d10/300	d10/300
	d16/200	d16/200	d20/200	d20/200	d10/300	d10/300
	d16/100	d16/100	d16/200	d16/200	d10/300	d10/300
	d16/100	d16/100	d16/100	d16/100	d10/300	d10/300
	d16/100	d16/100	d20/200	d20/200	d10/300	d10/300
	d16/100	d16/100	d20/100	d20/100	d10/300	d10/300
	d20/100	d20/100	d12/200	d12/200	d10/300	d10/300
	d20/100	d20/100	d16/200	d16/200	d10/300	d10/300
	d20/100	d20/100	d16/100	d16/100	d10/300	d10/300
	d20/100	d20/100	d20/200	d20/200	d10/300	d10/300
	d20/100	d20/100	d20/100	d20/100	d10/300	d10/300
	d25/100	d25/100	d12/200	d12/200	d10/300	d10/300
	d25/100	d25/100	d16/200	d16/200	d10/300	d10/300
	d25/100	d25/100	d16/100	d16/100	d10/300	d10/300
	d25/100	d25/100	d20/100	d20/100	d10/300	d10/300
	d32/100	d32/100	d16/200	d16/200	d10/300	d10/300
	d40/100	d40/100	d16/200	d16/200	d10/300	d10/300
	d16/200	d16/200	d12/200	d12/200	d10/300	d10/300
	d16/100	d16/100	d12/200	d12/200	d10/300	d10/300
	d25/100	d25/100	d12/200	d12/200	d10/300	d10/300
	d25/100	d25/100	d12/200	d12/200	d10/300	d10/300

Figure 6. Wall reinforcement in Block 1 model

RESULTS

Results of the conducted analyses exhibited consistent distribution of displacements and forces (Figs. 7, 8, 9) in foundation and superstructure structural elements of the Choreographic Academy blocks under special load combinations including the seismic load.

It was determined that design parameters of the building (geometry (layout and cross-sections), material properties, characteristics of element connections, values and combinations of loads) provided compliance with the requirements concerning strength, stability and limited deformations of the structural system and its individual elements.

Nonlinear dynamic analysis of the building response to the special load combination including the maximum considered earthquake applied in the form of the ground motion history (see Fig.5) revealed its spatial and time complexity. Nevertheless, the design reinforcement with the structural solutions compensating extra factor K_2=1.2 taken into account appeared to be enough to provide structural safety.

Some of the results for the block 1 are presented in Figs. 7-11 below.

Zones where the reinforcement reached its yield stress are depicted in Fig. 10. Also, using the SCAD postprocessor tools normal stresses in the most severely strained cross-sections of individual reinforced concrete elements were determined (see Fig.11).

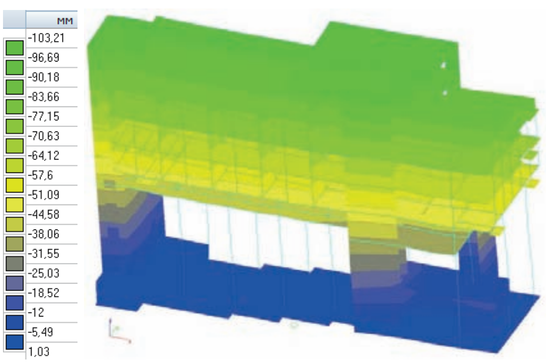

a) Ux, mm, time instant t = 14.20 s

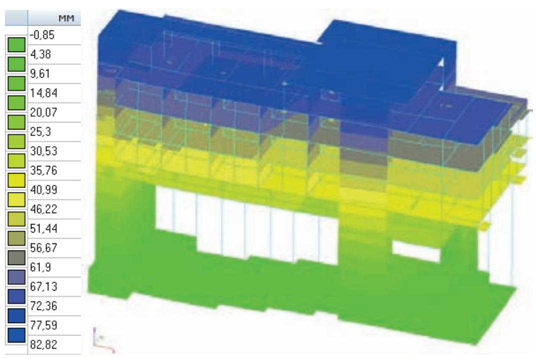

b) Uy, mm, time instant t = 12.70 s

Figure 7. Horizontal displacements induced by the special load combination including the maximum considered earthquake (the presented time instants correspond to the maximum absolute values of the displacement components)

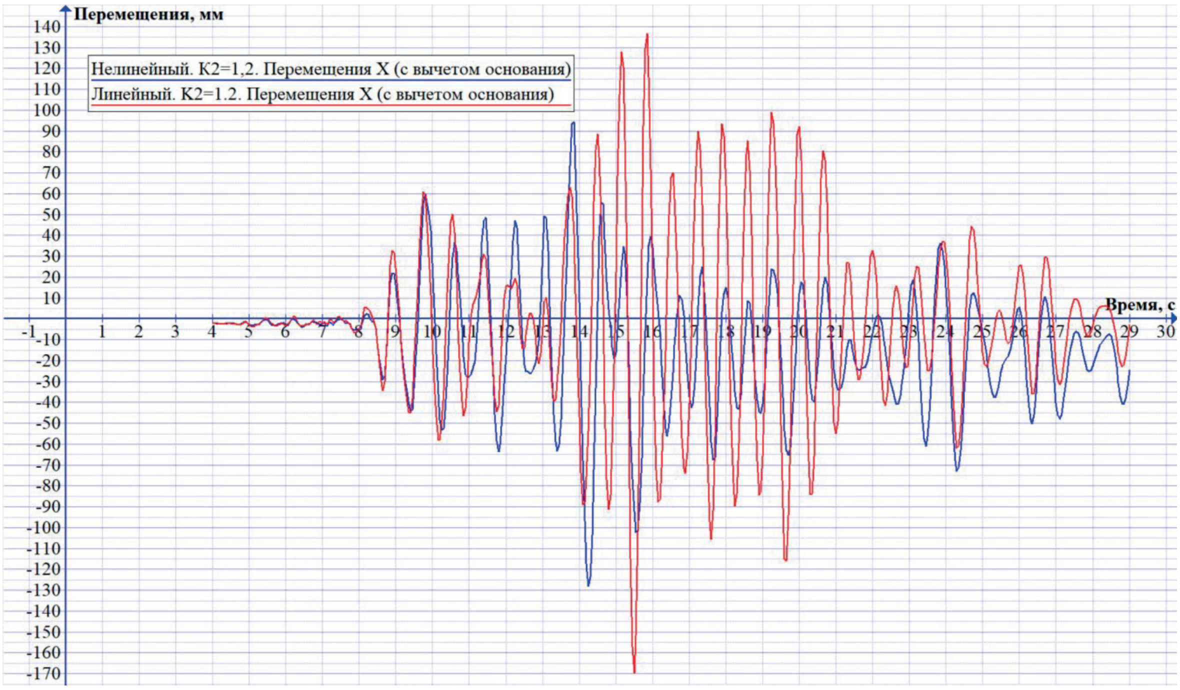

Figure 8. Horizontal displacements along X axis at the top of the block 1 induced by the special load combination including the maximum considered earthquake with the structural solutions extra factor K_2=1.2 taken into account

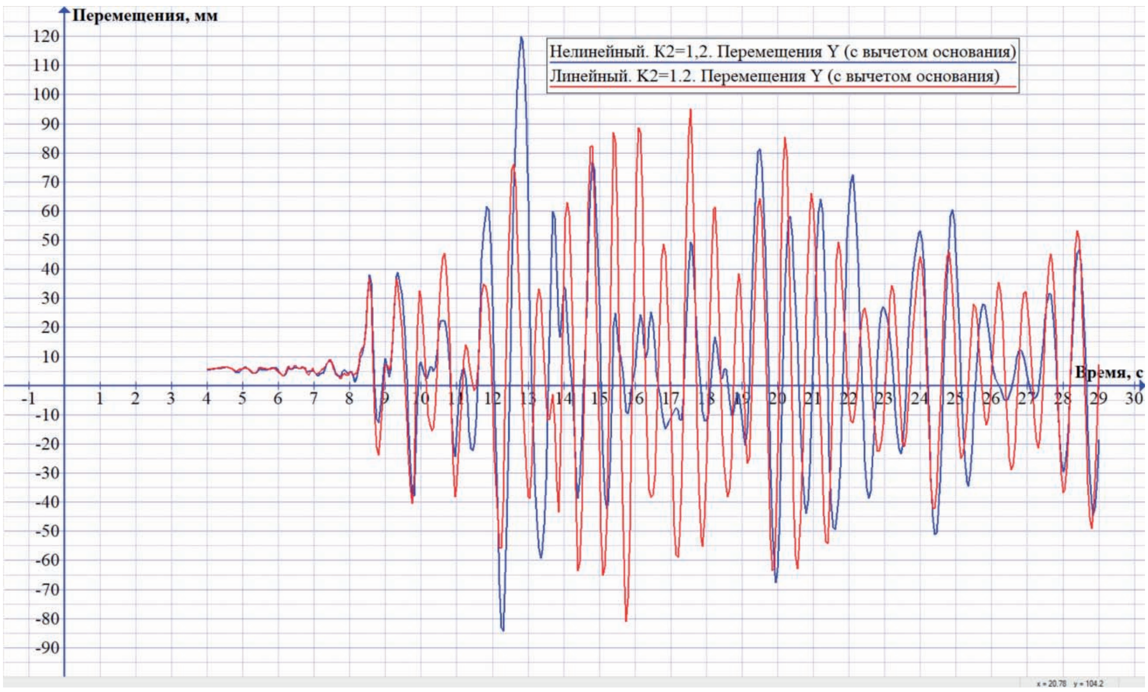

Figure 9. Horizontal displacements along Y axis at the top of the block 1 induced by the special load combination including the maximum considered earthquake with the structural solutions extra factor K_2=1.2 taken into account

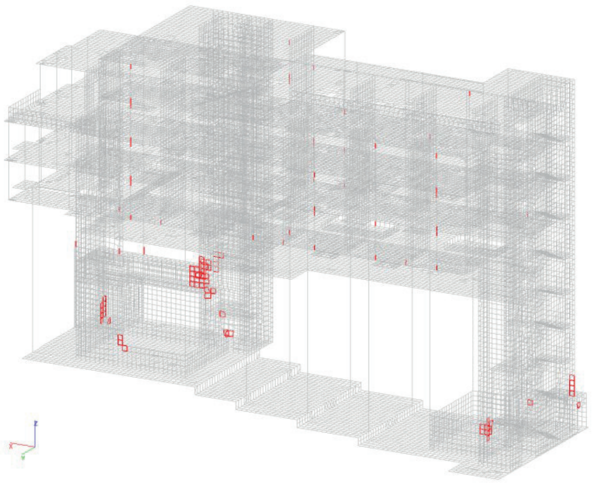

a) Finite elements in which the reinforcement reached its yield stress under tension

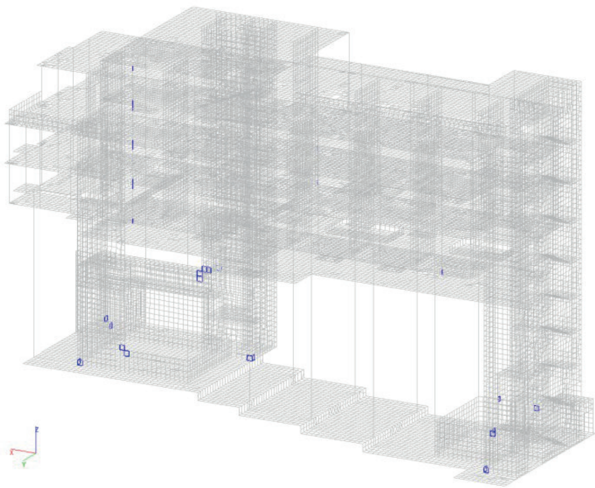

b) Finite elements in which the reinforcement reached its yield stress under compression

Figure 10. Finite elements in which the reinforcement reached its yield stress due to action of the special load combination including the maximum considered earthquake with the structural solutions extra factor K_2=1.2 taken into account

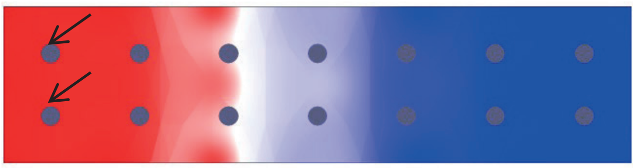

Concrete:
Compression. The minimum of -17.3 MPa
Tension. The maximum of 1.29 MPa
Reinforcement rods in which the yield stress of 522 MPa was reached are shown by the arrows

a) Column 800×200 mm on grid lines 16-17/E

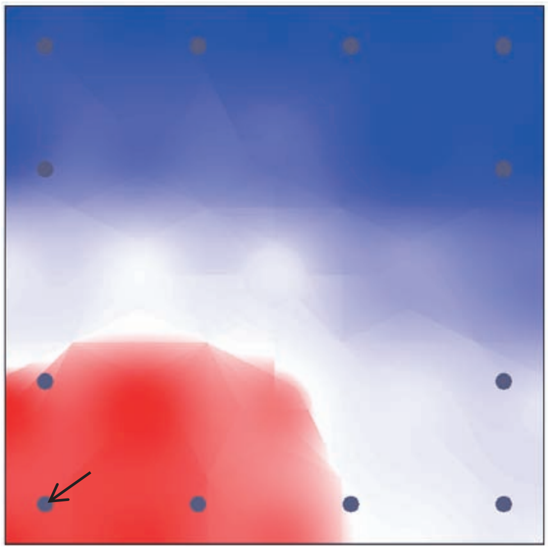

Concrete:
Compression. The minimum of -17.1 MPa
Tension. The maximum of 1.05 MPa
Reinforcement rods in which the yield stress of 522 MPa was reached are shown by the arrows

b) Column 800×800 mm on grid lines 18/D

Figure 11. Normal stresses in the cross-sections of the reinforced concrete elements induced by the special load combination including the maximum considered earthquake with the structural solutions extra factor K_2=1.2 taken into account

CONCLUSION

1. Nonlinear dynamic analysis of the Choreographic Academy response to the special load combination including the maximum considered earthquake (applied in the form of the ground motion history, see Fig.) conducted using elaborate three-dimensional finite element model revealed spatial and time complexity of the building response. Nevertheless, the design reinforcement with the structural solutions compensating extra factor K_2=1.2 taken into account appeared to be enough to provide structural safety (preventing progressive collapse of the building).
2. The very utilization of the “compensating measures” (we had not coined this term and believe there is a better one) which do not require mandatory seismic isolation enabled to perform the design and the scientific and technical support at a high level, and ensure the structural safety of the one considered within the present article and other truly unique buildings located in the earthquake-prone regions without groundless installation of a seismic isolation devices. Among famous and the latest approved by the FAI “Glavgosexpertiza of Russia” are the Opera and Ballet Theater located in Sevastopol city (in the immediate vicinity to the Choreographic Academy) and the Opera and Ballet Theater located in Kaliningrad city.
3. The structural safety of unique, highly dangerous, and technically sophisticated permanent facilities shall be substantiated by a real scientific and technical support including detailed and independent analysis of major structural safety parameters, not by its “imitation” usually come down to uncountable references to highly imperfect Russian building codes (a very gentle characteristic when considering its part related to the earthquake resistance of buildings and structures), and (or) “juggling” with regular “acts of the party and the government”.
4. The considered one and other plentiful examples of theoretical substantiation of the earthquake resistance of buildings and structures performed by NIC StaDyO JSC and Zolotov Research and Educational Center for Computational Modelling of the National Research Moscow State University of Civil Engineering state with absolute certainty that superiority of structural requirements over results of an elaborate theoretical analysis, which takes place in the current Russian seismic building design code [9], is desperately backward and hazardous. Perhaps, such requirements should be fulfilled only by underqualified design engineers; on second thoughts, it is more rational to keep such engineers off the substantiation of the earthquake resistance of permanent facilities.

ACKNOWLEDGEMENTS

This study was funded by the Ministry of Science and Higher Education of RF, project no. FSWG-2023-0004 “Territorial seismic protection system for critically important infrastructure based on granular metamaterials acting as broadband phononic crystals”.

REFERENCES

1. NIC StaDyO JSC proprietary standard. Scientific and technical support for design documentation of unique and critical permanent facilities (in regard to theoretical substantiation of structural safety). Scope, basic requirements, and formatting guidelines *(in Russian)*. Moscow, Russia: NIC StaDyo JSC, 2021, 80 p.
2. **Belostotsky, A., Pavlov, A., Nagibovich, A.** Numerical simulation of the stress-strain state of a large-span structure with joints with gap under the seismic loads in a transient dynamic. International Journal for Computational Civil and Structural Engineering, 2023, 19(3), 165-172. https://doi.org/10.22337/2587-9618-2023-19-3-165-172.
3. **Belostotsky, A.M., Akimov, P.A.** About some issues concerning finite element analysis of underground facilities response to seismic excitations *(in Russian)* // Proceed-

ings of the XX International Conference "Current Issues in Construction, Building Industry and Architecture", Tula, Russia, Jun 28-29, 2019. – Tula, Russia: Tula State University, 2019, pp. 67-70.

4. **Belostotsky, A.M., Akimov, P.A., Luong, N.T.N**. About some issues concerning numerical simulation of three-dimensional stress-strain state of "foundation – dam – reservoir" systems under seismic excitations *(in Russian)* // Proceedings of the XX International Conference "Current Issues in Construction, Building Industry and Architecture", Tula, Russia, Jun 28-29, 2019. – Tula, Russia: Tula State University, 2019, pp. 88-94.
5. **Travush, V.I., Belostotsky, A.M., Vershinin, V.V., Ostrovsky, K.I., Petryashev, N.O., Petryashev, S.O.** Numerical simulation of physically non-linear dynamic response of high-rise buildings under maximum design earthquake excitation *(in Russian)*. International Journal for Computational Civil and Structural Engineering, 2016, 12(1), 117-139.
6. **Belostotsky, A.M., Luong, N.T.N., Dmitriev, D.S., Scherbina, S.V**. Comparative analysis of numerical simulation methods of dynamic analysis of three-dimensional system "foundation – reservoir – dam" at seismic impacts *(in Russian)*. International Journal for Computational Civil and Structural Engineering, 2016, 12(2), 65-74.
7. **Belostotsky, A.M., Dmitriev, D.S., Luong, N.T.N.** Numerical method modeling of strain-stress state system "foundation – dam – reservoir" at seismic impacts. International Journal for Computational Civil and Structural Engineering, 2016, 12(4), 80-86.
8. **Belostotsky, A.M., Akimov, P.A., Afanasyeva, I.N., Kaytukov, T.B., Vershinin, V.V., Scherbina, S.V.** Article series on earthquake resistance analysis of large volume storage tanks with floating roofs (*in Russian*). Problems of Applied Mathematics and Computational Mechanics. MSUCE, Transactions No. 18, 2015, pp. 6-232.
9. SP 14.13330.2018 Seismic building design code. Revised edition of SNiP II-7-81* – Put into execution on Nov 25, 2018. – Moscow, Russia: Standartinform, 2018.

СПИСОК ЛИТЕРАТУРЫ

1. СТО АО НИЦ СтаДиО. Научно-техническое сопровождение проектной документации уникальных и особо ответственных объектов строительства (в части расчетного обоснования механической безопасности). Состав, основные требования и правила оформления, М., НИЦ СтаДиО, 2021, 80 с.
2. **Белостоцкий А.М., Павлов А.С., Нагибович А.Н.** Численное моделирование напряженно-деформированного состояния большепролетного сооружения с люфтами в опорах с учетом сейсмического воздействия в нелинейной динамической постановке // International Journal for Computational Civil and Structural Engineering, 2023, Том 19 № 3, pp. 165-172.
3. **Белостоцкий А. М., Акимов П. А.** О некоторых вопросах расчета подземных сооружений на сейсмические воздействия методом конечных элементов. // Сборник материалов XX Международной конференции «Актуальные проблемы строительства, строительной индустрии и архитектуры» (28-29 июня 2019 г.). – Тула, Тульский государственный университет, 2019, с. 67-70.
4. **Белостоцкий А. М., Акимов П. А., Нгуен Тай Нанг Лыонг**. О некоторых вопросах численного моделирования трехмерного динамического напряженно-деформированного состояния систем «основание – плотина – водохранилище» при сейсмических воздействиях. // Сборник материалов XX Международной конференции «Актуальные проблемы строительства, строительной индустрии и архитектуры“ (28-29 июня 2019

г.). – Тула, Тульский государственный университет, 2019, с. 88-94.

5. **Травуш В. И., Белостоцкий А. М., Вершинин В. В., Островский К. И., Петряшев Н. О. Петряшев С. О.** Численное моделирование физически нелинейной динамической реакции высотных зданий при сейсмических воздействиях уровня МРЗ // International Journal for Computational Civil and Structural Engineering / Международный журнал по расчету гражданских и строительных конструкций, Volume 12, Issue 1, 2016, pp. 117-139.
6. **Белостоцкий А.М., Нгуен Тай Нанг Лыонг, Д.С. Дмитриев, С.В. Щербина.** Сравнительный анализ методик численного моделирования динамики трехмерных систем «основание – арочная плотина – водохранилище» при сейсмических воздействиях // International Journal for Computational Civil and Structural Engineering / Международный журнал по расчету гражданских и строительных конструкций, Volume 12, Issue 2, 2016, pp. 65-74.
7. **Белостоцкий А. М., Нгуен Тай Нанг Лыонг, Д.С. Дмитриев.** Методика численного моделирования НДС системы «основание — плотина — водохранилище» при сейсмических воздействиях // Journal for Computational Civil and Structural Engineering / Международный журнал по расчету гражданских и строительных конструкций, Volume 12, Issue 4, 2016, pp. 80-86.
8. **Белостоцкий А.М., Акимов П. А., Афанасьева И.Н., Кайтуков Т. Б., Вершинин В.В., Щербина С.В.** Цикл статей о сейсмических расчетах резервуаров большой емкости с понтонами (плавающими крышами). Вопросы прикладной математики и вычислительной механики. МГСУ, Сборник трудов № 18, 2015, с. 6-232.
9. СП 14.13330.2018 Строительство в сейсмических районах. Актуализированная редакция СПиП II-7-81* – Введ. 2018-11-25. – М.: Стандартинформ, 2018.

Alexander M Belostotsky – DSc, Professor, Full Member of the Russian Academy of Architecture and Construction Sciences, Scientific adviser at A.B. Zolotov REC CM of the National Research Moscow State University of Civil Engineering; 129337, Russia, Moscow, Yaroslavskoe shosse, 26. e-mail: amb@stadyo.ru

Alexander I. Nagibovich – CSc, Director at A.B. Zolotov REC CM of the National Research Moscow Stale University of Civil Engineering; 129337, Russia, Moscow, Yaroslavskoe shosse, 26. e-mail: nagibovich@yandex.ru

Pavel I. Novikov – CSc, Senior Researcher at A.B. Zolotov REC CM of the National Research Moscow Stale University of Civil Engineering; 129337, Russia, Moscow, Yaroslavskoe shosse, 26. e-mail: novikov.mgsu@gmail.com

Vladislav V. Vershinin – Senior Lecturer at the Department of Structural Metal and Timber of the National Research Moscow Stale University of Civil Engineering; 129337, Russia, Moscow, Yaroslavskoe shosse, 26. e-mail: vlodya_91@mail.ru

Белостоцкий Александр Михайлович – д.т.н., профессор, академик РААСН, научный руководитель НОЦ КМ им. А.Б. Золотова Национального исследовательского Московского государственного строительного университета; 129337, Россия, г. Москва, Ярославское шоссе, д. 26. e-mail: amb@stadyo.ru

Нагибович Александр Игоревич – к.т.н, директор НОЦ КМ им. А.Б. Золотова Национального исследовательского Московского государственного строительного университета; 129337, Россия, г. Москва, Ярославское шоссе, д. 26. e-mail: nagibovich@yandex.ru

Новиков Павел Игоревич – к.т.н., старший научный сотрудник НОЦ КМ им. А.Б. Золотова Национального исследовательского Московского государственного строительного университета; 129337, Россия, г. Москва, Ярославское шоссе, д. 26. e-mail: novikov.mgsu@gmail.com

Вершинин Владислав Владимирович – старший преподаватель кафедры Металлических и деревянных конструкций Национального исследовательского Московского государственного строительного университета; 129337, Россия, г. Москва, Ярославское шоссе, д. 26. e-mail: vlodya_91@mail.ru